frontiers | Research Topics

Women in microbial physiology and metabolism 2023

Edited by
Jie Xiao, Ilana Kolodkin-Gal and Maria Filippa Addis

Published in
Frontiers in Microbiology

ISSN 1664-8714
ISBN 978-2-8325-5074-8
DOI 10.3389/978-2-8325-5074-8

About Frontiers

Frontiers is more than just an open access publisher of scholarly articles: it is a pioneering approach to the world of academia, radically improving the way scholarly research is managed. The grand vision of Frontiers is a world where all people have an equal opportunity to seek, share and generate knowledge. Frontiers provides immediate and permanent online open access to all its publications, but this alone is not enough to realize our grand goals.

Frontiers journal series

The Frontiers journal series is a multi-tier and interdisciplinary set of open-access, online journals, promising a paradigm shift from the current review, selection and dissemination processes in academic publishing. All Frontiers journals are driven by researchers for researchers; therefore, they constitute a service to the scholarly community. At the same time, the *Frontiers journal series* operates on a revolutionary invention, the tiered publishing system, initially addressing specific communities of scholars, and gradually climbing up to broader public understanding, thus serving the interests of the lay society, too.

Dedication to quality

Each Frontiers article is a landmark of the highest quality, thanks to genuinely collaborative interactions between authors and review editors, who include some of the world's best academicians. Research must be certified by peers before entering a stream of knowledge that may eventually reach the public - and shape society; therefore, Frontiers only applies the most rigorous and unbiased reviews. Frontiers revolutionizes research publishing by freely delivering the most outstanding research, evaluated with no bias from both the academic and social point of view. By applying the most advanced information technologies, Frontiers is catapulting scholarly publishing into a new generation.

What are Frontiers Research Topics?

Frontiers Research Topics are very popular trademarks of the *Frontiers journals series*: they are collections of at least ten articles, all centered on a particular subject. With their unique mix of varied contributions from Original Research to Review Articles, Frontiers Research Topics unify the most influential researchers, the latest key findings and historical advances in a hot research area.

Find out more on how to host your own Frontiers Research Topic or contribute to one as an author by contacting the Frontiers editorial office: frontiersin.org/about/contact

Women in microbial physiology and metabolism: 2023

Topic editors

Jie Xiao — Johns Hopkins University, United States
Ilana Kolodkin-Gal — Reichman University, Israel
Maria Filippa Addis — University of Milan, Italy

Citation

Xiao, J., Kolodkin-Gal, I., Addis, M. F., eds. (2024). *Women in microbial physiology and metabolism: 2023*. Lausanne: Frontiers Media SA.
doi: 10.3389/978-2-8325-5074-8

Table of contents

frontiers | Frontiers in Microbiology

TYPE Editorial
PUBLISHED 14 June 2024
DOI 10.3389/fmicb.2024.1437794

OPEN ACCESS

EDITED AND REVIEWED BY
Biswarup Mukhopadhyay,
Virginia Tech, United States

*CORRESPONDENCE
Maria Filippa Addis
✉ filippa.addis@unimi.it
Jie Xiao
✉ xiao@jhmi.edu
Ilana Kolodkin-Gal
✉ ilana.kolodkin@runi.ac.il

RECEIVED 24 May 2024
ACCEPTED 03 June 2024
PUBLISHED 14 June 2024

CITATION
Addis MF, Xiao J and Kolodkin-Gal I (2024) Editorial: Women in microbial physiology and metabolism: 2023.
Front. Microbiol. 15:1437794.
doi: 10.3389/fmicb.2024.1437794

Editorial: Women in microbial physiology and metabolism: 2023

Maria Filippa Addis[1]*, Jie Xiao[2]* and Ilana Kolodkin-Gal[3]*

[1]Department of Veterinary Medicine and Animal Science, University of Milan, Milan, Italy, [2]Department of Biophysics and Biophysical Chemistry, Johns Hopkins School of Medicine, Baltimore, MD, United States, [3]Scojen Institue for Synthetic Biology, Reichman University, Herzliya, Israel

KEYWORDS

metabolism, microbial diversity, microbial genetics, microbial physiology, antibiotics, food microbes, women scientists

Editorial on the Research Topic
Women in microbial physiology and metabolism: 2023

There is overwhelming evidence that female scientists have shaped modern microbiology in general and the study of microbial physiology and metabolism. In 1928, Marjory Stephenson isolated a bacterial enzyme, lactic dehydrogenase, from *Escherichia coli*. In the 1930s, the German-Jewish bacteriologist Emmy Klieneberger-Nobel developed a unique nutrient agar blend and culturing technique that allowed the bacteria that caused bronchopneumonia in rats and mice to grow in a lab for the first time and later isolated and identified several pathogenic species of mycoplasma—*Mycoplasma arthritidis* and *Mycoplasma pneumoniae*. In 1944, Elizabeth Bugie, an American microbiologist and biochemist, contributed significantly to the breakthrough discovery of the antibiotic streptomycin. Besides these fundamental discoveries, female scientists have also contributed overwhelmingly to the evolution of molecular approaches, the fundamental understanding of bacterial genetics, and the development of accurate tools to study the physiology of microorganisms. These scientists span from the unsung hero of her time, Rosalind Franklin, who played a vital role in generating an X-ray diffraction analysis of the DNA's double-helical structure, leading to the resolution of the double helix, to the American Jewish scientist Esther Lederberg, who discovered the Lambda (λ) phage and gene transfers between bacteria through a process called "specialized transduction," and to recent microbiologists Jennifer Doudna and Emmanuelle Charpentier who won the Nobel prize for CRISPR, a bacterial immune system for self-defense, in 2020 (Nature Microbiology, 2022). Out of unending respect for the contributions of female scientists to the field, we had the distinct honor of editing this year's Research Topic of Women in Metabolism and Physiology. Accepted manuscripts in this Research Topic represent a collection of outstanding works led by female scientists in the field, including but not limited to the investigation of microbial strategies for resistance, communication, cooperation, and survival in extreme environments, the application of novel physical chemistry and omic approaches to resolving microbial metabolism, and a novel discovery that *B. subtilis* histone-like protein is involved in antibiotic tolerance. Below, we provide a glimpse of these exciting studies.

Xenobiotics often challenge the principle of microbial infallibility. One example is acesulfame. Introduced in the 1980s as a zero-calorie sweetener, it was recalcitrant in wastewater treatment plants until the early 2010s. By studying acesulfame metabolism in alphaproteobacterial degraders of the genera *Bosea*

and *Chelatococcus*, Bonatelli et al. experimentally confirmed the previously postulated route of two subsequent hydrolysis steps of acesulfame to acetoacetate and sulfamate *via* acetoacetamide-N-sulfonate. By applying comparative genomics, heterologous expression, and biochemical analysis, the authors identified genes responsible for acesulfame anion degradation and surveyed their distributions in public sequence databases. The authors discuss that this pathway may be established by combining preexisting catabolic genes; horizontal gene transfer may facilitate its fast distribution. The authors conclude that structurally related natural and anthropogenic compounds, such as aminoacyl sulfamate ribonucleotide or sulfonamide antibiotics, may have supported the evolution of the acesulfame degradation pathway.

The study by González-Orozco et al. explored microbial metabolism in the context of bacterial interactions. The research delves into the interactions between the probiotic lactic acid bacterium (LAB) *Lactobacillus kefiranofaciens* from Kefir and the yeast *Kluyveromyces marxianus*. The findings suggest that co-culturing these two microorganisms enhances their survival in gastrointestinal conditions and improves their adhesion to epithelial cells. These findings indicate that the combination enhances the probiotic potential of both species. The authors highlight the potential of using co-cultures of yeast and lactic acid bacteria in creating novel fermented functional products that support human health. The contribution of the food microbiome to our health is also manifested in a review by Eicher et al. where the role of citrate is thoroughly discussed with the LAB bacterium *Oenococcus oeni,* which is involved in the second step in wine fermentation.

Haenelt et al. provide an interesting insight into the communal genetics of wastewater. In their research, the authors shed light on antibiotic-resistant bacteria, their resistance genes (ARGs), and their dynamics in untreated and treated wastewater. The authors reveal that higher proportions of wastewater rivers increased the absolute and relative abundance of ARGs encoding for sulfonamide resistance genes and that this effect was season-dependent. Moreover, they obtain evidence that biofilms in wastewater may serve as a reservoir for ARGs, in agreement with the dense growth of microorganisms in a biofilm, where limited diffusion of small molecules may provide biofilm microenvironments with altered antibiotic concentrations. The community contribution to genomic evolution toward environmental resistance is also reflected in Pagnucco et al., who explore metal tolerance and biosorption of four bacterial environmental strains of *Serratia*, *Raoultella*, and *Klebsiella* isolated from Saint Clair River sediments. The effective removal of various metal cations (As^{3+}, Pb^{2+}, Cu^{2+}, Mn^{2+}, Zn^{2+}, Cd^{2+}, Cr^{6+}, and Ni^{2+}) by these strains confirmed that that metal absorption involves interactions between metal ions and functional groups on the surface of the strains. Moreover, the study revealed a variation in specifications of metal absorption between strains, highlighting the importance of tailoring selected strains and species to suit the environment's metal composition.

Our understanding of microbial metabolism fundamentally relies on technologies that can sensitively and accurately measure metabolites. Kassem et al. review how Fourier Transform-Infrared (FT-IR) spectroscopy can be a powerful tool to resolve the physiology of microorganisms and their responses to the environment. The applications of FT-IR spectroscopy open new fronts in analyzing microbial composition, functions, and interactions and have significantly advanced our understanding of microbial communities and their interactions within complex ecosystems. Key challenges in harnessing the full potential of FT-IR are thoroughly discussed. The review describes how qualitative insights into microbial composition and functional groups can be obtained with FT-IR spectroscopy and provides a comprehensive summary of data interpretation, analysis, and handling. Moreover, the authors discuss future aspects of standardization of FT-IR spectroscopy for microbial identification and the integration of FT-IR with complementary techniques, such as Raman spectroscopy, mass spectrometry, and genomics, which may revolutionize the study and resolution of complex metabolic pathways and molecular interactions.

Bacterial communication is a fundamental process synchronizing gene expression and collective behavior within the bacterial population. The most studied bacterial communication system is quorum sensing, a cell density system in which the concentration of inducers increases to a threshold level, allowing detection by specific receptors. As a result, bacteria can change their behavior in a coordinated way. In *Pseudomonas* spp., quorum sensing based on the synthesis of N-acyl homoserine lactone molecules is well studied. However, volatile organic compounds, although considered communication signals in the rhizosphere, are understudied. In their research article, Dupont et al. explore the role of the volatile organic compound 1-undecene in the communication of *Pseudomonas fluorescens* MFE01, a strain with a very active Type VI secretion system that can kill some competitive bacteria, by constructing defective mutants. Using this approach, they demonstrate that *P. fluorescens* MFE01 uses 1-undecene emission for aerial communication, reporting this volatile organic compound as a bacterial intraspecific communication signal for the first time.

Pectobacterium is considered one of the top ten bacterial pathogens that causes harvest loss of potatoes and other vegetables in the field and during transport or storage. These bacteria can cause soft rot disease in various plants due to the secretion of cell wall degrading enzymes. *Pectobacterium betavasculorum* is a member of the *Pectobacerium* genus that inhabits a variety of niches and is found in all climates. It is responsible for the vascular necrosis of sugar beet and soft rot of many vegetables. In their original research article, Smoktunowicz et al. investigated the metabolism of *P. betavasculorum* in the presence of sucrose and xylose, the two main sugars of sugar beet and artichoke, by applying untargeted metabolomics coupled with genomics. The authors confirmed the ability of the strains to use various sugars as the only carbon source, and provided information on the active metabolic pathways for their degradation.

Extreme environments are challenging for life, yet bacteria have developed strategies for survival. The Atacama Desert, located in northern Chile at the border with Bolivia and Argentina, is the driest, with the highest radiation, and one of the most ancient deserts in the world. In their original research article, Reverdy et al. provide a comprehensive

picture of microbial diversity and investigate the survival strategies of bacteria living in this hostile habitat. Upon sampling 18 locations and cultivating 74 unique isolates, the authors characterized pigment production, biofilm formation, production of inhibitory substances, and antibiotic resistance as probable survival mechanisms, providing insights into bacterial diversity and the strategies that bacteria use to survive in extreme environments. These functional characterizations create opportunities for their exploitation in agriculture, healthcare, or biotechnological applications.

Lastly, Carr et al. reveal a novel role of a histone-like protein in microbial tolerance to antibiotics. Unlike archaea and eukaryotes, in which DNA is wrapped around in a nucleosome-like structure, bacteria use histone-like proteins to control the condensation of the microbial chromosome. In *Bacillus subtilis*, the histone-like protein HBsu is acetylated at seven sites, which regulates DNA compaction and the process of sporulation. The authors analyzed a collection of HBsu mutants to reveal the potential roles of this protein in response to antibiotics. The authors demonstrated that the acetylation status of HBsu led to an increase in persister cell formation. Moreover, deacetylation-mimic mutants with compacted nucleoids delayed in resuming growth after antibiotic removal. This work suggests that histone acetylation is required to escape the persistent state, which may play an important role in the epigenetic machinery of bacteria in the response to antibiotics.

Collectively, these discoveries highlight the significant contributions of femal scientsits to the field of microbial sciences with their broad scope and depth, emphasizing the importance of diversity and inclusion in our scientific community.

References

Nature Microbiology (2022). Breaking the bias in microbiology. *Nat. Microbiol.* 7, 341–342. doi: 10.1038/s41564-022-01086-z

Author contributions

MA: Writing – original draft, Writing – review & editing. JX: Writing – original draft, Writing – review & editing. IK-G: Writing – original draft, Writing – review & editing. All authors contributed equally to this work.

Funding

The author(s) declare that no financial support was received for the research, authorship, and/or publication of this article.

Conflict of interest

The authors declare that the research was conducted in the absence of any commercial or financial relationships that could be construed as a potential conflict of interest.

The author(s) declared that they were an editorial board member of Frontiers, at the time of submission. This had no impact on the peer review process and the final decision.

Publisher's note

frontiers | Frontiers in Microbiology

TYPE Original Research
PUBLISHED 27 July 2023
DOI 10.3389/fmicb.2023.1223838

OPEN ACCESS

EDITED BY
Maria Filippa Addis,
University of Milan, Italy

REVIEWED BY
Gao Chen,
The University of Tennessee, Knoxville, United States
Hong-Jun Chao,
Wuhan Polytechnic University, China

*CORRESPONDENCE
Thore Rohwerder
✉ thore.rohwerder@ufz.de
Sabine Kleinsteuber
✉ sabine.kleinsteuber@ufz.de

†PRESENT ADDRESSES
Denny Popp,
Institute of Human Genetics, University of Leipzig Medical Center, Leipzig, Germany
Kuan-Po Liao,
Fraunhofer Institute for Interfacial Engineering and Biotechnology, Stuttgart, Germany

RECEIVED 16 May 2023
ACCEPTED 27 June 2023
PUBLISHED 27 July 2023

CITATION
Bonatelli ML, Rohwerder T, Popp D, Liu Y, Akay C, Schultz C, Liao K-P, Ding C, Reemtsma T, Adrian L and Kleinsteuber S (2023) Recently evolved combination of unique sulfatase and amidase genes enables bacterial degradation of the wastewater micropollutant acesulfame worldwide.
Front. Microbiol. 14:1223838.
doi: 10.3389/fmicb.2023.1223838

Recently evolved combination of unique sulfatase and amidase genes enables bacterial degradation of the wastewater micropollutant acesulfame worldwide

Maria L. Bonatelli[1], Thore Rohwerder[1]*, Denny Popp[1†], Yu Liu[2], Caglar Akay[2], Carolyn Schultz[1], Kuan-Po Liao[1†], Chang Ding[2], Thorsten Reemtsma[3,4], Lorenz Adrian[2,5] and Sabine Kleinsteuber[1]*

[1]Department of Environmental Microbiology, Helmholtz Centre for Environmental Research—UFZ, Leipzig, Germany, [2]Department of Environmental Biotechnology, Helmholtz Centre for Environmental Research—UFZ, Leipzig, Germany, [3]Department of Analytical Chemistry, Helmholtz Centre for Environmental Research—UFZ, Leipzig, Germany, [4]Institute of Analytical Chemistry, University of Leipzig, Leipzig, Germany, [5]Chair for Geobiotechnology, Technische Universität Berlin, Berlin, Germany

Xenobiotics often challenge the principle of microbial infallibility. One example is acesulfame introduced in the 1980s as zero-calorie sweetener, which was recalcitrant in wastewater treatment plants until the early 2010s. Then, efficient removal has been reported with increasing frequency. By studying acesulfame metabolism in alphaproteobacterial degraders of the genera *Bosea* and *Chelatococcus*, we experimentally confirmed the previously postulated route of two subsequent hydrolysis steps via acetoacetamide-N-sulfonate (ANSA) to acetoacetate and sulfamate. Genome comparison of wildtype *Bosea* sp. 100-5 and an acesulfame degradation-defective mutant revealed the involvement of two plasmid-borne gene clusters. The acesulfame-hydrolyzing sulfatase is strictly manganese-dependent and belongs to the metallo beta-lactamase family. In all degraders analyzed, it is encoded on a highly conserved gene cluster embedded in a composite transposon. The ANSA amidase, on the other hand, is an amidase signature domain enzyme encoded in another gene cluster showing variable length among degrading strains. Transposition of the sulfatase gene cluster between chromosome and plasmid explains how the two catabolic gene clusters recently combined for the degradation of acesulfame. Searching available genomes and metagenomes for the two hydrolases and associated genes indicates that the acesulfame plasmid evolved and spread worldwide in short time. While the sulfatase is unprecedented and unique for acesulfame degraders, the amidase occurs in different genetic environments and likely evolved for the degradation of other substrates. Evolution of the acesulfame degradation pathway might have been supported by the presence of structurally related natural and anthropogenic compounds, such as aminoacyl sulfamate ribonucleotide or sulfonamide antibiotics.

KEYWORDS

pathway evolution, treatment wetland, sulfamic acid derivative, mobile genetic element, horizontal gene transfer

1. Introduction

Acesulfame potassium (ACE-K) is an artificial sweetener used in food and beverages, pharmaceuticals and personal care products. It was discovered in the late 1960s (Clauß and Harald, 1973) and is a zero-calorie, high-potency sweetener that is 200 times sweeter than sucrose, with good storage and temperature stabilities (Klug and von Rymon Lipinski, 2012). It received its first approval of use in the UK in 1983 and has been used worldwide since the 1990s (Klug and von Rymon Lipinski, 2012). After human consumption, the acesulfame anion (ACE) is readily absorbed but not metabolized, and eventually excreted unchanged via the urinary tract. Consequently, ACE is present in domestic wastewater in a range between 10 and 100 $\mu g\,L^{-1}$ (Lange et al., 2012) and can reach other aquatic environments (Buerge et al., 2009). Due to its hydrophilicity and persistence, ACE became an ideal anthropogenic wastewater tracer (Lange et al., 2012). Recalcitrance of ACE in wastewater treatment plants (WWTPs) was reported first in 2009 (Buerge et al., 2009), and its persistence in surface waters, groundwater and even tap water was observed in the USA (Subedi and Kannan, 2014; Schaider et al., 2016), Canada (Liu et al., 2014), China (Gan et al., 2013), Germany (Nodler et al., 2013) and other countries in the early 2010s. However, reports on ACE biodegradation in WWTPs started to appear in the later 2010s. Two studies conducted in Australia (Cardenas et al., 2016) and China (Yang et al., 2017) revealed high percentages (92% and 85%, respectively) of ACE removal in WWTPs. When analyzing 13 WWTPs in Switzerland and Germany, Castronovo et al. (2017) noticed 57 to 97% ACE removal and identified sulfamic acid/the sulfamate ion as the transformation product. Likewise, Kahl et al. (2018) reported biodegradation of >85% in nine WWTPs in Germany and observed a seasonality of ACE removal with highest efficiency in summer and autumn. These results challenged the perception of ACE recalcitrance and clearly indicated biodegradation as the removal mechanism.

The reports on emerging ACE biodegradability in WWTPs inspired research on the microorganisms and metabolic pathways involved with this process. In a first study of our lab (Kahl et al., 2018), ACE-degrading bacteria were enriched from sludge sampled from a treatment wetland in 2015 (located in Mockrehna, Germany). We used mineral medium with 125 $\mu g\,L^{-1}$ to 125 $mg\,L^{-1}$ ACE-K as sole carbon source and showed evidence for its complete mineralization. From the resulting community, which was dominated by *Alpha-and Gammaproteobacteria* (Kahl et al., 2018), we isolated a pure culture identified as *Bosea* sp. 3-1B (Kleinsteuber et al., 2019). Three more strains (*Bosea* sp. 100-5, *Chelatococcus* sp. 1 g-2 and 1 g-11) were isolated later using fresh samples from the same wetland by direct enrichment on 0.1 to 1 $g\,L^{-1}$ ACE-K (Kleinsteuber et al., 2019). The latter three strains completely degraded 1 $g\,L^{-1}$ ACE-K within 8 to 9 days and formed sulfamate in stoichiometric amounts during batch cultivation. Additionally, acetoacetamide-N-sulfonate (ANSA) was detected transiently in culture supernatants, confirming the assumption of Castronovo et al. (2017) who suggested ANSA as an intermediate of ACE degradation. Based on this finding, we proposed a catabolic pathway of two subsequent hydrolysis steps via ANSA to acetoacetate as shown in Figure 1 (Kleinsteuber et al., 2019).

Another group investigated ACE-degrading communities enriched from activated sludge (sampled at a WWTP located in Hong Kong, China) and found that the most abundant metagenome-assembled genomes (MAGs) belonged to *Planctomycetes*, *Alpha- and Gammaproteobacteria* (Huang et al., 2021). These authors also isolated two ACE-mineralizing *Chelatococcus* strains (YT9 and HY11) and compared their genomes with those of two *Chelatococcus* type strains that do not degrade ACE. They found a total of 812 protein-coding genes that were present in both ACE-degrading strains but not in *Chelatococcus* type strains DSM 6462 and DSM 101465. However, they could not further narrow down the ACE degradation genes. Recently, the group of bacterial genera with representatives capable of ACE mineralization was extended by *Shinella*, and based on comparative genomics it was speculated that the degradation is a plasmid-mediated process (Huang et al., 2022).

Despite these advances in isolating ACE-degrading pure cultures and sequencing the genomes of a few strains, the ACE-degrading enzymes have not yet been identified, and the proposed pathway still needs to be confirmed. Hence, the genetic background of this recently emerged catabolic trait and its evolutionary origin remained elusive. The present study aimed to elucidate the ACE metabolism in our previously isolated strains (Kleinsteuber et al., 2019) and some other ACE degraders that we have isolated from WWTPs located in Germany. Based on comparative genomics, heterologous expression and biochemical analysis, we identified the genes responsible for ACE degradation and surveyed their distribution in public sequence databases. Additionally, we discuss the mechanisms that might have established this pathway by combination of preexisting catabolic genes and facilitated its fast distribution by horizontal gene transfer.

2. Materials and methods

2.1. Isolation and cultivation of bacterial strains

Bosea sp. 3-1B was previously isolated from an ACE-degrading enrichment culture (Kahl et al., 2018; inoculum sludge sampled in July 2015, see also Table 1). *Bosea* sp. 100-5, *Chelatococcus* sp. 1 g-2 and *Chelatococcus* sp. 1 g-11 originated from the same treatment wetland sampled in February 2019. The strains were isolated by plating on R2A agar (Reasoner and Geldreich, 1985) after enrichment in DSMZ 462 mineral medium (see Supplementary material for recipe) with 0.5 or 5 mM ACE as sole carbon source (Kleinsteuber et al., 2019). *Chelatococcus asaccharovorans* WSA4-1, *Chelatococcus* sp. WSC3-1, *Chelatococcus asaccharovorans* WSD1-1, *Chelatococcus* sp. WSG2-a and *Shinella* sp. WSC3-e were isolated from enrichment cultures in DSMZ 461 mineral medium (see Supplementary material for recipe) with 5 mM ACE inoculated with activated sludge from four WWTPs in Germany (sampled in 2020, see Table 1). The strains were identified by Sanger sequencing of 16S rRNA genes (Lane, 1991) and maintained on DSMZ 461 agar with 5 mM ACE incubated at 30°C. Liquid cultures to study growth and degradation kinetics or for enzyme assays and DNA extraction were set up in DSMZ 461 or DSMZ 462 medium with the respective carbon source (2.5 to 10 mM ACE, 10 mM 3-hydroxybutyrate or 10 mM succinate; supplied by Sigma-Aldrich as potassium or sodium salts). Inability of *Paraburkholderia sartisoli* LMG 24000 (obtained as DSM 23088 from DSMZ, Braunschweig, Germany) to degrade ACE was tested at 30°C during growth on DSMZ 461 with 3-hydroxybutyrate (2.5 mM ACE not degraded) and

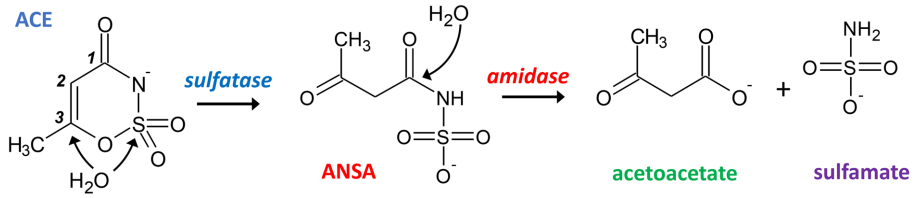

FIGURE 1
Proposed hydrolytic pathway for bacterial degradation of ACE. Initially, a sulfatase catalyzes the attack of either the sulfur or C3 atom of ACE resulting in the formation of ANSA. In a subsequent step, an amidase hydrolyzes the linear amide intermediate to acetoacetate and sulfamate.

by incubation on DSMZ 461 with 5 mM ACE as only substrate (no growth observed).

To select an ACE degradation-defective mutant, *Bosea* sp. 100-5 was grown in R2A medium for 12 transfers and plated on R2A agar in dilution series to obtain single colonies. Isolates were screened for growth in liquid culture on either ACE or succinate as sole carbon source. One isolate that grew on succinate but not on ACE was identified and designated as *Bosea* sp. 100-5 Mut1.

2.2. Genome sequencing

Genomic DNA was extracted from ACE-grown cells (DSMZ medium 461 with 5 mM ACE) with the NucleoSpin Microbial DNA kit (Macherey-Nagel, Düren, Germany) according to the manual and using wide-bore tips. DNA concentration was measured with the Qubit dsDNA BR Assay Kit (Thermo Fisher Scientific, Rockford, IL, United States); DNA integrity was checked by gel electrophoresis.

Genomes of all strains except *Bosea* sp. 100-5 Mut1 were sequenced using a combination of long-read and short-read approaches. Long-read sequencing was done on the MinION MK1b platform (Oxford Nanopore Technologies, Oxford, United Kingdom) as previously described (Liu et al., 2020) using Guppy v4.0.15 for basecalling. Nanopore read data was downsampled per isolate to about 150x coverage using filtlong v0.2.0[1] with a priority on read length (—length_weight 10). Short-read sequencing of strain 3-1B was conducted on the Illumina MiSeq platform (Illumina, San Diego, CA, United States) using the NEBNext Ultra II FS DNA library prep kit (New England Biolabs, Frankfurt, Germany) to prepare a 2 × 300 bp library. Short-read sequencing of the other strains was performed on the Illumina NovaSeq platform (2 × 150 bp; Genewiz, Leipzig, Germany). Short and long reads were assembled with a hybrid approach using Unicycler v0.4.9 (Wick et al., 2017) with default parameters.

Genome sequencing of *Bosea* sp. 100-5 Mut1 was conducted on the Illumina NextSeq 2000 platform (2 × 150 bp; StarSeq, Mainz, Germany). After assembly with SPAdes version 3.15.2 (Prjibelski et al., 2020), contigs smaller than 500 bp were excluded from the assembly. Platanus v1.2.1 (Kajitani et al., 2014) was used for scaffolding and Mauve 20150226 (Darling et al., 2004) for reordering the contigs using the wildtype genome of *Bosea* sp. 100-5 as reference.

2.3. Genome annotation and comparative genomics

The MicroScope pipeline was used for the prediction and functional annotation of coding sequences (CDS; Vallenet et al., 2020). The tools GTDB-tk 1.1.2 (Chaumeil et al., 2019) and CheckM 1.3.0 (Parks et al., 2015) were used for taxonomic classification and estimating genome completeness and contamination, respectively. Genome metrics is provided in Supplementary Table S1. To compare the genome of *Bosea* sp. 100-5 with *Bosea* sp. 100-5 Mut1, we used Geneious 10.0.9 (Kearse et al., 2012), Mauve and Proksee 1.1.3 (Stothard and Wishart, 2005). Additionally, the Synteny Statistics tool of MicroScope was used to explore the similarity between the two genomes. Gene clusters of interest and surrounding genes were investigated in all genomes with cblaster version 1.3.11 (Gilchrist et al., 2021). Besides the genomes sequenced in this study, we included the genomes of five isolates and the MAG sequences of the corresponding BioProjects (PRJNA725625, PRJNA749893; Huang et al., 2021, 2022). Briefly, protein sequences of >100 amino acids were searched against a database built from genomes annotated with MicroScope applying default parameters, except for minimal nucleotide identity of 90%. For the genomes that did not present the gene clusters, tblastn was used to manually search for BOSEA1005_40015.

To look for genes related to BOSEA1005_40015 in public databases, we searched the NCBI and the JGI[2] databases (both June 2023) using different strategies. In NCBI, we used tblastn with both nr and env_nr databases and with the whole-genome shotgun contigs (WGS) database. The tblastn search was limited to the following metagenomes: activated sludge (taxid:942017), aquatic (taxid:1169740), aquifer (taxid:1704045), bioreactor (taxid:1076179), bioreactor sludge (taxid:412754), drinking water (taxid:2651591), freshwater (taxid:449393), groundwater (taxid:717931), lagoon (taxid:1763544), lake water (taxid:1647806), pond (taxid:1851193), sludge (taxid:1592332) and wastewater (taxid:527639). In JGI, blastp search (E-value < 1 e-40) was done in the metagenome datasets wastewater treatment plant (365) and wastewater (439), and in the metatranscriptome datasets wastewater treatment plant (43) and wastewater (20). Metagenome dataset bioreactor (816) and metatranscriptome dataset bioreactor (259) were also investigated. For datasets presenting hits for the query sequence BOSEA1005_40015, we searched for other elements of the *Bosea* sp. 100-5 plasmid and

1 https://github.com/rrwick/Filtlong

2 https://img.jgi.doe.gov

TABLE 1 Information on the bacterial genomes analyzed in this study.

Strain	Sampling site/isolation origin	Sampling date	Localization of ACE clusters 1 and 2	Size of contigs with ACE clusters (bp)	Assembly accession	References
Bosea sp. 100-5	Treatment wetland Langenreichenbach, Mockrehna, Germany (51°30′N 12°53′E)	2019	Contig 4	40,931	GCA_930633465	Kleinsteuber et al. (2019)
Bosea sp. 100-5 Mut1	Spontaneous mutant of *Bosea* sp. 100-5	Isolated in 2021	Contig 56 (only cluster 2)	9,696 (only cluster 2)	GCA_946047605	This work
Bosea sp. 3-1B	Treatment wetland Langenreichenbach, Mockrehna, Germany (51°30′N 12°53′E)	2015	Contig 3	43,141	GCA_930633495	Kleinsteuber et al. (2019)
Chelatococcus sp. 1 g-2	Treatment wetland Langenreichenbach, Mockrehna, Germany (51°30′N 12°53′E)	2019	Contig 3	41,507	GCA_930633515	Kleinsteuber et al. (2019)
Chelatococcus sp. 1 g-11	Treatment wetland Langenreichenbach, Mockrehna, Germany (51°30′N 12°53′E)	2019	Contig 6	45,665	GCA_930633505	Kleinsteuber et al. (2019)
Chelatococcus asaccharovorans WSA4-1	WWTP Markranstädt, Germany (51°18′N 12°12′E)	2020	Contig 5	45,942	GCA_930633525	This work
Chelatococcus sp. WSC3-1	WWTP Rosental, Leipzig, Germany (51°21′N 12°20′E)	2020	Contig 2	45,505	GCA_930633455	This work
Chelatococcus asaccharovorans WSD1-1	WWTP Markkleeberg, Germany (51°17′N 12°21′E)	2020	Contig 6	41,507	GCA_930633485	This work
Chelatococcus sp. WSG2-a	WWTP Wiedemar, Germany (51°28′N 12°11′E)	2020	Contig 1	45,506	GCA_930633475	This work
Chelatococcus sp. YT9	WWTP Sha Tin, Hong Kong, China	2018	Contig 1 (cluster1) Contig 5 (cluster 2)	4,368,288 (cluster 1) 16,496 (cluster 2)	GCA_018398315	Huang et al. (2021)
Chelatococcus sp. HY11	WWTP Sha Tin, Hong Kong, China	2018	Contig 6 (only cluster 2)	18,060 (only cluster 2)	GCA_018398335	Huang et al. (2021)
Shinella sp. WSC3-e	WWTP Rosental, Leipzig, Germany (51°21′N 12°20′E)	2020	Contig 2 (only cluster 2)	41,586 (only cluster 2)	GCA_945994535	This work
Shinella sp. HY16	WWTP Sha Tin, Hong Kong, China (22.17 N 114.08 E)	2021	Contig 11 (only cluster 2)	41,603 (only cluster 2)	GCA_028534175	Huang et al. (2022)
Shinella sp. YE25	WWTP Sha Tin, Hong Kong, China (22.17 N 114.08 E)	2021	Contig 13 (only cluster 2)	41,586 (only cluster 2)	GCA_028534295	Huang et al. (2022)
Shinella sp. YZ44	WWTP Sha Tin, Hong Kong, China (22.17 N 114.08 E)	2021	Contig 11 (only cluster 2)	41,603 (only cluster 2)	GCA_028534455	Huang et al. (2022)

used Geneious and Proksee to compare them. Predicted proteins with ambiguous annotation were searched for functional sites with the NCBI Conserved Domains tool (Lu et al., 2020) using CDD v3.20 and InterPro 93.0 (Finn et al., 2017).

2.4. Biochemical analyses

Crude extracts from bacterial cells were prepared in lysis buffer (10 mM Tris–HCl with 10% glycerol, pH 7.8) applying French press or disruption in a mixer mill with glass beads (Becher et al., 2018). Extracts were obtained by centrifugation at 20,000 x g and 4°C for 20 min. For removal of low molecular weight compounds interfering with HPLC analysis, protein extracts were purified with 10 kDa Amicon filters (Merck, Darmstadt, Germany). Protein concentration was determined with Pierce BCA Protein Assay Kit (Thermo Fisher Scientific) or Bradford reagent (AppliChem, Darmstadt, Germany) using bovine serum albumin as standard. For degradation assays and as analytical standards, ACE potassium salt (99% pure, Merck) and acetoacetate lithium salt (95% pure; abcr GmbH, Karlsruhe, Germany) were used. As ANSA is not commercially available, it was prepared employing the

ACE-hydrolyzing activity of *Bosea* sp. 100-5. To separate ACE and ANSA hydrolase activities, size exclusion chromatography was used with protein crude extracts of ACE-grown cells, a Superdex 200 10/300 column (Cytiva, Marlborough, MA, United States) and 100 mM ammonium hydrogen carbonate buffer pH 7.82 as eluent. Fractions showing ACE hydrolytic activity were directly used to prepare up to 20 mM ANSA at 2-mL scale (for details see Supplementary material). The conversion was stoichiometric enabling calibration for ANSA (Supplementary Figure S1). ACE and ANSA hydrolysis activities were quantified in discontinuous HPLC-based assays at 30°C in lysis buffer. Samples were diluted in stop buffer (10 mM malonate, pH 4.0, 60°C) prior to HPLC analysis.

2.5. Heterologous expression of the hydrolase genes

Genes were synthesized and cloned into expression vector pET-28a(+)-TEV (BOSEA1005_40015 via *Bmt*I/*Bam*HI sites; BOSEA1005_40016 and BOSEA1005_40030 via *Nde*I/*Bam*HI sites; GenScript, Oxford, United Kingdom). Recombinant plasmids were transformed into *E. coli* Lemo21 (DE3; New England Biolabs). Resulting strains were grown at 30°C in lysogeny broth with 30 ppm chloramphenicol and 50 ppm kanamycin at 30°C until an optical density (600 nm) of 0.5. Then, 0.4 mM isopropyl β-d-1-thiogalactopyranoside were added and incubation proceeded at 17°C for 20 h (40016 and 40030) or 30°C for 4 h (40015). For expression of 40016 and 40030, cultures were supplemented with 0.1 mM rhamnose and, after induction, with 2% (v/v) ethanol. Due to lack of Mn^{2+} in lysogeny broth (Anjem et al., 2009), $MnCl_2$ at 0.5 mM was added to cultures expressing 40015 as indicated in corresponding figure captions. Due to low yield of soluble heterologous protein, expression of BOSEA1005_40015, 40016, and 40030 genes was not routinely monitored by gel electrophoresis but by employing shotgun proteomics. Crude extracts from respective transformed *E. coli* strains obtained after heterologous expression were analyzed according to Schopper et al. (2017) with some modifications. Protein extracts were denatured by 5% (w/v final concentration) sodium deoxycholate (≥98%, Sigma-Aldrich) and sequentially treated with 12 mM dithiothreitol and 40 mM 2-iodacetamide before overnight digestion with trypsin (Promega). The desalting method for the digested peptides and also the nano-LC-MS/MS analysis were from Ding and Adrian (2020). Relative abundance of the heterologous BOSEA1005_40015, 40016, and 40030 proteins, other pET-28a(+)-TEV-related proteins (LacI and KanR) as well as a selection of endogenous *E. coli* proteins is compared in Supplementary Table S2.

2.6. Analytics

ACE, ANSA and acetoacetate were quantified by HPLC (Shimadzu) with a photodiode array detector employing a Nucleosil 100-5 C18 HD column (240/3 mm, Macherey-Nagel) and an eluent at 0.5 mL min^{-1} containing 100 mM NaH_2PO_4 and 10 mM tetrabutylammoniumhydrogensulfate, pH 4.5, and an acetonitrile gradient (% v/v): 2 min 7.5, linear increase to 27.5 in 2 min, 6 min 27.5, linear decrease to 7.5 in 2 min, 12 min 7.5. ACE and ANSA peaks were analyzed at 260 nm, acetoacetate at 274 nm.

Identity of enzymatically prepared ANSA was validated by LC–MS/MS (Agilent) operated with electrospray ionization in negative polarity and equipped with a Zorbax Eclipse Plus Rapid Resolution HT-C18 column (100 × 3 mm, 1.8 µm, Agilent) at 30°C. A binary mobile phase at 0.4 mL min^{-1} consisted of 0.2% formic acid and a methanol gradient: 1 min equilibration at 10%, 2 min linear increase to 55%, 7 min linear increase to 95%, 2 min hold at 95%, 0.5 min decrease to 10% and 3.5 min hold at 10%. See Supplementary material for further details.

3. Results

3.1. Enzymatic ACE hydrolysis in *Bosea* sp. 100-5 proceeds via ANSA to acetoacetate and strongly depends on Mn^{2+} ions

ACE degradation to acetoacetate via ANSA (Figure 1) was experimentally confirmed with strain *Bosea* sp. 100-5. Protein crude extracts from ACE-grown cells readily degraded ACE to acetoacetate (Figure 2A) with transient accumulation of ANSA (Figure 2B). Enzyme activity did not depend on addition of any cosubstrates, such as NADH or ATP, confirming that ACE degradation to acetoacetate is a two-step hydrolytic reaction as already postulated (Kleinsteuber et al., 2019). Moreover, growth on ACE as sole source of carbon and energy was strongly dependent on supplementation with Mn^{2+} ions. In mineral medium with excess Mn^{2+}, ACE degradation allowed exponential growth with doubling times of about 19 h (Figure 2C). In contrast, growth and ACE turnover was substantially reduced in Mn^{2+}-limited medium (Figure 2D; Supplementary Figure S2A). Supplementation with other divalent metals, such as Zn^{2+}, Fe^{2+}, Cu^{2+}, or Co^{2+}, did not reverse this effect. However, *Bosea* sp. 100-5 grew well in Mn^{2+}-limited medium on alternative carbon sources, such as succinate or 3-hydroxybutyrate. The latter substrate is likely metabolized through the same route employed for the carbon skeleton of ACE, i.e., via acetoacetate, acetoacetyl-CoA and acetyl-CoA. Hence, the observed metal dependence is specific for growth on ACE, indicating that one or both hydrolytic steps leading to the intermediate acetoacetate are Mn^{2+}-dependent.

3.2. Two plasmid-borne gene clusters are involved in ACE degradation

The ACE degradation trait seemed to be unstable in *Bosea* sp. 100-5 and was lost after prolonged cultivation in complex medium without ACE. After several generations in R2A medium, a mutant strain *Bosea* sp. 100-5 Mut1 was isolated that could neither grow on ACE nor consume it in the presence of the alternative carbon source 3-hydroxybutyrate. Moreover, crude extracts did not transform ACE, confirming the lack of the initial hydrolytic enzyme in the mutant.

Mapping the genome of *Bosea* sp. 100-5 Mut1 on the corresponding wildtype genome revealed that only 2.5% of the nucleotides are missing in the mutant and 98.15% of the CDS are conserved among both strains. The wildtype genome comprises a contig of 40,931 bp that was annotated as a plasmid (Figure 3; Table 2). A gap of 26,252 bp was found in the corresponding region of the

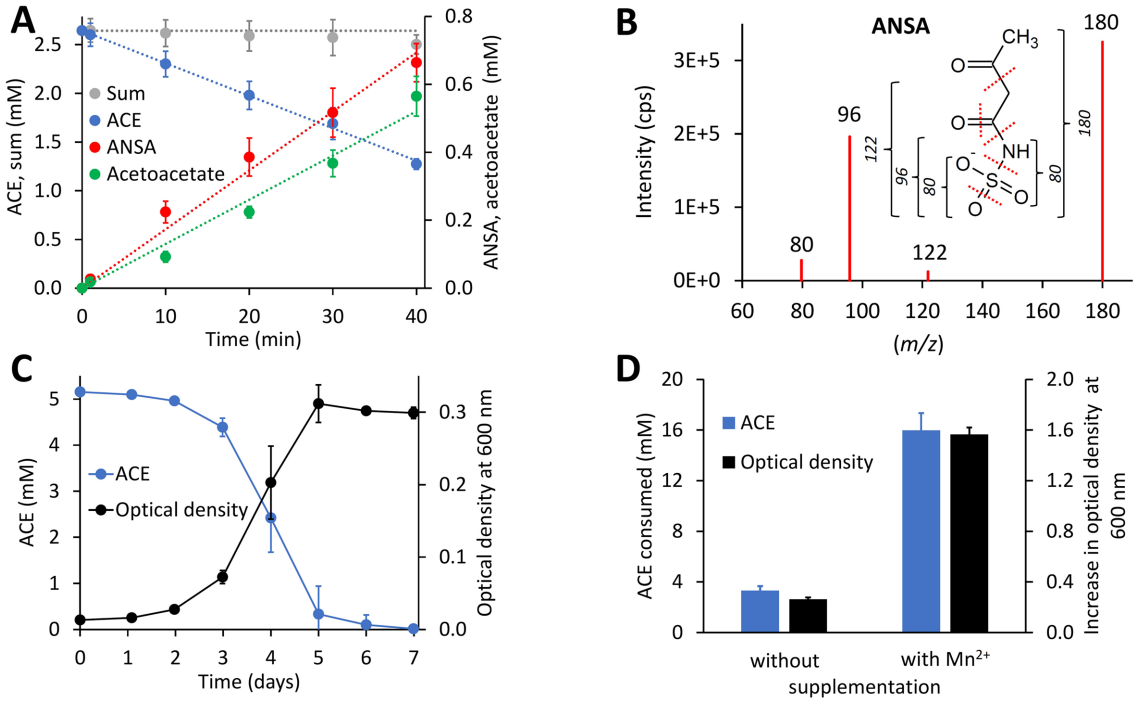

FIGURE 2
Physiological and biochemical characteristics of bacterial ACE degradation. **(A)** ACE degradation assay at 30°C with crude protein extract (470 µg mL^{-1} total protein) obtained from *Bosea* sp. 100-5 cells grown on ACE as sole source of carbon and energy. **(B)** Identification of ANSA (anion $[H_6C_4NSO_5]^-$ with mass-to-charge ratio *m/z* = 180) as product of enzymatic ACE hydrolysis. Enhanced product ion spectrum obtained by LC–MS/MS analysis with electrospray ionization in negative polarity (cps, counts per second). Formation of characteristic products $([SO_3]^-$ or $[H_2NSO_2]^-$ with *m/z* = 80, $[H_2NSO_3]^-$ with *m/z* = 96 and $[H_4C_2NSO_3]^-$ with *m/z* = 122) is indicated. **(C)** Batch growth of *Bosea* sp. 100-5 on 5 mM ACE at 30°C in Mn^{2+}-rich mineral medium (66.7 µM Mn^{2+}) allowing doubling times as low as 19 h. **(D)** Metal dependence of fed-batch growth and degradation of ACE in *Bosea* sp. 100-5 cultivated in Mn^{2+}-limited mineral medium (0.15 µM Mn^{2+}) without or with Mn^{2+} supplementation (3.7 µM Mn^{2+}). Cultures were incubated for 5 days at 30°C with a total amount of 20 mM ACE (see also Supplementary Figure S2A). Values given represent mean and SD of at least five independent experiments.

mutant genome (Figure 3; Supplementary Figure S3). This deletion comprises a putative metabolic gene cluster of six CDS encoding two hydrolases and four transport proteins, flanked by several CDS typically associated with a composite transposon, such as genes encoding transposases, integrases and transposase-assisting ATPases (Figure 3; Table 2).

Three CDS of the identified cluster (BOSEA1005_40011, 40012, and 40013) encode the essential components of an ATP-binding cassette (ABC) transport system with BOSEA1005_40011 encoding the ATP-binding protein, BOSEA1005_40012 the transmembrane subunit and BOSEA1005_40013 the periplasmic substrate-binding protein. The two hydrolases encoded by BOSEA1005_40015 and 40016 belong to the metallo beta-lactamase (MBL)-type and amidase signature sequence enzyme families, respectively. BOSEA1005_40018 encodes a protein related to the TauE-like anion transport system, which might be responsible for the removal of the ANSA hydrolysis product sulfamate.

Catalytic activity of MBL-type hydrolases depends on divalent metal ions coordinated by highly conserved active site His and Asp residues (Gonzalez, 2021). Considering the observed Mn^{2+} dependence of ACE degradation in *Bosea* sp. 100-5 (Figure 2D; Supplementary Figure S2A), the BOSEA1005_40015 enzyme was the most likely candidate for the initial attack on ACE. This assumption was proven by heterologous expression in *E. coli* (Supplementary Table S2), which also confirmed the Mn^{2+} dependence of the enzyme (Figure 4A; Supplementary Figure S2B). The ACE sulfatase encoded by BOSEA1005_40015 has 283 aa with a predicted molecular weight of 31.9 kDa. Conserved residues for coordination of two divalent metal ions per subunit are H61, H63, D65, H66, H172, and H251.

Enzymes with amidase signature sequence do not show any specific metal dependence but possess a unique Ser Ser Lys (SSK) catalytic triad for the nucleophilic attack of the carbonyl carbon found in amide groups (Shin et al., 2002). BOSEA1005_40016 encodes a protein of 465 aa with a molecular weight of 49.3 kDa bearing the amidase signature sequence in residues K81, S156, and S180. Consequently, it was tempting to assign the hydrolytic activity for ANSA degradation to BOSEA1005_40016. However, directly downstream of the composite transposon, a second metabolic gene cluster was found (Figure 3) encoding a LysR-like transcriptional regulator (BOSEA1005_40029) and a second enzyme of the SSK triad amidase signature family (BOSEA1005_40030, 39% amino acid identity with BOSEA1005_40016). The latter genes are still present in the mutant plasmid (Figure 3). In crude extracts from 3-hydroxybutyrate-grown Mut1 cells, ANSA was readily converted to acetoacetate (Supplementary Figure S4), ruling out the BOSEA1005_40016 enzyme as the primary ANSA amidase. Moreover, although both amidases showed similar relative abundance after heterologous expression (Supplementary Table S2), crude extracts of *E. coli* with heterologous BOSEA1005_40030 protein

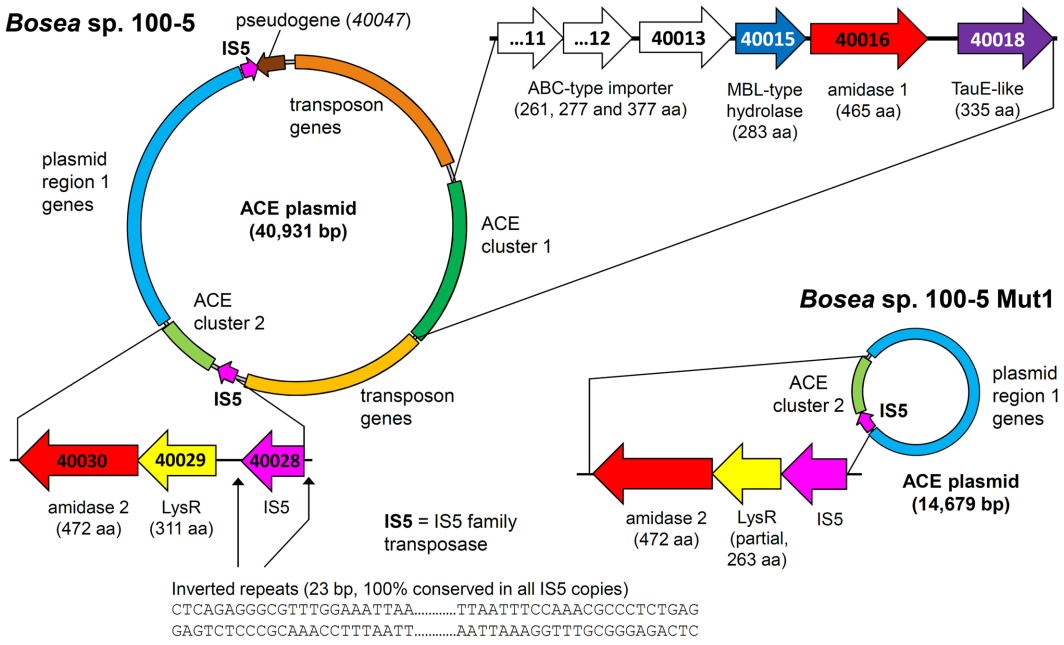

FIGURE 3
Deletion of the 22.5-kb composite transposon and additional genes from the 40.9-kb ACE plasmid found in *Bosea* sp. 100-5. Within the transposon, the wildtype plasmid bears a gene cluster (ACE cluster 1) encoding two hydrolases and four transport proteins. Additionally, a second gene cluster encoding another hydrolase (ACE cluster 2), other plasmid genes (named "plasmid region 1 genes") and two copies of an IS5 family transposase (IS5) with inverted repeats as indicated are present. In the mutant strain *Bosea* sp. 100-5 Mut1, a 14.7-kb plasmid containing the genes from plasmid region 1 and ACE cluster 2 remained. The plasmid was manually reconstructed from contigs 56, 57, and 70 of the Mut1 genome sequence (GCA_946047605). Numbers in genes refer to locus tags in *Bosea* sp. 100−5 (prefix BOSEA1005_). Both plasmids are shown true to scale. Detailed map and annotations of the wildtype ACE plasmid can be found in Figure 6 and Table 2, respectively.

showed high ANSA-hydrolyzing activity, whereas heterologous BOSEA1005_40016 protein did not confirm ANSA hydrolysis (Figure 4B). Phylogenetic relationships between BOSEA1005_40030 and other amidase genes are illustrated in Supplementary Figure S5. The tree clearly shows that the amidase encoded by BOSEA1005_40016 clusters distantly from the putative ANSA amidase cluster. However, its closest relatives are not characterized and their substrates are unknown.

Taken together, the genome comparison between *Bosea* sp. 100-5 and its deletion mutant Mut1 as well as the heterologous expression of the three hydrolases confirmed that the two-step hydrolysis of ACE to acetoacetate and sulfamate is encoded by two different gene clusters located on one plasmid in *Bosea* sp. 100-5 (Figure 3; Table 2).

3.3. The plasmid-borne metabolic genes found in *Bosea* sp. 100-5 are highly conserved among ACE degraders

In addition to the previously described strains *Bosea* sp. 100-5, *Bosea* sp. 3-1B, *Chelatococcus* sp. 1 g-11, and *Chelatococcus* sp. 1 g-2 (Kleinsteuber et al., 2019), we isolated several other ACE-degrading *Chelatococcus* strains and one *Shinella* strain from samples collected in WWTPs from different locations in Germany (Table 1) and sequenced the genomes of all these strains. Supplementary Table S1 summarizes the genomic features of the nine ACE degraders and the degradation-defective mutant *Bosea* sp. 100-5 Mut1. All strains have large genomes (5.9 Mb for the *Bosea* strains, 7 to 7.3 Mb for the *Chelatococcus* strains, and 7.8 Mb for *Shinella* sp. WSC3-e). Five other ACE-degrading strains isolated from a WWTP in Hong Kong (Huang et al., 2021, 2022) were included in genome comparison (Table 1). In agreement with their proposed role in ACE degradation, the two gene clusters were found in all genomes on plasmid-like contigs ranging from 41,507 to 45,942 bp, except for the *Shinella* strains and strain HY11, which harbor only ACE cluster 2, and strain YT9, which has both clusters but only cluster 2 on a plasmid (Table 1). While ACE cluster 1 (sulfatase cluster) together with its flanking transposon-related CDS is highly conserved (>99% nucleotide identity) among all these strains, ACE cluster 2 (amidase cluster) is variable in size (two to four CDS) but always contains the conserved CDS for the ANSA amidase and the LysR-like transcriptional regulator. The ACE plasmid of *Chelatococcus* sp. 1 g-11 is exemplarily shown in Figure 5 (see Supplementary Figure S6 for a detailed plasmid map and annotations).

3.4. Putative ACE degradation gene clusters in public sequence databases

The ACE sulfatase (BOSEA1005_40015) appears to be a unique feature of the pathway. While its gene is ≥99% conserved among all genome-sequenced ACE degraders thus far (Table 1), only very distantly related sequences (with <30% amino acid identity at ≥80% coverage) were found in other published genomes (bacterial isolates and MAGs). Therefore, we surveyed public metagenomes and metatranscriptomes from wastewater environments and found the ACE sulfatase gene in sequence datasets from activated sludge

10.3389/fmicb.2023.1223838

TABLE 2 CDS of the ACE plasmid from *Bosea* sp. 100-5 with predicted functions (locus tag prefix BOSEA1005_).

Locus tag	Gene length (bp)	Predicted function of gene product	Plasmid region
40001	1,497[a]	Transposase	Transposon
40002	759	AAA family ATPase	Transposon
40004	777	Putative RNA-directed DNA polymerase	Transposon
40006	1,083	Transposase	Transposon
40007	1,032	Transposase	Transposon
40011	786	ABC type import system, ATP-binding subunit	ACE cluster 1
40012	834	ABC type import system, transmembrane subunit	ACE cluster 1
40013	1,134	ABC type import system, substrate-binding subunit	ACE cluster 1
40015	852	MBL-type hydrolase, ACE sulfatase	ACE cluster 1
40016	1,398	Amidase 1, unknown substrate	ACE cluster 1
40018	1,008	TauE-like small molecular weight anion export system	ACE cluster 1
40019	1,110	Transposase	Transposon
40022	1,512	Transposase	Transposon
40023	756	Insertion sequence ATP-binding protein	Transposon
40025	1,404	Integrase/recombinase	Transposon
40028	783	Transposase	IS5 family element
40029	936	LysR-like transcriptional regulator	ACE cluster 2
40030	1,419	Amidase 2, ANSA amidase	ACE cluster 2
40032	747	Family of unknown function (DUF6118)	Plasmid region 1
40033	3,777	Conjugal transfer protein TraA	Plasmid region 1
40034	291	Mobilization protein, MobC-like	Plasmid region 1
40035	1,779	Type IV secretion system protein TraG	Plasmid region 1
40037	318	Helix-turn-helix protein, antitoxin for 40,038	Plasmid region 1
40038	390	Type II toxin-antitoxin system RelE/ParE family toxin	Plasmid region 1
40039	282	Ribbon-helix–helix protein, CopG family	Plasmid region 1
40040	624	Chromosome partitioning protein ParA	Plasmid region 1
40041	882	Replication protein A	Plasmid region 1
40042	321	Protein of unknown function	Plasmid region 1
40043	252	Protein of unknown function	Plasmid region 1
40044	336	Protein of unknown function	Plasmid region 1
40045	432	Protein of unknown function	Plasmid region 1
40046	783	Transposase	IS5 family element
40047	1,179	low molecular weight anion importer, partial CDS/pseudogene[b]	

[a]Complete CDS after manually circularizing the contig, identical to the homologous CDS of strain 1 g-11 (CHELA1G11_60037).
[b]Complete CDS present in strain 1 g-11 (CHELA1G11_60039).

sampled in Austria, China, Germany, Netherlands, Taiwan, and USA (Figure 6). As the samples were collected between 2015 and 2018, the first record of the ACE sulfatase gene in 2015 can be traced back to the Klosterneuburg WWTP in Austria (Supplementary Table S3).

In some datasets that presented the ACE sulfatase gene, other elements of the ACE plasmid from *Bosea* sp. 100-5 were also found. In the metatranscriptome from the Weurt WWTP in Nijmegen (Netherlands), genes of ACE cluster 1 corresponding to BOSEA_40011 to 40016 were detected, and the metagenome from the Wenshan WWTP (Taiwan) was shown to contain fragments of all ACE cluster 1 genes. In the latter dataset, we also found contigs related to the transposon and other genes of the *Bosea* sp. 100-5 ACE plasmid (Figure 6). While likewise including fragments of 40012 and 40016 of cluster 1, the metagenome from the Virginia WWTP is one of the two datasets representing part of the 40030 gene of ACE cluster 2, and a particularly high coverage of 75% of the *Bosea* sp. 100-5 ACE plasmid was detected in the dataset from activated sludge microbial communities from an anaerobic bioreactor operated at Hunan University (Changsha, China).

4. Discussion

The artificial sweetener ACE was once considered recalcitrant in WWTPs (Buerge et al., 2009) but recently its emerging

biodegradability was reported (Cardenas et al., 2016; Castronovo et al., 2017; Kahl et al., 2018). The earliest indication for biodegradation based on ACE monitoring in wastewater was found in WWTPs located in Queensland, Australia (Cardenas et al., 2016) and Eriskirch, Germany (Castronovo et al., 2017), demonstrating removal efficiencies of about 90% in the sampling campaign years 2012 and 2013, respectively. Microbial community surveys highlighted the importance of *Alphaproteobacteria* for ACE degradation (Kahl et al., 2018; Huang et al., 2021). In particular, representatives of the genera *Bosea*, *Chelatococcus* and *Shinella* capable of degrading ACE were isolated recently (Kleinsteuber et al., 2019; Huang et al., 2021, 2022). Our present study revealed the enzymatic and genetic background of ACE degradation and offers a glimpse of the evolutionary mechanisms driving the fast and worldwide spread of this novel xenobiotics degradation trait.

The comparison of the wildtype *Bosea* sp. 100-5 and its ACE degradation-defective mutant clearly revealed the involvement of a plasmid-borne gene cluster (ACE cluster 1) encoding an MBL-type hydrolase (BOSEA1005_40015) in ACE degradation. The heterologous expression of the latter enzyme corroborates its function as ACE sulfatase. Recently, Castronovo et al. (2023) confirmed the presence of the MBL-type hydrolase in the metaproteome of an ACE-degrading enrichment culture dominated by *Chelatococcus*. Accordingly, the complete gene cluster including the flanking transposon-related CDS is highly conserved among the ACE-degrading strains analyzed in the present study. However, BOSEA1005_40015 appears to be unique and unprecedented, as the gene was not found in any other genomic context, and no closely related enzyme has been characterized thus far. In analogy to the distantly related hydrolases attacking phosphate ester bonds in nucleotides, the BOSEA1005_40015 enzyme might attack the sulfonyloxy group in ACE. Substantial sequence coverage with the BOSEA1005_40015 protein was only found for Apyc1 from *Bacillus* phage BSP38 (PDB ID 7T28) showing 26% identity (at 90% query coverage). The phage protein catalyzes the hydrolysis of cyclic mononucleotides involved in the antiphage defense system of its host. Its di-metal center is occupied by Zn^{2+} ions (Hobbs et al., 2022). Other distantly related hydrolases (only <30% identical residues at >80% query coverage) are often annotated as the short form of ribonuclease Z (consisting of 300 to 400 aa) that removes extra 3′ nucleotides from tRNA precursors (Takaku et al., 2004). From the specific metal dependence of the ACE degradation observed in *Bosea* sp. 100-5 (Figure 2D; Supplementary Figure S2A) and the heterologous BOSEA1005_40015 enzyme (Figure 4A; Supplementary Figure S2B), it can be concluded that the reaction center of the active MBL-type hydrolase is exclusively occupied by two Mn^{2+} ions. This is somewhat surprising, as MBL-type enzymes may be able to coordinate other divalent metal ions when the favored species is not available (Hu et al., 2009). Presumably, in the case of the ACE sulfatase, the substitution with other metals than Mn^{2+} results in a substantial reduction in activity. This might be explained by the ACE structure that obviously requires the full activity of the enzyme, as a nucleophilic attack toward the sulfur or C3 atom (Figure 1) is quite challenging due to the electron-richness of the ring system.

The required translocation of the negatively charged substrate into the cell across the cytoplasmic membrane and against the membrane potential is likely enabled by the ABC-type transporter encoded in ACE cluster 1 (Figures 3, 7). Protein sequences of the importer are distantly related to uptake systems associated with the transport of small inorganic or organic anions. However, only very low identity to thus far studied proteins can be found, e.g., the periplasmic substrate-binding protein shows 27% sequence identity at 18% query coverage to TauA from *E. coli* (UniProt ID Q47537), which was reported to bind preferentially the short-chain alkanesulfonate taurine (Qu et al., 2019). Finally, as the ACE hydrolysis product sulfamate formed in the cytoplasm is not used by ACE-degrading bacteria (Kleinsteuber et al., 2019), an export system is probably needed for the efficient removal of the waste product, which could be the BOSEA1005_40018 gene product. This protein belongs to the TauE/SafE family of transmembrane proteins involved in the export of small anions, such as sulfite, sulfoacetate, and 3-sulfolactate (Weinitschke et al., 2007; Mayer et al., 2012). Beyond this finding, the TauE/SafE system is not well characterized and the amino acid sequence is poorly conserved among representatives of the protein family, e.g., BOSEA1005_40018 does not show significant similarity (blastp) with WP_011617520.1 from *Cupriavidus necator* H16.

Together with BOSEA1005_40016 encoding an amidase, the gene cluster seems to be dedicated for the two-step hydrolytic degradation of a substrate sharing some features with ACE. However, BOSEA1005_40016 was lost in *Bosea* sp. 100-5 Mut1 but protein extracts still hydrolyzed ANSA. Moreover, heterologous expression of another amidase gene (BOSEA1005_40030) in *E. coli* identified its function in ANSA hydrolysis and disproved the involvement of BOSEA1005_40016. Related sequences of BOSEA1005_40016 (about 60% identity at 96% query coverage) are present in gene environments other than the ACE degradation gene cluster 1, e.g., WP_013973238.1 (nicotine-degrading *Pseudomonas putida* S16) and WP_244145082.1 (root nodule bacterium *Paraburkholderia tuberum* LMG 21444). However, as these matches lack biochemical characterization, no conclusion on substrate preferences can be drawn. Therefore, the genetic makeup of ACE cluster 1 implies that it originally evolved for a different function than ACE degradation.

The ANSA amidase gene BOSEA1005_40030 is located in a second gene cluster on the ACE plasmid. In *Bosea* sp. 100-5, this cluster only consists of CDS for a transcriptional regulator (LysR) and the ANSA amidase. In *Chelatococcus* sp. 1g-11, additional genes encoding an anion import system (CHELA1G11_60039) and another TauE/SafE-like exporter (CHELA1G11_60040) are present (Figure 5; Supplementary Figure S7). In contrast to BOSEA1005_40015, sequences closely related to BOSEA1005_40030 can be found in genomes of bacteria that do not degrade ACE, e.g., WP_176954172.1 from *Paraburkholderia sartisoli* LMG 24000 showing 66% amino acid identity at 99% coverage. Interestingly, the gene clusters in strains 1g-11 and LMG 24000 do not only share the amidase gene but also that encoding the anion import system (75% amino acid identity at 93% coverage; Supplementary Figure S7). Additionally, a TauE/SafE system is present in strain LMG 24000, albeit not closely related to the ones encoded on the ACE plasmids. This constellation appears to have evolved for uptake of an extracellular amide that is hydrolyzed in the cytoplasm. *Bosea* sp. 100-5 lacks the TauE/SafE system, likely due to insertions of the IS5 family transposase and subsequent rearrangements, and the anion transport gene is only present as a pseudogene outside ACE cluster 2 (Figure 3; Table 2). Hence, only the BOSEA1005_40030 amidase is needed for ANSA degradation but not the anion import system present in strain *Chelatococcus* sp. 1g-11.

Intriguingly, ACE cluster 1 has been found only in the genera *Bosea* and *Chelatococcus* thus far. The specific physiological

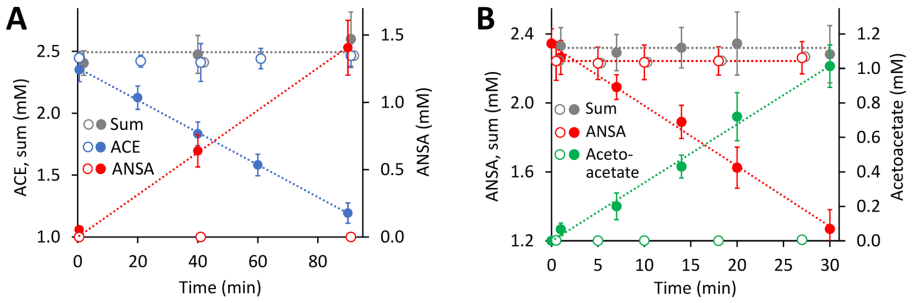

FIGURE 4
Both hydrolase-encoding gene clusters found on the 40.9-kb ACE plasmid of the wildtype *Bosea* sp. 100-5 are involved in ACE degradation. **(A)** Conversion of ACE to ANSA in crude extracts from *E. coli* Lemo21 (DE3) expressing either BOSEA1005_40016 or 40030 amidase genes (open symbols, 1,330 μg mL^{-1} total protein) or BOSEA1005_40015 hydrolase gene (closed symbols, 1,330 μg mL^{-1} total protein). Expression medium and assay buffer were supplemented with 0.5 and 1 mM $MnCl_2$, respectively. ANSA formation from ACE in the presence of the amidases was below 0.2 μM (LC–MS/MS). **(B)** Conversion of ANSA to acetoacetate in crude extracts from *E. coli* Lemo21 (DE3) expressing either BOSEA1005_40016 (open symbols, 74 to 370 μg mL^{-1} total protein) or 40030 amidase (closed symbols, 74 μg mL^{-1} total protein) genes. Acetoacetate formation with BOSEA1005_40016 was below 10 μM (HPLC). Values given represent mean and SD of at least four independent experiments.

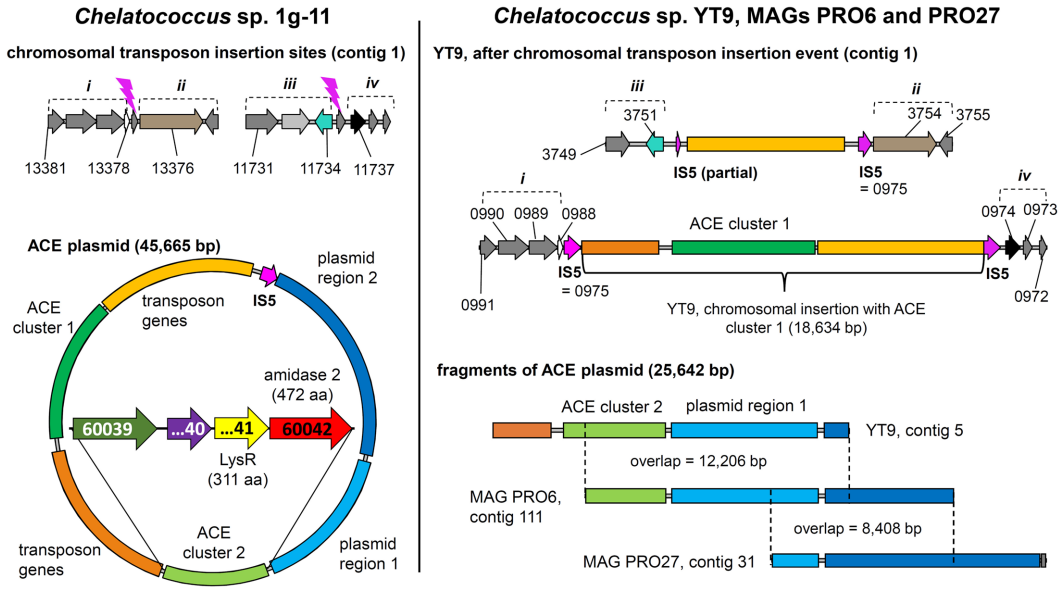

FIGURE 5
Tracing back the transposition event resulting in the insertion of the transposon bearing the ACE cluster 1 into the chromosome of strain *Chelatococcus* sp. YT9. (Left) *Chelatococcus* sp. 1g-11, chromosomal insertion sites (assembly accession GCA_930633515, contig 1, locus tag prefix CHELA1G11_) for the IS5 family transposase (IS5) encoded on the 45.7-kb ACE plasmid (contig 6) that also bears the ACE sulfatase and ANSA amidase ("amidase 2") genes on ACE clusters 1 and 2, respectively. Compared to the corresponding plasmid found in wildtype *Bosea* sp. 100-5 (Figure 3), only a part of the plasmid region 1 genes is shared ("plasmid region 1"), whereas other genes are only present in strain 1g-11 ("plasmid region 2"). Regions describing the chromosomal rearrangement are labeled *i* to *iv*. Detailed ACE plasmid map and annotations can be found in Supplementary Figure S6. (Right) *Chelatococcus* sp. YT9, chromosomal sites affected by the transposon insertion event (NZ_JAHBRW010000001.1, locus tag prefix WP_21332). At one site, the transposon with ACE cluster 1 is integrated. Due to the insertion event, identical copies of the IS5 family transposase gene frame the whole gene cluster (WP_213320975.1; 100% identical with BOSEA1005_40028 and BOSEA1005_40046 IS5 genes). From the ACE plasmid itself, however, only a small fragment is present in the genome of strain YT9 (NZ_JAHBRW010000005.1). Additional fragments can be found in MAGs (JAHBYS010000111.1, JAHBYU010000031.1) obtained from the ACE-degrading enrichment cultures from which also strain YT9 was isolated. Numbers marking genes refer to locus tags (with prefix as indicated). Plasmids and DNA fragments are shown true to scale. Genes with the same color refer to identical or closely related sequence (≥80% amino acid identity in predicted gene product, in most cases > 99%).

background making these genera suitable hosts of ACE cluster 1 could be related to their ability to accumulate high intracellular manganese concentrations (Fredrickson et al., 2008). On the other hand, the genomes of recently isolated *Shinella* strains harbor only ACE cluster 2 (Table 1), which might imply the involvement of other sulfatases catalyzing the initial hydrolysis reaction in these strains.

Compounds structurally related to ACE that could be likewise attacked by the MBL-type hydrolase are other natural or synthetic sulfamic acid derivatives (Spillane and Malaubier, 2014; Awakawa et al., 2021), in particular, O- and N-substituted sulfamates. In this context, Supplementary Figure S8A proposes a two-step enzymatic hydrolysis of ascamycin and other natural or synthetic aminoacyl

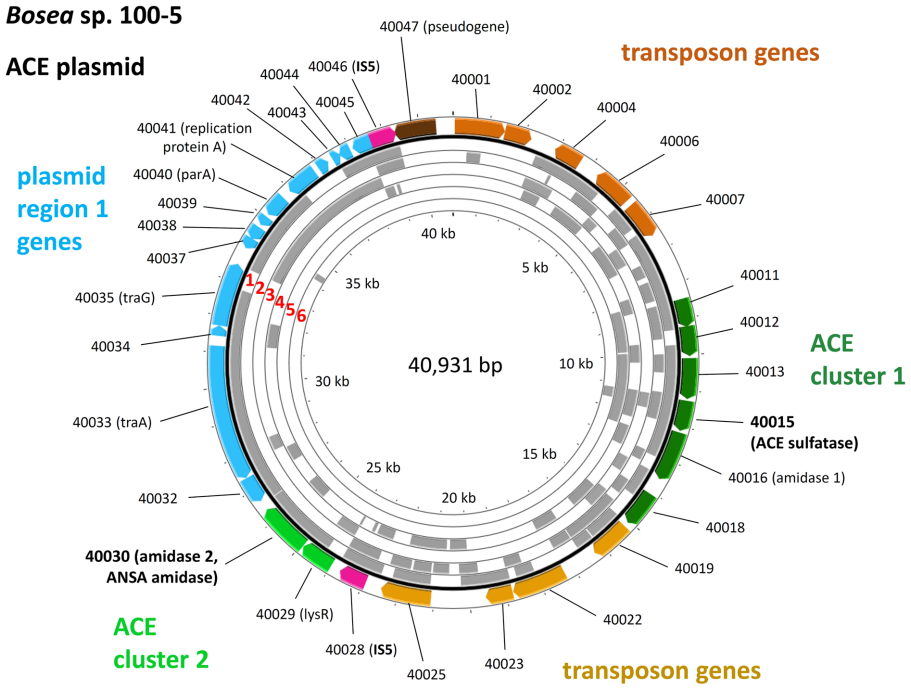

FIGURE 6
Mapping of the ACE plasmid genes on metagenome and metatranscriptome datasets associated with wastewater, bioreactors and WWTPs. These findings indicate the worldwide distribution and genetic conservation of the ACE degradation gene clusters and the ACE plasmid. The outer colored ring shows the genes on the *Bosea* sp. 100-5 ACE plasmid (color code as in Figure 3; locus tag prefix is BOSEA1005_). For complete annotation, see Table 2. Gray areas show hits (≥98% nucleotide identity) within the following metagenome and metatranscriptome datasets (numbering highlighted in red): 1 = Anaerobic bioreactor from Hunan University (sample 11), China; 2 = Wenshan WWTP, Taiwan; 3 = Linkou WWTP, Taiwan; 4 = WWTP in Virginia, United States; 5 = Weurt WWTP, The Netherlands; 6 = Klosterneuburg WWTP (sample MT KNB_C2_LD), Austria. For complete matches from datasets, see Supplementary Table S3. The figure was generated with Proksee.

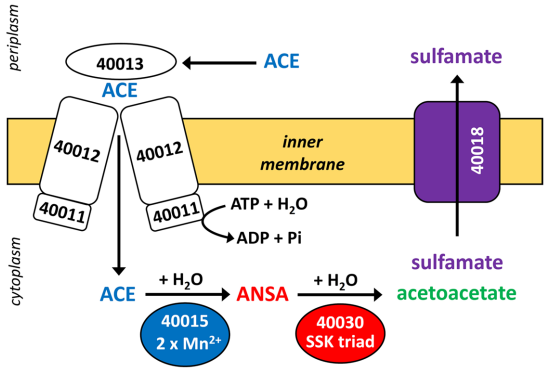

FIGURE 7
Proposed scheme of the two-step hydrolysis of ACE catalyzed by cytoplasmic MBL-type hydrolase BOSEA1005_40015 (from ACE cluster 1) and amidase BOSEA1005_40030 (from ACE cluster 2). Likely, ACE and its final hydrolysis product sulfamate are taken up and removed, respectively, by the transport systems encoded in ACE cluster 1 (see Figure 3), but both assumptions need experimental support. Numbers shown refer to locus tags in *Bosea* sp. 100–5 (prefix BOSEA1005_).

sulfamate ribonulceoside antibiotics (Isono et al., 1984), involving sulfatase and amidase activities. Also sulfonamide antibiotics might be relevant, albeit having a deviating structure compared to sulfamates, as the sulfur atom of the sulfonyl group is directly linked to an aniline ring system (Supplementary Figure S8B). Although bacterial degradation seems to proceed mainly via ipso-hydroxylation leading to the decomposition of the resulting intermediates and the release of sulfite (Ricken et al., 2013), alternatively, enzymatic hydrolysis by attacking the sulfur atom of, e.g., sulfacetamide, might lead to the release of aniline and an ANSA-related N-sulfonated acyl amide (Supplementary Figure S8B). In support, aniline as degradation product not compatible with the ipso-hydroxylation mechanism has been reported for *Pseudomonas psychrophila* HA-4 incubated with the sulfonamide antibiotic sulfamethoxazole (Jiang et al., 2014). Interestingly, the latter and other sulfonamides are partially removed from municipal wastewater concomitantly with ACE (Yang et al., 2017).

Metabolic genes embedded in transposons and their location on a conjugative plasmid are typical features of bacterial pathways involved in degradation of xenobiotics, such as antibiotics and pesticides (Springael and Top, 2004). This enables the evolution and distribution of novel degradation pathways or other functional traits that facilitate niche adaptation. In case of ACE, mediated by the IS5 family transposase, ACE cluster 1 can easily transpose between different replicons (Figure 5), which might have supported the recruitment of metabolic genes for ACE degradation. A potential scenario of the genetic rearrangements that might have led from an ancestral plasmid to the ACE plasmids currently found in the various *Bosea* and *Chelatococcus* strains is illustrated in Figure 8. In the mutant strain *Bosea* sp. 100-5 Mut1, the composite transposon comprising ACE cluster 1 has been completely deleted

from the plasmid. A similar situation was found in the published genome of the ACE-degrading strain *Chelatococcus* sp. HY11 isolated from a WWTP in Hong Kong (Huang et al., 2021). Here, ACE cluster 1 is also missing, like most of the other CDS of the composite transposon. However, some other genes corresponding to the ACE plasmid are located on a short contig of the HY11 genome (JAHBRX010000006.1). Likewise, various fragments of the rudimentary plasmid, lacking most of the 26-kb region associated with ACE hydrolysis, are present in the MAG sequences PRO6 and PRO27 (Figure 5). The corresponding metagenome was obtained from samples of ACE-degrading consortia seeded with activated sludge from the WWTP in Hong Kong from which also the ACE degraders *Chelatococcus* sp. HY11 and YT9 were isolated (Huang et al., 2021). It is worth mentioning that the gene for the type IV secretion system protein TraG (Figure 8; Table 2) is disrupted by a Tn3 family transposase gene (WP_113946498) in strain HY11, indicating some recombination events in this genomic region that identically occurred in our strain *Chelatococcus* sp. WSC3-1 isolated from a WWTP located in Leipzig, Germany (Table 1).

While the genome sequences of *Bosea* sp. 100-5 Mut1 and likely also of *Chelatococcus* sp. HY11 document the loss of ACE cluster 1, the genome of *Chelatococcus* sp. YT9 gives evidence for the insertion of the composite transposon into the chromosome. Here, ACE cluster 1 is flanked by almost all transposon components found in the 26 kb region of *Bosea* sp. 100-5 (Figure 5). As the insertion sites are well conserved in *Chelatococcus* sp. 1 g-11, the event can be reconstructed. Likely, the mobile element was originally located on a plasmid as the ones found in our ACE-degrading isolates (Figure 8). Accordingly, short contigs of strain YT9 and MAGs PRO6 and PRO27 harbor parts of the transposon genes, ACE cluster 2 and some other genes of the ACE plasmid found in *Chelatococcus* sp. 1 g-11 (Figure 5). The genome rearrangements in *Bosea* and *Chelatococcus* strains illustrate the genetic plasticity of the ACE degradation trait and suggest that the

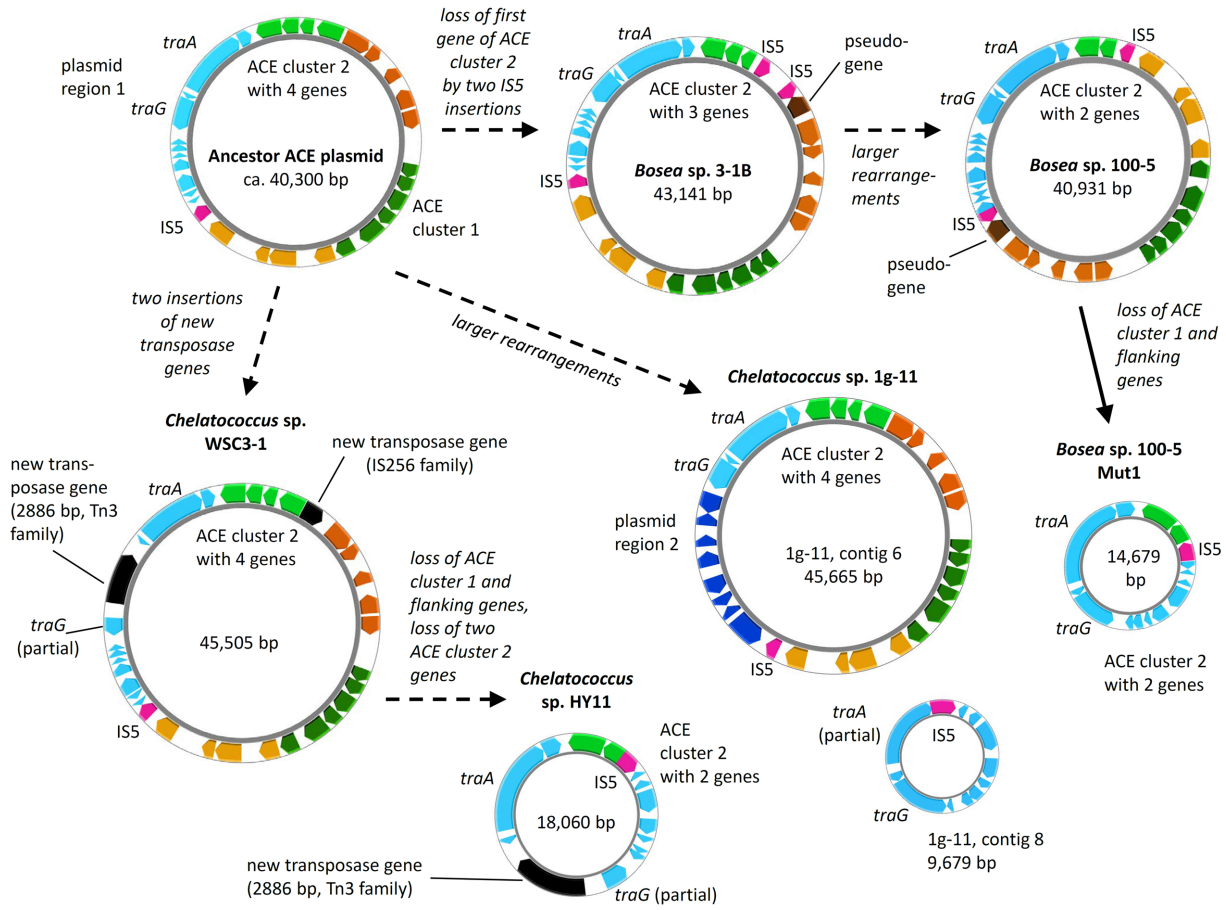

FIGURE 8
Diversity of ACE plasmids in isolated *Bosea* and *Chelatococcus* strains. Inspection of the ACE cluster 2 genes and a plasmid region consisting of genes encoding conjugative transfer (e.g., *traA* and *traG*) and other functions ("plasmid region 1") indicates a possible ancestor closely related to the plasmids from *Bosea* sp. 3–1B and *Chelatococcus* sp. WSC3-1. Only in *Chelatococcus* sp. 1 g-11, plasmid region 1 is substantially smaller, while new genes ("plasmid region 2") not present in the other plasmids are found. However, strain 1 g-11 still harbors an almost complete region 1 on a separate plasmid (contig 8), deviating only by a new insertion of the IS5 family element (IS5) in the Ti-type conjugative transfer relaxase gene *traA*. On the other hand, ACE plasmids of strains WSC3-1 and HY11 share the disruption of the type IV secretory system conjugative DNA transfer family protein gene *traG* by a 2,886-bp Tn3 family transposase gene (WP_113946498) not present in the other plasmids. Dashed arrows propose the plasmid evolution mainly induced by the IS5 element, whereas the event indicated by the solid arrow was demonstrated experimentally in this study. Gene rearrangements might include transpositions into the chromosome as shown in Figure 5. Smaller plasmids (<20 kb) are not true to scale but about 150% to 200% enlarged. Color code as used in Figure 5. The figure was generated with Proksee.

pathway recruitment is not yet completed since the ANSA amidase gene is located in another plasmid-borne cluster.

From the biochemist's perspective, ACE represents a challenging molecule combining features of a carboxylic acid amide and a sulfamic acid ester in an electron-rich ring system. Particularly, nucleophilic attack of the amide is difficult due to the localization of the negative charge mainly at the nitrogen atom (Popova et al., 2012). Furthermore, even when used for productive degradation, growth yields on ACE would be low, as (i) its uptake likely depends on ATP hydrolysis and (ii) only the carbon skeleton could be used for assimilation and dissimilation (representing only 50% of the molecular weight). Hence, it can be concluded that nature lacked an appropriate degradation mechanism when ACE was introduced into the environment for the first time in the 1980s (Klug and von Rymon Lipinski, 2012). In agreement, the artificial sweetener was long time considered recalcitrant against enzymatic attack (Buerge et al., 2009). The unprecedented high removal efficiency monitored in WWTPs since 2012 (Cardenas et al., 2016) points to the evolution of an ACE degradation pathway within a 30-years period. However, considering its low concentration in wastewater [typically <100 $\mu g L^{-1}$ in Europe, China and Australia (Buerge et al., 2009; Gan et al., 2013; Cardenas et al., 2016; Castronovo et al., 2017)], ACE is a rather poor substrate. Consequently, its utilization is likely not a sufficient driving force for the evolution of such a well-coordinated degradation pathway as depicted in Figure 7. Rather, co-metabolism with more dominant environmental chemicals can be expected (Kennes-Veiga et al., 2022). In line with this, no earlier stage or any other evolution of ACE cluster 1 was traceable in genomes and metagenomes. However, older metagenome datasets might have insufficient sequencing depth to cover such rare genes. Moreover, MAGs are prone to miss variable genes of natural populations (Meziti et al., 2021). Accordingly, matches for the genes of the ACE clusters were only found in partially assembled metagenome and metatranscriptome data (Figure 6; Supplementary Table S3) but not in MAGs. Direct and systematic Sequence Read Archive (SRA) search would be needed for tracing gene fragments that are discarded by assembly algorithms. As exemplarily shown for the metagenome dataset from the WWTP in Virginia (Figure 6; Supplementary Table S3), we could map SRA datasets on the entire ACE clusters (Supplementary Figures S9, S10). Mapping of another SRA dataset from a WWTP in Christchurch, New Zealand, on ACE cluster 1 and 2 sequences is illustrated in Supplementary Figure S11.

The evolution and distribution of the individual ACE clusters likely started much earlier than in the 2010s, possibly triggered by other natural or anthropogenic chemicals that exerted higher selective pressure than the non-toxic ACE. However, the last evolutionary step of combining the two gene clusters in one genome can be attributed to the recent bacterial adaptation to ACE as energy and carbon source. Due to the low ACE concentration in wastewater, this evolution might have occurred in rather oligotrophic environments, such as the late sections of treatment wetlands (Kahl et al., 2017, 2018) and biofilms thriving in receiving waters. The concomitant occurrence of identical gene clusters in Germany and China (Figures 5, 6) suggests that the ACE plasmid formed first at one site and then was distributed rapidly among WWTPs. Further isolation studies and molecular surveys using the ACE and ANSA hydrolases as genetic markers could reveal the origin of the ACE degradation trait and how it has spread in aquatic environments worldwide.

Data availability statement

The datasets presented in this study can be found in online repositories. The names of the repository/repositories and accession number(s) can be found in the article/Supplementary material.

Author contributions

SK, TRo, TRe, LA, and CD conceived and directed the project. DP, MB, K-PL, CS, TRo, YL, and CA performed the experiments and were involved in method design as well as data analysis. MB, TRo, and SK wrote the manuscript with substantial input of MB, TRo, DP, YL, CA, CS, K-PL, CD, TRe, LA, and SK. All authors contributed to the article and approved the submitted version.

Funding

Cloud computing facilities used for the bioinformatics analyses were provided by the BMBF-funded de.NBI Cloud within the German Network for Bioinformatics Infrastructure (de.NBI) (031A537B, 031A533A, 031A538A, 031A533B, 031A535A, 031A537C, 031A534A, and 031A532B). YL wishes to thank the CSC for the doctoral fellowship (202004910433).

Acknowledgments

The authors thank Ute Lohse (UFZ) for excellent technical assistance, particularly, in strain cultivation and genome sequencing. A preprint of this article has been published at bioRxiv (Bonatelli et al., 2022).

Conflict of interest

The authors declare that the research was conducted in the absence of any commercial or financial relationships that could be construed as a potential conflict of interest.

Publisher's note

Supplementary material

The Supplementary material for this article can be found online at: https://www.frontiersin.org/articles/10.3389/fmicb.2023.1223838/full#supplementary-material

References

Anjem, A., Varghese, S., and Imlay, J. A. (2009). Manganese import is a key element of the oxy R response to hydrogen peroxide in *Escherichia coli*. *Mol. Microbiol.* 72, 844–858. doi: 10.1111/j.1365-2958.2009.06699.x

Awakawa, T., Barra, L., and Abe, I. (2021). Biosynthesis of sulfonamide and sulfamate antibiotics in actinomycete. *J. Ind. Microbiol. Biotechnol.* 48:kuab001. doi: 10.1093/jimb/kuab001

Becher, E., Heese, A., Claußen, L., Eisen, S., Jehmlich, N., Rohwerder, T., et al. (2018). Active site alanine preceding catalytic cysteine determines unique substrate specificity in bacterial CoA-acylating prenal dehydrogenase. *FEBS Lett.* 592, 1150–1160. doi: 10.1002/1873-3468.13019

Bonatelli, M. L., Rohwerder, T., Popp, D., Liu, Y., Akay, C., Schultz, C., et al. (2022). Recently evolved combination of unique sulfatase and amidase genes enables bacterial degradation of the wastewater micropollutant acesulfame worldwide. bioRxiv [Preprint]. bioRxiv: 2022.2008.2017.504299.

Buerge, I. J., Buser, H.-R., Kahle, M., Müller, M. D., and Poiger, T. (2009). Ubiquitous occurance of the artificial sweetener acesulfame in the aquatic environment: an ideal chemical marker of domestic wastewater in groundwater. *Environ. Sci. Technol.* 43, 4381–4385. doi: 10.1021/es900126x

Cardenas, M. A. R., Ali, I., Lai, F. Y., Dawes, L., Thier, R., and Rajapakse, J. (2016). Removal of micropollutants through a biological wastewater treatment plant in a subtropical climate, Queensland-Australia. *J. Environ. Health Sci. Eng.* 14:14. doi: 10.1186/s40201-016-0257-8

Castronovo, S., Helmholz, L., Wolff, D., Poulsen, J. S., Nielsen, J. L., Ternes, T. A., et al. (2023). Protein fractionation and shotgun proteomics analysis of enriched bacterial cultures shed new light on the enzymatically catalyzed degradation of acesulfame. *Water Res.* 230:119535. doi: 10.1016/j.watres.2022.119535

Castronovo, S., Wick, A., Scheurer, M., Nodler, K., Schulz, M., and Ternes, T. A. (2017). Biodegradation of the artificial sweetener acesulfame in biological wastewater treatment and sandfilters. *Water Res.* 110, 342–353. doi: 10.1016/j.watres.2016.11.041

Chaumeil, P. A., Mussig, A. J., Hugenholtz, P., and Parks, D. H. (2019). GTDB-Tk: a toolkit to classify genomes with the genome taxonomy database. *Bioinformatics* 36, 1925–1927. doi: 10.1093/bioinformatics/btz848

Clauß, K., and Harald, J. (1973). Oxathiazinondioxide, eine neue Gruppe von Süßstoffen. *Angew. Chem.* 85, 965–973. doi: 10.1002/ange.19730852202

Darling, A. C., Mau, B., Blattner, F. R., and Perna, N. T. (2004). Mauve: multiple alignment of conserved genomic sequence with rearrangements. *Genome Res.* 14, 1394–1403. doi: 10.1101/gr.2289704

Ding, C., and Adrian, L. (2020). Comparative genomics in "Candidatus Kuenenia stuttgartiensis" reveal high genomic plasticity in the overall genome structure, CRISPR loci and surface proteins. *BMC Genomics* 21:851. doi: 10.1186/s12864-020-07242-1

Finn, R. D., Attwood, T. K., Babbitt, P. C., Bateman, A., Bork, P., Bridge, A. J., et al. (2017). InterPro in 2017-beyond protein family and domain annotations. *Nucleic Acids Res.* 45, D190–d199. doi: 10.1093/nar/gkw1107

Fredrickson, J. K., Li, S. M., Gaidamakova, E. K., Matrosova, V. Y., Zhai, M., Sulloway, H. M., et al. (2008). Protein oxidation: key to bacterial desiccation resistance? *ISME J.* 2, 393–403. doi: 10.1038/ismej.2007.116

Gan, Z., Sun, H., Feng, B., Wang, R., and Zhang, Y. (2013). Occurrence of seven artificial sweeteners in the aquatic environment and precipitation of Tianjin, China. *Water Res.* 47, 4928–4937. doi: 10.1016/j.watres.2013.05.038

Gilchrist, C. L. M., Booth, T. J., van Wersch, B., van Grieken, L., Medema, M. H., and Chooi, Y. H. (2021). Cblaster: a remote search tool for rapid identification and visualization of homologous gene clusters. *Bioinform Adv* 1–10. doi: 10.1093/bioadv/vbab016

Gonzalez, J. M. (2021). Visualizing the superfamily of metallo-beta-lactamases through sequence similarity network neighborhood connectivity analysis. *Heliyon* 7:e05867. doi: 10.1016/j.heliyon.2020.e05867

Hobbs, S. J., Wein, T., Lu, A., Morehouse, B. R., Schnabel, J., Leavitt, A., et al. (2022). Phage anti-CBASS and anti-Pycsar nucleases subvert bacterial immunity. *Nature* 605, 522–526. doi: 10.1038/s41586-022-04716-y

Hu, Z., Spadafora, L. J., Hajdin, C. E., Bennett, B., and Crowder, M. W. (2009). Structure and mechanism of copper-and nickel-substituted analogues of Metallo-β-lactamase L1. *Biochemistry* 48, 2981–2989. doi: 10.1021/bi802295z

Huang, Y., Deng, Y., Law, J. C.-F., Yang, Y., Ding, J., Leung, K. S.-Y., et al. (2021). Acesulfame aerobic biodegradation by enriched consortia and Chelatococcus spp.: kinetics, transformation products, and genomic characterization. *Water Res.* 202:117454. doi: 10.1016/j.watres.2021.117454

Huang, Y., Yu, Z., Liu, L., Che, Y., and Zhang, T. (2022). Acesulfame anoxic biodegradation coupled to nitrate reduction by enriched consortia and isolated Shinella spp. *Environ. Sci. Technol.* 56, 13096–13106. doi: 10.1021/acs.est.2c03656

Isono, K., Uramoto, M., Kusakabe, H., Miyata, N., Koyama, T., Ubukata, M., et al. (1984). Ascamycin and dealanylascamycin, nucleoside antibiotics from streptomyces sp. *J. Antibiot.* 37, 670–672. doi: 10.7164/antibiotics.37.670

Jiang, B., Li, A., Cui, D., Cai, R., Ma, F., and Wang, Y. (2014). Biodegradation and metabolic pathway of sulfamethoxazole by *Pseudomonas psychrophila* HA-4, a newly isolated cold-adapted sulfamethoxazole-degrading bacterium. *Appl. Microbiol. Biotechnol.* 98, 4671–4681. doi: 10.1007/s00253-013-5488-3

Kahl, S., Kleinsteuber, S., Nivala, J., van Afferden, M., and Reemtsma, T. (2018). Emerging biodegradation of the previously persistent artificial sweetener acesulfame in biological wastewater treatment. *Environ. Sci. Technol.* 52, 2717–2725. doi: 10.1021/acs.est.7b05619

Kahl, S., Nivala, J., van Afferden, M., Müller, R. A., and Reemtsma, T. (2017). Effect of design and operational conditions on the performance of subsurface flow treatment wetlands: emerging organic contaminants as indicators. *Water Res.* 125, 490–500. doi: 10.1016/j.watres.2017.09.004

Kajitani, R., Toshimoto, K., Noguchi, H., Toyoda, A., Ogura, Y., Okuno, M., et al. (2014). Efficient de novo assembly of highly heterozygous genomes from whole-genome shotgun short reads. *Genome Res.* 24, 1384–1395. doi: 10.1101/gr.170720.113

Kearse, M., Moir, R., Wilson, A., Stones-Havas, S., Cheung, M., Sturrock, S., et al. (2012). Geneious basic: an integrated and extendable desktop software platform for the organization and analysis of sequence data. *Bioinformatics* 28, 1647–1649. doi: 10.1093/bioinformatics/bts199

Kennes-Veiga, D. M., Gonzalez-Gil, L., Carballa, M., and Lema, J. M. (2022). Enzymatic cometabolic biotransformation of organic micropollutants in wastewater treatment plants: a review. *Bioresour. Technol.* 344:126291. doi: 10.1016/j.biortech.2021.126291

Kleinsteuber, S., Rohwerder, T., Lohse, U., Seiwert, B., and Reemtsma, T. (2019). Sated by a zero-calorie sweetener: wastewater bacteria can feed on acesulfame. *Front. Microbiol.* 10:2606. doi: 10.3389/fmicb.2019.02606

Klug, C., and von Rymon Lipinski, G. -W. (2012). "Acesulfame K" in *Sweeteners and sugar alternatives in food technology. 2nd Edn.* eds. K. O'Donnell and M. W. Kearsley (Chichester, UK: Wiley-Blackwell), 93–115.

Lane, D. J. (1991). "16S/23S rRNA sequencing" in *Nucleic acid techniques in bacterial systematics*. eds. E. Stackebrandt and M. Goodfellow (Chichester: John Wiley & Sons Ltd), 115–175.

Lange, F. T., Scheurer, M., and Brauch, H. J. (2012). Artificial sweeteners--a recently recognized class of emerging environmental contaminants: a review. *Anal. Bioanal. Chem.* 403, 2503–2518. doi: 10.1007/s00216-012-5892-z

Liu, Y., Blowes, D. W., Groza, L., Sabourin, M. J., and Ptacek, C. J. (2014). Acesulfame-K and pharmaceuticals as co-tracers of municipal wastewater in a receiving river. *Environ Sci Process Impacts* 16, 2789–2795. doi: 10.1039/c4em00237g

Liu, B., Popp, D., Sträuber, H., Harms, H., and Kleinsteuber, S. (2020). Draft genome sequences of three clostridia isolates involved in lactate-based chain elongation. *Microbiol Resour Announc* 9, e00679–20. doi: 10.1128/mra.00679-20

Lu, S., Wang, J., Chitsaz, F., Derbyshire, M. K., Geer, R. C., Gonzales, N. R., et al. (2020). CDD/SPARCLE: the conserved domain database in 2020. *Nucleic Acids Res.* 48, D265–d268. doi: 10.1093/nar/gkz991

Mayer, J., Denger, K., Hollemeyer, K., Schleheck, D., and Cook, A. M. (2012). (R)-Cysteate-nitrogen assimilation by *Cupriavidus necator* H16 with excretion of 3-sulfolactate: a patchwork pathway. *Arch. Microbiol.* 194, 949–957. doi: 10.1007/s00203-012-0825-y

Meziti, A., Rodriguez, R. L., Hatt, J. K., Peña-Gonzalez, A., Levy, K., and Konstantinidis, K. T. (2021). The reliability of metagenome-assembled genomes (MAGs) in representing natural populations: insights from comparing MAGs against isolate genomes derived from the same Fecal sample. *Appl. Environ. Microbiol.* 87:20. doi: 10.1128/aem.02593-20

Nodler, K., Hillebrand, O., Idzik, K., Strathmann, M., Schiperski, F., Zirlewagen, J., et al. (2013). Occurrence and fate of the angiotensin II receptor antagonist transformation product valsartan acid in the water cycle--a comparative study with selected beta-blockers and the persistent anthropogenic wastewater indicators carbamazepine and acesulfame. *Water Res.* 47, 6650–6659. doi: 10.1016/j.watres.2013.08.034

Parks, D. H., Imelfort, M., Skennerton, C. T., Hugenholtz, P., and Tyson, G. W. (2015). CheckM: assessing the quality of microbial genomes recovered from isolates, single cells, and metagenomes. *Genome Res.* 25, 1043–1055. doi: 10.1101/gr.186072.114

Popova, A. D., Velcheva, E. A., and Stamboliyska, B. A. (2012). DFT and experimental study on the IR spectra and structure of acesulfame sweetener. *J. Mol. Struct.* 1009, 23–29. doi: 10.1016/j.molstruc.2011.07.039

Prjibelski, A., Antipov, D., Meleshko, D., Lapidus, A., and Korobeynikov, A. (2020). Using SPAdes De Novo Assembler. *Curr. Protoc. Bioinformatics* 70:e102. doi: 10.1002/cpbi.102

Qu, F., ElOmari, K., Wagner, A., De Simone, A., and Beis, K. (2019). Desolvation of the substrate-binding protein TauA dictates ligand specificity for the alkanesulfonate ABC importer TauABC. *Biochem. J.* 476, 3649–3660. doi: 10.1042/bcj20190779

Reasoner, D. J., and Geldreich, E. E. (1985). A new medium for the enumeration and subculture of bacteria from potable water. *Appl. Environ. Microbiol.* 49, 1–7. doi: 10.1128/aem.49.1.1-7.1985

Ricken, B., Corvini, P. F., Cichocka, D., Parisi, M., Lenz, M., Wyss, D., et al. (2013). Ipso-hydroxylation and subsequent fragmentation: a novel microbial strategy to eliminate sulfonamide antibiotics. *Appl. Environ. Microbiol.* 79, 5550–5558. doi: 10.1128/aem.00911-13

Schaider, L. A., Ackerman, J. M., and Rudel, R. A. (2016). Septic systems as sources of organic wastewater compounds in domestic drinking water wells in a shallow sand and gravel aquifer. *Sci. Total Environ.* 547, 470–481. doi: 10.1016/j.scitotenv.2015.12.081

Schopper, S., Kahraman, A., Leuenberger, P., Feng, Y., Piazza, I., Müller, O., et al. (2017). Measuring protein structural changes on a proteome-wide scale using limited proteolysis-coupled mass spectrometry. *Nat. Protoc.* 12, 2391–2410. doi: 10.1038/nprot.2017.100

Shin, S., Lee, T. H., Ha, N. C., Koo, H. M., Kim, S. Y., Lee, H. S., et al. (2002). Structure of malonamidase E2 reveals a novel ser-cisSer-Lys catalytic triad in a new serine hydrolase fold that is prevalent in nature. *EMBO J.* 21, 2509–2516. doi: 10.1093/emboj/21.11.2509

Spillane, W., and Malaubier, J. B. (2014). Sulfamic acid and its N-and O-substituted derivatives. *Chem. Rev.* 114, 2507–2586. doi: 10.1021/cr400230c

Springael, D., and Top, E. M. (2004). Horizontal gene transfer and microbial adaptation to xenobiotics: new types of mobile genetic elements and lessons from ecological studies. *Trends Microbiol.* 12, 53–58. doi: 10.1016/j.tim.2003.12.010

Stothard, P., and Wishart, D. S. (2005). Circular genome visualization and exploration using CGView. *Bioinformatics* 21, 537–539. doi: 10.1093/bioinformatics/bti054

Subedi, B., and Kannan, K. (2014). Fate of artificial sweeteners in wastewater treatment plants in New York state, U.S.A. *Environ. Sci. Technol.* 48, 13668–13674. doi: 10.1021/es504769c

Takaku, H., Minagawa, A., Takagi, M., and Nashimoto, M. (2004). The N-terminal half-domain of the long form of tRNase Z is required for the RNase 65 activity. *Nucleic Acids Res.* 32, 4429–4438. doi: 10.1093/nar/gkh774

Vallenet, D., Calteau, A., Dubois, M., Amours, P., Bazin, A., Beuvin, M., et al. (2020). MicroScope: an integrated platform for the annotation and exploration of microbial gene functions through genomic, pangenomic and metabolic comparative analysis. *Nucleic Acids Res.* 48, D579–d589. doi: 10.1093/nar/gkz926

Weinitschke, S., Denger, K., Cook, A. M., and Smits, T. H. M. (2007). The DUF81 protein TauE in *Cupriavidus necator* H16, a sulfite exporter in the metabolism of C2 sulfonates. *Microbiology* 153, 3055–3060. doi: 10.1099/mic.0.2007/009845-0

Wick, R. R., Judd, L. M., Gorrie, C. L., and Holt, K. E. (2017). Unicycler: Resolving bacterial genome assemblies from short and long sequencing reads. *PLoS Comput Biol.* 13: e1005595. doi: 10.1371/journal.pcbi.1005595

Yang, Y. Y., Liu, W. R., Liu, Y. S., Zhao, J. L., Zhang, Q. Q., Zhang, M., et al. (2017). Suitability of pharmaceuticals and personal care products (PPCPs) and artificial sweeteners (ASs) as wastewater indicators in the Pearl River Delta, South China. *Sci. Total Environ.* 590-591, 611–619. doi: 10.1016/j.scitotenv.2017.03.001

frontiers | Frontiers in Microbiology

TYPE Original Research
PUBLISHED 03 August 2023
DOI 10.3389/fmicb.2023.1236634

OPEN ACCESS

EDITED BY
Ilana Kolodkin-Gal,
Hebrew University of Jerusalem, Israel

REVIEWED BY
Graciela Liliana Garrote,
National University of La Plata, Argentina
Tingting Guo,
Shandong University, China

*CORRESPONDENCE
Valente B. Alvarez
✉ alvarez.23@osu.edu

RECEIVED 08 June 2023
ACCEPTED 21 July 2023
PUBLISHED 03 August 2023

CITATION
González-Orozco BD, Kosmerl E, Jiménez-Flores R and Alvarez VB (2023) Enhanced probiotic potential of *Lactobacillus kefiranofaciens* OSU-BDGOA1 through co-culture with *Kluyveromyces marxianus* bdgo-ym6.
Front. Microbiol. 14:1236634.
doi: 10.3389/fmicb.2023.1236634

Enhanced probiotic potential of *Lactobacillus kefiranofaciens* OSU-BDGOA1 through co-culture with *Kluyveromyces marxianus* bdgo-ym6

Brianda D. González-Orozco, Erica Kosmerl, Rafael Jiménez-Flores and Valente B. Alvarez*

Department of Food Science and Technology, The Ohio State University, Columbus, OH, United States

Introduction: Due to the increasing consumer demand for the development and improvement of functional foods containing probiotics, new probiotic candidates need to be explored as well as novel means to enhance their beneficial effects. *Lactobacillus kefiranofaciens* OSU-BDGOA1 is a strain isolated from kefir grains that has demonstrated probiotic traits. This species is the main inhabitant of kefir grains and is responsible for the production of an exopolysaccharide (EPS) whit vast technological applications and potential bioactivities. Research has shown that interkingdom interactions of yeast and lactic acid bacteria can enhance metabolic activities and promote resistance to environmental stressors.

Methods: Comparative genomic analyses were performed to distinguish OSU-BDGOA1 from other strains of the same species, and the genome was mined to provide molecular evidence for relevant probiotic properties. We further assessed the cumulative effect on the probiotic properties of OSU-BDGOA1 and *Kluyveromyces marxianus bdgo-ym6* yeast co-culture compared to monocultures.

Results: Survival during simulated digestion assessed by the INFOGEST digestion model showed higher survival of OSU-BDGOA1 and *bdgo-ym6* in co-culture. The adhesion to intestinal cells assessed with the Caco-2 intestinal cell model revealed enhanced adhesion of OSU-BDGOA1 in co-culture. The observed increase in survival during digestion could be associated with the increased production of EPS during the late exponential and early stationary phases of co-culture that, by enhancing co-aggregation between the yeast and the bacterium, protects the microorganisms from severe gastrointestinal conditions as observed by SEM images. Immune modulation and barrier function for recovery and prevention of flagellin-mediated inflammation by *Salmonella* Typhimurium heat-killed cells (HKSC) in Caco-2 cells were also measured. OSU-BDGOA1 in mono- and co-culture regulated inflammation through downregulation of pro-inflammatory cytokine expression and increased membrane barrier integrity assessed by TEER, FD4 permeability, and expression of tight junctions.

Discussion: The results of the study warrant further research into the application of co-cultures of yeast and LAB in functional probiotic products and the potential to increase EPS production by co-culture strategies.

KEYWORDS

co-culture, probiotics, exopolysaccharides (EPS), kefir, *in vitro* digestion, heat-killed *Salmonella* Typhimurium cells (HKSC)

1. Introduction

Probiotic microorganisms are widely consumed around the world and have gained popularity for their potential to improve human health (Ailioaie and Litscher, 2021; Cunningham et al., 2021). The most recent definition of probiotics is "live microorganisms, which when administered in adequate amounts confer a health benefit on the host" (Hill et al., 2014). Probiotics exert their beneficial effects through different mechanisms including supporting the gut microbiota, producing antibacterial peptides, outcompeting pathogens for nutrients and preventing their adhesion to intestinal cells, modulating the immune system, enhancing intestinal barrier function, and reducing inflammation. However, these properties are strain-specific and a comprehensive genetic and phenotypic characterization of potential probiotic strains and their associated health benefits is required (Liu et al., 2018; Raheem et al., 2021).

The most widely used probiotic bacteria for human consumption include members of the *Lactobacillus* and *Bifidobacterium* genera. Further, dairy products are the most common vehicles for delivery to consumers due to their complex nutritional profiles (Gullo and Zotta, 2022). With increasing consumer demand for the development and improvement of functional foods containing probiotics, new probiotic candidates need to be explored as well as novel means to enhance their probiotic properties.

Kefir is a fermented dairy product originating from the Caucasus mountains that has been consumed for centuries due to its associated health benefits. Traditional kefir is produced from the fermentation of milk with kefir grains, which are complex microbial communities of lactic acid bacteria (LAB), acetic acid bacteria, and yeast embedded in an exopolysaccharide (EPS) matrix known as kefiran (Nejati et al., 2020). During kefir production, EPS-producing bacteria play an important role in traditional kefir production, as they acidify and improve the viscosity and texture of the fermented product. Recently, EPS from probiotic bacteria are receiving renewed interest due to their potential functional and bioactive properties. Several studies have demonstrated the biological activities of EPS, including prebiotic effects, modulation of the host immune response, antagonism of pathogens in the gut, and increasing barrier integrity (Jurášková et al., 2022; Sørensen et al., 2022). However, due to the complexity of the kefir grains and unique fermentation dynamics, the production of a stable kefir product remains unfeasible at a commercial level (Yilmaz et al., 2022). Therefore, there is a significant opportunity to isolate, identify, and characterize specific EPS-producing kefir strains with functional benefits, and a need for understanding the detailed mechanisms underlying their probiotic effects.

Lactobacillus kefiranofaciens is the main habitant of kefir grains and is responsible for the production of a unique EPS known as kefiran. Kefiran has multiple potential technological applications as a thickener and texture-modifier, and also exhibits various bioactivities, including antibacterial, antioxidant, and immune regulatory properties (Vinderola et al., 2006; Wang X. et al., 2018). Several strains of *L. kefiranofaciens* isolated from various kefir grain origins have shown probiotic traits; however, genotypic characterization is restricted due to the limited number of genome sequences available. *Lactobacillus kefiranofaciens* OSU-BDGOA1 (GenBank number: JARJVW01) is a strain previously isolated by our group and has shown activity against indicator microorganisms, resistance to gastrointestinal tract conditions, lack of blood hemolysis, and absence of antibiotic resistance to common antibiotics (González-Orozco et al., 2023).

Kluyveromyces marxianus is the predominant yeast found in kefir grains and plays a crucial role in the production of desirable flavor compounds (e.g., ethyl acetate and phenylethanol) in milk kefir. Relative to other yeast species, such as *Saccharomyces cerevisiae*, *K. marxianus* has several physiological advantages due to its ability to ferment a wide variety of sugars and its thermotolerance, with a maximum growth temperature of 52°C (Ahtesh et al., 2018). Furthermore, *K. marxianus* strains have exhibited probiotic traits (Maccaferri et al., 2012; Diosma et al., 2014). *Kluyveromyces marxianus* bdgo-ym6 (GenBank number: MZ927822.1) was previously isolated by our group from kefir grains. In a preliminary screening, this strain showed potential in resisting gastrointestinal tract conditions, surface hydrophobicity, auto-aggregation ability, and proteolytic activity (González-Orozco et al., 2023).

In natural environments, including the human gut, microorganisms exist as part of complex communities consisting of hundreds or thousands of strains that form unique networks of relationships. For instance, a consortium of microorganisms may provide crucial benefits like the division of labor toward a metabolic purpose where more than one strain is involved (Canon et al., 2020b). The value of co-cultivation has been exploited in many fields including the production of vitamins and enzymes, wastewater treatments, in the bioenergy sector, and to enhance flavor and rheological properties of fermented foods (Kapoore et al., 2022).

In food applications, usually microbial consortia of different probiotic LAB are used with the purpose of enhancing probiotic traits and metabolic capacities. Bolla et al. (2013) showed that the co-culture of lactic acid bacteria (*L. plantarum, L. kefir, L. lactis*) and yeast (*K. marxianus, S. cerevisiae*) reduced the levels of a *C. difficile*-induced enterocolitis in a hamster model. Another co-culture of kefir microorganisms (*Lactiplantibacillus plantarum* CIDCA 8327, *Lentilactobacillus kefiri* CIDCA 8348, and *K. marxianus* CIDCA 8154) showed positive effects against *Salmonella* spp. in Caco-2/TC7 cells in an *in vitro* model (Londero et al., 2015). Overall, these studies suggest that the use of a co-culture of probiotic strains could trigger beneficial effects through metabolic cooperation through division of labor and removal of inhibitory metabolites (Canon et al., 2020a). However, designing and controlling a synthetic consortium of different LAB to achieve a metabolic goal is challenging due to competitive exclusion, in which two non-interbreeding populations competing for the same ecological niche and nutritional requirements cannot coexist (Grandel et al., 2021). As many LAB utilize the same nutrients, combining strains with similar metabolic dependencies in a co-culture can result in the faster growing population completely overtaking the slower growing population. Therefore, understanding the positive microbial interactions among members of the consortium is essential and a consortia of a single LAB strain and a single yeast with different ecological niches may overcome these challenges (Giri et al., 2020).

Interkingdom consortia of yeasts and LAB are of key importance in natural fermented products such as kefir, kimchi, beer, kombucha, sourdough, etc. (Tamang et al., 2016). As shown by Ponomarova et al. (2017), by-products of yeast metabolism such as amino acids and small peptides can render new metabolic niches for LAB. Additionally, lactic acid accumulation during fermentation inhibits growth of LAB and results in a decrease in productivity of metabolites like EPS. Sieuwerts et al. (2008) showed that in kefir grains *S. cerevisiae*

raises the pH by utilizing the lactic acid produced by *L. kefiranofaciens* as a carbon source and enables prolonged growth of the bacterium. Bertsch et al. (2019) reported that co-culturing *S. cerevisiae* with *Lactobacillus delbrueckii* increased kefiran production and bacteriocin (nisin) production.

Therefore, we hypothesized that a co-culture of *L. kefiranofaciens* OSU-BDGOA1 and *K. marxianus* bdgo-ym6 will enhance probiotic traits through positive symbiotic microbial interactions using a model system. In the present study, we assessed the cumulative effect of co-culturing kefir microorganisms *L. kefiranofaciens* OSU-BDGOA1 and *K. marxianus* bdgo-ym6 compared to single strains on the resistance to simulated digestion, adhesion to epithelial cells, EPS production, antibacterial activity, and regulation of the gut-associated immune system and membrane barrier upon flagellin-mediated inflammation by *Salmonella enterica* serovar Typhimurium LT2 heat-killed cells in a Caco-2 intestinal cell model.

2. Materials and methods

2.1. Genomic comparison of *Lactobacillus kefiranofaciens* strains

For a comparative analysis between *L. kefiranofaciens* strains, the genome sequence of OSU-BDGOA1 was compared to three other *L. kefiranofaciens* strains (1,207, ZW3, LKK75) from GenBank (Supplementary Table S1). To estimate differential gene content of the genomes and other comparison metrics, we used the comparative genomics platform EDGAR (Blom et al., 2009).

2.2. Genotypic characterization based on screening of targeted functions

Lactobacillus kefiranofaciens OSU-BDGOA1 was previously identified by PCR amplification of a major part of the 16 s rRNA gene, as described in González-Orozco et al. (2023). Identity confirmation was performed by whole genome sequencing (BioSample ID: SAMN31370630). The genome of OSU-BDGOA1 was mined for genes associated with bacteriocin production using BAGEL4 (van Heel et al., 2018) and for potential phages using Prophage Hunter (Song et al., 2019). Genomic islands of virulence factors, resistance genes, and pathogen-associated genes were tracked with IslandViewer4 (Bertelli et al., 2017) and compared with other *L. kefiranofaciens* strains (1,207, ZW3, and LKK75). Additionally, genes encoding for specific functions (i.e., the genes encoding carbohydrate metabolism, genes for resistance to gastric tract conditions, and EPS production) were also mined from the annotation with IslandViewer4 (Supplementary Table S2).

2.3. Co-culture growth conditions

Preliminary experiments for *L. kefiranofaciens* and *K. marxianus* growth in co-culture showed fitness of growth of both microorganisms in co-culture at 30°C in aerobic conditions when cultivated in MRS broth (Sigma Aldrich, St. Louis, MO) (Supplementary Table S3). *Lactobacillus kefiranofaciens* and *Kluyveromyces marxianus* strains were stored with 20% glycerol (Thermo Fisher, Waltham, MA) in De Man Rogosa Sharpe (MRS) broth and Yeast Extract Peptone Dextrose (YEPD) broth, respectively, at −80°*C. prior* to each experiment, the strains were activated from the glycerol stocks in 5 mL of either MRS or YEPD broth and incubated aerobically for 16 h at 30°C. Liquid cultures were sub-cultured twice before the start of all experiments.

2.4. Survival during *in vitro* INFOGEST digestion

Survival during digestion was assessed following the static INFOGEST 2.0 digestion model consisting of oral, gastric, and intestinal phases (Brodkorb et al., 2019) with slight modifications. All digestion reagents were purchased from Sigma Aldrich. *L. kefiranofaciens* and *Kluyveromyces marxianus* were pre-cultured as described previously in MRS and YEPD broth, respectively. Stationary phase cultures were centrifuged (4,200 × g, 4°C, 10 min), washed twice with saline solution (0.85% NaCl, pH 7.0) and resuspended to an optical density (OD) of 0.1 at 600 nm, corresponding to approximately 10^8 CFU/mL for bacteria and 10^6 CFU/mL for yeast. The OD = 0.1 suspensions were inoculated at a ratio of 10% of the final volume in MRS broth for each monoculture control. For the co-culture, the OD-adjusted suspensions were mixed 1:1 (v/v) and inoculated at a ratio of 10% of the final volume in MRS broth based on the ratio of these strains present in kefir. The cultures were then incubated aerobically for 16 h at 30°C. Immediately before the start of simulated digestion, the OD of each monoculture and the co-culture were adjusted to 0.1 at 600 nm in saline solution and 5 mL of each suspension was used at the start of digestion. At the end of the gastric and intestinal phases, the digesta was centrifuged (3,500 × g, 4°C, 10 min) and the supernatant was removed, the microbial pellet was resuspended in 5 mL of saline solution and serial dilutions were made. CFUs of the monoculture and co-culture at the end of the gastric and intestinal phases were counted by plating onto selective media: MRS supplemented with 0.02 g/L cycloheximide were used to selectively estimate *L. kefiranofaciens* and potato dextrose agar (PDA) supplemented with 0.1 g/L chloramphenicol was used to selectively estimate *K. marxianus* yeast in the co-culture. For monocultures MRS agar was used for *L kefiranofaciens* and PDA for *K. marxianus*. Plates were incubated for 2 days at 30°C before counting. Survival percentage was determined as follows:

$$Survival\ (\%) = \left(\frac{\frac{CFU}{mL}\ of\ survivors\ in\ each\ phase}{\frac{CFU}{mL}\ pre-digestion\ control} \right) \times 100$$

2.5. Caco-2 cell culture

The human colorectal adenocarcinoma Caco-2 cell line (HTB37, American Type Culture Collection) was used as a model of intestinal epithelium cells. Cells were seeded in T-75 cm^2 flasks (Corning) with complete Dulbecco's modified Eagle's medium (cDMEM) supplemented with 10% heat-inactivated fetal bovine serum, 1%

penicillin–streptomycin (100 units/mL penicillin and 100 units/mL streptomycin), 1% non-essential amino acids (100X), and 1% 200 mM L-glutamine in a humidified atmosphere of air and CO_2 (95:5, vol/vol) for 4 h at 37°C. Cells were passaged by trypsinization at 70–90% confluence (6 ± 1-day post-seeding) and passages between 23 and 35 were utilized for the experiments. Spent medium was replaced every 48 h. Media was replaced with serum- and antibiotic-free media one day prior to all experiments. All cell culture reagents were purchased from Thermo Fisher (Gibco).

2.6. Adhesion to Caco-2 cells

Caco-2 cells were seeded at a density of 1×10^5 cells per well in a 12-well culture plate (Corning) and cultured for 14 days post-confluency for adequate differentiation. Caco-2 cells were incubated with 1.5 mL of mono- and co-culture stationary-phase suspensions ($OD_{600} = 0.1$) for 4 h at 37°C. To account for changes in microbial growth in the presence of cDMEM, both mono- and co-culture suspensions without Caco-2 cells were simultaneously incubated in cDMEM. These suspensions served as the control for added microorganisms. At the end of the incubation time, Caco-2 cells were washed two times with sterile PBS to remove non-adherent bacteria and lysed with 1% Triton X-100 (v/v) for 30 min at 4°C to release adherent microorganisms. Samples were centrifuged (8,000 × g, 4°C, 10 min) and washed twice before resuspending in 1.0 mL of saline solution. Adhesion of the monoculture and co-culture were determined by plating serial dilutions on selective media as explained above. Adhesion percentage was determined as follows:

$$Adhesion\,(\%) = \left(\frac{CFU}{mL} of\ adhered\ microorganisms \Big/ \frac{CFU}{mL} added\ microorganisms \right) \times 100.$$

Adhesion assays were carried out in three independent experiments, each containing three replicates.

2.7. Growth and exopolysaccharides (EPS) production

For the production of EPS in co-culture and monoculture of *L. kefiranofaciens,* we determined the EPS concentration at different time points (4, 8, 12, 20, 24, and 48 h) during incubation at 30°C. At the same time, the growth curves were prepared by incubating 20 µL of mono- and co-culture suspensions ($OD_{600} = 0.1$) in 180 µL MRS media in a sterile 96-well plate in triplicate. The OD_{600} was recorded every 2 h over the aerobic incubation time with 5 s of low-speed shaking prior to each read.

Based on previous reports that address the overestimation of bacterial EPS production by the subsequent extraction of medium constituents such as beef and yeast extract during EPS characterization and quantification, we adjusted the methodology to account for these limitations. Specifically, we use a modified version of Casein Glucose Broth (mCGB) replacing yeast extract with yeast nitrogen base (YNB) and peptone with casein acid hydrolysate (Sigma Aldrich) according to Alhudhud et al. (2014). We also determined that the mCGB was able to support the growth of the co-culture and monocultures. The EPS extraction was performed using the methods of Ferrari et al. (2022) with modifications. Briefly, 9 mL of fresh medium was inoculated with 1 mL of co-culture and monoculture suspensions ($OD_{600} = 0.1$) and incubated aerobically at 30°C. Separate tubes were prepared for each time point. At each time point, cells were harvested by centrifugation at (4,200 × g, 4°C, 10 min), the supernatants were treated with trichloroacetic acid (TCA) at a final concentration of 12% (v/v) and incubated at −20°C for 30 min. After centrifugation (7,000 × g, 4°C, 20 min), the pH of the supernatants was adjusted to ~7 by addition of 5 M NaOH, the polysaccharides were precipitated with two volumes of EtOH after overnight incubation at −20°C. Pellets were collected by centrifugation (9,000 × g, 4°C, 30 min) and resuspended in MilliQ water (18.2 MΩ • cm).

Total EPS in mg/mL was determined by subtracting the total sugar content assessed by the phenol sulfuric acid assay with glucose as a standard (Dubois et al., 1956) from the reducing sugars estimated by the DNSA (Dinitrosalicylic acid) method (Gonçalves et al., 2010). Additionally, protein quantification was performed with the Pierce micro-BCA kit (Thermo Fisher).

2.8. Monosaccharide composition and quantification by HPLC-CAD

EPS were extracted as previously described from 200 mL of the co-culture and monoculture in mCGB media after 16 h of incubation at 30°C. Following extraction, EPS were dialyzed with a 3.5 kDa MWCO Amicon Ultra-15 Centrifugal Filter Unit (Millipore) and lyophilized. EPS were hydrolyzed to monosaccharides using the method of Zajšek et al. (2013) with modifications. Briefly, 25 mg of lyophilized EPS powder were dissolved in 2 mL of MilliQ water and sonicated for 10 min to completely dissolve the sugars. Next, 1-mL of the sample was transferred to a 2 mL tube and treated with 0.5 mL of 0.5 M H_2SO_4 for 1.5 h at 100°C. Samples were diluted by adding 1.5 mL of water, pH was adjusted with 5 M NaOH, and further diluted to a final concentration of 4 mg/mL in MilliQ water.

High-purity HPLC-grade solvents, triethylamine, ammonium acetate, and the carbohydrates (glucose, galactose, and mannose) analytical standards were obtained from either Sigma-Aldrich or Fisher Scientific. The analysis was conducted on an XBridge Amide 3.5 µm (4.6 × 250 mm) column (Waters) equipped with a guard column of the same filling on a Dionex Ultimate 3,000 HPLC system with a charged aerosol detector (CAD; Thermo Fisher). A column temperature of 80°C was maintained throughout the run. The volume injected was 50 µL of samples prepared in 60% (v/v) ACN. Elution of monosaccharides was performed at a flow rate of 0.5 mL/min with a multi-step-gradient using two mobile phases. Solvent B consisted of 90% ACN +10% H_2O + 0.2% TEA +25 mM ammonium acetate. Solvent A consisted of 50% ACN + 50% H_2O with 0.2% v/v TEA and 25 mM of ammonium acetate. The isocratic conditions used were as follows: 90% Solvent B (t = 0–32 min), followed by column washing and equilibration. Separation and elution of the carbohydrates analyzed occurred within the first 20 min. The CAD evaporator temperature was set to 35°C with a data collection rate of 10 Hz and filter constant of 1.0. HPLC-grade glucose (D-Glu), galactose (D-Gal),

and mannose (D-Man) standards were used for quantification. The system was controlled by Chromeleon 7.2.9 software. The final sugar quantification was normalized by CFU/mL of the bacterium.

2.9. Scanning electron microscopy

To visualize the EPS produced during the mono and co-culture and analyze their physical and structural properties, the stationary-phase cultures of the mono and co-culture and the lyophilized EPS were imaged using a Schottky Field Emission Scanning Electron Microscope (Hitachi High Technologies America, Inc., Schaumburg, IL, United States) at the Molecular and Cellular Imaging Center (MICI) at The Ohio State University (Wooster, OH). For the fixation process, the microbial pellets were resuspended in 1 mL of fixative (3% glutaraldehyde, 2% paraformaldehyde in 0.1 M of PBS buffer) and incubated at 25°C for 2 h. After centrifugation, the obtained pellet was resuspended in PBS buffer for further addition to a silicon chip and dehydration in acetone.

2.10. Antibacterial activity and sensitivity of antibacterial substances to catalase and proteases

The agar well diffusion method was used to test the antibacterial activity of cell free supernatants (CFS) of the co-culture and monocultures against indicator strains (*Escherichia coli* ATCC 25922 and *Listeria innocua* ATCC 51742). Briefly, CFS were collected by centrifugation (4000 × g, 10 min, 4°C), adjusted to a pH of 7.00 ± 0.05 using 5 M NaOH, and filtered through a nitrocellulose membrane (0.22 μm). Tryptic soy agar plates were overlaid with 10 mL of soft TSA medium (0.75%) and seeded with 10 μL of indicator strains (~10^6–10^7 CFU ml^{-1}). After solidification, 9-mm diameter wells were cut from the agar and 50 μL of the CFS were spotted and maintained at 25°C for 2 h to allow diffusion before incubation at 37°C for 16–18 h. The agar plates were then examined to detect the formation of a clear zone of inhibition around the wells. To determine that the antibacterial activity was not associated with production of hydrogen peroxide and the susceptibility of antibacterial substances to proteases, supernatants were treated with catalase, and trypsin according to the methods followed by Wang et al. (2019). CFS from each strain were incubated for 2 h at 37°C with catalase (3000 U/mg) and trypsin (250 U/mg). The enzymes were used at a final concentration of 1 mg/mL in 50 mM sodium phosphate buffer (pH = 7.00). After incubation, the enzymes were inactivated at 80°C for 10 min. After treatment, the antibacterial ability was determined as described before. A heat control of the CFS was also evaluated to determine sensitivity of the CFS to the heat treatment.

2.11. Study of the regulation of the immune response and membrane barrier in Caco-2 cells

2.11.1. Inflammation induction by heat-killed *Salmonella* Typhimurium cells (HKSC)

Salmonella enterica serovar Typhimurium LT2 heat-killed cells (HKSC, kindly donated by Dr. Ahmed Yousef, The Ohio State University, Columbus, OH, United States) were used to study the effect on the immune responses of the mono- and co-cultures at prevention and recovery upon flagellin-mediated inflammation by *Salmonella* Typhimurium in Caco-2 cells. *Salmonella* Typhimurium cells were activated from glycerol stocks in TSA (1.5%) plates. Liquid cultures were sub-cultured twice before the inactivation experiment. Pellets OD_{600nm} = 0.5 were recover by centrifugation, washed twice, and resuspend in PBS buffer. HKSC were prepared by heat treatment at 65°C for 1 h. To ensure complete cell inactivation the resulting suspension was plated in TSA plates and incubated for 24 h at 37°C in aerobic conditions. The inflammatory response was measured by the gene expression of pro- and anti-inflammatory cytokines (*Il-8, Mcp-1, Il-6,* and *Il-10*), as these are key modulators of the inflammatory response. Since the time of administration of probiotics is crucial in determining their response (Liu et al., 2018; Milner et al., 2021), the effect of the mono and co-culture before (preventive group) and after (recovery group) the HKSC-induced inflammation was evaluated.

To determine the concentration of HKSC that will induce an inflammation response in Caco-2 cells, preliminary experiments testing different concentrations and times of exposure were conducted and the inflammation response evaluated by expression of pro-inflammatory cytokines. Cytotoxicity to the mammalian cells for all the treatments was also determined with the lactose dehydrogenase (LDH) assay using a commercial kit (Sigma-Aldrich) (data not shown).

For the recovery group, fully-differentiated Caco-2 cells seeded in 24 well plates (Corning) were washed with sterile DPBS and replaced with 500 μL of a suspension HKSC (MOI ≈ 100) in serum- and antibiotic-free media and incubated for 4 h at 37°C. Subsequently, 500 μL of stationary phase suspensions of mono- and co-cultures in serum- and antibiotic-free media were added to the wells and incubated for an additional 4 h. For the preventive group, the stationary phase suspensions of mono- and co-culture were first added to the cells, incubated for 4 h at 37°C, and then treated with 500 μL of HKSC (MOI ≈ 100) in serum- and antibiotic-free media for an additional 4 h. At the end of the experiment, Caco-2 cells were washed twice with DPBS (pH 7.0) and harvested with 200 μL of Trizol reagent (Sigma-Aldrich). Samples were stored at −80°C until further RNA extraction. Wells treated with HKSC for 8 h were used as positive controls, untreated Caco-2 cells in serum- and antibiotic-free media were used as negative controls. Additionally, to account for the effect of the co-culture and respective monocultures and in the mammalian cells, controls without HKSC were also evaluated. The layout of the experimental design, including the different treatments and time points is shown in Figure 1.

2.11.2. Gene expression by qPCR

RNA was extracted from Caco-2 cells after treatment using Trizol according to the manufacturer's protocol (Sigma Aldrich). Reverse transcription of RNA was performed with the iScript Reverse Transcription Supermix kit (Bio-Rad) and the cDNA was subsequently diluted ten times. Amplification of primer-specific cDNA was achieved using the SsoAdvanced Universal SYBR Green Supermix (Bio-Rad). Primers for the human inflammatory cytokines (*Il-8, Mcp-1, Il-6*) and anti-inflammatory cytokines (*IL-10*) were amplified using PrimerPCR SYBR Green Assays (Bio-Rad) in a CFX96 Touch System with expression being normalized to actin. Primer specificity and efficiency was assessed from the melt curves. Analysis was performed using CFX Maestro Software (Bio-Rad).

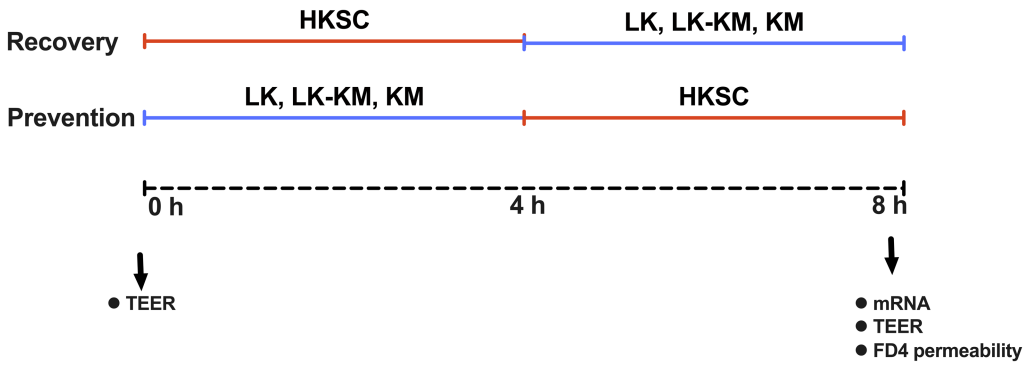

FIGURE 1
Experimental design used to test the immune regulation capacity of *Lactobacillus kefiranofaciens* (LK) and *Kluyveromyces marxianus* (KM) in mono- and co-culture at prevention and recovery upon flagellin-mediated inflammation by heat-killed *Salmonella* Typhimurium cells (HKSC) in Caco-2 intestinal cells model. Recovery group: 4 h of inflammation induction with HKSC followed by 4 h treatment with monocultures (LK, KM) and co-culture (LK-KM). Prevention group: 4 h treatment with monocultures (LK, KM) and co-culture (LK-KM) followed by 4 h of inflammation induction with HKSC.

2.11.3. Determination of monolayer integrity of Caco-2 cells

Experiments to determine the effect of mono- and co-culture on the prevention and recovery of HKSC-induced disruptions of monolayer integrity were performed on 6-well membrane inserts with a 0.4 µm PET tracked-etched membrane (Corning). Inserts were seeded apically with 1.5 mL of cDMEM containing 2×10^5 cells per insert and maintained for 21 days for complete differentiation of Caco-2 cells. Only the monolayers with epithelial resistance reaching $\geq 300\,\Omega\,cm^2$ were used for experiments (21 days post-confluency).

2.11.4. Trans-Epithelial Electrical Resistance (TEER) and paracellular permeability

Caco-2 cells were washed with sterile DPBS and 750 µL of HKSC (MOI ≈ l00) or co-culture and monocultures suspensions in serum- and antibiotic-free media were added apically according to the experimental design and incubated for 4 h at 37°C. After the first incubation time, additional 750 µL suspensions of HKSC or monocultures and co-culture were added to the inserts and incubated for an additional 4 h at 37°C.

TEER was measured using a EVOM Epithelial Voltohmmeter with an STX2 probe (Millipore) in sterile DPBS after a washing step to remove old medium breakdown products that can affect the TEER measurements as described by Hubatsch et al. (2007). TEER change was expressed as the ratio of the TEER at the end of the treatments compared to the initial value. The paracellular permeability of the Caco-2 monolayers was determined by the transport of fluorescein isothiocyanate (FITC)-labeled dextran (FD4, MW = 4,000 Da; Sigma Aldrich) according to Yuan et al. (2020). FD4 was dissolved in phenol red-free DMEM for a final concentration of 2 mg/mL and 100 µL of the dextran solution were added to the apical side of the inserts. Aliquots of 100 µL were taken from basolateral side after a 2 h incubation at 37°C in the dark. Fluorescence was measured using a fluorescence microplate reader (490 nm excitation/520 nm emission). FD4 transport across the monolayer was quantified using a calibration curve of fluorescence intensity of different FD4 concentrations. Gene expression of tight junction proteins claudin-1 (*Cldn-1*), occludin-1 (*Ocl-1*), and zonula occludens (*Zo-1*) was also determined with Primer PCR SYBR Green Assays as explained above.

2.12. Statistical analysis

All data presented are represented as the mean ± standard deviation of at least three replicates. Differences of $p < 0.05$ were considered statistically significant. All statistical analysis was performed in GraphPad Prism V9.4. The survival during digestion was analyzed by a 2-way analysis of variance (ANOVA) and multiple comparison by *post hoc* Tukey test. Adhesion data, qPCR gene expression data, trans-epithelial electrical resistance, and paracellular permeability of FITC-dextran were analyzed with an ordinary one-way ANOVA and *post hoc* Tukey test. EPS production and monosaccharide composition data were analyzed with an unpaired *t*-test.

3. Results

3.1. Genotypic characterization

Conducting gene mining and genome comparison between the strain of interest and related species prior to phenotypic characterization allows for the identification of genetic differences that may be associated with specific traits or functions and therefore guide the experimental design to confirm predictions. The EDGAR comparison revealed 1,575 coding sequences (CDS) shared between *L. kefiranofaciens* OSU-BDGOA1 and *L. kefiranofaciens* 1,207 compared to 1,516 shared CDS with *L. kefiranofaciens* ZW3, and 1,528 shared CDS with *L. kefiranofaciens* LKK75. The average amino acid identity (AAI) between all the tested strains was higher that 99%, indicating a close evolutionary relationship between the given strains. The percentage of conserved proteins (POCP) was higher for the 1,207 strain and the mean nucleotide identity of orthologous genes (FastANI) was higher for the LKK75 strain (Supplementary Figure S1). Furthermore, the gene distribution among the four strains by a Venn diagram revealed that OSU-BDGOA1 has the highest number of unique genes (239) followed by the 1,207 strain (167 unique genes), suggesting that these strains possess greater genomic diversity. Out of the 239 unique genes in OSU-BDGOA1, we found genes encoding polysaccharide synthesis, S-layer, S-layer associated proteins (SLAP), transposases, helveticin J bacteriocin, and genes associated with resistance to acidic conditions. All analyzed *L. kefiranofaciens* strains

showed a gene cluster for a bacteriocin III and a bacteriocin immunity protein. The functional categories of the genome were determined using KEGG (Kyoto Encyclopedia of Genes and Genomes) and COG (clusters of orthologous genes database), which enable better understanding of the high-level functions and utilities within the genomes. Figure 2 shows the 10,484 and 8,472 functional gene categories by KEGG and COG, respectively, that were found in all the strains using *L. kefiranofaciens* LKK75 as reference genome.

Genes encoding for an Enterolysin A and a helveticin-J were mined by BAGEL4, while Phage Hunter identified a *Lactobacillus* phage Lfelnf (74% identity) in the OSU-BDGA1 genome that has been reported to infect *Lactobacillus fermentum* (Liu et al., 2015). No genomic islands of virulence factors, resistance genes, or pathogen-associated genes were found in the genome by IslandViewer4. Supplementary Table S2 lists the genes encoding for specific functions that were mined in the genome. The presence of genes associated with bile salt tolerance and resistance to acidic pH, as well as genes associated with EPS production, were identified.

3.2. Co-culture increased survival of *Lactobacillus kefiranofaciens* OSU-BDGOA1 during simulated digestion and adhesion to intestinal cells

To determine whether the functional characteristics found in the genome of *L. kefiranofaciens* OSU-BDGOA1 are associated with the

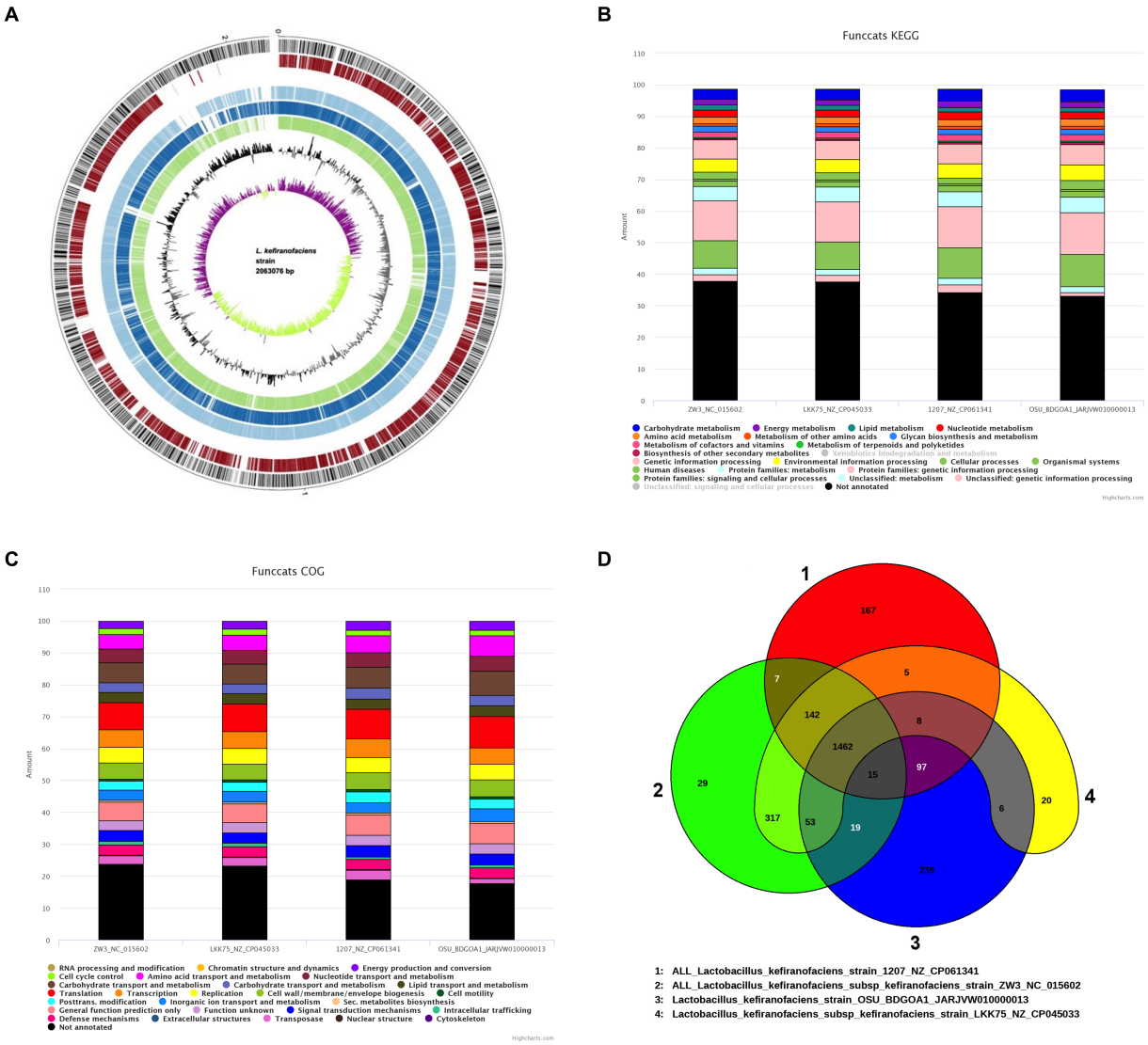

FIGURE 2
Genomic-based comparison of *Lactobacillus kefiranofaciens* OSU-BDGOA1 and closely related strains of the same species. Circular genome plot **(A)** generated by BioCircos within the EDGAR software comparing four *L. kefiranofaciens* genomes arranged from outer to inner circle as follows: Circles 1–4 showed coding sequences (CDSs) on the forward and reverse strands of *L. kefiranofaciens* OSU-BDGOA1 (reference genome), *L. kefiranofaciens* subsp. *kefiranofaciens* LKK75, *L. kefiranofaciens* 1,207, and *L. kefiranofaciens* subsp. *kefiranofaciens* ZW3, respectively. Circles 5 and 6 represent the RNA features (green) and the GC content. Circle 6 represents the GC skew [(C – G) / (C + G)] curve, above mean GC skew (violet), below mean GC Skew (green). Functional annotation comparison by KEGG **(B)** and COG (clusters of orthologous genes database) **(C)**. Venn diagrams of coding sequences for the four *L. kefiranofaciens* strains evaluated **(D)**.

10.3389/fmicb.2023.1236634

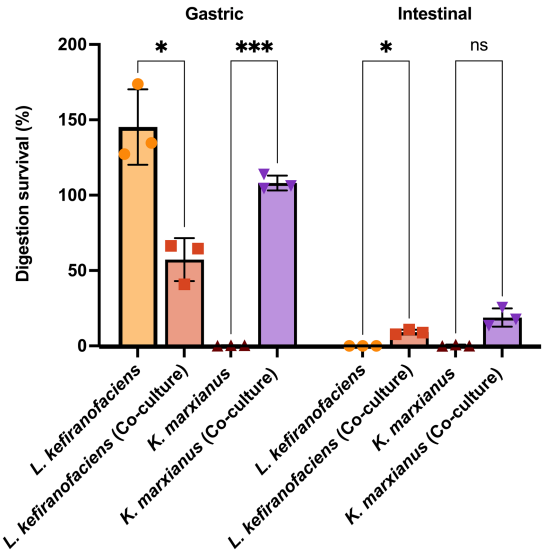

FIGURE 3
Survival (%) of *L. kefiranofaciens* and *K. marxianus* in mono- and co-culture across the gastric and intestinal phases using the INFOGEST static simulated digestion model. Statistical difference between treatments is denoted as $*p < 0.05$, $**p < 0.01$, $***p < 0.0005$ by 2-way ANOVA with *post hoc* Tukey test.

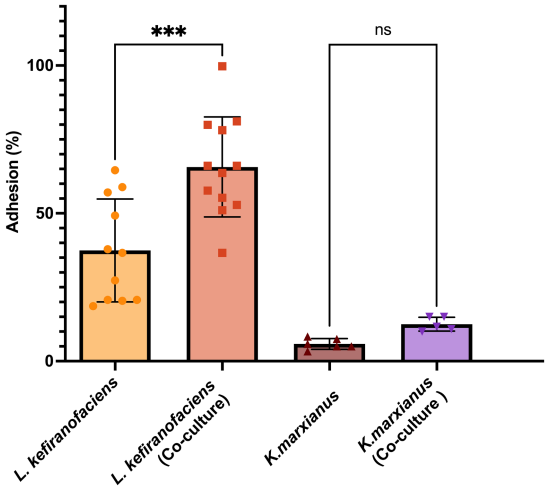

FIGURE 4
Adhesion (%) of *L. kefiranofaciens* and *K. marxianus* in mono- and co-culture to Caco-2 intestinal cells. Values represent the mean ± SD of at least three replicates. Statistical difference denoted as $***p < 0.0005$ by one-way ANOVA with post hoc Tukey test.

expressed phenotype and whether they are influenced by co-culturing with *K. marxianus*, we screened for several key probiotic properties, including survival during digestive stress and adhesion to intestinal cell culture. During simulated digestion, the survival of *L. kefiranofaciens* significantly increased from 0.003 to 9.14% ($p < 0.05$) at the end of the intestinal phase when co-cultured with *K. marxianus* bdgo-ym6. For *K. marxianus,* the survival was significantly greater in co-culture in the gastric phase (109% vs. 0.31%); however, at the end of the intestinal phase, the difference between co-culture and monoculture was not significant (18.8 and 0.35%, respectively) (Figure 3). The effect of the co-culture in modifying the adhesion phenomenon of these microorganisms to intestinal cells was assessed with the Caco-2 cell culture model using a 4 h incubation to simulate gastrointestinal transit time. The co-culture condition enhanced adhesion of *L. kefiranofaciens* compared to the monoculture (65.68, and 37.47%, respectively). This result represents a 1.7-fold increase in adhesion to intestinal cells. However, the adhesion of *K. marxianus* was not enhanced, with a 12.5% adhesion in the co-culture to 5.8% in the monoculture condition (Figure 4).

3.3. EPS production increased in the co-culture using mCGB in a time-dependent manner

EPS production in the co-culture and monoculture was determined throughout microbial growth in mCGB. The growth of the microorganisms was determined by plate count on selective media and the EPS production was normalized for bacterium number. EPS production in co-culture peaked at 8 h in the exponential phase and was higher than in the *L. kefiranofaciens* monoculture (0.73 and 0.44 mg/mL, respectively). However, in the late exponential phase ($t = 12$ h) the EPS production was significantly reduced in the co-culture compared to the monoculture, with values of 0.4 mg/mL for co-culture to 0.60 mg/mL for the monoculture ($p < 0.05$) (Figure 5A). The decreasing trend in EPS production for the co-culture was maintained for the remaining hours of the fermentation, although after 20 h no significant differences were observed between both conditions. Since carbohydrates from peptidoglycan and glycoproteins may be co-extracted and contribute to the EPS quantification, the protein content was monitored and compared to the EPS production at each time point. The protein quantification did not significantly change during microbial growth under any of the conditions (Figure 5B).

As a secondary approach, and to determine the monosaccharide composition of the EPS produced in the co-culture and monoculture at the stationary phase (16 h), we used HPLC-CAD. Carbohydrates extracted from both the co-culture and monoculture displayed similar neutral sugar profiles comprising of D-Glucose (D-Glu), D-Galactose (D-Gal), and D-Mannose (D-Man) (Table 1). Total sugars were higher in the co-culture compared to the monoculture, consisting of 139.1 and 81.9 g/100 g freeze-dried powder, respectively ($p < 0.05$). The ratio of D-Glu to D-Gal was significantly different in the monoculture condition as compared to the co-culture (1:0.9 and 1:1.5, respectively). The results are in alignment with the observed increased in the EPS production at the early and late stationary phases of the microbial growth (Figure 5A). The visualization of the mono and co-culture via SEM revealed co-aggregation between bacteria and yeast cells in microbial clusters surrounded by EPS layers (Figures 6A,B). The EPS may act as a protective layer and provide mechanical stability to the consortium by serving as a network to maintain a close association between both species. This association may facilitate cross-talk between the cells and activation of genes that allow the co-culture to survive stressful environmental conditions (Kapoore et al., 2022).

10.3389/fmicb.2023.1236634

3.4. Antibacterial activity in cell-free supernatant comes from a proteinaceous compound

To determine whether the co-culture exerted an impact on the antibacterial activity against indicator strains, and to gain insight into the nature of the inhibitory compounds, we treated the CFS of *L. kefiranofaciens* OSU-BDGOA1 in mono- and co-culture with catalase and trypsin. The antibacterial effects depicted by the CFS against *Escherichia coli* ATCC 25922 and *Listeria innocua* ATCC 51742 were not affected by the co-culture conditions (Table 2; Supplementary Figure 2). Conversely, the antibacterial effect was not influenced by catalase treatment, indicating that hydrogen peroxide could not be responsible for the observed effect. However, when the CFS was treated with trypsin, the antibacterial effects against both microorganisms were completely depleted. The heat control also retained the effect, which suggests that the compound responsible for the antibacterial activity is likely proteinaceous in nature, and that upon proteolysis it loses its effect.

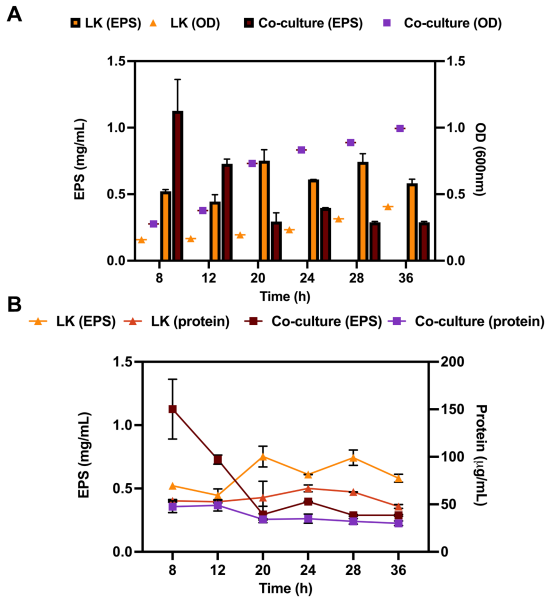

FIGURE 5
Exopolysaccharide production curves (left y-axis) compared to protein quantification curves (right y-axis) of *L. kefiranofaciens* in mono and co-culture with *K. marxianus* during 36 h at 30°C **(A)**. Exopolysaccharide production curves (left y-axis) compared to growth curve (right y-axis) of *L. kefiranofaciens* in mono and co-culture with *K. marxianus* during 36 h at 30°C **(B)**. Values represent the mean ± SD of at least three replicates.

3.5. The monoculture and co-culture of *Lactobacillus kefiranofaciens* OSU-BDGOA1 prevents and ameliorates *Kluyveromyces marxianus* monoculture exacerbation of HKSC-induced inflammation in Caco-2 cells

The potential protective effect of the co-culture and monocultures at preventing and resolving HKSC-induced inflammation was assessed in Caco-2 cells. Treatment with the co-culture (LK-KM) and *L. kefiranofaciens* monoculture (LK) in both the recovery and prevention groups resulted in significant downregulation of the pro-inflammatory cytokines *Il-8* and *Mcp-1* gene expression, with values similar to those of the untreated cells control ($p < 0.05$) (Figures 7A,B,E,F). Interestingly, the monoculture of *K. marxianus* (KM) in the recovery group significantly upregulated the expression of *Il-8*, *Mcp-1*, and *Il-6* to levels similar to the HKSC. *Il-6* expression levels in the prevention group were not significantly affected by any of the treatments ($p < 0.05$) (Figure 7G), whereas in the recovery group the KM monoculture significantly induced *Il-6* expression as compared to the HKSC and untreated cells control (Figure 7C). *Il-10* expression was not induced by any of the treatments as compared to the untreated cells control.

3.6. *Lactobacillus kefiranofaciens* OSU-BDGOA1 in mono- and co-culture protects against HKSC-induced disruption of intestinal barrier function by regulating tight junction proteins expression

In the recovery group, treatment with HKSC led to a 14% decrease in TEER in Caco-2 cells. However, when treated with *K. marxianus* monoculture (HKSC+KM), TEER was markedly more decreased, with a 35% TEER reduction compared to the untreated cells control. In the prevention group, treatment with LK in monoculture significantly increased TEER compared to the HKSC ($p < 0.05$) (Figures 8A,B).

In the paracellular permeability assay, the FD4 concentration across the membrane increased by 3.5-fold in cells treated with HKSC, and remarkably by 14.6-fold in the *K. marxianus* prevention group (KM + HKSC), and by 14.7-fold in the *K. marxianus* recovery group (HKSC+KM). These results suggest a significant reduction in the membrane barrier integrity in these treatments by loss of Caco-2 cell junctions. Treatment with *L. kefiranofaciens* co-culture in the recovery group (HKSC+LK-KM) and with monoculture in the prevention group (LK + HKSC) significantly reduced FD4 paracellular transport compared to HKSC ($p < 0.05$). Furthermore, in both the recovery and prevention groups *L. kefiranofaciens* mono- and co-culture showed

TABLE 1 Monosaccharide composition of the exopolysaccharide (EPS) produced by *Lactobacillus kefiranofaciens* (LK) monoculture and co-culture (LK-KM) after 16 h of incubation at 30°C.

Treatment	Total Sugars (g/100 g freeze-dried powder)*	D-Glu g/100 g	D-Gal g/100	D-Man g/100	Ratio Glu:Gal:Man
LK	81.9 ± 3.7[b]	25.3 ± 8.5[b]	23.3 ± 5.1[b]	33.3 ± 1.1[b]	1:0.9:1.3
LK + KM	139.1 ± 2.5[a]	33.6 ± 2.2[a]	50.4 ± 6.2[a]	55.1 ± 6.7[a]	1:1.5:1.6

*Values correspond to the mean ± SD. Means without common letter between treatments are significantly different ($p < 0.05$), Student's *t*-test.

10.3389/fmicb.2023.1236634

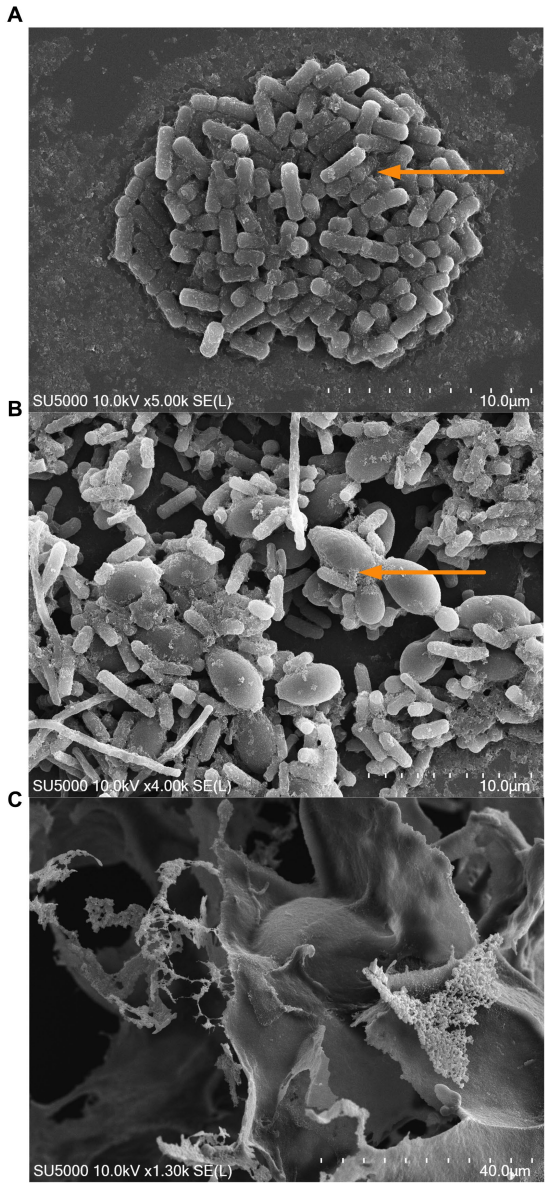

FIGURE 6
Scanning electron microscopy (SEM) images of *L. kefiranofaciens* monoculture **(A)**, *L. kefiranofaciens* and *K. marxianus* co-culture **(B)**, and exopolysaccharide produced by *L. kefiranofaciens* **(C)**. Arrow indicates the exopolysaccharide network observed in the mono- and co-culture.

values similar to those of the untreated control cells, indicating conservation of Caco-2 cell junctions (Figures 8C,D).

To determine if the disruption of the intestinal barrier was associated with altered gene expression of tight junctions, we analyzed the expression of *Cldn-1*, *Ocl-1*, and *Zo-1*. In both the recovery and prevention groups, treatment with HKSC did not reduce the expression of the three tight junction proteins as compared to the untreated cells (Figure 9). In the recovery group, the gene expression of *Ocl-1* and *Zo-1* was not affected by any of the treatments, including HKSC (Figures 9B,C). However, there was a significant induction in *Cldn-1* expression in the *K. marxianus* monoculture in both the recovery and the prevention group ($p < 0.05$) (Figures 9A,D).

TABLE 2 Antibacterial activity of cell-free supernatants (CFS) from *L. kefiranofaciens* (LK) in mono- and co-culture with *K. marxianus* (LK-KM) against indicator strains by the agar well diffusion assay*.

Treatment	*E. coli* ATCC 25922		*L. innocua* ATCC 51742	
	LK	LK-KM	LK	LK-KM
CFS	16.05 ± 0.07	14.15 ± 1.63	14.15 ± 0.49	14.05 ± 0.71
CFS + catalase	12.4 ± 0.14	12.2 ± 0.28	13.65 ± 0.21	12.75 ± 1.06
CFS + trypsin	ND	ND	ND	ND
CFS heat control	13.25 ± 0.35	13.5 ± 0.71	12.75 ± 0.35	12.0 ± 0.0

*Values correspond to the mean ± SD of the diameter of the inhibition halo (mm). ND: not detected antibacterial activity.

Furthermore, in the prevention group, treatment with *L. kefiranofaciens* monoculture (LK + HKSC) showed significantly higher expression levels of *Ocl-1* and *Zo-1* as compared to the co-culture (LK-KM + HKSC) ($p < 0.05$) (Figures 9E,F).

4. Discussion

In the present study, the effect of co-culturing *L. kefiranofaciens* OSU-BDGOA1 with *K. marxianus* bdgo-ym6 was compared to the respective monocultures. The survival of probiotic strains throughout gastrointestinal transit and their adhesive ability to epithelial cells are key factors that determine their beneficial effects. Survival of various *L. kefiranofaciens* strains isolated from kefir and kefir grains in gastrointestinal conditions has been reported by other authors. Kim et al. (2017) reported that two *L. kefiranofaciens* strains isolated from kefir displayed high survival and growth (final bacteria growth exceeded the initial count) during gastrointestinal conditions. In our study, *L. kefiranofaciens* OSU-BDGOA1 in monoculture exceeded the initial counts at the gastric phase; however, at the end of the intestinal phase, the survival was significantly reduced. Evidence of survival capacity in gastrointestinal conditions was found in the genome of *L. kefiranofaciens* OSU-BDGOA1 with genes encoding for resistance to acid and bile salt conditions. Survival of *K. marxianus* in gastrointestinal conditions had been previously reported by others, Fadda et al. (2017) showed that four strains isolated from Fiore Sardo cheese showed higher survival as compared to the probiotic commercial yeast *Saccharomyces boulardii* CODEX SB1with survival rates from 83 to 100%, and adhesion to Caco-2 cells ranging from 4 to 68%. Recently, another study evaluated the survival of five *K. marxianus* strains isolated from kefir in different gastrointestinal environments and compared it to the survival depicted by *S. boulardii* MYA-796. The authors observed not only survival but yeast growth from 1.1 to 11.2 fold (Youn et al., 2022). However, comparing survival in gastrointestinal conditions among different studies is challenging due to the different protocols and conditions that try to simulate the complex gastrointestinal environment (Brodkorb et al., 2019). The highest survival in the present study showed by the co-culture of *L. kefiranofaciens* OSU-BDGOA1 and *K. marxianus* bdgo-ym6 could be associated with the increased production of EPS during the late exponential and early stationary phases of co-culture growth. It has been shown that EPS can enhance the viability of probiotics in the gastrointestinal tract by acting as a protective layer during gastrointestinal transit (Lebeer et al., 2011).

10.3389/fmicb.2023.1236634

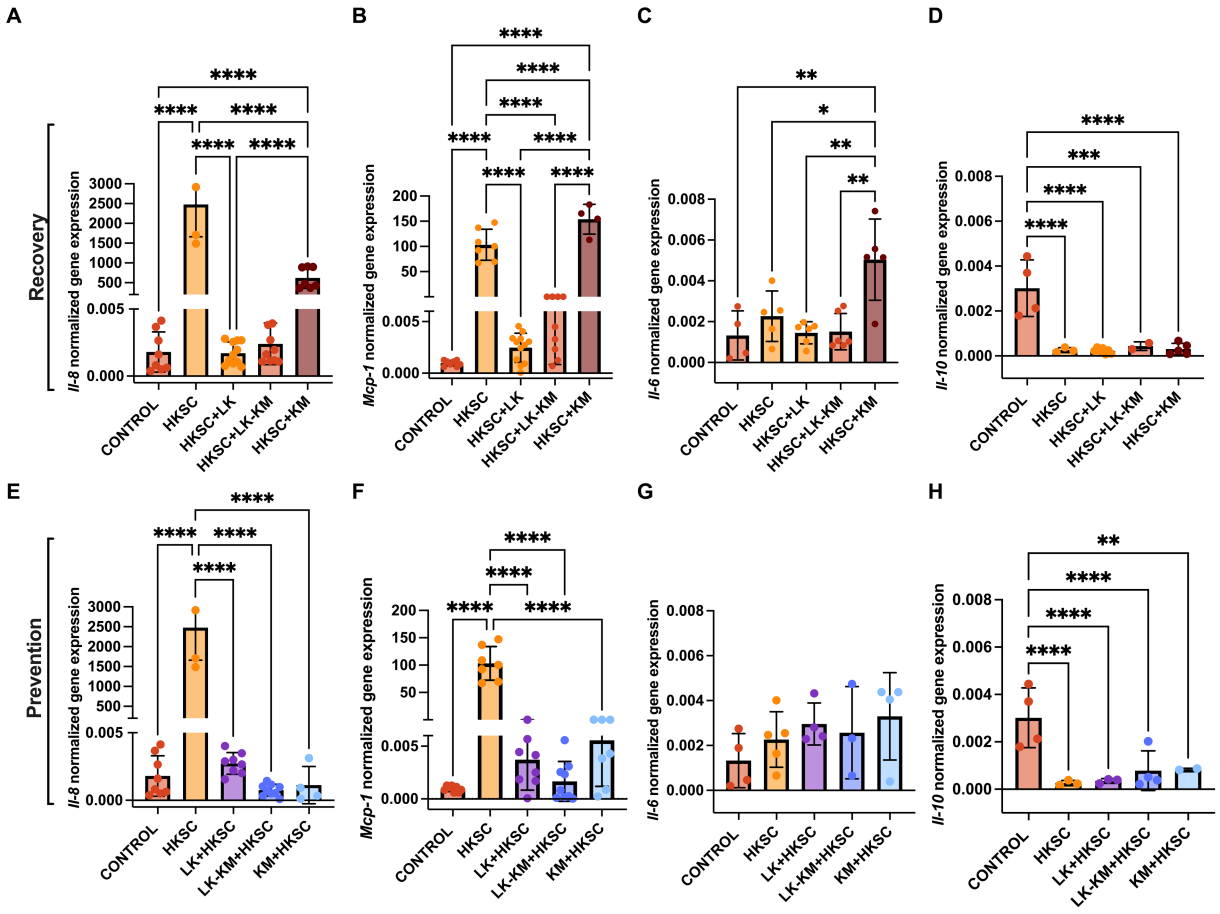

FIGURE 7
Effect of co-culture (LK-KM) and monocultures (LK, KM) on the gene expression of cytokines (*Il-8, Mcp-1, Il-6, Il-10*) for recovery **(A–D)** and prevention **(E–H)** of HKSC-induced inflammation in Caco-2 cells. Values represent the mean ± SD of at least three replicates. Statistical difference denoted as $*p < 0.05$, $**p < 0.01$, $****p < 0.0001$ by one-way ANOVA with *post hoc* Tukey test.

In this study, the observed decrease in EPS in the co-culture after 12 h may be attributed to the limited availability of nutrients in the medium. To minimize the interference of other medium components containing reducing sugars, mCGB was used, which allowed specific quantification of bacterial EPS. However, the removal of yeast extract and beef extract had an impact on the growth of both mono- and co-cultures. Under these restricted nutrient conditions, it is possible that the yeast and bacterium are utilizing the EPS as a fermentable nutrient source to support their growth. This is considered a potential benefit of the EPS in the gut, as they can serve as a fermentable substrate for the gut microbiota (Oerlemans et al., 2021). The monosaccharide composition of the EPS produced by *L. kefiranofaciens* has been previously described as a glucogalactan with a glucose and galactose ratio of approximately 1:1 (Exarhopoulos et al., 2018). While co-culturing *L. kefiranofaciens* with non-EPS producing yogurt bacteria has been shown to alter the EPS composition by adding additional sugars such as xylose and arabinose (Ahmed et al., 2013), no changes in the EPS composition between mono- and co-culture were observed based on the limited neutral sugars we analyzed by HPLC-CAD. However, potential changes in other neutral sugars may have occurred.

Previously, kefiran production by *L. kefiranofaciens* was enhanced by a co-culture system of yeast-LAB, the authors observed that the yeast prevents lactic acid accumulation allowing LAB growth and therefore increasing EPS production (Tada et al., 2007). Previous research reported that the ideal pH for maximum kefiran production lies between 5 and 6 (Cheirsilp and Radchabut, 2011; Zajšek et al., 2013). In our study, the pH in the co-culture at 12 h was 5.22, compared to 4.28 in the monoculture (Supplementary Table S3), supporting the important role of the yeast in enhancing EPS production by regulating media pH. Additionally, yeast can support the growth of LAB through production of diffusible growth-promoting factors, with amino acids being particularly important since most of LAB are auxotrophic for important amino acids (Ponomarova et al., 2017; Liu et al., 2022). In particular, *S. cerevisiae* EC118 has been shown to supply alanine to *L. delbrueckii* when cultivated in co-culture, leading to increased viability of *Lactobacillus rhamnosus* HN001 and *Lacticaseibacillus paracasei* H9 under gastrointestinal conditions and improved adhesion to intestinal cells (Lim et al., 2015).

The SEM images of the co-culture also showed cell–cell interactions between bacteria and yeast cells that could be attributed to the potential increase in survival during gastrointestinal conditions. Previous studies have reported that direct cell contact between *L. rhamnosus* and *S. cerevisiae* in co-culture can increase viability

10.3389/fmicb.2023.1236634

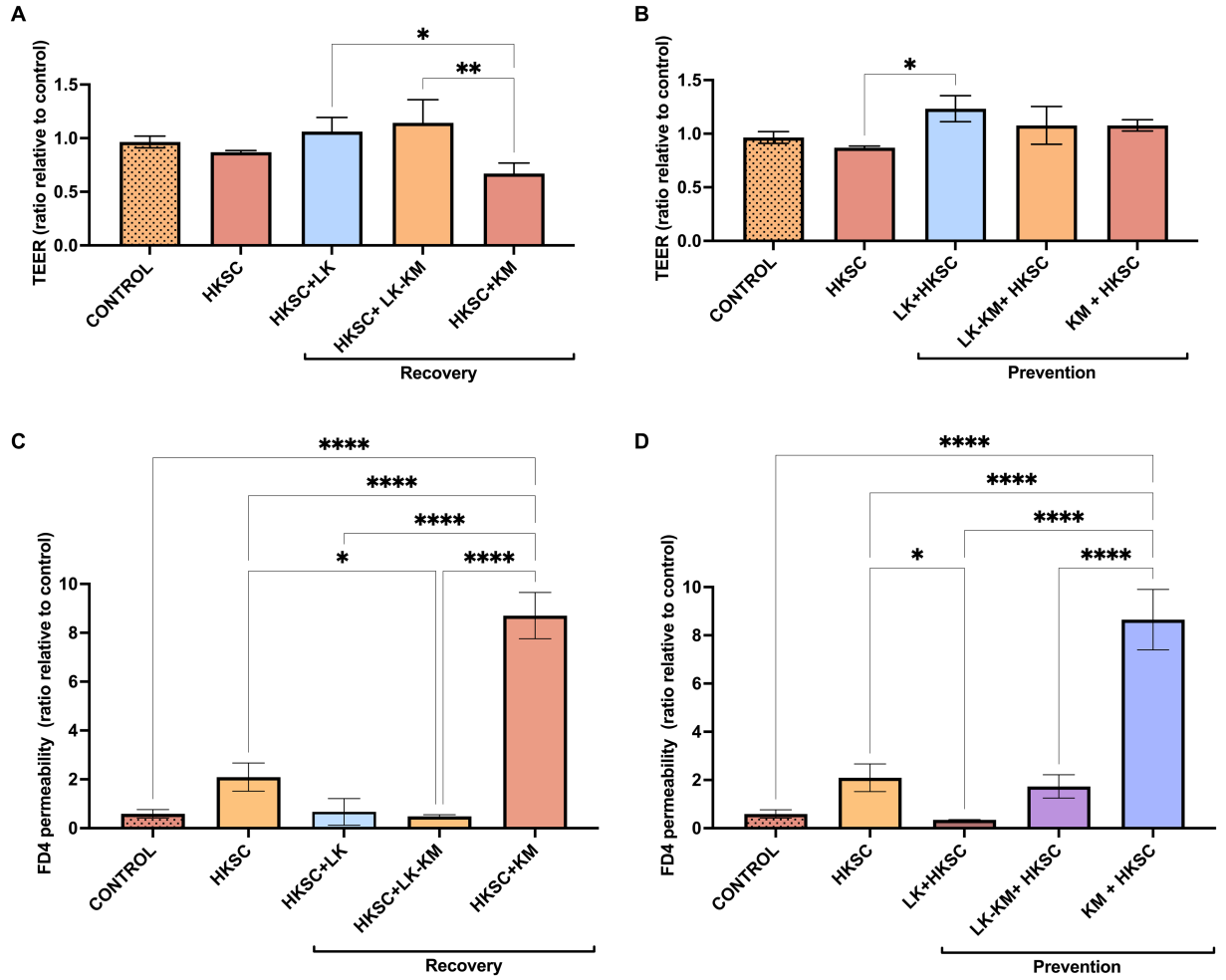

FIGURE 8
Effect of co-culture (LK-KM) and monocultures (LK, KM) on trans-epithelial electrical resistance (TEER) and paracellular permeability of FITC-dextran (FD4) for recovery **(A,C)** and prevention **(B,D)** of HKSC-induced barrier damage. Statistical difference denoted as *$p < 0.05$, **$p < 0.01$,****$p < 0.0001$ by one-way ANOVA with *post hoc* Tukey test.

through cell wall components and metabolites (Xu et al., 2021). Furthermore, yeast cell wall components can also play a significant role in increasing adhesion to intestinal cells. The co-aggregation of *Lactobacillus* spp. and *S. cerevisiae* via mannose-specific adhesin (Msa) and surface layer proteins (S-layer proteins) can mediate adhesion to intestinal cells (Xu et al., 2021). In a study by Wang et al. (2023), increased adhesion to Caco-2 cells of kefir grain isolates *Lactobacillus helveticus* SNA12 and *K. marxianus* GY1 in co-culture was attributed to the presence of proteins and polysaccharides in the yeast cell wall. Furthermore, co-aggregation has been shown to induce overproduction of EPS by *L. kefiranofaciens* in co-culture with *S. cerevisiae* (Benjamas et al., 2003).

Genome mining of *L. kefiranofaciens* OSU-BDGOA1 for genes associated with bacteriocin production revealed the presence of genes that encode class III bacteriocins; Enterolysin- A, a cell wall degrading bacteriocin with broad spectrum activity against Gram-positive and Gram-negative bacteria (Nilsen et al., 2003) and helveticin J, a bacteriocin with a narrow antibacterial spectrum against Gram-positive bacteria including *Listeria monocytogenes* (Joerger and Klaenhammer, 1986), and that has been previously found in other *L. kefiranofaciens* strains (Xing et al., 2017; Georgalaki et al., 2021). However, we cannot directly attribute the observed *in vitro* antibacterial activity to the bacteriocins mined from the genome. The production of bacteriocins *in vivo* is regulated by complex signaling pathways that may not be expressed in experimental conditions. Additionally, post-translational modifications can affect the stability and activity of the bacteriocins, leading to different activities. Finally, other proteins/peptides that are not of bacteriocin nature could be associated with the observed activity (Huang et al., 2021).

In this study, we used an inflammation model using HKSC in Caco-2 epithelial cells to study the immune responses of the co-culture and respective monocultures. Previous research reported that some commonly used inflammation inducers such as bacterial lipopolysaccharide (LPS) did not induce an IL-8 response in *in vitro* intestinal cell models including Caco-2 cells, indicating that the Toll-like receptors (TLRs) that recognize these pathogen-associated molecular patterns (PAMPs) are either not present or not functional in these models. However, flagellin from *Salmonella* Typhimurium significantly increased IL-8 in the apical side of a Caco-2 cells, suggesting that TLR5, which recognizes flagellin, is present and functional in this cell culture model (Grouls et al., 2022). Carasi et al. (2014) induced inflammation in Caco-2 cells by using flagellin from

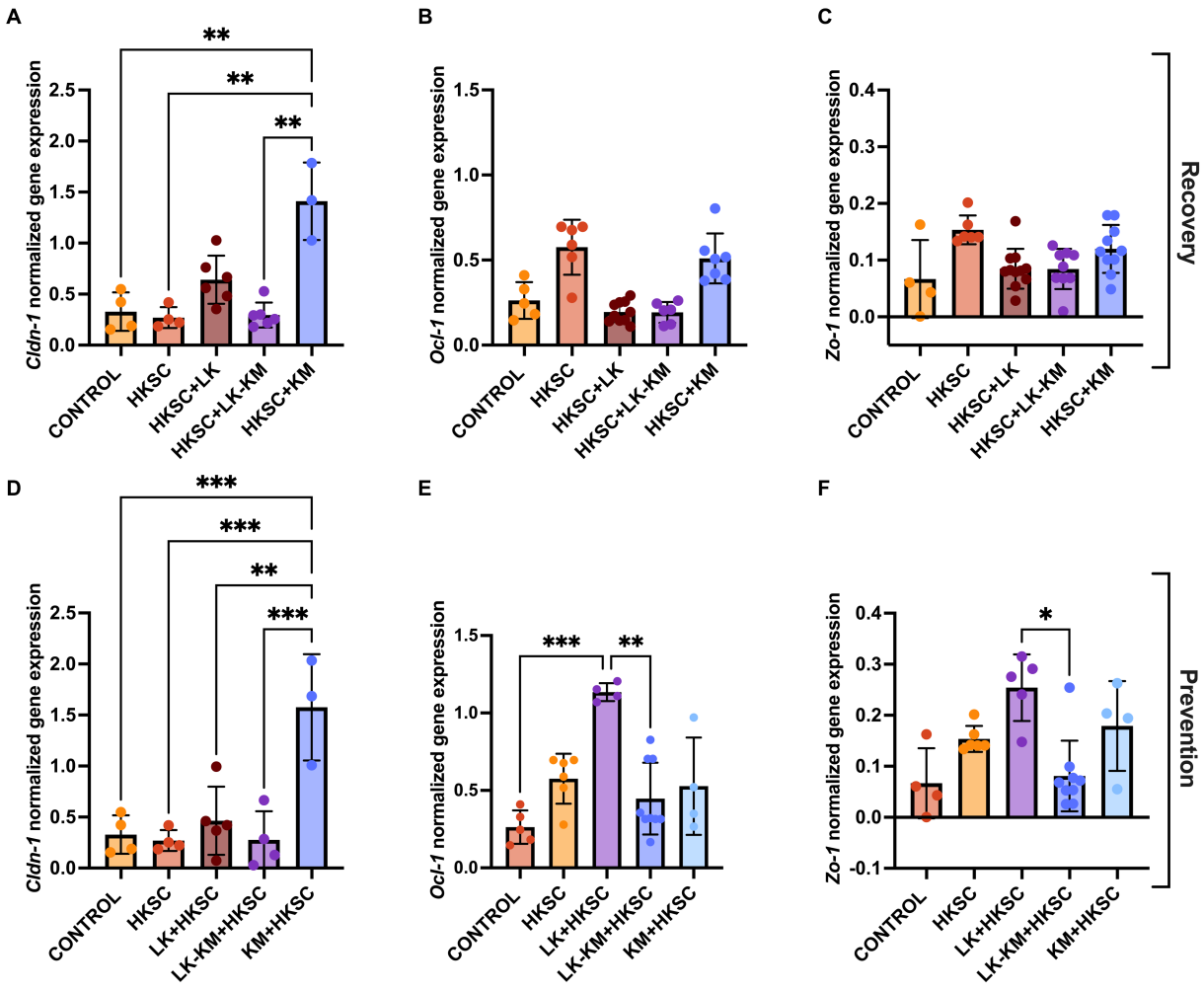

FIGURE 9
Effect of co-culture (LK-KM) and monocultures (LK, KM) on the expression of tight junctions (*Cldn-1-1, Ocl-1, Zo-1*) for recovery **(A–C)** and prevention **(D–F)** of HKSC-induced barrier damage in Caco-2 cells. Values represent the mean ± SD of at least three replicates. Statistical difference denoted as $*p < 0.05$, $**p < 0.01$,$***p < 0.0005$ by one-way ANOVA with *post hoc* Tukey test.

Salmonella Typhimurium (FliC) to study the immune response of different *Lentilactobacillus kefiri* strains after 6 h of treatment. However, utilization of HKSC is a cost-effective and less hazardous way to study inflammation in cell-culture models. As Kalupahana et al. (2005) reported, the viability of *Salmonella* Typhimurium is not essential for the activation of the inflammatory pathways as a 2 h stimulation of HKSC induced inflammation in macrophage-like and dendritic cell lines. Activation of the immune response after *Salmonella* invasion is mainly associated with stimulation of CCL20 chemokine by flagellin, which triggers dendritic cell chemotaxis and secretion of IL-8 (Sierro et al., 2001).

Previous studies have shown the *in vitro* anti-inflammatory effects and membrane barrier properties of *L. kefiranofaciens* and *K. marxianus* strains in monoculture using different models of inflammation (Chen et al., 2013; Romanin et al., 2016; Smith et al., 2016; Xing et al., 2017). However, there is limited research on the potential regulation of inflammation by a co-culture of these microorganisms. Recently, kefir grain isolates *L. kefiranofaciens* and *S. cerevisiae* in mono- and co-culture enhanced the gut barrier and decreased the expression of pro-inflammatory cytokines in a colon inflammation and colorectal carcinogenesis mouse model (Zeng et al., 2022). In the present study, we observed a decrease in the expression of pro-inflammatory cytokines *Il-8* and *Mcp-1* by *L. kefiranofaciens* in both mono- and co-culture with *K. marxianus* as a preventative and restorative treatment as compared to the expression induced by HKSC. These findings could potentially help the host immune response upon an inflammatory event. Interestingly, treatment with *K. marxianus* monoculture in the recovery group showed markedly higher expression of *Il-8* and *Mcp-1*. Yeast cell wall components can have beneficial or adverse effects in a strain-dependent manner on intestinal inflammation upon recognition by TLRs. Furthermore, fungal microbiota are important regulators of gut dysbiosis and their interaction with bacteria in the gut are important regulators of disease (Hall and Noverr, 2017). Cell wall β-glucans of various *S. cerevisiae* strains showed exacerbation of the inflammatory response in a mice model, whereas *S. boulardii* CNC I-3799 down-regulated the pro-inflammatory response (Jawhara et al., 2012). Although the mechanisms by which *K. marxianus* bdgo-ym6 seems to exacerbate the inflammation induced by HKSC remain to be elucidated, the understanding of these complex interactions and the role of the yeast cell wall components on the inflammation mechanisms may provide a rational for future studies in yeast-LAB co-cultures. While in this

study only the gene expression of the cytokines was evaluated, a similar study reported a correlation between gene expression and protein levels of cytokines (Zeng et al., 2022).

The intestinal epithelial cells and cell connections are the first barrier of defense against invasion of pathogenic microorganisms and toxic compounds, and its disruption implies entrance to the gut lumen and ultimately circulatory and tissue invasion (Slifer and Blikslager, 2020). Tight junctions (TJ) composed of transmembrane proteins such as claudins, occludin (OCL), and zonula occludens (ZO) play a crucial role in regulating paracellular pathway transport and in maintaining intestinal barrier integrity (Li et al., 2021). TJ play a key role in the proper functioning of the epithelial barrier and exposure to foreign substances can compromise their function, causing a decrease in epithelial resistance and increase in paracellular permeability. This disruption subsequently leads to activation of inflammatory pathways and elevated levels of pro-inflammatory cytokines (Bhat et al., 2019). In the present study, the expression levels of *claudin-1*, *Ocl-1*, and *Zo-1* were evaluated in the different treatment groups. Overall, the expression levels were not affected by HKSC as compared to the untreated control cells. *Salmonella* Typhimurium disrupts TJ by type 3 secretion system (T3SS) protein complexes that translocate specific proteins directly in the host cells (Anderson and Kendall, 2017). In the case of HKSC, this activation was not achieved, however, flagellin has been shown to disrupt membrane barrier by disruption of TJ organization and structure, which would explain the reduced TEER and increased FD4 permeability but negligible effect on TJ gene expression. Varying effects of different probiotic strains on the expression levels of TJ proteins have been reported. Previous exposure to *Lactobacillus acidophilus*, *L. rhamnosus*, and *L. casei* to HT29-MTX intestinal cells had a protective effect against *Salmonella enterica* ser. Javiana invasion and cell damage (Burkholder et al., 2019), while treatment with *L. plantarum* with prior challenge by enterotoxigenic *Escherichia coli* (ETEC) increased expression of *Cldn-1*, *Ocl-1*, and *Zo-1* and protected against membrane barrier disruption in IPEC-J2 cells (Wang J. et al., 2018). Zeng et al. (2022) reported that the oral administration of *L. kefiranofaciens* JKSP109 and *S. cerevisiae* JKSP39 in mono- and co-culture alleviated the effects of dextran sulfate sodium (DSS)-induced colorectal cancer in mice by increasing the expression and protein levels of tight junction proteins to various degrees. In the present study, *Ocl-1* and *Zo-1* expression was upregulated by *L. kefiranofaciens* monoculture as a preventative treatment, which may be associated with higher TEER and reduced FD4 permeability observed by this treatment. Importantly, the maintenance of membrane barrier could be also mediated by the postbiotic effects of EPS, as it has been reported that EPS protect against membrane disruption by upregulation of tight junction protein expression (Oerlemans et al., 2021).

Of notable interest is the increase in *Cldn-1* gene expression in the *K. marxianus* monoculture in both the recovery and prevention groups, along with the concomitant increase in FD4 permeability. Similarly, Poritz et al. (2011) reported an increase in *Cldn-1* expression while *Ocl-1* expression and TEER levels decreased during an inflammation induction with TNF-α in IEC-18 cells. These results are in alignment with the hypothesis that the increased expression of TJ proteins may actually be a protective response provoked by initial degradation of the TJs as suggested by Rose et al. (2021). These authors observed that treatment with *L. plantarum* in Caco-2 cells resulted in increased transcription of genes involved in tight junction disassembly and occludin-1 degradation. Therefore, a clear association between expression of TJ proteins and membrane barrier upon probiotic treatments remains unclear.

5. Conclusion

The complex microbial interactions that take place within co-cultures and the complex dynamics between bacteria and yeast play a significant role in the fermentation of traditional milk kefir. Understanding the interactions between *L. kefiranofaciens* and *K. marxianus* in co-culture, can provide valuable insights for development of a standardized commercial product with active core kefir microorganisms. Collectively the data presented in this study shows that co-culturing *L. kefiranofaciens* OSU-BDGOA1 with *K. marxianus* bdgo-ym6 in MRS medium enhances the probiotic potential of these strains, as evidenced by the increased survival during gastrointestinal conditions and enhanced adhesion to epithelial cells. These results, along with the modulation of the immune response in intestinal cells, highlights the opportunity to use co-cultures of yeast and LAB in novel fermented functional products that support human health. However, further research is required with an *in vivo* model to validate the observed effects. In addition, the potential of increasing EPS production through co-culture strategies is promising, considering the technological and prebiotic benefits associated with bacterial EPS.

Data availability statement

The datasets presented in this study can be found in online repositories. The names of the repository/repositories and accession number(s) can be found in the article/Supplementary material.

Author contributions

BDGO and EK: investigation, formal analysis, conceptualization, methodology, writing – original draft, reviewing and editing. RJ-F: funding acquisition, resources, supervision, conceptualization, and formal analysis. VA: supervision, resources, review and editing. All authors contributed to the article and approved the submitted version.

Funding

This project was funded by the Wilbur A. Gould Food Industries Center and the J.T. "Stubby" Parker Endowment in Dairy Foods at The Ohio State University (Columbus, OH).

Acknowledgments

The authors would like to thank Ahmed Yousef and Post-Doctoral Researcher Ahmed Abdelhamid for providing *Salmonella enterica* serovar Typhimurium LT2 strain and for allowing us to work in their BSL-2 laboratory. They also would like to thank Tea Meulia for her expertise in SEM and help in analyzing the samples, Tasha Santiago-Rodriguez for her help with the genomic analysis, and finally Molly J. Davis for editing the manuscript.

Conflict of interest

The authors declare that the research was conducted in the absence of any commercial or financial relationships that could be construed as a potential conflict of interest.

Publisher's note

All claims expressed in this article are solely those of the authors and do not necessarily represent those of their affiliated organizations, or those of the publisher, the editors and the reviewers. Any product that may be evaluated in this article, or claim that may be made by its manufacturer, is not guaranteed or endorsed by the publisher.

Supplementary material

The Supplementary material for this article can be found online at: https://www.frontiersin.org/articles/10.3389/fmicb.2023.1236634/full#supplementary-material

References

Ahmed, Z., Wang, Y., Anjum, N., Ahmad, H., Ahmad, A., and Raza, M. (2013). Characterization of new exopolysaccharides produced by coculturing of *L. kefiranofaciens* with yoghurt strains. *Int. J. Biol. Macromol.* 59, 377–383. doi: 10.1016/j.ijbiomac.2013.04.075

Ahtesh, F. B., Apostolopoulos, V., Stojanovska, L., Shah, N. P., and Mishra, V. K. (2018). Effects of fermented skim milk drink by Kluyveromyces marxianus LAF4 co-cultured with lactic acid bacteria to release angiotensin-converting enzyme inhibitory activities. *Int. J. Dairy Technol.* 71, 130–140. doi: 10.1111/1471-0307.12425

Ailioaie, L., and Litscher, G. (2021). Probiotics, Photobiomodulation, and disease management: controversies and challenges. *IJMS* 22:4942. doi: 10.3390/ijms22094942

Alhudhud, M., Humphreys, P., and Laws, A. (2014). Development of a growth medium suitable for exopolysaccharide production and structural characterisation by *Bifidobacterium animalis* ssp. lactis AD011. *J. Microbiol. Methods* 100, 93–98. doi: 10.1016/j.mimet.2014.02.021

Anderson, C. J., and Kendall, M. M. (2017). *Salmonella enterica* Serovar typhimurium strategies for host adaptation. *Front. Microbiol.* 8:1983. doi: 10.3389/fmicb.2017.01983

Benjamas, C., Shoji, H., Shimizu, H., and Shioya, S. (2003). Interactions between lactobacillus kefiranofaciens and *Saccharomyces cerevisiae* in mixed culture for kefiran production - ScienceDirect. *J. Biosci. Bioeng.* 96, 279–284. doi: 10.1016/S1389-1723(03)80194-9

Bertelli, C., Laird, M. R., Williams, K. P., Simon Fraser University Research Computing GroupLau, B. Y., Hoad, G., et al. (2017). IslandViewer 4: expanded prediction of genomic islands for larger-scale datasets. *Nucleic Acids Res.* 45, W30–W35. doi: 10.1093/nar/gkx343

Bertsch, A., Roy, D., and LaPointe, G. (2019). Enhanced exopolysaccharide production by *Lactobacillus rhamnosus* in co-culture with *Saccharomyces cerevisiae*. *Appl. Sci. (Switzerland)* 9. doi: 10.3390/app9194026

Bhat, A. A., Uppada, S., Achkar, I. W., Hashem, S., Yadav, S. K., Shanmugakonar, M., et al. (2019). Tight junction proteins and Signaling pathways in cancer and inflammation: A functional crosstalk. *Front. Physiol.* 9:1942. doi: 10.3389/fphys.2018.01942

Blom, J., Albaum, S. P., Doppmeier, D., Pühler, A., Vorhölter, F.-J., Zakrzewski, M., et al. (2009). EDGAR: A software framework for the comparative analysis of prokaryotic genomes. *BMC Bioinform.* 10:154. doi: 10.1186/1471-2105-10-154

Bolla, P. A., Carasi, P., Bolla, M. D. L. A., De Antoni, G. L., and Serradell, M. D. L. A. (2013). Protective effect of a mixture of kefir-isolated lactic acid bacteria and yeasts in a hamster model of *Clostridium difficile* infection. *Anaerobe* 21, 28–33. doi: 10.1016/j.anaerobe.2013.03.010

Brodkorb, A., Egger, L., Alminger, M., Alvito, P., Assunção, R., Ballance, S., et al. (2019). INFOGEST static in vitro simulation of gastrointestinal food digestion. *Nat. Protoc.* 14, 991–1014. doi: 10.1038/s41596-018-0119-1

Burkholder, K. M., Fletcher, D. H., Gileau, L., and Kandolo, A. (2019). Lactic acid bacteria decrease *Salmonella enterica* Javiana virulence and modulate host inflammation during infection of an intestinal epithelial cell line. *Pathogens and Disease* 77:ftz025. doi: 10.1093/femspd/ftz025

Canon, F., Mariadassou, M., Maillard, M.-B., Falentin, H., Parayre, S., Madec, M.-N., et al. (2020a). Function-driven Design of Lactic Acid Bacteria co-cultures to produce new fermented food associating Milk and Lupin. *Front. Microbiol.* 11:584163. doi: 10.3389/fmicb.2020.584163

Canon, F., Nidelet, T., Guédon, E., Thierry, A., and Gagnaire, V. (2020b). Understanding the mechanisms of positive microbial interactions that benefit lactic acid bacteria co-cultures. *Front. Microbiol.* 11:2088. doi: 10.3389/fmicb.2020.02088

Carasi, P., Díaz, M., Racedo, S. M., De Antoni, G., and Urdaci, M. C., and Serradell, M. de los A., (2014). Safety characterization and antimicrobial properties of kefir-isolated *Lactobacillus kefiri*. *Biomed. Res. Int.* 2014,:e208974. doi:10.1155/2014/208974.

Cheirsilp, B., and Radchabut, S. (2011). Use of whey lactose from dairy industry for economical kefiran production by *Lactobacillus kefiranofaciens* in mixed cultures with yeasts. *New Biotechnol.* 28, 574–580. doi: 10.1016/j.nbt.2011.01.009

Chen, Y. P., Lee, T. Y., Hong, W. S., Hsieh, H. H., and Chen, M. J. (2013). Effects of *Lactobacillus kefiranofaciens* M1 isolated from kefir grains on enterohemorrhagic *Escherichia coli* infection using mouse and intestinal cell models. *J. Dairy Sci.* 96, 7467–7477. doi: 10.3168/jds.2013-7015

Cunningham, M., Azcarate-Peril, M. A., Barnard, A., Benoit, V., Grimaldi, R., Guyonnet, D., et al. (2021). Shaping the future of probiotics and prebiotics. *Trends Microbiol.* 29, 667–685. doi: 10.1016/J.TIM.2021.01.003

Diosma, G., Romanin, D. E., Rey-Burusco, M. F., Londero, A., and Garrote, G. L. (2014). Yeasts from kefir grains: isolation, identification, and probiotic characterization. *World J. Microbiol. Biotechnol.* 30, 43–53. doi: 10.1007/s11274-013-1419-9

Dubois, M., Gilles, K. A., Hamilton, J. K., Rebers, P. A., and Smith, F. (1956). Colorimetric method for determination of sugars and related substances. *Anal. Chem.* 28, 350–356. doi: 10.1021/ac60111a017

Exarhopoulos, S., Raphaelides, S. N., and Kontominas, M. G. (2018). Conformational studies and molecular characterization of the polysaccharide kefiran. *Food Hydrocoll.* 77, 347–356. doi: 10.1016/j.foodhyd.2017.10.011

Fadda, M. E., Mossa, V., Deplano, M., Pisano, M. B., and Cosentino, S. (2017). In vitro screening of Kluyveromyces strains isolated from Fiore Sardo cheese for potential use as probiotics. *LWT* 75, 100–106. doi: 10.1016/j.lwt.2016.08.020

Ferrari, M., Hameleers, L., Stuart, M. C. A., Oerlemans, M. M. P., de Vos, P., Jurak, E., et al. (2022). Efficient isolation of membrane-associated exopolysaccharides of four commercial bifidobacterial strains. *Carbohydr. Polym.* 278:118913. doi: 10.1016/j.carbpol.2021.118913

Georgalaki, M., Zoumpopoulou, G., Anastasiou, R., Kazou, M., and Tsakalidou, E. (2021). *Lactobacillus kefiranofaciens*: from isolation and taxonomy to probiotic properties and applications. *Microorganisms* 9:2158. doi: 10.3390/microorganisms9102158

Giri, S., Oña, L., Waschina, S., Shitut, S., Yousif, G., Kaleta, C., et al. (2020). Metabolic dissimilarity determines the establishment of cross-feeding interactions in bacteria. *bioRxiv*:2020.10.09.333336. doi: 10.1101/2020.10.09.333336

Gonçalves, C., Rodriguez-Jasso, R. M., Gomes, N., Teixeira, J. A., and Belo, I. (2010). Adaptation of dinitrosalicylic acid method to microtiter plates. *Anal. Methods* 2:2046. doi: 10.1039/c0ay00525h

González-Orozco, B. D., García-Cano, I., and Escobar-Zepeda, A. (2023). Metagenomic analysis and antibacterial activity of kefir microorganisms. *J. Food Sci.* 88, 2933–2949. doi: 10.1111/1750-3841.16614

Grandel, N. E., Reyes Gamas, K., and Bennett, M. R. (2021). Control of synthetic microbial consortia in time, space, and composition. *Trends Microbiol.* 29, 1095–1105. doi: 10.1016/j.tim.2021.04.001

Grouls, M., van der Zande, M., de Haan, L., and Bouwmeester, H. (2022). Responses of increasingly complex intestinal epithelium in vitro models to bacterial toll-like receptor agonists. *Toxicol. In Vitro* 79:105280. doi: 10.1016/j.tiv.2021.105280

Gullo, M., and Zotta, T. (2022). Probiotics in dairy products: microencapsulation and delivery. *Adv. Dairy Microbial Products*, 271–285. doi: 10.1016/B978-0-323-85793-2.00032-1

Hall, R. A., and Noverr, M. C. (2017). Fungal interactions with the human host: exploring the spectrum of symbiosis. *Curr. Opin. Microbiol.* 40, 58–64. doi: 10.1016/j.mib.2017.10.020

Hill, C., Guarner, F., Reid, G., Gibson, G. R., Merenstein, D. J., Pot, B., et al. (2014). The international scientific Association for Probiotics and Prebiotics consensus statement on the scope and appropriate use of the term probiotic. *Nat. Rev. Gastroenterol. Hepatol.* 11, 506–514. doi: 10.1038/nrgastro.2014.66

Huang, F., Teng, K., Liu, Y., Cao, Y., Wang, T., Ma, C., et al. (2021). Bacteriocins: potential for human health. *Oxidative Med. Cell. Longev.* 2021, 1–17. doi: 10.1155/2021/5518825

Hubatsch, I., Ragnarsson, E. G. E., and Artursson, P. (2007). Determination of drug permeability and prediction of drug absorption in Caco-2 monolayers. *Nat. Protoc.* 2, 2111–2119. doi: 10.1038/nprot.2007.303

Jawhara, S., Habib, K., Maggiotto, F., Pignede, G., Vandekerckove, P., Maes, E., et al. (2012). Modulation of intestinal inflammation by yeasts and Cell Wall extracts: strain dependence and unexpected anti-inflammatory role of glucan fractions. *PLoS One* 7:e40648. doi: 10.1371/journal.pone.0040648

Joerger, M. C., and Klaenhammer, T. R. (1986). Characterization and purification of Helveticin J and evidence for a chromosomally determined Bacteriocin produced by *Lactobacillus helveticus* 481t. *J. Bacteriol.* 167:439:446. doi: 10.1128/jb.167.2.439-446.1986

Jurášková, D., Ribeiro, S. C., and Silva, C. C. G. (2022). Exopolysaccharides produced by lactic acid bacteria: from biosynthesis to health-promoting properties. *Foods* 11:156. doi: 10.3390/foods11020156

Kalupahana, R. S., Mastroeni, P., Maskell, D., and Blacklaws, B. A. (2005). Activation of murine dendritic cells and macrophages induced by *Salmonella enterica* serovar typhimurium. *Immunology* 115, 462–472. doi: 10.1111/j.1365-2567.2005.02180.x

Kapoore, R. V., Padmaperuma, G., Maneein, S., and Vaidyanathan, S. (2022). Co-culturing microbial consortia: approaches for applications in biomanufacturing and bioprocessing. *Crit. Rev. Biotechnol.* 42, 46–72. doi: 10.1080/07388551.2021.1921691

Kim, D. H., Kim, H., Jeong, D., Kang, I. B., Chon, J. W., Kim, H. S., et al. (2017). Kefir alleviates obesity and hepatic steatosis in high-fat diet-fed mice by modulation of gut microbiota and mycobiota: targeted and untargeted community analysis with correlation of biomarkers. *J. Nutr. Biochem.* 44, 35–43. doi: 10.1016/J.JNUTBIO.2017.02.014

Lebeer, S., Claes, I. J. J., Verhoeven, T. L. A., Vanderleyden, J., and De Keersmaecker, S. C. J. (2011). Exopolysaccharides of *Lactobacillus rhamnosus* GG form a protective shield against innate immune factors in the intestine: EPS as adaptation factor of *L. rhamnosus* GG. *Microb. Biotechnol.* 4, 368–374. doi: 10.1111/j.1751-7915.2010.00199.x

Li, C., Bai, X., Liu, X., Zhang, Y., Liu, L., Zhang, L., et al. (2021). Disruption of epithelial barrier of Caco-2 cell monolayers by excretory secretory products of Trichinella spiralis might be related to serine protease. *Front. Microbiol.* 12:634185. doi: 10.3389/fmicb.2021.634185

Lim, P. L., Toh, M., and Liu, S. Q. (2015). *Saccharomyces cerevisiae* EC-1118 enhances the survivability of probiotic *Lactobacillus rhamnosus* HN001 in an acidic environment. *Appl. Microbiol. Biotechnol.* 99, 6803–6811. doi: 10.1007/s00253-015-6560-y

Liu, M., Bischoff, K. M., Gill, J. J., Mire-Criscione, M. D., Berry, J. D., Young, R., et al. (2015). Bacteriophage application restores ethanol fermentation characteristics disrupted by *Lactobacillus fermentum*. *Biotechnol. Biofuels* 8:132. doi: 10.1186/s13068-015-0325-9

Liu, Y., Tran, D. Q., and Rhoads, J. M. (2018). Probiotics in disease prevention and treatment. *J. Clin. Pharmacol.* 58, S164–S179. doi: 10.1002/jcph.1121

Liu, Y., Wan, B., Yang, F., Zhang, X., Li, J., Du, G., et al. (2022). Metabolomics-driven elucidation of interactions between Saccharomyces cerevisiae and *Lactobacillus panis* from Chinese baijiu fermentation microbiome. *Fermentation* 8:33. doi: 10.3390/fermentation8010033

Londero, A., Iraporda, C., Garrote, G. L., and Abraham, A. G. (2015). Cheese whey fermented with kefir micro-organisms: antagonism against salmonella and immunomodulatory capacity. *Int. J. Dairy Technol.* 68, 118–126. doi: 10.1111/1471-0307.12161

Maccaferri, S., Klinder, A., Brigidi, P., Cavina, P., and Costabile, A. (2012). Potential probiotic Kluyveromyces marxianus B0399 modulates the immune response in Caco-2 cells and peripheral blood mononuclear cells and impacts the human gut microbiota in an in vitro colonic model system. *Appl. Environ. Microbiol.* 78, 956–964. doi: 10.1128/AEM.06385-11

Milner, E., Stevens, B., An, M., Lam, V., Ainsworth, M., Dihle, P., et al. (2021). Utilizing probiotics for the prevention and treatment of gastrointestinal diseases. *Front. Microbiol.* 12:689958. doi: 10.3389/fmicb.2021.689958

Nejati, F., Junne, S., and Neubauer, P. (2020). A big world in small grain: A review of natural milk kefir starters. *Microorganisms* 8. doi: 10.3390/microorganisms8020192

Nilsen, T., Nes, I. F., and Holo, H. (2003). Enterolysin A, a Cell Wall-degrading Bacteriocin from *Enterococcus faecalis* LMG 2333. *Appl. Environ. Microbiol.* 69, 2975–2984. doi: 10.1128/AEM.69.5.2975-2984.2003

Oerlemans, M. M. P., Akkerman, R., Ferrari, M., Walvoort, M. T. C., and de Vos, P. (2021). Benefits of bacteria-derived exopolysaccharides on gastrointestinal microbiota, immunity and health. *J. Funct. Foods* 76:104289. doi: 10.1016/j.jff.2020.104289

Ponomarova, O., Gabrielli, N., Sévin, D. C., Mülleder, M., Zirngibl, K., Bulyha, K., et al. (2017). Yeast creates a niche for symbiotic lactic acid bacteria through nitrogen overflow. *Cell Sys.* 5, 345–357.e6. doi: 10.1016/j.cels.2017.09.002

Poritz, L. S., Harris, L. R., Kelly, A. A., and Koltun, W. A. (2011). Increase in the tight junction protein Claudin-1 in intestinal inflammation. *Dig. Dis. Sci.* 56:2802. doi: 10.1007/s10620-011-1688-9

Raheem, A., Liang, L., Zhang, G., and Cui, S. (2021). Modulatory effects of probiotics during pathogenic infections with emphasis on immune regulation. *Front. Immunol.* 12:616713. doi: 10.3389/fimmu.2021.616713

Romanin, D. E., Llopis, S., Genovés, S., Martorell, P., Ramón, V. D., Garrote, G. L., et al. (2016). Probiotic yeast Kluyveromyces marxianus CIDCA 8154 shows anti-inflammatory and anti-oxidative stress properties in in vivo models. *Benefic. Microbes* 7, 83–93. doi: 10.3920/BM2015.0066

Rose, E. C., Odle, J., Blikslager, A. T., and Ziegler, A. L. (2021). Probiotics, prebiotics and epithelial tight junctions: A promising approach to modulate intestinal barrier function. *IJMS* 22:6729. doi: 10.3390/ijms22136729

Sierro, F., Dubois, B., Coste, A., Kaiserlian, D., Kraehenbuhl, J.-P., and Sirard, J.-C. (2001). Flagellin stimulation of intestinal epithelial cells triggers CCL20-mediated migration of dendritic cells. *Proc. Natl. Acad. Sci. U. S. A.* 98, 13722–13727. doi: 10.1073/pnas.241308598

Sieuwerts, S., de Bok, F. A. M., Hugenholtz, J., and van Hylckama Vlieg, J. E. T. (2008). Unraveling microbial interactions in food fermentations: from classical to genomics approaches. *Appl. Environ. Microbiol.* 74, 4997–5007. doi: 10.1128/AEM.00113-08

Slifer, Z. M., and Blikslager, A. T. (2020). The integral role of tight junction proteins in the repair of injured intestinal epithelium. *IJMS* 21:972. doi: 10.3390/ijms21030972

Smith, I. M., Baker, A., Christensen, J. E., Boekhout, T., Frøkiær, H., Arneborg, N., et al. (2016). Kluyveromyces marxianus and saccharomyces boulardii induce distinct levels of dendritic cell cytokine secretion and significantly different T cell responses in vitro. *PLoS One* 11:e0167410. doi: 10.1371/journal.pone.0167410

Song, W., Sun, H.-X., Zhang, C., Cheng, L., Peng, Y., Deng, Z., et al. (2019). Prophage hunter: an integrative hunting tool for active prophages. *Nucleic Acids Res.* 47, W74–W80. doi: 10.1093/nar/gkz380

Sørensen, H. M., Rochfort, K. D., Maye, S., MacLeod, G., Brabazon, D., Loscher, C., et al. (2022). Exopolysaccharides of lactic acid bacteria: production, purification and health benefits towards functional food. *Nutrients* 14:2938. doi: 10.3390/nu14142938

Tada, S., Katakura, Y., Ninomiya, K., and Shioya, S. (2007). Fed-batch coculture of *Lactobacillus kefiranofaciens* with *Saccharomyces cerevisiae* for effective production of kefiran. *J. Biosci. Bioeng.* 103, 557–562. doi: 10.1263/jbb.103.557

Tamang, J. P., Watanabe, K., and Holzapfel, W. H. (2016). Review: diversity of microorganisms in global fermented foods and beverages. *Front. Microbiol.* 7. doi: 10.3389/fmicb.2016.00377

van Heel, A. J., de Jong, A., Song, C., Viel, J. H., Kok, J., and Kuipers, O. P. (2018). BAGEL4: a user-friendly web server to thoroughly mine RiPPs and bacteriocins. *Nucleic Acids Res.* 46, W278–W281. doi: 10.1093/nar/gky383

Vinderola, G., Perdigón, G., Duarte, J., Farnworth, E., and Matar, C. (2006). Effects of the oral administration of the exopolysaccharide produced by *Lactobacillus kefiranofaciens* on the gut mucosal immunity. *Cytokine* 36, 254–260. doi: 10.1016/J.CYTO.2007.01.003

Wang, G., Yu, Y., Garcia-Gutierrez, E., Jin, X., He, Y., Wang, L., et al. (2019). *Lactobacillus acidophilus* JCM 1132 strain and its mutant with different Bacteriocin-producing behaviour have various in situ effects on the gut microbiota of healthy mice. *Microorganisms* 8:49. doi: 10.3390/microorganisms8010049

Wang, J., Ji, H., Wang, S., Liu, H., Zhang, W., Zhang, D., et al. (2018). Probiotic *Lactobacillus plantarum* promotes intestinal barrier function by strengthening the epithelium and modulating gut microbiota. *Front. Microbiol.* 9:1953. doi: 10.3389/fmicb.2018.01953

Wang, X., Li, W., Mahsa, G. C., Zhang, C., Ma, K., Rui, X., et al. (2023). Co-cultivation effects of *Lactobacillus helveticus* SNA12 and Kluveromyces marxiensis GY1 on the probiotic properties, flavor, and digestion in fermented milk. *Food Res. Int.* 112843. doi: 10.1016/j.foodres.2023.112843

Wang, X., Xiao, J., Jia, Y., Pan, Y., and Wang, Y. (2018). *Lactobacillus kefiranofaciens*, the sole dominant and stable bacterial species, exhibits distinct morphotypes upon colonization in Tibetan kefir grains. *Heliyon* 4:649. doi: 10.1016/J.HELIYON.2018.E00649

Xing, Z., Tang, W., Geng, W., Zheng, Y., and Wang, Y. (2017). In vitro and in vivo evaluation of the probiotic attributes of *Lactobacillus kefiranofaciens* XL10 isolated from Tibetan kefir grain. *Appl. Microbiol. Biotechnol.* 101, 2467–2477. doi: 10.1007/s00253-016-7956-z

Xu, Z., Lu, Z., Soteyome, T., Ye, Y., Huang, T., Liu, J., et al. (2021). Polymicrobial interaction between lactobacillus and *Saccharomyces cerevisiae*: coexistence-relevant mechanisms. *Crit. Rev. Microbiol.* 47, 386–396. doi: 10.1080/1040841X.2021.1893265

Yilmaz, B., Sharma, H., Melekoglu, E., and Ozogul, F. (2022). Recent developments in dairy kefir-derived lactic acid bacteria and their health benefits. *Food Biosci.* 46:101592. doi: 10.1016/j.fbio.2022.101592

Youn, H.-Y., Kim, D.-H., Kim, H.-J., Bae, D., Song, K.-Y., Kim, H., et al. (2022). Survivability of Kluyveromyces marxianus isolated from Korean kefir in a simulated gastrointestinal environment. *Front. Microbiol.* 13:842097. doi: 10.3389/fmicb.2022.842097

Yuan, L., van der Mei, H. C., Busscher, H. J., and Peterson, B. W. (2020). Two-stage interpretation of changes in TEER of intestinal epithelial layers protected by adhering Bifidobacteria during *E. coli* challenges. *Front. Microbiol.* 11:599555. doi: 10.3389/fmicb.2020.599555

Zajšek, K., Goršek, A., and Kolar, M. (2013). Cultivating conditions effects on kefiran production by the mixed culture of lactic acid bacteria imbedded within kefir grains. *Food Chem.* 139, 970–977. doi: 10.1016/j.foodchem.2012.11.142

Zeng, X., Jia, H., Shi, Y., Chen, K., Wang, Z., Gao, Z., et al. (2022). *Lactobacillus kefiranofaciens* JKSP109 and *Saccharomyces cerevisiae* JKSP39 isolated from Tibetan kefir grain co-alleviated AOM/DSS induced inflammation and colorectal carcinogenesis. *Food Funct.* 13, 6947–6961. doi: 10.1039/D1FO02939H

frontiers | Frontiers in Microbiology

TYPE Original Research
PUBLISHED 05 September 2023
DOI 10.3389/fmicb.2023.1252870

OPEN ACCESS

EDITED BY
Ilana Kolodkin-Gal,
The Hebrew University of Jerusalem, Israel

REVIEWED BY
Shuyu Jia,
Nanjing Agricultural University, China
John J. Kelly,
Loyola University Chicago, United States

*CORRESPONDENCE
Sarah Haenelt
✉ sarah.haenelt@ufz.de

RECEIVED 04 July 2023
ACCEPTED 22 August 2023
PUBLISHED 05 September 2023

CITATION
Haenelt S, Richnow H-H, Müller JA and Musat N (2023) Antibiotic resistance indicator genes in biofilm and planktonic microbial communities after wastewater discharge. *Front. Microbiol.* 14:1252870. doi: 10.3389/fmicb.2023.1252870

Antibiotic resistance indicator genes in biofilm and planktonic microbial communities after wastewater discharge

Sarah Haenelt[1]*, Hans-Hermann Richnow[1], Jochen A. Müller[2] and Niculina Musat[1,3]

[1]Department of Isotope Biogeochemistry, Helmholtz Centre for Environmental Research, Leipzig, Germany, [2]Institute for Biological Interfaces (IBG 5), Karlsruhe Institute of Technology, Eggenstein-Leopoldshafen, Germany, [3]Department of Biology, Section for Microbiology, Aarhus University, Aarhus, Denmark

The spread of bacteria with antibiotic resistance genes (ARGs) in aquatic ecosystems is of growing concern as this can pose a risk of transmission to humans and animals. While the impact of wastewater treatment plant (WWTP) effluent on ARG abundance in surface waters has been studied extensively, less is known about the fate of ARGs in biofilms. The proximity and dense growth of microorganisms in combination with the accumulation of higher antibiotic concentrations in biofilms might render biofilms a reservoir for ARGs. Seasonal parameters such as water temperature, precipitation, and antibiotic concentrations should be considered as well, as they may further influence the fate of ARGs in aquatic ecosystems. Here we investigated the effect of WWTP effluent on the abundance of the sulfonamide resistance genes *sul1* and *sul2*, and the integrase gene *intI1* in biofilm and surface water compartments of a river in Germany with a gradient of anthropogenic impact using quantitative PCR. Furthermore, we analyzed the bacterial community structure in both compartments via 16S rRNA gene amplicon sequencing, following the river downstream. Additionally, conventional water parameters and sulfonamide concentrations were measured, and seasonal aspects were considered by comparing the fate of ARGs and bacterial community diversity in the surface water compartment between the summer and winter season. Our results show that biofilm compartments near the WWTP had a higher relative abundance of ARGs (up to 4.7%) than surface waters (<2.8%). Sulfonamide resistance genes were more persistent further downstream (>10 km) of the WWTP in the hot and dry summer season than in winter. This finding is likely a consequence of the higher proportion of wastewater and thus wastewater-derived microorganisms in the river during summer periods. We observed distinct bacterial communities and ARG abundance between the biofilm and surface water compartment, but even greater variations when considering seasonal and spatiotemporal parameters. This underscores the need to consider seasonal aspects when studying the fate of ARGs in aquatic ecosystems.

KEYWORDS

biofilm, surface water, spatiotemporal monitoring, *sul1*, *sul2*, *intI1*, aquatic ecosystem, One Health

Introduction

As a step toward limiting the global spread of antimicrobial resistance, it is crucial to remind ourselves that humans, animals, and the environment are interconnected, which has already been well expressed as the basis of the One Health approach (The World Health Organization et al., 2019). The freshwater environment links all terrestrial life, and can therefore be a dissemination route of antibiotic-resistant bacteria and the resistance genes (ARGs) they carry (Berendonk et al., 2015; Larsson and Flach, 2022). The flux of clinically relevant ARGs and the dynamics of their pool sizes in anthropogenically impacted waterbodies are less certain, rendering it important to better understand the mechanisms and factors that influence the fate of these genes in such ecosystems. A key source of ARGs and antibiotics pollution in aquatic ecosystems is untreated and treated wastewater (Proia et al., 2016; Wang et al., 2020). Well-operated wastewater treatment plants (WWTP) are efficient in attenuating concentrations of phosphorous and fixed nitrogen compounds, but they are not specifically designed to remove antibiotic-resistant bacteria, ARGs, and antibiotics (Chaturvedi et al., 2021). Modifying existing or constructing new WWTPs with improved capability for their removal is a substantial task. In the EU, for example, with its comparatively extensive treatment infrastructure, the wastewater of 447 million people is treated in about 26,500 WWTP at investment and operational costs of €39 billion per year (OECD, 2020). Further monitoring of the level of ARG contamination of surface waters will be helpful to guide stakeholders on whether, where, and when to implement improved wastewater treatment.

Cost-effective assessment of ARG contamination can be achieved by quantification of marker genes (Berendonk et al., 2015). The *sul1* and *sul2* genes, which confer resistance to sulfonamides, are among the earliest used markers and most frequently detected ARGs in WWTP effluent (Pruden et al., 2006; Wang et al., 2020). The environmental presence of these ARGs mirrors the common prescription of sulfonamides in human medicine and food animal production, as well as their chemical stability (Martin-Laurent et al., 2019). Likewise, the abundance of the integrase gene *intI1* of the clinical class 1 integron has increased globally in natural environments as a result of anthropogenic activities (Gillings et al., 2008). The genes *intI1* and *sul1* usually show a strong positive correlation in environmental samples, as both co-occur in the classical class 1 integron (Gillings et al., 2015). However, some studies show an independent trend, such as an increase in the relative abundance of *intI1* without a concomitant increase in *sul1* relative abundance (Koczura et al., 2016; Haenelt et al., 2023). While the biological reason for this observation remains to be elucidated, it is an example of how genes associated with antimicrobial resistance that share the same point source can have different environmental fates. Therefore, site monitoring ideally includes the enumeration of several ARGs. In our study, we have chosen *sul1* and *sul2* to assess the antimicrobial resistance status in the Holtemme river, due to their widespread occurrence in aquatic ecosystems globally and their established recognition as indicator genes over many years (Pruden et al., 2006). Furthermore, the prevalence of the *intI1* gene was monitored as a proxy for anthropogenic pollution (Gillings et al., 2015; Yue et al., 2021).

Multiple studies have focused on the fate of ARGs and the effect of anthropogenic pollution on planktonic microorganisms in the surface water or sediment compartment of rivers downstream WWTPs (e.g., Harnisz et al., 2020; Borsetto et al., 2021; Chaturvedi et al., 2021; Hutinel et al., 2021; Pesce et al., 2021; Kasuga et al., 2022). Less attention has been given to the fate of ARGs and the effect of WWTP effluent on bacterial communities in the biofilm compartment of rivers, which we define here as the biological interface between the sediment and the overlaying surface water compartment (Luo et al., 2020). Biofilms are known to play an important role in the functioning of aquatic ecosystems, e.g., in nutrient cycling, transformation of pollutants, and as reservoirs of microorganisms (Flemming et al., 2016). The proximity and dense growth of microorganisms within biofilms, the accumulation of antibiotics resulting in higher concentrations than in the surrounding environment, and their ability to accumulate mobile elements make them a favorable environment for the spread of ARGs (Proia et al., 2016; Flores-Vargas et al., 2021). In addition, sediment samples contain material collected some distance below the surface of the riverbed, where ambient conditions are likely different from those in the biofilm, and hence ARG prevalence could be different in the two compartments.

Furthermore, the effect of seasonal variations on the abundance of *sul1*, *sul2*, and *intI1* in WWTP effluent-impacted streams is currently uncertain. For example, Sabri et al. (2020) reported slightly higher concentrations of these marker genes in a Dutch river during the summer season, while Koczura et al. (2016) found a higher occurrence of the genes in a Polish river during cold months. The latter authors hypothesized that higher antibiotic consumption during colder months might have contributed to the higher ARG concentrations. In contrast, studies targeting the wet and dry seasons in China have not shown significant seasonal differences in the occurrence of ARGs (Chen et al., 2013; Yuan et al., 2014; Mao et al., 2015). Since multiple environmental parameters including water temperature and availability of nutrients vary throughout the year, it is difficult to determine their individual impact. Moreover, the urban discharge fraction, i.e., the proportion of WWTP effluent relative to the total volume of a stream, can be substantially different in summer and winter season, which likely has a strong effect on the spread of ARG. The effect could be exacerbated in regions of the world where climate change is expected to cause more frequent hot and dry summer seasons in the future (Gudmundsson et al., 2021).

This study aimed to assess the effect of wastewater discharge on *sul1*, *sul2*, and *intI1* prevalence comparatively in biofilm and surface water compartments at six sampling sites in a small river along its gradient of anthropogenic impact. We aimed to elucidate the role of the riverine biofilm compartment as a reservoir for ARGs in the aquatic environment, with special emphasis on the effect of wastewater discharge. Furthermore, we investigated the effects of seasonality on the abundance of ARGs and bacterial community diversity in surface waters by comparing results obtained during the current summer sampling campaign with data from a previous study conducted in a winter season (Haenelt et al., 2023).

Materials and methods

Study region and sampling sites

This study investigated the Holtemme, a 47 km long river originating in the Harz mountains of Saxony-Anhalt, Germany. The river is considered near-pristine in the mountainous region, while downstream anthropogenic impact increases due to wastewater discharge, rectification, settlements, and widespread farming activities (Inostroza et al., 2016; Karthe et al., 2017; Wollschläger et al., 2017). In the mountainous region, low concentrations of caffeine and the insecticide diethyltoluamide indicate a mild impact by hikers (Weitere et al., 2021). The sediment in the Holtemme is mostly sandy with pebbles and cobbles (Kunz et al., 2017). Five small streams flow into the Holtemme in the study area, all of which contribute little to the water volume of the river. During the sampling period in the summer season of 2022, a stream entering the Holtemme between Site 5 and 6 had dried up completely. For this study, two sampling sites were selected in the "pristine" part of the river, one directly at the discharge point of an activated sludge-based, tertiary WWTP, one about 150 m downstream of the WWTP, and two others 8 and 13 km further downstream. The latter site is at the upstream outskirts of the next city (Halberstadt), which has its own WWTP. All six sampling sites have been previously described in detail (Haenelt et al., 2023).

Sampling and sample preparation

Planktonic and biofilm samples were collected during a dry period in the summer season of 2022 on five sampling days (August 9th, three consecutive days from August 23rd to 25th, and September 1st) at all six sites. Rain events were rare and the average rainfall was less than 2.3 mm per day (**Supplementary Figure 1**). Water temperature and pH were measured at all sites using a SenTix41 probe (Xylem Analytics, Germany). NO_3-N, total phosphorous, and water depth were obtained from the MOBICOS stations located at Sites 1 and 5 (Fink et al., 2020), and physicochemical parameters from Site 3 (WWTP discharge) were kindly provided by the WWTP Silstedt.[1]

Planktonic samples were collected in sterilized and pre-rinsed 1-L glass flasks at an approximate water depth of 5 cm. Biofilm samples were collected with a spatula from the water-facing side of stones covering the riverbed and transferred into tubes containing 1 mL 1xPBS. To obtain a sufficient amount of biomass, approximately 10 cm^2 of surface area was used for biofilm sampling at Sites 1, 2, 5, and 6. At Sites 3 and 4, which were characterized by dense biofilms, approximately 1 cm^2 was sampled. All samples were stored in a thermobox with cold packs and transported to the laboratory within 3 h. Immediately upon arrival, biofilm samples were stored at 8°C until DNA extraction within the next 2 days. Planktonic samples were further treated as follows. One liter of river water from each site except Site 3 (500 mL) was filtered using 0.22 μm pore size PSE PALL filters (diameter 47 mm, Pall Corporation, New York, NY, USA) and stored at −20°C until DNA extraction. Additionally, 100 mL flow-through was collected for each site and stored at 8°C overnight before solid phase extraction (SPE) and sulfonamide concentration measurements via HPLC-MS.

SPE and HPLC-MS analysis

Flow-through was concentrated 100-fold using SPE with Oasis HLB 6cc 500 mg columns (Waters, CT USA) before HPLC-MS was carried out as described in Haenelt et al. (2023). In brief, a calibration curve from 0.01 μg/L to 2 μg/L of a sulfonamide mixture containing sulfamethoxazole (SMX), sulfadiazine (SDZ), and sulfamethazine (SMZ) was generated, and all samples were measured in technical triplicates. HPLC-MS analysis was carried out using a Zorbax Eclipse Plus Rapid Resolution HT-C18 (100 mm × 3 mm, 1.8 μm) column on a 1,260 Infinity II HPLC (Agilent Technologies, Santa Clara, CA, USA) coupled to a QTRAO 6500 + MS/MS (AB Sciex, UK).

DNA extraction

The biofilm samples were vortexed and centrifuged for 5 min at 13,000 *g* to harvest microorganisms. The supernatant was discarded and the sediment was resuspended in 100 μL BE buffer (Macherey Nagel, Germany). For planktonic samples, filters were cut into small pieces and divided into two parallel 2-mL tubes containing 200 μL BE buffer and approximately 0.15 g of 1-mm zirconium beads (Carl Roth, Germany) each. The individual tubes were agitated for 20 s at 4 m/s on a FastPrep 24 instrument (MP Biomedicals, Germany) and centrifuged in a benchtop centrifuge (neoLab, Germany). The supernatant from parallel tubes was collected and pooled. To maximize the final DNA yield, an additional 100 μL of BE buffer was added to the tubes containing the filter pieces, vortexed, and centrifuged again, and the supernatant was pooled with the previous one. DNA extraction was performed using the NucleoSpin Microbial DNA Kit (Macherey Nagel, Germany) following the manufacturer's protocol.

16S rRNA gene amplicon sequencing

The diversity of bacterial communities in planktonic and biofilm samples was determined for all sites and sampling campaigns by preparing a 16S rRNA gene amplicon library as described (Haenelt et al., 2023). We conducted a nested PCR of the variable region V3 using the primer pairs specified in **Supplementary Table 1**. Performing a nested PCR was necessary to obtain sufficient DNA yield for the planktonic samples. Amplicons were sequenced with the NextSeq 500/550 High Output Kit v2.5 on an Illumina NextSeq 550 instrument. Bacterial community analysis was performed using QIIME 2 (Bolyen et al., 2019), DADA2 (Callahan et al., 2016), and the taxonomic classifier "Silva 138 99% OTU full-length sequences" (Bokulich et al., 2018; Robeson et al., 2021). Phyloseq (McMurdie and Holmes, 2013) was used for further data analysis in R. The dataset for Site 1 on

1 https://www.wahb.eu/

August 9th was removed due to low sequencing depth. Rarefaction curves can be found in **Supplementary Figure 2**. For statistical analyses of alpha diversity measurements, we performed Kruskal-Wallis and Dunn's tests using the package rstatix (Kassambara, 2023). An overview of the statistical significance of differences in alpha diversity, both between sampling sites and within each sampling site, comparing planktonic and biofilm samples, can be found in **Supplementary Table 2**. To compare microbial beta diversity in biofilm and planktonic samples, we applied non-metric multidimensional scaling (NMDS) of Bray-Curtis dissimilarities using the vegan package (Oksanen et al., 2022). To assess seasonal influences on bacterial community structure and diversity in the surface water compartment, we did NMDS with data obtained for planktonic samples in this study and data from our previous study from the 2020/2021 winter season (Haenelt et al., 2023). PERMANOVA tests were performed to evaluate the statistical significance of differences in beta diversity between sampling sites, within each sampling site comparing both surface water and biofilm compartments (**Supplementary Table 3**), as well as between the summer and winter season.

Quantitative PCR

Absolute abundances of *sul1*, *sul2*, *intI1*, and the 16S rRNA gene were determined with SYBR Green-based quantitative real-time PCR using established primers (**Supplementary Table 1**) and a protocol from Haenelt et al. (2023). For planktonic samples, copy numbers (CN) were normalized to CN/100 mL river water. For biofilm samples, CN were normalized to CN/sample and are therefore not directly comparable with each other. Relative abundances of *sul1*, *sul2*, and *intI1* were calculated by dividing their absolute abundances by those of the 16S rRNA gene. The statistical significance of differences in absolute and relative ARG abundances between sampling sites and seasons was determined using the package rstatix (Kassambara, 2023). We performed statistical analyses employing Kruskal-Wallis and Dunn's tests using the package rstatix (Kassambara, 2023). Results for the relative abundance of the target genes, encompassing comparisons of both sampling sites and riverine compartments within each sampling site can be found in **Supplementary Table 4**. Additionally, we compared the abundance of all four target genes quantified in the current study with data acquired during a winter season in our previous study (Haenelt et al., 2023). We aimed to identify notable differences in both absolute and relative abundance between the two seasons for each sampling site using Dunn's test, and the outcome of these analyses is depicted in **Supplementary Table 5**.

Results and discussion

Physicochemical parameters

Our monitoring study showed that WWTP effluent was the primary source of SMX, nitrogen, and phosphorus pollution. Downstream of the discharge point, our data show decreasing SMX as well as nutrient concentrations. The highest SMX concentration was found at Site 3, with a median concentration of 20 ng/L, resulting in 17.7 ng/L SMX at Site 4. This finding is in line with previous studies on the Holtemme (Krauss et al., 2019; Beckers et al., 2020; Švara et al., 2021) and with numerous publications which showed that WWTP effluent is the primary source of antibiotic pollution in aquatic ecosystems (Carvalho and Santos, 2016; Rodriguez-Mozaz et al., 2020; Zhuang et al., 2021; Larsson and Flach, 2022). Sulfonamides are typically found at concentrations below 100 ng/L in anthropogenically impacted river waters (Li et al., 2022). In our previous study during the 2020/2021 winter season (Haenelt et al., 2023), the median SMX concentration at Site 3 was 8.6 ng/L and therefore lower than during the summer season. Lower antibiotic concentrations in the effluent during the winter season could be explained by dilution effects due to precipitation in the WWTP catchment (Hong et al., 2018). Taking the SMX concentration as an indicator of the proportion of wastewater in the river, WWTP effluent would account for nearly 90% of the river water at Site 4 in the summer season of 2022. This value is similar to the value of 75% estimated on the basis of the flow rates provided by the State Office for Flood Protection and Water Management Saxony-Anhalt.[2] Downstream of the discharge point, SMX concentration decreased. However, the decrease was not statistically significant and the decline rate of SMX concentration (11% from Site 3 to Site 6) was lower than during the winter season (73%), presumably because of high water evaporation together with the lack of precipitation. SDZ and SMZ concentrations did not exceed 1.3 ng/L at any of the sampling sites (**Figure 1A**). SMX and SMZ concentrations at Site 4 are consistent with a previous study conducted on the Holtemme (Tousova et al., 2017). There, samples were taken approximately 1 km downstream from our Site 4, the mean SMX concentration was 8 ng/L and SMZ concentrations were below the limit of quantification. SDZ concentrations were previously not quantified.

During the hot and dry summer season in 2022, water depth was on average below 10 cm in the Holtemme. Water temperature upstream of the WWTP varied between 13 and 16°C, while wastewater discharge at Site 3 (21°C) resulted in an elevated water temperature of 19°C at Site 4. Downstream at Site 5 (17°C), water temperature increased further, peaking at 22°C at Site 6. The pH in the river changed from pH 7.3 at Site 1 to pH 8.8 at Site 6. Nitrate concentrations were 1.2 mg/L upstream of the WWTP, 4 mg/L in the wastewater effluent, and 2.8 mg/L downstream at Site 5. These values are in the lower range of previously reported nitrate concentrations along the river stretch (Brase et al., 2018). Total phosphorous showed a similar pattern with low concentrations of 0.02 mg/L at Site 1 and an increase to 0.1 mg/L at Site 5 after WWTP discharge of 1 mg/L (**Figure 1B**).

Bacterial community structure

The bacterial community structures of planktonic and biofilm samples are reported individually, using Shannon index and species richness based on the number of observed Amplicon Sequence Variants (ASVs) to assess bacterial diversity (**Figure 2**). In planktonic samples, both indices showed the same trend. Highest

2 https://hochwasservorhersage.sachsen-anhalt.de/messwerte/wasserstand

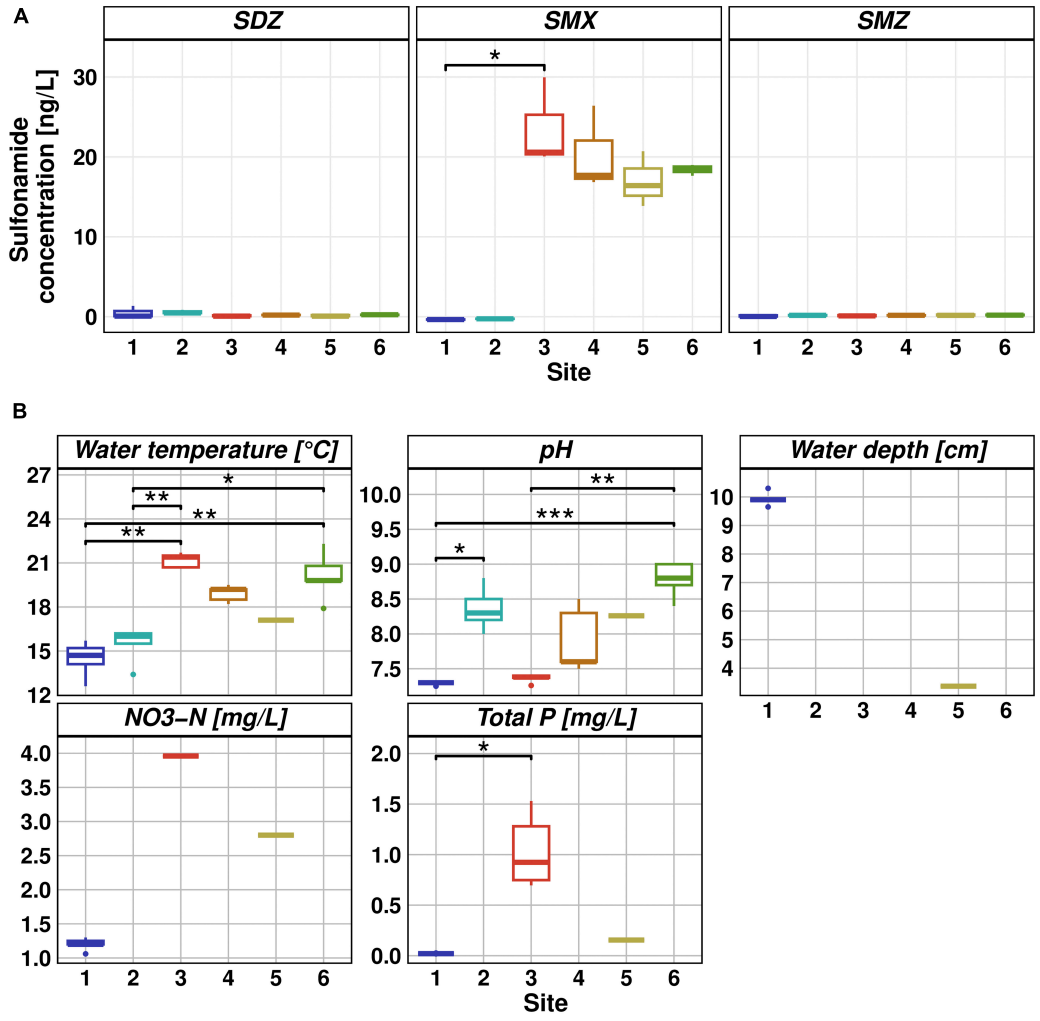

FIGURE 1
(A) Sulfonamide concentrations measured via HPLC-MS. Measurement was done in five replicates and sulfadiazine (left), sulfamethoxazole (middle) and sulfamethazine (right) concentrations are reported as box whisker plots for each site. **(B)** Physicochemical parameters. Measurements were obtained from MOBICOS monitoring stations (Site 1 and 5, https://www.ufz.de/index.php?en=39611), WWTP Silstedt (Site 3, https://www.wahb.eu/) and manually using a SenTix41 probe (Site 2, 4, and 6). From left to right and top to bottom: water temperature [°C], pH, water depth [cm], NO_3-N [mg/L], and total P [mg/L]. Significant differences between sampling sites are represented by asterisks (Dunn's test, * ≤ 0.05, ** ≤ 0.01, *** ≤ 0.001).

median values of 6.4 and 1,379 were found at Site 1, whereas lowest values were found at Site 3 (median 5.5 and 1,113). The decrease in Shannon index from Site 1 and 2 to Site 3 was statistically significant (Dunn's test: $p \leq 0.01$ for Site 1, $p \leq 0.05$ for Site 2). Downstream of the WWTP, both indices increased steadily, reaching values of 6 and 1,354 at Site 6. The steady increase of both indices downstream the discharge point indicates a recovery of the riverine bacterial community, which was demonstrated in our previous winter monitoring study on the Holtemme using a microbiome recovery model (Haenelt et al., 2023). In contrast to planktonic samples, both indices decreased in the biofilm samples from Site 1 (5.8 and 1,038) to Site 2 (5 and 782). Values at Site 3 (5.7 and 1,157) and nearby Site 4 (5.9 and 1,334) are similar to those at near-pristine Site 1, while further downstream the WWTP, both indices again decreased in a statistically significant manner (Dunn's test: $p \leq 0.05$) with medians of 5.3 and 803 at Site 6. Notably, the biofilm communities at Sites 1, 2, 5, and 6 showed significantly lower alpha diversity in comparison to the corresponding planktonic samples (Dunn's test: $p \leq 0.05$). The number of observed ASVs at Site 1 was the only exception, showing a non-significant difference. Conversely, polluted Sites 3 and 4 show much more uniform alpha diversity in both planktonic and biofilm-forming bacterial communities. We hypothesize that the increase in both indices in the surface water compartment downstream from the WWTP might be attributed to biases during rarefaction of the sequencing data. The high abundance of certain taxa in wastewater may have prevented detection of rare taxa, which were found further downstream in the river with higher evenness (Cameron et al., 2021).

The composition of bacterial communities along the river stretch was impacted by anthropogenic pollution. This is evident in the dissimilarities of beta diversity across different sites, as shown in the NMDS plot in **Figure 2C**. Influencing factors could be foremost the discharge of wastewater, flow rate, physicochemical parameters, and rectification (Luo et al., 2020). A clear trend could be observed with Sites 1 and 2 on one side and WWTP effluent

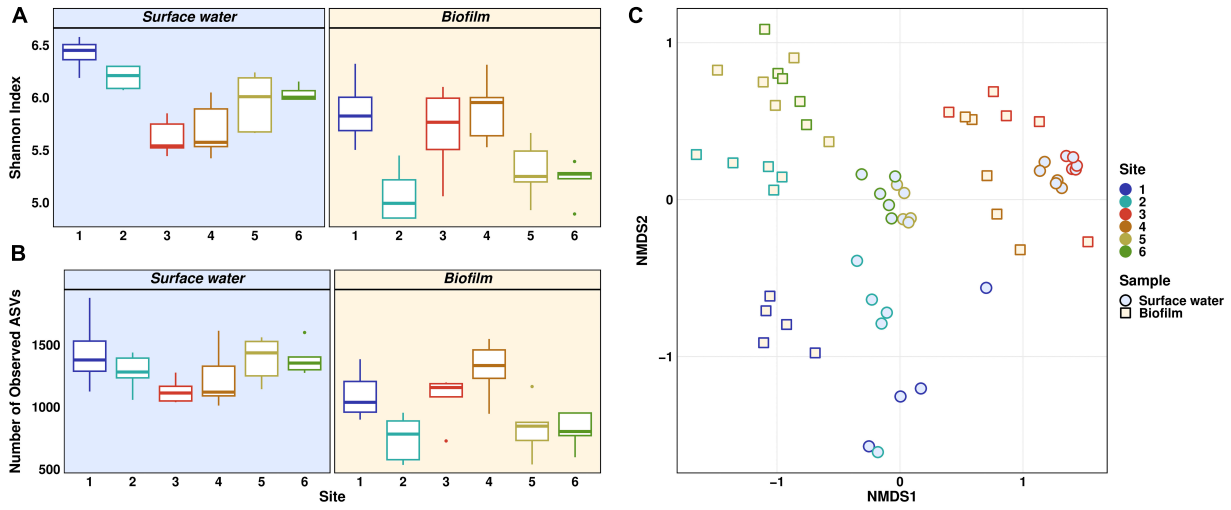

FIGURE 2
Microbial community structure and diversity based on 16S rRNA gene amplicon sequencing. Alpha diversity is given using Shannon measurement **(A)** and Number of observed ASVs **(B)**. Beta diversity is displayed as NMDS plot of Bray-Curtis-dissimilarities **(C)**. Distinct colors represent different sites. Light yellow background **(A,B)** and squares **(C)** represent biofilm samples, light blue background **(A,B)** and circles **(C)** represent surface water samples.

and nearby Site 4 on the other side of the plot, whereas Sites 5 and 6 showed very similar community structure and are positioned in between the upstream and WWTP-impacted sites. Significantly distinct beta diversity was observed in both planktonic and biofilm-forming microbial communities across all sampling sites, except when comparing Site 3 to Site 4 (PERMANOVA: $p \leq 0.05$). NMDS analysis also revealed a statistically significant separation between planktonic and biofilm-forming bacterial communities at all sampling sites (PERMANOVA: $p \leq 0.01$). However, the change in community composition seemed to be driven more by the anthropogenic pollution rather than the type of compartment, i.e., surface water vs. biofilm.

The taxonomic compositions of the samples corresponded to the degree of anthropogenic influence along the river. The 50 most abundant phylotypes for each site and their corresponding relative abundances can be found in **Supplementary Table 6**. Biofilm and planktonic communities at Site 1 were dominated by members of the classes *Alphaproteobacteria*, *Gammaproteobacteria*, *Clostridia*, and *Bacilli*. In the biofilm samples, approximately 4% of the high-quality reads were derived from *Cyanobacteria*, whereas in the planktonic samples, *Cyanobacteria* were not among the 50 most abundant phylotypes (>0.26% of total read abundance). At the family level, bacteria typically exhibiting an aerobic, heterotrophic metabolism predominated in both compartments (e.g., *Chitinophagaceae*, *Comamonadaceae*, and *Xanthobacteraceae*). Noteworthy, we found an ASV affiliated with *Escherichia-Shigella* in every sample from the surface water compartment at Site 1 (average read abundance of 0.3%). Since identical or similar ASVs were not found in any of the other 55 samples from our campaign, it seems unlikely that they are sampling/laboratory contaminants in the planktonic samples from Site 1. While it remains to be elucidated to which genus the *Escherichia-Shigella* ASV belonged, and whether it was derived from an autochthonous population, the members of that genus could be a source of the occasionally detected *sul1*, *sul2*, and *intI1* genes at the site (see below). At Site 2 just downstream the city of Wernigerode, the communities of the surface water and biofilm compartments included several phylotypes often associated with warm-blooded animals (e.g., various *Ruminococcaceae*) in addition to those found at Site 1. The WWTP effluent at Site 3 was dominated by phylotypes of the family *Peptostreptococcaceae* and the order *Lactobacillales* in planktonic samples, while in biofilm samples most abundant phylotypes were associated with *Peptostreptococcaceae*, *Nitrospiraceae,* and *Rhodobacteraceae*. Downstream the discharge point, *Peptostreptococcaceae* remained a dominant family, but *Sphingomonadaceae* and *Xenococcaceae* were also detected with increasing abundance. *Arcobacteraceae* (phylum *Campilobacterota*) became highly abundant in biofilm samples (**Figure 3**). Members of this family have been identified as predominate hosts of *sul1*, *sul2*, *intI1*, and probably class 1 integrons in sewage-impacted water (Hultman et al., 2018; Knecht et al., 2023). Overall, the relative abundance of families with known hosts of integrons slightly decreased from 17% in both biofilm and surface water compartment at Site 1 to an average relative abundance of 12% downstream the WWTP, thus potential hosts for ARGs were already present upstream the WWTP in an area with little anthropogenic impact. Some of these families such as *Aeromonadaceae* and *Rhodocyclaceae* have been implicated as prevalent carriers of the indicator genes in and downstream of wastewater treatment systems (Zhang et al., 2018; Lo et al., 2022; Knecht et al., 2023).

Differences in beta diversity of planktonic communities from this sampling campaign and those analyzed in our study of the winter season 2020/2021 (Haenelt et al., 2023) are shown in **Figure 4**. Bacterial communities in summer and winter season were distinct, with statistically significant differences at all sampling sites (PERMANOVA: $p \leq 0.05$). Summer communities cluster more than those acquired in winter season, which is most likely related to the shorter sampling period. This becomes evident in the spatial arrangement of data points in the NMDS plot depending on the

10.3389/fmicb.2023.1252870

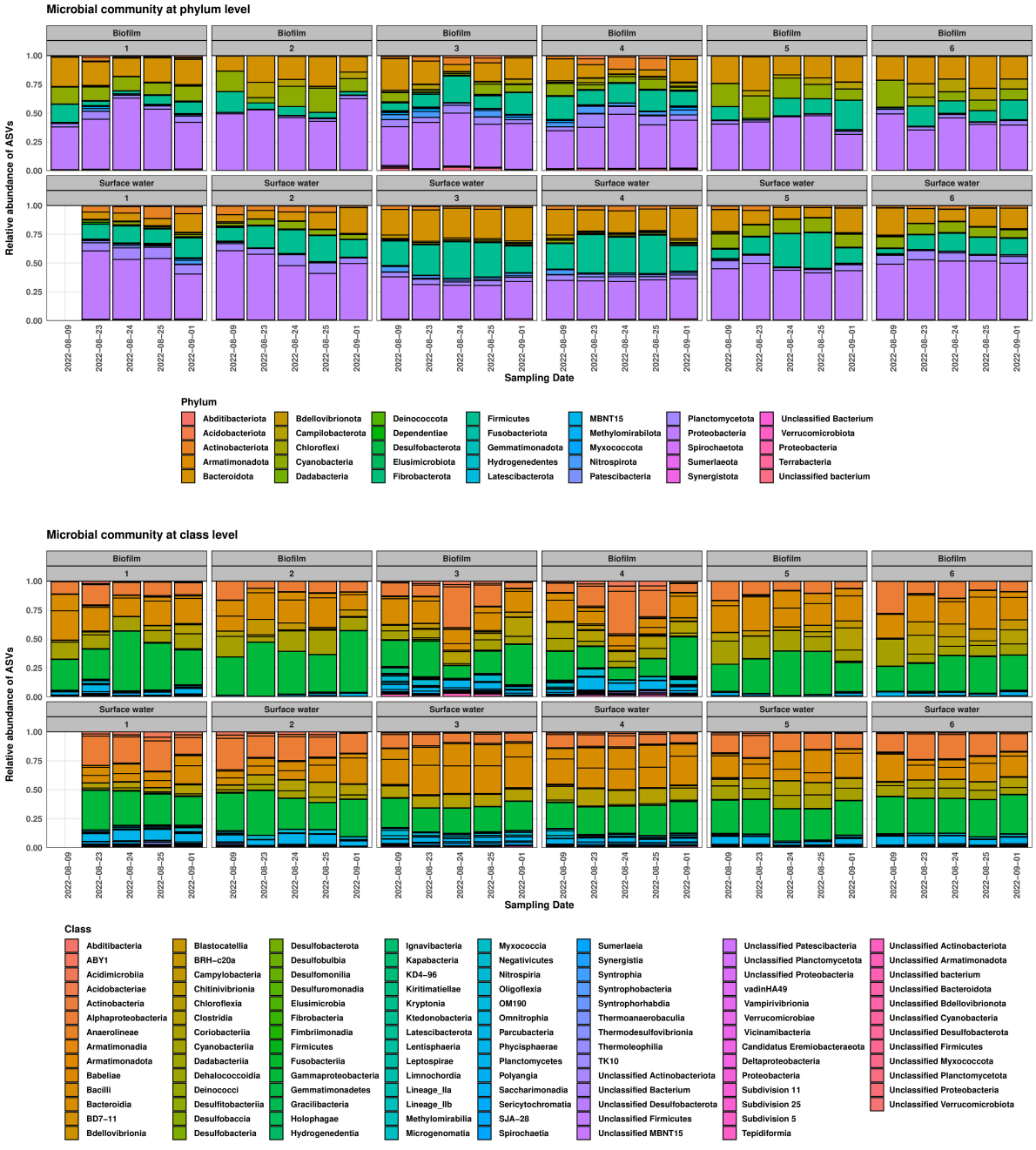

FIGURE 3
Microbial community structure at phylum **(top)** and class level **(bottom)** for each site. Sampling dates are displayed on the *x*-axis. Sample for Site 1, 8th August 2022 was removed before analysis due to low sampling depth.

sampling date in the winter season, where samples were collected over approximately 3 months. The summer sampling campaign lasted only about 1 month. In contrast to upstream sites, the bacterial community in the WWTP effluent were more stable over time and in between seasons, as data points are located close to each other in the plot. As WWTP performances are often stable over time, one would expect the bacterial community structure to be distributed more closely around an average, as previously shown by Wang et al. (2021). At downstream Sites 4, 5, and 6, site-specific distances are much smaller than the time-specific differences. These findings are consistent with a monitoring study conducted on a river in southern Germany (Reichert et al., 2021), illustrating the substantial impact of seasonality on bacterial community structure and diversity.

ARG abundance

The anthropogenic pollution pattern in the Holtemme is evident from the prevalence of *sul1*, *sul2*, *intI1*, and the 16S rRNA gene in planktonic samples. All four genes showed a similar pattern with low CN or CN below limit of quantification at Sites 1 and

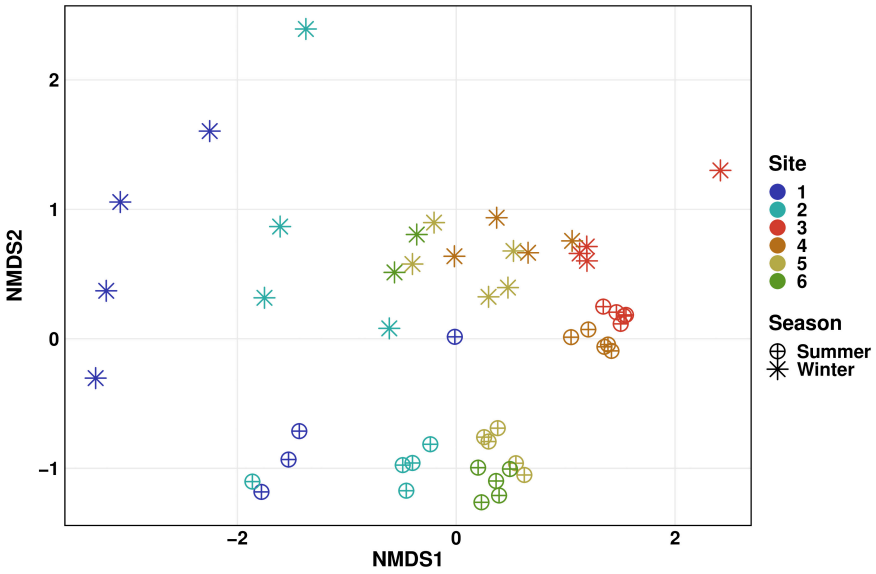

FIGURE 4
Seasonal comparison (winter vs. summer) of microbial community diversity in surface water displayed as NMDS plot of Bray-Curtis-dissimilarities. Distinct colors represent different sites. Stars represent samples taken during an earlier monitoring study in the winter season 2020/2021 (**Figure 2C**, Water), circles represent samples taken in this study in the summer season 2022 (Haenelt et al., 2023). Differences were statistically different between both seasons for all sampling sites, with Sites 3, 4, and 5 showing higher significance levels (PERMANOVA: $p \leq 0.01$) than Sites 1, 2, and 6 (PERMANOVA: $p \leq 0.05$).

2, highest CN in wastewater and decreasing CN downstream of the WWTP (**Supplementary Figure 3**). The increase in absolute abundance was statistically significant for *sul1*, *sul2* and 16S rRNA gene from upstream Sites 1 and 2 to heavily wastewater-impacted Sites 3 and 4 (Dunn's test: $p \leq 0.01$). The median CN of 16S rRNA gene at Site 6 was only 16% of the CN at Site 4. Similar declines were observed for *sul1*, *sul2*, and *intI1* (12, 10, and 6%, respectively). The absolute CN of the 16S rRNA gene was higher at the wastewater discharge point (median 4.1×10^7 CN/100 mL) than in the river water with a median of 4.3×10^6 CN/100 mL at Site 5. In contrast to our previous monitoring study in the winter season 2020/2021, the absolute abundance of all four target genes in summer season declined more rapidly from Site 4 to 5. This observation is of special interest, as we would have expected the opposite, a faster decrease in the absolute abundance during winter season, due to dilution effects. Absolute abundance for biofilm samples is not depicted because a normalization to CN/sample does not allow for direct comparison between different sampling sites. In the summer season, relative abundance against 16S rRNA gene showed a similar pattern for all three target genes *sul1*, *sul2*, and *intI1* in planktonic samples, with the highest relative abundance at Site 3 (median 2.8, 2.6, and 1.3%, respectively) and decreasing relative abundance from Site 4 to 5 (**Figure 5**). Wastewater discharge at Site 3 resulted in significantly increased relative abundances of *sul1* and *sul2* when compared to both upstream sites (Dunn's test: $p \leq 0.05$). The decrease in absolute and relative abundance downstream the WWTP is most likely attributed to dilution effects, but additional removal mechanisms like sedimentation, cell death by predation or inactivation by UV light might also occur (Lee et al., 2021).

Although both, the relative and absolute abundances of these genes are decreasing, the median values remain largely unchanged 8 km (Site 5) and 13 km (Site 6) downstream the WWTP. These observations show that ARGs can be persistent in the aquatic environment even far downstream the point source of pollution (>10 km). Sabri et al. (2020) measured the abundance of several ARGs in a Dutch river and absolute abundances of *sul1*, *sul2*, and *intI1* gene copy numbers remained constant over 20 km of the river stretch regardless of the season. These findings differ from our previous monitoring study in winter season 2020/2021, where absolute abundances of *sul1* and *sul2* decreased to copy numbers below the limit of quantification at Site 6, 13 km downstream the WWTP. Potential causes for differing observations could be the fraction of wastewater discharge, and the amount of precipitation and additional inflow from tributaries depending on the season. In addition, the absolute abundance of the 16S rRNA and sulfonamide resistance genes was significantly higher in the WWTP effluent and at all sampling sites downstream the WWTP in the summer compared to the winter season (Dunn's test: $p \leq 0.05$). This increase is most likely a consequence of higher abundance of microorganisms in the WWTP during summer season. The relative abundance of *sul1* and *sul2* was also higher in the summer season at Site 3 and downstream the WWTP. For *sul2* the difference was statistically significant (Dunn's test: $p \leq 0.05$). We estimate an increase in the proportion of WWTP effluent at Site 4 from ~27% in winter to about 75% in the summer season (see above). Therefore, seasonal differences like the increased proportion of wastewater and thus ARG-carrying wastewater-derived microorganisms in the river increased the abundance of sulfonamide resistance genes. In the face of climate change with less average precipitation in summer seasons in Europe, one must assume that the proportion of wastewater in rivers will increase even further (European Environment Agency, 2021), leading to an increase of ARGs in rivers.

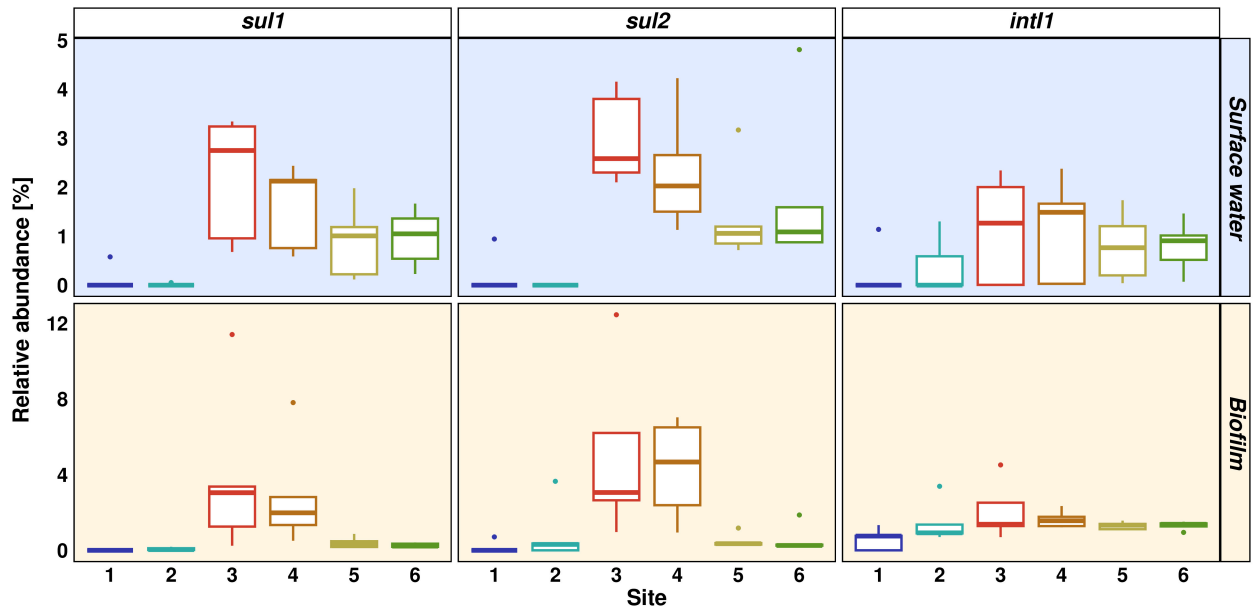

FIGURE 5
Abundance of *sul1*, *sul2*, and *intI1* relative to 16S rRNA gene. Distinct colors represent different sites. Light yellow background represents biofilm samples, light blue background represents surface water samples.

In biofilm samples, similar relative abundances were observed for *sul1* and *sul2*, however, at higher relative abundance at Site 3 (both genes at 3%) and Site 4 (2 and 4.7%) and a more rapid drop from Site 4 to Site 5 (both 0.3%). The relative abundance of both genes was significantly increased at Site 3 and 4 when compared to the pristine Site 1 (Dunn's test: $p \leq 0.01$). The elevated relative abundance in vicinity to the discharge point indicates that ARG-carrying microorganisms were mainly accumulated in biofilm directly at the WWTP, whereas those remaining in surface waters over longer distance did not or only barely enter biofilms at a later stage. Similar findings were reported by Guo et al. (2018), where the authors found higher ARG abundances and detection frequencies in biofilm compared to planktonic samples. The accumulation of antibiotics in the biofilm compartment, in combination with dense microbial growth and accumulation of mobile genetic elements might render biofilms an important reservoir for ARGs downstream WWTPs (Gillings et al., 2009). However, the spatially restricted occurrence of sulfonamide resistance genes *sul1* and *sul2* in biofilms in close vicinity to the discharge point suggests that this was not the case in our study.

In contrast to the sulfonamide resistance genes, *intI1* was detectable upstream and downstream of the WWTP without significant differences in the relative abundance between sampling sites. However, wastewater discharge increased its relative abundance from a median of 0.9% at Site 2 to 1.5% at Site 4. All anthropogenically impacted ecosystems have become polluted with the clinical class 1 integron in recent years (Gillings, 2018). For example, Cacace et al. (2019) conducted a study on the abundance of nine ARGs and the *intI1* gene in 16 WWTP effluents from 10 European countries. Similar to the biofilm samples we studied, they found a background level of *intI1* resistance already present upstream of the WWTP, which further increased when wastewater entered the river. Possible reasons for the occurrence upstream of a WWTP could be anthropogenic impact from the city of Wernigerode or leisure activities at the river (Weitere et al., 2021). The prevalence of the *intI1* gene in biofilm throughout the river stretch is of concern if correlating with the abundance of class 1 integron, as the integron could potentially carry various ARGs as gene cassettes, and biofilms provide suitable conditions for horizontal gene transfer (Gillings et al., 2008; Chaturvedi et al., 2021).

During our monitoring study, we were limited in information regarding flow rates for all sampling sites, which would have been needed to calculate the loads of ARGs in CN/day as previously done by Lee et al. (2021). This would have further enabled us to determine the environmental fate of ARGs (e.g., dilution of wastewater in the river vs. additional removal mechanism) more precisely. In addition, single-cell approaches such as epicPCR or directGeneFISH (Moraru et al., 2010; Spencer et al., 2016) could be implemented in future studies to link the host phylotypes with the ARGs type and to better assess the risk of ARG transfer to human pathogens.

Conclusion

The findings of this study emphasize the importance of spatiotemporal monitoring of anthropogenic pollution on both planktonic and biofilm-forming bacterial communities in aquatic ecosystems. Higher proportions of wastewater in the river increased the absolute and relative abundance of sulfonamide resistance genes in summer when compared with previously published data obtained during the winter season. Even though we observed a more rapid decline of absolute abundances after wastewater discharge in the summer season, we found that the indicator

genes *sul1*, *sul2*, and *intI1* were persistent in river water and remained detectable even 13 km downstream of the pollution source, which was not the case in our previous study in the winter season. In light of climate change, where forecasts predict even hotter and drier summers and therefore greater urban discharge fractions in streams (European Environment Agency, 2021), this finding become of great concern. Moreover, resistance genes were found to be higher abundant in biofilms located near the WWTP in comparison to the surrounding water, suggesting the possible accumulation of antibiotic-resistant bacteria derived from wastewater in biofilms. Further research is needed to understand the underlying mechanisms responsible for the accumulation of ARGs in biofilms and to gain better insights into the influence of seasonal variations on bacterial community alteration and ARG persistence in aquatic environments. It is already certain that higher proportions of wastewater in rivers and the resulting high occurrence of wastewater-derived microorganisms lead to the increased abundance and persistence of ARGs in the aquatic environment.

Data availability statement

The datasets presented in this study can be found in online repositories. The names of the repository/repositories and accession number(s) can be found below: https://www.ncbi.nlm.nih.gov/, PRJNA962299.

Author contributions

SH, NM, JM, and H-HR conceived the study and the experimental design. SH performed the sampling, sample treatment, and data analysis and wrote the manuscript with contributions from NM and JM. NM and SH supervised during the whole study duration. All authors contributed to the manuscript revision and read and approved the submitted version.

Acknowledgments

We would like to thank the Helmholtz Centre for Environmental Research for funding this Ph.D project through the Ph.D college initiative–FATE (Fate and effects of antibiotics from sources to sinks: Bridging the scale from molecular-level processes to large-scale observations in engineered and natural systems). We appreciate the support of Florian Tschernikl during the sampling campaign. We would like to thank David Thiele and Florian Lenk at KIT for library preparation and Illumina sequencing. We extend special thanks to Caglar Akay for providing us with the HPLC-MS method for the measurement of sulfadiazine and sulfamethazine and to Patrick Fink, Mario Brauns, and Florian Zander for their continuous effort in maintaining the MOBICOS stations.

Conflict of interest

The authors declare that the research was conducted in the absence of any commercial or financial relationships that could be construed as a potential conflict of interest.

Publisher's note

Supplementary material

The Supplementary Material for this article can be found online at: https://www.frontiersin.org/articles/10.3389/fmicb.2023.1252870/full#supplementary-material

References

Beckers, L.-M., Brack, W., Dann, J. P., Krauss, M., Müller, E., and Schulze, T. (2020). Unraveling longitudinal pollution patterns of organic micropollutants in a river by non-target screening and cluster analysis. *Sci. Total Environ.* 727:138388.

Berendonk, T. U., Manaia, C. M., Merlin, C., Fatta-Kassinos, D., Cytryn, E., Walsh, F., et al. (2015). Tackling antibiotic resistance: the environmental framework. *Nat. Rev. Microbiol.* 13, 310–317. doi: 10.1038/nrmicro3439

Bokulich, N. A., Kaehler, B. D., Rideout, J. R., Dillon, M., Bolyen, E., Knight, R., et al. (2018). Optimizing taxonomic classification of marker-gene amplicon sequences with QIIME 2's q2-feature-classifier plugin. *Microbiome* 6:90. doi: 10.1186/s40168-018-0470-z

Bolyen, E., Rideout, J. R., Dillon, M. R., Bokulich, N. A., Abnet, C. C., Al-Ghalith, G. A., et al. (2019). Reproducible, interactive, scalable and extensible microbiome data science using QIIME 2. *Nat. Biotechnol.* 37, 852–857. doi: 10.1038/s41587-019-0209-9

Borsetto, C., Raguideau, S., Travis, E., Kim, D. W., Lee, D. H., Bottrill, A., et al. (2021). Impact of sulfamethoxazole on a riverine microbiome. *Water Res.* 201:117382. doi: 10.1016/j.watres.2021.117382

Brase, L., Sanders, T., and Dähnke, K. (2018). Anthropogenic changes of nitrogen loads in a small river: External nutrient sources vs. internal turnover processes. *Isotopes Environ. Health Stud.* 54, 168–184. doi: 10.1080/10256016.2018.1428580

Cacace, D., Fatta-Kassinos, D., Manaia, C. M., Cytryn, E., Kreuzinger, N., Rizzo, L., et al. (2019). Antibiotic resistance genes in treated wastewater and in the receiving water bodies: A pan-European survey of urban settings. *Water Res.* 162, 320–330. doi: 10.1016/j.watres.2019.06.039

Callahan, B. J., McMurdie, P. J., Rosen, M. J., Han, A. W., Johnson, A. J. A., and Holmes, S. P. (2016). DADA2: High-resolution sample inference from Illumina amplicon data. *Nat. Methods* 13, 581–583. doi: 10.1038/nmeth.3869

Cameron, E. S., Schmidt, P. J., Tremblay, B. J.-M., Emelko, M. B., and Müller, K. M. (2021). Enhancing diversity analysis by repeatedly rarefying next generation sequencing data describing microbial communities. *Sci. Rep.* 11:22302. doi: 10.1038/s41598-021-01636-1

Carvalho, I. T., and Santos, L. (2016). Antibiotics in the aquatic environments: A review of the European scenario. *Environ. Int.* 94, 736–757. doi: 10.1016/j.envint.2016.06.025

Chaturvedi, P., Shukla, P., Giri, B. S., Chowdhary, P., Chandra, R., Gupta, P., et al. (2021). Prevalence and hazardous impact of pharmaceutical and personal care products and antibiotics in environment: A review on emerging contaminants. *Environ. Res.* 194:110664. doi: 10.1016/j.envres.2020.110664

Chen, B., Liang, X., Huang, X., Zhang, T., and Li, X. (2013). Differentiating anthropogenic impacts on ARGs in the Pearl River Estuary by using suitable gene indicators. *Water Res.* 47, 2811–2820. doi: 10.1016/j.watres.2013.02.042

European Environment Agency (2021). *Europe's changing climate hazards - an index-based interactive EEA report*. Copenhagen: European Environment Agency.

Fink, P., Norf, H., Anlanger, C., Brauns, M., Kamjunke, N., Risse-Buhl, U., et al. (2020). Streamside mobile mesocosms (MOBICOS): A new modular research infrastructure for hydro-ecological process studies across catchment-scale gradients. *Int. Rev. Hydrobiol.* 105, 63–73. doi: 10.1002/iroh.201902009

Flemming, H.-C., Wingender, J., Szewzyk, U., Steinberg, P., Rice, S. A., and Kjelleberg, S. (2016). Biofilms: An emergent form of bacterial life. *Nat. Rev. Microbiol.* 14, 563–575. doi: 10.1038/nrmicro.2016.94

Flores-Vargas, G., Bergsveinson, J., Lawrence, J. R., and Korber, D. R. (2021). Environmental biofilms as reservoirs for antimicrobial resistance. *Front. Microbiol.* 12:766242. doi: 10.3389/fmicb.2021.766242

Gillings, M. R. (2018). DNA as a pollutant: The clinical class 1 integron. *Curr. Pollut. Rep.* 4, 49–55. doi: 10.1007/s40726-018-0076-x

Gillings, M. R., Gaze, W. H., Pruden, A., Smalla, K., Tiedje, J. M., and Zhu, Y.-G. (2015). Using the class 1 integron-integrase gene as a proxy for anthropogenic pollution. *ISME J.* 9, 1269–1279. doi: 10.1038/ismej.2014.226

Gillings, M. R., Holley, M. P., and Stokes, H. W. (2009). Evidence for dynamic exchange of qac gene cassettes between class 1 integrons and other integrons in freshwater biofilms. *FEMS Microbiol. Lett.* 296, 282–288. doi: 10.1111/j.1574-6968.2009.01646.x

Gillings, M., Boucher, Y., Labbate, M., Holmes, A., Krishnan, S., Holley, M., et al. (2008). The evolution of class 1 integrons and the rise of antibiotic resistance. *J. Bacteriol.* 190, 5095–5100. doi: 10.1128/JB.00152-08

Gudmundsson, L., Boulange, J., Do, H. X., Gosling, S. N., Grillakis, M. G., Koutroulis, A. G., et al. (2021). Globally observed trends in mean and extreme river flow attributed to climate change. *Science* 371, 1159–1162. doi: 10.1126/science.aba3996

Guo, X., Yang, Y., Lu, D., Niu, Z., Feng, J., Chen, Y., et al. (2018). Biofilms as a sink for antibiotic resistance genes (ARGs) in the Yangtze Estuary. *Water Res.* 129, 277–286. doi: 10.1016/j.watres.2017.11.029

Haenelt, S., Wang, G., Kasmanas, J. C., Musat, F., Richnow, H. H., da Rocha, U. N., et al. (2023). The fate of sulfonamide resistance genes and anthropogenic pollution marker intI1 after discharge of wastewater into a pristine river stream. *Front. Microbiol.* 14:1058350. doi: 10.3389/fmicb.2023.1058350

Harnisz, M., Kiedrzynska, E., Kiedrzynski, M., Korzeniewska, E., Czatzkowska, M., Koniuszewska, I., et al. (2020). The impact of WWTP size and sampling season on the prevalence of antibiotic resistance genes in wastewater and the river system. *Sci. Total Environ.* 741:140466. doi: 10.1016/j.scitotenv.2020.140466

Hong, B., Lin, Q., Yu, S., Chen, Y., Chen, Y., and Chiang, P. (2018). Urbanization gradient of selected pharmaceuticals in surface water at a watershed scale. *Sci. Total Environ.* 634, 448–458. doi: 10.1016/j.scitotenv.2018.03.392

Hultman, J., Tamminen, M., Pärnänen, K., Cairns, J., Karkman, A., and Virta, M. (2018). Host range of antibiotic resistance genes in wastewater treatment plant influent and effluent. *FEMS Microbiol. Ecol.* 94:fiy038. doi: 10.1093/femsec/fiy038

Hutinel, M., Fick, J., Larsson, D. G. J., and Flach, C.-F. (2021). Investigating the effects of municipal and hospital wastewaters on horizontal gene transfer. *Environ. Pollut.* 276:116733. doi: 10.1016/j.envpol.2021.116733

Inostroza, P. A., Vera-Escalona, I., Wicht, A.-J., Krauss, M., Brack, W., and Norf, H. (2016). Anthropogenic stressors shape genetic structure: Insights from a model freshwater population along a land use gradient. *Environ. Sci. Technol.* 50, 11346–11356. doi: 10.1021/acs.est.6b04629

Karthe, D., Lin, P.-Y., and Westphal, K. (2017). Instream coliform gradients in the Holtemme, a small headwater stream in the Elbe River Basin, Northern Germany. *Front. Earth Sci.* 11:544–553. doi: 10.1007/s11707-017-0648-x

Kassambara, A. (2023). *rstatix: Pipe-friendly framework for basic statistical tests. R package version 0.7.2.*

Kasuga, I., Nagasawa, K., Suzuki, M., Kurisu, F., and Furumai, H. (2022). High-throughput screening of antimicrobial resistance genes and their association with class 1 integrons in urban rivers in Japan. *Front. Environ. Sci.* 10:825372. doi: 10.3389/fenvs.2022.825372

Knecht, C. A., Hinkel, M., Mäusezahl, I., Kaster, A.-K., Nivala, J., and Müller, J. A. (2023). Identification of antibiotic resistance gene hosts in treatment wetlands using a single-cell based high-throughput approach. *Water* 15:2432. doi: 10.3390/w15132432

Koczura, R., Mokracka, J., Taraszewska, A., and Łopacinska, N. (2016). Abundance of class 1 integron-integrase and sulfonamide resistance genes in river water and sediment is affected by anthropogenic pressure and environmental factors. *Microb. Ecol.* 72, 909–916. doi: 10.1007/s00248-016-0843-4

Krauss, M., Hug, C., Bloch, R., Schulze, T., and Brack, W. (2019). Prioritising site-specific micropollutants in surface water from LC-HRMS non-target screening data using a rarity score. *Environ. Sci. Eur.* 31:45. doi: 10.1186/s12302-019-0231-z

Kunz, J. V., Annable, M. D., Rao, S., Rode, M., and Borchardt, D. (2017). Hyporheic passive flux meters reveal inverse vertical zonation and high seasonality of nitrogen processing in an anthropogenically modified stream (Holtemme, Germany). *Water Resour. Res.* 53, 10155–10172. doi: 10.1002/2017WR020709

Larsson, D. G. J., and Flach, C.-F. (2022). Antibiotic resistance in the environment. *Nat. Rev. Microbiol.* 20, 257–269. doi: 10.1038/s41579-021-00649-x

Lee, J., Ju, F., Maile-Moskowitz, A., Beck, K., Maccagnan, A., McArdell, C. S., et al. (2021). Unraveling the riverine antibiotic resistome: The downstream fate of anthropogenic inputs. *Water Res.* 197:117050. doi: 10.1016/j.watres.2021.117050

Li, S., Liu, Y., Wu, Y., Hu, J., Zhang, Y., Sun, Q., et al. (2022). Antibiotics in global rivers. *Natl. Sci. Open* 1:20220029. doi: 10.1360/nso/20220029

Lo, H.-Y., Martínez-Lavanchy, P. M., Goris, T., Heider, J., Boll, M., Kaster, A.-K., et al. (2022). IncP-type plasmids carrying genes for antibiotic resistance or for aromatic compound degradation are prevalent in sequenced *Aromatoleum* and *Thauera* strains. *Environ. Microbiol.* 24, 6411–6425. doi: 10.1111/1462-2920.16262

Luo, X., Xiang, X., Yang, Y., Huang, G., Fu, K., Che, R., et al. (2020). Seasonal effects of river flow on microbial community coalescence and diversity in a riverine network. *FEMS Microbiol. Ecol.* 96, 1–13. doi: 10.1093/femsec/fiaa132

Mao, D., Yu, S., Rysz, M., Luo, Y., Yang, F., Li, F., et al. (2015). Prevalence and proliferation of antibiotic resistance genes in two municipal wastewater treatment plants. *Water Res.* 85, 458–466. doi: 10.1016/j.watres.2015.09.010

Martin-Laurent, F., Topp, E., Billet, L., Batisson, I., Malandain, C., Besse-Hoggan, P., et al. (2019). Environmental risk assessment of antibiotics in agroecosystems: Ecotoxicological effects on aquatic microbial communities and dissemination of antimicrobial resistances and antibiotic biodegradation potential along the soil-water continuum. *Environ. Sci. Pollut. Res. Int.* 26, 18930–18937. doi: 10.1007/s11356-019-05122-0

McMurdie, P. J., and Holmes, S. (2013). phyloseq: An R package for reproducible interactive analysis and graphics of microbiome census data. *PLoS One* 8:e61217. doi: 10.1371/journal.pone.0061217

Moraru, C., Lam, P., Fuchs, B. M., Kuypers, M. M. M., and Amann, R. (2010). GeneFISH–an in situ technique for linking gene presence and cell identity in environmental microorganisms. *Environ. Microbiol.* 12, 3057–3073. doi: 10.1111/j.1462-2920.2010.02281.x

OECD (2020). *Financing water supply, sanitation and flood protection: Challenges in EU member states and policy options*. Paris: OECD Publishing.

Oksanen, J., Simpson, G. L., Blanchet, F. G., Kindt, R., Legendre, P., Minchin, P. R., et al. (2022). *vegan: Community ecology package. R package version 2.6-0.*

Pesce, S., Kergoat, L., Paris, L., Billet, L., Besse-Hoggan, P., and Bonnineau, C. (2021). Contrasting effects of environmental concentrations of sulfonamides on microbial heterotrophic activities in freshwater sediments. *Front. Microbiol.* 12:753647. doi: 10.3389/fmicb.2021.753647

Proia, L., von Schiller, D., Sànchez-Melsió, A., Sabater, S., Borrego, C. M., Rodríguez-Mozaz, S., et al. (2016). Occurrence and persistence of antibiotic resistance genes in river biofilms after wastewater inputs in small rivers. *Environ. Pollut.* 210, 121–128. doi: 10.1016/j.envpol.2015.11.035

Pruden, A., Pei, R., Storteboom, H., and Carlson, K. H. (2006). Antibiotic resistance genes as emerging contaminants: Studies in Northern Colorado. *Environ. Sci. Technol.* 40, 7445–7450. doi: 10.1021/es060413l

Reichert, G., Hilgert, S., Alexander, J., Rodrigues de Azevedo, J. C., Morck, T., Fuchs, S., et al. (2021). Determination of antibiotic resistance genes in a WWTP-impacted river in surface water, sediment, and biofilm: Influence of seasonality and water quality. *Sci. Total Environ.* 768:144526. doi: 10.1016/j.scitotenv.2020.144526

Robeson, M. S., O'Rourke, D. R., Kaehler, B. D., Ziemski, M., Dillon, M. R., Foster, J. T., et al. (2021). RESCRIPt: Reproducible sequence taxonomy reference database management. *PLoS Comput. Biol.* 17:e1009581. doi: 10.1371/journal.pcbi.1009581

Rodriguez-Mozaz, S., Vaz-Moreira, I., Della Varela Giustina, S., Llorca, M., Barceló, D., Schubert, S., et al. (2020). Antibiotic residues in final effluents of European wastewater treatment plants and their impact on the aquatic environment. *Environ. Int.* 140:105733. doi: 10.1016/j.envint.2020.105733

Sabri, N. A., Schmitt, H., van der Zaan, B., Gerritsen, H. W., Zuidema, T., Rijnaarts, H., et al. (2020). Prevalence of antibiotics and antibiotic resistance genes in a wastewater effluent-receiving river in the Netherlands. *J. Environ. Chem. Eng.* 8:102245. doi: 10.1016/j.jece.2018.03.004

Spencer, S. J., Tamminen, M. V., Preheim, S. P., Guo, M. T., Briggs, A. W., Brito, I. L., et al. (2016). Massively parallel sequencing of single cells by epicPCR links functional genes with phylogenetic markers. *ISME J.* 10, 427–436. doi: 10.1038/ismej.2015.124

Švara, V., Krauss, M., Michalski, S. G., Altenburger, R., Brack, W., and Luckenbach, T. (2021). Chemical pollution levels in a river explain site-specific sensitivities to micropollutants within a genetically homogeneous population of freshwater amphipods. *Environ. Sci. Technol.* 55, 6087–6096. doi: 10.1021/acs.est.0c07839

The World Health Organization, The Food and Agriculture Organization of the United Nations, and The World Organisation for Animal Health (2019). *Taking a multisectoral, one health approach: A tripartite guide to addressing zoonotic diseases in countries*. Geneva: World Health Organization.

Tousova, Z., Oswald, P., Slobodnik, J., Blaha, L., Muz, M., Hu, M., et al. (2017). European demonstration program on the effect-based and chemical identification and monitoring of organic pollutants in European surface waters. *Sci. Total Environ.* 601-602, 1849–1868. doi: 10.1016/j.scitotenv.2017.06.032

Wang, J., Chu, L., Wojnárovits, L., and Takács, E. (2020). Occurrence and fate of antibiotics, antibiotic resistant genes (ARGs) and antibiotic resistant bacteria (ARB) in municipal wastewater treatment plant: An overview. *Sci. Total Environ.* 744:140997. doi: 10.1016/j.scitotenv.2020.140997

Wang, Y., Ye, J., Ju, F., Liu, L., Boyd, J. A., Deng, Y., et al. (2021). Successional dynamics and alternative stable states in a saline activated sludge microbial community over 9 years. *Microbiome* 9:199. doi: 10.1186/s40168-021-01151-5

Weitere, M., Altenburger, R., Anlanger, C., Baborowski, M., Bärlund, I., Beckers, L.-M., et al. (2021). Disentangling multiple chemical and non-chemical stressors in a lotic ecosystem using a longitudinal approach. *Sci. Total Environ.* 769:144324. doi: 10.1016/j.scitotenv.2020.144324

Wollschläger, U., Attinger, S., Borchardt, D., Brauns, M., Cuntz, M., Dietrich, P., et al. (2017). The bode hydrological observatory: A platform for integrated, interdisciplinary hydro-ecological research within the TERENO Harz/Central German Lowland Observatory. *Environ. Earth Sci.* 76:29. doi: 10.1007/s12665-016-6327-5

Yuan, Q.-B., Guo, M.-T., and Yang, J. (2014). Monitoring and assessing the impact of wastewater treatment on release of both antibiotic-resistant bacteria and their typical genes in a Chinese municipal wastewater treatment plant. *Environ. Sci. Process Impacts* 16, 1930–1937. doi: 10.1039/c4em00208c

Yue, Z., Zhang, J., Zhou, Z., Ding, C., Wan, L., Liu, J., et al. (2021). Pollution characteristics of livestock faeces and the key driver of the spread of antibiotic resistance genes. *J. Hazard Mater.* 409:124957. doi: 10.1016/j.jhazmat.2020.124957

Zhang, A. N., Li, L.-G., Ma, L., Gillings, M. R., Tiedje, J. M., and Zhang, T. (2018). Conserved phylogenetic distribution and limited antibiotic resistance of class 1 integrons revealed by assessing the bacterial genome and plasmid collection. *Microbiome* 6:130. doi: 10.1186/s40168-018-0516-2

Zhuang, M., Achmon, Y., Cao, Y., Liang, X., Chen, L., Wang, H., et al. (2021). Distribution of antibiotic resistance genes in the environment. *Environ. Pollut.* 285:117402. doi: 10.1016/j.envpol.2021.117402

frontiers | Frontiers in Microbiology

TYPE Original Research
PUBLISHED 16 October 2023
DOI 10.3389/fmicb.2023.1264801

OPEN ACCESS

EDITED BY
Maria Filippa Addis,
University of Milan, Italy

REVIEWED BY
Eunhye Goo,
Seoul National University, Republic of Korea
Bodo Philipp,
University of Münster, Germany

*CORRESPONDENCE
Annabelle Merieau
✉ annabelle.merieau@univ-rouen.fr

RECEIVED 21 July 2023
ACCEPTED 27 September 2023
PUBLISHED 16 October 2023

CITATION
Dupont CA, Bourigault Y, Osmond T, Nier M, Barbey C, Latour X, Konto-Ghiorghi Y, Verdon J and Merieau A (2023) *Pseudomonas fluorescens* MFE01 uses 1-undecene as aerial communication molecule.
Front. Microbiol. 14:1264801.
doi: 10.3389/fmicb.2023.1264801

Pseudomonas fluorescens MFE01 uses 1-undecene as aerial communication molecule

Charly A. Dupont[1,2], Yvann Bourigault[1,2], Théo Osmond[1,2], Maëva Nier[3], Corinne Barbey[1,2], Xavier Latour[1,2], Yoan Konto-Ghiorghi[1,2], Julien Verdon[3] and Annabelle Merieau[1,2]*

[1]Laboratoire de Communication Bactérienne et Stratégies Anti-infectieuses (CBSA UR), Univ Rouen Normandie, Université Caen Normandie, Normandie Univ, Rouen, France, [2]Structure Fédérative de Recherche Normandie Végétale and Entente Franco-Québécoise NOR-SEVE, NORVEGE, Rouen, France, [3]Laboratoire Ecologie and Biologie des Interactions, Université de Poitiers, Poitiers, France

Bacterial communication is a fundamental process used to synchronize gene expression and collective behavior among the bacterial population. The most studied bacterial communication system is quorum sensing, a cell density system, in which the concentration of inductors increases to a threshold level allowing detection by specific receptors. As a result, bacteria can change their behavior in a coordinated way. While in *Pseudomonas* quorum sensing based on the synthesis of *N*-acyl homoserine lactone molecules is well studied, volatile organic compounds, although considered to be communication signals in the rhizosphere, are understudied. The *Pseudomonas fluorescens* MFE01 strain has a very active type six secretion system that can kill some competitive bacteria. Furthermore, MFE01 emits numerous volatile organic compounds, including 1-undecene, which contributes to the aerial inhibition of *Legionella pneumophila* growth. Finally, MFE01 appears to be deprived of *N*-acyl homoserine lactone synthase. The main objective of this study was to explore the role of 1-undecene in the communication of MFE01. We constructed a mutant affected in *undA* gene encoding the enzyme responsible for 1-undecene synthesis to provide further insight into the role of 1-undecene in MFE01. First, we studied the impacts of this mutation both on volatile organic compounds emission, using headspace solid-phase microextraction combined with gas chromatography-mass spectrometry and on *L. pneumophila* long-range inhibition. Then, we analyzed influence of 1-undecene on MFE01 coordinated phenotypes, including type six secretion system activity and biofilm formation. Next, to test the ability of MFE01 to synthesize *N*-acyl homoserine lactones in our conditions, we investigated *in silico* the presence of corresponding genes across the MFE01 genome and we exposed its biofilms to an *N*-acyl homoserine lactone-degrading enzyme. Finally, we examined the effects of 1-undecene emission on MFE01 biofilm maturation and aerial communication using an original experimental set-up. This study demonstrated that the Δ*undA* mutant is impaired in biofilm maturation. An exposure of the Δ*undA* mutant to the volatile compounds emitted by MFE01 during the biofilm development restored the biofilm maturation process. These findings indicate that *P. fluorescens* MFE01 uses 1-undecene emission for aerial communication, reporting for the first time this volatile organic compound as bacterial intraspecific communication signal.

KEYWORDS

bacterial communication, *Pseudomonas fluorescens* MFE01, volatile compounds, biofilm, type six secretion system

1. Introduction

Bacteria exchange chemical signals to communicate with each other (Miller and Bassler, 2001). These signals are used to coordinate gene expression and collective behaviors, including those involved in virulence, at a community level. Consequently, understanding bacterial communication is of the greatest interest for the development of new strategies to control bacterial populations and preventing infections (Waters and Bassler, 2005).

The most studied bacterial communication system is quorum sensing (QS), defined as a population-density-responsive gene regulation system allowing bacteria to sense population density and to act only when a quorum of cells is reached (Waters and Bassler, 2005). The chemical signals used in QS (i.e., autoinducers) are small molecules released and accumulated into the environment by bacteria. The concentration of autoinducers increases with bacterial growth until a threshold level is reached. At this point, these signals molecules are detected by specific receptors and their binding activates positive feedback and change in gene expression, allowing bacteria to adjust their behavior accordingly (Fuqua et al., 1994). In some *Pseudomonas*, QS is mainly based on the synthesis of *N*-acyl homoserine lactone molecules (AHLs) and their perception by a dedicated sensor (Papenfort and Bassler, 2016). In *Pseudomonas aeruginosa* a QS system based on alkyl-quinolone is also present (Papenfort and Bassler, 2016).

QS is a key factor for biofilm development, notably in *P. aeruginosa* (De Kievit, 2009). Biofilms are complex communities of microorganisms embedded in a matrix of extracellular polymeric substances (EPS) (Flemming et al., 2016). These complex structures are commonly found in natural and man-made environments and can have both beneficial and harmful effects, depending on the context (Hall-Stoodley et al., 2004). In addition to biofilm formation, QS regulates other behaviors such as motility or type six secretion systems (T6SSs) (Papenfort and Bassler, 2016; Gallique et al., 2017a).

T6SSs are nanomachines that use a contractile mechanism to propel an effector-loaded needle into target cells (Brackmann et al., 2017; Cherrak et al., 2019; Coulthurst, 2019; Wang et al., 2019). In most *Pseudomonas*, a functional T6SS requires at least 14 core proteins, which assemble onto a membrane complex and a tail structure (Brackmann et al., 2017; Cherrak et al., 2019; Coulthurst, 2019). The tail structure is made of a needle wrapped by a contractile sheath (Basler et al., 2012). The needle comprises the inner tube constituted of Hcp protein hexamers and by a spike complex made of a trimer of VgrG sharpened by PAAR protein that serves as prey cell penetrating device (Leiman et al., 2009; Shneider et al., 2013). The sheath is made of the TssB and TssC subunits and its contraction leads to the expulsion of the needle carrying T6SS effectors (Kapitein and Mogk, 2013). T6SSs are capable to inject a broad repertoire of toxins as anti-bacterial specific effectors, anti-eukaryotic specific effectors or trans-kingdom effectors (Hernandez et al., 2020; Monjarás Feria and Valvano, 2020; Jurėnas and Journet, 2021). In environmental *Pseudomonas,* T6SS plays an essential role in interbacterial competition, allowing bacteria to acquire extracellular elements such as DNA, metallic ions, and participates to bacteria communication (Ho et al., 2014; Hachani et al., 2016; Gallique et al., 2017a).

Volatile compounds (VCs), including volatile organic compounds (VOCs) are also considered to be communication signals within the rhizosphere (Ninkovic et al., 2021). VOCs are byproducts of the primary and secondary metabolism. These molecules are small (molecular weight <500 Daltons), with a high vapor pressure, low boiling point, and a lipophilic part. These physicochemical properties enable these molecules to be in the gaseous state under environmental conditions (Schmidt et al., 2015). Numerous studies have reported interaction between bacteria with plants, fungi, or other bacteria via VOCs emission (Kim et al., 2013; Létoffé et al., 2014; Schmidt et al., 2015; Raza et al., 2016; Netzker et al., 2020; Weisskopf et al., 2021; Vlot and Rosenkranz, 2022).

The *Pseudomonas fluorescens* MFE01 strain is able to protect potato-tuber from soft-rot against the phytopathogen *Pectobacterium atrosepticum* via its T6SS (Smadja et al., 2004; Decoin et al., 2014). Like in other *P. fluorescens* strains, no AHL-based QS system has been detected in MFE01 using biosensor-based assays (Wei and Zhang, 2006; Martins et al., 2014; Gallique et al., 2017b). Nevertheless, MFE01 strain coordinates its population during biofilm formation and swimming when its T6SS is functional (Decoin et al., 2015; Gallique et al., 2017b; Bouteiller et al., 2020). Previous works showed that MFE01, like other *Pseudomonas*, emits a broad range of VOCs (Corre et al., 2021). Among the VOCs emitted on lysogenic broth (LB) medium, MFE01 generates a high amount of 1-undecene which exerts long-range growth inhibition against *Legionella pneumophila*, the etiological agent of legionellosis (Bigot et al., 2013; Corre et al., 2021). A transposition mutant from this previous study suggested a link between T6SS activity and 1-undecene emission. Unfortunately, polar effects caused by transposon insertion did not allow to confirm these observations (Corre et al., 2021).

In this study, we constructed a mutant affected in *undA* gene encoding the enzyme responsible for 1-undecene synthesis to provide further insight onto the physiological role of 1-undecene in MFE01. First, we studied impact of this mutation on MFE01 VOCs emission, using headspace solid-phase microextraction combined with gas chromatography-mass spectrometry (HS-SPME/GC-MS). Then, the *undA* mutation effect was investigated on *L. pneumophila* long-range growth inhibition. We also analyzed influence of 1-undecene on the coordinated phenotypes of MFE01, including biofilm formation and T6SS antibacterial activity. Next, to confirm the inability of MFE01 to produce AHLs, we investigated *in silico* the presence of corresponding genes across its genome and we exposed its biofilms to an AHLs-degrading enzyme. Finally, we characterized the effect of 1-undecene emission on the maturation of MFE01 biofilms.

2. Materials and methods

2.1. Bacterial strains, plasmids, culture conditions and chemicals

All strains and plasmids used in this study are listed in Supplementary Table S1. *P. fluorescens*, *P. aeruginosa*, *Escherichia coli* and *P. atrosepticum* strains were grown in lysogenic broth (LB) medium and *L. pneumophila* lens strain in buffered yeast extract medium or on buffered charcoal yeast extract (BCYE) agar plates (Corre et al., 2019). *P. fluorescens* strains were grown at 28°C, *P. atrosepticum* strain at 25°C, *P. aeruginosa*, *E. coli* and *L. pneumophila* lens strains at 37°C. All liquid cultures were grown under constant rotary shaker at 180 rpm. Media were supplemented with antibiotics, as appropriate: 15 μg/mL tetracycline; 20 μg/mL

or 50 μg/mL gentamycin for *E. coli* or *P. fluorescens*, respectively. Cultures carrying pJN105 plasmid were supplemented with 0.2% L-arabinose for gene expression. All chemicals were purchased from Sigma-Aldrich (St. Louis, MO, United States) unless otherwise stated.

2.2. General molecular biology procedures

PCR reactions were performed under standard conditions using Phusion® high-fidelity DNA polymerase (NEB) in high fidelity buffer. The temperature of primer hybridization was calculated using NEB Tm calculator.[1] Primers listed in Supplementary Table S2 were purchased from Eurogentec, Belgium. Restriction enzymes and T4 DNA ligase were used according to manufacturer's instructions. Genomic DNA extraction and purification were performed using the "Genejet Genomic DNA purification Kit" (Thermo Fisher). PCR products were purified using the "PCR purification Kit" (Qiagen) or the "Gel purification Kit" (Qiagen) from agarose gels. All kits were used accordingly to manufacturers' instructions.

2.3. Construction of the MFE01 Δ*undA* mutant strain

The markerless *undA* in-frame deletion mutant (Δ*undA*) contains a deletion of 762 base pairs (bp) in the *undA* gene. To obtain this deletion, the upstream and downstream regions of *undA* were amplified by PCR with the two primer pairs M1-*undA*/M2QC-*undA* (977 bp) and M3QC-*undA*/M4-*undA* (1,146 bp) respectively. Amplicons were used in overlap-PCR and re-amplified using M1-*undA*/M4-*undA* primers. The deleted *undA* gene construction was introduced into pAKE604 suicide vector (El-Sayed et al., 2001) digested by SmaI via blunt-ended ligation using T4 DNA ligase (NEB) and transformed in *E. coli* top 10 strain (Thermo Fisher Scientific). This construction was verified by Sanger-sequencing (Genewiz, Germany) and introduced into *E. coli* S17.1 strain (Simon et al., 1983). This plasmid was transferred in MFE01 by biparental mating as described by Bouteiller et al. (2020), and double recombination event was selected. The *in frame undA* deletion mutant was checked by PCR analysis and DNA sequencing.

2.4. Insertion of *undA* into pJN105 expression vector

The *undA*-EcoRI-F/*undA*-XbaI-R primers were used to amplify *undA* gene. The amplified fragment (856 bp) and the pJN05 vector were digested with *EcoRI* and *XbaI* to generate cohesive ends. Then, *undA* gene was ligated into the pJN105 plasmid (Newman and Fuqua, 1999), under the L-arabinose-inducible promoter control. The resulting plasmid was checked by sequencing.

1 https://tmcalculator.neb.com/#!/main

2.5. MFE01 transformation by electroporation

Fresh colonies of MFE01 or mutants were resuspended in cold sterile 300 mM sucrose solution (Fisher Chemicals), washed two times, and resuspended in 100 μL of 300 mM sucrose. These competent cells and 150 ng of plasmid were added in 1 mm gap electroporation cuvettes (Fisher brand), electroporated at 1.8 kV for 5 ms, 200 Ω resistance and 25 μF capacitance. LB was added and mixtures were incubated for 1 h 30 min at 28°C with shaking. Transformed bacteria were plating on gentamycin supplemented LB agar.

2.6. Anti-*Legionella* activity tests

L. pneumophila inhibition by MFE01 or mutants was tested using a 6-well plate qualitative long-range inhibition assay as previously described by Corre et al. (2019). Three independents assays were performed for each condition.

2.7. HS-SPME/ GC-MS

VOCs were analyzed as previously described (Corre et al., 2021) with minor modifications. Briefly, an overnight culture of bacteria was inoculated (40 μL adjusted at $OD_{580} = 1$) in sterile headspace screw-cap vial (20 mL) and containing 10 mL of inclined LB agar. Vials were incubated for 24 h at 28°C to allow bacterial growth. Prior to analysis, the 100 μm SPME polydimethylsiloxane (PDMS) fiber (Shimadzu) was preconditioned in the bake-out oven of the injector as recommended by the manufacturer (250°C for 30 min). Extraction duration profiles were carried out for 30 min at 37°C under agitation (250 rpm). Desorption time was set at 5 min in the GC injection port sets at 250°C. GC-MS analyses were performed in a gas chromatograph GC-2010 Plus (Shimadzu). Helium was used as the carrier gas at a constant flow rate of 1.2 mL/min. The injector operated in the spitless mode and its temperature was set at 250°C. The separation of volatile compounds was performed on a SH-Rxi-5 ms column (30 m × 0.25 mmID, 0.25 mm; Shimadzu). The oven temperature program started at 40°C (held for 5 min), was raised at a rate of 4°C/min to 140°C (held for 2 min), raised at a rate of 6°C/min to 190°C (held for 2 min), and then raised at a rate of 15°C/min to 230°C (held for 1 min). The detection was performed by a QP2010 SE mass spectrometer sets in positive electron impact mode (EI) with 70 eV of electron energy. The electron multiplier was set by the auto-tune procedure. MS data were collected in a full scan mode over the *m*/*z* range from 35 to 400 (0.3 s/scan) Transfer line temperature was set at 230°C. At least three independent samples were analyzed for each condition. Once the raw data had been acquired, the peaks were automatically integrated on the basis of the area. Volatile compounds were identified using the NIST20 spectral library, based on the mass spectrum with the highest similarity score (minimum 87%). This is achieved by comparing the mass fingerprints of the unknown compounds eluted with those of 300,000 references. The identity of 1-undecene has already been confirmed by the use of an analytical standard in one of our previous studies (Corre et al., 2021). Only compounds systematically detected in all wild type samples were reported.

2.8. Biofilm culture and staining

Biofilm were developed in 24-well microplates with glass bottoms (Sensoplate, Greiner Bio-One). Overnight culture of MFE01 or mutants were adjusted at $OD_{580} = 1$ in LB and wells were filled with 1 mL of bacterial suspension. Plates were incubated at 28°C (*P. fluorescens*) or 37°C (*P. aeruginosa*) for 48 h and the medium was renewed after 24 h of incubation. When needed, biofilms were developed in separated plates to avoid volatile compounds interferences between cultures. The effect of QsdA on MFE01 biofilm structure was studied by adding 24 µg (i.e., 6.74 10–4 µmol) of QsdA to MFE01 cultures. After incubation, biofilms were washed twice with saline water (NaCl 9 gL^{-1}) and stained with 5 µM Syto9 green-fluorescent dye (Invitrogen) for 15 min at room temperature. Five independent assays were performed for each condition.

2.9. Adhesion assay

Bacterial cultures were centrifuged 3 min at 8000 g and pellets were resuspended in saline water. Bacterial suspensions were then equilibrated at $OD_{580} = 0.1$ and 1 mL was deposited in a well of a 24-well polystyrene plate (Thermo Fisher Scientific). A 10 mm diameter sterile coverslip (Epredia) was deposited on the bottom of each well. After 2 h of incubation at 28°C in separate plates to avoid interferences by volatile compounds, each well was washed once with saline water and cells were stained with 5 µM Syto9 green-fluorescent dye for 15 min at room temperature. After one additional wash with saline water, coverslip was positioned between slide (VWR) and cover-slide (VWR) using ProlongDiamond® (Invitrogen) as mounting medium. Three independent assays were performed for each condition.

2.10. Biofilm exposition to volatile compounds

To expose biofilm to MFE01 or mutants' volatile compounds, two wells of a 24-well glass bottom plate were filled with 2 mL of LB agar (LBg). Then, 10 µL of a bacterial suspension equilibrated at $OD_{580} = 10$ were deposited on LBg and plates were incubated overnight prior to start biofilm culture. Each biofilm culture was adjacent to two LBg-filled wells. To expose biofilm to pure 1-undecene, the same protocol was used with modifications. A mixed cellulose membrane (Merk) was deposited on each LBg-filled well. A 220 µM 1-undecene solution in 100% ethanol was prepared from pure 1-undecene. 2 µL of this solution were deposited on membranes at the beginning of biofilm cultures. After 24 h of incubation, 1-undecene was renewed.

2.11. Confocal laser scanning microscopy

Biofilm observation and quantification of average thickness and biovolume were performed as described by Bourigault et al. (2021) using the Comstat 2.0 software (Heydorn et al., 2000). Surface coverage was determined as described by Cambronel et al. (2019) using the ImageJ software (Schneider et al., 2012).

2.12. Supernatant protein extraction

Overnight cultures (5 mL) were centrifuged at 7,500 g for 5 min at room temperature. 2 mL of supernatant were filtered through a 0.22 µm Millipore membrane (Merck). Trichloroacetic acid was added to 10% final concentration and mixture was incubated at 4°C overnight. Solution was then centrifuged at 13,000 g for 30 min at 4°C and supernatant was discarded. The pellet was washed twice with 2 mL cold 100% acetone (VWR chemicals) and centrifuged at 13,000 g, for 30 min at 4°C. Finally, the pellet was air dried for 30 min and resuspended with 20 µL of 2X Laemmli buffer (Nupage®, Invitrogen) containing 5% β-mercapto-ethanol. Three independent assays were performed for each condition.

2.13. SDS-PAGE analysis

Protein solutions were incubated for 5 min at 95°C and proteins corresponding to 1 mL of supernatant were separated on a 12% bis-acrylamide (Biorad) gel. Protein electrophoresis and visualization were performed as previously described (Bouteiller et al., 2020). Hcp identification by MALDI-TOF was carried out as previously described (Decoin et al., 2014).

2.14. Killing assay, mucoid phenotype and swimming motility

Killing assays, mucoid and swimming phenotypes were performed as previously described using *tssC* mutant strain, defective for T6SS activity, as negative control (Maurhofer et al., 1998; Decoin et al., 2014, 2015; Chane et al., 2019; Bouteiller et al., 2020). Three independent assays were performed for each condition.

3. Results

3.1. The *undA* deletion impairs 1-undecene emission and *Legionella pneumophila* aerial inhibition

In order to investigate impacts of 1-undecene emission on the physiology of MFE01, we managed to construct a MFE01 mutant unable to emit 1-undecene. The UndA enzyme was previously described in the *P. fluorescens* Pf-5 strain to catalyze 1-undecene synthesis by oxidative decarboxylation of cytoplasmic lauric acid (Rui et al., 2014) (Supplementary Figure S1). The presence of a single copy of *undA* gene (GenBank accession number: OQ434583.1) in MFE01 genome led to the construction of a MFE01 *undA* in frame deletion mutant, named Δ*undA*. In LB medium the Δ*undA* mutant showed no difference in growth compared to the wild type (WT) strain (Supplementary Figure S2). By using HS-SPME/GC–MS analysis, we analyzed VOCs emitted by MFE01 (WT) (Supplementary Figure S3A) and the Δ*undA* mutant. We defined a "core volatilome" in the WT strain as the VOCs systematically detected in our conditions. VOCs emitted with lower reproducibility were not considered here. Seven VOCs composed this "core volatilome," belonging to the alkene, alkane, methyl ketone and

10.3389/fmicb.2023.1264801

alcohol chemical classes (Figure 1A). In the Δ*undA* mutant, the 1-undecene was never detected whereas the other VOCs were emitted in a similar amount comparatively to the WT strain (Figure 1A). Detection of 1-undecene by HS-SPME/GC-MS demonstrated that *ΔundA* mutant containing the empty pJN105 vector (*ΔundA* + EV) was not able to emit 1-undecene, in contrast to the WT strain containing the empty pJN105 vector (WT + EV) (Figure 1B; Supplementary Figure S3). In order to confirm the role of *undA* in 1-undecene emission, we cloned the *undA* gene in the L-arabinose inducible pJN105 plasmid (Newman and Fuqua, 1999). *In trans* expression of the *undA* gene in *ΔundA* mutant (*ΔundA* + *undA*) restored 1-undecene emission (Figure 1B). These results demonstrated that 1-undecene synthesis in MFE01 only occurs via UndA in our conditions. Interestingly, the overexpression of *undA* in the *ΔundA* + *undA* strain lead to an increase of 1-undecene emission (approximately a 5 folds increase in arbitrary units A.U.) and a weak

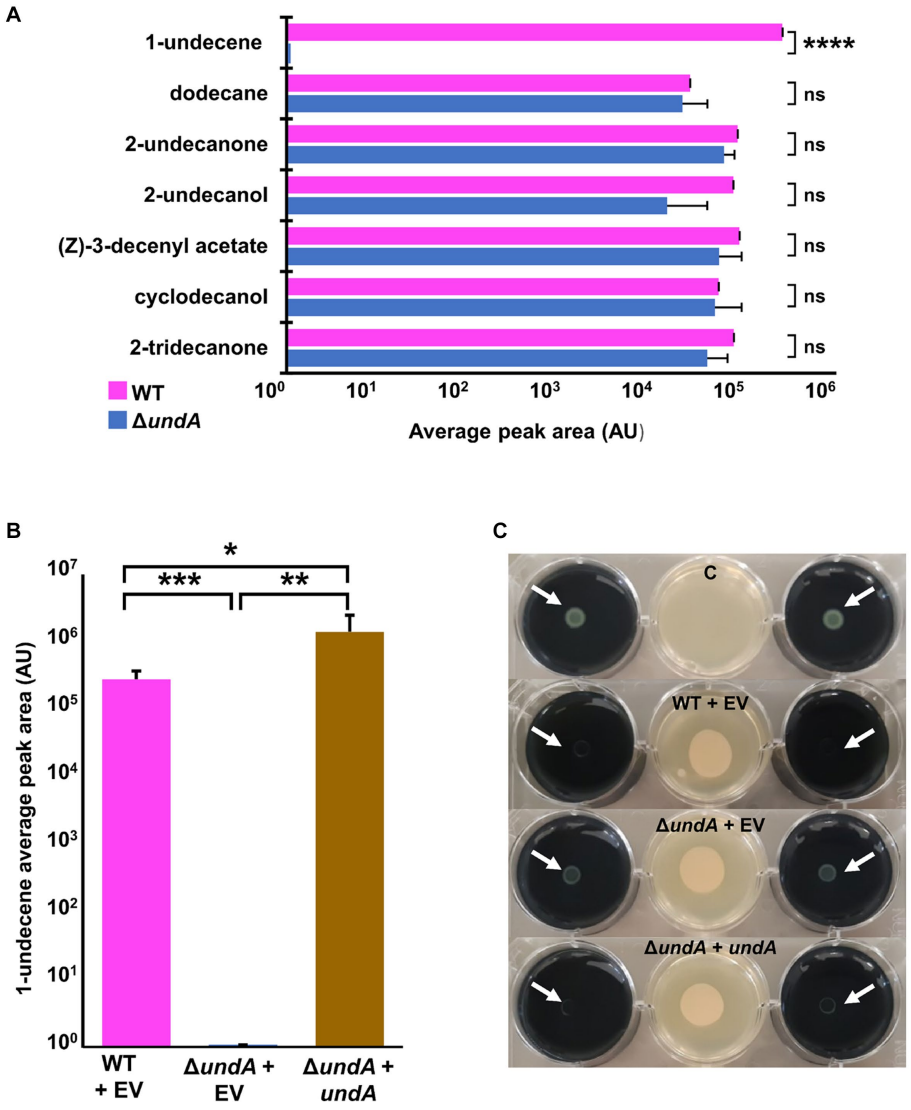

FIGURE 1
Emission of VOCs and *L. pneumophila* long-range inhibition. **(A)** Detection of main VOCs emitted from *P. fluorescens* MFE01 (WT) and its Δ*undA* mutant was realized by headspace SPME/GC-MS. Each strain was cultured in LB medium for 24 h and a suspension diluted at OD_{580} = 1 was deposited on a sterile GC vial filled with LB. Vials were then incubated for 24 h at 28°C and analyzed by SPME/GC–MS. VOCs detected from the Δ*undA* mutant headspace were compared to the VOCs systematically detected from the WT strain headspace. **(B)** Detection of 1-undecene emission from *P. fluorescens* MFE01 and mutants was realized by headspace SPME/GC-MS. Each strain was cultured in LB medium for 24 h and a suspension diluted at OD_{580} = 1 was deposited on a sterile GC vial filled with LB agar supplemented with 0.2% L-arabinose. Vials were then incubated for 24 h at 28°C and analyzed by SPME/GC-MS. ns, not significant; *$p < 0.05$, **$p < 0.01$, ***$p < 0.001$, and ****$p < 0.001$ (*t*-test). Data represent the mean of at least 3 independent experiments. Error bars indicate standard deviations. A.U. means arbitrary units. GC spectrum is in Supplementary Figure S2. **(C)** Volatile interference between *P. fluorescens* MFE01 containing pJN105 empty vector (WT + EV), *undA* mutant containing pJN105 empty vector (Δ*undA* + EV) or *undA* mutant containing *undA* cloned into pJN105 (Δ*undA* + *undA*) and GFP-tagged *L. pneumophila* Lens growth was determined using the 6-well plate assay. Growth of *L. pneumophila* Lens was monitored after 96 h of incubation at 28°C in absence or in presence of MFE01 or its mutants spread on the center of a 6-well plate. The absence of *L. pneumophila* lens growth indicates a volatile-dependent inhibitory phenotype. C means control without MFE01 or its mutants, EV means empty pJN105 vector. Initial plating of *L. pneumophila* Lens suspension on the agar plate is indicated by white arrows. Images are representative of three independent experiments.

additional synthesis of 1-4-undecadiene, a C11:1,4 alkadiene (Supplementary Figures S3B, S4). Then, the Δ*undA* mutant was tested to gain insight into the role of 1-undecene in *L. pneumophila* growth inhibition. Compared to the WT + EV strain, the Δ*undA* + EV mutant was attenuated in its ability to inhibit the growth of *L. pneumophila* (Figure 1C). Moreover, overexpression of *undA* in the Δ*undA* mutant restored antagonizing capacity of MFE01, confirming that *undA* gene expression in MFE01, and consequently 1-undecene emission, is important for the growth inhibition of *L. pneumophila* at distance. Interestingly, it appeared that the growth of *L. pneumophila* was still weakly inhibited by the (VCs) emitted by the Δ*undA* + EV mutant comparatively to the control condition (Figure 1C).

3.2. The T6SS of MFE01 and related phenotypes are not regulated by 1-undecene

In previous work, we identified a potential link between 1-undecene emission and T6SS activity in a transposition mutant, but we were unable to explain this crosstalk (Corre et al., 2021). Moreover, previous studies demonstrated that T6SS is essential for antibacterial activity, swimming and mucoid phenotype in MFE01 (Decoin et al., 2014, 2015; Gallique et al., 2017b; Bouteiller et al., 2020). Then, we compared the Δ*undA* mutant with the WT strain and the MFE01 Δ*tssC* mutant (T6SS-inactivated mutant) (Decoin et al., 2015) for Hcp-secretion, antibacterial activity, mucoidy and swimming (Figures 2A–D, respectively). The secretion of Hcp proteins into the medium is described as the "hallmark" of a functional T6SS (Pukatzki et al., 2009). SDS-PAGE analysis of Δ*undA* mutant supernatant proteins revealed an Hcp secretion equivalent to that observed for the WT strain, corresponding to an active T6SS (Figure 2A). To confirm these results, we managed MFE01 or Δ*undA* killing assays against *P. atrosepticum* (*Pca*) (Decoin et al., 2014). After 4 h of contact, MFE01 and Δ*undA* killed in the same efficiency *P. atrosepticum in vitro*, decreasing cell counts by five-log compared to *Pca* counting without predatory cells (Figure 2B). During this experiment, each killing assay was performed in separate plates to avoid VCs interference between strains. Mucoid and swimming phenotypes were impaired in the T6SS-inactivated Δ*tssC* mutant while the Δ*undA* mutant was not impacted in its mucoid and swimming phenotype, whether in the same box or in a separate box from the WT strain (Figures 2C,D). These results indicated that 1-undecene does not regulate T6SS activity and related phenotypes.

3.3. The *undA* gene expression modulates biofilm maturation in *Pseudomonas fluorescens* MFE01

To test 1-undecene impact on MFE01 coordinated phenotypes, we investigated biofilm formation and maturation in MFE01 and Δ*undA* mutant (Figure 3), and in the presence of the empty vector pJN105 or the *undA* gene cloned in the pJN105 vector (Figure 4). Biofilm formation assays were carried out on glass surface. To avoid VCs interferences, each biofilm assay was performed in separate compartment in the same incubator. Biofilms were visualized using confocal laser scanning microscopy (CLSM) after Syto9 nucleic acid-staining. The WT strain (Figure 3A) formed an aerial biofilm with cells dispersed in the matrix. These biofilms were heterogenous, containing aggregate in no mushroom-like structure and flatter zones. In contrast, the Δ*undA* mutant formed a flatter and non-matured biofilm, without notable cell aggregate. Biovolumes and average thicknesses were quantified by Comstat 2.0 analysis and corroborated these observations with a 60% and 50% decrease for each parameter, respectively (Figures 3B,C). Moreover, we evaluated the surface adhesion capacity of both WT and Δ*undA* strains. The two strains adhered on the surface equivalently, with an average surface covered corresponding to 6% of the total surface area (Supplementary Figure S5). As a result, *undA* gene seems to be implicated in biofilm maturation process and not in the ability to adhere on glass surface. In the presence of the pJN105 plasmid, the WT strain produced heterogenous mature biofilms in static conditions and contained cell-aggregates without mushroom like structures, while the Δ*undA* mutant formed a flatter non-maturated biofilm (Figure 4A). In these assays, the medium was supplemented with 0.2% L-arabinose and 50 μg mL^{-1} gentamycin sulfate. *In trans* overexpression of *undA* in Δ*undA* mutant restored the biofilm maturation but biofilms contained more aggregates than the WT strain biofilms. These observations were correlated by quantification of biovolume and average thickness using Comstat 2.0. The *undA* mutation did not significantly affect the biofilm biovolume (Figure 4B) but significantly reduced the average thickness (60% decrease). Intriguingly, in these conditions (with L-arabinose), the biofilm biovolume was not impacted by the *undA* deletion, contrary to that observed for the plasmid-free strains (Figure 3). We measured the impact of L-arabinose and pJN105 plasmid on 1-undecene emission in WT using HS-SPME/GC-MS. The presence of L-arabinose or plasmid did not alter the amount of 1-undecene emitted by MFE01 (Supplementary Figure S6).

3.4. In our conditions, biofilm maturation seems not AHL dependent in MFE01

A previous work using biosensor strains to detect AHL signals indicated the absence of medium or long chain AHL production by MFE01 (Gallique et al., 2017b). Since AHL-based QS is considered a key factor for biofilm development for many bacterial species, we wanted to test if MFE01 produced AHL in our conditions. However, biosensors are limited in the range of detectable molecules, and other lactone-containing QS molecules might be produced by MFE01. To challenge this possibility, we performed *in silico* detection of putative QS system's genes in MFE01 genome using the tblastn software on the Basic Local Alignment Search Tool (BLAST) (Altschul et al., 1990). We searched for genes encoding AHLs synthesis proteins. Comparison using tblastn with RhlI (AAC44037.1), LasI (WP_134630090.1), LuxI (AAP22376.1) and TraI (AAZ50473.1) protein sequences versus MFE01 translated genome did not provide any results, suggesting an absence of gene encoding AHLs synthesis protein in MFE01 genome. The same method was applied to identify AHLs receptors homologous to *P. aeruginosa* RhlR (WP_003119559.1), LasR (WP_003082999.1) and QscR (WP_003118960.1) or *Alivibrio fischeri* LuxR receptor (WP_011263745.1), *Agrobacterium tumefaciens* TraR receptor (WP_010974900.1) and *E. coli* SdiA receptor (WP_001152715.1). Each of these proteins matched with a putative protein encoded by a single gene in MFE01 genome with an identity

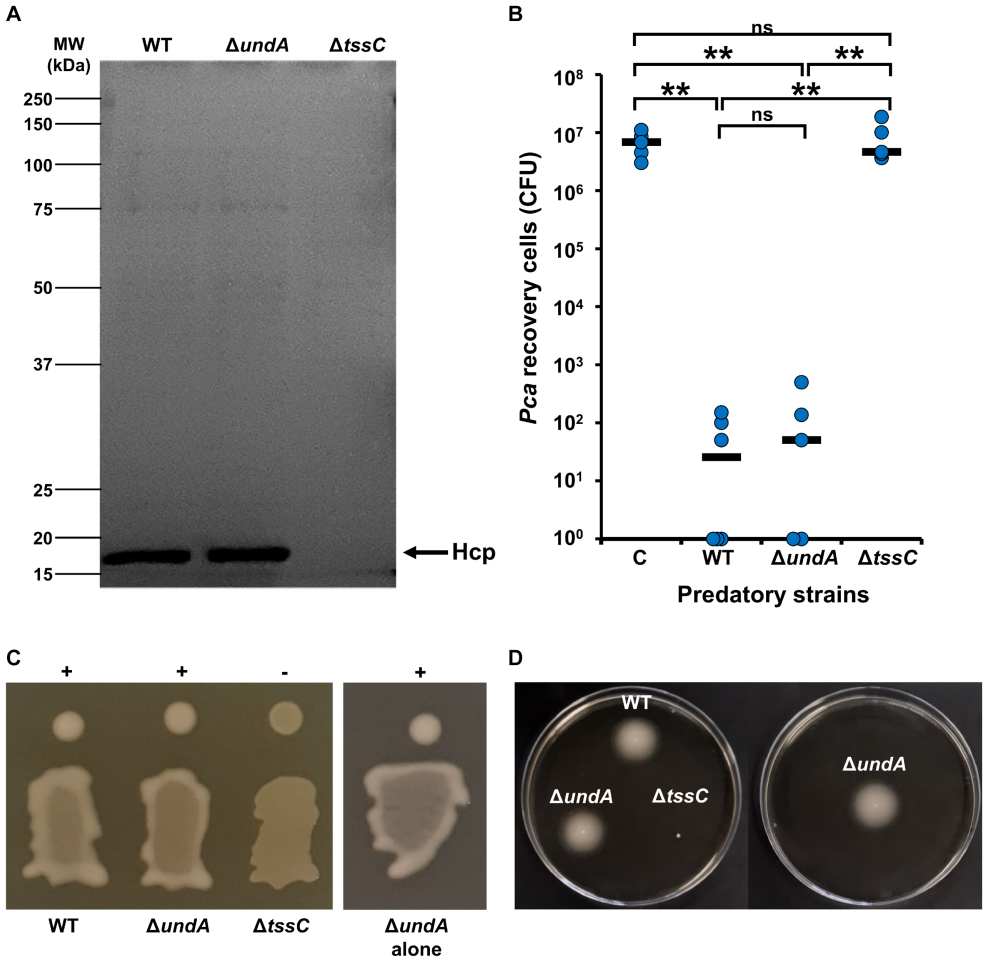

FIGURE 2
T6SS activity, mucoïdy and swimming motility. **(A)** Hcp secretion analysis. Supernatant of culture in stationary phase were concentrated and analyzed by SDS-PAGE (12% separation gel) and Coomassie staining. Arrows indicate the Hcp band, identified by Maldi/ToF. The image shown is representative of 3 assays ($n = 3$). **(B)** Killing activity of MFE01 and mutants. Contacts between the prey *P. atrosepticum* + PME6000: sfGFP-*mcherry* and the indicated predatory strains were performed. After 4 h of incubation at 28°C, number of recovered *Pca* were counted. $^{**}p < 0.01$; ns, not significant (*t*-test). C means control condition without predatory strain. WT: MFE01 Wild-type strain as predator. Δ*undA*: Δ*undA* strain as predator. Δ*tssC*: Δ*tssC* strain as predator. Horizontal bars represent median of 5 independent experiments. **(C)** Mucoidy was assessed on LB agar after 24 h of incubation at 28°C. +: mucoid. –: mucoid. Mucoidy of Δ*undA* mutant was performed in the same plate that the WT strain and alone. **(D)** Swimming assays were performed on 0.3% LB agar for 24 h at 28°C.

percentage in a range from 19.18% (TraR) to 30.8% (QscR) (Supplementary Figure S7A). Analysis of the putative protein sequence with Interproscan software (Jones et al., 2014) revealed that the corresponding putative protein contains two domains. The N-terminal domain (amino acids 4 to 166) belongs to the "Transcription factor LuxR-like, autoinducer-binding domain superfamily (IPR036693)" and the C-terminal to the "Winged helix-like DNA-binding domain superfamily (IPR036388)" (Supplementary Figure S7B). Thus, it appeared that this gene may encode an autoinducer-binding-domain-containing protein, able to bind to AHLs and to bind to DNA after homodimerization. Interestingly, this putative protein is identical to a protein of *Pseudomonas moraviensis* (MBH3446738.1) (Supplementary Figure S7C).

To determine if biofilm formation is AHLs-dependent in MFE01, under our conditions, i.e., in the absence of exogenous AHLs, we performed biofilm assays in presence of the lactonase QsdA. QsdA is an enzyme able to hydrolyze the lactone ring of a wide range of AHLs (Barbey et al., 2018), impairing biofilm formation of γ-proteobacteria using AHLs-based QS (Bourigault et al., 2021). No difference was observed on biofilm architecture, biovolume and average thickness by the QsdA addition to MFE01 cultures, suggesting that AHLs are not produced or do not influence MFE01 biofilm in our conditions (Figures 5A–C). On the contrary, *P. aeruginosa* H103 (AHLs producer) (Hancock and Carey, 1979; Tahrioui et al., 2019) exposure to QsdA caused a decrease in biofilm formation (Supplementary Figure S8).

3.5. 1-undecene is a potential aerial communication molecule

To test whether 1-undecene might be an aerial communication molecule, we performed biofilm assays using a specific experimental

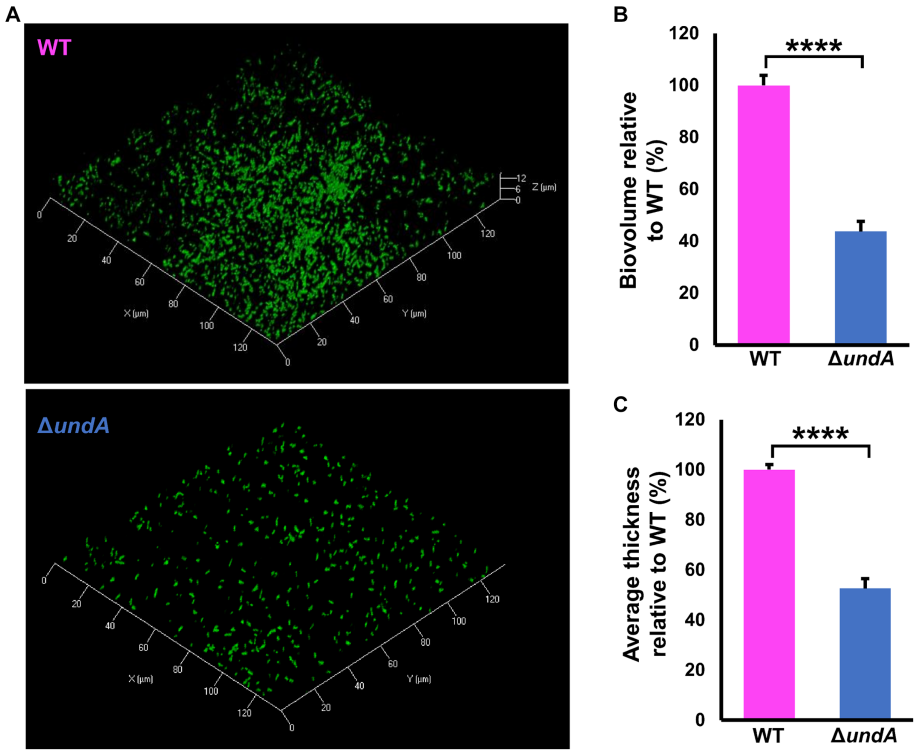

FIGURE 3
1-undecene emission and biofilm maturation. Biofilms were grown in static condition on a glass surface of a 24 well plate for 48 h at 28°C in LB medium containing 0.2% L-arabinose. **(A)** Confocal laser scanning microscopy analysis of MFE01 + pJN105, Δ*undA* + EV and Δ*undA* + *undA* mutants. Representative biofilm 3D shadow representations are shown. Bacteria were visualized with the Syto 9® green fluorescent nucleic acid stain. **(B)** Comstat analyses of biofilms biovolume. **(C)** Comstat analyses of biofilm average thickness. *$p < 0.05$ and **$p < 0.01$; ns, not significant (*t*-test). Data represent the mean of 5 independent experiments. Error bars represent standard error of the mean. EV means empty pJN105 vector.

setup (Figures 6A–D, left panels and Supplementary Figure S9). In each microtiter plate used for biofilm culture, two wells adjacent to the well exploited for biofilm development were filled with 2 mL of LB agar. Depending on the conditions, 10 µL of a bacterial suspension adjusted to $OD_{580} = 10$ of the WT or the Δ*undA* mutant or 2 µL of 220 µM 1-undecene solution were spotted on the LB agar. This setup allowed an exposure of the biofilm culture to the VCs emitted by the bacteria spotted on the LB agar or to pure 1-undecene. The quantity of pure 1-undecene used in this assay corresponds to 1-undecene measured in GC-vial after MFE01 growth during 24 h as described by Corre et al. (2021). The WT strain exposed to the VCs emitted by the LB (WT + LB VCs, Figure 6A, middle panel) formed a thick biofilm with mushroom-like aggregates while the Δ*undA* strain (Δ*undA* + LB VCs, Figure 6A, right panel) made a non-structured biofilm with numerous aggregates dispersed on the surface. The WT strain and the Δ*undA* mutant exposed to VCs emitted by the WT strain constituted homogenous biofilms with few non-mushroom aggregates, like the WT strain biofilm shown in Figures 3, 6B. In Figure 6C, MFE01 and Δ*undA* exposed to VCs emitted by the Δ*undA* mutant did not form similar biofilms. In this setup, the WT strain (Figure 6C, middle panel) developed a biofilm with some "hairy" microcolonies and surface adherent cells, whereas the Δ*undA* mutant formed a sparse biofilm with smaller number and size of microcolonies (Figure 6C, right panel). Exposed to pure 1-undecene, MFE01 and Δ*undA* formed biofilms that appear identical (Figure 6D) and similar to those visualized when *undA* was overexpressed (Figure 4C). Comstat 2.0 analysis (Figure 7) revealed that the Δ*undA* mutant (Figures 7A,B) built a biofilm reduced in its biovolume (50% decrease) without impact on the average thickness. In this experimental setup, biofilms seem to be slightly modified by the volatile compounds emitted by the LB agar medium in comparison with the biofilm developed by the WT strain showed in Figure 3. When exposed to MFE01's VCs, the Comstat 2.0 analysis (Figures 7C,D) did not reveal any difference on biofilm biovolume or average thickness between the WT and Δ*undA* strains. Then it appeared that volatile compounds emitted by MFE01 restored the biofilm development of the Δ*undA* 1-undecene deficient strain. The Comstat 2.0 analysis during Δ*undA* mutant's VCs exposition (Figures 7E,F) showed a decrease of biofilm biovolume and average thickness for the Δ*undA* mutant comparatively to the WT strain (50%). These observations confirmed that VCs, emitted by MFE01 and lacking in Δ*undA*, modulate biofilm maturation. No significant difference in biovolume or mean biofilm thickness was obtained after Comstat 2.0 analysis between WT and Δ*undA* mutant during 1-undecene exposure (Figures 7G,H). Thus, the presence of pure 1-undecene seems sufficient to restore the maturation of the biofilm.

4. Discussion

The UndA and UndB enzymes that catalyze 1-undecene synthesis by oxidative decarboxylation of lauric acid were previously studied by

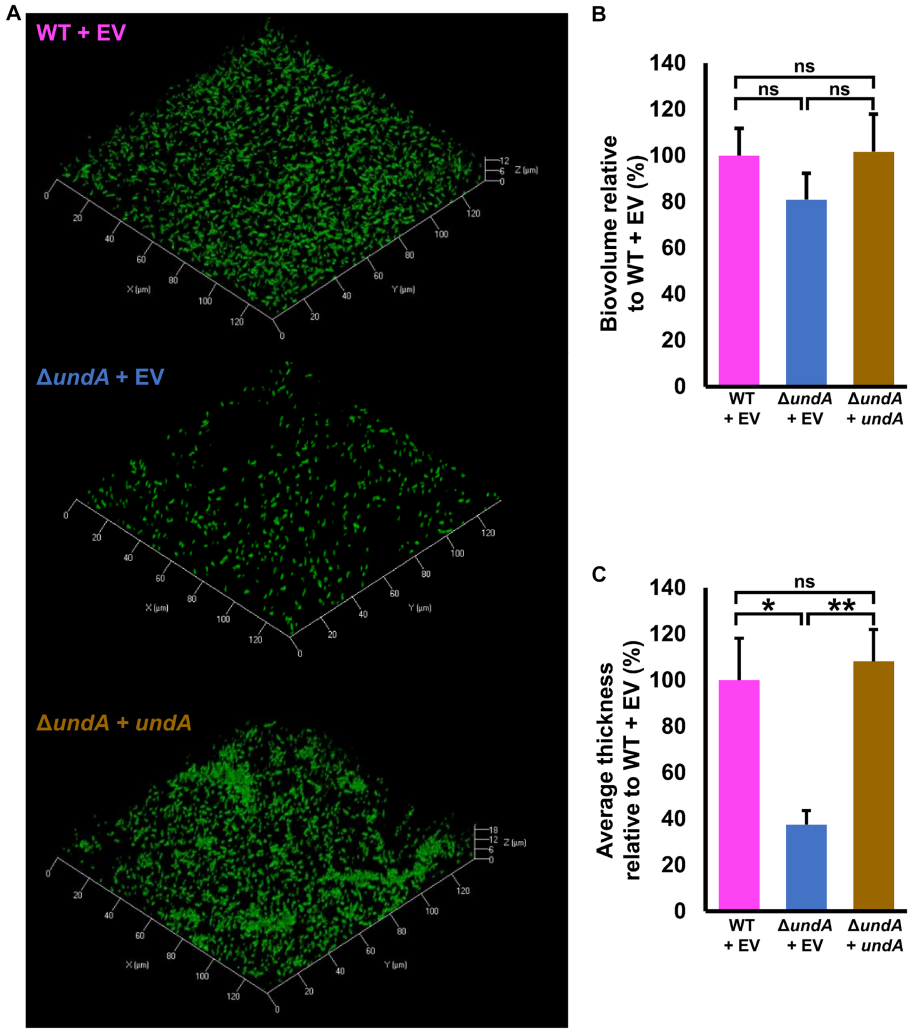

FIGURE 4
Effect of *undA* mutation on biofilm maturation. Biofilms were grown in static condition on glass surface of a 24 well plate for 48 h at 28°C in LB medium. **(A)** Confocal laser scanning microscopy analysis of MFE01 and its Δ*undA* deletion mutant. Representative biofilm 3D shadow representations are shown. **(B)** Comstat analyses of biofilms biovolume **(C)** Comstat analyses of biofilm average thickness. ****$p < 0.0001$; ns, not significant; (*t*-test). Data represent the mean of 5 independent experiments. Error bars indicate standard error of the mean.

Rui et al. (2014, 2015). Currently, they are mainly studied in synthetic biology field for their high value in biofuel production, allowing valorization of multiple pollutants and wastes via various metabolic engineering strategies (Herman and Zhang, 2016; Chatterjee et al., 2018; Wang et al., 2018; Luo et al., 2019; Liu and Li, 2020; Salmela et al., 2020; Khanongnuch et al., 2022). Bioinformatical predictions designated UndB as a membrane bound desaturase (Rui et al., 2015). UndB is active on a broad range of free fatty acids (from C4:0 to C18:0), with a maximal affinity for lauric acid (C12:0) (Yunus et al., 2018, 2022). UndB allows emission of alkene in *Saccharomyces cerevisiae* which suggests UndB ability to translocate alkene across the membrane along with decarboxylation. In contrast the *undA* gene need co-expression of the human long-chain fatty acid transporter FATP1 to allow efficient 1-undecene emission in *S. cerevisiae* (Zhou et al., 2018). UndA is described as a cytoplasmic oxygen-activating nonheme iron-containing oxidoreductase. The reaction is probably catalyzed via substrate binding (i.e., free fatty acid from C10:0 to C14:0) to the Fe^{2+} center, which triggers electron transfer, leading to substrate oxidation, Fe^{2+} reduction and formation of H_2O and CO_2 (Rui et al., 2014). In *E. coli*, *undA* heterologous expression resulted in 1-undecene emission on LB medium (Rui et al., 2014) while medium supplementation in lauric acid is required for 1-undecene production during *undB* heterologous expression (Rui et al., 2015). These results indicate that in bacteria UndA decarboxylates fatty acid synthesized by cell metabolism while UndB decarboxylates fatty acids from the external environment. Our results confirmed the UndA requirement for 1-undecene emission by MFE01 and demonstrated that an overexpression of *undA* lead to an increase of 1-4-undecadiene emission. The role of UndA in 1-4-undecadiene synthesis was never stated but is consistent with UndA ability to bind to multiple substrates (Rui et al., 2014). Despite a low affinity, when UndA is present in large quantities, it could bind to dodec-4-enoic acid, allowing the synthesis of 1-4-undecadiene.

In this study, lack of 1-undecene emission decreased *L. pneumophila* aerial killing, even if slight inhibitory activity was still observed. We concluded that MFE01 may emit other VC able to limit

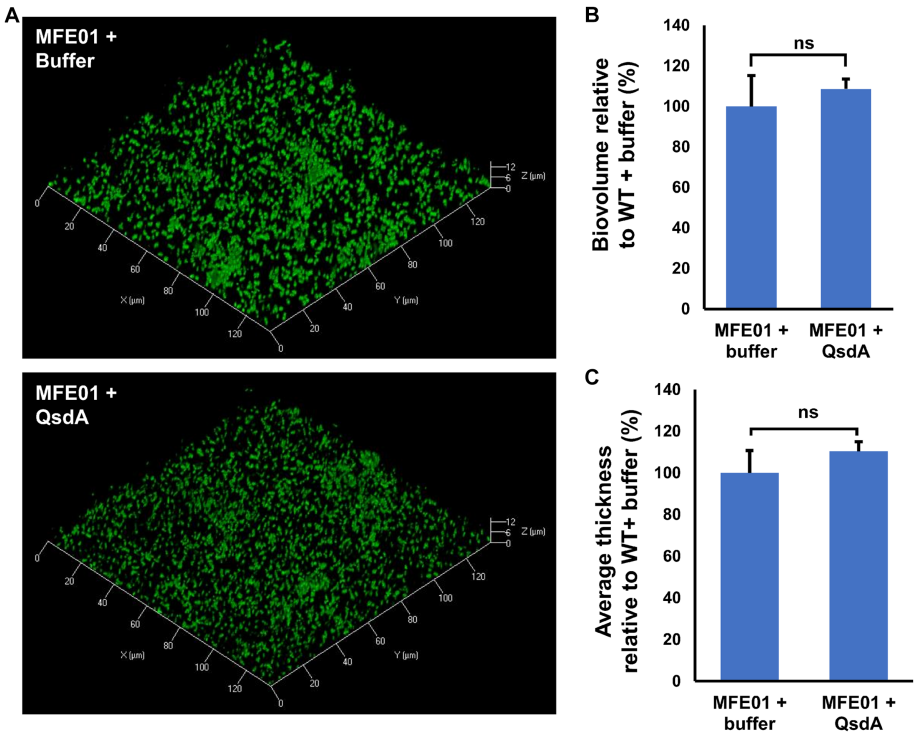

FIGURE 5
Effect of QsdA lactonase on MFE01 biofilm maturation. Biofilms were grown in static condition on a glass surface of a 24 well plate for 48 h at 28°C in LB medium. Medium was supplemented with 50 µL of buffer containing or not 24 µg of purified QsdA. **(A)** Confocal laser scanning microscopy analysis of MFE01 + Buffer or MFE01 + QsdA. Representative biofilm 3D shadow representations are shown. Bacteria were visualized with the Syto 9® green fluorescent nucleic acid stain. **(B)** Comstat analyses of biofilms biovolume. **(C)** Comstat analyses of biofilm average thickness. ns, not significant; (*t*-test). Data represent the mean of 3 independent experiments. Error bars indicate standard error of the mean.

L. pneumophila growth. Concordantly, in a previous work, one of the MFE01 transposition mutants was unable to inhibit the growth *L. pneumophila* (Corre et al., 2021). This mutant was impaired in emission of 1-undecene, 2-undecanone and 2-tridecanone. Purified 2-undecanone is described to possess nematocidal, antifungal and antibacterial activities (Gu et al., 2007; Popova et al., 2014; Giorgio et al., 2015; Lemfack et al., 2018), while 2-tridecanone has been associated with nematocidal activity, plant-bacteria communication and interference with bacterial social phenotypes (Ryu et al., 2004; Xu et al., 2015; Lemfack et al., 2018; López-Lara et al., 2018). Thus, it is probable that MFE01 inhibits *L. pneumophila* growth using a VCs cocktail, including mostly 1-undecene and likely 2-undecanone and/or 2-tridecanone.

Here, we demonstrated that the T6SS activity of MFE01 and related phenotypes, i.e., Hcp proteins secretion, killing activity, swimming and mucoidy, are not regulated by 1-undecene emission. These results thus invalidate our previous hypothesis formulated during the study of a transposition mutant impaired for VOCs emission and T6SS activity (Corre et al., 2021). This mutant contained an insertion of the transposon into one of the genes of tryptophan metabolism (the *trpE* gene). As a different phenotype was observed with an *in-frame* mutation in the *trpE* gene, we had also hypothesized a polar effect of the transposon insertion, resulting in an unexplained disturbance of a common regulatory pathway for the T6SS and the emission of VOCs. In literature, several studies report regulations of VOC emission and T6SSs by the two-component system (TCS) GacA/GacS (Cheng et al., 2013, 2016; Allsopp et al., 2017). Therefore, it seems relevant to study the impact of this TCS on MFE01 phenotypes. Experimentations concerning the role of the GacA/GacS system on 1-undecene emission and T6SS activity in MFE01 are underway in our laboratory.

One of our major findings is the key role of the *undA* expression, and therefore the 1-undecene synthesis, in the maturation of the MFE01 biofilm. This result is consistent with previously 1-undecene detection from *P. aeruginosa* biofilms (Koehler et al., 2020). Moreover, Rui and collaborators reported that *undA* gene is always associated with *rbdA* gene among various *Pseudomonas* genomes (Rui et al., 2014). RbdA seems to be implicated in signal recognition and biofilm modulation by modifying the ci-di-GMP homeostasis (An et al., 2010; Roy et al., 2012; Eilers et al., 2022). Work is planned to study the involvement of RbdA in maturation of biofilm during 1-undecene emission.

MFE01 genome analyses did not revealed any gene encoding AHLs synthesis protein and the addition of QsdA lactonase, purified from the quorum quenching agent *Rhodococcus erythropolis* R138, did not affect the maturation of biofilm in MFE01. It was previously demonstrated that QsdA both silences AHL communication from diverse bacteria and prevents biofilm formation in *Rhizobium rhizogenes* 5520^T (Barbey et al., 2018; Bourigault et al., 2021). These results are consistent with previously published infructive detection of AHL by biosensors (Gallique et al., 2017b), suggesting that MFE01 does not use AHLs-based QS system in our conditions. The lack of AHL-based QS and the key role of *undA* in biofilm maturation allow

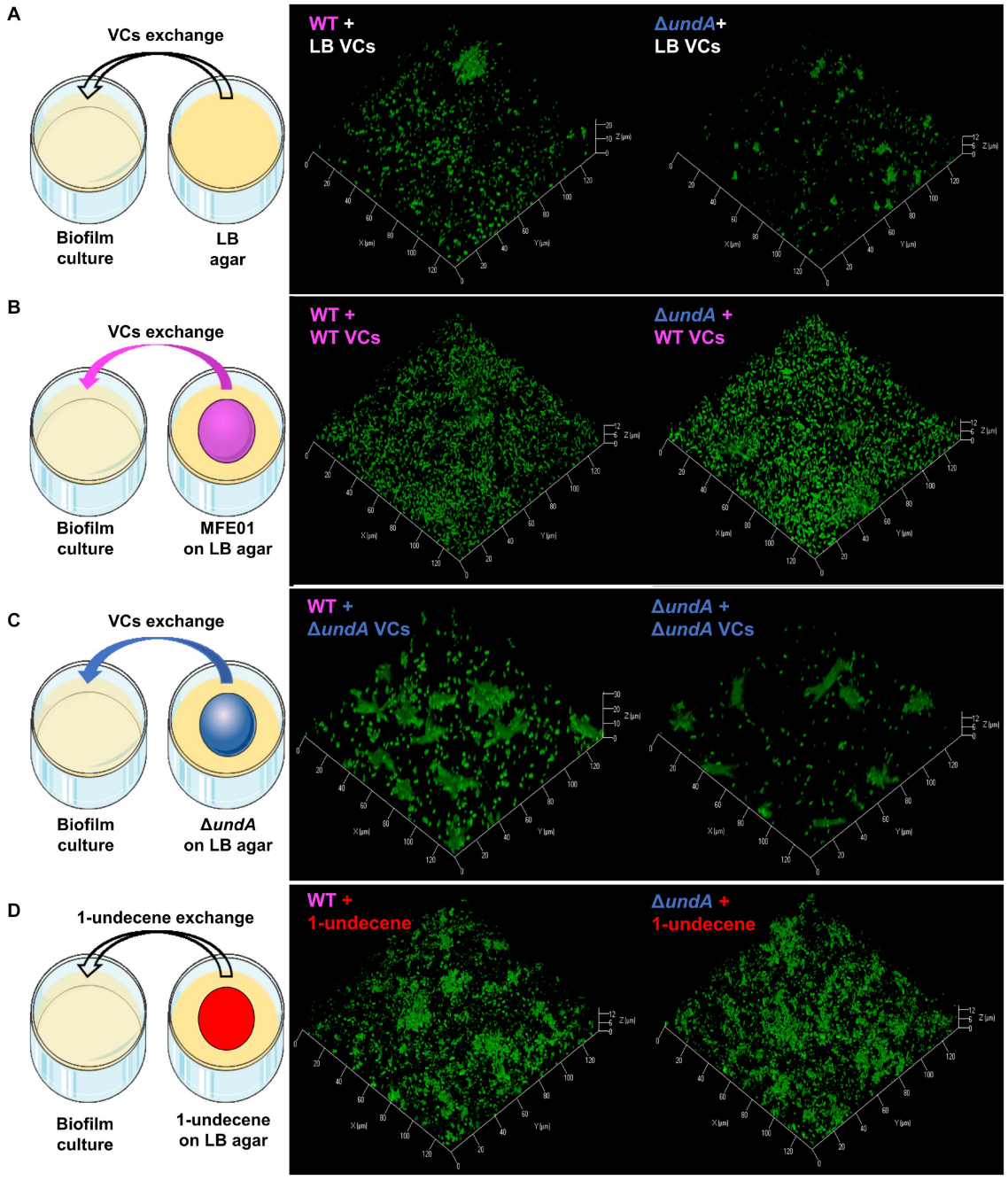

FIGURE 6
Biofilm maturation modulation by volatile compounds. **(A)** Exposition of biofilm to LB volatile compounds. **(B)** Exposition of biofilm to volatile compounds of MFE01 on LB. **(C)** Exposition of biofilm to volatile compounds of Δ*undA* mutant on LB. **(D)** Exposition of biofilm to pure 1-undecene. VCs means volatile compounds. The left panels correspond to schematic representations of experimental setups used for volatile compounds exposure, middle panels are confocal laser scanning microscopy analysis of MFE01 and right panels are confocal laser scanning microscopy analysis of Δ*undA* mutant exposed to the volatile compounds. Representative biofilm 3D shadow representations are shown. Biofilms were grown in static condition on a glass surface of a 24 well plate for 48 h at 28°C in LB medium. In each plate, 2 wells were filled with 2 mL of LB agar with or without 10 µL of MFE01 or Δ*undA* mutant culture at OD_{580nm} = 10 or 2 µL of 220 µM 1-undecene solution.

us to hypothesize that MFE01 may use 1-undecene as volatile communication molecule.

For this study, a novel experimental device was developed to analyze the effect of emitted volatile compounds on biofilm maturation. In this setup, the emission rate and the accumulation of VCs are continuous and biologically relevant. We think this device is more suitable for the study of aerial communication by VCs than other commonly performed experiments. In fact, several studies are based on the use of purified volatile compounds added at the outset of the experiment to evaluate their toxicity (Popova et al., 2014; De Vrieze et al., 2015; Lo Cantore et al., 2015; Corre et al., 2021). This may lead to a massive accumulation of volatile compounds in the first

10.3389/fmicb.2023.1264801

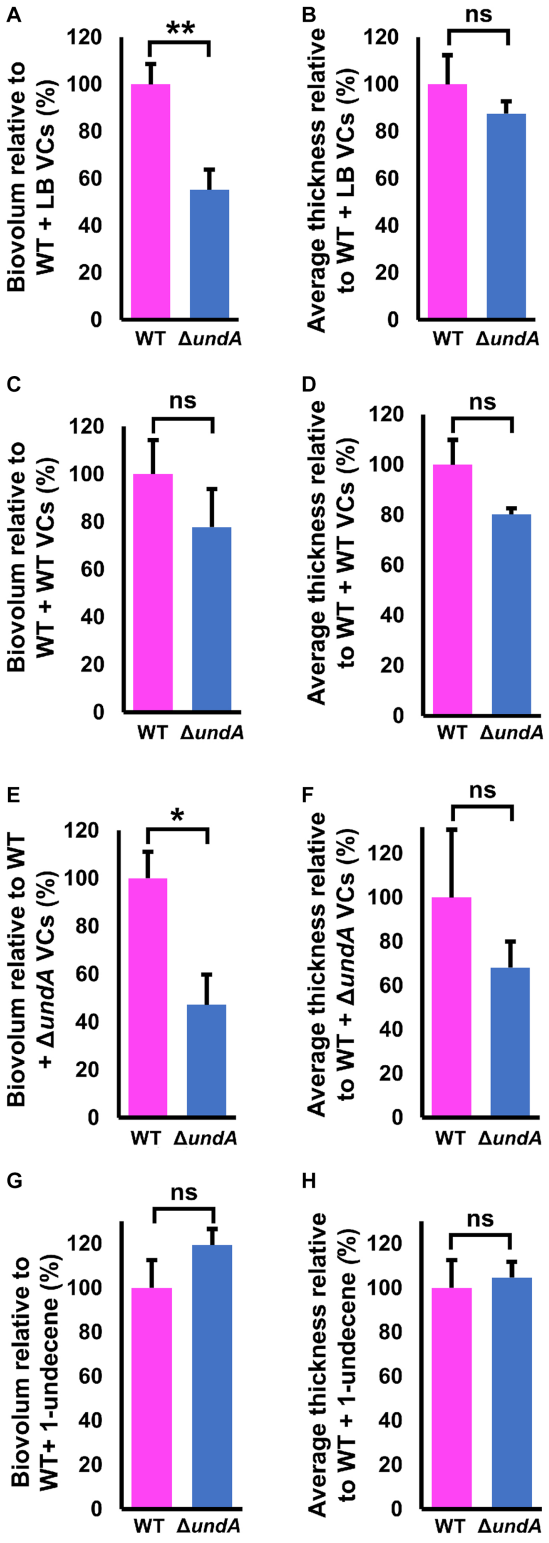

FIGURE 7
Quantitative analysis of biofilms developed after exposure to volatile compounds. **(A,B)** Comstat analysis of biofilms biovolume and average thickness of MFE01 and Δ*undA* mutant exposed to the LB volatile compounds. **(C,D)** Comstat analysis of biofilms biovolume and average thickness of MFE01 and Δ*undA* mutant exposed to the MFE01 volatile compounds. **(E,F)** Comstat analysis of biofilms biovolume (right panel) and average thickness of MFE01 and Δ*undA* mutant exposed to the Δ*undA* Volatile Compounds. **(G,H)** Comstat analysis of biofilms biovolume and average thickness of MFE01 and Δ*undA* mutant exposed to 2 µL of 220 µM 1-undecene solution, corresponding to 1-undecene quantity emitted by MFE01 in 24 h in LB medium. *$p < 0.05$ and **$p < 0.01$; ns, not significant (*t*-test). Data represent the mean of 5 independent experiments. Error bars indicate standard error of the mean.

hours of experimentation followed by a dispersion. While these experiments are suited to demonstrate the toxicity of a VC, they do not seem to be appropriate for investigating the role of VCs in communication.

According to our experimental results, despite its hydrophobic part, 1-undecene remains sufficiently soluble in the aqueous phase of the biofilm to modify its maturation. This is coherent with VOCs detection in different sources of water (Chary and Fernandez-Alba, 2012) and the 1-undecene solubility in water of 0.3432 mg/L, corresponding to 2.22 µmol per liter, accordingly to the PubChem database.[2] Another volatile communication molecule, the 3-hydroxypalmitic acid methyl ester (3-OH PAME), was previously described for its implication in gaseous and water phase communication (Clough et al., 1994; Flavier et al., 1997). This VOC is synthesized by the *Ralstonia solanacearum* PhcB enzyme and is detected by the PhcR sensor histidine kinase, leading to expression of genes involved in virulence towards *Solanum tuberosum* (Clough et al., 1994, 1997; Flavier et al., 1997; Schell, 2000). Schell (2000) proposed the Phc system as a confinement sensing system. In this pathosystem, the accumulation of 3-OH PAME produced by *R. solanacearum* is detected as a signal indicating a confined space that is a favorable niche to trigger virulence. Here we report that the environmental strain *P. fluorescens* MFE01 could use 1-undecene as an aerial communication signal. Indeed, the Δ*undA* mutant was not able to mature its biofilm, but the 1-undecene emitted by the wild strain or exposure to pure 1-undecene at biologically relevant concentration restored its biofilm maturation capacity. These finding suggest that during 1-undecene emission, by an unknown mechanism, MFE01 detects it, leading biofilm formation modulation. To our knowledge, this is the first description of 1-undecene as intraspecific bacterial aerial communication molecule. This leads us to propose 1-undecene as a member of the restrictive list of volatiles autoinducers, as well as 3-OH PAME (Clough et al., 1994, 1997; Flavier et al., 1997; Schell, 2000) and indole (Wang et al., 2001; Lee et al., 2007, 2009; Lee and Lee, 2010; DeJong et al., 2017). Then, it appears that volatile compounds, including 1-undecene, may act as indicator for a high cell density or confined space. Characterization of other volatile autoinducers and their detection systems seems to be essential for identifying the biological roles of VOCs-based communication. Interestingly, Prakash et al. (2021) have already demonstrated that 1-undecene plays a role in interspecific communication. Indeed, the nematode *Caenorhabditis elegans* can specifically detect the 1-undecene emitted by *P. aeruginosa*, leading to a flight and early triggering of the immune response. Taken together, these results suggest that 1-undecene may be used as a toolbox by *Pseudomonas*, during competition, virulence or inter- and intra-species communication.

Surprisingly, VCs emitted by the LB medium modulated MFE01 biofilm. This unexpected finding highlights MFE01 ability to integrate signal from various VCs. Another interesting result was the modification of biofilm maturation in presence of L-arabinose in the medium, despite the lack of effect on 1-undecene emission. This may be explained by the ability of *P. fluorescens* bacteria to catabolize arabinose (Lockwood and Nelson, 1946), and to integrate it in its biofilm matrix (Hung et al., 2005; Raza et al., 2012). Thereby, arabinose supplementation, used for activation of pJN105 promotor, may modify MFE01 metabolism and EPS matrix of biofilm, explaining the observed differences.

To conclude, *P. fluorescens* MFE01 seems to use its own main VOCs (i.e., 1-undecene) as an aerial communication molecule. We hypothesize that MFE01 may possess dedicated receptors for different VCs. This confirms that bacterial communication is a complex network of multiplex chemical signals detected by specific receptors. An environmental strain such as *P. fluorescens* MFE01, lacking AHL-based QS, appears to be a suitable model for studying undervalued modes of communication to date.

Data availability statement

The datasets presented in this study can be found in online repositories. The names of the repository/repositories and accession number(s) can be found at: https://www.ncbi.nlm.nih.gov/genbank/, OQ434583.

Author contributions

CD: Conceptualization, Data curation, Formal analysis, Investigation, Methodology, Visualization, Writing – original draft, Writing – review & editing. YB: Formal analysis, Investigation, Methodology, Writing – review & editing. TO: Formal analysis, Investigation, Methodology, Writing – review & editing. MN: Formal analysis, Investigation, Methodology, Writing – review & editing. CB: Investigation, Methodology, Writing – review & editing. XL: Funding acquisition, Writing – review & editing. Y-KG: Writing – review & editing. JV: Conceptualization, Formal analysis, Funding acquisition, Investigation, Methodology, Supervision, Writing – original draft, Writing – review & editing. AM: Conceptualization, Formal analysis, Funding acquisition, Investigation, Project administration, Supervision, Validation, Visualization, Writing – original draft, Writing – review & editing.

Funding

The author(s) declare financial support was received for the research, authorship, and/or publication of this article. This research was supported by grant from Rouen Normandie Université. This work was supported by Structure Fédérative de Recherche Normandie Végétal NORVEGE Fed4277, FEDER (European Union) and the Société Française de Phytopathologie.

Acknowledgments

The authors thank Magalie Robert, Florian Defontaine, and Amine Boukerb and Olivier Maillot for technical assistance. The authors thank the Ecole Normande de Biologie Intégrative Santé et Environnement for kindly providing help for mobility.

2 https://pubchem.ncbi.nlm.nih.gov/compound/1-Undecene

Conflict of interest

The authors declare that the research was conducted in the absence of any commercial or financial relationships that could be construed as a potential conflict of interest.

Publisher's note

All claims expressed in this article are solely those of the authors and do not necessarily represent those of their affiliated organizations, or those of the publisher, the editors and the reviewers. Any product that may be evaluated in this article, or claim that may be made by its manufacturer, is not guaranteed or endorsed by the publisher.

Supplementary material

The Supplementary material for this article can be found online at: https://www.frontiersin.org/articles/10.3389/fmicb.2023.1264801/full#supplementary-material

References

Allsopp, L. P., Wood, T. E., Howard, S. A., Maggiorelli, F., Nolan, L. M., Wettstadt, S., et al. (2017). RsmA and AmrZ orchestrate the assembly of all three type VI secretion systems in *Pseudomonas aeruginosa*. *Proc. Natl. Acad. Sci. U.S.A.* 114, 7707–7712. doi: 10.1073/pnas.1700286114

Altschul, S. F., Gish, W., Miller, W., Myers, E. W., and Lipman, D. J. (1990). Basic local alignment search tool. *J. Mol. Biol.* 215, 403–410. doi: 10.1016/S0022-2836(05)80360-2

An, S., Wu, J., and Zhang, L.-H. (2010). Modulation of *Pseudomonas aeruginosa* biofilm dispersal by a cyclic-Di-GMP phosphodiesterase with a putative hypoxia-sensing domain. *Appl. Environ. Microbiol.* 76, 8160–8173. doi: 10.1128/AEM.01233-10

Barbey, C., Chane, A., Burini, J.-F., Maillot, O., Merieau, A., Gallique, M., et al. (2018). A rhodococcal transcriptional regulatory mechanism detects the common lactone ring of AHL quorum-sensing signals and triggers the quorum-quenching response. *Front. Microbiol.* 9:2800. doi: 10.3389/fmicb.2018.02800

Basler, M., Pilhofer, M., Henderson, G. P., Jensen, G. J., and Mekalanos, J. J. (2012). Type VI secretion requires a dynamic contractile phage tail-like structure. *Nature* 483, 182–186. doi: 10.1038/nature10846

Bigot, R., Bertaux, J., Frere, J., and Berjeaud, J.-M. (2013). Intra-amoeba multiplication induces chemotaxis and biofilm colonization and formation for *Legionella*. *PLoS One* 8:e77875. doi: 10.1371/journal.pone.0077875

Bourigault, Y., Rodrigues, S., Crépin, A., Chane, A., Taupin, L., Bouteiller, M., et al. (2021). Biocontrol of biofilm formation: jamming of sessile-associated rhizobial communication by rhodococcal quorum-quenching. *Int. J. Mol. Sci.* 22:8241. doi: 10.3390/ijms22158241

Bouteiller, M., Gallique, M., Bourigault, Y., Kosta, A., Hardouin, J., Massier, S., et al. (2020). Crosstalk between the type VI secretion system and the expression of class IV flagellar genes in the *Pseudomonas fluorescens* MFE01 strain. *Microorganisms* 8:622. doi: 10.3390/microorganisms8050622

Brackmann, M., Nazarov, S., Wang, J., and Basler, M. (2017). Using force to punch holes: mechanics of contractile nanomachines. *Trends Cell Biol.* 27, 623–632. doi: 10.1016/j.tcb.2017.05.003

Cambronel, M., Tortuel, D., Biaggini, K., Maillot, O., Taupin, L., Réhel, K., et al. (2019). Epinephrine affects motility, and increases adhesion, biofilm and virulence of *Pseudomonas aeruginosa* H103. *Sci. Rep.* 9:20203. doi: 10.1038/s41598-019-56666-7

Chane, A., Barbey, C., Robert, M., Merieau, A., Konto-Ghiorghi, Y., Beury-Cirou, A., et al. (2019). Biocontrol of soft rot: confocal microscopy highlights virulent pectobacterial communication and its jamming by rhodococcal quorum-quenching. *Mol. Plant Microbe. Interact.* 32, 802–812. doi: 10.1094/MPMI-11-18-0314-R

Chary, N. S., and Fernandez-Alba, A. R. (2012). Determination of volatile organic compounds in drinking and environmental waters. *Trends Anal. Chem.* 32, 60–75. doi: 10.1016/j.trac.2011.08.011

Chatterjee, A., Eliasson, S. H. H., and Jensen, V. R. (2018). Selective production of linear α-olefins via catalytic deoxygenation of fatty acids and derivatives. *Catal. Sci. Technol.* 8, 1487–1499. doi: 10.1039/C7CY02580G

Cheng, X., Cordovez, V., Etalo, D. W., van der Voort, M., and Raaijmakers, J. M. (2016). Role of the GacS sensor kinase in the regulation of volatile production by plant growth-promoting *Pseudomonas fluorescens* SBW25. *Front. Plant Sci.* 7:1706. doi: 10.3389/fpls.2016.01706

Cheng, X., de Bruijn, I., van der Voort, M., Loper, J. E., and Raaijmakers, J. M. (2013). The Gac regulon of *Pseudomonas fluorescens* SBW25. *Environ. Microbiol. Rep.* 5, 608–619. doi: 10.1111/1758-2229.12061

Cherrak, Y., Flaugnatti, N., Durand, E., Journet, L., and Cascales, E. (2019). Structure and activity of the type VI secretion system. *Microbiol. Spectr.* 7. doi: 10.1128/microbiolspec.psib-0031-2019

Clough, S. J., Lee, K. E., Schell, M. A., and Denny, T. P. (1997). A two-component system in *Ralstonia* (*Pseudomonas*) solanacearum modulates production of Phc A-regulated virulence factors in response to 3-hydroxypalmitic acid methyl ester. *J. Bacteriol.* 179, 3639–3648. doi: 10.1128/jb.179.11.3639-3648.1997

Clough, S. J., Schell, M. A., and Denny, T. P. (1994). Evidence for involvement of a volatile extracellular factor in *Pseudomonas solanacearum* virulence gene expression. *Mol. Plant Microbe. Interact.* 7, 621–630. doi: 10.1094/MPMI-7-0621

Corre, M.-H., Delafont, V., Legrand, A., Berjeaud, J.-M., and Verdon, J. (2019). Exploiting the richness of environmental waterborne bacterial species to find natural *Legionella pneumophila* competitors. *Front. Microbiol.* 9:3360. doi: 10.3389/fmicb.2018.03360

Corre, M.-H., Mercier, A., Bouteiller, M., Khalil, A., Ginevra, C., Depayras, S., et al. (2021). Bacterial long-range warfare: aerial killing of *Legionella pneumophila* by *Pseudomonas fluorescens*. *Microbiol. Spectr.* 9:e0040421. doi: 10.1128/Spectrum.00404-21

Coulthurst, S. (2019). The type VI secretion system: a versatile bacterial weapon. *Microbiology* 165, 503–515. doi: 10.1099/mic.0.000789

De Kievit, T. R. (2009). Quorum sensing in *Pseudomonas aeruginosa* biofilms. *Environ. Microbiol.* 11, 279–288. doi: 10.1111/j.1462-2920.2008.01792.x

De Vrieze, M., Pandey, P., Bucheli, T. D., Varadarajan, A. R., Ahrens, C. H., Weisskopf, L., et al. (2015). Volatile organic compounds from native potato-associated *Pseudomonas* as potential anti-oomycete agents. *Front. Microbiol.* 6:1295. doi: 10.3389/fmicb.2015.01295

Decoin, V., Barbey, C., Bergeau, D., Latour, X., Feuilloley, M. G. J., Orange, N., et al. (2014). A type VI secretion system is involved in *Pseudomonas fluorescens* bacterial competition. *PLoS One* 9:e89411. doi: 10.1371/journal.pone.0089411

Decoin, V., Gallique, M., Barbey, C., Le Mauff, F., Poc, C. D., Feuilloley, M. G., et al. (2015). A *Pseudomonas fluorescens* type 6 secretion system is related to mucoidy, motility and bacterial competition. *BMC Microbiol.* 15:72. doi: 10.1186/s12866-015-0405-9

DeJong, C. S., Wang, D. I., Polyakov, A., Rogacs, A., Simske, S. J., and Shkolnikov, V. (2017). Bacterial detection and differentiation via direct volatile organic compound sensing with surface enhanced Raman spectroscopy. *ChemistrySelect* 2, 8431–8435. doi: 10.1002/slct.201701669

Eilers, K., Kuok Hoong Yam, J., Morton, R., Mei Hui Yong, A., Brizuela, J., Hadjicharalambous, C., et al. (2022). Phenotypic and integrated analysis of a comprehensive *Pseudomonas aeruginosa* PAO1 library of mutants lacking cyclic-di-GMP-related genes. *Front. Microbiol.* 13:949597. doi: 10.3389/fmicb.2022.949597

El-Sayed, A. K., Hothersall, J., and Thomas, C. M. (2001). Quorum-sensing-dependent regulation of biosynthesis of the polyketide antibiotic mupirocin in *Pseudomonas fluorescens* NCIMB 10586. *Microbiology* 147, 2127–2139. doi: 10.1099/00221287-147-8-2127

Flavier, A. B., Clough, S. J., Schell, M. A., and Denny, T. P. (1997). Identification of 3-hydroxypalmitic acid methyl ester as a novel autoregulator controlling virulence in *Ralstonia solanacearum*. *Mol. Microbiol.* 26, 251–259. doi: 10.1046/j.1365-2958.1997.5661945.x

Flemming, H.-C., Wingender, J., Szewzyk, U., Steinberg, P., Rice, S. A., and Kjelleberg, S. (2016). Biofilms: an emergent form of bacterial life. *Nat. Rev. Microbiol.* 14, 563–575. doi: 10.1038/nrmicro.2016.94

Fuqua, W. C., Winans, S. C., and Greenberg, E. P. (1994). Quorum sensing in bacteria: the lux R-lux I family of cell density-responsive transcriptional regulators. *J. Bacteriol.* 176, 269–275. doi: 10.1128/jb.176.2.269-275.1994

Gallique, M., Bouteiller, M., and Merieau, A. (2017a). The type VI secretion system: a dynamic system for bacterial communication? *Front. Microbiol.* 8:1454. doi: 10.3389/fmicb.2017.01454

Gallique, M., Decoin, V., Barbey, C., Rosay, T., Feuilloley, M. G. J., Orange, N., et al. (2017b). Contribution of the *Pseudomonas fluorescens* MFE01 type VI secretion system to biofilm formation. *PLoS One* 12:e0170770. doi: 10.1371/journal.pone.0170770

Giorgio, A., De Stradis, A., Lo Cantore, P., and Iacobellis, N. S. (2015). Biocide effects of volatile organic compounds produced by potential biocontrol rhizobacteria on *Sclerotinia sclerotiorum*. *Front. Microbiol.* 6:1056. doi: 10.3389/fmicb.2015.01056

Gu, Y.-Q., Mo, M.-H., Zhou, J.-P., Zou, C.-S., and Zhang, K.-Q. (2007). Evaluation and identification of potential organic nematicidal volatiles from soil bacteria. *Soil Biol. Biochem.* 39, 2567–2575. doi: 10.1016/j.soilbio.2007.05.011

Hachani, A., Wood, T. E., and Filloux, A. (2016). Type VI secretion and anti-host effectors. *Curr. Opin. Microbiol.* 29, 81–93. doi: 10.1016/j.mib.2015.11.006

Hall-Stoodley, L., Costerton, J. W., and Stoodley, P. (2004). Bacterial biofilms: from the natural environment to infectious diseases. *Nat. Rev. Microbiol.* 2, 95–108. doi: 10.1038/nrmicro821

Hancock, R. E., and Carey, A. M. (1979). Outer membrane of *Pseudomonas aeruginosa*: heat-2-mercaptoethanol-modifiable proteins. *J. Bacteriol.* 140, 902–910. doi: 10.1128/jb.140.3.902-910.1979

Herman, N. A., and Zhang, W. (2016). Enzymes for fatty acid-based hydrocarbon biosynthesis. *Curr. Opin. Chem. Biol.* 35, 22–28. doi: 10.1016/j.cbpa.2016.08.009

Hernandez, R. E., Gallegos-Monterrosa, R., and Coulthurst, S. J. (2020). Type VI secretion system effector proteins: effective weapons for bacterial competitiveness. *Cell. Microbiol.* 22:e13241. doi: 10.1111/cmi.13241

Heydorn, A., Nielsen, A. T., Hentzer, M., Sternberg, C., Givskov, M., Ersbøll, B. K., et al. (2000). Quantification of biofilm structures by the novel computer program comstat. *Microbiology* 146, 2395–2407. doi: 10.1099/00221287-146-10-2395

Ho, B. T., Dong, T. G., and Mekalanos, J. J. (2014). A view to a kill: the bacterial type VI secretion system. *Cell Host Microbe* 15, 9–21. doi: 10.1016/j.chom.2013.11.008

Hung, C.-C., Santschi, P. H., and Gillow, J. B. (2005). Isolation and characterization of extracellular polysaccharides produced by *Pseudomonas fluorescens* biovar II. *Carbohydr. Polym.* 61, 141–147. doi: 10.1016/j.carbpol.2005.04.008

Jones, P., Binns, D., Chang, H.-Y., Fraser, M., Li, W., McAnulla, C., et al. (2014). Inter pro scan 5: genome-scale protein function classification. *Bioinformatics* 30, 1236–1240. doi: 10.1093/bioinformatics/btu031

Jurėnas, D., and Journet, L. (2021). Activity, delivery, and diversity of type VI secretion effectors. *Mol. Microbiol.* 115, 383–394. doi: 10.1111/mmi.14648

Kapitein, N., and Mogk, A. (2013). Deadly syringes: type VI secretion system activities in pathogenicity and interbacterial competition. *Curr. Opin. Microbiol.* 16, 52–58. doi: 10.1016/j.mib.2012.11.009

Khanongnuch, R., Mangayil, R., Santala, V., Hestnes, A. G., Svenning, M. M., and Rissanen, A. J. (2022). Batch experiments demonstrating a two-stage bacterial process coupling methanotrophic and heterotrophic bacteria for 1-alkene production from methane. *Front. Microbiol.* 13:874627. doi: 10.3389/fmicb.2022.874627

Kim, K., Lee, S., and Ryu, C.-M. (2013). Interspecific bacterial sensing through airborne signals modulates locomotion and drug resistance. *Nat. Commun.* 4:1809. doi: 10.1038/ncomms2789

Koehler, T., Ackermann, I., Brecht, D., Uteschil, F., Wingender, J., Telgheder, U., et al. (2020). Analysis of volatile metabolites from in vitro biofilms of *Pseudomonas aeruginosa* with thin-film microextraction by thermal desorption gas chromatography-mass spectrometry. *Anal. Bioanal. Chem.* 412, 2881–2892. doi: 10.1007/s00216-020-02529-4

Lee, J., Jayaraman, A., and Wood, T. K. (2007). Indole is an inter-species biofilm signal mediated by SdiA. *BMC Microbiol.* 7:42. doi: 10.1186/1471-2180-7-42

Lee, J.-H., and Lee, J. (2010). Indole as an intercellular signal in microbial communities. *FEMS Microbiol. Rev.* 34, 426–444. doi: 10.1111/j.1574-6976.2009.00204.x

Lee, J., Maeda, T., Hong, S. H., and Wood, T. K. (2009). Reconfiguring the quorum-sensing regulator SdiA of *Escherichia coli* to control biofilm formation via indole and N-acylhomoserine lactones. *Appl. Environ. Microbiol.* 75, 1703–1716. doi: 10.1128/AEM.02081-08

Leiman, P. G., Basler, M., Ramagopal, U. A., Bonanno, J. B., Sauder, J. M., Pukatzki, S., et al. (2009). Type VI secretion apparatus and phage tail-associated protein complexes share a common evolutionary origin. *Proc. Natl. Acad. Sci. U.S.A.* 106, 4154–4159. doi: 10.1073/pnas.0813360106

Lemfack, M. C., Gohlke, B.-O., Toguem, S. M. T., Preissner, S., Piechulla, B., and Preissner, R. (2018). mVOC 2.0: a database of microbial volatiles. *Nucleic Acids Res.* 46, D1261–D1265. doi: 10.1093/nar/gkx1016

Létoffé, S., Audrain, B., Bernier, S. P., Delepierre, M., and Ghigo, J.-M. (2014). Aerial exposure to the bacterial volatile compound trimethylamine modifies antibiotic resistance of physically separated bacteria by raising culture medium pH. *mBio* 5, e00944–e00913. doi: 10.1128/mBio.00944-13

Liu, K., and Li, S. (2020). Biosynthesis of fatty acid-derived hydrocarbons: perspectives on enzymology and enzyme engineering. *Curr. Opin. Biotechnol.* 62, 7–14. doi: 10.1016/j.copbio.2019.07.005

Lo Cantore, P., Giorgio, A., and Iacobellis, N. S. (2015). Bioactivity of volatile organic compounds produced by *Pseudomonas tolaasii*. *Front. Microbiol.* 6:1082. doi: 10.3389/fmicb.2015.01082

Lockwood, L. B., and Nelson, G. E. N. (1946). The oxidation of pentoses by *Pseudomonas*. *J. Bacteriol.* 52, 581–586. doi: 10.1128/jb.52.5.581-586.1946

López-Lara, I. M., Nogales, J., Pech-Canul, Á., Calatrava-Morales, N., Bernabéu-Roda, L. M., Durán, P., et al. (2018). 2-tridecanone impacts surface-associated bacterial behaviours and hinders plant-bacteria interactions. *Environ. Microbiol.* 20, 2049–2065. doi: 10.1111/1462-2920.14083

Luo, J., Lehtinen, T., Efimova, E., Santala, V., and Santala, S. (2019). Synthetic metabolic pathway for the production of 1-alkenes from lignin-derived molecules. *Microb. Cell Factories* 18:48. doi: 10.1186/s12934-019-1097-x

Martins, M. L., Uelinton, M. P., Riedel, K., Vanetti, M. C. D., Mantovani, H. C., and de Araújo, E. F. (2014). Lack of AHL-based quorum sensing in *Pseudomonas fluorescens* isolated from milk. *Braz. J. Microbiol.* 45, 1039–1046. doi: 10.1590/S1517-83822014000300037

Maurhofer, M., Reimmann, C., Schmidli-Sacherer, P., Heeb, S., Haas, D., and Défago, G. (1998). Salicylic acid biosynthetic genes expressed in *Pseudomonas fluorescens* strain P 3 improve the induction of systemic resistance in tobacco against tobacco necrosis virus. *Phytopathology* 88, 678–684. doi: 10.1094/PHYTO.1998.88.7.678

Miller, M. B., and Bassler, B. L. (2001). Quorum sensing in bacteria. *Annu. Rev. Microbiol.* 55, 165–199. doi: 10.1146/annurev.micro.55.1.165

Monjarás Feria, J., and Valvano, M. A. (2020). An overview of anti-eukaryotic T6SS effectors. *Front. Cell. Infect. Microbiol.* 10:584751. doi: 10.3389/fcimb.2020.584751

Netzker, T., Shepherdson, E. M. F., Zambri, M. P., and Elliot, M. A. (2020). Bacterial volatile compounds: functions in communication, cooperation, and competition. *Annu. Rev. Microbiol.* 74, 409–430. doi: 10.1146/annurev-micro-011320-015542

Newman, J. R., and Fuqua, C. (1999). Broad-host-range expression vectors that carry the l-arabinose-inducible *Escherichia coli* ara BAD promoter and the ara C regulator. *Gene* 227, 197–203. doi: 10.1016/S0378-1119(98)00601-5

Ninkovic, V., Markovic, D., and Rensing, M. (2021). Plant volatiles as cues and signals in plant communication. *Plant Cell Environ.* 44, 1030–1043. doi: 10.1111/pce.13910

Papenfort, K., and Bassler, B. L. (2016). Quorum sensing signal-response systems in gram-negative bacteria. *Nat. Rev. Microbiol.* 14, 576–588. doi: 10.1038/nrmicro.2016.89

Popova, A. A., Koksharova, O. A., Lipasova, V. A., Zaitseva, J. V., Katkova-Zhukotskaya, O. A., Eremina, S. I., et al. (2014). Inhibitory and toxic effects of volatiles emitted by strains of *Pseudomonas* and *Serratia* on growth and survival of selected microorganisms, *Caenorhabditis elegans*, and *Drosophila melanogaster*. *Biomed. Res. Int.* 2014:125704. doi: 10.1155/2014/125704

Prakash, D., Ms, A., Radhika, B., Venkatesan, R., Chalasani, S. H., and Singh, V. (2021). 1-undecene from *Pseudomonas aeruginosa* is an olfactory signal for flight-or-fight response in *Caenorhabditis elegans*. *EMBO J.* 40:e106938. doi: 10.15252/embj.2020106938

Pukatzki, S., McAuley, S. B., and Miyata, S. T. (2009). The type VI secretion system: translocation of effectors and effector-domains. *Curr. Opin. Microbiol.* 12, 11–17. doi: 10.1016/j.mib.2008.11.010

Raza, W., Ling, N., Liu, D., Wei, Z., Huang, Q., and Shen, Q. (2016). Volatile organic compounds produced by *Pseudomonas fluorescens* WR-1 restrict the growth and virulence traits of *Ralstonia solanacearum*. *Microbiol. Res.* 192, 103–113. doi: 10.1016/j.micres.2016.05.014

Raza, W., Yang, W., Jun, Y., Shakoor, F., Huang, Q., and Shen, Q. (2012). Optimization and characterization of a polysaccharide produced by *Pseudomonas fluorescens* WR-1 and its antioxidant activity. *Carbohydr. Polym.* 90, 921–929. doi: 10.1016/j.carbpol.2012.06.021

Roy, A. B., Petrova, O. E., and Sauer, K. (2012). The phosphodiesterase DipA (PA5017) is essential for *Pseudomonas aeruginosa* biofilm dispersion. *J. Bacteriol.* 194, 2904–2915. doi: 10.1128/JB.05346-11

Rui, Z., Harris, N. C., Zhu, X., Huang, W., and Zhang, W. (2015). Discovery of a family of desaturase-like enzymes for 1-alkene biosynthesis. *ACS Catal.* 5, 7091–7094. doi: 10.1021/acscatal.5b01842

Rui, Z., Li, X., Zhu, X., Liu, J., Domigan, B., Barr, I., et al. (2014). Microbial biosynthesis of medium-chain 1-alkenes by a nonheme iron oxidase. *Proc. Natl. Acad. Sci. U.S.A.* 111, 18237–18242. doi: 10.1073/pnas.1419701112

Ryu, C.-M., Farag, M. A., Hu, C.-H., Reddy, M. S., Kloepper, J. W., and Paré, P. W. (2004). Bacterial volatiles induce systemic resistance in *Arabidopsis*. *Plant Physiol.* 134, 1017–1026. doi: 10.1104/pp.103.026583

Salmela, M., Lehtinen, T., Efimova, E., Santala, S., and Santala, V. (2020). Towards bioproduction of poly-α-olefins from lignocellulose. *Green Chem.* 22, 5067–5076. doi: 10.1039/D0GC01617A

Schell, M. A. (2000). Control of virulence and pathogenicity genes of *Ralstonia Solanacearum* by an elaborate sensory network. *Annu. Rev. Phytopathol.* 38, 263–292. doi: 10.1146/annurev.phyto.38.1.263

Schmidt, R., Cordovez, V., de Boer, W., Raaijmakers, J., and Garbeva, P. (2015). Volatile affairs in microbial interactions. *ISME J.* 9, 2329–2335. doi: 10.1038/ismej.2015.42

Schneider, C. A., Rasband, W. S., and Eliceiri, K. W. (2012). NIH image to ImageJ: 25 years of image analysis. *Nat. Methods* 9, 671–675. doi: 10.1038/nmeth.2089

Shneider, M. M., Buth, S. A., Ho, B. T., Basler, M., Mekalanos, J. J., and Leiman, P. G. (2013). PAAR-repeat proteins sharpen and diversify the type VI secretion system spike. *Nature* 500, 350–353. doi: 10.1038/nature12453

Simon, R., Priefer, U., and Pühler, A. (1983). A broad host range mobilization system for in vivo genetic engineering: transposon mutagenesis in gram negative Bacteria. *Nat. Biotechnol.* 1, 784–791. doi: 10.1038/nbt1183-784

Smadja, B., Latour, X., Trigui, S., Burini, J. F., Chevalier, S., and Orange, N. (2004). Thermodependence of growth and enzymatic activities implicated in pathogenicity of two *Erwinia carotovora* subspecies (*Pectobacterium* spp.). *Can. J. Microbiol.* 50, 19–27. doi: 10.1139/w03-099

Tahrioui, A., Duchesne, R., Bouffartigues, E., Rodrigues, S., Maillot, O., Tortuel, D., et al. (2019). Extracellular DNA release, quorum sensing, and PrrF1/F2 small RNAs are key players in *Pseudomonas aeruginosa* tobramycin-enhanced biofilm formation. *npj Biofilms Microbiomes* 5, 15–11. doi: 10.1038/s41522-019-0088-3

Vlot, A. C., and Rosenkranz, M. (2022). Volatile compounds—the language of all kingdoms? *J. Exp. Bot.* 73, 445–448. doi: 10.1093/jxb/erab528

Wang, J., Brodmann, M., and Basler, M. (2019). Assembly and subcellular localization of bacterial type VI secretion systems. *Annu. Rev. Microbiol.* 73, 621–638. doi: 10.1146/annurev-micro-020518-115420

Wang, D., Ding, X., and Rather, P. N. (2001). Indole can act as an extracellular signal in *Escherichia coli*. *J. Bacteriol.* 183, 4210–4216. doi: 10.1128/jb.183.14.4210-4216.2001

Wang, J., Yu, H., and Zhu, K. (2018). Employing metabolic engineered lipolytic microbial platform for 1-alkene one-step conversion. *Bioresour. Technol.* 263, 172–179. doi: 10.1016/j.biortech.2018.04.119

Waters, C. M., and Bassler, B. L. (2005). Quorum sensing: cell-to-cell communication in bacteria. *Annu. Rev. Cell Dev. Biol.* 21, 319–346. doi: 10.1146/annurev.cellbio.21.012704.131001

Wei, H.-L., and Zhang, L.-Q. (2006). Quorum-sensing system influences root colonization and biological control ability in *Pseudomonas fluorescens* 2P24. *Antonie Van Leeuwenhoek* 89, 267–280. doi: 10.1007/s10482-005-9028-8

Weisskopf, L., Schulz, S., and Garbeva, P. (2021). Microbial volatile organic compounds in intra-kingdom and inter-kingdom interactions. *Microbiology* 19, 391–404. doi: 10.1038/s41579-020-00508-1

Xu, Y.-Y., Lu, H., Wang, X., Zhang, K.-Q., and Li, G.-H. (2015). Effect of volatile organic compounds from bacteria on nematodes. *Chem. Biodivers.* 12, 1415–1421. doi: 10.1002/cbdv.201400342

Yunus, I. S., Anfelt, J., Sporre, E., Miao, R., Hudson, E. P., and Jones, P. R. (2022). Synthetic metabolic pathways for conversion of CO_2 into secreted short-to medium-chain hydrocarbons using cyanobacteria. *Metab. Eng.* 72, 14–23. doi: 10.1016/j.ymben.2022.01.017

Yunus, I. S., Wichmann, J., Wördenweber, R., Lauersen, K. J., Kruse, O., and Jones, P. R. (2018). Synthetic metabolic pathways for photobiological conversion of CO2 into hydrocarbon fuel. *Metab. Eng.* 49, 201–211. doi: 10.1016/j.ymben.2018.08.008

Zhou, Y. J., Hu, Y., Zhu, Z., Siewers, V., and Nielsen, J. (2018). Engineering 1-alkene biosynthesis and secretion by dynamic regulation in yeast. *ACS Synth. Biol.* 7, 584–590. doi: 10.1021/acssynbio.7b00338

frontiers | Frontiers in Microbiology

TYPE Original Research
PUBLISHED 23 October 2023
DOI 10.3389/fmicb.2023.1278886

OPEN ACCESS

EDITED BY
Ilana Kolodkin-Gal,
Reichman University, Israel

REVIEWED BY
Edwin Hualpa Cutipa,
National University of San Marcos, Peru
Shafinaz Shahir,
University of Technology Malaysia, Malaysia

*CORRESPONDENCE
Sonia M. Tiquia-Arashiro
✉ smtiquia@umich.edu

RECEIVED 17 August 2023
ACCEPTED 10 October 2023
PUBLISHED 23 October 2023

CITATION
Pagnucco G, Overfield D, Chamlee Y, Shuler C, Kassem A, Opara S, Najaf H, Abbas L, Coutinho O, Fortuna A, Sulaiman F, Farinas J, Schittenhelm R, Catalfano B, Li X and Tiquia-Arashiro SM (2023) Metal tolerance and biosorption capacities of bacterial strains isolated from an urban watershed. *Front. Microbiol.* 14:1278886. doi: 10.3389/fmicb.2023.1278886

Metal tolerance and biosorption capacities of bacterial strains isolated from an urban watershed

Grace Pagnucco, Dustin Overfield, Yanesa Chamlee, Claudia Shuler, Amin Kassem, Somie Opara, Hawraa Najaf, Lana Abbas, Oliver Coutinho, Aleksa Fortuna, Fatima Sulaiman, James Farinas, Reis Schittenhelm, Brian Catalfano, Xiaohua Li and Sonia M. Tiquia-Arashiro*

Department of Natural Sciences, University of Michigan-Dearborn, Dearborn, MI, United States

Rapid industrialization and urbanization have led to widespread metal contamination in aquatic ecosystems. This study explores the metal tolerance and biosorption characteristics of four bacterial strains (*Serratia* sp. L2, *Raoultella* sp. L30, *Klebsiella* sp. R3, and *Klebsiella* sp. R19) isolated from Saint Clair River sediments. These strains effectively removed various metal cations (As^{3+}, Pb^{2+}, Cu^{2+}, Mn^{2+}, Zn^{2+}, Cd^{2+}, Cr^{6+}, and Ni^{2+}) in single and multi-metal solutions. Minimum inhibitory concentration (MIC) assays revealed strain-specific variations in metal tolerance, with L2 and L30 exhibiting higher tolerance. Surprisingly, R3 and R19, despite lower tolerance, demonstrated superior metal removal efficiency, challenging the notion that tolerance dictates removal efficacy. In single-metal solutions, R3 and R19 excelled at extracting various metal ions, while competitive binding in multi-metal solutions hindered removal. However, R3 and R19 retained higher removal efficiencies, possibly due to enhanced flocculation activities facilitating metal-ion contact. Comprehensive Fourier-transform infrared (FTIR) analysis highlighted the strains' metal-binding capabilities, with novel peaks emerging after metal exposure, indicative of extracellular polymeric substance (EPS) production. Scanning electron microscopy (SEM) and energy-dispersive X-ray spectroscopy (EDX) confirmed metal accumulation on bacterial surfaces and within cytoplasmic regions and revealed morphological changes and metal adsorption patterns, emphasizing the strains' ability to adapt to metal stress. Scanning transmission microscopy (STEM) and EDX analysis uncovered metal accumulation within bacterial cells, underscoring the complexity of microbial-metal interactions. This study also confirms that the simultaneous presence of an aqueous solution may cause a mutual inhibition in the adsorption of each metal to the EPS resulting in reduced metal uptake, which emphasizes the need to select specific bacterial strains for a given metal-containing effluent. The differences in metal distribution patterns between *Klebsiella* sp. R19 and *Raoultella* sp. L30 suggest species-specific metal accumulation strategies driven by environmental conditions and metal availability. The heavy metal-removing capabilities and the ability to grow over a wide range of metal concentrations of the strains used in this study may offer an advantage to employ these organisms for metal remediation in bioreactors or *in situ*.

KEYWORDS

biosorption, metal-resistant microbes, metal selectivity, exopolysaccharide-producing bacteria, heavy metal removal, Fourier-transform infrared analysis, scanning electron microscopy, transmission electron microscopy

1. Introduction

Wastewater contamination has emerged as a critical environmental concern in recent years. The escalating processes of industrialization and urbanization have contributed to the significant release of heavy metals into aquatic ecosystems (Boening, 2000; Zamora-Ledezma et al., 2021; Goswami and Neog, 2023). The release of heavy metals into aquatic environments arises from a variety of sources, including industrial discharges, urban runoff, and agricultural activities (Tiquia, 2010; Oest et al., 2018; Patel et al., 2019; Narwal et al., 2023). These pollutants pose a substantial threat to both aquatic ecosystems and human health due to their persistence and potential toxicity (Goswami and Neog, 2023). As heavy metals accumulate in aquatic environments, they can disrupt the delicate balance of these ecosystems, causing harm to aquatic life and endangering the health of humans who rely on these water bodies for various purposes, including drinking water and recreational activities (Tiquia, 2011; Sharma et al., 2023). Additionally, heavy metal contamination can have far-reaching ecological implications, affecting the food chain and ultimately impacting terrestrial ecosystems as well (Ledin, 2000; Ahmad et al., 2021). Among the heavy metals under rigorous investigation are chromium (Cr), cadmium (Cd), copper (Cu), zinc (Zn), mercury (Hg), lead (Pb), nickel (Ni), manganese (Mn), and arsenic (As), primarily due to their pronounced threats to both public health and the environment (Boulanger and Nikolaidis, 2003; Tchounwou et al., 2012; Queiroz et al., 2021). These heavy metals find their way into the environment through human-driven activities like mining and agriculture (Goswami and Neog, 2023). Traditional techniques such as reverse osmosis, ion exchange, precipitation, and solvent extraction have been utilized to treat wastewater before discharge into natural ecosystems. However, these methods either incur substantial costs or fall short in terms of efficacy (Volesky, 1990; Qasem et al., 2021). In response, the employment of microorganisms for heavy metal removal has emerged as a highly promising alternative. This approach holds advantages by preventing secondary pollution and offering cost-effectiveness through the avoidance of sludge disposal requirements (Kim et al., 1996; Bruins et al., 2000; Lakherwal, 2014).

Bioremediation processes using microorganisms are cost effective and are highly efficient as compared to physicochemical methods mentioned above; therefore, over the last several decades attention has focused toward exploiting microbes for heavy metal bioremediation (Tiquia-Arashiro, 2018). The bioremediation of heavy metals can be categorized into two main approaches: bioaccumulation, which is an actively controlled process necessitating the uptake of heavy metal ions by living biomass, and biosorption, a passive process where metal cations are adhered to non-living biomass (Razzak et al., 2022; Jeyakumari et al., 2023). In the context of bioaccumulation, energy is expended for the absorption of metal ions, usually achieved through interactions with the cell wall. Following this, intracellular uptake takes place, with metal ions permeating the cell membrane and binding to active sites provided by polysaccharides and proteins. In contrast, biosorption capitalizes on the presence of functional groups in the cell wall or exported metabolites within the external environment. The mechanisms behind biosorption include ion exchange, complexation, precipitation, reduction, and chelation (Vishan et al., 2017; Priya et al., 2022; Sreedevi et al., 2022).

Accordingly, understanding the mechanisms by which microorganisms sequester toxic heavy metals is crucial to the development of microbial processes that will concentrate, remove, and recover metals from industrial effluents. The bioavailability of metals in the environment is an important factor for metal toxicity since soluble metals can readily penetrate cell membranes (Roane, 1999; Tiquia-Arashiro, 2018; Jeong et al., 2023). To counteract this, bacteria employ immobilization strategies to counteract the toxic effect of heavy metals, which includes precipitation, intracellular accumulation, and extracellular sequestration in exopolysaccharides (EPSs) (Higham and Sadler, 1984; Roane, 1999; van Hullebusch et al., 2003; Tiquia-Arashiro, 2018; Vandana et al., 2023). EPSs typically consist of polysaccharides featuring ionizable functional groups that can bind to anionic species. This transformation facilitates electrostatic interactions with cationic metal ions, ultimately leading to the immobilization of heavy metals within the EPS matrix (Saba et al., 2019). The effectiveness of EPS-mediated biosorption in efficiently sequestering toxic metals has led to its extensive investigation (Shameer, 2016; Vishan et al., 2017; Saba et al., 2019; Sharma and Saraf, 2023). As a result, biosorption via EPS has garnered substantial research attention. Heavy metals do not only need to be remediated from the ecosystem but are also required to be recovered from every possible source given their importance in commercial and industrial applications. The interaction between several metal cations and the EPS-producing microorganisms combined with their potential for removing heavy metals from polluted waters has stimulated scientific interests due to their ecological importance and practical implications.

Despite the isolation of diverse bacterial strains, the significance of isolating and characterizing indigenous bacteria remains paramount. This approach is not only environmentally sound but also preserves the ecological balance within their specific habitats. This assertion is corroborated by studies that have harnessed metal-tolerant bacteria sourced from industrial effluents (Mishra et al., 2013; Bhatt et al., 2023). In our previous study (Bowman et al., 2018), we isolated Pb-resistant bacterial strains, *Klebsiella* sp. R3, *Klebsiella* sp. R19, *Serratia* sp. L2, and *Raoultella* sp. L30 from sediments of the Saint Clair River. These bacterial strains remove large amounts of Pb^{2+} from solution and produce a high rate of flocculation activity (Bowman et al., 2018). Furthermore, these bacterial strains are well adapted to unfavorable conditions due to their resistance to metals (e.g., Pb) and antibiotics and can grow in a wide range of temperatures. These characteristics may help in developing an effective process for wastewater treatment. However, the metal removal of these strains in aqueous multi-metal solutions has not been investigated in detail, which is particularly useful for building up processes aimed at recovering metals from industrial wastewaters. This study aims to (1) assess the selective metal removal abilities of the bacterial strains in the presence of multiple heavy metals (As^{3+}, Pb^{2+}, Cu^{2+}, Mn^{2+}, Zn^{2+}, Cd^{2+}, Cr^{6+}), (2) investigate the interactions between these metals during the sorption process, and (3) uncover mechanisms of the biosorption process using FT-IR, SEM–EDX, and STEM-EDX techniques.

2. Materials and methods

2.1. Bacterial strains

In this study, the strains were grown on M9 minimal media (M9 salts [BD Difco, Franklin Lakes, NJ], 20% glucose, 1 M $MgSO_4$, 1 M

$CaCl_2$). The biochemical properties of bacterial strains were characterized using the API 20E system (Bio-Mérieux, Marcy-l'Étoile, France). Furthermore, the 16S rRNA sequence of the bacterial strains were determined by direct sequencing of the PCR product. DNA extracts from each strain were prepared using the DNEasy kit (Qiagen, Inc., Valencia, CA). Genomic DNA from these isolates were extracted using the DNEasy kit. Identification of isolates was performed by amplifying the full-length 16S rRNA genes using bacteria-specific primers sequence FD1 (5′ AGA GTT TGA TCC TGG CTC AG 3′) and 1540r (5′ > AAG GAG GTG ATC CAG CC < 3′) (Weisburg et al., 1991) with cycling conditions described previously (Tiquia et al., 2007, 2008; Cho et al., 2012; Nguyen et al., 2013; Plecha et al., 2013). The purified PCR products were sequenced and analyzed directly without cloning. Sequence fragments generated from a given template were edited against electropherograms and then assembled into contigs using SeqMan (Lasergene DNASTAR, Inc., Madison, WI). Two to four overlapping fragments (from both coding and noncoding strand) were used to assemble the contigs. Chimeric sequences were checked by the Check_Chimera program available at the Ribosomal Database Project (RDP II) (Hugenholtz and Huber, 2003). Complete 16S rRNA gene sequences were compared with other reference sequences as available in the NCBI database using the Basic Local Alignment Search Tool (BLAST) algorithm. Closely related sequences were retrieved from Genbank and were aligned along with the 16S rRNA gene sequences of the bacterial strains using the ClustalW program. Phylogenetic trees (Supplementary Figure S1) were constructed from the evolutionary distance matrix calculated through the neighbor-joining method (Saitou and Nei, 1987). Neighbor joining analysis was performed using MEGA 11 (Tamura et al., 2021). Based on the morphological, physiological, biochemical characteristics (Supplementary Table S1) and comparative analysis of the sequence to references retrieved from the NCBI database, the strains were found to be similar to the 16S rRNA sequences of *Klebsiella* sp. (strain R2), *Klebsiella* sp. (strain R19), *Serratia* sp. (strain L2) and *Raoultella* sp. (strain L30).

2.2. Determination of minimum inhibitory concentrations to metals

The bacterial strains used in this study are resistant to Pb and grew in enrichment cultures containing high concentrations (1.25 or 1.5 g L^{-1}) of Pb $(NO_3)_2$ (Bowman et al., 2018). To determine their resistance to other metals (As^{3+}, Pb^{2+}, Cu^{2+}, Mn^{2+}, Zn^{2+}, Cd, $^{2+}$ Cr^{6+}, or Ni^{2+}), the MIC on the strains to these metals was carried out. Stock solutions of As ($NaAsO_2$), Cr ($K_2Cr_2O_7$), Cd ($CdCl_2$), Cu ($CuCl_2.2H_20$), Pb (Pb $[NO_3]_2$), Mn ($MnCl_2.4H_2O$), Ni ($NiCl_2.6H_2O$), and Zn ($ZnSO_4.7H_2O$) were prepared to achieve the final concentration of 1,000 and 10,000 mg L^{-1} with distilled water. The metal solutions were filter sterilized using 0.2 µm Nalgene vacuum filtration system (Thermo Scientific, Waltham, MA). Polycarbonate filters were required for the Cu study. For other metals, polysulfone filters were used to prevent sorption of metals to the filter apparatus (Shuttleworth and Unz, 1993; Wu et al., 2005). Susceptibility testing of the strains to eight different metals was conducted in M9 minimal media amended with metals. Metal-amended media were prepared by adding increasing amounts of metal stock solutions to the autoclaved media. The broth media (200 µL) were poured into 96-well plates and inoculated with mid-logarithmic-phase cultures (20 µL). The plates were incubated at room temperature with shaking (SBT1500 Microplate Shaker, Southwest Science, Hamilton, NJ) at 150 rpm. The MICs (minimal inhibitory concentrations) reported in this study were the lowest concentration of the metal that inhibited bacterial growth after an incubation of 24 h at room temperature in the dark. Growth media inoculated with bacterial strains without metals were used as positive controls. Growth of the strains was monitored by optical density at 595 nm with Sunrise microwell plate reader (Tecan, Research Triangle Park, NC). The absence of growth was determined by the detection threshold of the plate reader.

2.3. Metal removal assay in aqueous solutions

Cells of each culture (100 mL) were confined in dialysis tubing (12–14 kDa of molecular weight cut-off; Spektra/por 5, Spectrum Laboratories, CA) and pretreated with 0.1 N HCl to remove the metal ions possibly bound to the negatively charged groups of the cell envelopes. After 30 min of soaking in 0.1 N HCl, the cell cultures were dialyzed against deionized water for 24 h with continuous stirring at 100 rpm, to remove residual HCl from the treated cultures. In the mono-metal systems, dialyzed cultures were subsequently transferred in 1 L aqueous solutions containing 10 mg L^{-1} of As^{3+}, Pb^{2+}, Cu^{2+}, Mn^{2+}, Zn^{2+}, Cd^{2+}, Cr^{6+}, or Ni^{2+} for 24 h. This metal concentration (10 mg L^{-1}) is like that used in other dialysis assays to investigate the binding capacity of bacterial cells or bacterial EPS with metals (Perez et al., 2008; Pereira et al., 2011; Wang et al., 2014; Bowman et al., 2018). To avoid any possible hydroxide precipitation, the pH of the system (biosorbent + metal solution) was adjusted to 4.5–5.5 by addition of either 1 N HCl or 1 N NaOH. The experiment was performed at room temperature. For the multi-metal systems, 10 mg L^{-1} of each metal was used. Such concentration was used for each metal to be consistent with the concentrations used for the single-metal assays.

Ten mL of the aqueous solutions were withdrawn at different time intervals over 24 h and filtered through 0.2 µm Acrodisc syringe filters (Sigma-Aldrich, Saint Louis, MO). The metal uptake by the bacterial strains was determined from the difference between the concentration of the metals in solution using an atomic absorption spectrometer (PinAAcle 900 T, Perkin Elmer, MA). The As^{3+}, Pb^{2+}, Cu^{2+}, Mn^{2+}, Zn^{2+}, Cd^{2+}, Cr^{6+}, and Ni^{2+} were determined at 193.70, 283.31, 324.75, 279.48, 213.86, 228.00, 357.87, and 232.0 nm, respectively. The amount of metal uptake in blanks (carried out in parallel with just 100 mL of culture media without cells) was also monitored to confirm that negligible metal was lost from solution. The amount of metals removed in blanks, which ranged from 0.1 to 0.2 mg L^{-1}, was subtracted from the experimental values obtained in the tests with the bacterial cultures.

Specific metal uptake (q) was expressed as mg metal removed per g of dry biomass. The dry weight (g L^{-1}) was determined by centrifugation 10 mL of the dialyzed cultures, followed by drying at 50°C until a constant weight was reached (Volesky and May-Philips, 1995). The experiments were performed in triplicates and the data were reported as mean values ± standard deviation. As metal sorption was followed, cell viability was also determined at the beginning and at 24 h using the plate count method (Gerhardt et al., 1994).

2.4. FT-IR analysis of bacterial biomass

Fourier transform infrared spectroscopy (FT-IR) was performed to identify the functional groups in the bacterial strains that might be involved in metal uptake during the biosorption process. This technique has proven to be effective in providing structural information on metal cation binding in microbes (Gupta et al., 2020). FT-IR analysis was carried out on cells before and after metal uptake in aqueous solution containing the 8 metals (As^{3+}, Pb^{2+}, Cu^{2+}, Mn^{2+}, Zn^{2+}, Cd^{2+}, Cr^{6+}, and Ni^{2+}), each had a concentration of 10 mg/L. The infrared spectra of the control before and after metal uptake were analyzed on lyophilized cells using Attenuated Total Reflection (ATR).

2.5. SEM–EDX analysis

Field emission scanning electron microscopy (Tescan Mira3 FEG SEM, Tescan USA, Inc., Pleasanton, CA 94588, United States) coupled with energy dispersive X-ray spectroscopy was carried out to examine the outer morphology of the bacterial cells (Raoultella sp. L30 and *Klebsiella* R19) grown without metal stress and bacterial cells grown with metals. Samples were fixed in 2.5% glutaraldehyde in Sorensen phosphate buffer (pH 7.2), dehydrated with increasing solutions of ethanol (30, 50, 70, 80, 90, 95, and 100%) and HDMS. Prepared samples were placed on the sample holder (stub) with carbon tape. To improve electron conduction, the samples were sputter coated with carbon.

2.6. STEM-EDX analysis

Scanning Transmission electron microscopy with energy dispersive X-ray (EDS) analysis (Thermo Fisher Talos F200X G2, Waltham, Massachusetts, United States) was used to determine the location of the metals in the cell. Strains R19 and L30 were washed with phosphate buffer saline (pH 6.8). After washing, the samples were embedded in agarose and then fixed in 3% Glutaraldehyde +3% paraformaldehyde solutions in 0.1 M Cacodylate buffer (pH 7.2). After 24 h, the cells were fixed with osmium tetroxide (2%) and potassium ferrocyanide (1%) 0.1 M carbonate buffer for 1 h and then washed with 0.1 M carbonate buffer and 0.1 M Na_2 + acetate buffer (pH 5.2) before en-bloc staining for 1 h. Using an automated tissue processor (Leica EM TP, Leica Biosystems, Deerfield, Illinois, USA) the samples were washed with 0.1 M carbonate buffer and 0.1 M Na_2 + acetate buffer (pH 5.2) and then dehydrated with increasing concentrations of ethanol before infiltrated with acetone and Spurr's resin. Thin sections of 60–80 nm thick were obtained using an ultramicrotome (Leica EM UC7, Leica Biosystems, Deerfield, Illinois, United States) and stained with uranyl acetate. The section was fixed on a carbon grid and examined TEM.

2.7. Nucleotide sequence accession numbers and taxon numbers

The nucleotide sequence coding for 16S rRNA genes of *Klebsiella* sp. R3, *Klebsiella* sp. R19, *Serratia* sp. L2, and *Raoultella* sp. L30 were submitted to the GenBank database under the accession numbers OR143353, MG022653, OR143351, and OR143352, respectively. The respective digital protologue database (DPD) Taxon Number were: TA00308 (*Klebsiella* sp. R3), TA00308 (*Klebsiella* sp. R19), TA00309 (*Serratia* sp. L2), and TA00310 (*Raoultella* sp. L30).

3. Results

3.1. Tolerance to metals of the bacterial strains

Table 1 provides the minimum inhibitory concentrations (MICs) of the eight different metals for the respective bacterial strains. Overall, strains L2 and L30 (*Serratia* sp. strain L2 and *Raoultella* sp. strain L30) exhibited higher metal tolerance compared to strains R3 (*Klebsiella* sp.) and R19 (*Klebsiella* sp.). In a broader perspective, the strains demonstrated greater resilience against As^{3+} (ranging from 250 to 450 mg L^{-1}), Pb^{2+} (ranging from 700 to 800 g mL^{-1}), Mn^{2+} (>2,000 mg L^{-1}), and Zn^{2+} (ranging from 500 to 1,100 mg L^{-1}), in contrast to Cd^{2+} (ranging from 20 to 75 mg L^{-1}), Cr^{6+} (ranging from 5 to 10 mg L^{-1}), Cu^{2+} (ranging from 20 to 50 mg L^{-1}), and Ni^{2+} (ranging from 50 to 75 mg L^{-1}).

The hierarchy of metal tolerance for each bacterial strain was as follows: for *Klebsiella* sp. R3, it was $Mn^{2+} > Zn^{2+} > Pb^{2+} > As^{3+} > Cu^{2+} = Ni^{2+} > Cd^{2+} > Cr^{6+}$; for *Klebsiella* sp. R19, it was $Mn^{2+} > Pb^{2+} > Zn^{2+} > As^{3+} > Cu^{2+} = Ni^{2+} > Cd^{2+} > Cr^{6+}$; for *Serratia* sp. L2, it was $Mn^{2+} > Zn^{2+} > Pb^{2+} > As^{3+} > Ni^{2+} = Cd^{2+} > Cu^{2+} > Cr^{6+}$; and for *Raoultella* sp. L30, it was Mn > Zn > Pb > As > Cd > Ni = Cu > Cr (Table 1).

3.2. Metal removal in single-metal and multi-metal systems

The investigation into the specific metal removal capabilities of the bacterial strains was conducted using individual single-metal solutions, each containing 10 mg L^{-1} of As^{3+}, Pb^{2+}, Cu^{2+}, Mn^{2+}, Zn^{2+}, Cd^{2+}, Cr^{6+}, or Ni^{2+}. The study spanned various time intervals over a 24-h period (as demonstrated in Supplementary Figure S2). Over time, the metals were gradually extracted from the solutions, with saturation of the metal removal capacity achieved within approximately 4 to 5 h (Supplementary Figure S2), except for As^{3+} (notably for strains L2 and L30) and Cr^{6+}, for which minimal or negligible removal occurred. Generally, the metal removal efficiency was more pronounced for *Klebsiella* sp. R3 and *Klebsiella* sp. R19 (ranging from 4.4 to 318 mg g^{-1} dry mass) compared to *Serratia* sp. L2 and *Raoultella* sp. L30 (ranging from 0 to 155.42 mg g^{-1} dry mass) (Supplementary Figure S2).

Comparatively, the efficiency of metal removal in single-metal solutions was notably higher than that in mixed solutions containing all eight metal cations (as depicted in Figure 1). Notably, in single-metal solutions, *Klebsiella* sp. R3 exhibited removal efficiencies of ≥150 mg g^{-1} dry mass for Pb^{2+}, Cu^{2+}, and Zn^{2+} (Figure 1A). Similarly, *Klebsiella* sp. R19 displayed high removal efficiency for Pb^{2+}, Cd^{2+}, Cu^{2+}, Mn^{2+}, and Zn^{2+} (Figure 1B), while *Raoultella* sp. L30 showed effective removal of Pb^{2+} (Figure 1D). In the presence of all eight metal cations, the binding process was primarily inhibitory rather than stimulatory, as the cations competed for binding sites on the bacterial cells. Unexpectedly, a stimulatory effect on the removal efficiency of

10.3389/fmicb.2023.1278886

TABLE 1 Minimum inhibitory concentrations of metals.

Minimum inhibitory concentrations (MIC) (mg L^{-1})	Strains			
	Klebsiella sp. strain R3	*Klebsiella* sp. strain R19	*Serratia* sp. strain L2	*Raoultella* sp. strain L30
As	250	350	350	450
Cd	20	20	75	75
Cr	10	15	15	15
Cu	50	50	20	50
Pb	700	800	800	800
Mn	>2,000	>2,000	>2,000	>2,000
Ni	50	50	75	50
Zn	1,000	500	1,100	1,100

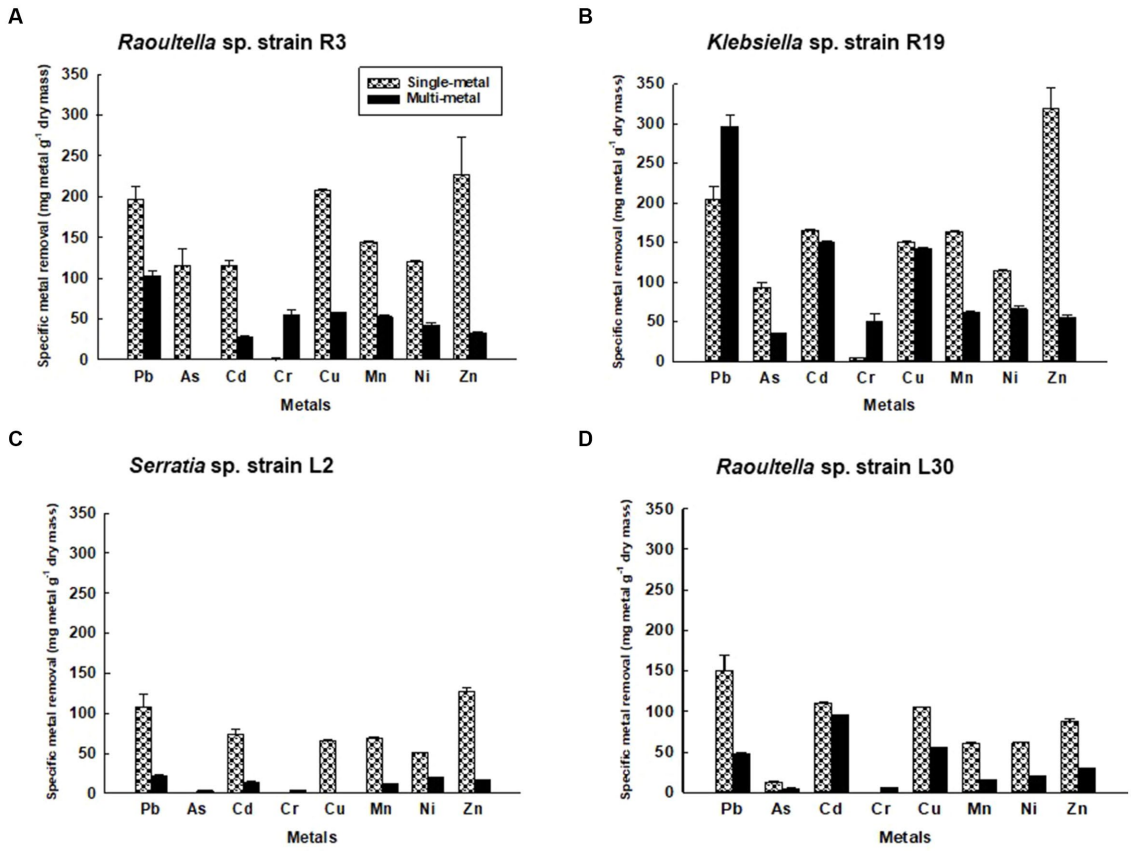

FIGURE 1
Metal removal by **(A)** *Klebsiella* sp. R3; **(B)** *Klebsiella* sp. R19; **(C)** *Serratia* sp. L2; and **(D)** *Raoultella* sp. L30 in single- (dotted bars) and multiple- (black bars) metal solutions. All the values are the mean of three replicates ± standard deviation.

Pb^{2+} and Cr^{6+} was observed in strain R19 (Figure 1B) in the presence of multiple metal cations. Specifically, Pb^{2+} removal in the multi-metal solution was 31% higher compared to the solution with only Pb^{2+}, and 91% higher compared to the solution with only Cr^{6+}. A lesser stimulatory effect was observed for Cr^{6+} removal in strains L2 and L30 (Figures 1C,D).

Notably, the kinetics of metal uptake in the eight-metal solutions did not significantly deviate from those observed in the single-metal solutions. The saturation of metal removal capacity occurred within 4–5 h in the presence of all eight metals (Supplementary Figure S3). Moreover, the viability of the strains remained unaffected by the presence of metals in both single-metal and multi-metal solutions. The number of viable cells was consistent, ranging from 7.3 to 8.9 Log10 CFU g^{-1} of dry cell mass for strains R3 and R19, and from 8.0 to 9.7 Log10 CFU g^{-1} of dry cell mass for strains L2 and L30 throughout the 24-h metal binding assay (Supplementary Figure S4). There was no statistically significant difference ($p \leq 0.05$) in the number of viable cells between the single-metal and multi-metal solutions.

3.3. FT-IR

FTIR spectra were acquired for bacterial strains before and after the uptake of a combination of eight metals, spanning the range of 4,000 to 400 cm^{-1} (depicted in Figure 2). The FT-IR profiles of metal-free bacterial strains exhibited diverse peaks, revealing the intricate nature of the bacterial cell surface. Common bands were evident in the strains prior to metal uptake across all four bacterial types, albeit with fewer IR peaks observed in the *Serratia* sp. L2 and *Raoultella* sp. L30 strains (illustrated in Figures 2A,B) compared to the *Klebsiella* sp. R3 and *Klebsiella* sp. R19 strains (shown in Figures 2C,D). These IR bands corresponded to functional groups including amino (N-H, NH_2), alkyne (C ≡ C), carbonyl (C=O), carboxylic (C-O), hydroxyl (-OH), and phosphate (P=O) groups (depicted in Figure 2). The assignments of these bands and the specific functional groups for each of the four strains are detailed in Tables 2–5. Upon exposure to metals, alterations in the intensity of bands became apparent, accompanied by shifts in absorption bands and the emergence of new peaks. The number of IR bands expanded as the strains encountered the multi-metal environment. Notably, the occurrences of IR shifts and new peaks were more pronounced in *Klebsiella* sp. R3 and *Klebsiella* sp. R19 than in *Serratia* sp. L2 and *Raoultella* sp. L30 strains. In the metal-loaded L2 and L30 strains, IR spectra shifts indicated the involvement of functional groups linked to aromatic organics, alkynes (C ≡ C), and alkanes (C-H). Conversely, the R3 and R19 strains demonstrated shifts associated with aromatic organics, alkynes (C ≡ C), alkanes (C-H), as well as hydroxyl, amine, and aldehyde functional groups. Moreover, new peaks emerged in the spectra of the R3 and R19 metal-loaded strains, indicating the presence of aromatic compounds, alkanes (C-H), carboxyl (C-C), alkynes (C ≡ C), alcohol (R-CHO), amine (P-NH, NH_2), and hydroxyl (O-H) functional groups. These observations underscored the intricate alterations in the bacterial cell surfaces induced by the uptake of multiple metals, with distinct variations based on bacterial strain type.

3.4. SEM–EDX

Examination of SEM micrographs revealed alterations in both size and morphology of *Klebsiella* sp. R19 (depicted in Figure 3) and *Raoultella* sp. L30 (depicted in Figure 4) before and after metal adsorption. Initially, *Klebsiella* sp. R19 exhibited an average length of 1.78 ± 0.40 μm and an average width of 0.71 ± 0.12 μm (Figure 3A). Subsequent to the biosorption process in an aqueous solution containing eight metals, its dimensions were diminished to 1.32 ± 0.27 μm x 0.70 ± 0.11 μm (Figure 3B), reflecting reductions of 26% in length and 3% in width. A parallel outcome was observed for *Raoultella* sp. L30, wherein its size underwent a decrease from 1.53 ± 0.34 μm x 0.65

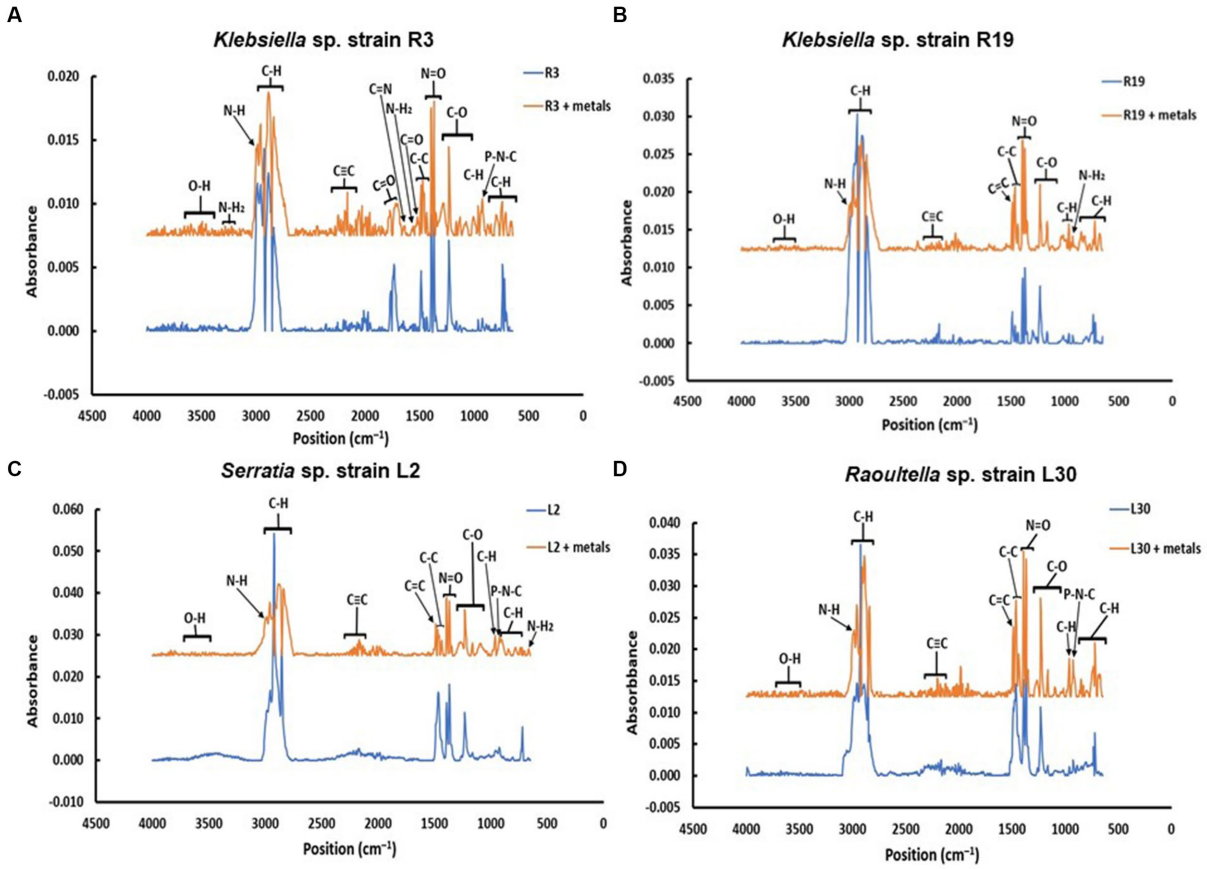

FIGURE 2
Comparison of the IR spectra of **(A)** *Klebsiella* sp. R19; **(B)** *Klebsiella* sp. R19; **(C)** *Serratia* sp. L2; and **(D)** *Raoultella* sp. L30 before and after absorption of mixed metals.

10.3389/fmicb.2023.1278886

TABLE 2 IR absorption band changes and possible assignment for the metal-free and metal-loaded *Klebsiella* strain sp. R3.

FTIR peak	*Klebsiella* sp. strain R3					
	Metal-free	Metal-loaded	Displacement*	Functional groups	Bond	Assignment
1		667	667	$C_2H_2R_2$	C-H out-of-plane-bend	Alkene
2	719	712	7	1,3-Disubstituted (Aromatic compounds)	C-H out-of-plane-bends	Aromatic
3	738	742	4	1,2-Disubstituted (Aromatic compounds)	C-H out-of-plane-bend	Aromatic
4	805	798	7	C_2HR_3	C-H out-of-plane-bend	Alkene
5		846	846	1,4-Disubstituted (Aromatic compounds)	C-H out-of-plane-bend	Aromatic
6		876	876	1,3-Disubstituted (Aromatic compounds)	C-H out-of-plane-bend	Aromatic
7		1,003	1,003	$(RCO)_2O$	C-O stretch	Carbonyl
8		1,128	1,128	R-OH	C-O stretches	Alcohol
9		1,282	1,282	RCOOR'	C-O stretch	Carbonyl
10	1,457	1,469	12	C-C	C-C bend	Alkane
11	1,558	1,557	1	P-NH_2	NH_2	Amine
12	1,647	1,640	7	R_2C=NR or R_2C=NH	C=N stretch	Imine and Oxime
13		1,700	1,700	R_2C=O or RCOOH	C=O stretch	Ketone or carboxylic acid
14		1,718	1,718	R_2C=O or RCOOH	C=O stretch	Ketone or carboxylic acid
15		1,770	1,770	RCOC1	C=O stretch	Acid Chloride
16	2,121	2,117	4	C≡C	C≡C stretch	Alkyne
17	2,147	2,136	11	C≡C	C≡C stretch	Alkyne
18		2,162	2,162	C≡C	C≡C stretch	Alkyne
19	2,177	2,184	7	C≡C	C≡C stretch	Alkyne
20	2,195	2,199	4	C≡C	C≡C stretch	Alkyne
21	2,251	2,259	8	RC≡N	C≡N stretch	Nitrile
22	2,859	2,861	3	C-H	C-H stretch	Alkane
23	2,986	2,984	2	P-NH	NH	Amine
24		3,120	3,120	C=C-H	C-H stretch	Alkene
25		3,224	3,224	P-NH_2	NH_2	Amine
26		3,280	3,280	P-NH_2	NH_2	Amine
27		3,493	3,493	RO-H hydrogen bond	O-H stretch	Hydroxyl
28		3,993	3,593	RO-H free	O-H stretch	Hydroxyl
29	3,630	3,623	7	RO-H free	O-H stretch	Hydroxyl

*IR band shifts in red; new bands in blue.

± 0.09 µm (Figure 4A) to 1.17 ± 0.27 µm x 0.70 ± 0.07 µm (Figure 4B). SEM analysis also provided insights into notable modifications observed on the cell surfaces of both *Klebsiella* sp. R19 and *Raoultella* sp. L30 bacteria Following the process of metal biosorption. The cell surfaces of *Klebsiella* sp. R19 exhibited a distinctive texture characterized by irregularities, including dents, wrinkles, and elongations (Figures 3C,D). These surface features appeared to be a direct consequence of the interaction between the bacterial cells and the adsorbed metals. The metals' toxic influence appeared to induce these alterations in the cell surface structure. Additionally, a considerable amount of flocculation was evident on the cell surfaces. This phenomenon could be attributed to the secretion of extracellular polysaccharides prompted by the presence of metals. The extracellular polysaccharides might have contributed to the aggregation of bacterial cells, leading to the formation of these flocculent clusters (Figure 3C). The cell surfaces of *Raoultella* sp. exhibited varying degrees of deformations, creases, or elongations due to the adverse impact of the metals. Additionally, a notable amount of flocculation emerged on the cell surfaces, prompting cellular aggregation (Figures 4C,D). This phenomenon might be attributed to the metal-induced secretion of extracellular polysaccharides (Gupta and Diwan, 2017).

The energy-dispersive X-ray spectroscopy (EDX) analysis of *Klebsiella* sp. R19 and *Serratia* sp. L30 (Figure 5) affirmed the presence of adsorbed metals on the cell surfaces. The quantified outcomes, illustrating the distribution of the eight metals on the cell surfaces of *Klebsiella* sp. R19 and *Raoultella* sp. L30, are presented in Figure 5. Among these eight metals, Cd^{2+} predominated the cell surface of *Klebsiella* sp. followed by Cu^{2+}, Zn^{2+} and Pb^{2+} (Figure 5A), while Cu^{2+} stood out as the foremost element, followed by Zn^{2+}, Cd^{2+}, and As^{3+} (Figure 5B).

10.3389/fmicb.2023.1278886

TABLE 3 IR absorption band changes and possible assignment for the metal-free and metal-loaded *Klebsiella* sp. strain R19.

FTIR peak	*Klebsiella* sp. strain R19					
	Metal-free	Metal-loaded	Displacement*	Functional groups	Bond	Assignment
1		675	675	$C_2H_2R_2$	C-H out-of-plane bend	Alkene
2	716	719	3	1,3-Disubstituted (Aromatic compounds)	C-H out-of-plane bend	Aromatic
3	734	737	4	Monosubstituted	C-H out-of-plane bend	Aromatic
4		768	768	1,2-Disubstituted (Aromatic compounds)	C-H out-of-plane bend	Aromatic
5	801	813	12	C_2HR_3	C-H out-of-plane-bend	Alkene
6		846	846	1,4-Disubstituted (Aromatic compounds)	C-H out-of-plane-bend	Aromatic
7		924	924	P-NH_2	NH_2	Amine
8		939	939	P-NH_2	NH_2	Amine
9	962	964	2	$C_2H_2R_2$	C-H out-of-plane-bend	Alkene
10		988	988	C_2H_3R	C-H out-of-plane-bends	Alkene
11		1,118	1,118	R-OH	C-O stretches	Alcohol
12	1,230	1,238	8	R-OH	C-O stretches	Alcohol
13	1,368	1,373	5	R-NO_2	N=O	Nitro
14	1,390	1,393	3	R-NO_2	N=O	Nitro
15	1,435	1,434	1	C-C	C-C bend	Alkane
16	1,457	1,461	4	C-C	C-C bend	Alkane
17	1,487	1,490	2	C=C	C=C	Aromatic
18		2,147	2,147	C≡C	C≡C stretch	Alkyne
19	2,166	2,162	4	C≡C	C≡C stretch	Alkyne
20	2,188	2,193	5	C≡C	C≡C stretch	Alkyne
21		2,210	2,210	C≡C	C≡C stretch	Alkyne
22		2,230	2,230	C≡C	C≡C stretch	Alkyne
23		2,232	2,232	C≡C	C≡C stretch	Alkyne
24	2,837	2,840	3	RCHO	C-H stretch	Aldehyde
25	2,881	2,889	8	C-H	C-H stretch	Alkane
26		2,911	2,911	C-H	C-H stretch	Alkane
27		2,930	2,930	C-H	C-H stretch	Alkane
28	2,926	2,960	34	C-H	C-H stretch	Alkane
29		2,986	2,986	P-NH	NH	Amine
30		2,997	2,997	P-NH	NH	Amine

*IR band shifts in red; new bands in blue.

3.5. STEM-EDX

STEM images unveiled the accumulation of metals within both the cytoplasm and cell walls of *Klebsiella* sp. R19 (depicted in Figures 6, 7) and *Raoultella* sp. L30 (illustrated in Figures 8, 9). Numerous electron-dense granules were discernible, situated across cell walls, membrane fractions, and within the cytoplasm. These electron-dense granules appeared vividly in the STEM-HAADF image. The granules exhibited three distinct types: sizable and compact granules (indicated by blue arrows), smaller granules (marked by green arrows), and saturation clustering around storage granules (designated by purple arrow) (depicted in Figure 7). Interestingly, *Raoultella* sp. L30 did not exhibit evident storage granules. The verification via EDX analysis affirmed the presence of metal accumulation on the cell wall, cell membrane, and cytoplasm. The position beam spectra clearly indicated the detection of all eight metals within the electron-dense granules for both strains (portrayed in Figures 6–9). These electron-dense granules encapsulate metal complexes, effectively binding the metals. To determine the relative distribution of the eight metals within the electron-dense granules, the atomic percentages (atm %) of As^{3+}, Pb^{2+}, Cu^{2+}, Mn^{2+}, Zn^{2+}, Cd^{2+}, Cr^{6+}, and Ni^{2+} were normalized to 100%, after excluding contaminants (such as C, O, etc.).

For *Klebsiella* sp. R19, Cd overwhelmingly dominated the electron-dense granules within the cell wall and cell membrane. The order of metal distribution was as follows: $Cd^{2+} > Cu^{2+} > Pb^{2+} > As^{3+} > Zn^{2+} > Ni^{2+} > Mn^{2+} > Cr^{6+}$ (depicted in Figure 6). A similar pattern emerged for the electron-dense granules within the cytoplasm (illustrated in

10.3389/fmicb.2023.1278886

TABLE 4 IR absorption band changes and possible assignment for the metal-free and metal-loaded *Serratia* sp. strain L2.

FTIR peak	*Serratia* sp. strain L2					
	Metal-free	Metal-loaded	Displacement*	Functional groups	Bond	Assignment
1		663	663	P-NH	NH_2	Amine
2		704	704	Monosubstituted (aromatic compound)	C-H out-of-plane-bends	Aromatic
3	719	723	4	1,3-Disubstituted (aromatic compound)	C-H out-of-plane-bend	Aromatic
4		846	846	1,4-Disubstituted (aromatic compound)	C-H out-of-plane-bend	Aromatic
5		909	909	C_2H_3R	C-H out-of-plane-bends	Alkene
6		1,092	1,092	R-OH	C-O stretches	Alcohol
7		1,435	1,435	C-C	C-C bend	Alkane
8		1,469	1,469	C-C	C-C bend	Alkane
9	2,132	2,134	4	C≡C	C≡C stretch	Alkyne
10	2,154	2,158	4	C≡C	C≡C stretch	Alkyne
11	2,195	2,184	11	C≡C	C≡C stretch	Alkyne
12	2,218	2,214	4	C≡C	C≡C stretch	Alkyne
13		2,837	2,837	RCHO	C-H stretch	Aldehyde
14	2,851	2,885	34	C-H	C-H stretch	Alkane
15	2,922	2,930	8	C-H	C-H stretch	Alkane
16	2,956	2,960	4	C-H	C-H stretch	Alkane
17		2,986	2,986	P-NH	NH	Amine
18		3,496	3,496	RO-H hydrogen bond	O-H stretch	Hydroxyl
19		3,623	3,623	RO-H free	O-H stretch	Hydroxyl

*IR band shifts in red; new bands in blue.

Figure 4). Meanwhile, in the case of *Raoultella* sp. L30, the electron-dense granules in the cell wall [$Cu^{2+} > Cd^{2+} > Pb^{2+} = Zn^{2+} > Cr^{6+} > Ni^{2+} > Mn^{2+} > As^{3+}$] and cell membrane [$Cu^{2+} > Pb^{2+} > Cd^{2+} > Zn^{2+} > Cr^{6+} > Ni^{2+} > Mn^{2+} > As^{3+}$] were notably enriched in Cu^{2+} (depicted in Figure 8). While the relative metal distribution in the electron-dense granules within the cytoplasm of *Raoultella* sp. L30 exhibited some variability (shown in Figure 9), the dominant metal consistently observed in these granules was Cu^{2+} (as shown in Figure 9).

4. Discussion

Metal tolerance in bacteria is an essential trait and may help in developing an effective process for the treatment of heavy metal contaminated wastewaters. The results of the MIC assay provided insights into the range of metal concentrations at which these strains could withstand metal exposure. The strains were adapted to high concentrations of not only Pb but also As^{3+}, Mn^{2+}, and Zn^{2+} (Table 1). From a broader perspective, it is notable that the bacterial strains exhibited considerable resistance against certain metals. Specifically, they demonstrated robust resilience against As^{3+}, with MICs ranging from 250 to 450 mg L^{-1}. Similarly, they showcased noteworthy tolerance against Pb^{2+}, spanning from 700 to 800 g L^{-1}. Moreover, the strains exhibited impressive resilience against Mn concentrations exceeding 2,000 mg L^{-1}, as well as Zn^{2+} concentrations ranging from 500 to 1,100 mg L^{-1}. These findings suggest that these bacterial strains have evolved mechanisms to withstand and adapt to these specific heavy metals. Conversely, the strains exhibited comparatively lower tolerance toward other heavy metals. Cd^{2+}, Cr^{6+}, Cu^{2+}, and Ni^{2+} elicited relatively lower MIC values, indicating that the bacterial strains are more sensitive to these metals. This variability in sensitivity across different metals underscores the complexity of bacterial responses to heavy metal exposure. it becomes evident that strains L2 and L30 (*Serratia* sp. strain L2 and *Raoultella* sp. strain L30) displayed heightened levels of metal tolerance compared to strains R3 (*Klebsiella* sp.) and R19 (*Klebsiella* sp.). This disparity in metal tolerance could stem from a multitude of factors, such as variations in the strains' genetic makeup, metabolic pathways, and the presence of specific metal detoxification mechanisms (Rosen, 1995; Silver, 1996; Nies, 1999; Rensing and Grass, 2003; Silver and Phung, 2005; Helbig and Grass, 2017).

The biosorption abilities of bacterial isolates in both single metal and multi-metal solutions, shedding light on their potential effectiveness in metal removal and the intricate dynamics of simultaneous metal exposure. In the context of single metal solutions, Within the realm of single metal solutions, the capabilities of four metal-tolerant strains emerge prominently. These strains demonstrated impressive efficacy in extracting substantial concentrations of diverse metal ions, including Pb^{2+}, As^{2+}, Zn^{2+}, Cd^{2+}, Cr^{6+}, and Mn^{2+}—each exceeding 50 mg of metal per gram of cell dry mass. Notably, strains R3 and R19 exhibited heightened metal cation removal compared to L2 and L30. These findings underscore the strains' adaptability and potential applicability in targeted scenarios where specific metal pollutants predominate. Transitioning into solutions encompassing eight metals, a more intricate picture unfolds. The co-presence of multiple metal cations elicited inhibitory effects in the cation binding process, stemming from the

10.3389/fmicb.2023.1278886

TABLE 5 IR absorption band changes and possible assignment for the metal-free and metal-loaded *Raoultella* sp. strain L30 strain.

FTIR peak	*Raoultella* sp. strain L30					
	Metal-free	Metal-loaded	Displacement*	Functional groups	Bond	Assignment
1		678	678	$C_2H_2R_2$	C-H out-of-plane bend	Alkene
2	734	738	4	Monosubstituted (Aromatic Compound)	C-H out-of-plane bends	Aromatic
3	805	809	4	C_2HR_3	C-H out-of-plane bends	Alkene
4	846	848	2	1,4-Disubstituted (Aromatic Compound)	C-H out-of-plane bends	Aromatic
5	887	886	1	$C_2H_2R_2$	C-H out-of-plane bend	Alkene
6		1,066	1,066	$(RCO)_2O$	C-O stretch	Carbonyl
7		1,260	1,260	R-OH	C-O stretches	Alcohol
8	1,461	1,465	4	C-C	C-C bend	Alkane
9		1,562	1,562	P-NH_2	NH_2	Amine
10		1,640	1,640	R_2C=NR or R_2C=NH	C=N stretch	Imine and Oxime
11		2,147	2,147	C≡C	C≡C stretch	Alkyne
12		2,162	2,162	C≡C	C≡C stretch	Alkyne
13	2,188	2,190	2	C≡C	C≡C stretch	Alkyne
14		2,210	2,210	C≡C	C≡C stretch	Alkyne
15		2,230	2,230	C≡C	C≡C stretch	Alkyne
16		2,840	2,840	RCHO	C-H stretch	Aldehyde
17	2,855	2,859	4	C-H	C-H stretch	Alkane
18	2,922	2,930	8	C-H	C-H stretch	Alkane
19		2,986	2,986	P-NH	NH	Amine
20		2,997	2,996	P-NH	NH	Amine
21		3,493	3,493	RO-H hydrogen bond	O-H stretch	Hydroxyl
22		3,586	3,586	RO-H free	O-H stretch	Hydroxyl

*IR band shifts in red; new bands in blue.

competition for binding sites on both bacterial cell surfaces and extracellular polymeric substances (EPS). It has been reported that in solutions containing multiple metals, some of the metal cations already bound on the EPS exert a strong hindrance to the access of other cations at the adjacent adsorption sites (Sag et al., 2000; Micheletti et al., 2008; Pradhan and Rai, 2011; Lu et al., 2021). This steric effect results in EPS conformational change (Huang et al., 2022) that leads to the general reduction in metal removal. *Klebsiella* sp. R19 showed the highest affinity to Pb^{2+} in mixed metal solutions with q value even higher than in single-metal solutions (Supplementary Figure S2). In contrast to Pb^{2+} the other seven metals performed poorer in the multiple-metal tests. The reduction in metal removal could be because the presence of many metals may have overwhelmed the cells and EPS to a point that they cannot bind to as many metal cations as in the single-metal tests. Nonetheless, *Klebsiella* sp. R19 was the strain that removed the most metal cations of all the four bacterial strains tested. In the mixed metal solutions, *Klebsiella* sp. R3, *Klebsiella* sp. R19 showed higher metal cation removal efficiencies than *Serratia* sp. L2 and *Raoultella* sp. L30. Insights from the study align with Bowman et al.'s (2018) observations, linking higher flocculation activities of bacterial strains to enhanced metal cation removal capacity. Both *Klebsiella* sp. R3 and *Klebsiella* sp. R19 exhibited superior flocculation activities (79 and 71%, respectively) compared to *Serratia* sp. L2 and *Raoultella* sp. L30 (L2 = 56%; L30 = 67%). This correlation underscores that flocculation activity directly influences the EPS's ability to bind metal ions, thus strengthening the strains' metal removal potential.

Surprisingly, despite R3 and R19 strains showcasing lower metal tolerance than L2 and L30 strains (Table 1), they exhibit a remarkable ability to efficiently remove a greater quantity of metals (Figure 10). Overall, *Klebsiella* sp. R3, *Klebsiella* sp. R19 had higher metal cation removal efficiencies than *Serratia* sp. L2 and *Raoultella* sp. L30 in single- and multi-metal solutions. These findings challenge the conventional belief that metal tolerance dictates the efficacy of metal removal by bacterial strains. The results underline that metal removal efficiency is a complex phenomenon, shaped not only by a strain's ability to endure metal stress but also by its capacity to effectively bind metal cations. The high flocculant-production ability of R3 and R19 strains (Bowman et al., 2018) emerges as a crucial factor, enabling them to interact with a higher number of metal cations in aqueous solutions. Bowman et al. (2018) suggest that the efficiency of metal removal is linked to the strains' capability to create contact with metal cations, a vital aspect often overshadowed by metal tolerance considerations. A pertinent facet of metal resistance is its association with decreased metal uptake or impermeability, as discussed by Gadd (1990). The lower overall metal uptake observed in the L2 and L30 strains may be attributed to their metal resistance mechanisms, which inadvertently diminish their metal uptake capacity. Conversely, R3 and R19 strains' ability to effectively remove metals could be attributed

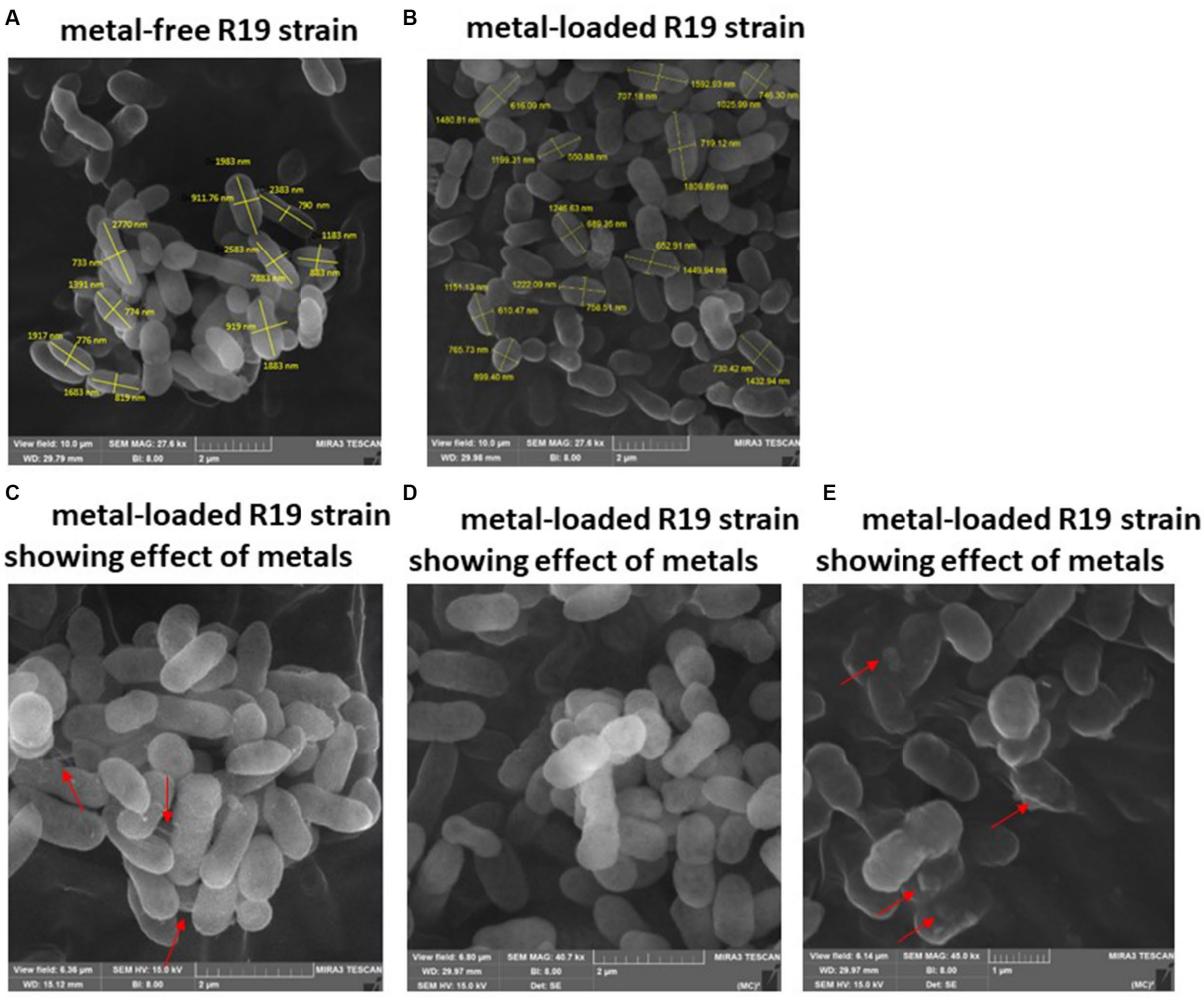

FIGURE 3
SEM images of *Klebsiella* sp. R19 before **(A)** and after absorption of mixed metals **(B)** and morphological changes when exposed to the eight metals **(C–E)**. The size (length and width) and cells are shown in nm. The red arrows point to the presence of flocs on the cell surface.

to their dynamic interaction with metal cations, potentially due to a different balance between metal resistance and efficient metal removal strategies. R3 and R19 strains might possess a higher number or more accessible functional groups, recognized as crucial metal binding sites.

To understand the interactions between bacterial cell surfaces and multiple metal ions, the four strains were subjected to a comprehensive FTIR analysis, both before and after exposure to a complex blend of eight metal ions. When metals first interact with the cell surface, they get sequestered on the surface via adsorption. This could be a result of surface complexation of the metals with the functional groups present on the cell wall (Wang et al., 2021). As a result, changes in the absorption peaks of the spectrum were witnessed in this study (Tables 2–5). The bacterial strains devoid of metal ions revealed a nuanced spectrum, marked by a multitude of absorption peaks. This intricate profile reflects the complex composition of the cellular biomass. A robust and expansive FTIR region, spanning from 3,600 to 2,500 cm^{-1}, is emblematic of the vibrational stretches encompassing C-H (alkane), OH (hydroxyl), and N-H (amine) stretches (Panda et al., 2007). The distinctive C ≡ C stretch between 2,260 and 2,100 cm^{-1} aligns with alkynes, while the span from, while the span from 1,500 to 900 cm^{-1} encapsulates the overlap of C-C, C-O, and C-O-P stretches, characteristic of cellular polysaccharides (Wolkers et al., 2004). Notably, bands resonating within the range of 860 to 700 cm^{-1} correspond to aromatic organic components, further mirroring the intricate nature of cellular constitution (Grube et al., 2008). It is important to note that the appearance of a new peak at 3,496 cm^{-1} for *Serratia* sp. L2 and 3,493 for *Raoultella* sp. L30 appeared after contact with metals and these shifts may be due to Cd^{+2}, Cr^{2+}, Cu^{2+}, or Ni^{2+} cationic interaction with the hydroxyl group for metal oxygen binding (Panda et al., 2007). The appearance of new peaks at 3,224 and 3,280 cm^{-1} for *Klebsiella* sp. R3, and 1,118, 2,986, and 2,997 cm^{-1} for *Klebsiella* sp. R19 can be attributed to the presence of phosphate and amino groups and are linked to the presence of phosphate and amino groups, playing a pivotal role in the biosorption of metals (Sodhi et al., 2020).

The appearance of new IR peaks within the spectra can be attributed to the dynamic response of bacterial strains to metal exposure, resulting in the production of extracellular polymeric substances (EPS). This phenomenon has garnered the attention of numerous researchers who have noted enhanced EPS production in

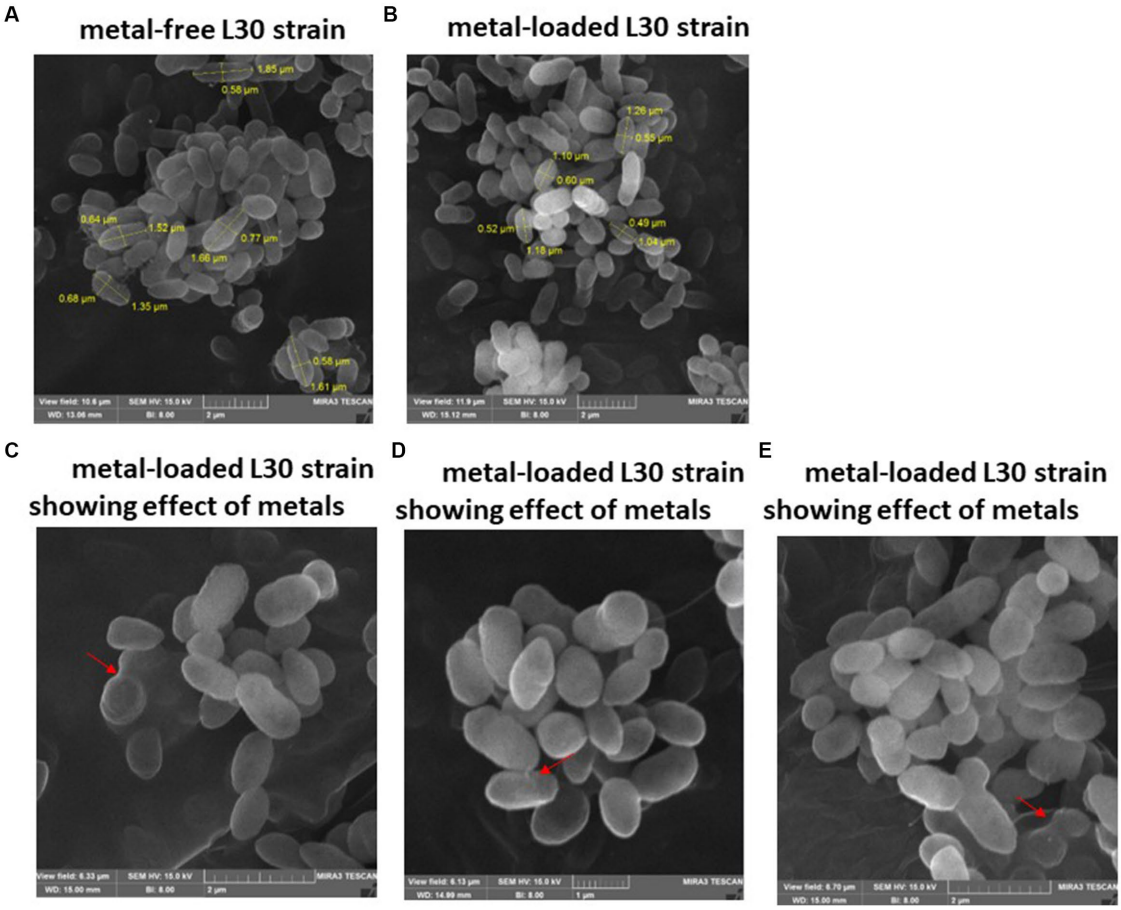

FIGURE 4
SEM images of *Raoultella* sp. L30 L30 before **(A)** and after absorption of mixed metals **(B)** and morphological changes when exposed to the eight metals **(C–E)**. The size (length and width) and cells are shown in μm. The red arrows point to the presence of flocs on the cell surface.

bacterial cells under metal-amended conditions (Redmile-Gordon and Chen, 2017; Rizvi et al., 2019a). This observation underscores the notion that metal-induced stress triggers heightened EPS production, potentially acting as a protective layer against the deleterious effects of metal toxicity (Mathivanan et al., 2021a). EPS are such complex blends of high molecular weight polyanionic polymers, such as proteins, humic acids, polysaccharides, and nucleic acids that bind cationic metals with different degrees of specificity and affinity (Bhaskar and Bhosle, 2006; Pal and Paul, 2008; Tiquia-Arashiro, 2018; Pagliaccia et al., 2022). The multifaceted functions of EPS span beyond metal binding, extending to the safeguarding of cells against environmental stressors and the augmentation of metal biosorption capabilities (Planchon et al., 2013; Rajaram et al., 2013; Deepika et al., 2016). Notably, Mathivanan et al. (2021b) conducted FT-IR analysis on EPS produced by *Bacillus cereus* KMS3-1, revealing the presence of hydroxyl, carboxyl, or carbonyl groups and glycosidic bonds—a testament to the diversity of functional groups contributing to metal binding. Insightful research by Shuhong et al. (2014) shed light on the metal-binding mechanism, emphasizing that this process occurs on the EPS surface. Their findings indicated the pivotal roles of functional groups such as O–H, CH, C=O, C–O, and C–C=O in the binding of metal ions like Cd^{+2}, Cu^{2+}, and Pb^{2}. Notably, these very functional groups were evident in the metal-loaded bacterial cells in the current study, as exemplified in Tables 2–5. The distinctive spectrum alterations and emergence of new bands, particularly prominent in *Klebsiella* sp. R3 and *Klebsiella* sp. R19 (Tables 2, 3), allude to the abundance of binding sites on the cell surface for metal interactions. Consequently, this abundance of interaction sites aligns with the higher observed metal removal capacity in these strains compared to *Serratia* sp. L2 and *Raoultella* sp. L30 (Figure 1). In essence, the appearance of novel IR peaks underscores the dynamic interplay between bacterial strains and metal ions, triggering EPS production and instigating a repertoire of metal-binding functional groups. This mechanism not only shields cells against metal toxicity but also enhances their metal removal prowess, accentuating the multifaceted nature of microbial-metal interactions.

The investigation into the effects of metal exposure on bacterial strains was enriched by employing SEM and EDX analyses. These techniques provided valuable insights into the morphological changes and metal adsorption patterns exhibited by the bacterial strains *Klebsiella* sp. R19 and *Raoultella* sp. L30, both before and after exposure to a complex mixture of eight metal ions. The SEM micrographs unveiled significant alterations in the size and morphology of the bacterial strains following metal adsorption. The initial dimensions of *Klebsiella* sp. R19 and *Raoultella* sp. L30 were reduced after the biosorption process, indicating a potential

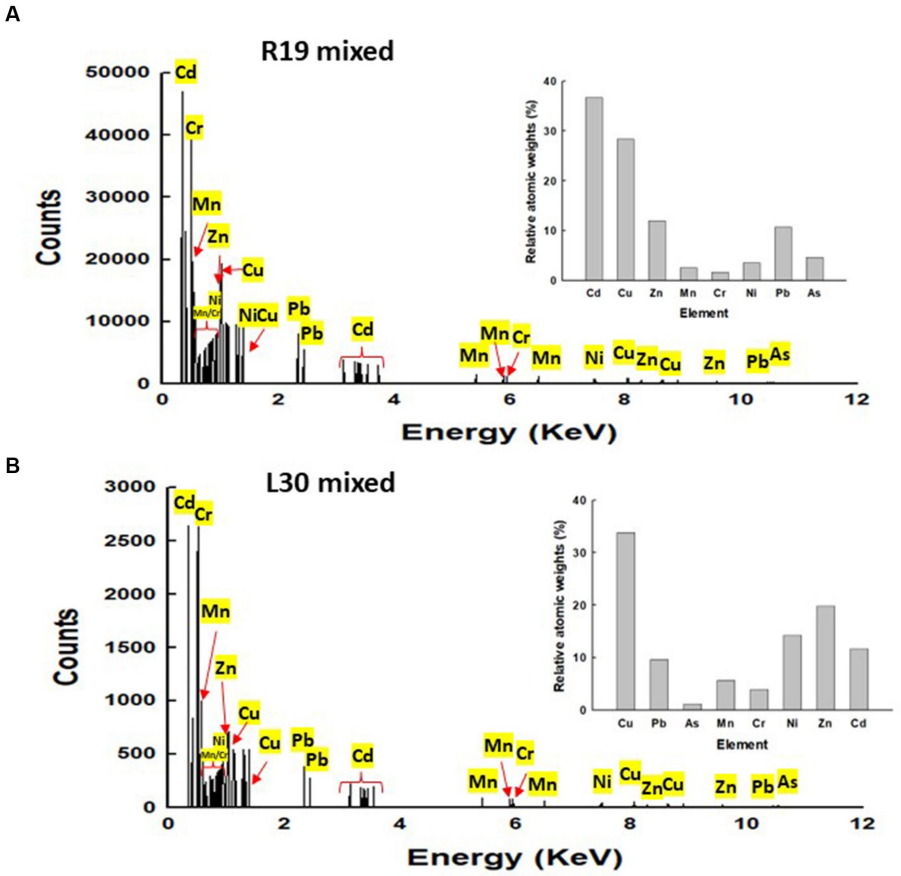

FIGURE 5
Energy dispersive X-ray spectroscopy (EDX) results for **(A)** *Klebsiella* sp. R19 and *Serratia* sp. L30 after absorption of mixed metals **(B)**. Quantification results of Pb, As, Cd, Cr, Cu, Mn, Ni or Zn in *Klebsiella* sp. R19 and *Serratia* sp. L30 strains at 15 kV.

interaction between the bacterial cells and the adsorbed metals. These changes in size could be attributed to the toxic effects of metals on the cells, leading to structural modifications on the cell surface (Rizvi et al., 2019b). Particularly noteworthy were the distinct textures observed on the cell surfaces of both strains. The irregularities such as dents, wrinkles, and elongations reflected the complex interplay between bacterial cells and metal ions. The appearance of these surface features was likely driven by the binding of metals to specific functional groups on the bacterial cell surfaces. Dadrasnia et al. (2015) noted that the roughness and wrinkling of the cells could also be due to sequestration and precipitation of functional groups on the cell wall. The EDX analysis confirmed the presence of metals on the surface of the cells. The observed phenomenon of flocculation on the cell surfaces of both strains further underscored the intricate response to metal exposure. This flocculation could be linked to the secretion of extracellular polysaccharides as a protective mechanism against metal toxicity. The aggregation of bacterial cells resulting from this flocculation indicated a dynamic adaptation to the metal stress environment. The SEM analysis thus provided a visual representation of the cellular changes induced by metal exposure, shedding light on the intricate dynamics of bacterial response to multi-metal conditions. Moreover, EDX analysis validated the presence of adsorbed metals on the cell surfaces. The quantification of metal distribution further illuminated the preference of certain metals for binding to the cell surfaces. The dominance of specific elements on the cell surface, such as Cd^{2+} and Cu^{2+}, highlighted the varying degrees of metal binding affinity exhibited by the strains. These findings corroborated the importance of examining the interaction between bacterial cell surfaces and metal ions in multi-metal environments.

The comprehensive understanding of metal uptake and accumulation within bacterial cells has been facilitated by STEM EDX analysis. This advanced analytical approach not only confirmed the presence of metals on the cell surface but also provided valuable insights into the intracellular accumulation of these metals. The coexistence of metal ions on both the cell wall and within the cytoplasm suggests intricate interactions and potential bioaccumulation mechanisms at play. The identification of metal accumulation within the cytoplasm holds significance as it hints at the presence of internalized mechanisms for metal uptake. This phenomenon has been reported in various microorganisms and underpins the complexity of microbial-metal interactions. This is particularly evident from studies conducted by different researchers (Perdrial et al., 2008; Ozdemir et al., 2012; Diba et al., 2021; Li et al., 2021), indicating the universality of intracellular metal accumulation mechanisms. However, the process of intracellular absorption is considered slower and more intricate compared to the relatively straightforward cell surface absorption (Ma et al., 2022). The initial binding of metal ions to

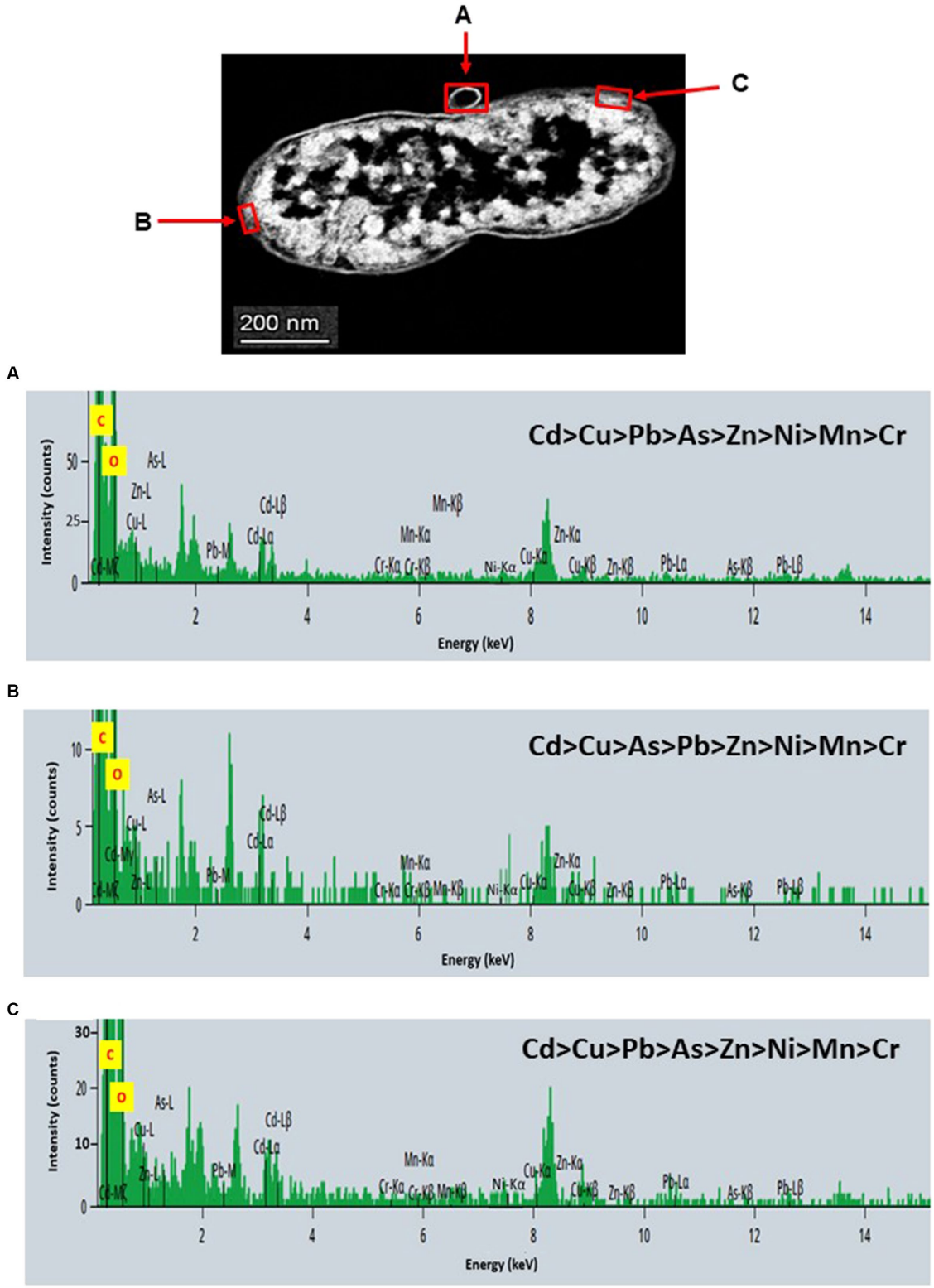

FIGURE 6
Scanning transmission electron micrographs (STEM) off a thin section of metal-loaded *Klebsiella* sp. R19 and the location of metals. **(A–C)** Energy dispersive X-ray spectra of the surface biosorption of metals acquired from the region indicated by arrow A, B, and C. The electron-dense granules appear bright on the STEM-HAADF image.

10.3389/fmicb.2023.1278886

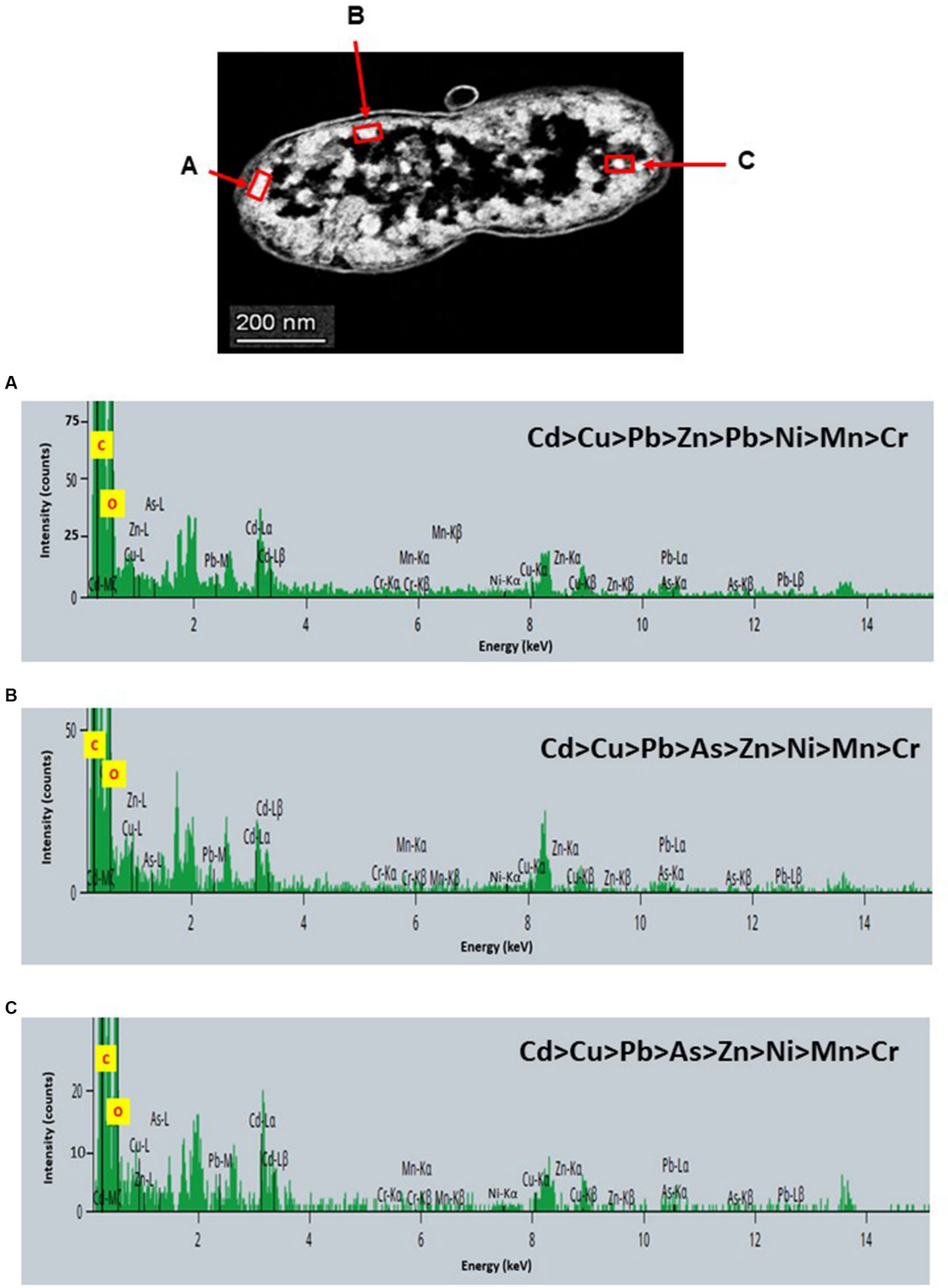

FIGURE 7
Scanning transmission electron micrographs (STEM) off a thin section of metal-loaded *Klebsiella* sp. R19 and the location of metals. **(A–C)** Energy dispersive X-ray spectra of the intracellular accumulation of metals acquired from the region indicated by arrow A, B, and C. The electron-dense granules appear bright on the STEM-HAADF image. Granules are of three types: large and compact (blue arrows), small (green arrows), and saturated around storage granules (purple arrow).

10.3389/fmicb.2023.1278886

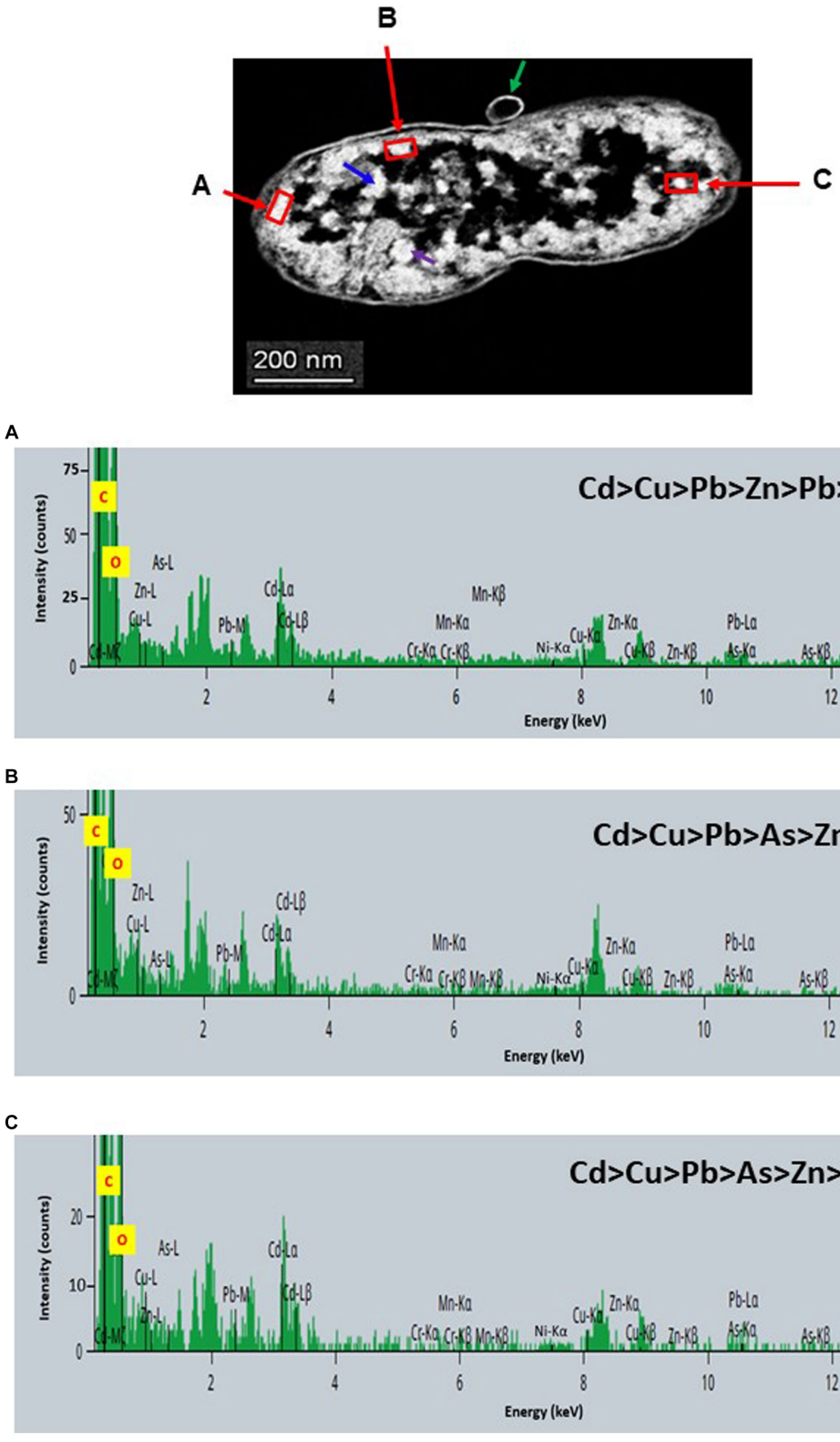

FIGURE 8
Scanning transmission electron micrographs (STEM) off a thin section of metal-loaded *Raoultella* sp. L30 and the location of metals. **(A–C)** Energy dispersive X-ray spectra of the surface biosorption of metals acquired from the region indicated by arrow A, B, and C. The electron-dense granules appear bright on the STEM-HAADF image.

the cell surface is often a precursor to their subsequent transport into the cell. Many established mechanisms of metal transport hinge upon the electrochemical proton gradient existing across the cell membrane. This gradient, comprising a chemical component in the form of the pH gradient and a membrane potential, actively facilitates the transport of ionized solutes across cellular

10.3389/fmicb.2023.1278886

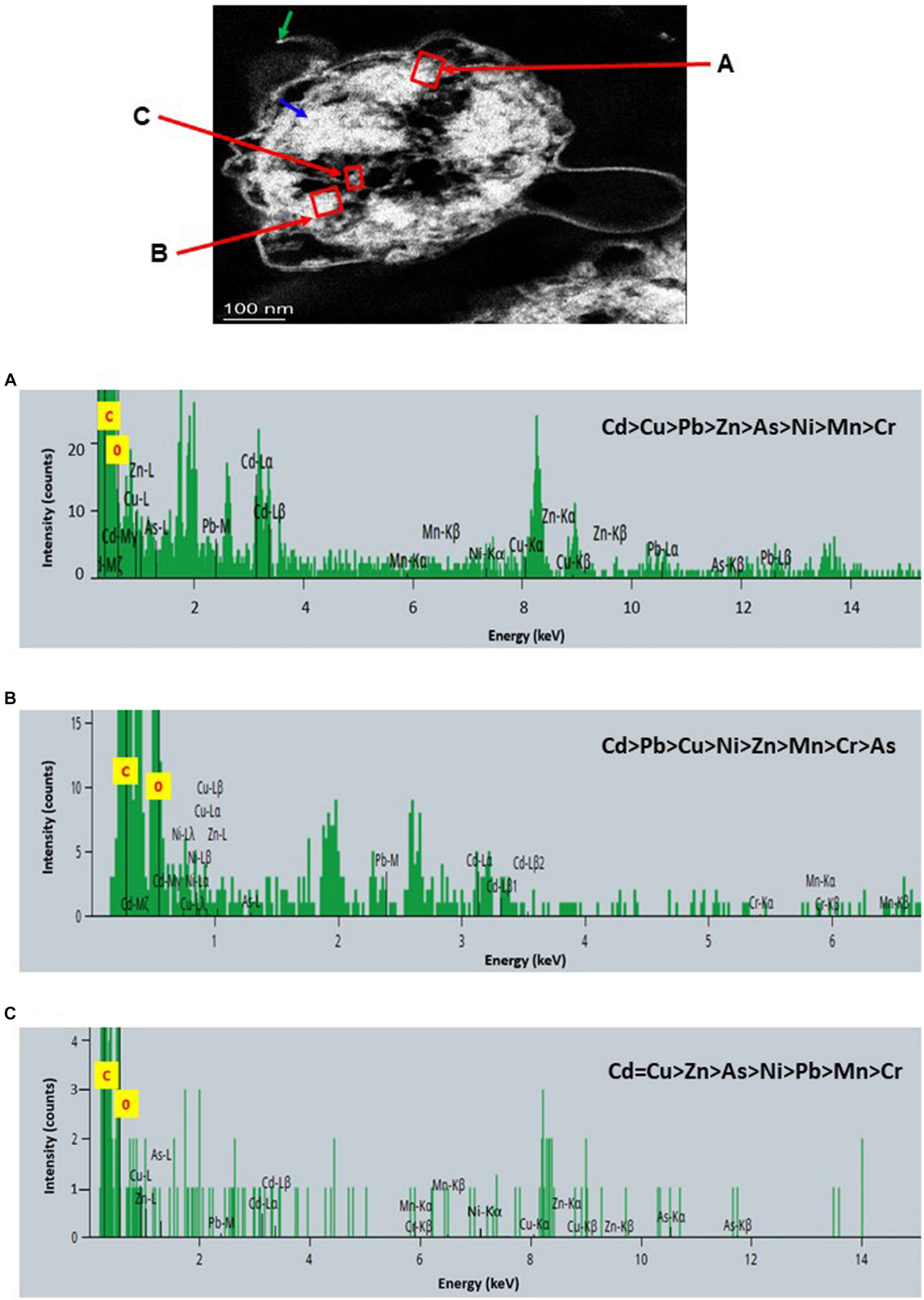

FIGURE 9
Scanning transmission electron micrographs (STEM) off a thin section of metal-loaded *Raoultella* sp. L30 and the location of metals. **(A–C)** Energy dispersive X-ray spectra of the intracellular accumulation of metals acquired from the region indicated by arrow A, B, and C. The electron-dense granules appear bright on the STEM-HAADF image. Granules are of three types: large and compact (blue arrows), small (green arrows), and saturated around storage granules (purple arrow).

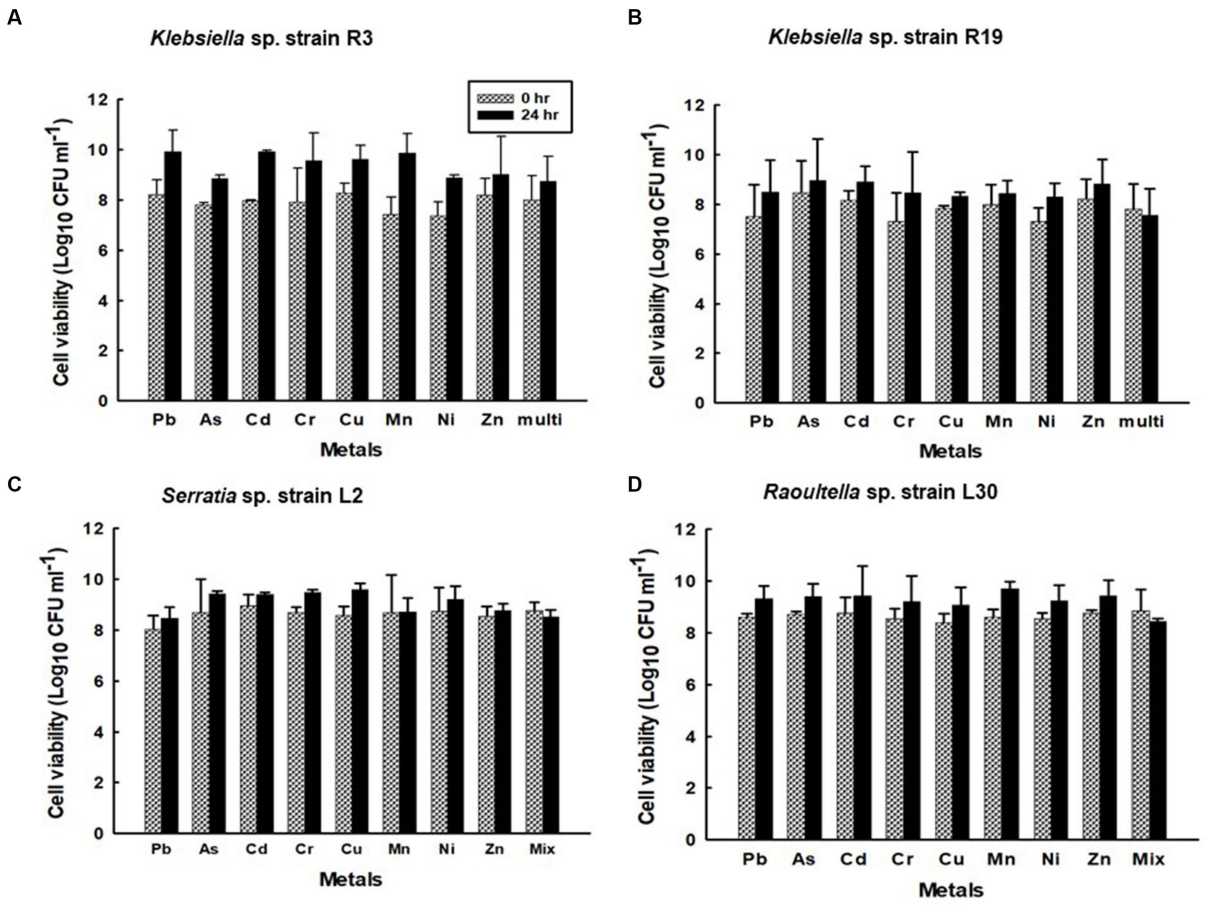

FIGURE 10
Viability of the confined **(A)** *Klebsiella* sp. R3; **(B)** *Klebsiella* sp. R19; **(C)** *Serratia* sp. L2; and **(D)** *Raoultella* sp. L30 strains during sorption in aqueous solutions single metal solutions containing Pb, Cu, Cd, Ni, As, Zn, Cr, Mn, or in mixed metal solutions containing eight metals.

membranes. This process has been explored in prior research (Borst-Pauwels, 1981; Ma et al., 2022), underscoring the critical role of membrane electrochemistry in mediating metal movement within cells. It's noteworthy that intracellular metal uptake may also transpire via diffusion, especially in scenarios where the toxic influence of the metal leads to alterations in membrane permeability. These adaptive changes in cellular structure may inadvertently facilitate metal penetration, a phenomenon explored in studies by Gadd (1988). This underscores the multifaceted nature of microbial responses to metal exposure, wherein cells dynamically adjust their mechanisms to counteract toxicity. Comparing the metal distribution patterns between *Klebsiella* sp. R19 and *Raoultella* sp. L30 reveals intriguing differences. While both species exhibit a preference for Cu^{2+} accumulation, *Klebsiella* sp. R19 displays a unique preference for Cd^{2+}, whereas *Raoultella* sp. L30 shows a more varied distribution in the cytoplasmic granules. These patterns might reflect the adaptation of each species to its specific environmental conditions, suggesting that metal availability and toxicity play crucial roles in shaping their metal accumulation strategies. The observed metal distribution patterns could be attributed to the presence of specialized metal transporters or binding proteins within these bacteria. The differences in distribution might also arise from variations in the metal-binding affinities of their cellular components.

5. Conclusion

The bacterial strains in the study effectively removed various metal cations, both in single- and multi-metal solutions. They exhibited both heavy metal-removing capabilities and the ability to thrive over a wide range of metal concentrations, making them suitable for potential use in metal remediation in bioreactors or *in situ* applications. Strains R3 and R19, despite being less metal-tolerant than L2 and L30 strains, demonstrated efficient metal removal because possess a higher number and more accessible carboxyl and amide functional groups, which are crucial for metal binding. This study confirmed that the simultaneous presence of multiple metals in an aqueous solution can lead to mutual inhibition in metal adsorption by the extracellular polymeric substance (EPS), resulting in reduced overall metal uptake. FTIR and SEM–EDX techniques confirmed the interactions between metal ions and functional groups on the surface of the strains. Moreover, TEM-EDX analysis showed the presence of metals on the cell surface and the cytoplasm.

Collectively, these findings advance our understanding of the metal removal capabilities and adaptive mechanisms of bacterial strains. They underscore the potential of these strains for applications in environmental remediation and the treatment of metal-contaminated effluents. Furthermore, the study emphasizes the critical role of tailoring strain selection to suit the specific metal composition

of effluent environments, thus enhancing the efficiency and effectiveness of metal removal strategies.

6. Future studies

Future research should explore the practical applications of the highly efficient metal-resistant bacterial strains identified in this study by conducting pilot-scale studies and field trials to assess their real-world performance in diverse contaminated environments. Additionally, efforts should be directed toward optimizing bioremediation techniques and strategies that harness these strains, including the design of specialized bioreactor systems and the evaluation of scalability. Finally, investigating genetic and metabolic engineering approaches to enhance the metal-binding capabilities of these strains could lead to the development of even more specialized and efficient bioremediation tools.

Data availability statement

The datasets presented in this study can be found in online repositories. The names of the repository/repositories and accession number(s) can be found in the article/Supplementary material.

Author contributions

GP: Data curation, Formal analysis, Investigation, Software, Validation, Writing – original draft. DO: Data curation, Formal analysis, Investigation, Methodology, Writing – review & editing. YC: Data curation, Formal analysis, Investigation, Methodology, Validation, Writing – review & editing. AF: Formal analysis, Investigation, Methodology, Validation, Writing – review & editing. FS: Data curation, Formal analysis, Investigation, Methodology, Validation, Writing – review & editing. JF: Data curation, Formal analysis, Investigation, Methodology, Software, Writing – review & editing. RS: Data curation, Formal analysis, Methodology, Writing – review & editing. CS: Data curation, Formal analysis, Investigation, Methodology, Software, Validation, Writing – review & editing. AK: Data curation, Formal analysis, Investigation, Methodology, Software, Validation, Writing – review & editing. SO: Data curation, Formal analysis, Investigation, Methodology, Software, Validation, Writing – review & editing. HN: Data curation, Formal analysis, Investigation, Methodology, Validation, Writing – review & editing. LA: Data curation, Formal analysis, Investigation, Methodology, Validation, Writing – review & editing. OC: Formal analysis, Investigation, Methodology, Writing – review & editing, Data curation, Software. BC: Data curation, Formal analysis, Investigation, Methodology, Validation, Writing – review & editing. XL: Investigation, Resources, Supervision, Validation, Writing – review & editing. ST-A: Conceptualization, Formal analysis, Funding acquisition, Investigation, Methodology, Project administration, Resources, Supervision, Validation, Visualization, Writing – original draft, Writing – review & editing.

Funding

The author(s) declare financial support was received for the research, authorship, and/or publication of this article. This work was financially supported by the University of Michigan-Dearborn. Office of Research and Sponsored Programs (Research Initiation and Development Grant). GP, YC, and BC were supported by the Summer Undergraduate Research Experience (SURE) Program at the University of Michigan-Dearborn.

Acknowledgments

The authors like to express their sincere thanks and deep gratitude to Haiping Sun of Michigan Center for Materials Characterization and the staff at the Microscopy Core at University of Michigan-Ann Arbor for SEM and TEM training to ST-A's undergraduate students.

Conflict of interest

The authors declare that the research was conducted in the absence of any commercial or financial relationships that could be construed as a potential conflict of interest.

Publisher's note

Supplementary material

The Supplementary material for this article can be found online at: https://www.frontiersin.org/articles/10.3389/fmicb.2023.1278886/full#supplementary-material

References

Ahmad, W., Alharthy, R. D., Zubair, M., Ahmed, M., Hameed, A., and Rafique, S. (2021). Toxic and heavy metals contamination assessment in soil and water to evaluate human health risk. *Sci. Rep.* 11:17006. doi: 10.1038/s41598-021-94616-4

Bhaskar, P. V., and Bhosle, N. B. (2006). Bacterial extracellular polymeric substances (EPS) a carrier of heavy metals in the marine food-chain. *Environ. Int.* 32, 191–198. doi: 10.1016/J.ENVINT.2005.08.010

Bhatt, J., Desai, S., Wagh, N. S., and Lakkakula, J. (2023). "New bioremediation technologies to remove heavy metals and radionuclides" in *Industrial wastewater reuse*. ed. M. P. Shah (Singapore: Springer) doi: 10.1007/978-981-99-2489-9_14

Boening, D. W. (2000). Ecological effects, transport, and fate of mercury: a general review. *Chemosphere* 40, 1335–1351. doi: 10.1016/S0045-6535(99)00283-0

Borst-Pauwels, G. (1981). Ion transport in yeast. *Biochim. Biophys. Acta* 650, 88–127. doi: 10.1016/0304-4157(81)90002-2

Boulanger, B., and Nikolaidis, N. P. (2003). Mobility and aquatic toxicity of copper in an urban watershed. *J. Am. Water Resour. Assoc.* 39, 325–336. doi: 10.1111/j.1752-1688.2003.tb04387.x

Bowman, N., Patel, P., Xu, W., Alsaffar, A., and Tiquia-Arashiro, S. M. (2018). Enrichment and isolation of Pb-resistant bacteria from Saint Clair River sediments and their potential for Pb removal in aqueous solutions. *Appl. Microbiol. Biotechnol.* 102, 2391–2398. doi: 10.1007/s00253-018-8772-4

Bruins, M. R., Kapil, S., and Oehme, F. W. (2000). Microbial resistance to metals in the environment. *Ecotoxicol. Environ. Saf.* 45, 198–207. doi: 10.1006/eesa.1999.1860

Cho, K., Zholi, A., Frabutt, D., Flood, M., Floyd, D., and Tiquia, S. M. (2012). Linking bacterial diversity and geochemistry of uranium-contaminated groundwater. *Environ. Technol.* 33, 1629–1640. doi: 10.1080/09593330.2011.641036

Dadrasnia, A., Chuan Wei, K. S., Shahsavari, N., Azirun, M. S., and Ismail, S. (2015). Biosorption potential of Bacillus salmalaya strain 139SI for removal of Cr(VI) from aqueous solution. *Int. J. Environ. Res. Public Health* 12, 15321–15338. doi: 10.3390/ijerph121214985

Deepika, K. V., Raghuram, M., Kariali, E., and Bramhachari, P. V. (2016). Biological responses of symbiotic *Rhizobium radiobacter* strain VBCK1062 to the arsenic contaminated rhizosphere soils of mung bean. *Ecotoxicol. Environ. Saf.* 134, 1–10. doi: 10.1016/j.ecoenv.2016.08.008

Diba, F., Khan, M. Z. H., Uddin, S. Z., Istiaq, A., Shuvo, M. S. R., Ul Alam, A. S. M. R., et al. (2021). Bioaccumulation and detoxification of trivalent arsenic by *Achromobacter xylosoxidans* BHW-15 and electrochemical detection of its transformation efficiency. *Sci. Rep.* 11:21312. doi: 10.1038/s41598-021-00745-1

Gadd, G. M. (1988). "Accumulation of metals by microorganisms and algae" in *Biotechnology a comprehensive treatise*, vol. *6* (Weinheim: VCH Yerlagsgesellschaft), 401–433.

Gadd, G. M. (1990). Heavy metal accumulation by bacteria and other microorganisms. *Experientia* 46, 834–840. doi: 10.1007/BF01935534

Gerhardt, P., Murray, R. G. E., Costilow, R. N., Nester, E. W., Wood, W. A., Kreig, N. R., et al. *Manual of methods for general bacteriology*. Washington, DC: American Society for Microbiology. (1994); *40*: 791.

Goswami, R., and Neog, N. (2023). "Heavy metal pollution in the environment: impact on air quality and human health implications" in *Heavy metal toxicity: Environmental concerns, remediation and opportunities*. eds. R. P. Singh, P. Singh and A. Srivastava (Singapore: Springer) doi: 10.1007/978-981-99-0397-9_4

Grube, M., Muter, O., Strikauska, S., Gavare, M., and Limane, B. (2008). Application of FT-IR spectroscopy for control of the medium composition during the biodegradation of nitro aromatic compounds. *J. Ind. Microbiol. Biotechnol.* 35, 1545–1549. doi: 10.1007/s10295-008-0456-0

Gupta, P., and Diwan, B. (2017). Bacterial exopolysaccharide mediated heavy metal removal: a review on biosynthesis, mechanism and remediation strategies. *Biotechnol. Rep.* 13, 58–71. doi: 10.1016/j.btre.2016.12.006

Gupta, A. D., Kavitha, E., Singh, S., and Karthikeyan, S. (2020). Toxicity mechanism of Cu^{2+} ion individually and in combination with Zn^{2+} ion in characterizing the molecular changes of *Staphylococcus aureus* studied using FTIR coupled with chemometric analysis. *J. Biol. Phys.* 46, 395–414. doi: 10.1007/s10867-020-09560-7

Helbig, K., and Grass, G. (2017). Mechanisms of copper homeostasis in bacteria. *Front. Cell. Infect. Microbiol.* 287, 13549–13555. doi: 10.1074/jbc.R111.316406

Higham, D. P., and Sadler, P. J. (1984). Scawen MO. Cadmium resistant Pseudomas putida synthesizes novel cadmium binding proteins. *Science* 225, 1043–1046. doi: 10.1126/science.225.4666.1043

Huang, L., Jin, Y., Zhou, D., Liu, L., Huang, S., Zhao, Y., et al. (2022). A review of the role of extracellular polymeric substances (EPS) in wastewater treatment systems. *Int. J. Environ. Res. Public Health* 19:12191. doi: 10.3390/ijerph191912191

Hugenholtz, P., and Huber, T. (2003). Chimeric 16S rDNA sequences of diverse origin are accumulating in public databases. *Int. J. Syst. Evol. Microbiol.* 53, 289–293. doi: 10.1099/ijs.0.02441-0

Jeong, H., Byeon, E., Kim, D. H., Maszczyk, P., and Lee, J. S. (2023). Heavy metals and metalloid in aquatic invertebrates: a review of single/mixed forms, combination with other pollutants, and environmental factors. *Mar. Pollut. Bull.* 191:114959. doi: 10.1016/j.marpolbul.2023.114959

Jeyakumari, P., Debnath, C., Vijayaaraghavan, R., and Muthura, M. (2023). Trends in bioremediation of heavy metal contaminations. *Environ. Eng. Res.* 28:220631, –220630. doi: 10.4491/eer.2021.631

Kim, S. Y., Kim, J. H., Kim, C. I., and Oh, O. (1996). Metal adsorption of the polysaccharide produced from *Methylobacterium organophilum*. *Biotechnol. Lett.* 18, 1161–1164. doi: 10.1007/BF00128585

Lakherwal, D. (2014). Adsorption of heavy metals: a review. *Int. J. Environ. Res. Dev.* 18, 4745–4750. doi: 10.1016/j.matpr.2019.07.462

Ledin, M. (2000). Accumulation of metals by microorganisms: processes and importance for soil systems. *Earth Sci. Rev.* 51, 1–31. doi: 10.1016/S0012-8252(00)00008-8

Li, N., Qin, L., Jin, M., Zhang, L., Geng, W., and Xiao, X. (2021). Extracellular adsorption, intracellular accumulation and tolerance mechanisms of Cyclotella sp. to Cr(VI) stress. *Chemosphere* 270:128662. doi: 10.1016/j.chemosphere.2020.128662

Lu, S., Li, X., Xi, Y., Liu, H., Zhang, Z., Huang, Y., et al. (2021). Insight the roles of loosely bound and tightly-bound extracellular polymeric substances on Cu^{2+}, Zn^{2+} and Pb^{2+} biosorption process with *Desulfovibrio vulgaris*. *J. Colloid Interface Sci.* 596, 408–419. doi: 10.1016/j.jcis.2021.03.152

Ma, Y., Bantec, T. N., Oliveira, R. S., Coutinho, A., Zhang, C., and Freitas, H. (2022). "The role of bacteria in metal bioaccumulation and biosorption" in *Advances in microbe-assisted phytoremediation of polluted sites*. eds. K. Bauddh and Y. Ma (New York, USA: Elsevier), 103–112.

Mathivanan, K., Chandirika, J. U., Mathimani, T., Rajaram, R., Annadurai, G., and Yin, H. (2021b). Production and functionality of exopolysaccharides in bacteria exposed to a toxic metal environment. *Ecotoxicol. Environ. Safety* 208:111567. doi: 10.1016/j.ecoenv.2020.111567

Mathivanan, K., Chandirika, J. U., Vinothkanna, A., Yin, H., Liu, X., and Meng, D. (2021a). Bacterial adaptive strategies to cope with metal toxicity in the contaminated environment-a review. *Ecotoxicol. Environ. Saf.* 226:112863. doi: 10.1016/j.ecoenv.2021.112863

Micheletti, E., Colica, G., Viti, C., Tamagnini, P., and De Philippis, R. (2008). Selectivity in the heavy metal removal by exopolysaccharide-producing cyanobacteria. *J. Appl. Microbiol.* 105, 88–94. doi: 10.1111/j.1365-2672.2008.03728.x

Mishra, V., Balomajumder, C., and Agarwal, V. K. (2013). Biological removal of heavy metal zinc from industrial effluent by zinc sequestering bacterium VMSDCM. *Clean Techn. Environ. Policy* 16, 555–568. doi: 10.1007/s10098-013-0655-x

Narwal, N., Katyal, D., Kataria, N., Rose, P. K., Warkar, S. G., Pugazhendhi, A., et al. (2023). (2023) emerging micropollutants in aquatic ecosystems and nanotechnology-based removal alternatives: a review. *Chemosphere* 341:139945. doi: 10.1016/j.chemosphere.2023.139945

Nguyen, S., Ala, F., Cardwell, C., Cai, D., McKindles, K. M., Lotvola, A., et al. (2013). Isolation and screening of carboxydotrophs isolated from composts and their potential for butanol synthesis. *Environ. Technol.* 34, 1995–2007. doi: 10.1080/09593330.2013.795987

Nies, D. H. (1999). Microbial heavy-metal resistance. *Appl. Microbiol. Biotechnol.* 51, 730–750. doi: 10.1007/s002530051457

Oest, A., Alsaffar, A., Fenner, M., Azzopardi, D., and Tiquia-Arashiro, S. M. (2018). Patterns of change in metabolic capabilities of sediment microbial communities in river and lake ecosystems. *Int. J. Microbiol.* 2018, 1–15. doi: 10.1155/2018/6234931

Ozdemir, S., Kilinc, E., Poli, A., Nicolaus, B., and Güven, K. (2012). Cd, cu, Ni, Mn and Zn resistance and bioaccumulation by thermophilic bacteria, *Geobacillus toebii* subsp. decanicus and *Geobacillus thermoleovorans* subsp. stromboliensis. *World J. Microbiol. Biotechnol.* 28, 155–163. doi: 10.1007/s11274-011-0804-5

Pagliaccia, B., Carretti, E., Severi, M., Berti, D., Lubello, C., and Lotti, T. (2022). Heavy metal biosorption by extracellular polymeric substances (EPS) recovered from anammox granular sludge. *J. Haz. Mat.* 424:126661. doi: 10.1016/j.jhazmat.2021.126661

Pal, A., and Paul, A. K. (2008). Microbial extracellular polymeric substances: central elements in heavy metal bioremediation. *Indian J. Microbiol.* 48, 49–64. doi: 10.1007/s12088-008-0006-5

Panda, G., Das, S., Bandopadhyay, T., and Guha, A. (2007). Adsorption of nickel on husk of *Lathyrus sativus*: behavior and binding mechanism. *Colloids Surf. B Biointerfaces* 57, 135–142. doi: 10.1016/j.colsurfb.2007.01.022

Patel, D., Gismondi, R., Alsaffar, A., and Tiquia-Arashiro, S. M. (2019). (2019) applicability of API ZYM to capture seasonal and spatial variabilities in lake and river sediments. *Environ. Technol.* 40, 3227–3239. doi: 10.1080/09593330.2018.1468492

Perdrial, N., Liewig, N., Delphin, J. E., and Elsass, F. (2008). TEM evidence for intracellular accumulation of lead by bacteria in subsurface environments. *Chem. Geol.* 253, 196–204. doi: 10.1016/j.chemgeo.2008.05.008

Pereira, S., Micheletti, E., Zille, A., Santos, A., Moradas-Ferreira, P., Tamagnini, P., et al. (2011). Using extracellular polymeric substances (EPS)- producing cyanobacteria for the bioremediation of heavy metals: do cations compete for the EPS functional groups and also accumulate inside the cell? *Microbiology* 157, 451–458. doi: 10.1099/mic.0.041038-0

Perez, J. A. M., Garcia-Ribera, R., Quesada, T., Aguilera, M., Ramos-Cormenzana, A., and Monteoliva-Sanchez, M. (2008). Biosorption of heavy metals by exopolysaccharide produced by *Paenibacillus jamilae*. *World J. Microbiol. Biotechnol.* 24, 2699–2704. doi: 10.1007/s11274-008-9800-9

Planchon, M., Jittawuttipoka, T., Cassier-Chauvat, C., Guyot, F., Gelabert, A., Benedetti, M. F., et al. (2013). Exopolysaccharides protect Synechocystis against the deleterious effects of titanium dioxide nanoparticles in natural and artificial waters. *J. Colloid Interface Sci.* 405, 35–43. doi: 10.1016/j.jcis.2013.05.061

Plecha, S., Hall, D., and Tiquia-Arashiro, S. M. (2013). Screening for novel bacteria from the bioenergy feedstock switchgrass (Panicum virgatum L.). *Environ. Technol.* 34, 1895–1904. doi: 10.1080/09593330.2013.818701

Pradhan, S., and Rai, L. C. (2011). Biotechnological potential of Microcystis sp. in cu, Zn and cd biosorption from single and multimetallic systems. *Biometals* 14, 67–74. doi: 10.1023/a:1016607729691

Priya, A. K., Gnanasekaran, L., Dutta, K., Rajendran, S., Balakrishnan, D., and Soto-Moscoso, M. (2022). Biosorption of heavy metals by microorganisms: evaluation of different underlying mechanisms. *Chemosphere* 307:135957. doi: 10.1016/j.chemosphere.2022.135957

Qasem, N. A. A., Mohammed, R. H., and Lawal, D. U. (2021). Removal of heavy metal ions from wastewater: a comprehensive and critical review. *NPI Clean Water* 4:36. doi: 10.1038/s41545-021-00127-0

Queiroz, H. M., Ying, S. C., Abernathy, M., Barcellos, D., Gabriel, F. A., Otero, X. L., et al. (2021). Manganese: the overlooked contaminant in the world largest mine tailings dam collapse. *Environ. Int.* 146, 146:106284. doi: 10.1016/j.envint.2020.106284

Rajaram, R., Banu, J. S., and Mathivanan, K. (2013). Biosorption of cu (II) ions by indigenous copper-resistant bacteria isolated from polluted coastal environments. *Toxicol. Environ. Chem.* 95, 590–604. doi: 10.1080/02772248.2013.801979

Razzak, S. A., Faruque, M. O., Alsheikh, Z., Alsheikhmohamad, L., Alkuroud, D., Alfayez, A., et al. (2022). A comprehensive review on conventional and biological-driven heavy metals removal from industrial wastewater. *Environ. Adv.* 7:100168. doi: 10.1016/j.envadv.2022.100168

Redmile-Gordon, M., and Chen, L. (2017). Zinc toxicity stimulates microbial production of extracellular polymers in a copiotrophic acid soil. *Int. Biodeterior. Biodegrad.* 119, 413–418. doi: 10.1016/j.ibiod.2016.10.004

Rensing, C., and Grass, G. (2003). *Escherichia coli* mechanisms of copper homeostasis in a changing environment. *FEMS Microbiol. Rev.* 27, 197–213. doi: 10.1016/S0168-6445(03)00049-4

Rizvi, A., Ahmed, B., Zaidi, A., and Khan, M. S. (2019a). Heavy metal mediated phytotoxic impact on winter wheat: oxidative stress and microbial management of toxicity by *Bacillus subtilis* BM2. *RSC Adv.* 9, 6125–6142. doi: 10.1039/c9ra00333a

Rizvi, A., Ahmed, B., Zaidi, A., and Khan, M. S. (2019b). Bioreduction of toxicity influenced by bioactive molecules secreted under metal stress by *Azotobacter chroococcum*. *Ecotoxicology* 28, 302–322. doi: 10.1007/s10646-019-02023-3

Roane, T. M. (1999). Lead resistance in two bacterial isolates from heavy metal-contaminated soils. *Microb. Ecol.* 37, 218–224. doi: 10.1007/s002489900145

Rosen, B. P. (1995). Resistance mechanisms to arsenicals and antimonials. *J. Basic Microbiol.* 35, 453–460.

Saba, Y. R., Ahmed, M., and Sabri, A. N. (2019). Potential role of bacterial extracellular polymeric substances as biosorbent material for arsenic bioremediation. *Biorem. J.* 23, 72–81. doi: 10.1080/10889868.2019.1602107

Sag, Y., Kaya, A., and Kutsal, T. (2000). (2000) Lead, copper and zinc biosorption from bicomponent systems modelled by empirical Freundlich isotherm. *Appl. Microbiol. Biotechnol.* 53, 338–341. doi: 10.1007/s002530050031

Saitou, N., and Nei, M. (1987). The neighbor-joining method: a new method for reconstructing phylogenetic trees. *Mol. Biol. Evol.* 4, 406–425. doi: 10.1093/oxfordjournals.molbev.a040454

Shameer, S. (2016). Biosorption of lead, copper and cadmium using the extracellular polysaccharides (EPS) of Bacillus sp., from solar salterns. *Biotech* 6, 194–110. doi: 10.1007/s13205-016-0498-3

Sharma, A., Grewal, A. S., Sharma, D., and Srivastav, A. L. (2023). "Chapter 3- heavy metal contamination in water: Consequences on human health and environment" in *Advances in environmental pollution research, metals in water*. eds. S. K. Shukla, S. Kumar, S. Madhav and P. K. Mishra (New York, USA: Elsevier), 39–52.

Sharma, S., and Saraf, M. (2023). Enhanced exopolysaccharide production by multi metal tolerant *Klebsiella variicola* SMHMZ46 isolated from mines area and application in metal bioremediation. *Int. Microbiol.* doi: 10.1007/s10123-023-00366-w

Shuhong, Y., Meiping, Z., Hong, Y., Han, W., Shan, X., Yan, L., et al. (2014). Biosorption of Cu^{2+}, Pb^{2+} and Cr^{6+} by a novel exopolysaccharide from Arthrobacter ps-5. *Carbohydr. Polym.* 101, 50–56. doi: 10.1016/j.carbpol.2013.09.021

Shuttleworth, K. L., and Unz, R. F. (1993). Sorption of heavy metal to the filamentous bacterium Thiothrix strain A1. *Appl. Environ. Microbiol.* 59, 1274–1282. doi: 10.1128/aem.59.5.1274-1282.1993

Silver, S. (1996). Bacterial resistances to toxic metal ions—a review. *Gene* 179, 9–19. doi: 10.1016/S0378-1119(96)00323-X

Silver, S., and Phung, L. T. (2005). Bacterial heavy metal resistance: new surprises. *Annu. Rev. Microbiol.* 59, 273–298. doi: 10.1146/annurev.micro.50.1.753

Sodhi, K. K., Kumar, M., and Singh, D. K. (2020). Multi-metal resistance and potential of Alcaligenes sp. MMA for the removal of heavy metals. SN. *Appl. Sci.* 2, 1–13. doi: 10.1007/s42452-020-03583-4

Sreedevi, P. R., Suresh, K., and Jiang, G. (2022). Bacterial bioremediation of heavy metals in wastewater: a review of processes and applications. *J. Wat. Process Eng.* 48:102884. doi: 10.1016/j.jwpe.2022.102884

Tamura, K., Stecher, G., and Kumar, S. (2021). MEGA11: molecular evolutionary genetics analysis. *Mol. Biol. Evol.* 38, 3022–3027. doi: 10.1093/molbev/msab120

Tchounwou, P. B., Yedjou, C. G., Patlolla, A. K., and Sutton, D. J. (2012). Heavy metal toxicity and the environment. *Exp. Suppl.* 101, 133–164. doi: 10.1007/978-3-7643-8340-4_6

Tiquia, S. M. (2010). Metabolic diversity of the heterotrophic microorganisms and potential link to pollution of the Rouge River. *Environ. Pollut.* 158, 1435–1443. doi: 10.1016/j.envpol.2009.12.035

Tiquia, S. M. (2011). Extracellular hydrolytic enzyme activities of the heterotrophic microbial communities of the Rouge River: an approach to evaluate ecosystem response to urbanization. *Microb. Ecol.* 62, 679–689. doi: 10.1007/s00248-011-9871-2

Tiquia, S. M., Davis, D., Hadid, H., Kasparian, S., Ismail, M., and Murray, K. S. (2007). Halotolerant bacteria from river waters and shallow groundwater along the Rouge River of southeastern Michigan. *Environ. Technol.* 28, 297–307. doi: 10.1080/09593332808618789

Tiquia, S. M., Schleibak, M., Schlaff, J., Floyd, J. C., Benipal, B., Zakhem, E., et al. (2008). Microbial community profiling and characterization of some heterotrophic bacterial isolates from river waters and shallow groundwater wells along the Rouge River, Southeast Michigan. *Environ. Technol.* 29, 651–663. doi: 10.1080/09593330801986998

Tiquia-Arashiro, S. M. (2018). Lead absorption mechanisms in bacteria as strategies for lead bioremediation. *Appl. Microbiol. Biotechnol.* 102, 5437–5444. doi: 10.1007/s00253-018-8969-6

van Hullebusch, E. D., Zandvoort, M. H., and Lens, P. N. L. (2003). Metal immobilization by biofilms: mechanisms and analytical tools. *Rev. Environ. Sci. Biotechnol.* 2, 9–33. doi: 10.1023/B:RESB.0000022995.48330.55

Vandana, M., Priyadarshanee, M., and Das, S. (2023). Bacterial extracellular polymeric substances: biosynthesis and interaction with environmental pollutants. *Chemosphere* 332:138876. doi: 10.1016/j.chemosphere.2023.138876

Vishan, I., Laha, A., and Kalamdhad, A. (2017). Biosorption of Pb(II) by *Bacillus badius* AK strain originating from rotary drum compost of water hyacinth. *Water Sci. Technol.* 75, 1071–1083. doi: 10.2166/wst.2016.590

Volesky, B. (1990) *Biosorption of heavy metals*. CRC Press, Boc Raton, FL. 408.

Volesky, B., and May-Philips, H. A. (1995). Biosorption of heavy metals by *Saccharomyces cerevisiae*. *Appl. Microbiol. Biotechnol.* 42, 797–806. doi: 10.1007/bf00171964

Wang, J., Li, Q., Li, M. M., Chen, T. H., Zhou, Y. F., and Yue, Z. B. (2014). Competitive adsorption of heavy metal by extracellular polymeric substances (EPS) extracted from sulfate reducing bacteria. *Bioresour. Technol.* 163, 374–376. doi: 10.1016/j.biortech.2014.04.073

Wang, Z., Xu, W., Jie, F., Zhao, Z., Zhou, K., and Liu, H. (2021). The selective adsorption performance and mechanism of multiwall magnetic carbon nanotubes for heavy metals in wastewater. *Sci. Rep.* 11:16878. doi: 10.1038/s41598-021-96465-7

Weisburg, W. W., Barns, S. M., Pelletier, D. A., and Lane, D. J. (1991). SSU ribosomal DNA amplification for phylogenetic study. *J. Bacteriol.* 173, 697–703. doi: 10.1128/jb.173.2.697-703.1991

Wolkers, W. F., Oliver, A. E., Tablin, F., and Crowe, J. H. (2004). A Fourier-transform infrared spectroscopy study of sugar glasses. *Carbohydr. Res.* 339, 1077–1085. doi: 10.1016/j.carres.2004.01.016

Wu, W., Gu, B., Fields, M. W., Gentile, M., Ku, Y.-K., Yan, H., et al. (2005). Uranium (VI) reduction by denitrifying biomass. *Biorem. J.* 9, 49–61. doi: 10.1080/10889860590929628

Zamora-Ledezma, C., Negrete-Bolagay, D., Figueroa, F., Zamora-Ledezma, E., Ni, M., Alexis, F., et al. (2021). Heavy metal water pollution: a fresh look about hazards, novel and conventional remediation methods. *Environ. Tech. Innov.* 22:101504. doi: 10.1016/j.eti.2021.101504

frontiers | Frontiers in Microbiology

TYPE Review
PUBLISHED 21 November 2023
DOI 10.3389/fmicb.2023.1304081

OPEN ACCESS

EDITED BY
Ilana Kolodkin-Gal,
Reichman University, Israel

REVIEWED BY
Luca Roscini,
University of Perugia, Italy
Peng Zhang,
Xiangtan University, China

*CORRESPONDENCE
Sonia Tiquia-Arashiro
✉ smtiquia@umich.edu

RECEIVED 28 September 2023
ACCEPTED 03 November 2023
PUBLISHED 21 November 2023

CITATION
Kassem A, Abbas L, Coutinho O, Opara S, Najaf H, Kasperek D, Pokhrel K, Li X and Tiquia-Arashiro S (2023) Applications of Fourier Transform-Infrared spectroscopy in microbial cell biology and environmental microbiology: advances, challenges, and future perspectives. *Front. Microbiol.* 14:1304081. doi: 10.3389/fmicb.2023.1304081

Applications of Fourier Transform-Infrared spectroscopy in microbial cell biology and environmental microbiology: advances, challenges, and future perspectives

Amin Kassem[1], Lana Abbas[1], Oliver Coutinho[1], Somie Opara[1], Hawraa Najaf[1], Diana Kasperek[1], Keshav Pokhrel[2], Xiaohua Li[1] and Sonia Tiquia-Arashiro[1]*

[1]Department of Natural Sciences, University of Michigan-Dearborn, Dearborn, MI, United States, [2]Department of Mathematics and Statistics, University of Michigan-Dearborn, Dearborn, MI, United States

Microorganisms play pivotal roles in shaping ecosystems and biogeochemical cycles. Their intricate interactions involve complex biochemical processes. Fourier Transform-Infrared (FT-IR) spectroscopy is a powerful tool for monitoring these interactions, revealing microorganism composition and responses to the environment. This review explores the diversity of applications of FT-IR spectroscopy within the field of microbiology, highlighting its specific utility in microbial cell biology and environmental microbiology. It emphasizes key applications such as microbial identification, process monitoring, cell wall analysis, biofilm examination, stress response assessment, and environmental interaction investigation, showcasing the crucial role of FT-IR in advancing our understanding of microbial systems. Furthermore, we address challenges including sample complexity, data interpretation nuances, and the need for integration with complementary techniques. Future prospects for FT-IR in environmental microbiology include a wide range of transformative applications and advancements. These include the development of comprehensive and standardized FT-IR libraries for precise microbial identification, the integration of advanced analytical techniques, the adoption of high-throughput and single-cell analysis, real-time environmental monitoring using portable FT-IR systems and the incorporation of FT-IR data into ecological modeling for predictive insights into microbial responses to environmental changes. These innovative avenues promise to significantly advance our understanding of microorganisms and their complex interactions within various ecosystems.

KEYWORDS

Fourier transform infrared spectroscopy, cellular structures, metabolic activities, bacteria, microbial stress, cell membrane, population dynamics

1 Introduction

Fourier Transform-Infrared (FTIR) spectroscopy has emerged as an exceptionally versatile and indispensable tool, revolutionizing molecular analysis across a spectrum of scientific domains, including microbiology (Beekes et al., 2007; Baker et al., 2014; Zarnowiec et al., 2015; Nandiyanto et al., 2019; He et al., 2022; Koczoń et al., 2023). This analytical technique operates on the principle that molecules absorb specific frequencies of infrared light, which correspond to the vibrational frequencies of their chemical bonds (Griffiths, 1983; Nandiyanto et al., 2019; He et al., 2022; Lilo et al., 2022; Weber et al., 2023). The absorption produces a characteristic spectrum that can be used to identify the functional groups and molecular structures present in a sample.

FTIR spectroscopy has been a valuable tool in various biological studies across different scientific areas. In the field of microbiology, it has significantly aided in the rapid and accurate identification of microorganisms (Helm et al., 1991; Wenning and Scherer, 2013; Corte et al., 2014; Câmara et al., 2020; Feng et al., 2020; Brito and Lourenço, 2021; Smirnova et al., 2022; Kamnev et al., 2023; Tata et al., 2023; Tessaro et al., 2023), contributing to timely infection diagnosis and the implementation of appropriate treatment methods. This technique has also allowed for in-depth analyses of microbial structures, metabolic activities, and responses to environmental changes, leading to a better understanding of microbial physiology and behavior (Corte et al., 2014; Câmara et al., 2020; Smirnova et al., 2022; Tessaro et al., 2023). Moreover, FTIR spectroscopy has played a crucial role in monitoring and evaluating the dynamics of microbial communities in different environments (Kamnev et al., 2023; Marques et al., 2023). This has contributed to the management of water quality, assessment of ecosystem health, and the detection of microbial pollution. In the context of metal-pollutant bioremediation, FTIR has enabled the comprehensive analysis of how microorganisms interact with metal contaminants (Pagnucco et al., 2023). This has helped in understanding the mechanisms involved in metal sequestration, transformation, and detoxification. Furthermore, in the domain of organic pollutant bioremediation, FTIR has served as a valuable tool in investigating the interactions between microorganisms and organic contaminants. It has provided insights into the biochemical transformations and degradation pathways involved in the bioremediation process (Aziz et al., 2020).

This review explores the diverse applications of FT-IR spectroscopy in microbiology, with a particular emphasis on its use in microbial cell biology and environmental microbiology. While previous reviews on FT-IR have provided valuable insights into the general principles and applications of the technology, our study seeks to differentiate itself by focusing on its applications in microbial cell biology and environmental microbiology. Additionally, this review addresses the limitations of FT-IR in these disciplines and the challenges that researchers encounter when practically employing FT-IR technology. The review also outlines potential avenues for future research and development, laying the groundwork for further advancements in the field of microbiology and FT-IR technology.

2 Basic principles of FTIR

FT-IR spectroscopy is based on the principle that molecules absorb specific frequencies of infrared light, corresponding to the vibrational frequencies of their chemical bonds. When a sample is exposed to infrared light, the molecules within the sample absorb this light at characteristic frequencies, causing the bonds within the molecules to vibrate. Different types of bonds, such as C-H, O-H, and N-H bonds, have distinct vibrational frequencies, leading to unique patterns in the absorption of infrared light. By measuring the intensity of the absorbed light at various wavelengths, an FT-IR spectrometer produces a characteristic spectrum for the sample. This spectrum can be used to identify the functional groups and molecular structures present in the sample, essentially providing a "fingerprint" that can be used for qualitative and quantitative analysis. FT-IR spectroscopy can be used to study a diverse array of specimens, including solids, liquids, and gases, and it has applications across various scientific domains, including chemistry, physics, materials science, and biology (Griffiths, 1983; Koczoń et al., 2023).

The range of IR radiation encompasses electromagnetic radiation with frequencies between 14,300 and 20 cm^{-1}, with the most significant vibrational frequencies for most molecules falling within the mid IR spectrum, ranging between 4,000 and 400 cm^{-1} (Griffiths, 1983). Within this specific range, there are four different regions: (1) the single bond region (2,500–4,000 cm^{-1}), (2) the triple bond region (2,000–2,500 cm^{-1}), (3) the double bond region (1,500–2,000 cm^{-1}), and (4) the fingerprint region (600–1,500 cm^{-1}) (Figure 1). Table 1 shows some common peaks observed in FT-IR spectra, along with their corresponding functional groups and reference wavenumbers. Far-and near-IR ranges are less frequently employed, primarily because these regions register overtone (secondary) vibrations and combination vibrations, making them analytically challenging to study and interpret (Nandiyanto et al., 2019; Pirutin et al., 2023).

Within the mid IR spectrum, researchers commonly use five distinct spectral windows (Figure 1). The first window, ranging from 3,000 to 2,800 cm^{-1}, is primarily influenced by specific functional groups like membrane fatty acids and certain amino acid side-chain vibrations, dominated by C-H stretching vibrations of CH_3 and CH_2 functional groups. The second window, between 1,800 and 1,500 cm^{-1}, is affected by amide I and amide II groups in proteins and peptides, showcasing intense peaks providing comprehensive insights into protein structure, along with vibrations of ester functional groups in lipids and nucleic acid absorptions. The third window, spanning 1,500 to 1,200 cm^{-1}, represents a mixed region influenced by proteins, fatty acids, and compounds with phosphate groups, affected by CH_2 and CH_3 bending modes. The fourth window, from 1,200 to 900 cm^{-1}, is characterized by symmetric stretching vibrations of PO_2^- groups in nucleic acids, along with vibrations related to carbohydrates, polysaccharides, and nucleic acids. Lastly, the fifth window, between 900 and 700 cm^{-1}, known as the true fingerprint region, demonstrates subtle spectral patterns arising from vibrations of aromatic rings in specific amino acids and nucleotides.

The spectrum's peaks serve as identifiers for functional groups in both organic and inorganic compounds, utilizing their characteristic absorption bands within the infrared region of the electromagnetic spectrum (Griffiths, 1983; El-Azazy et al., 2021). These functional groups, linked to specific vibrational modes resulting from atomic movements within the groups (Griffiths, 1983; Smith, 1998; El-Azazy et al., 2021), encompass stretching, bending, and combination bands. Expressing the frequencies of these vibrations in wavenumbers (cm^{-1}) enables the identification of particular functional groups. For instance, the C=O stretching vibration of a carbonyl group, typically found in ketones and aldehydes, appears around 1,700–1,750 cm^{-1} (Table 1). Meanwhile, the

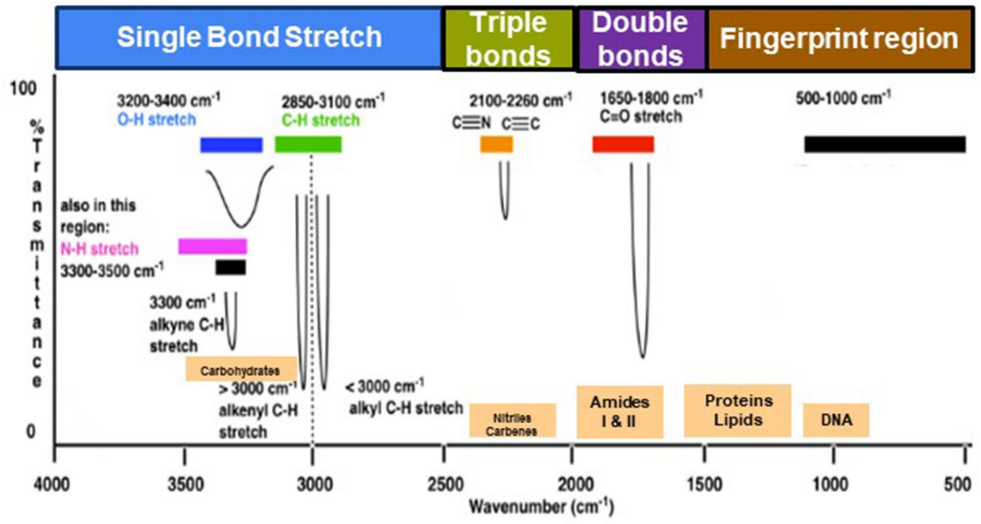

FIGURE 1
Typical infrared values for various types of bonds. The region 500–1,500 cm^{-1}, which is in the mid-IR region, is called the fingerprint region and provides molecular fingerprints unique to specific compounds. Reproduced from Master Organic Chemistry (https://www.masterorganicchemistry.com/2016/11/23/quick_analysis_of_ir_spectra/) (accessed on 28 September 2023), with kind permission from James Ashenhurst.

O-H stretching vibration of alcohols typically appears around 3,200–3,600 cm^{-1} (Table 1). By comparing the absorption bands' positions and intensities in the sample's spectrum to known reference spectra, analysts can determine the presence of specific functional groups in the sample (Silverstein et al., 2014). Notably, complex and distinctive patterns within the ~1,500–400 cm^{-1} region are highly specific to the compound's molecular structure. However, peak positions may vary due to factors such as the molecular environment, sample preparation, and instrument settings, underscoring the importance of consulting reliable databases and literature for accurate peak assignments (Griffiths, 1983; Silverstein et al., 2014; He et al., 2022).

3 Types of FT-IR used in microbiology

In microbiology, various forms of Fourier Transform Infrared (FT-IR) spectroscopy serve different research purposes. Transmission FT-IR involves transmitting infrared light through a sample to measure the transmitted light and absorption spectrum, proving valuable for analyzing solid samples like microbial cell walls or biofilm components. Attenuated Total Reflection (ATR) FT-IR is used for liquid and solid samples unsuitable for transmission FT-IR, enabling analysis without extensive sample preparation by measuring the sample's infrared spectrum in contact with an ATR crystal. Micro-FTIR Spectroscopy allows microscopic analysis of small sample areas, providing high spatial resolution and detailed information about the molecular composition of specific microorganisms or microbial components within a sample. Diffuse Reflectance Fourier Transform Infrared (DRIFT) spectroscopy is ideal for analyzing powdered or granulated samples, including microbial samples, without demanding extensive sample preparation.

In the case of ATR FT-IR, the sample is situated on a densely refractive crystal, usually of higher refractive index (Figure 2A). This method requires minimal or no sample preparation. The IR beam reflects off the crystal's inner surface, giving rise to an evanescent wave that extends beyond the crystal's surface and interacts with the sample in intimate contact with the ATR crystal (Baker et al., 2014; Bottum et al., 2023). The sample absorbs some of the evanescent wave's energy, and the resulting reflected radiation reaches the IR spectrometer's detector upon exiting the crystal. DRIFT involves directing the IR beam into the sample, where it is reflected, scattered, and transmitted through the sample material (Figure 2B). The IR light that becomes diffusely scattered within the sample and returns to the detector optics is termed diffuse reflection. Lastly, FT-IR micro-spectroscopy is an innovative technique that combines an FT-IR spectrometer with a microscope (Figure 2C). This approach enables the examination of limited areas on surfaces, such as agar plates, and facilitates the acquisition of reflectance or transmittance spectra from samples consisting of a few hundred cells, like microcolonies that develop within 6 to 10 h (Bhargava, 2012; Watanabe et al., 2023).

When subjecting a sample of a substance to continuous infrared (IR) light radiation, a distinctive resonance absorption band with intricate, fingerprint-like characteristics is obtained. The intensity of these absorption bands arises from scanning before and after the IR beam traverses the substance. Instead of isolated peaks, the frequencies and intensities of the IR bands exhibit distinctive, broad, and intricate profiles. These profiles serve as signatures that can be harnessed for the identification, characterization, and quantification of the sample. Upon radiating a sample containing bacterial cells, the resulting IR spectrum encapsulates the overall chemical composition of the sample. This spectrum holds the capability to provide insights into taxonomic variations due to inherent chemical distinctions or to identify chemical alterations resulting from exposure to challenging environments.

4 Applications of FT-IR in microbial cell biology

FT-IR spectroscopy has found numerous applications in the field of microbiology due to its ability to provide rapid and non-destructive

TABLE 1 Possible assignment of some bands frequently found in microbial IR spectra (peak frequencies have been obtained from the second derivative spectra).

Assignment	Frequency (cm^{-1})
C-H stretching peaks	
Alkane C-H stretching	2,850–2,960
Alkene C-H stretching	3,010–3,100
Alkyne C-H stretching	3,300
O-H and N-H stretching peaks	
Alcohols and phenols O-H stretching	3,200–3,600
Carboxylic acids O-H stretching	2,500–3,300
Amines N-H stretching	3,300–3,500
C=O stretching peaks	
Ketones and aldehydes C=O stretching	1,680–1,750
Carboxylic acids C=O stretching	1,700–1,750
Amides C=O stretching	1,630–1,690
C-N stretching peaks	
Aromatic C-N stretching	1,300–1,350
Aliphatic C-N stretching	1,000–1,300
C=C stretching peaks	
Alkene C=C stretching	1,620–1,680
Aromatic C=C stretching	1,450–1,600
N-H bending peaks	
Amines N-H bending	1,560–1,640
Amides N-H bending	1,550–1,670
C-H bending peaks	
Alkanes C-H bending	1,370–1,470
Alkenes C-H bending	960–1,200
O-H bending peaks	
Alcohols and phenols O-H bending	1,350–1,450
Fingerprint region peaks	700–900

Adapted from Smith (1998) and Silverstein et al. (2014).

information about the molecular composition of microorganisms. It is also used to investigate bacterial cell wall composition, studies biofilm formation and antibiotic resistance, monitor microbial growth and metabolic activity, and explore microbial community dynamics in complex environments. Furthermore, FT-IR spectroscopy provides insights into bacterial interactions with other microorganisms, host cells, and environmental factors, offering valuable information about microbial physiology and behavior. Thus, this technique finds widespread applications in microbiology, providing valuable insights into bacterial physiology, ecology, and interactions (Maquelin et al., 2000; Tiquia-Arashiro, 2019a; Jansson et al., 2023). Below reviews key applications of FT-IR in microbiology:

4.1 Microbial identification

FT-IR spectroscopy has been used for the identification of microorganisms based on their unique spectral fingerprints (Table 2). The FT-IR spectra of microbial cells, including bacteria, yeast, and fungi, contain characteristic peaks that reflect the presence of specific biomolecules (lipids, proteins, carbohydrates) and their functional groups. These spectral patterns can be compared to reference spectra in databases to identify the microorganisms. Microorganisms contain diverse biomolecules like proteins, lipids, nucleic acids, and carbohydrates, which exhibit characteristic absorption bands in the infrared spectrum. For bacterial identification, the FT-IR spectra of bacterial samples can be compared to spectral databases or reference spectra, researchers can identify bacterial species or strains based on their unique spectral features (Lin et al., 1998; Naumann et al., 2001; Dziuba et al., 2007; Rebuffo-Scheer et al., 2008; Novais et al., 2019; Feng et al., 2020; Brito and Lourenço, 2021). The ability of FT-IR spectroscopy to detect bacteria relies on the fact that the chemical composition and structure of bacterial biomolecules vary among different species and strains, resulting in distinct infrared absorption patterns. These patterns enable differences and identification. To enhance the accuracy and efficiency of bacterial detection and classification using FT-IR spectroscopy, researchers employ advanced statistical analysis methods like Principal Component Analysis (PCA) (Lasch et al., 2004; Bombalska et al., 2011), hierarchical clustering analysis (HCA) (Lasch et al., 2004; Dziuba et al., 2007; Bombalska et al., 2011; Feng et al., 2020), linear discriminant analysis (LDA) (Brito and Lourenço, 2021), stepwise discriminant analysis (SDA) (Lasch et al., 2004), and Ward's algorithm (Dziuba et al., 2007; Table 2). By developing spectral libraries or databases that encompass a wide range of bacterial species, robust and reliable models for bacterial identification can be established (Martak et al., 2019; Tessaro et al., 2023; Yang et al., 2023). In bacterial identification, most analyses of bacterial samples have been observed to fall within the mid-IR region (4,000 to 600 cm^{-1}) mainly because absorption patterns of functional groups in biological molecules are observed in this particular region as sharp fundamental vibrations, rather than broad overtones or harmonics which are found in the near-IR (AlMasoud et al., 2021).

One of the key challenges in the use of FT-IR for microbial identification is the complexity of microbial samples, leading to the potential for overlapping spectral signals and difficulties in accurate identification (Wenning and Scherer, 2013). Moreover, the lack of standardized protocols and extensive databases can impede consistent and reliable microbial identification, particularly for less studied or newly discovered microorganisms (Franco-Duarte et al., 2019; Feng et al., 2020). In certain cases, the resolution of infrared spectroscopy might not be adequate to distinguish between closely related microbial species or strains, limiting its efficacy in precise microbial identification (AlMasoud et al., 2021). Microbial species exhibit considerable diversity, and within each species, there can be substantial variability due to genetic, environmental, and phenotypic factors (Feng et al., 2020).

Capturing this diversity in an FT-IR library would necessitate the inclusion of a wide range of strains and conditions, requiring extensive sampling and data collection efforts. Ensuring the standardization of sample preparation, data acquisition, and analytical protocols across different laboratories is crucial for the reproducibility and comparability of spectral data. Variations in experimental procedures can lead to inconsistencies in spectral profiles, making it challenging to build a reliable and consistent FT-IR library. Moreover, analyzing and interpreting complex spectral data from diverse microbial species requires advanced computational tools and expertise. Developing

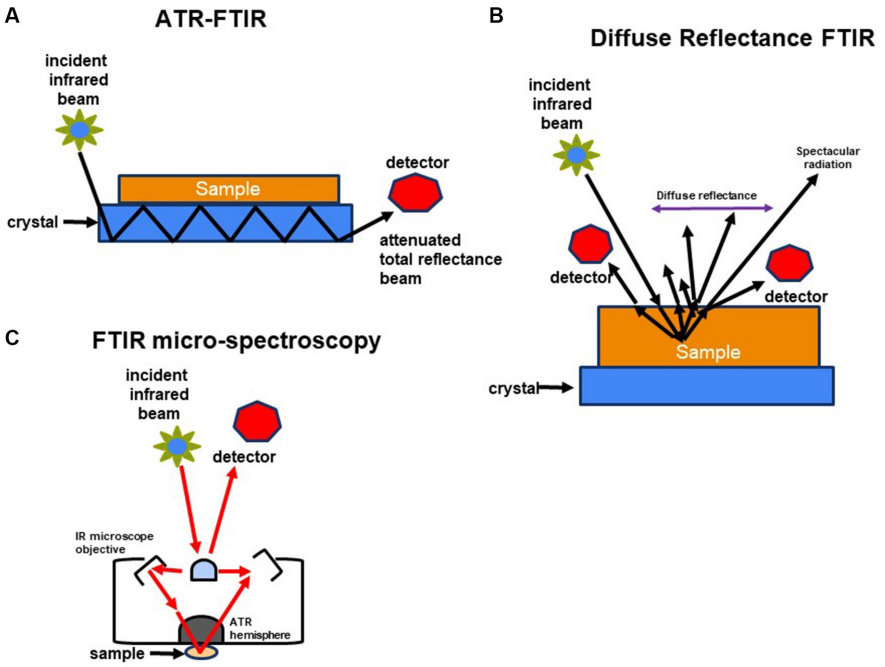

FIGURE 2
Schematic representation of methods used to characterize molecular composition of microorganisms: **(A)** FTIR-attenuated total reflectance, **(B)** diffuse reflectance FT-IR (DRIFT), and **(C)** FTIR-microspectroscopy.

robust algorithms and software for efficient data processing, feature extraction, and classification of microbial spectra is essential for effective library management and utilization. However, despite these limitations, infrared spectroscopy remains instrumental in the rapid and non-destructive identification of microorganisms, aiding in the timely diagnosis of infections and the implementation of appropriate treatment strategies. Furthermore, it contributes to environmental monitoring and various biotechnological applications, demonstrating its significant role in the field of microbial identification despite its shortcomings.

4.2 Bacterial typing

FT-IR can differentiate bacterial strains and classify them into different groups or species based on their spectral profiles. This aids in bacterial typing, strain characterization, and epidemiological studies (Goodacre et al., 2000; Perkins et al., 2005; Yu, 2005; Wang et al., 2019; Feng et al., 2020; AlMasoud et al., 2021; Table 3). Whole living cells can be analyzed non-destructively, which allows *in vivo* investigations. As an example, diffuse reflectance infrared spectroscopy (DRIFT) was used to discriminate among 36 strains of vegetative *Bacillus* cells and their spores (Goodacre et al., 2000; Table 3). Different serovars of *Salmonella enterica* have been discriminated by mid-FTIR in attenuated total reflection (ATR) mode applying soft independent modeling of class analogy (SIMCA modeling) (Perkins et al., 2005; Glassford et al., 2013). Discrimination of endospores by mid-FTIR in ATR mode followed by the application of PCA (Goodacre et al., 2000; Perkins et al., 2005; Yu, 2005; Wang et al., 2019; Feng et al., 2020), hierarchical cluster analysis (HCA) (Perkins et al., 2005; Wang et al., 2019; Feng et al., 2020), canonical variates analysis (CVA/DFC) (Goodacre et al., 2000), correlation analysis (Feng et al., 2020), and SIMCA (Perkins et al., 2005) remained possible even after autoclaving of the samples (Perkins et al., 2005; Table 3). Libraries have been developed to relate spectral absorbance peaks of key functional groups present in proteins, carbohydrates, lipids, or nucleic acids (Yu and Irudayaraj, 2005; Fadlelmoula et al., 2022). Spectra of biological samples can be divided into different regions or windows. The typical fingerprint region for microorganisms is between wavenumbers of 650 cm^{-1} and 1,800 cm^{-1} originating from cellular carbohydrate compounds and proteins.

Discrimination of vegetative cells and spores of *Bacillus circulans* was possible using FT-IR and subsequent chemometrical analysis of the spectra (Fadlelmoula et al., 2022). By FT-IR spectroscopy, spores of *Bacillus thuringiensis*, *B. subtilis*, and *B. megaterium* were easily distinguished. In some cases, however, IR fingerprints obtained by chemometrical analysis of spores of *B. atrophaeus*, *B. brevis*, *B. circulans*, and *B. lentus* clustered close together making discrimination difficult. The distance trees resulting from HCA based on FT-IR investigations of pure cultures agreed to phylogenetic trees derived from classical molecular methods based on 16S rRNA gene sequences (Zhao et al., 2006). Brandes and Brandl (2011) showed that spores originating from different *Bacillus species* can be discriminated against by applying FT-IR and subsequent multi-scaling chemometrical data treatment (Brandes and Brandl, 2011). A study carried out by Wang et al. (2019) proved the ability of FT-IR to distinguish between 16 types of foodborne pathogenic bacterial strains and was supported by multivariate analysis such as PCA and HCA of FT-IR data. In this study the authors found that a specific spectral region from 1,300 to 1,000 cm^{-1} which corresponds to phosphate and polysaccharide vibrations was successfully employed to discriminate bacterial strains (Smith, 2011; Wang et al., 2019).

TABLE 2 Applications of FT-IR in microbial identification.

Research goal	Microorganism	Data analysis	Reference
Compare the macrosample and microsample methods to evaluate which approach is more suited to the identification of *Listeria* spp. based on FT-IR spectra.	*Listeria* spp.	Leave-one-out method	Rebuffo-Scheer et al. (2008)
Determine the suitability of FT-IR as a supplement to MALDI-TOF MS for the identification and typing and identification microorganisms	*Escherichia coli* and *Shigella* species.	Correlation analysis, Principal component analysis (PCA), and hierarchical clustering analysis (HCA).	Feng et al. (2020)
Develop and validate an FTIR-ATR method for rapid identification of contaminants in pharmaceutical products	*Bacillus subtilis, Candida albicans, Enterococcus faecium, Escherichia coli, Micrococcus luteus, Pseudomonas aeruginosa, Salmonella typhimurium, Staphylococcus aureus,* and *Staphylococcus epidermidis.*	PCA and linear discriminant analysis (LDA).	Brito and Lourenço (2021)
Evaluate the potential of FT-IR for rapid identification of *Bacillus* isolates	*Bacillus cereus, Bacillus mycoides, Bacillus thuringiensis,* and other *Bacillus*, and non-*Bacillus* species.	-	Lin et al. (1998)
Differentiate and identify different lactic and propionic acid bacteria using (artificial neural networks) ANNs and FT-IR analysis; Expand the library of FTIR spectra of microorganisms	*Lactobacillus, Lactococcus, Leuconostoc, Propionibacterium, Streptococcus,* and *Lactobacillus.*	Custer analysis, Pearson's correlation coefficient and Ward's algorithm	Dziuba et al. (2007)
Study isolates belonging to the species *Campylobacter coli* and *Campylobacter jejuni* and to compare FT-IR typing schemes with established genomic profiles based on enterobacterial repetitive intergenic consensus PCR (ERIC-PCR)	*Campylobacter coli* and *Campylobacter jejuni*	HCA, stepwise discriminant analysis (SDA)	Lasch et al. (2004)
Use FTIR spectroscopy for the detection of the spectral parameters representing biochemical differences between species of the bacteria and fungi as well as different physiological states of the bacteria, i.e., endospores and vegetative cells of Bacillus spp.	*Bacillus cereus, Bacillus atrophaeus, Bacillus megaterium, Bacillus subtilis, Escherichia coli, Micrococus luteus, Pantoea agglomerans, Alternaria alternata, Candida albicans, Cladosporium herbarum, Penicillium brevicompactum* and *Penicillium chrysogenum*	PCA, HCA	Bombalska et al. (2011)

One of the primary limitations in bacterial typing is related to the need for high resolution to differentiate between closely related strains or species, which may not always be achievable with standard infrared spectroscopy (AlMasoud et al., 2021). Moreover, the technique might struggle with complex microbial samples, leading to overlapping signals and difficulties in accurately distinguishing between different bacterial types (Perkins et al., 2005; AlMasoud et al., 2021). To address this challenge of achieving high resolution and differentiating closely related bacterial strains or species in bacterial typing using infrared spectroscopy, the integration of advanced data processing techniques such as machine learning algorithms and multivariate analysis could be beneficial (AlMasoud et al., 2021). These methods can enhance the spectral analysis by enabling the identification of subtle differences and patterns within complex microbial samples, thereby improving the accuracy of bacterial classification. Leveraging these computational tools alongside infrared spectroscopy can provide a comprehensive and robust framework for precise bacterial typing, allowing for the differentiation of closely related strains with greater resolution and reliability.

4.3 Microbial growth phases monitoring

FT-IR can monitor changes in microbial growth phases by tracking alterations in the spectral profiles of cells during different growth stages (Portenier et al., 2005; AlQadiri et al., 2008; Corte et al., 2011; Grace et al., 2020; Kochan et al., 2020; Spain and Funk, 2022; Table 4). This helps in understanding microbial physiology and metabolism (Tiquia-Arashiro, 2014). In batch cultures, bacterial growth is usually accompanied by four distinct stages which are clearly visible on the growth curve: (1) lag, (2) exponential (log), (3) stationary and (4) death phase (Cooper, 1991; Tiquia et al., 2004, 2008; Rolfe et al., 2012; Wang et al., 2015; Kochan et al., 2020). Knowledge of the bacterial growth stage, bacterial numbers and growth kinetics is needed in research and commercial applications. The basis of the traditional methods to determine growth phase is cell numbers which

can be established using standard plate counting or by optical density (Stuart, 2004; Tiquia, 2010a; Nguyen et al., 2013; Plecha et al., 2013; Patel et al., 2019). However, any biochemical changes that could reflect microbial physiology cannot be described by these methods (Stuart, 2004; Tiquia, 2010a; Oest et al., 2018).

FT-IR spectroscopy detected significant changes in the chemical composition of bacteria through its different growth stages (Stuart, 2004; Spain and Funk, 2022). For the lag and log phases, these changes were mainly related to the various relative amounts of nucleic acid, accompanied by changes in protein composition (Kochan et al., 2020; Semeraro et al., 2023). The dominant spectral differences were associated with relative nucleic acid content, which reached its highest level after 60 and 90 min (Stuart, 2004; Kochan et al., 2020). This was expressed by bands at 1,215, 1,085, and 965 cm^{-1} in ATR. Further to that, an alteration in the protein composition (Amide II/Amide I) and substantial changes in relative carbohydrate content, visible via bands at 1,035 cm^{-1} (ATR) were observed. These changes may reflect the cellular activity aimed at adaptation to a new environment or in preparation for division (Stuart, 2004; AlQadiri et al., 2008; Spain and Funk, 2022). The results demonstrate the possibilities offered by multimodal vibrational spectroscopies (e.g., ATR-FTIR) toward providing a biochemical characterization, enabling the study of microbial physiology even given low bacterial numbers. Such biochemical probing opens a new door toward studying lag-phase related events (Stuart, 2004; Kochan et al., 2020; Spain and Funk, 2022). So, FT-IR demonstrates changes in the overall chemical composition of bacterial populations during growth (Zeroual et al., 1994; Stuart, 2004; Corte et al., 2011; Kochan et al., 2020; Tata et al., 2023).

FT-IR spectroscopy has been proven essential in elucidating bacterial chemical changes and understanding microbial physiology during different growth stages. However, its limited ability to capture subtle cellular composition changes and challenges in data interpretation pose constraints for comprehensive monitoring of microbial growth phases. Spectral overlap and diverse biochemical compositions across microbial species further complicate the establishment of a universal standard for interpreting FT-IR spectra. Additionally, the technique's incapacity to capture rapid changes in cellular composition restricts its effectiveness for real-time analysis of microbial growth in dynamic environments. To overcome the challenges associated with using FT-IR spectroscopy to monitor microbial growth phases, the integration of complementary techniques and advanced data analysis methods can enhance the depth and accuracy of the analysis. Coupling FT-IR with high-resolution microscopy and flow cytometry can provide additional spatial and temporal information, enabling a more comprehensive understanding of cellular changes during different growth stages. Leveraging multivariate data analysis approaches, such as PCA and partial least squares regression (PLSR), can facilitate the deconvolution of complex spectral data and enable the identification and quantification of individual biochemical constituents, addressing the challenge of spectral overlap and variability across microbial species. Furthermore, the development of standardized protocols and reference databases specific to different microbial growth phases can aid in the interpretation and comparison of FT-IR spectra, fostering a more consistent and reliable analysis framework. Integration of these strategies can enhance the utility of FT-IR spectroscopy in monitoring microbial growth phases, providing a more holistic and detailed understanding of microbial physiology and metabolism.

4.4 Characterization of microbial cell wall components

FT-IR has been used to analyze the composition of microbial cell walls (Table 5), to study changes in cell phenotype (Galichet et al., 2001), elucidate changes in functional groups among Gram-positive and Gram-negative bacteria (Jiang et al., 2004; Tang et al., 2013; Zhang et al., 2023), determine the interactions with nanoparticles with the cell wall (Nadtochenko et al., 2005; Huang et al., 2017), monitor drug interactions with bacteria cells (Zlotnikov et al., 2023), characterize the functional role of extracellular polysaccharides and lipopolysaccharide (LPS) extracted from endophytic *Pseudomonas putida* against rice blast (Ashajyothi et al., 2023), and compare structural components of the cell wall of different algal strains logarithmic and stationary growth phases (Spain and Funk, 2022; Table 5). Changes in these structural components (e.g., peptidoglycan, lipopolysaccharides) can indicate bacterial responses to various conditions.

One study utilized FT-IR and other spectroscopic methods to investigate the cell surface properties of *Aquabacterium commune* (Ojeda et al., 2008). The FT-IR signals revealed the presence of carbon, phosphorus, and nitrogen atoms in the bacterial cell wall, with specific signals demonstrating variations in response to changes in pH. These variations were linked to acid–base reactive carboxyl, phosphoryl, and amine functional groups, suggesting their involvement in the acid–base exchange reactivity observed during titration experiments. In a separate study, FT-IR spectroscopy was employed to analyze the isolated cell wall material of four algal strains (*Chlorella vulgaris*, *Coelastrella* sp., *Scendesmus* sp. B2-2, and *Haematococcus pluvialis*) during logarithmic or stationary growth phases (Spain and Funk, 2022). The spectral shape indicated typical carbohydrate (960–1,180 cm^{-1}) and protein (amide II; 1,475–1,620 cm^{-1} and amide I; 1,620–1,710 cm^{-1}) regions, while the lipid fraction (around 1,740 cm^{-1}) showed minimal absorption, suggesting a low presence of fatty acids in the cell walls. For strain comparison, the FTIR spectra were normalized to the amide I band (indicating protein content) (Spain and Funk, 2022).

Another study (Huang et al., 2017) utilized two-dimensional Correlation Fourier Transformation Infrared spectroscopy (2D-FTIR-COS) to investigate the interaction between TiO_2 nanoparticles and bacterial cell membranes using bacterial ghosts (BGs), which are non-living bacterial cell envelopes. The results suggested that the proteins in BGs exhibited a strong preference for interacting with TiO_2 nanoparticles, while the interaction with characteristic functionalities in polysaccharides (C-OH) and phospholipids (P=O) was minimal. This observation was further confirmed by the settlement of TiO_2 nanoparticles in the presence of specific biomolecules such as bovine serum albumin (BSA), alginate, and phosphatidylethanolamine (PE). The asynchronous map of 2D-FTIR-COS indicated a sequential bonding order of COO- > aromatic C=C stretching > NH, amide II > C=O, ketone, shedding light on the interaction between TiO_2 nanoparticles and bacterial cell membranes in aquatic environments.

TABLE 3 Applications of FT-IR in bacterial typing.

Research goal	Microorganism	Data analysis	Reference
Typing of 36 *Bacillus* spp. and rapid detection of bacterial spores	*Bacillus* spp.	Principal component analysis (PCA) and Canonical variates analysis (CVA/DFA)	Goodacre et al. (2000)
Classification of bacterial endospores	*Bacillus* and *Clostridium* spores.	PCA, hierarchical clustering analysis (HCA), and Soft independent method of class analogy (SIMCA).	Perkins et al. (2005)
Use FT-IR microspectroscopy to whole microbial cells establish a spectroscopic fingerprinting basis for effective discrimination of microbial cells	*Salmonella, Escherichia coli, Yersinia enterocolitis,* and *Shigella boydii.*	PCA and CVA	Yu (2005)
Application of synchrotron radiation-based FTIR (SR-FTIR) spectroscopy to discriminate 10 bacterial strains in combination with chemometric methods.	*Salmonella, Shigella, Rhodococcus, Listeria, Yersinia, Vibrio,* and *Staphylococcus* strains.	PCA and HCA	Wang et al. (2019)
Determine the suitability of FT-IR as a supplement to MALDI-TOF MS for the identification and typing and identification microorganisms.	*Escherichia coli* and *Shigella* species.	Correlation analysis, PCA, and HCA.	Feng et al. (2020)
Develop a fast and reproducible non-molecular method to differentiate pure samples of *Bacillus* spores originating from different species as well as to identify spores in a simple matrix, such as the clay mineral, bentonite.	*Bacillus atrophaeus, Bacillus brevis, Bacillus circulans, Bacillus lentus, Bacillus megaterium, Bacillus subtilis* and *B. thuringiensis*	PCA, HCA, and SIMCA	Brandes and Brandl (2011)

Zhang et al. (2023) determined the impact of reactive oxygen species on cell activity and structural integrity of Gram-positive and Gram-negative bacteria in electrochemical disinfection system. Around 70% of the cell wall mass is composed of -CH_3- and -CH_2- vibrational stretching bands, with changes in their positions suggesting alterations in the cell wall layers. Notably, *Staphylococcus aureus* (a Gram-positive bacterium) exhibited a pronounced blue shift trend in the -CH_2 and -CH_3 peaks, indicating increased fluidity in the cell wall bilayer, potentially induced by peroxidation. Conversely, *E. coli* (A Gram-negative bacterium) showed no significant dependency in peak positions despite disorder in cell wall components. Analysis within the 2,000–1,000 cm^{-1} region identified five prominent peaks, including amides, nucleic acids, lipid, and protein vibrations, PO_2-profiles, and C–O–P symmetric stretches from oligo/polysaccharides. Changes in peak positions and intensities of amide and C–O–P suggested modifications in cell wall proteins and oligosaccharides. While the C–O–P band weakening in *E. coli* indicated potential damage due to electrochemical oxidation, *S. aureus* exhibited slight changes after 60 min. Damage to the C–O–P band, a vital component in lipopolysaccharides (LPS), could lead to LPS degradation and subsequent cell structure failure. The decrease in C–O–P intensity served as an indicator of cell damage, corroborated by inactivation efficiency results. Furthermore, changes in the PO_2-band near 1,245 cm^{-1} suggested the disruption of the hydrogen phosphate group during the electrochemical oxidation process. However, the detection of specific C=O peaks representing peroxidation products might require extended treatment time for accurate identification.

Fourier-transform infrared (FT-IR) spectroscopy has been widely used to investigate microbial cell walls, yet its application faces notable limitations. Interpreting FT-IR data is complex and demands specialized expertise, posing a significant challenge. Sample preparation sensitivity can affect spectra quality, with issues like sample thickness and uniformity leading to potential distortions. Limited spatial resolution restricts the observation of microscopic cell wall variations. Overlapping peaks within spectra can complicate the identification of specific functional groups, potentially leading to misinterpretations. Dependence on reference spectra, particularly for scarce data, may hinder compound characterization. FT-IR spectroscopy's sensitivity to environmental factors, such as temperature and humidity, can introduce variability in results. While offering insights into cell wall chemical composition, it may lack the resolution required for understanding intricate cell wall interactions, limiting its use in certain research contexts. Considering these limitations is crucial for ensuring accurate and meaningful interpretation of FT-IR results in cell wall analysis. Standardizing sample preparation protocols, including precise control of sample thickness, uniformity, and purity, can minimize variability and ensure the reproducibility of spectral results. Building comprehensive reference databases for microbial cell wall components can facilitate more accurate comparison and interpretation of FT-IR results. Implementing rigorous environmental controls during data acquisition, such as temperature and humidity regulation, can help mitigate variations in spectral data. Furthermore, combining FT-IR with other high-resolution structural analysis techniques, such as electron microscopy and atomic force microscopy, can provide a more

TABLE 4 Applications of FT-IR in monitoring microbial growth phases.

Research goal	Microorganism	Data analysis	Reference
Detect biochemical changes that occur during bacterial growth phases in batch culture.	*Escherichia coli* and *Listeria innocua*	Soft independent method of class analogy (SIMCA) and Principal component analysis (PCA)	AlQadiri et al. (2008)
Study the changes in nordic microalgal strains in relation with the logarithmic and stationary growth phases.	*Chlorella vulgaris, Scenedesmus* sp., *Haematococcus pluvialis* and *Coelastrella* sp.	-	Spain and Funk (2022)
Determine the susceptibility of bacterial cells to three endodontic medicaments during exponential growth, stationary phase and starvation phase	*Enterococcus faecalis*	-	Portenier et al. (2005)
Detect the chemical composition of bacteria within the same phase (intra-phase).	*Staphylococcus aureus*	Student's *t*-test	Kochan et al. (2020)
Analyze the molecular transitions and lipid accumulation in freshwater green microalgal species during their growth phases.	*Monoraphidium contortum, Pseudomuriella* sp. and *Chlamydomonas* sp.	PCA	Grace et al. (2020)

comprehensive understanding of the complex interactions within microbial cell walls.

5 Use of FT-IR spectroscopy in environmental microbiology

The study of microbial ecology has undergone transformative advancements due to innovative analytical techniques. Among these, Fourier Transform-Infrared (FT-IR) spectroscopy has emerged as a pivotal tool, enabling researchers to delve into the world of microorganisms with unprecedented precision and depth. FT-IR spectroscopy holds the potential to unravel the complexities of microbial communities, shedding light on their composition, metabolic activities, and responses to environmental changes. It also offers insights into the molecular signatures that characterize microorganisms, paving the way for a comprehensive understanding of microbial ecosystems and their vital roles in various habitats. This exploration into the utilization of FT-IR spectroscopy in microbial ecology opens new avenues for deciphering the hidden dynamics that govern microbial interactions and their impact on broader ecological systems.

5.1 Monitoring microbial biofilms

Microbial biofilms, complex communities of microorganisms adhering to surfaces and encased in self-produced extracellular polymeric substances (EPS), have garnered significant attention due to their diverse roles and impact on various fields, including medicine, industry, and environmental science (Schmitt et al., 1995; Schmitt and Flemming, 1998; Bosch et al., 2006; Mukherjee et al., 2011; Quilès et al., 2016; Tugarova et al., 2017; Di Martino, 2018; Miao et al., 2019; Gieroba et al., 2020; Cheah and Chan, 2022).

The use of Fourier Transform-Infrared (FT-IR) spectroscopy has proven to be a valuable and versatile approach in monitoring bacterial (Bosch et al., 2006; Elzinga et al., 2012; Quilès et al., 2016; Tugarova et al., 2017; Singhalage et al., 2018; Cheeseman et al., 2021; Kamnev et al., 2023), fungal (Singhalage et al., 2018; Cheeseman et al., 2021; Dimopoulou et al., 2021), algal (Tong and Derek, 2021; Wang et al., 2021) and microbial community (Schmitt and Flemming, 1998; Oberbeckmann et al., 2014; Gong et al., 2019; Miao et al., 2019) biofilms (Table 6). As an analytical tool, the attenuated total reflection (ATR) offers a further possibility to directly investigate the chemical composition of smooth surfaces of various materials (Smith, 1998; Elzinga et al., 2012; Cheeseman et al., 2021; Tong and Derek, 2021; Watanabe et al., 2023). This can be achieved practically without any sample preparation. With respect to biofilm research, this offers the significant advantage that the sample can be investigated in a relatively undisturbed state. Especially for membrane and polymer investigations, ATR is a helpful analytical tool. A further advantage of FTIR-ATR-spectroscopy in biofilm research is the possibility of measuring in aqueous media as well as investigating the development of a biofilm *in situ*, non-destructively and in real time directly at the substratum/liquid interface (Schmitt et al., 1995; Schmitt and Flemming, 1998; Oberbeckmann et al., 2014; Miao et al., 2019; Jansson et al., 2023). The major advantage of the ATR method is that the biofilm can be observed non-destructively, directly, on-line and in real time (Schmitt and Flemming, 1998; Tiquia-Arashiro, 2012). FT-IR can provide useful information on the functional groups of EPS that play an adhesive and cohesive role in maintaining biofilms (Geoghegan et al., 2008; Di Martino, 2018). The EPS matrix plays a pivotal role in biofilm formation, stability, and protection. FT-IR spectroscopy assists in elucidating the composition of EPS, which includes polysaccharides, proteins, and other biomolecules. By studying changes in specific bands related to carbohydrate and protein vibrations, researchers can assess the dynamic nature of EPS as biofilms develop, mature, and respond to environmental cues (Bosch et al., 2006; Ojeda et al., 2008; Mukherjee et al., 2011; Bowman et al., 2018; Cheeseman et al., 2021; Cheah and Chan, 2022).

The complex composition of biofilms can lead to challenges in identifying specific components due to overlapping spectral bands and the heterogeneous mixture of biomolecules and extracellular polymeric substances (EPS). Advanced spectral deconvolution techniques are necessary for accurate analysis. The inherent heterogeneity of biofilm structures introduces variability in FT-IR signals, making it difficult to establish consistent baseline data for comparison and identify subtle changes during biofilm development

TABLE 5 Applications of FT-IR in characterization of microbial cell wall components.

Research goal	Microorganism	Data analysis	Reference
Understand the relation of the functional groups on the cell wall with the changes observed in the chemical cell surface properties in aqueous electrolyte solutions at different pH values.	*Aquabacterium commune*	-	Ojeda et al. (2008)
Assess the cell wall compositions of nordic microalgal strains.	*Chlorella vulgaris, Scenedesmus* sp., *Haematococcus pluvialis* and *Coelastrella* sp.	-	Spain and Funk (2022)
Determine the structural changes of the *Escherichia coli* cell membranes during TiO_2 photocatalysis.	*Escherichia coli*	-	Nadtochenko et al. (2005)
Discriminate mycobacteria and Gram-negative bacteria by assessing specific characteristic spectral features.	*Mycobacterium* spp. *Escherichia coli* strains, and *Pseudomonas putida.*	Direct classical least squares (DCLS)	Tang et al. (2013)
Investigate the effects of α-glucosidase on the cell wall of yeast bacteria.	*Saccharomyces cerevisiae*	-	Galichet et al. (2001)
Obtain functional group specific information on bacterial surfaces in aqueous solutions and observe their variation as a function of cell structure (Gram-positive versus Gram-negative cells) and solution composition.	*Bacillus subtilis, Bacillus licheniformis, Pseudomonas stutzeri* and *Pseudomonas aeruginosa*	-	Jiang et al. (2004)
Investigate the interaction between TiO_2 nanoparticles and cell membrane	*Escherichia coli* K-12	-	Huang et al. (2017)
Determine if cell wall-associated polysaccharides of *Pseudomonas putida* could elicit defense against rice blast.	*Pseudomonas putida*	-	Ashajyothi et al. (2023)
Monitor the drugs interaction with *Escherichia coli* cells localized in macrophages for diagnosis and treatment control of respiratory diseases	*Escherichia coli* JM109	-	Zlotnikov et al. (2023)
Determine the impact of reactive oxygen species on cell activity and structural integrity of Gram-positive and Gram-negative bacteria	*Staphylococcus aureus* and *Escherichia coli*	-	Zhang et al. (2023)

and responses to environmental stimuli. Environmental influences on biofilm formation and EPS composition, such as temperature and nutrient availability, require careful consideration and control during experimental design and data interpretation. Background signals and contaminants can interfere with the identification of specific biomolecules and functional groups within the biofilm, affecting the reliability of FT-IR analysis. The limited spatial resolution of traditional FT-IR spectroscopy may hinder precise characterization of localized changes within the biofilm matrix, emphasizing the need for complementary imaging techniques and high-resolution FT-IR imaging systems to enable more accurate spatial analysis of microbial biofilms. Employing advanced data processing and statistical modeling approaches, such as multivariate analysis and machine learning algorithms, can aid in interpreting complex FT-IR spectra and discerning subtle changes in biofilm development and response to environmental stimuli. Integration of complementary imaging techniques, such as confocal microscopy and atomic force microscopy, can provide spatially resolved information, complementing FT-IR spectroscopy and enabling more comprehensive characterization of localized biofilm structures and molecular distributions. Furthermore, the development of high-resolution FT-IR imaging systems and the incorporation of advanced data visualization tools can enhance spatial resolution and facilitate detailed mapping of biofilm composition and dynamics at the microscale level (Kamnev et al., 2023).

5.2 Functional profiling of microbial communities

Microbial communities within natural environments carry out a plethora of functions essential for nutrient cycling, organic matter decomposition, and ecosystem stability (Tiquia et al., 2006a,b; Tiquia, 2008, 2010b; Igisu et al., 2012; Mckindles and Tiquia-Arashiro, 2012; Flood et al., 2015; Tiquia-Arashiro and Grube, 2019; Duncan and Petrou, 2022; Naylor et al., 2022). The metabolic activities and functional profiles of the microbial communities are influenced by environmental factors, including temperature fluctuations, nutrient availability, and pollutant exposure (Liu et al., 2003; Wu et al., 2005; Gentile et al., 2006; Tiquia, 2010a, 2011; Dong et al., 2017; Qin et al., 2018; Tiquia-Arashiro, 2019b; Huang et al., 2020; Cabugao et al., 2022; Duncan and Petrou, 2022).

FT-IR spectroscopy has been crucial in comprehending the functional characteristics of microbial communities (Table 7). This method is commonly combined with genetic techniques like

TABLE 6 Applications of FT-IR in monitoring microbial biofilms.

Research goal	Microorganism	Data analysis	Reference
Determine the effect of pH and contact time on the attachment of bacteria to a surface of hematite in the process of biofilm formation	*Shewanella putrefaciens*	-	Elzinga et al. (2012)
Study the characteristics of a bacterial biofilm.	*Bordetella pertussis*	Analysis of variance (ANOVA) and Fisher's least significant difference (LSD)	Bosch et al. (2006)
Characterize biofilm formation on the surface of ZnSe discs by a rhizobacterium.	*Azospirillum brasilense*	-	Tugarova et al. (2017)
Analyze the effect of antimicrobial peptides on nascent bacterial biofilm.	*Pseudomonas fluorescens*	Sneddon model	Quilès et al. (2016)
Use FTIR spectroscopic analyses to study biofilms formed on a solid surface or liquid/air interface along with the macromolecular biofilm matrix and its main macrocomponents,	*Azospirillum baldaniorum*	-	Kamnev et al. (2023)
To confirm the value of FT-IR spectroscopy in biology, medicine, and pharmacy as effective tools for bacterial product characterization.	*Streptococcus* spp.	-	Gieroba et al. (2020)
Investigate the photosynthetic parameters, microstructures, biomass accumulation, and CO_2 fixation rate of *Chlorella* sp. biofilms cultured under a series of light intensities	*Chlorella* sp.	-	Wang et al. (2021)
Study the relationships between the algal attachment rate onto membranes via biofilm and the compositional changes of the extracellular polymeric substances in the biofilm	*Amphora coffeaeformis, Cylindrotheca fusiformis* and *Navicula incerta*	ANOVA	Tong and Derek (2021)
Show differences between biofilms formed by Gram-positive methicillin-resistant *Staphylococcus aureus* (MRSA), Gram-negative *Pseudomonas aeruginosa*, and the yeast-type *Candida albicans* using synchrotron macro attenuated total reflectance-Fourier transform infrared (ATR-FTIR) microspectroscopy.	*Staphylococcus aureus, Pseudomonas aeruginosa,* and *Candida albicans*	Hierarchical cluster analysis (HCA), Principal component analysis (PCA)	Cheeseman et al. (2021)
Determine the adhesion capacity of eleven strains of the species, compare the metabolic fingerprint of the attached vs. planktonic cells, reveal the compounds implicated in the biofilm formation associated with wine spoilage.	*Brettanomyces bruxellensis*	PCA	Dimopoulou et al. (2021)
Examine the structural attributes of fungal-bacterial biofilms in comparison to bacterial (BBs) and fungal (FBs) biofilms.	*Enterobacter* sp. and *Aspergillus* sp.	-	Singhalage et al. (2018)
Investigate the development and properties of biofilm.	Microbial communities	-	Schmitt and Flemming (1998)
Investigate the biofilm formation by microorganisms originating from lake water on low-density polyethylene	Microbial communities	ANOVA	Gong et al. (2019)
Understand the structural and taxonomical variation of microbial biofilm communities on plastic fragments in coastal and offshore Northern European waters, with respect to season, geographical location and plastic type.	Microbial communities	-	Oberbeckmann et al. (2014)

metagenomics and qPCR (Edwards et al., 2014; Lin et al., 2014; Andrei et al., 2015; Miao et al., 2019; Wang et al., 2021; Wilson et al., 2021 and Zada et al., 2021). Additionally, it is utilized alongside genetic fingerprinting techniques (Edwards et al., 2014), radioisotope labeling (Andrei et al., 2015; Wang et al., 2021; Wilson et al., 2021; Duncan and Petrou, 2022), as well as biochemical assays like community level physiological profiles (CLPP) (Artz et al., 2006) and enzyme assays (Miao et al., 2019). Other supporting analytical and imaging techniques include excitation emission matrix spectroscopy (EEMS) (Wilson et al., 2021) and scanning electron microscopy (SEM) (Miao et al., 2019).

TABLE 7 Applications of FT-IR in functional profiling of microbial communities.

Research goal	Microorganism	Data analysis	Reference
Investigate the genetic and functional diversity of bacteria and archaea in typical limestone (Kashmir Cave) and silicate-containing (Tiser Cave) caves.	Microbial communities	Nonmetric multidimensional scaling (NMDS)	Zada et al. (2021)
Evaluate community level physiological profiles of the microbial community in peat horizons of differing degrees of humification	Microbial communities	Principal components analysis (PCA), subsequent canonical variate analysis (CVA)	Artz et al. (2006)
Quantitatively link the abundance and distribution of specific microbial groups to the dynamics of specific plant-derived organic carbon compounds and environmental parameters at the ecosystem scale in a northern peatland	Microbial communities	paired *t* tests, chi-square test, distance-based linear model combined with a forward model selection method	Lin et al. (2014)
Determine the plasticity and taxonomic diversity of sea ice microalgae macromolecular composition, with a focus on how different environmental conditions influence macromolecular production and partitioning within cells and communities.	Microbial communities	Permutational multivariate ANOVA	Duncan and Petrou (2022)
Examine bacterial community structure and biochemical properties of organic matter by metabolite fingerprinting using FT-IR spectroscopy.	Microbial communities	Canonical correspondence analysis (CCA), Permutational multivariate ANOVA	Edwards et al. (2014)
Compare the prokaryotic assemblages from Ursu and Fara Fund hypersaline meromictic lakes (Transylvanian Basin, Romania) in relation to their limnological factors and infer their role in elemental cycling by matching taxa to known taxon-specific biogeochemical functions	Microbial communities	Correlation analysis, Permutational multivariate ANOVA	Andrei et al. (2015)
Probe the extent of environmental perturbations using high-resolution geochemical and microbial gene-based community profiling of anaerobically incubated material from three wetland habitats across a permafrost peatland	Microbial communities	Permutational multivariate ANOVA	Wilson et al. (2021)
Investigate the effects of copper oxide (CuO) NPs on freshwater sediment biofilms in terms of the functional properties and microbial community structure	Microbial communities	Linear discriminant analysis (LDA), Permutational multivariate ANOVA	Miao et al. (2019)
Stduy the transformation patterns of different S cycling microbial species in mangrove sediments amended with different microplastics and their associated microbial communities were investigated	Microbial communities	ANOVA	Wang et al. (2021)

The FT-IR protocol follows a structured process that involves sample preparation, data acquisition, and advanced data analysis techniques (Figure 3). To ensure accurate representation of microbial components, diverse samples are collected from various environments and undergo preparation steps such as cell lysis and extraction (Figure 3A). FT-IR spectroscopy generates unique spectral signatures revealing the biomolecular composition of the microbial samples, providing insights into lipids, proteins, carbohydrates, and nucleic acids (Figure 3B). The data analysis stage utilizes sophisticated tools like PCA and HCA and SIMCA (Figure 3C), enabling comparisons with reference databases to identify microbial taxa and their functional attributes (Figure 3D).

While FT-IR spectroscopy has proven to be a valuable tool for studying microbial functions in natural environments, it has encountered challenges in interpreting the complex data it generates. The acquired spectra demand a profound grasp of both spectroscopy and microbiology. To ensure meaningful comparisons and reliable findings across studies, standardized protocols and data analysis methods are imperative, given the diversity and variability in natural environments and microbial communities. Uniform protocols and robust analytical frameworks are essential for maintaining consistency and coherence in result interpretation, thereby bolstering the credibility and reproducibility of findings. Despite challenges, FT-IR spectroscopy serves as a bridge between molecular insights and ecosystem processes. By utilizing multivariate statistical tools such as PCA and cluster analysis, researchers can identify functional patterns and understand the roles of microorganisms in environmental dynamics. The integration of FTIR spectroscopy with other advanced techniques, including genetic analysis and stable isotope probing (Wang et al., 2023), holds promise for deeper insights into microbial functions, but requires careful consideration and methodological refinement to effectively merge these approaches.

5.3 Microbial stress and viability

The use of FT-IR spectroscopy for microbial stress and viability has emerged as a valuable approach for understanding the responses

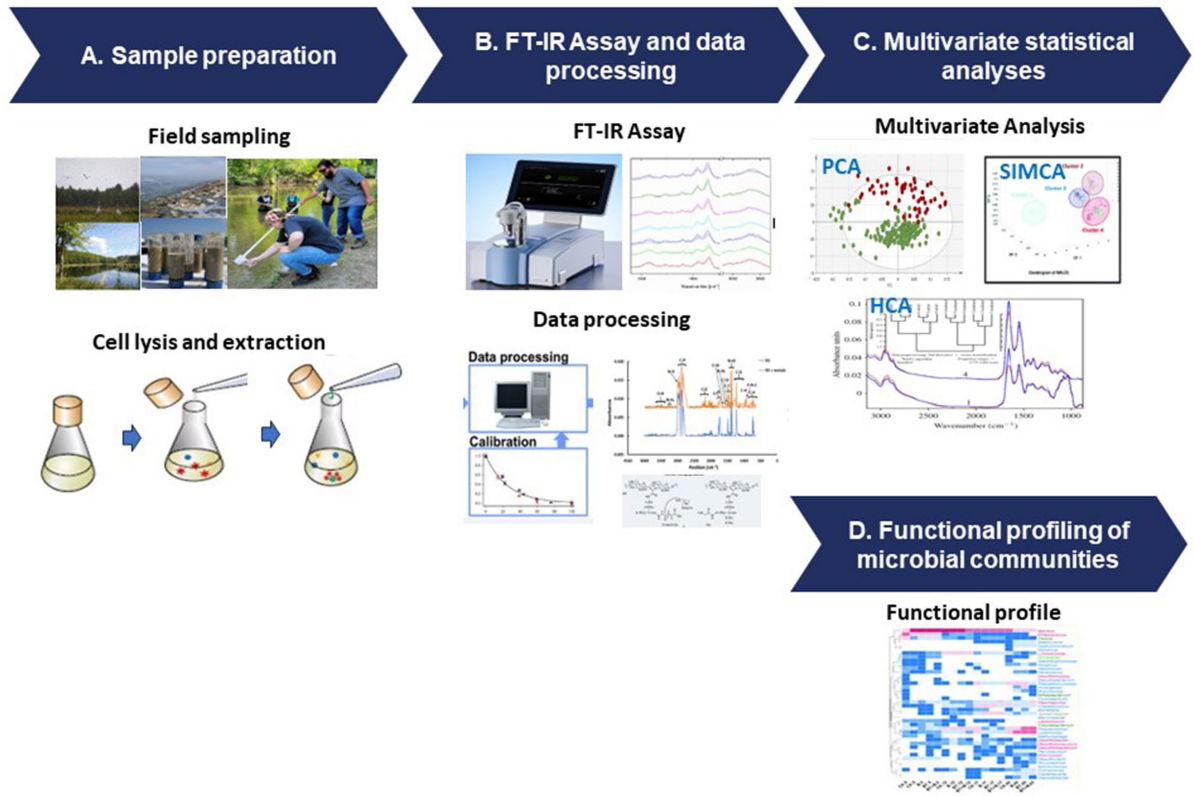

FIGURE 3
FT-IR protocol for microbial functional analysis. **(A)** Sample preparation, **(B)** FT-IR assay and data processing, **(C)** multivariate statistical analyses, and **(D)** functional profiling of the microbial communities.

of microorganisms to various stressors (Table 8). Microorganisms encounter a multitude of stressors, including changes in nutrient availability, temperature fluctuations, pH variations, exposure to toxins, and other environmental challenges. Traditional methods for assessing microbial stress and viability often involve time-consuming culturing procedures and may not accurately represent the real-time physiological state of microorganisms (Kumar and Ghosh, 2019). FT-IR spectroscopy offers a rapid and comprehensive alternative for studying these aspects. When microorganisms undergo stress or changes in their physiological state, alterations occur in their biochemical composition, resulting in shifts in FT-IR spectra. Researchers can analyze these changes to assess the stress levels and viability of microorganisms (Moen et al., 2005, 2009; Alvarez-Ordóñez et al., 2011; Câmara et al., 2020). Monitoring these shifts allows researchers to infer stress-induced modifications within cellular components, including protein denaturation, lipid peroxidation, and changes in carbohydrate content, offering insights into microbial adaptation mechanisms (Moen et al., 2005, 2009; Alvarez-Ordóñez et al., 2011; Câmara et al., 2020). Employing various modes of FT-IR spectroscopy, including transmission, DRIFT, and ATR, researchers have examined changes in the composition and structure of whole bacterial cells in response to specific stress factors and plant-derived signals (Kamnev, 2008; Meyvisch et al., 2022). Investigations using FT-IR spectroscopy have revealed distinctive metabolic variations between epiphytic and endophytic strains of the *Azospirillum brasilense* species under conditions of heavy-metal stress (Kamnev, 2008). Furthermore, FT-IR spectroscopy has been utilized to study the metabolomic stress responses triggered by N-alkylpyridinium bromide surfactants in yeast strains *Saccharomyces cerevisiae* and *Candida albicans*, demonstrating its utility in probing stress-induced metabolic alterations in various microorganisms (Corte et al., 2014). Studies involving FT-IR spectroscopy have highlighted its sensitivity in detecting stressful conditions or pathological states, ranging from bacterial reactions to antibiotics, responses to starvation and environmental stressors, to encounters with pollutants and gene mutations, underscoring its potential in diverse research contexts (Melin et al., 2001; Kamnev et al., 2005; Portenier et al., 2005; Stehfest et al., 2005; El-Bialy et al., 2019; Câmara et al., 2020; Ribeiro da Cunha et al., 2020; Scarsini et al., 2021; Soares et al., 2022; Table 8).

Microbial viability assessment is central to understanding the functional status of microbial populations in diverse environments (Braissant et al., 2020). It provides critical information about the metabolic activity, reproductive potential, and overall health of microorganisms (Nguyen et al., 2013; Pomaranski and Tiquia-Arashiro, 2016; Braissant et al., 2020). In microbial ecology, assessing viability aids in deciphering community responses to environmental fluctuations, resource availability, and biotic interactions (Tiquia et al., 2002; Cho et al., 2012; Berninger et al., 2018). Additionally, viability assessments are pivotal for monitoring the efficacy of antimicrobial treatments, studying microbial survival strategies, and predicting ecosystem responses to perturbations.

FT-IR spectroscopy has practical applications in discerning viable microbial cells and distinguishing between viable and non-viable ones

TABLE 8 Applications of FT-IR in microbial stress and viability assessment.

Research goal	Microorganism	Data analysis	Reference
Understand stress responses triggered by antibiotic exposure	*Escherichia coli*	Savitzky–Golay (SG) and Loopy Multiplicative Scatter Correction (LMSC), Partial Least Squares Discriminant Analysis (PLS-DA) predictive models.	Ribeiro da Cunha et al. (2020)
Modulating the synergistic response of antibiotics to circumvent the mechanisms of bacterial resistance	*Staphylococcus aureus*	Hierarchical Cluster Analysis (HCA)	Soares et al. (2022)
Confirm the metabolic plasticity of microalgae in response to environmental stress (nutrient stress)	*Phaeodactylum tricornutum*	Standard Normal Variate (SNV), ANOVA	Scarsini et al. (2021)
Understand the modifications of single-cells biophysical profiles during different dehydration conditions using synchrotron radiation-based Fourier-transform infrared (S-FTIR)	*Lachancea thermotolerans*	Principal component analysis (PCA)	Câmara et al. (2020)
Understand the effect of different environmental stresses including heavy metal, nutritional, plant stress-response protein stresses on soil bacteria	*Azospirillum* sp.	-	Kamnev (2008)
Assess the effect of N-tetradecyltropinium bromide surfactant and some of its variants on yeast bacteria and human pathogens.	*Saccharomyces cerevisiae* and *Candida albicans*	QUANT2 algorithm	Corte et al. (2014)
Investigate the susceptibility of bacterial cells to three endodontic medicaments	*Enterococcus faecalis*	Student's *t*-test	Portenier et al. (2005)
Determine the effect of nutrient stress on bacterial composition of phytoplankton algae	*Microcystis aeruginosa, Croococcus minutus, Nostoc* sp., *Cyclotella meneghiniana,* and *Phaeodactylum tricornutum*	-	Stehfest et al. (2005)
Characterize the effect of γ-irradiation on bacteria.	*Deinococcus radiodurans*	Savitsky–Golay algorithm and Ward's algorithm	Melin et al. (2001)
Develop FTIR micro-spectroscopy device for probing live bacteria and to compare the biochemical data obtained at the single-cell level with data obtained from clusters of thousands of cells	*Lactobacillus delbrueckii* subsp. *bulgaricus*	Savitzky–Golay algorithm, PCA	Meneghel et al. (2020)
Apply specific collection techniques and spectroscopy to differentiate between live and dead *Escherichia coli* O157:H7 cells, as well as cells subjected to various inactivation treatments, including heat, salt, UV, antibiotics and alcohol.	*Escherichia coli* O157:H7	Canonical variate analysis (CVA), Mahalanobis distances (MD)	Davis et al. (2012)
Determine if FT-IR could detect and differentiate between *Salmonella typhimurium* and *Salmonella enteritidis* live serotypes and between live and dead Salmonella cells.	*Salmonella typhimurium* MH 68123 and *Salmonella enteritidis* MH 42841	PCA, Mahalanobis distances, Soft independent modeling by class analogy (SIMCA)	Sundaram et al. (2012)

(Davis et al., 2012; Sundaram et al., 2012; Meneghel et al., 2020; Table 8). Meneghel et al. (2020) developed two distinct FT-IR systems for analyzing the infrared spectra of bacteria in water, operating at different spatial resolutions (Figure 4). The first system integrated a custom-built attenuated total reflection inverted microscope with a synchrotron-based FT-IR spectrometer (Figure 4A), enabling the acquisition of spectra at the individual-cell level within the 1,800–1,300 cm^{-1} range. The second system utilized a transmission FT-IR microscope with a specially designed sample holder for liquid samples (Figure 4B), allowing the examination of viable cells across the entire

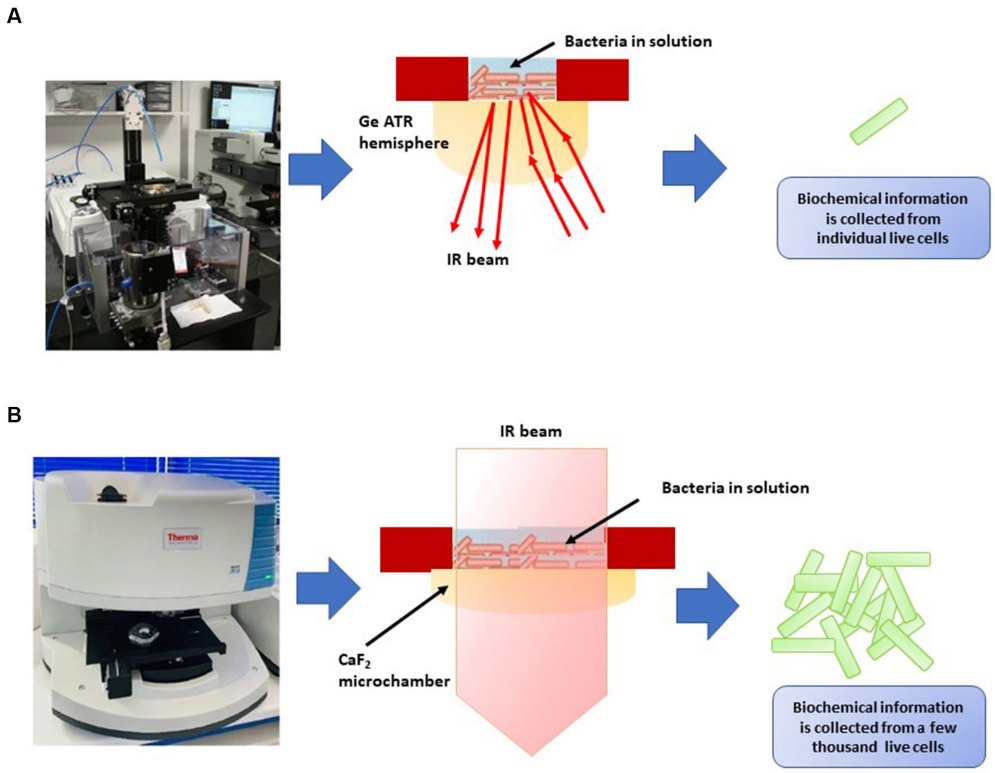

FIGURE 4
Two types of FT-IR developed by Meneghel et al. (2020). **(A)** Attenuated total reflectance-Fourier transform infrared (ATR-FTIR) inverted microscope for the analysis of individual bacterial cells in an aqueous environment using synchrotron radiation. An enlargement diagram of the liquid sampling area showing the ATR principle. **(B)** Thermal source-powered FTIR microscope for probing clusters of a few thousands of live cells in the mid-IR region (4,000–975 cm^{-1}). Diagram shows the demountable liquid micro-chamber.

mid-IR region by regulating the optical path length. These approaches helped identify potential cellular markers of bacterial populations, including the secondary structure of proteins, particularly the proportions of α-helix and β-sheet structures, as well as cell envelope components, specifically polar head groups of membrane phospholipids and complex sugars of the peptidoglycan cell wall. These components, already utilized for microbial identification, were also implicated in cryo-resistance mechanisms. Multivariate analysis of the spectra revealed that cryo-sensitive cells exhibited the highest cell heterogeneity and the highest content of proteins with the α-helix structure. Moreover, cluster analysis of bacterial cells highlighted phosphate and peptidoglycan vibrational bands associated with the cell envelope as potential markers of resistance to environmental conditions (Meneghel et al., 2020).

Sundaram et al. (2012) conducted research indicating the effectiveness of FT-IR in distinguishing between live and deceased cells of *Salmonella typhimurium* and *Salmonella enteritidis*. They discovered significant spectral variations in components such as the cell wall, cell membrane, cytoplasm, polysaccharides, proteins, peptides, amide bands, and nucleic acids. The Mahalanobis distance and SIMCA analysis yielded a perfect 100% accuracy in classifying live and dead cells of both *Salmonella* serotypes. However, the authors emphasized the need for further investigations to develop a comprehensive spectral library for different *Salmonella* serotypes and validate the method's sensitivity and selectivity using standard microbiological procedures. Davis et al. (2012) also utilized FT-IR spectroscopy to differentiate live and dead *Escherichia coli* O157:H7 cells and those treated with various inactivation methods (heat, salt, UV, antibiotics, and alcohol). The study demonstrated the efficacy of partial least squares analysis and canonical variate analysis (CVA) in rapidly distinguishing between live and dead cells. This approach shows promise in reducing detection time compared to other techniques like fluorescent microscopy and EMA-qPCR, which necessitate lengthier preparation and detection times. The findings suggest potential applications of this FT-IR approach in analyzing food samples subjected to different inactivation treatments.

In these studies, changes in spectral features, such as alterations in protein and lipid content, served as indicators of cellular viability. By comparing FT-IR spectra of viable and non-viable cells, researchers can develop spectral fingerprints that aid in rapid and non-destructive viability assessment. The viability of microbial cells influences their biochemical makeup, leading to variations in FT-IR spectra. Viable cells generally exhibit well-defined spectral bands associated with intact proteins, lipids, nucleic acids, and carbohydrates. In contrast, non-viable cells or cells undergoing stress may exhibit shifts or reductions in these bands due to protein denaturation, lipid degradation, and changes in cellular structure (Davis et al., 2012; Sundaram et al., 2012; Meneghel et al., 2020). By analyzing these spectral changes, researchers can establish viability indicators that aid in distinguishing between live and non-live cells. While FT-IR spectroscopy holds promise for microbial viability assessment, challenges remain. The interpretation of complex spectral data

requires advanced analytical techniques and expertise. Standardization of protocols and data analysis methods is essential for ensuring consistent results across studies. As technology advances, integrating FT-IR spectroscopy with other techniques, such as microscopy and flow cytometry, could provide a multi-faceted view of microbial viability and functional responses in ecological contexts.

5.4 Microbial biosorption studies with metals

Microbial biosorption has gained prominence as an environmentally friendly method for extracting heavy metals from water (Bowman et al., 2018; Tiquia-Arashiro, 2018, Pagnucco et al., 2023). This process involves a variety of interactions between microbial cell surfaces and metal ions, including physical adsorption, ion exchange, complexation, and surface precipitation (Tiquia-Arashiro, 2018; Tiquia-Arashiro and Pant, 2019; Pagnucco et al., 2023). FT-IR spectroscopy allows researchers to investigate the molecular-level alterations on microbial cell surfaces during metal binding. By examining the vibrational modes of functional groups like hydroxyl, carboxyl, and amino groups, FT-IR spectra offer insights into the chemical bonds formed between microorganisms and metal ions. The analysis of FT-IR spectra post-biosorption reveals shifts in peak positions or intensity, indicating changes in functional group vibrations. These modifications provide valuable information about the specific functional groups responsible for metal absorption and the ensuing chemical reactions on the microbial cell surface. Comprehensive analysis of biosorption of metal ions using FT-IR have been studied in bacteria (Pardo et al., 2003; Oh et al., 2009; Gutiérrez-Corona et al., 2016; Dhanwal et al., 2018; Saranya et al., 2018; Pagnucco et al., 2023), algae (Michalak et al., 2013; Gu and Lan, 2021) and fungi (George et al., 2012; Gutiérrez-Corona et al., 2016; Sundararaju et al., 2022; Table 9).

In Michalak et al.'s (2013) work, they investigated the biosorption of Cr^{3+}, Mn^{2+}, and Mg^{2+} by the freshwater macroalga *Cladophora glomerata*, using FT-IR spectroscopy. The FTIR analysis identified key functional groups involved in the process, primarily carboxyl and hydroxyl. In Gutiérrez-Corona et al.'s (2016) review, FT-IR spectroscopy was employed to examine the cell walls of microorganisms like *Streptomyces werraensis* LD22 and *Aspergillus niger*, highlighting the specific functional groups involved in binding with chromium (Cr^{6+}). The analysis revealed the participation of amine, hydroxyl, and carboxyl groups in Cr^{6+} binding within the cell walls of *S. werraensis* LD22, while in *Aspergillus niger*, hydroxyl, carboxyl, amino, and carbonyl groups were identified as instrumental in Cr^{6+} binding. Oh et al. (2009) utilized FT-IR spectroscopy to validate interactions between functional groups on the cell wall of *Pseudomonas stutzeri* and heavy metals Pb^{2+}, Cd^{2+}, and Cu^{2+}. The intricate mechanisms underlying metal removal by microorganisms were classified into three groups, involving biosorption of metal ions onto the cell surface, intracellular uptake of metal ions, and chemical transformation of metal ions by microorganisms. Various studies highlighted the role of functional groups, such as carboxylic, hydroxyl, and amino groups, in the biosorption process (Pardo et al., 2003; Oh et al., 2009; George et al., 2012; Michalak et al., 2013; Gu and Lan, 2021; Pagnucco et al., 2023).

Saranya et al. (2018) employed FT-IR spectroscopy to study the biosorption of multi-heavy metals by *Cronobacter muytjensii* KSCAS2. The analysis of both control and mixed heavy metals-treated bacterial cultures through FT-IR revealed that the biosorption capacity was influenced by the functional groups present on the active sites of bacterial cells, as confirmed by SEM results. Moreover, Dhanwal et al. (2018) examined FT-IR spectra of bacterial cells isolated from contaminated soil, identifying various absorption peaks indicating the involvement of multiple functional groups. These findings emphasize the valuable role of FT-IR spectroscopy in elucidating the intricate mechanisms of microbial biosorption processes and the significance of different functional groups. FT-IR spectroscopy aids in characterizing biosorption sites and the affinity of microorganisms for specific metals, providing insights into the nature of the binding sites. Furthermore, the quantification of metal-induced spectral changes can offer information on metal affinities and competitive binding behavior, enabling the optimization of biosorption processes and prediction of metal removal efficiency (Dhanwal et al., 2018; Pagnucco et al., 2023).

Pagnucco et al. (2023) note that biosorption can impact the biochemical composition of microbial cells. FT-IR spectroscopy, as highlighted by Ojeda and Dittrich (2012), enables the monitoring of changes in biomolecule vibrational modes, revealing alterations in cellular structure and function caused by metal stress. Analyzing FT-IR spectra provides valuable insights into the effects of biosorption on microbial physiology and viability (Meng et al., 2023). This technique finds applications in diverse metal-contaminated environments, including industrial effluents and mine tailings, as discussed by Tiquia-Arashiro (2012), Mudziwapasi et al. (2018), and Sundararaju et al. (2022). FT-IR-based analyses aid in optimizing biosorption conditions, understanding the influence of environmental parameters on metal uptake, and developing specialized microbial biosorbents for specific metals. The integration of FT-IR with other analytical techniques, such as X-ray absorption spectroscopy and microscopy, promises a holistic understanding of metal-microbe interactions across different scales.

The use of FT-IR spectroscopy in microbial biosorption studies of metals is valuable but not without limitations. While it enables the investigation of molecular-level changes during metal binding on microbial cell surfaces, the limited spatial resolution of FT-IR restricts the detailed examination of microscopic variations within cell wall structures, potentially overlooking crucial details. Moreover, while FT-IR provides valuable insights into the chemical composition of cell walls, it may not offer the high-resolution structural details required for understanding complex interactions between cell wall components and external factors. The integration of FT-IR alongside complementary analytical methods such as scanning electron microscopy with energy dispersive X-ray spectroscopy (SEM/EDX) and Transmission Electron Microscopy with EDX shows promise in comprehensively unraveling the complexities of metal-microbe interactions at different scales (Pagnucco et al., 2023).

5.5 Microbial degradation of organic pollutants

The application of FT-IR spectroscopy in the study of microbial interactions with organic pollutants, such as polycyclic aromatic hydrocarbons (PAHs), pesticides, and emerging contaminants like pharmaceuticals and personal care products, has garnered significant attention (Obinaju and Martin, 2016; Chakraborty and Das, 2017;

TABLE 9 Applications of FT-IR in microbial biosorption studies with metals.

Research goal	Microorganism	Data analysis	Reference
Study the biosorption process of Cr^{3+}, Mn^{2+} and Mg^{2+} ions by a freshwater macroalga	*Cladophora glomerata*	-	Michalak et al. (2013)
Unravel the interactions of bacteria with Cr^{6+}	*Streptomyces werraensis* and *Aspergillus niger*	-	Gutiérrez-Corona et al. (2016)
Assess the biosorptive capacity of Pb^{2+}, Cd^{2+} and Cu^{2+} by bacteria.	*Pseudomonas stutzeri*	Langmuir and Freundlich models.	Oh et al. (2009)
Determine the biosorption of Cd^{2+}, Cu^{2+}, Pb^{2+} and Zn^{2+} by bacteria.	*Pseudomonas putida*	Langmuir and Freundlich models.	Pardo et al. (2003)
Study the biosorption of Cd^{2+}, Cr^{6+}, Cu^{2+}, and Zn^{2+} by coral associated phosphate solubilizing bacteria.	*Cronobacter muytjensii*	Langmuir model.	Saranya et al. (2018)
Investigate the removal of Pb^{2+} and Hg^{2+} from aqueous solutions by bacteria isolated from estuarine sediments	*Aspergillus niger*	-	George et al. (2012)
Assess the biosorptive capacity of bacterial strains single and multi-metal solutions	*Klebsiella* spp. *Serratia* sp. and *Raoultella* sp.	-	Pagnucco et al. (2023)
Screened biosorption potential of bacteria isolated from soil contaminated with electroplating industrial effluents to multi-metals (Cu^{2+}, Ni^{2+}, Pb^{2+}, and $Cr6^{+}$)	*Bacillus cereus*	-	Dhanwal et al. (2018)
Evaluate the biomass of *Penicillium* sp. MRF1 as biosorbent for the removal of Ni^{2+} ions from electroplating industrial effluent.	*Penicillium* sp. MRF1	Analysis of variance (ANOVA); Freundlich isotherm model	Sundararaju et al. (2022)
Understand the functional groups at cell surface, and the interactions between metal ions (Cu^{2+}, Zn^{2+}, Pb^{2+}, Hg^{2+}, and Cd^{2+}) and biosorbents	*Neochloris oleoabundans*	Langmuir model	Gu and Lan (2021)
Determine the physiological characteristics of *Spirulina* strains, and their chromium (VI) adsorption capacities	*Spirulina* spp.	Principal components analysis (PCA)	Meng et al. (2023)

Monga et al., 2021; Kumar et al., 2022; Cáceda Quiroz et al., 2023; Chaudhary et al., 2023; Hosseini et al., 2023; Nor et al., 2023; Table 10).

Sharma et al. (2020) introduced a pioneering bioelectroremediation strategy for efficiently eliminating phenanthrene, a significant polycyclic aromatic hydrocarbon (PAH) pollutant, while concurrently generating power. This technique not only captured electrons released during microbial metabolism but also fostered the growth of microbial communities specializing in PAH degradation, including *Pseudomonas*, *Thauera*, and *Rhodococcus*. The researchers employed FT-IR to track the biodegradation process, identifying the presence of phenanthrene through distinct C–H out-of-plane stretching vibrations at approximately 730 cm^{-1} in the phenanthrene-loaded electrodes. Subsequent analysis after 50 days revealed the disappearance of the ~730 cm^{-1} band, suggesting the successful breakdown or elimination of phenanthrene from the sample. Moreover, a new major band emerged in the 1,170–980 cm^{-1} range, with a peak at approximately 1,030 cm^{-1}, indicating the potential involvement of various functional groups within the polysaccharides due to the biofilms formed by the microorganisms. These FT-IR findings provided robust evidence of phenanthrene degradation by the microbial communities.

Krishnaswamy (2021) delved into the efficient biotreatment techniques for methyl parathion, an agricultural pesticide designed to combat crop-damaging insects, using native strains of *Pseudomonas aeruginosa* and *Fusarium* spp. Through specific biotransformation experiments, various biodegradation compounds were identified. Gas chromatography–mass spectrometry (GCMS) analysis of the transformed compounds by the bacteria unveiled the presence of p-nitrophenol, dimethylaminophenol, and other derivatives. The study extensively utilized FT-IR spectroscopy to examine the structural changes of methyl parathion and its products. The spectra highlighted distinct bands corresponding to specific functional groups, including 2,955 cm^{-1} for CH_3, 837 cm^{-1} for CH in the outer plane of the aromatic ring, and 1,641 cm^{-1} for C=C. Furthermore, the presence of bands around 1,346 cm^{-1} and 1,047 cm^{-1} was associated with the aromatic NO_2 group and the P–OCH_3 group, respectively. Additionally, the phosphate group was identified through bands at 576 cm^{-1} and 1,036 cm^{-1} for P–O stretching and bending vibrations, and at 1,036 cm^{-1} and 767 cm^{-1} for P–O–C and P = S stretching, respectively. The spectral analysis provided crucial insights into the structural modifications occurring during the biotreatment processes.

Chang and Gupta (2022) demonstrated the degradation of Amphotericin B (AmB, an antifungal drug) in tandem with wastewater treatment within a Microbial Peroxide Producing Cell (MPPC). Two sets of MPPCs were employed for the oxidative degradation of AmB, one utilizing H_2O_2 and the other employing the microbial electro-Fenton process. FT-IR analysis of the treated samples unveiled the disappearance of characteristic bands such as the

TABLE 10 Applications of FT-IR in microbial degradation of organic pollutants.

Research goal	Microorganism	Data analysis	Reference
Use a novel approach of sequestering PAH, phenanthrene, onto a solid carbon matrix bioanode in a microbial fuel cell (MFC) to assess its biodegradation coupled with power generation.	Microbial communities	-	Sharma et al. (2020)
Determine effective biotreatment processes of aqueous methylparathion by competent potential indigenous strains of bacterium (*Pseudomonas aeruginosa* mpd5) and fungus (*Fusarium* spp. mpd1).	*Pseudomonas aeruginosa*, *Fusarium* spp.	-	Krishnaswamy (2021)
Investigate the degradation of amphotericin B (AmB) with simultaneous wastewater treatment in a microbial peroxide producing cell (MPPC)	Microbial communities	-	Chang and Gupta (2022)
Evaluate the biosurfactant property of an extremophilic microbe *Bacillus cereus* KH1 in decolorizing the textile dyes.	*Bacillus cereus* KH1	-	Nor et al. (2023)
Use FTIR spectroscopy to study the functional groups of compounds made during the biodegradation of alkaline cyanide to figure out the specific biochemical mechanisms and pathways involved	*Bacillus subtilis* strain TT10s	-	Cáceda Quiroz et al. (2023)
Investigate the capability and efficiency of co-contaminant bioremediation of phenol and tellurite as two models of aromatic compounds and metalloid oxyanions.	*Lysinibacillus* sp. EBL303	Kolmogorov–Smirnov and Levene's test, Analysis of variance (ANOVA)	Hosseini et al. (2023)
Evaluate volatile organic carbon (VOCs) removal efficiencies of VOC-degrading bacteria using diffusion bioreactor	*Pseudomonas* sp. DKR-23 and *Rhodococcus* sp. Korf-18	-	Chaudhary et al. (2023)

NH band at 1,556 cm^{-1} and the CH band in the Polyene ring at 3,358 cm^{-1}. This indicated the disruption of multiple double bonds in the polyene structure, resulting in the breakdown of the lactone ring. Liquid chromatography quadrupole time-of-flight confirmed the structural changes by revealing shifts in retention time and peak area compared to native AmB, leading to the loss of its antifungal action. The absence of zones of inhibition in an antimicrobial susceptibility test against *Candida albicans* corroborated this finding.

FT-IR analysis of microbial degradation of organic pollutants faces several limitations due to the intricate nature of microbial samples. Distinguishing specific functional groups within diverse microbial communities can be difficult (Sharma et al., 2020; Chang and Gupta, 2022), leading to potential misinterpretation of data. Inconsistent sample preparation techniques, such as variations in drying procedures, can introduce errors and hinder data reliability. Instrumental limitations, including resolution and sensitivity, may impede the detection of subtle spectral changes in complex samples, affecting the accuracy of results. Interference from other organic and inorganic components in the sample matrix can obscure the identification of target pollutants and their interactions with the microbial biomass. To address the challenges associated with FT-IR analysis of microbial degradation of organic pollutants, several potential solutions can be implemented. Advanced data processing methods such as peak fitting, baseline correction, and deconvolution can assist in discerning specific functional groups in complex microbial samples. Ensuring standardized sample preparation protocols, including consistent drying, presentation, and handling techniques, can reduce variability and ensure consistent spectral data. Regular calibration of FT-IR instruments, along with rigorous quality control measures, can improve the precision and accuracy of the analysis. Establishing comprehensive spectral databases covering diverse microbial samples and organic pollutants can aid in the precise identification of spectral signatures and facilitate data interpretation. Performing thorough sample matrix analyses and utilizing advanced spectral analysis techniques to isolate target pollutants from background noise and overlapping signals can help minimize spectral interference. Collaboration among experts in microbiology, chemistry, and spectroscopy can drive the development of integrated approaches, promoting innovative solutions for dependable FT-IR analysis and deeper insights into the intricate dynamics of microbial interactions with organic pollutants.

6 Challenges

The applications of Fourier Transform-Infrared (FT-IR) spectroscopy have ushered in new possibilities for understanding microbial composition, functions, and interactions and have brought about significant advancements in our understanding of microbial communities and their interactions within complex ecosystems. However, these applications are not without their challenges. Several

key challenges need to be addressed to harness the full potential of FT-IR in advancing microbiological research.

(1) *Sample complexity and heterogeneity:* Microbial communities are composed of diverse microorganisms with distinct cellular compositions. FT-IR spectra can be influenced by variations in biomass, cell size, and cellular content. Discriminating between different functional groups and their contributions within mixed microbial communities remains a challenge. In complex mixtures, functional groups can produce overlapping peaks, making it difficult to deconvolute and accurately identify individual components. This requires careful spectral interpretation and, in some cases, additional techniques to separate overlapping signals. Advances in single-cell FT-IR spectroscopy (Doherty et al., 2019) may facilitate the precise analysis of the biochemical constituents and functional attributes of individual microbial cells, enabling researchers to gain a comprehensive understanding of the intricate responses and behaviors exhibited by diverse microorganisms within complex microbial communities.

(2) *Quantitative analysis:* While FT-IR provides qualitative insights into microbial composition and functional groups, quantitative analysis remains a challenge. Factors like sample thickness, path length, and scattering can affect the accuracy of quantitative measurements (Wenning and Scherer, 2013; Watanabe et al., 2023). The development of robust calibration techniques and the establishment of reference standards are pivotal in ensuring the precise quantification of specific biomolecules and metabolites within microbial samples. These calibration methods are essential for translating the spectral data obtained from FT-IR analysis into quantifiable and meaningful information, enabling researchers to accurately assess the concentration of microbial biomass, monitor the production of key metabolic products, and quantify the levels of pollutants within diverse microbial systems. Overcoming the challenges associated with quantitative analysis in FT-IR spectroscopy is vital for enhancing the applicability and reliability of this analytical tool in the field of microbiology research.

(3) *Data interpretation and standardization:* Interpreting FT-IR spectra is a multidisciplinary task that demands expertise in both microbiology and spectroscopy. The complexity of microbial samples, which may contain a multitude of functional groups and biomolecules, can make deciphering the spectral information daunting. Standardization of protocols for sample preparation, data acquisition, and analysis is crucial to ensure consistent and comparable results across studies. Establishing clear guidelines for data interpretation will enhance the reliability and reproducibility of FT-IR-based microbiological studies.

(4) *Multivariate analysis and data handling:* FT-IR spectra generate large datasets containing intricate spectral information. Analyzing these datasets requires advanced multivariate analysis techniques, such as PCA and clustering algorithms like PCA, CVA, and SIMCA. Developing robust algorithms capable of extracting meaningful information from complex spectra is essential to unveil patterns, trends, and relationships within microbial data. Combining FT-IR with machine learning approaches could enhance our ability to distinguish microbial species, strains, and functional states accurately.

7 Future prospects

The challenges posed by FT-IR in microbiology also present opportunities for innovation and advancement. The future prospects of FT-IR applications in microbiology are promising and hold the potential to reshape how we perceive and study microorganisms.

(1) *Development of comprehensive and standardized FT-IR libraries for the identification of bacteria and fungi:* While the utilization of FT-IR spectroscopy for microbial identification has shown considerable potential, the establishment of extensive libraries could significantly enhance the accuracy, efficiency, and reliability of this identification method. One of the primary objectives in future research could be the creation of a universal, exhaustive, and well-curated spectral database that encompasses a diverse range of bacterial and fungal species. This library should include spectra obtained under varying growth conditions, substrates, and environmental factors to ensure robustness and applicability across different settings and contexts. To achieve this, collaborative efforts among researchers, microbiologists, and spectroscopy experts are essential. It is crucial to encourage data sharing and collaboration between different research groups and institutions to compile a diverse and representative collection of spectra. Furthermore, the inclusion of strains with clinical relevance, such as those associated with antibiotic resistance or pathogenicity, would enhance the practical utility of the library in clinical and diagnostic settings. In the process of building these libraries, it is important to consider the standardization of experimental protocols and data acquisition parameters to ensure consistency and comparability across different studies and laboratories. This includes defining standardized procedures for sample preparation, spectral acquisition, and data analysis to minimize variations and improve the reproducibility of results. Integration of advanced data analysis techniques, such as machine learning algorithms and pattern recognition methods, would further enhance the capabilities of FT-IR libraries for microbial identification. Leveraging these tools can enable the development of automated and efficient identification systems capable of handling large datasets and complex spectral information, thereby facilitating rapid and accurate microbial identification. Incorporating metadata, such as strain information, growth conditions, and environmental factors, into the spectral database would provide valuable insights into the effects of various parameters on microbial spectra, enabling a more comprehensive understanding of the relationships between microbial physiology and spectral fingerprints.

(2) *Integration of advanced analytical techniques:* The integration of FT-IR with other advanced analytical techniques, such as Raman spectroscopy, mass spectrometry, and genomics, represents a transformative approach in the study of microbial systems, enabling a comprehensive and multi-dimensional analysis of their intricate functionalities. By merging the capabilities of FT-IR with Raman spectroscopy, researchers can attain a more detailed understanding of molecular structures and spatial distributions within heterogeneous microbial samples. Simultaneously, the fusion of FT-IR with mass

spectrometry allows for the identification and quantification of specific biomolecules and metabolites, shedding light on complex metabolic pathways and molecular interactions. Additionally, coupling FT-IR with genomics and molecular biology techniques provides insights into the genetic underpinnings of microbial characteristics, facilitating the correlation of spectral data with specific genetic signatures and facilitating the identification of key biomarkers associated with distinct microbial phenotypes and environmental adaptations. This integrative analytical approach not only enhances microbial identification accuracy but also fosters a deeper comprehension of microbial behavior, offering significant implications for diverse fields such as biotechnology, medicine, environmental science, and bioprocess engineering.

(3) *High-throughput and single-cell analysis*: Technological advancements are paving the way for high-throughput FT-IR analysis, enabling rapid screening of microbial communities and dynamic responses. Additionally, single-cell FT-IR spectroscopy has the potential to achieve single-cell resolution. Recent advancements in the technology have enabled the development of methods for analyzing individual microbial cells (Saulou et al., 2013; Muhamadali et al., 2015; Harrison and Berry, 2017; Meneghel et al., 2020). The single-cell FT-IR approach can facilitate the study of diverse microbial properties, including metabolic activities, cellular responses to environmental stimuli, and the identification of specific biomolecules within a single microbial cell. This level of resolution is valuable for understanding the intricacies of microbial physiology and behavior at a microscale level, offering insights into cellular processes and enabling a more comprehensive understanding of microbial functionality.

(4) *Real-time environmental monitoring:* Portable FT-IR systems could revolutionize environmental monitoring by enabling real-time, *in situ* analysis of microbial communities. Such technology would allow researchers to track microbial responses to changing environmental conditions, detect pollution events, and assess ecosystem health promptly. Mitigating the interference of exogenous and endogenous substances remains a significant concern in environmental samples. Addressing this challenge necessitates the implementation of advanced data processing algorithms, signal deconvolution methods, and spectral library expansion to enable the accurate discrimination of target compounds from interfering substances. For example, comprehensive reference libraries containing spectral signatures of known exogenous and endogenous interfering substances can be established. This approach allows for the comparison of sample spectra with the reference database, aiding in the identification and correction of potential interferences during data analysis. Multivariate analysis techniques such as PCA and partial least squares regression (PLSR) to discern and account for the influence of interfering substances on the FT-IR spectra. These statistical methods enable the extraction of relevant spectral information and the identification of specific spectral patterns associated with target analytes, thereby reducing the impact of interferences. Moreover, the integration of complementary analytical techniques, such as chromatography and mass spectrometry, can enhance the selectivity and sensitivity of FT-IR in real-time environmental monitoring, allowing for the effective identification and quantification of specific pollutants amidst complex environmental matrices. These strategies, coupled with rigorous calibration and validation processes, can significantly contribute to minimizing the impact of interference and ensuring the reliability and accuracy of real-time environmental monitoring using FT-IR spectroscopy.

(5) *Functional metagenomics integration:* Integrating FT-IR data with functional metagenomics can link microbial metabolic activities to spectral changes, providing a deeper understanding of microbial contributions to ecosystem functions. This integration could elucidate the functional roles of specific microbial taxa in biogeochemical cycles. It can also facilitate the establishment of direct correlations between the spectral signatures captured by FT-IR and the underlying genetic mechanisms governing microbial functions.

(6) *Biosorption and bioremediation strategies:* Expanding FT-IR-based studies on microbial biosorption holds promise for developing efficient bioremediation strategies for metal removal. By utilizing FT-IR spectroscopy, researchers can investigate the molecular interactions between microorganisms and various contaminants, enabling a comprehensive understanding of biosorption mechanisms and bioremediation processes. Understanding the molecular-level interactions between microorganisms and metals could lead to the design of tailored biosorbents with enhanced metal-binding capacities.

(7) *Ecological modeling and predictive insights:* Integrating FT-IR data into ecological models can enhance our ability to predict microbial responses to environmental changes. For example, FT-IR spectroscopy assists in identifying key biomolecular signatures associated with microbial activities, enabling the development of predictive models that forecast ecosystem responses to environmental changes, such as shifts in nutrient availability, climate fluctuations, and anthropogenic disturbances. By coupling spectral information with ecological modeling approaches, researchers can gain insights into how microbial communities shape ecosystem dynamics and stability.

8 Conclusion

In conclusion, the challenges encountered in harnessing FT-IR in microbiology serve as catalysts for innovation and exploration of novel solutions. Addressing these challenges through interdisciplinary collaboration and technological advancements will pave the way for an exciting future in microbiological research. As FT-IR technology evolves and its integration with other techniques becomes more seamless, the scope of microbial analysis will expand, enabling us to uncover hidden insights into microbial communities, functions, and their roles in shaping our understanding of ecosystem dynamics and sustainability.

Author contributions

AK: Formal analysis, Validation, Writing – original draft, Writing – review & editing. LA: Methodology, Validation, Writing – original draft, Writing – review & editing. OC: Methodology, Validation, Writing – original draft, Writing – review & editing. SO: Methodology, Validation, Writing – original draft, Writing – review & editing. HN: Validation, Writing – original draft, Writing – review & editing. DK: Writing – original draft, Writing – review & editing. KP: Validation, Resources, Writing – review & editing. XL: Methodology, Supervision, Validation, Writing – original draft, Writing – review & editing. ST-A: Conceptualization, Funding acquisition, Project administration, Resources, Supervision, Validation, Visualization, Writing – original draft, Writing – review & editing.

Funding

The author(s) declare financial support was received for the research, authorship, and/or publication of this article. This work was financially supported by the University of Michigan-Dearborn. Office of Research and Sponsored Programs (Research Initiation and Development Grant) at the University of Michigan-Dearborn.

Conflict of interest

The authors declare that the research was conducted in the absence of any commercial or financial relationships that could be construed as a potential conflict of interest.

The author(s) declared that they were an editorial board member of Frontiers, at the time of submission. This had no impact on the peer review process and the final decision.

Publisher's note

References

AlMasoud, N., Muhamadali, H., Chisanga, M., AlRabiah, H., Lima, C. A., and Goodacre, R. (2021). Discrimination of bacteria using whole organism fingerprinting: the utility of modern physicochemical techniques for bacterial typing. *Analyst* 146, 770–788. doi: 10.1039/D0AN01482F

AlQadiri, M., Al-Alami, N. I., Lin, M., Al-Holy, M., Cavinato, A. G., and Rasco, B. A. (2008). Studying of the bacterial growth phases using fourier transform infrared spectroscopy and multivariate analysis. *J. Rapid Met. Autom. Microbiol.* 16, 73–89. doi: 10.1111/j.1745-4581.2008.00117.x

Alvarez-Ordóñez, A., Mouwen, D. J., López, M., and Prieto, M. (2011). Fourier transform infrared spectroscopy as a tool to characterize molecular composition and stress response in foodborne pathogenic bacteria. *J. Microbiol. Methods* 84, 369–378. doi: 10.1016/j.mimet.2011.01.009

Andrei, A. Ş., Robeson, M., Baricz, A., Coman, C., Muntean, V., Ionescu, A., et al. (2015). Contrasting taxonomic stratification of microbial communities in two hypersaline meromictic lakes. *ISME J.* 9, 2642–2656. doi: 10.1038/ismej.2015.60

Artz, R., Chapman, S. J., and Campbell, C. D. (2006). Substrate utilisation profiles of microbial communities in peat are depth dependent and correlate with whole soil FT-IR profiles. *Soil Biol. Biochem.* 38, 2958–2962. doi: 10.1016/j.soilbio.2006.04.017

Ashajyothi, M., Balamurugan, A., Patel, A., Krishnappa, C., Kumar, R., and Kumar, A. (2023). Cell wall polysaccharides of endophytic *Pseudomonas putida* elicit defense against rice blast disease. *J. Appl. Microbiol.* 134:lxac042. doi: 10.1093/jambio/lxac042

Aziz, S., Ali, M. I., Farooq, U., Jamal, A., Liu, F. J., He, H., et al. (2020). Enhanced bioremediation of diesel range hydrocarbons in soil using biochar made from organic wastes. *Environ. Monit. Assess.* 192:569. doi: 10.1007/s10661-020-08540-7

Baker, M. J., Trevisan, J., Bassan, P., Bhargava, R., Butler, H. J., Dorling, K. M., et al. (2014). Using Fourier transform IR spectroscopy to analyze biological materials. *Nate Protocols.* 9, 1771–1791. doi: 10.1038/nprot.2014.110

Beekes, M., Lasch, P., and Naumann, D. (2007). Analytical applications of Fourier transform-infrared (FT-IR) spectroscopy in microbiology and prion research. *Vet. Microbiol.* 123, 305–319. doi: 10.1016/j.vetmic.2007.04.010

Berninger, T., González López, Ó., Bejarano, A., Preininger, C., and Sessitsch, A. (2018). Maintenance and assessment of cell viability in formulation of non-sporulating bacterial inoculants. *Microb. Biotechnol.* 11, 277–301. doi: 10.1111/1751-7915.12880

Bhargava, R. (2012). Infrared spectroscopic imaging: the next generation. *Appl. Spectrosc.* 66, 1091–1120. doi: 10.1366/12-06801

Bombalska, A., Mularczyk-Oliwa, M., Kwaśny, M., Włodarski, M., Kaliszewski, M., Kopczyński, K., et al. (2011). Classification of the biological material with use of FT-IR spectroscopy and statistical analysis. *Spectrochim. Acta A Mol. Biomol. Spectrosc.* 78, 1221–1226. doi: 10.1016/j.saa.2010.10.025

Bosch, A., Serra, D., Prieto, C., Schmitt, J., Naumann, D., and Yantorno, O. (2006). Characterization of *Bordetella pertussis* growing as biofilm by chemical analysis and FT-IR spectroscopy. *Appl. Micro. Biotechnol.* 71, 736–747. doi: 10.1007/s00253-005-0202-8

Bottum, S. R., Teitsworth, T. S., Han, Q., Orr, A. D., Park, J. S., Jia, X., et al. (2023). *In situ* attenuated Total reflectance infrared Spectroelectrochemistry (ATR-IR-SEC) for the characterization of molecular redox processes on surface-proximal doped silicon ATR crystal working electrodes. *J. Phys. Chem. C.* 127, 6690–6701. doi: 10.1021/acs.jpcc.2c08991

Bowman, N., Patel, D., Sanchez, A., Xu, W., Alsaffar, A., and Tiquia-Arashiro, S. M. (2018). Lead-resistant bacteria from Saint Clair River sediments and Pb removal in aqueous solutions. *Appl. Microbiol. Biotechnol.* 102, 2391–2398. doi: 10.1007/s00253-018-8772-4

Braissant, O., Astasov-Frauenhoffer, M., Waltimo, T., and Bonkat, G. (2020). A review of methods to determine viability, vitality, and metabolic rates in microbiology. *Front. Microbiol.* 11:547458. doi: 10.3389/fmicb.2020.547458

Brandes, A., and Brandl, H. (2011). Detection and differentiation of bacterial spores in a mineral matrix by Fourier transform infrared spectroscopy (FT-IR) and chemometrical data treatment. *BMC Biophys.* 4, 1–8. doi: 10.1186/2046-1682-4-14

Brito, N. M. R. D., and Lourenço, F. R. (2021). Rapid identification of microbial contaminants in pharmaceutical products using a PCA/LDA-based FTIR-ATR method. *Brazilian J. Pharm. Sci.* 57:8899. doi: 10.1590/s2175-97902020000318899

Cabugao, K. G. M., Gushgari-Doyle, S., Chacon, S. S., Wu, X., Bhattacharyya, A., Bouskill, N., et al. (2022). Characterizing natural organic matter transformations by microbial communities in terrestrial subsurface ecosystems: a critical review of analytical techniques and challenges. *Front. Microbiol.* 13:864895. doi: 10.3389/fmicb.2022.864895

Cáceda Quiroz, C. J., Fora Quispe, G. L., Carpio Mamani, M., Maraza Choque, G. J., and Sacari Sacari, E. J. (2023). Cyanide bioremediation by *Bacillus subtilis* under alkaline conditions. *Water* 15:3645. doi: 10.3390/w15203645

Câmara, A. A. Jr., Nguyen, T. D., Saurel, R., Sandt, C., Peltier, C., Dujourdy, L., et al. (2020). Biophysical stress responses of the yeast Lachancea thermotolerans during dehydration using synchrotron-FTIR microspectroscopy. *Front. Microbiol.* 11:899. doi: 10.3389/fmicb.2020.00899

Chakraborty, J., and Das, S. (2017). Application of spectroscopic techniques for monitoring microbial diversity and bioremediation. *Appl. Spectr. Rev.* 52, 1–38. doi: 10.1080/05704928.2016.1199028

Chang, C., and Gupta, P. (2022). *In-situ* degradation of amphotericin B in a microbial electrochemical cell containing wastewater. *Chemosphere* 309:136726. doi: 10.1016/j.chemosphere.2022.136726

Chaudhary, D. K., Park, J. H., Kim, P. G., Ok, Y. S., and Hong, Y. (2023). Enrichment cultivation of VOC-degrading bacteria using diffusion bioreactor and development of bacterial-immobilized biochar for VOC bioremediation. *Environ. Pollut.* 320:121089. doi: 10.1016/j.envpol.2023.121089

Cheah, Y. T., and Chan, D. J. C. (2022). A methodological review on the characterization of microalgal biofilm and its extracellular polymeric substances. *J. Appl. Microbiol.* 132, 3490–3514. doi: 10.1111/jam.15455

Cheeseman, S., Shaw, Z. L., Vongsvivut, J., Crawford, R. J., Dupont, M. F., Boyce, K. J., et al. (2021). Analysis of pathogenic bacterial and yeast biofilms using the combination of synchrotron ATR-FTIR microspectroscopy and chemometric approaches. *Molecules* 26:3890. doi: 10.3390/molecules26133890

Cho, K., Zholi, A., Frabutt, D., Flood, M., Floyd, D., and Tiquia, S. M. (2012). Linking bacterial diversity and geochemistry of uranium-contaminated groundwater. *Environ. Technol.* 33, 1629–1640. doi: 10.1080/09593330.2011.641036

Cooper, S. *Bacterial growth and division: Biochemistry and regulation of prokaryotic and eukaryotic division cycles*. (1991). Elsevier Science: New York, NY. 501.

Corte, L., Antonielli, L., Roscini, L., Fatichenti, F., and Cardinali, G. (2011). Influence of cell parameters in Fourier transform infrared spectroscopy analysis of whole yeast cells. *Analyst* 136, 2339–2349. doi: 10.1039/c0an00515k

Corte, L., Tiecco, M., Roscini, L., Germani, R., and Cardinali, G. (2014). FT-IR analysis of the metabolomic stress response induced by N-alkyltropinium bromide surfactants in the yeasts Saccharomyces cerevisiae and *Candida albicans*. *Colloids Surf B Biointer.* 116, 761–771. doi: 10.1016/j.colsurfb.2014.01.054

Davis, R., Deering, A., Burgula, Y., Mauer, L. J., and Reuhs, B. L. (2012). Differentiation of live, dead and treated cells of *Escherichia coli* O157:H7 using FT-IR spectroscopy. *J. Appl. Microbiol.* 112, 743–751. doi: 10.1111/j.1365-2672.2011.05215.x

Dhanwal, P., Kumar, A., Dudeja, S., Badgujar, H., Chauhan, R., Kumar, A., et al. (2018). Biosorption of heavy metals from aqueous solution by bacteria isolated from contaminated soil. *Water Environ. Res.* 90, 424–430. doi: 10.2175/106143017X15131012152979

Di Martino, P. (2018). Extracellular polymeric substances, a key element in understanding biofilm phenotype. *AIMS Microbiol.* 4, 274–288. doi: 10.3934/microbiol.2018.2.274

Dimopoulou, M., Kefalloniti, V., Tsakanikas, P., Papanikolaou, S., and Nychas, G.-J. E. (2021). Assessing the biofilm formation capacity of the wine spoilage yeast Brettanomyces bruxellensis through FTIR spectroscopy. *Microorganisms* 9:587. doi: 10.3390/microorganisms9030587

Doherty, J., Raoof, A., Hussain, A., Wolna, M., Cinque, G., Brown, M., et al. (2019). Live single cell analysis using synchrotron FTIR microspectroscopy: development of a simple dynamic flow system for prolonged sample viability. *Analyst.* 144, 997–1007. doi: 10.1039/C8AN01566J

Dong, J., Zhang, Z., Yu, Z., Dai, X., Xu, X., Alvarez, P. J., et al. (2017). Evolution and functional analysis of extracellular polymeric substances during the granulation of aerobic sludge used to treat p-chloroaniline wastewater. *Chem. Engin. J.* 330, 596–604. doi: 10.1016/j.cej.2017.07.174

Douterelo, I., Boxall, J. B., Deines, P., Sekar, R., Fish, K. E., and Biggs, C. A. (2014). Methodological approaches for studying the microbial ecology of drinking water distribution systems. *Water Res.* 65, 134–156. doi: 10.1016/j.watres.2014.07.008

Duncan, R. J., and Petrou, K. (2022). Biomolecular composition of sea ice microalgae and its influence on marine biogeochemical cycling and carbon transfer through polar marine food webs. *Geosciences* 12:38. doi: 10.3390/geosciences12010038

Dziuba, B., Babuchowski, A., Nałęcz, D., and Niklewicz, M. (2007). Identification of lactic acid bacteria using FT-IR spectroscopy and cluster analysis. *Int. Dairy J.* 17, 183–189. doi: 10.1016/j.idairyj.2006.02.013

Edwards, A., Mur, L. A., Girdwood, S. E., Anesio, A. M., Stibal, M., Rassner, S. M., et al. (2014). Coupled cryoconite ecosystem structure-function relationships are revealed by comparing bacterial communities in alpine and Arctic glaciers. *FEMS Microbiol. Ecol.* 89, 222–237. doi: 10.1111/1574-6941.12283

El-Azazy, M., El-Shafie, A. S., and Al-Saad, K. (2021). Introductory chapter: infrared spectroscopy-principles and applications. Infrared spectroscopy-perspectives and applications. *Intech Open*. 1–13. doi: 10.5772/intechopen.109139

El-Bialy, H. A., El-Gamal, M. S., Elsayed, M. A., Saudi, H. A., and Khalifa, M. A. (2019). Microbial melanin physiology under stress conditions and gamma radiation protection studies. *Radiat. Phys. Chem.* 162, 178–186. doi: 10.1016/j.radphyschem.2019.05.002

Elzinga, E. J., Huang, J. H., Chorover, J., and Kretzschmar, R. (2012). ATR-FTIR spectroscopy study of the influence of pH and contact time on the adhesion of *Shewanella putrefaciens* bacterial cells to the surface of hematite. *Environ. Sci. Technol.* 46, 12848–12855. doi: 10.1021/es303318y

Fadlelmoula, A., Pinho, D., Carvalho, V. H., Catarino, S. O., and Minas, G. (2022). Fourier transform infrared (FTIR) spectroscopy to analyse human blood over the last 20 years: a review towards lab-on-a-Chip devices. *Micromachines* 13:187. doi: 10.3390/mi13020187

Feng, B., Shi, H., Xu, F., Hu, F., He, J., Yang, H., et al. (2020). FTIR-assisted MALDI-TOF MS for the identification and typing of bacteria. *Anal. Chim. Acta* 1111, 75–82. doi: 10.1016/j.aca.2020.03.037

Flood, M., Frabutt, D., Floyd, D., Powers, E. U., Devol, A., and Tiquia-Arashiro, S. M. (2015). Ammonia-oxidizing bacteria and archaea in sediments of the Gulf of Mexico. *Environ. Technol.* 36, 124–135. doi: 10.1080/09593330.2014.942385

Franco-Duarte, R., Černáková, L., Kadam, S., Kaushik, K., Salehi, B., Bevilacqua, A., et al. (2019). Advances in chemical and biological methods to identify microorganisms—from past to present. *Microorganisms* 7:130. doi: 10.3390/microorganisms7050130

Galichet, A., Sockalingum, G. D., Belarbi, A., and Manfait, M. (2001). FT-IR spectroscopic analysis of *Saccharomyces cerevisiae* cell walls: study of an anomalous strain exhibiting a pink-colored cell phenotype. *FEMS Microbiol. Lett.* 197, 179–186. doi: 10.1111/j.1574-6968.2001.tb10601.x

Gentile, M., Yan, T., Tiquia, S. M., Fields, M. W., Nyman, J., Zhou, J., et al. (2006). Stability and resilience in a denitrifying fluidized bed reactor. *Microb. Ecol.* 52, 311–321. doi: 10.1007/s00248-006-9024-1

Geoghegan, M., Andrews, J. S., Biggs, C. A., Eboigbodin, K. E., Elliott, D. R., Rolfe, S., et al. (2008). The polymer physics and chemistry of microbial cell attachment and adhesion. *Faraday Discuss.* 139, 85–103. doi: 10.1039/B717046G

George, B., Nirmal Kumar, J. I., Kumar, R. N., and Sajish, P. R. (2012). Biosorption potentiality of living aspergillus Niger Tiegh in removing heavy metal from aqueous solution. *Biorem. J.* 16, 195–203. doi: 10.1080/10889868.2012.731442

Gieroba, B., Krysa, M., Wojtowicz, K., Wiater, A., Pleszczyńska, M., Tomczyk, M., et al. (2020). The FT-IR and Raman spectroscopies as tools for biofilm characterization created by cariogenic streptococci. *Int. J. Mol. Sci.* 21:3811. doi: 10.3390/ijms21113811

Glassford, S. E., Byrne, B., and Kazarian, S. G. (2013). Recent applications of ATR FTIR spectroscopy and imaging to proteins. *Biochim et Biophys. Acta-Proteins Proteomics* 1834, 2849–2858. doi: 10.1016/j.bbapap.2013.07.015

Gong, M., Yang, G., Zhuang, L., and Zeng, E. Y. (2019). Microbial biofilm formation and community structure on low-density polyethylene microparticles in lake water microcosms. *Environ. Pollut.* 252, 94–102. doi: 10.1016/j.envpol.2019.05.090

Goodacre, R., Shann, B., Gilbert, R. J., Timmins, E. M., McGovern, A. C., Alsberg, B. K., et al. (2000). Detection of the dipicolinic acid biomarker in Bacillus spores using curie-point pyrolysis mass spectrometry and Fourier transform infrared spectroscopy. *Anal. Chem.* 72, 119–127. doi: 10.1021/ac990661i

Grace, C. E. E., Lakshmi, P. K., Meenakshi, S., Vaidyanathan, S., Srisudha, S., and Mary, M. B. (2020). Biomolecular transitions and lipid accumulation in green microalgae monitored by FT-IR and Raman analysis. *Spectrochimica Acta Part A* 224:117382. doi: 10.1016/j.saa.2019.117382

Griffiths, P. R. (1983). Fourier transform infrared spectrometry. *Science* 222, 297–302. doi: 10.1126/science.6623077

Gu, S., and Lan, C. Q. (2021). Biosorption of heavy metal ions by green alga *Neochloris oleoabundans*: effects of metal ion properties and cell wall structure. *J. Haz. Mat.* 418:126336. doi: 10.1016/j.jhazmat.2021.126336

Gutiérrez-Corona, J. F., Romo-Rodríguez, P., Santos-Escobar, F., Espino-Saldaña, A. E., and Hernández-Escoto, H. (2016). Microbial interactions with chromium: basic biological processes and applications in environmental biotechnology. *World J. Microbiol. Biotechnol.* 32, 191–199. doi: 10.1007/s11274-016-2150-0

Harrison, J. P., and Berry, D. (2017). Vibrational spectroscopy for imaging single microbial cells in complex biological samples. *Front. Microbiol.* 8:675. doi: 10.3389/fmicb.2017.00675

He, Z., Liu, Y., Kim, H. J., Tewolde, H., and Zhang, H. (2022). Fourier transform infrared spectral features of plant biomass components during cotton organ development and their biological implications. *J. Cotton Res.* 5:11. doi: 10.1186/s42397-022-00117-8

Helm, D., Labischinski, H., and Schallehn, G. (1991). Classification and identification of bacteria by Fourier-transform IR spectroscopy. *J. Gen. Microbiol.* 137, 69–79. doi: 10.1099/00221287-137-1-69

Hosseini, F., Lashani, E., and Moghimi, H. (2023). Simultaneous bioremediation of phenol and tellurite by Lysinibacillus sp. EBL303 and characterization of biosynthesized Te nanoparticles. *Sci. Rep.* 13:1243. doi: 10.1038/s41598-023-28468-5

Huang, G., Ng, T. W., An, T., Li, G., Wang, B., Wu, D., et al. (2017). Interaction between bacterial cell membranes and nano-TiO_2 revealed by two-dimensional FT-IR correlation spectroscopy using bacterial ghost as a model cell envelope. *Water Res.* 118, 104–113. doi: 10.1016/j.watres.2017.04.023

Huang, T., Zhang, W., Zhang, F., Feng, W., Li, C., and Zhang, Y. (2020). The role of microbial community composition in controlling soil respiration after organic matter addition revealed by FT-IR spectroscopy. *Soil Biol. Biochem.* 11:107752. doi: 10.1371/journal.pone.0165448

Igisu, M., Takai, K., Ueno, Y., Nishizawa, M., Nunoura, T., Hirai, M., et al. (2012). Domain-level identification and quantification of relative prokaryotic cell abundance in microbial communities by Micro-FTIR spectroscopy. *Environ. Microbiol. Rep.* 4, 42–49. doi: 10.1111/j.1758-2229.2011.00277.x

Jansson, M. M., Kögler, M., Hörkkö, S., Ala-Kokko, T., and Rieppo, L. (2023). Vibrational spectroscopy and its future applications in microbiology. *Appl. Spect. Rev.* 58, 132–158. doi: 10.1080/05704928.2021.1942894

Jiang, W., Saxena, A., Song, B., Ward, B. B., Beveridge, T. J., and Myneni, S. C. B. (2004). Elucidation of functional groups on gram-positive and gram-negative bacterial surfaces using infrared spectroscopy. *Langmuir* 20, 11433–11442. doi: 10.1021/la049043

Kamnev, A. A. (2008). FT-IR spectroscopic studies of bacterial cellular responses to environmental factors, plant-bacterial interactions and signalling. *Spectroscopy* 22, 83–95. doi: 10.3233/SPE-2008-0329

Kamnev, A. A., Dyatlova, Y. A., Kenzhegulov, O. A., Fedonenko, Y. P., Evstigneeva, S. S., and Tugarova, A. V. (2023). Fourier transform infrared (FT-IR) spectroscopic study of biofilms formed by the Rhizobacterium Azospirillum baldaniorum Sp245: aspects of

methodology and matrix composition. *Molecules* 28:1949. doi: 10.3390/molecules28041949

Kamnev, A. A., Tugarova, A. V., Antonyuk, L. P., Tarantilis, P. A., Polissiou, M. G., and Gardiner, P. H. (2005). Effects of heavy metals on plant-associated rhizobacteria: comparison of endophytic and non-endophytic strains of *Azospirillum brasilense*. *J. Trace Elem. Med. Biol.* 19, 91–95. doi: 10.1016/j.jtemb.2005.03.002

Kochan, K., Lai, E., Richardson, Z., Nethercott, C., Peleg, A. Y., Heraud, P., et al. (2020). Vibrational spectroscopy as a sensitive probe for the chemistry of intra-phase bacterial growth. *Sensors* 20:3452. doi: 10.3390/s20123452

Koczoń, P., Hołaj-Krzak, J. T., Palani, B. K., Bolewski, T., Dąbrowski, J., Bartyzel, B. J., et al. (2023). The analytical possibilities of FT-IR spectroscopy powered by vibrating molecules. *Int. J. Mol. Sci.* 24:1013. doi: 10.3390/ijms24021013

Krishnaswamy, U. (2021). GCMS and FT-IR spectral analysis of aqueous methylparathion biotransformation by the microbial mpd strains of Pseudomonas aeruginosa and fusarium spp. *Arch. Microbiol.* 203, 5763–5782. doi: 10.1007/s00203-021-02520-2

Kumar, S. S., and Ghosh, A. R. (2019). Assessment of bacterial viability: a comprehensive review on recent advances and challenges. *Microbiology* 165, 593–610. doi: 10.1099/mic.0.000786

Kumar, R., Vuppaladadiyam, A. K., Antunes, E., Whelan, A., Fearon, R., Sheehan, M., et al. (2022). Emerging contaminants in biosolids: presence, fate and analytical techniques. *Emerg. Cont.* 8, 162–194. doi: 10.1016/j.emcon.2022.03.004

Lasch, P., Beyer, W., Nattermann, H., Stämmler, M., and Naumann, D. (2004). Discrimination of *Campylobacter jejuni* strains by using polychromatic Fourier-transform infrared spectroscopy and multivariate statistics. *Appl. Environ. Microbiol.* 71, 4318–4324. doi: 10.1128/AEM.71.8.4318-4324.2005

Lilo, T., Morais, C., Shenton, C., Ray, A., and Gurusinghe, N. (2022). Revising Fourier-transform infrared (FT-IR) and Raman spectroscopy towards brain cancer detection. *Photodiag Photodyn Ther.* 38:102785. doi: 10.1016/j.pdpdt.2022.102785

Lin, S. F., Schraft, H., and Griffiths, M. W. (1998). Identification of *Bacillus cereus* by Fourier transform infrared spectroscopy (FT-IR). *J. Food Prot.* 61, 921–923. doi: 10.4315/0362-028x-61.7.921

Lin, X., Tfaily, M. M., Steinweg, J. M., Chanton, P., Esson, K., Yang, Z. K., et al. (2014). Microbial community stratification linked to utilization of carbohydrates and phosphorus limitation in a boreal peatland at Marcell experimental Forest, Minnesota, USA. *Appl. Environ. Microbiol.* 80, 3518–3530. doi: 10.1128/AEM.00205-14

Liu, X., Tiquia, S. M., Holguin, G., Wu, L., Nold, S. C., Devol, A. H., et al. (2003). Molecular diversity of denitrifying genes in continental margin sediments within the oxygen-deficient zone off the Pacific coast of Mexico. *Appl. Environ. Microbiol.* 69, 3549–3560. doi: 10.1128/AEM.69.6.3549-3560.2003

Maquelin, K., Choo-Smith, L. P., Endtz, H. P., Bruining, H. A., Puppels, G. J., and Naumann, D. (2000). Rapid identification of Candida species by confocal Raman microspectroscopy. *J. Clin. Microbiol.* 40, 594–600. doi: 10.1128/JCM.40.2.594-600.2002

Marques, J., Ares, A., Costa, J., Marques, M. P. M., de Carvalho, L. A. E. B., and Bessa, F. (2023). Plastisphere assemblages differ from the surrounding bacterial communities in transitional coastal environments. *Sci. Total Environ.* 869:161703. doi: 10.1016/j.scitotenv.2023.161703

Martak, D., Valot, B., Sauget, M., Cholley, P., Thouverez, M., Bertrand, X., et al. (2019). Fourier-transform infrared spectroscopy can quickly type gram-negative Bacilli responsible for hospital outbreaks. *Front. Microbiol.* 10:1440. doi: 10.3389/fmicb.2019.01440

McKindles, K. M., and Tiquia-Arashiro, S. M. (2012). "Functional gene arrays for analysis of microbial communities on ocean platform" in *Molecular biological Technologies for Ocean Sensing. Springer Protocols Handbooks*. ed. S. Tiquia-Arashiro (Totowa, NJ: Humana Press)

Melin, A. M., Perromat, A., and Déléris, G. (2001). Sensitivity of *Deinococcus radiodurans* to γ-irradiation: a novel approach by Fourier transform infrared spectroscopy. *Arch. Biochem. Biophys.* 394, 265–274. doi: 10.1006/abbi.2001.2533

Meneghel, J., Passot, S., Jamme, F., Lefrançois, S., Lieben, P., Dumas, P., et al. (2020). FT-IR micro-spectroscopy using synchrotron-based and thermal source-based radiation for probing live bacteria. *Anal. Bioanal. Chem.* 412, 7049–7061. doi: 10.1007/s00216-020-02835-x

Meng, G., Liu, J., Ma, J., Liu, X., Zhang, F., Guo, Y., et al. (2023). Biosorption and bioreduction of aqueous chromium (VI) by different Spirulina strains. *FEMS Microbiol. Lett.* 370:fnad070. doi: 10.1093/femsle/fnad070

Meyvisch, P., Gurdebeke, P. R., Vrielinck, H., Neil Mertens, K., Versteegh, G., and Louwye, S. (2022). Attenuated Total reflection (ATR) Micro-Fourier transform infrared (Micro-FT-IR) spectroscopy to enhance repeatability and reproducibility of spectra derived from single specimen organic-walled dinoflagellate cysts. *Appl. Spectrosc.* 76, 235–254. doi: 10.1177/00037028211041172

Miao, L., Wang, P., Hou, J., Yao, Y., Liu, Z., and Liu, S. (2019). Low concentrations of copper oxide nanoparticles alter microbial community structure and function of sediment biofilms. *Sci. Total Environ.* 653, 705–713. doi: 10.1016/j.scitotenv.2018.10.354

Michalak, I., Chojnacka, K., and Witek-Krowiak, A. (2013). State of the art for the biosorption process--a review. *Appl. Biochem. Biotechnol.* 170, 1389–1416. doi: 10.1007/s12010-013-0269-0

Moen, B., Janbu, A. O., Langsrud, S., Langsrud, O., Hobman, J. L., Constantinidou, C., et al. (2009). Global responses of *Escherichia coli* to adverse conditions determined by microarrays and FT-IR spectroscopy. *Can. J. Microbiol.* 55, 714–728. doi: 10.1139/w09-016

Moen, B., Oust, A., Langsrud, Ø., Dorrell, N., Marsden, G. L., Hinds, J., et al. (2005). Explorative multifactor approach for investigating global survival mechanisms of *Campylobacter jejuni* under environmental conditions. *Appl. Environ. Microbiol.* 71, 2086–2094. doi: 10.1128/AEM.71.4.2086-2094.2005

Monga, D., Kaur, P., and Singh, B. (2021). Microbe mediated remediation of dyes, explosive waste and polyaromatic hydrocarbons, pesticides and pharmaceuticals. *Curr. Res. Microb. Sci.* 3:100092. doi: 10.1016/j.crmicr.2021.100092

Mudziwapasi, J., Peter, M., and Madzivire, G. (2018). Biosorption of heavy metals in polluted water using microorganisms: progresses and challenges. *J. Chem.* 307, 135957–135911. doi: 10.1016/j.chemosphere.2022.135957

Muhamadali, H., Chisanga, M., Subaihi, A., and Goodacre, R. (2015). Combining Raman and FT-IR spectroscopy with quantitative isotopic labeling for differentiation of *E. coli* cells at community and single cell levels. *Anal. Chem.* 87, 4578–4586. doi: 10.1021/acs.analchem.5b00892

Mukherjee, J., Ow, S. Y., Noirel, J., and Biggs, C. A. (2011). Quantitative protein expression and cell surface characteristics of *Escherichia coli* MG1655 biofilms. *Proteomics* 11, 339–351. doi: 10.1002/pmic.201000386

Nadtochenko, V. A., Rincon, A. G., Stanca, S. E., and Kiwi, J. (2005). Dynamics of *E. coli* membrane cell peroxidation during TiO_2 photocatalysis studied by ATR-FTIR spectroscopy and AFM microscopy. *J. Photochem. Photobiol. A Chem.* 169, 131–137. doi: 10.1016/j.jphotochem.2004.06.011

Nandiyanto, A. B. D., Oktiani, R., and Ragadhita, R. (2019). How to read and interpret FT-IR spectroscopy of organic material. *Indo. J. Sci. Technol.* 4, 97–118. doi: 10.17509/ijost.v4i1.15806

Naumann, D., Helm, D., and Labischinski, H. (2001). Microbiological characterizations by FT-IR spectroscopy. *Nat. Protoc.* 351, 81–82. doi: 10.1038/351081a0

Naylor, D., McClure, R., and Jansson, J. (2022). Trends in microbial community composition and function by soil depth. *Microorganisms* 10:540. doi: 10.3390/microorganisms10030540

Nguyen, S., Ala, F., Cardwell, C., Cai, D., McKindles, K. M., Lotvola, A., et al. (2013). Isolation and screening of carboxydotrophs isolated from composts and their potential for butanol synthesis. *Environ. Technol.* 34, 1995–2007. doi: 10.1080/09593330.2013.795987

Nor, F. H. M., Abdullah, S., Ibrahim, Z., Nor, M. H. M., Osman, M. I., al Farraj, D. A., et al. (2023). Role of extremophilic *Bacillus cereus* KH1 and its lipopeptide in treatment of organic pollutant in wastewater. *Bioprocess Biosyst. Eng.* 46, 381–391. doi: 10.1007/s00449-022-02749-1

Novais, Â., Freitas, A. R., Rodrigues, C., and Peixe, L. (2019). Fourier transform infrared spectroscopy: unlocking fundamentals and prospects for bacterial strain typing. *Eur. J. Clin. Microbiol. Infect. Dis.* 38, 427–448. doi: 10.1007/s10096-018-3431-3

Oberbeckmann, S., Loeder, M., Gerdts, G., and Osborn, A. M. (2014). Spatial and seasonal variation in diversity and structure of microbial biofilms on marine plastics in northern European waters. *FEMS Microbiol. Ecol.* 90, 478–492. doi: 10.1111/1574-6941.12409

Obinaju, B. E., and Martin, F. L. (2016). ATR-FTIR spectroscopy reveals polycyclic aromatic hydrocarbon contamination despite relatively pristine site characteristics: results of a field study in the Niger Delta. *Environ. Int.* 89-90, 93–101. doi: 10.1016/j.envint.2016.01.012

Oest, A., Fenner, M., Azzopardi, D., Alsaffar, A., and Tiquia-Arashiro, S. M. (2018). Patterns of change in metabolic capabilities of sediment microbial communities along river and lake ecosystems. *J. Inter. Microbiol.* 2018:6234931. doi: 10.1155/2018/6234931

Oh, S. E., Hassan, S. H., and Joo, J. H. (2009). Biosorption of heavy metals by lyophilized cells of *Pseudomonas stutzeri*. *World J. Microbiol. Biotechnol.* 25, 1771–1778. doi: 10.1007/s11274-009-0075-6

Ojeda, J. J., and Dittrich, M. (2012). "Fourier transform infrared spectroscopy for molecular analysis of microbial cells" in *Microbial systems biology. Methods in molecular biology*. ed. A. Navid, vol. *881* (Totowa, NJ: Humana Press)

Ojeda, J. J., Romero-Gonzalez, M. E., Bachmann, R. T., Edyvean, R. G., and Banwart, S. A. (2008). Characterization of the cell surface and cell wall chemistry of drinking water bacteria by combining XPS, FT-IR spectroscopy, modeling, and potentiometric titrations. *Langmuir* 24, 4032–4040. doi: 10.1021/la702284b

Pagnucco, G., Overfield, D., Chamlee, Y., Fortuna, A., Sulaiman, F., Farinas, J., et al. (2023). Metal tolerance and biosorption capacities of bacterial strains isolated from an urban watershed. *Front. Microbiol.* 14:1278886. doi: 10.3389/fmicb.2023.1278886

Pardo, R., Herguedas, M., Barrado, E., and Vega, M. (2003). Biosorption of cadmium, copper, lead and zinc by inactive biomass of *Pseudomonas putida*. *Anal. Bioanal. Chem.* 376, 26–32. doi: 10.1007/s00216-003-1843-z

Patel, D., Gismondi, R., Alsaffar, A., and Tiquia-Arashiro, S. M. (2019). Applicability of API ZYM to capture seasonal and spatial variabilities in lake and river sediments. *Environ. Technol.* 40, 3227–3239. doi: 10.1080/09593330.2018.1468492

Perkins, D. L., Lovell, C. R., Bronk, B. V., Setlow, B., Setlow, P., and Myrick, M. L. Classification of endospores of Bacillus and Clostridium species by FT-IR reflectance microspectroscopy and autoclaving. IM S 2005- IEEE international workshop on measurement Systems for Homeland Security, contraband detection and personal safety. (2005). Orlando, FL. 81–87

Pirutin, S. K., Jia, S., Yusipovich, A. I., Shank, M. A., Parshina, E. Y., and Rubin, A. B. (2023). Vibrational spectroscopy as a tool for bioanalytical and biomonitoring studies. *Int. J. Mol. Sci.* 24:6947. doi: 10.3390/ijms24086947

Plecha, S., Hall, D., and Tiquia-Arashiro, S. M. (2013). Screening for novel bacteria from the bioenergy feedstock switchgrass (*Panicum virgatum* L.). *Environ. Technol.* 34, 1895–1904. doi: 10.1080/09593330.2013.818701

Pomaranski, E., and Tiquia-Arashiro, S. M. (2016). Butanol tolerance of carboxydotrophic bacteria isolated from manure composts. *Environ. Technol.* 37, 1970–1982. doi: 10.1080/09593330.2015.1137360

Portenier, I., Waltimo, T., Ørstavik, D., and Haapasalo, M. (2005). The susceptibility of starved, stationary phase, and growing cells of *Enterococcus faecalis* to endodontic medicaments. *J. Endod.* 31, 380–386. doi: 10.1097/01.don.0000145421.84121.c8

Qin, W., Amin, S. A., Lundeen, R. A., Heal, K. R., Martens-Habbena, W., Turkarslan, S., et al. (2018). Stress response of a marine ammonia-oxidizing archaeon informs physiological status of environmental populations. *ISME J.* 12, 508–519. doi: 10.1038/ismej.2017.186

Quilès, F., Saadi, S., Francius, G., Bacharouche, J., and Humbert, F. (2016). *In situ* and real time investigation of the evolution of a *Pseudomonas fluorescens* nascent biofilm in the presence of an antimicrobial peptide. *Biochim Biophy Acta* 1858, 75–84. doi: 10.1016/j.bbamem.2015.10.015

Rebuffo-Scheer, C. A., Dietrich, J., Wenning, M., and Scherer, S. (2008). Identification of five Listeria species based on infrared spectra (FT-IR) using macrosamples is superior to a microsample approach. *Anal. Bioanal. Chem.* 390, 1629–1635. doi: 10.1007/s00216-008-1834-1

Ribeiro da Cunha, B., Fonseca, L. P., and Calado, C. R. C. (2020). Metabolic fingerprinting with Fourier-transform infrared (FT-IR) spectroscopy: towards a high-throughput screening assay for antibiotic discovery and mechanism-of-action elucidation. *Meta* 10:145. doi: 10.3390/metabo10040145

Rolfe, M. D., Rice, C. J., Lucchini, S., Pin, C., Thompson, A., Cameron, A. D., et al. (2012). Lag phase is a distinct growth phase that prepares bacteria for exponential growth and involves transient metal accumulation. *J. Bacteriol.* 194, 686–701. doi: 10.1128/JB.06112-11

Saranya, K., Sundaramanickam, A., Shekhar, S., Meena, M., Sathishkumar, R. S., and Balasubramanian, T. (2018). Biosorption of multi-heavy metals by coral associated phosphate solubilising bacteria *Cronobacter muytjensii* KSCAS2. *J. Environ. Manag.* 222, 396–401. doi: 10.1016/j.jenvman.2018.05.083

Saulou, C., Jamme, F., Girbal, L., Maranges, C., Fourquaux, I., Cocaign-Bousquet, M., et al. (2013). Synchrotron FT-IR microspectroscopy of *Escherichia coli* at single-cell scale under silver-induced stress conditions. *Anal. Bioanal. Chem.* 405, 2685–2697. doi: 10.1007/s00216-013-6725-4

Scarsini, M., Thurotte, A., Veidl, B., Amiard, F., Niepceron, F., Badawi, M., et al. (2021). Metabolite quantification by Fourier transform infrared spectroscopy in diatoms: proof of concept on *Phaeodactylum tricornutum*. *Front. Plant Sci.* 12:756421. doi: 10.3389/fpls.2021.756421

Schmitt, J., and Flemming, H. C. (1998). FTIR-spectroscopy in microbial and material analysis. *Int. Biodeter. Biodeg.* 41, 1–11. doi: 10.1016/S0964-8305(98)80002-4

Schmitt, J., Nivens, D., White, D. C., and Flemming, H. C. (1995). Changes of biofilm properties in response to sorbed substances – an FTIR-ATR study. *Wat. Sci. Technol.* 32, 149–155. doi: 10.1016/0273-1223(96)00019-4

Semeraro, P., Giotta, L., Talà, A., Tufariello, M., D'Elia, M., Milano, F., et al. (2023). A simple strategy based on ATR-FTIR difference spectroscopy to monitor substrate intake and metabolite release by growing bacteria. *Spectrochimica Acta Part A* 302:123031. doi: 10.1016/j.saa.2023.123031

Sharma, M., Nandy, A., Taylor, N., Venkatesan, S. V., Ozhukil Kollath, V., Karan, K., et al. (2020). Bioelectrochemical remediation of phenanthrene in a microbial fuel cell using an anaerobic consortium enriched from a hydrocarbon-contaminated site. *J. Hazard. Mater.* 389:121845. doi: 10.1016/j.jhazmat.2019.121845

Silverstein, R. M., Webster, F. X., and Kiemle, D. J. *Spectrometric identification of organic compounds. Eight edition*. (2014). New York: John Wiley & Sons. 464.

Singhalage, I. D., Seneviratne, G., Madawala, H., and Manawasinghe, I. S. (2018). Characterization of structural properties of fungal-bacterial biofilms by Fourier transform infrared spectroscopy. *Ceylon J. Sci.* 47, 77–83. doi: 10.4038/cjs.v47i1.7490

Smirnova, M., Tafintseva, V., Kohler, A., Miamin, U., and Shapaval, V. (2022). Temperature-and nutrients-induced phenotypic changes of Antarctic green snow bacteria probed by high-throughput FTIR spectroscopy. *Biology* 11:890. doi: 10.3390/biology11060890

Smith, B. C. *Infrared spectral interpretation: A systematic approach*. (1998). CRC Press: Boca Raton, FL. 288.

Smith, B. C. *Fundamentals of Fourier transform infrared spectroscopy*. (2011). CRC Press, Boca Raton, FL. 207.

Soares, J. M., Guimarães, F. E. G., Yakovlev, V. V., Bagnato, V. S., and Blanco, K. C. (2022). Physicochemical mechanisms of bacterial response in the photodynamic potentiation of antibiotic effects. *Sci. Rep.* 12:21146. doi: 10.1038/s41598-022-25546-y

Spain, O., and Funk, C. (2022). Detailed characterization of the cell wall structure and composition of nordic green microalgae. *J. Agric. Food Chem.* 70, 9711–9721. doi: 10.1021/acs.jafc.2c02783

Stehfest, K., Toepel, J., and Wilhelm, C. (2005). The application of micro-FTIR spectroscopy to analyze nutrient stress-related changes in biomass composition of phytoplankton algae. *Plant Physiol. Biochem.* 43, 717–726. doi: 10.1016/j.plaphy.2005.07.001

Stuart, B. *Infrared spectroscopy: Fundamentals and applications*. (2004). New York: John Wiley & Sons. p 224.

Sundaram, J., Park, B., Hinton, A. Jr., Yoon, S. C., Windham, W. R., and Lawrence, K. C. (2012). Classification and structural analysis of live and dead Salmonella cells using Fourier transform infrared spectroscopy and principal component analysis. *J. Agric. Food Chem.* 60, 991–1004. doi: 10.1021/jf204081g

Sundararaju, S., Manjula, A., Kumaravel, V., Muneeswaran, T., and Vennila, T. (2022). Biosorption of nickel ions using fungal biomass Penicillium sp. MRF1 for the treatment of nickel electroplating industrial effluent. *Biomass Conv. Bioref.* 12, 1059–1068. doi: 10.1007/s13399-020-00679-0

Tang, M., McEwen, G. D., Wu, Y., Miller, C. D., and Zhou, A. (2013). Characterization and analysis of mycobacteria and gram-negative bacteria and co-culture mixtures by Raman microspectroscopy, FTIR, and atomic force microscopy. *Anal. Bioanal. Chem.* 405, 1577–1591. doi: 10.1007/s00216-012-6556-8

Tata, A., Marzoli, F., Cordovana, M., Tiengo, A., Zacometti, C., Massaro, A., et al. (2023). A multi-center validation study on the discrimination of *Legionella pneumophila* sg. 1, *Legionella pneumophila* sg. 2-15 and Legionella non-pneumophila isolates from water by FT-IR spectroscopy. *Front. Microbiol.* 14:1150942. doi: 10.3389/fmicb.2023.1150942

Tessaro, L., Mutz, Y. D. S., Andrade, J. C., Aquino, A., Belem, N. K. R., Silva, F. G. S., et al. (2023). ATR-FTIR spectroscopy and chemometrics as a quick and simple alternative for discrimination of SARS-CoV-2 infected food of animal origin. *Spectrochim. Acta A Mol. Biomol. Spectrosc.* 285:121883. doi: 10.1016/j.saa.2022.121883

Tiquia, S. M. (2008). Diversity of sulfate-reducing genes (dsrAB) in sediments from Puget Sound. *Environ. Technol.* 29, 1095–1108. doi: 10.1080/09593330802190608

Tiquia, S. M. (2010a). Metabolic diversity of the heterotrophic microorganisms and potential link to pollution of the Rouge River. *Environ. Pollut.* 158, 1435–1443. doi: 10.1016/j.envpol.2009.12.035

Tiquia, S. M. (2010b). Salt-adapted bacteria isolated from the Rouge River and potential for degradation of contaminants and biotechnological applications. *Environ. Technol.* 31, 967–978. doi: 10.1080/09593331003706226

Tiquia, S. M. (2011). Extracellular hydrolytic enzyme activities of the heterotrophic microbial communities of the Rouge River: An approach to evaluate ecosystem response to urbanization. *Microb. Ecol.* 62, 679–689. doi: 10.1007/s00248-011-9871-2

Tiquia, S. M., Chong, S. C., Fields, M. W., and Zhou, J. Oligonucleotide-based functional gene arrays for analysis of microbial communities in the environment. In: G. G. Kowalchuk, BruijnF. J. de, I. M. Head, A. D. Akkermans and ElsasJ. D. van, editors. *Molecular microbial ecology manual*. Kluwer Academic Publishers: Netherlands. (2004). p. 1743–1763.

Tiquia, S. M., Gurczynski, S., Zholi, A., and Devol, A. (2006a). Diversity of biogeochemical cycling genes from Puget Sound sediments using DNA microarrays. *Environ. Technol.* 27, 1377–1389. doi: 10.1080/09593332708618756

Tiquia, S. M., Masson, S. A., and Devol, A. (2006b). Vertical distribution of nitrite reductase genes (nirS) in continental margin sediments of the Gulf of Mexico. *FEMS Microbiol. Ecol.* 58, 464–475. doi: 10.1111/j.1574-6941.2006.00173.x

Tiquia, S. M., Schleibak, M., Schlaff, J., Floyd, J. C., Benipal, B., Zakhem, E., et al. (2008). Microbial community profiling and characterization of some heterotrophic bacterial isolates from river waters and shallow groundwater wells along the Rouge River, Southeast Michigan. *Environ. Technol.* 29, 651–663. doi: 10.1080/09593330801986998

Tiquia, S. M., Wan, H. C., and Tam, N. F. Y. (2002). Microbial population dynamics and enzyme activities during composting. *Compost. Sci. Utilization* 10, 150–161. doi: 10.1080/1065657X.2002.10702075

Tiquia-Arashiro, S. M. (2012) *Molecular biological Technologies for Ocean Sensing. Springer Protocols Handbooks*. Humana Press, Totowa, NJ. 307.

Tiquia-Arashiro, S. M. (2014). "Microbial CO metabolism" in *Thermophilic Carboxydotrophs and their Applications in Biotechnology. Springer Briefs in Microbiology*. Tiquia-Arashiro SM, editor. (Cham: Springer)

Tiquia-Arashiro, S. M. (2018). Lead absorption mechanisms in bacteria as strategies for lead bioremediation. *Appl. Microbiol. Biotechnol.* 102, 5437–5444. doi: 10.1007/s00253-018-8969-6

Tiquia-Arashiro, S. M. (2019a). "Synthesis of metallic nanoparticles by halotolerant fungi" in *Fungi in extreme environments: Ecological role and biotechnological significance*. eds. S. Tiquia-Arashiro and M. Grube (Cham: Springer)

Tiquia-Arashiro, S. M. (2019b). "Thermophilic fungi in composts: their role in composting and industrial processes" in *Fungi in extreme environments: Ecological role and biotechnological significance*. eds. S. Tiquia-Arashiro and M. Grube (Cham: Springer)

Tiquia-Arashiro, S. M., and Grube, M. (2019). *Fungi in extreme environments: Ecological role and biotechnological significance*. Basel: Springer Nature Switzerland AG. 626.

Tiquia-Arashiro, S. M., and Pant, D. (2019). *Microbial electrochemical technologies*. CRC Press, Boca Raton, FL. 518.

Tong, C. Y., and Derek, C. J. C. (2021). Biofilm formation of benthic diatoms on commercial polyvinylidene fluoride membrane. *Algal Res.* 55:102260. doi: 10.1016/j.algal.2021.102260

Tugarova, A. V., Scheludko, A. V., Dyatlova, Y. A., Filip'echeva, Y. A., and Kamnev, A. A. (2017). FTIR spectroscopic study of biofilms formed by the rhizobacterium *Azospirillum brasilense* Sp245 and its mutant *Azospirillum brasilense* Sp245. 1610. *J. Mol Struc.* 1140, 142–147. doi: 10.1016/j.molstruc.2016.12.063

Wang, L., Fan, D., Chen, W., and Terentjev, E. M. (2015). Bacterial growth, detachment, and cell size control on polyethylene terephthalate surfaces. *Sci. Rep.* 5:15159. doi: 10.1038/srep15159

Wang, Y., Jiang, Z., Lai, Z., Yuan, H., Zhang, X., Jia, Y., et al. (2021). The self-adaption capability of microalgal biofilm under different light intensities: photosynthetic parameters and biofilm microstructures. *Algal Res.* 58:102383. doi: 10.1016/j.algal.2021.102383

Wang, Y. D., Li, X. L., Hu, J., and Lü, J. H. (2019). Synchrotron infrared spectral regions as signatures for foodborne bacterial typing. *Nucl. Sci. Techniques* 30:25. doi: 10.1007/s41365-019-0554-x

Wang, H., Yang, Q., Li, D., Wu, J., Yang, S., Deng, Y., et al. (2023). Stable isotopic and metagenomic analyses reveal microbial-mediated effects of microplastics on sulfur cycling in coastal sediments. *Environ. Sci. Technol.* 57, 1167–1176. doi: 10.1021/acs.est.2c06546

Watanabe, R., Sugahara, A., Shinzawa, H., Yamane, S., Nakamura, S., Sato, H., et al. (2023). Photodegradation behavior of polyethylene terephthalate analyzed by MALDI-TOFMS and ATR-FTIR microscopic analysis in combination with two-trace two-dimensional (2T2D) correlation mapping. *Polym. Degr. Stabil.* 208:110246. doi: 10.1016/j.polymdegradstab.2022.110246

Weber, A., Hoplight, B., Ogilvie, R., Muro, C., Khandasammy, S. R., Pérez-Almodóvar, L., et al. (2023). Innovative vibrational spectroscopy research for forensic application. *Anal. Chem.* 95, 167–205. doi: 10.1021/acs.analchem.2c05094

Wenning, M., and Scherer, S. (2013). Identification of microorganisms by FTIR spectroscopy: perspectives and limitations of the method. *Appl. Microbiol. Biotechnol.* 97, 7111–7120. doi: 10.1007/s00253-013-5087-3

Wilson, R. M., Zayed, A. A., Crossen, K. B., Woodcroft, B., Tfaily, M. M., Emerson, J., et al. (2021). Functional capacities of microbial communities to carry out large scale geochemical processes are maintained during ex situ anaerobic incubation. *PLoS One* 16:e0245857. doi: 10.1371/journal.pone.0245857

Wu, W., Gu, B., Fields, M. W., Gentile, M., Ku, Y.-K., Yan, H., et al. (2005). Uranium (VI) reduction by denitrifying biomass. *Biorem. J.* 9, 49–61. doi: 10.1080/10889860590929628

Yang, H., Shi, H., Feng, B., Wang, L., Chen, L., Alvarez-Ordóñez, A., et al. (2023). Protocol for bacterial typing using Fourier transform infrared spectroscopy. *STAR Protoc.* 4:102223. doi: 10.1016/j.xpro.2023.102223

Yu, P. (2005). Applications of hierarchical cluster analysis (CLA) and principal component analysis (PCA) in feed structure and feed molecular chemistry research, using synchrotron-based Fourier transform infrared (FTIR) microspectroscopy. *J. Agric. Food Chem.* 53, 7115–7127. doi: 10.1021/jf050959b

Yu, C., and Irudayaraj, J. (2005). Spectroscopic characterization of microorganisms by Fourier transform infrared microspectroscopy. *Biopolymers* 77, 368–377. doi: 10.1002/bip.20247

Zada, S., Xie, J., Yang, M., Yang, X., Sajjad, W., Rafiq, M., et al. (2021). Composition and functional profiles of microbial communities in two geochemically and mineralogically different caves. *Appl. Microbiol. Biotechnol.* 105, 8921–8936. doi: 10.1007/s00253-021-11658-4

Zarnowiec, P., Lechowicz, Ł., Czerwonka, G., and Kaca, W. (2015). Fourier transform infrared spectroscopy (FTIR) as a tool for the identification and differentiation of pathogenic bacteria. *Curr. Med. Chem.* 22, 1710–1718. doi: 10.2174/0929867322666150311152800

Zeroual, W., Choisy, C., Doglia, S. M., Bobichon, H., Angiboust, J. F., and Manfait, M. (1994). Monitoring of bacterial growth and structural analysis as probed by FT-IR spectroscopy. *Biochimica et Biophysica Acta-Mol Cell Res* 1222, 171–178. doi: 10.1016/0167-4889(94)90166-X

Zhang, J., Su, P., Chen, H., Qiao, M., Yang, B., and Xu, Z. (2023). Impact of reactive oxygen species on cell activity and structural integrity of gram-positive and gram-negative bacteria in electrochemical disinfection system. *Chem. Eng. J.* 451:138879. doi: 10.1016/j.cej.2022.138879

Zhao, H., Parry, R. L., Ellis, D. I., Griffith, G. W., and Goodacre, R. (2006). The rapid differentiation of Streptomyces isolates using Fourier transform infrared spectroscopy. *Vibrational Spectroscopy.* 40:213–218. doi: 10.1016/j.vibspec.2005.09.006

Zlotnikov, I. D., Ezhov, A. A., Vigovskiy, M. A., Grigorieva, O. A., Dyachkova, U. D., Belogurova, N. G., et al. (2023). Application prospects of FTIR spectroscopy and CLSM to monitor the drugs interaction with bacteria cells localized in macrophages for diagnosis and treatment control of respiratory diseases. *Diagnostics* 13:698. doi: 10.3390/diagnostics13040698

frontiers | Frontiers in Microbiology

TYPE Correction
PUBLISHED 13 December 2023
DOI 10.3389/fmicb.2023.1342406

OPEN ACCESS

APPROVED BY
Frontiers Editorial Office,
Frontiers Media SA, Switzerland

*CORRESPONDENCE
Sonia Tiquia-Arashiro
✉ smtiquia@umich.edu

RECEIVED 21 November 2023
ACCEPTED 01 December 2023
PUBLISHED 13 December 2023

CITATION
Kassem A, Abbas L, Coutinho O, Opara S, Najaf H, Kasperek D, Pokhrel K, Li X and Tiquia-Arashiro S (2023) Corrigendum: Applications of Fourier Transform-Infrared spectroscopy in microbial cell biology and environmental microbiology: advances, challenges, and future perspectives. *Front. Microbiol.* 14:1342406. doi: 10.3389/fmicb.2023.1342406

Corrigendum: Applications of Fourier Transform-Infrared spectroscopy in microbial cell biology and environmental microbiology: advances, challenges, and future perspectives

Amin Kassem[1], Lana Abbas[1], Oliver Coutinho[1], Somie Opara[1], Hawraa Najaf[1], Diana Kasperek[1], Keshav Pokhrel[2], Xiaohua Li[1] and Sonia Tiquia-Arashiro[1]*

[1]Department of Natural Sciences, University of Michigan-Dearborn, Dearborn, MI, United States, [2]Department of Mathematics and Statistics, University of Michigan-Dearborn, Dearborn, MI, United States

KEYWORDS

Fourier transform infrared spectroscopy, cellular structures, metabolic activities, bacteria, microbial stress, cell membrane, population dynamics

A corrigendum on
Applications of Fourier Transform-Infrared spectroscopy in microbial cell biology and environmental microbiology: advances, challenges, and future perspectives

by Kassem, A., Abbas, L., Coutinho, O., Opara, S., Najaf, H., Kasperek, D., Pokhrel, K., Li, X., and Tiquia-Arashiro, S. (2023). *Front. Microbiol.* 14:1304081. doi: 10.3389/fmicb.2023.1304081

In the published article, there was an error in the author list, and the sequence of authors was incorrectly listed. The corrected author list appears below.

"Amin Kassem[1], Lana Abbas[1], Oliver Coutinho[1], Somie Opara[1], Hawraa Najaf[1], Diana Kasperek[1], Keshav Pokhrel[2], Xiaohua Li[1] and Sonia Tiquia-Arashiro[1*]"

The authors apologize for this error and state that this does not change the scientific conclusions of the article in any way. The original article has been updated.

Publisher's note

All claims expressed in this article are solely those of the authors and do not necessarily represent those of their affiliated organizations, or those of the publisher, the editors and the reviewers. Any product that may be evaluated in this article, or claim that may be made by its manufacturer, is not guaranteed or endorsed by the publisher.

frontiers | Frontiers in Microbiology

TYPE Review
PUBLISHED 04 January 2024
DOI 10.3389/fmicb.2023.1283220

OPEN ACCESS

EDITED BY
Ilana Kolodkin-Gal,
Reichman University, Israel

REVIEWED BY
Severino Zara,
University of Sassari, Italy
Maret Du Toit,
Stellenbosch University, South Africa

*CORRESPONDENCE
Camille Eicher
✉ camille.eicher@gmail.com
Cosette Grandvalet
✉ cosette.grandvalet@institut-agro.fr

RECEIVED 25 August 2023
ACCEPTED 08 December 2023
PUBLISHED 04 January 2024

CITATION
Eicher C, Coulon J, Favier M, Alexandre H, Reguant C and Grandvalet C (2024) Citrate metabolism in lactic acid bacteria: is there a beneficial effect for *Oenococcus oeni* in wine?
Front. Microbiol. 14:1283220.
doi: 10.3389/fmicb.2023.1283220

Citrate metabolism in lactic acid bacteria: is there a beneficial effect for *Oenococcus oeni* in wine?

Camille Eicher[1]*, Joana Coulon[2], Marion Favier[2], Hervé Alexandre[1], Cristina Reguant[3] and Cosette Grandvalet[1]*

[1]UMR PAM, Université de Bourgogne Franche-Comté, Institut Agro, Université de Bourgogne, INRAE, Dijon, France, [2]Biolaffort, Floirac, France, [3]Universitat Rovira i Virgili, Grup de Biotecnologia Enològica, Departament de Bioquímica i Biotecnologia, Tarragona, Catalonia, Spain

Lactic acid bacteria (LAB) are Gram positive bacteria frequently used in the food industry for fermentation, mainly transformation of carbohydrates into lactic acid. In addition, these bacteria also have the capacity to metabolize citrate, an organic acid commonly found in food products. Its fermentation leads to the production of 4-carbon compounds such as diacetyl, resulting in a buttery flavor desired in dairy products. Citrate metabolism is known to have several beneficial effects on LAB physiology. Nevertheless, a controversial effect of citrate has been described on the acid tolerance of the wine bacterium *Oenococcus oeni*. This observation raises questions about the effect of citrate on the capacity of *O. oeni* to conduct malolactic fermentation in highly acidic wines. This review aims to summarize the current understanding of citrate metabolism in LAB, with a focus on the wine bacterium *O. oeni*. Metabolism with the related enzymes is detailed, as are the involved genes organized in *cit* loci. The known systems of *cit* locus expression regulation are also described. Finally, the beneficial effects of citrate catabolism on LAB physiology are reported and the negative impact observed in *O. oeni* is discussed.

KEYWORDS

lactic acid bacteria, citrate, *Oenococcus oeni*, metabolic engineering, citrate locus, proton motive force

1 Introduction

Citrate is an organic acid commonly found in food products like fruits, vegetables or milk. This organic acid can be metabolized by lactic acid bacteria (LAB) into aromatic compounds including diacetyl which is responsible for the buttery aroma which is desirable in dairy products such as butter, acid cream and cottage cheese, etc. In addition, CO_2 produced from this metabolism contributes to the formation of "eyes" in certain types of cheese. Nevertheless, not all LAB can consume this organic acid. Indeed, its consumption depends on the presence of genes encoding a citrate permease and a citrate lyase enabling the internalization of citrate in the cell and the catabolism of citrate into oxaloacetate, respectively (Hugenholtz, 1993; Bekal et al., 1998a; Drider et al., 2004). In some species, these genes are plasmid-encoded, which explains the instability of this metabolic trait in LAB (Drider et al., 2004).

Several previous studies have reported the beneficial effect of citrate on the growth of LAB (Hugenholtz, 1993; Lolkema et al., 1995; Ramos and Santos, 1996; Magni et al., 1999; Kang et al., 2013). Indeed, the internalization of citrate and the conversion of oxaloacetate into pyruvate, leading to the consumption of one scalar proton, create a transmembrane proton motive force (PMF) which triggers the production of ATP through the F_0-F_1 ATPase (Ramos et al., 1994; Lolkema et al., 1995; Marty-Tesset et al., 1996). This mechanism participates in intracellular pH (pHi) homeostasis and consequently plays a role in the resistance of LAB to acid stress. In addition, in heterofermentative bacteria, citrate can be co-metabolized with sugars to facilitate the reoxidation of cofactors generated by hexose fermentation (Ramos and Santos, 1996; Zaunmüller et al., 2006; Kang et al., 2013). This co-metabolism results in an increased growth rate and the achievement of a higher final biomass (Ramos and Santos, 1996; Zaunmüller et al., 2006).

Oenococcus oeni is a LAB which come into play during the second step in wine fermentation. It has the capacity to consume malic acid to produce a weaker acid, namely lactic acid, in a process which deacidifies wine. In addition, by consuming all nutrient sources, the development of this bacterium in wine results in microbial stability. *Oenococcus oeni* improves the organoleptic properties of wine thanks to secondary metabolisms such as citrate metabolism (Bartowsky, 2005). Citrate is naturally present in small quantities in grape must (0.13 to 0.90 g/L; Alexandre et al., 2008). Its metabolism in *O. oeni* can lead to the production of acetate and lactate but also 4-carbon compounds: diacetyl, acetoin and 2,3-butanediol. Diacetyl synthesis is only desirable in very small quantities in wine. Indeed, its production is responsible for the development of a "buttery" character in wines that is undesirable beyond a certain threshold (Bartowsky and Henschke, 2004). Therefore, controlling its production is of interest, especially in wine, in order to avoid alteration of the final product.

As described above, citrate metabolism is known to have a beneficial effect on both the growth and the acid stress resistance of LAB. However, Augagneur et al. (2007b) have reported a dual effect of citrate on the *O. oeni* strain ATCC BAA-1163. Indeed, they reported that while the addition of citrate in a culture medium had a beneficial effect on the growth of the bacterium at optimal pH, it completely impaired the growth at low pH. This observation is comforted by a recent study, in which an adaptive evolution to low pH has been performed on this strain and triggered the appearance of mutation in the *cit* locus. The mutations acquired by these evolved populations enabled them to growth under low pH in presence of citrate, while the ancestral strain was not able (Julliat et al., 2023). There is therefore no consensus on the effect of citrate on bacterial physiology, at least in *O. oeni*. In this review, citrate metabolism in LAB and its related citrate locus will be described with a focus on *O. oeni*. Subsequently, a genomic insight into citrate metabolism will be provided by describing the known regulatory mechanisms in different LAB. Finally, the beneficial effect of citrate on LAB will be described in more detail and the controversial effect on the acidic stress response in *O. oeni* referred to above will be discussed.

2 Citrate metabolism in LAB

Citrate metabolism in LAB includes three major steps, the first of which involves the uptake of citrate in its anionic or dianionic form through a specific permease called citrate permease. Citrate is then converted to acetate and oxaloacetate under the action of a citrate lyase and finally, oxaloacetate is degraded into pyruvate by an oxaloacetate decarboxylase. Pyruvate can then be reoriented to different pathways which will be more fully examined in the second part of this section. The enzymes described above are encoded by different genes organized in one or two citrate clusters depending on the LAB. Typical LAB citrate clusters are reported below.

2.1 Citrate cluster organizations

As mentioned above, not all LAB are able to metabolize citrate. Such metabolism implies the presence of genes encoding a citrate permease and a citrate lyase. These genes can either be localized in a plasmid or be integrated in the chromosome, depending on the LAB. Figure 1 represents different *cit* cluster organizations found in *Lactococcus lactis* subsp. *lactis* biovar diacetylactis, *Weissella paramesenteroides, Enterococcus faecalis*, and *O. oeni.* All these species shares common genes on their citrate locus: *citI,* which encodes a transcriptional activator of the operon belonging to the SorC/DeoR family (Martin et al., 2005), *mae/citM* encoding a soluble oxaloacetate decarboxylase enabling the conversion of oxaloacetate into pyruvate (Sender et al., 2004), *citP/maeP* encoding the citrate transporter (Ramos et al., 1994; García-Quintáns et al., 2008) and the *citC, D, E, F, X, G* genes which produce the different subunits of the citrate lyase and its activator components (Bekal et al., 1998a). This type of citrate cluster has been characterized in *L. lactis* bv. diacetylactis, *W. paramesenteroides, Leuconostoc mesenteroides* and *O. oeni* (Figure 1; Bekal-Si Ali et al., 1999; Martín et al., 2000; Mills et al., 2005). It should be noted that different names have been given to the citrate genes according to the LAB species, whereas in fact they share identical functions, a situation which may lead to confusion.

In other LAB, including *E. faecalis* and *Lacticaseibacillus casei,* certain variations in the *cit* cluster are noted. Indeed, the citrate cluster contains the gene *citO* encoding a transcriptional activator of the GntR family instead of *citI*, and the membrane-bound oxaloacetate decarboxylase is encoded by the *oadA,B,D* and *H* genes (Blancato et al., 2008; Mortera et al., 2013; Repizo et al., 2013). It will also be noted that certain LAB possess two genes encoding proteins with similar functions. This is the case for *L. lactis* bv. diacetylactis and *W. paramesenteroides* which possess two different genes encoding regulators: *citI* and *citR*. *E. faecalis* may also be cited in this regard as it possesses both the *citM* gene encoding the soluble oxaloacetate decarboxylase and the cluster *oadHDBA*, encoding the membrane-bound oxaloacetate decarboxylase complex. Furthermore, a pseudogene is found after *citM* on the *cit* locus of *L. lactis* bv. diacetylactis. Its sequence is similar to that of the *maeP* gene found in *O. oeni* but several frameshift mutations render it an unfunctional gene (Martín et al., 2004).

2.2 Citrate utilization pathways in LAB: catabolism of citrate into pyruvate

Citrate metabolism in LAB most commonly leads to the production of pyruvate, acetate and CO_2. Three steps are necessary: first, citrate is taken up by the citrate permease encoded by the *citP,*

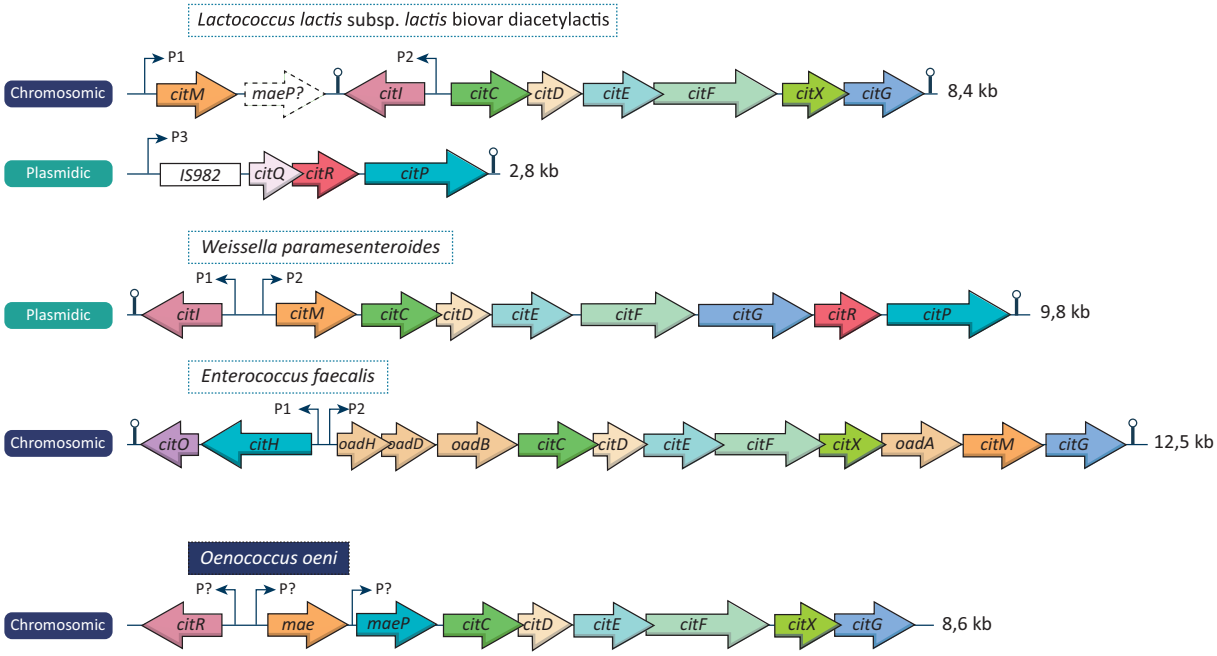

FIGURE 1
Organization of the citrate cluster from different LAB species. The citrate locus of *Lactococcus lactis* bv. diacetylactis, *Weissella paramesenteroides*, *Enterococcus faecalis* and *Oenococcus oeni* are represented and the size of each one is indicated. Thin arrows localize identified promotors (except for *O. oeni* in which putative promotors are represented). Air-pin structures represent identified rho-independent terminators. Dashed arrow represents a pseudogene founded on the citrate locus of *L lactis* bv. diacetylactis.

citH or maeP gene depending on the LAB. In *L. lactis* bv. diacetylactis, *Lc. mesenteroides W. paramesenteroides* and *Lactiplantibacillus plantarum,* the *citP* gene encodes a transporter belonging to the 2-hydroxy-carboxylate transporter family (García-Quintáns et al., 2008; Yang et al., 2022). This antiporter catalyzes the exchange of the di-anionic form of citrate against lactate in most cases (Marty-Tesset et al., 1996; Bandell et al., 1998; Drider et al., 2004). In *La. casei*, citrate is taken up in complex with Ca^{2+} by a transporter belonging to the citrate-divalent metal ion family (CitMHS) encoded by the *citH* gene (Mortera et al., 2013). Finally, in *O. oeni*, the *maeP* gene encodes a uniport belonging to the Metabolite/H^+ symporter family, enabling the uptake of citrate in its anionic form (Ramos et al., 1994). In this bacterium, another citrate transporter was suggested in the findings of Augagneur et al. (2007b) as its expression is positively regulated by the presence of citrate. This transporter is encoded by the *yaeP* gene but has not been characterized yet. Heterologous expression of this gene was carried out in order to characterize its function but was unsuccessful (Bonnin-Jusserand, 2011).

Citrate conversion into oxaloacetate and acetate is then initiated by the citrate lyase complex. This multimeric enzyme is composed by 3 subunits: γ (acyl carrier protein (ACP) containing the prosthetic group, EC: 4.1.3.6), α (acetyl-ACP:citrate ACP-transferase, EC:2.8.3.10) and β (citryl-S-ACP oxaloacetate-lyase, EC:4.1.3.34; 14, 55 and 34 kDa in *Lc. mesenteroides*, respectively; Bekal et al., 1998b). These subunits are encoded by the *citD, F* and *E* genes in LAB. Figure 2 illustrates the different steps required for the catabolism of citrate into acetate and oxaloacetate.

First, the α subunit of the citrate lyase catalyze the exchange of the citryl group (from citrate) with the acetyl group (linked to the prosthetic group of the ACP, the γ subunit of the citrate lyase) releasing acetate and citryl-S-ACP. Finally, the β subunit of the citrate lyase cleaves the citryl-S-ACP into oxaloacetate and acetyl-S-ACP, regenerating the acetyl group (Bekal et al., 1998a). This enzymatic activity is possible thanks to the action of three additional proteins: CitX (apo-citrate lyase phosphoribosyl-dephospho-coenzyme A, EC:2.7.7.61), CitG (triphosphoribosyl-dephospho-coenzyme A synthase, EC:2.4.2.52) and CitC (acetate:SH-citrate lyase ligase, EC:6.2.1.22), encoded by the *citX, citG*, and *citC* genes, respectively (Bott, 1997; Schneider et al., 2000). CitG and CitX participate in the formation of the prosthetic group from ATP and dephospho-coenzyme A, and CitC enables the activation of the latter via acetylation (García-Quintáns et al., 2008).

Acetate produced by citrate catabolism is released into the extracellular medium via passive diffusion or through a permease depending on the pHi of the bacteria, which can differ from one species to another. For example, in *L. lactis* bv. diacetylactis, it has been demonstrated that acetate can serve as the substrate of the citrate permease CitP and consequently be exchanged against citrate (Pudlik and Lolkema, 2011a). However, no exchange of citrate against one of its metabolic products by the permease MaeP could be demonstrated in *O. oeni* (Ramos et al., 1994). Another unidentified transporter of acetate presumably exists in this bacterium. While acetate is released, oxaloacetate, the second product of citrate, is metabolized into pyruvate and CO_2 by an oxaloacetate decarboxylase (EC:1.1.1.38). The reaction leads to the consumption of one proton, generating a ΔpH which is one of the key steps in generating PMF (Lolkema et al., 1995). In many LAB, this reaction is catalyzed by a soluble oxaloacetate decarboxylase belonging to the malic enzyme family and encoded by the *citM* gene, also named *mae* depending on the LAB (Sender et al., 2004; García-Quintáns et al., 2008). In other LAB including *E. faecalis,*

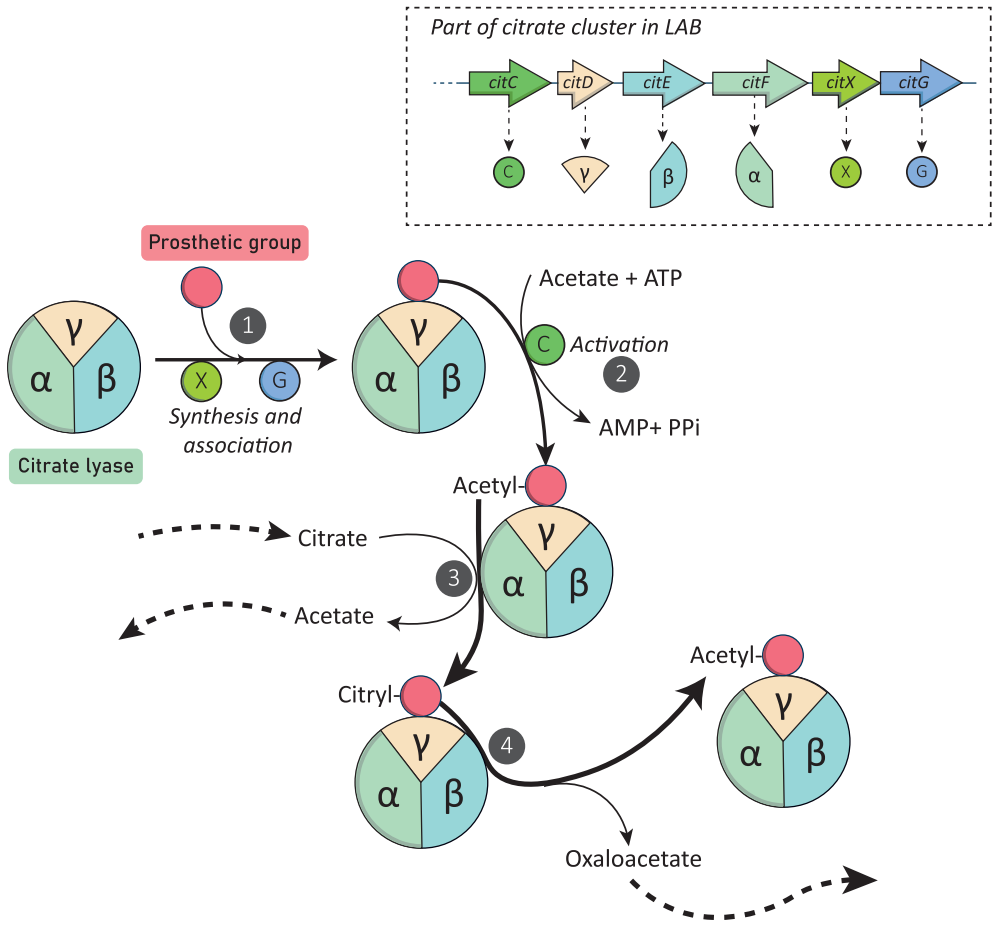

FIGURE 2
Citrate Lyase synthesis and catabolism of citrate mediated by this enzyme. Genes encoding the different citrate lyase (CL) subunits and the three additional proteins involved in this metabolism are showed. Arrows with solid lines represent enzymatic reactions, arrows with dashed lines represent the provenance or redirection of metabolites to other pathways. (1) CitX (apo-citrate lyase phosphoribosyl-dephospho-coenzyme A) and CitG (triphosphoribosyl-dephospho-coenzyme A synthase) synthetize the prosthetic group from ATP and dephospho-coenzyme A. (2) Activation by acetylation of the prosthetic group by CitC (acetate:SH-citrate lyase ligase). (3) Exchange of the acetyl group with the citryl group of citrate catalyzed by the α-subunit of the CL (acetyl-ACP:citrate ACP-transferase) and formation of acetate. (4) Clivage of the citryl group by the β-subunit of the CL (citryl-S-ACP oxaloacetate-lyase) releasing oxaloacetate and enable the acetyl group regeneration.

the reaction implies a membrane-bound oxaloacetate decarboxylase complex encoded by the *oadA, oadB, oadD*, and *oadH* genes (Repizo et al., 2013). Nevertheless, oxaloacetate is known to be unstable and can spontaneously decarboxylate into pyruvate by catalysis with a divalent metal ion (Sender et al., 2004; Pudlik and Lolkema, 2011b).

In the genus *Lactiplantibacillus*, oxaloacetate from citrate catabolism can also be metabolized into succinate using a part of the reductive Tricarboxylic Acid (TCA) cycle (Hugenholtz, 1993).

2.3 Fate of pyruvate

Pyruvate is at the crossroads of several metabolic pathways known as the pyruvate node (Figure 3). Its metabolism can defer between heterofermentative and homofermentative LAB and the difference between the two has previously been reviewed (Gemelas et al., 2014). In the case of heterofermentative LAB such as *O. oeni* and *W. paramesenteroides,* pyruvate produced from citrate catabolism can be reoriented toward different pathways depending on the growth conditions (Contreras et al., 2018). In the presence of hexoses, it can be metabolized into D-lactate by a lactate dehydrogenase (EC:1.1.1.28) in order to reoxidize NADH coming from the phosphoketolase pathway (Zaunmüller et al., 2006). *In O. oeni*, the gene commonly linked to the lactate dehydrogenase is the *ldhD* gene (locus tag OEOE_0413 in PSU-1 genome; Kim et al., 2011; Yang et al., 2019). However, five other genes have been annotated as putative lactate dehydrogenases in this bacterium: OEOE_0025, OEOE_0701, OEOE_1182, OEOE_1672, and OEOE_1709. Nevertheless, only the products of the OEOE_0413 and OEOE_1672 genes have been detected in the proteome of the PSU-1 strain of *O. oeni* (Zaunmüller, 2008).

Pyruvate can also be used to produce ATP. In this way, pyruvate is decarboxylated into acetyl-CoA under the action of the pyruvate dehydrogenase, which strongly depends on the presence of coenzyme A and thiamin diphosphate (Hugenholtz, 1993). This reaction generates one molecule of CO_2 and the reduction of one NAD^+ into NADH + H^+ which has to be reoxidize thanks to the transformation of another molecule of pyruvate into D-lactate by lactate

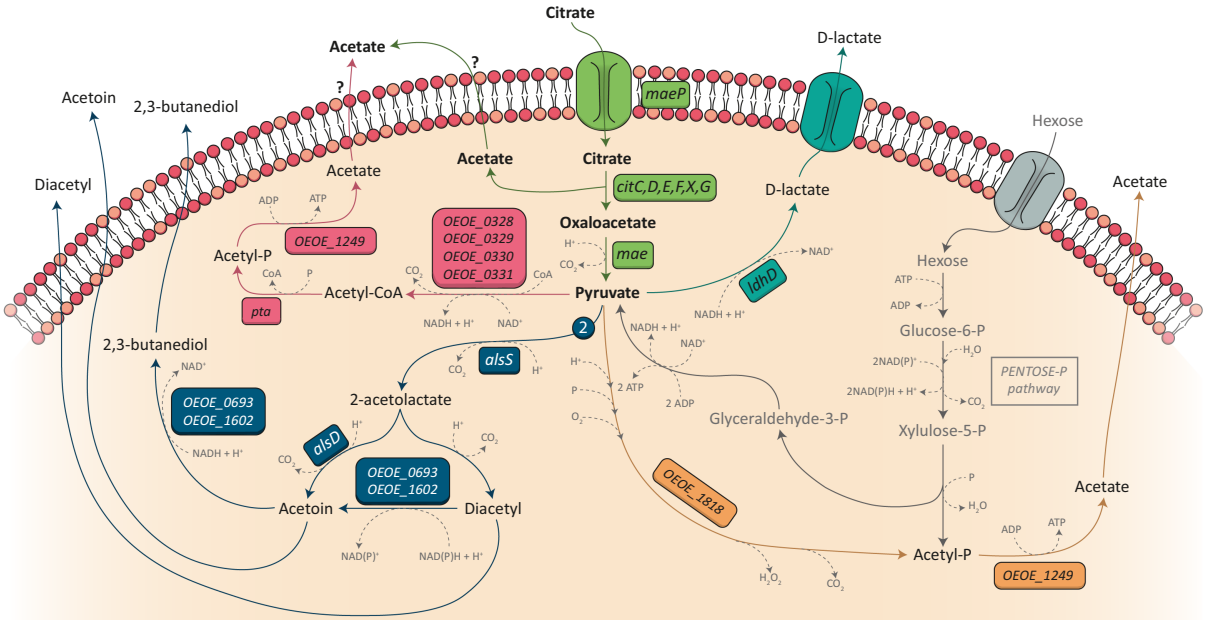

FIGURE 3
Citrate metabolism and becoming of pyruvate in *Oenococcus oeni*. Pyruvate produced by the citrate catabolism (green part) can be metabolized into D-lactate (blue pathway) for the reoxidation of co-factors generated by sugar metabolism (Pentose-P pathway, represented in gray). It can also be used for the production of acetate through the pyruvate dehydrogenase pathway (represented in pink) or through the pyruvate oxidase pathway (represented in orange). Finally, two molecules of pyruvate (symbolized by the number 2 on the figure) can be metabolized into α-acetolactate under the action of the acetolactate synthase (ALS) (dark blue pathway) which leads to the production of diacetyl, acetoin and 2,3-butanediol. Genes encoding the different enzymes are indicated in colored boxes. When no name was attributed to a gene, its locus tag from the PSU-1 strain is indicated. As the transport mechanism of acetate has not been characterized in *O. oeni*, question marks are represented.

dehydrogenase (Wagner et al., 2005; Zaunmüller et al., 2006). *Oenococcus oeni* possesses a pyruvate dehydrogenase which is annotated as the acetoin/pyruvate dehydrogenase complex (EC:1.2.4.1/2.3.1.12/1.8.1.4) encoded by the OEOE_0328, OEOE_0329, OEOE_0330, and OEOE_0331 genes. The acetyl-CoA produced is then metabolized into acetyl-P by a phosphotransacetylase (EC:2.3.1.8, encoded by OEOE_1435) which is then used by an acetate kinase (EC:2.7.2.1, encoded by OEOE_1249) to produce acetate and ATP (Wagner et al., 2005).

Another way to produce ATP from pyruvate without reducing co-factors is possible thanks to the action of the pyruvate oxidase (EC:1.2.3.3) encoded by OEOE_1818 in the *O. oeni* PSU-I strain. Indeed, this enzyme catalyze the conversion of pyruvate, inorganic phosphate and oxygen into acetyl-P, H_2O_2 and CO_2, leading to the production of acetate and ATP from acetyl-P (Wagner et al., 2005). This reaction is only possible under aerobic conditions. It has recently been demonstrated that the channeling of pyruvate to acetyl-P production via the pyruvate oxidase pathway is greatly increased under acidic conditions (pH = 3) in *O. oeni* (Qi et al., 2021). However, this pathway must not be privileged in oenological conditions, as access to oxygen is limited.

Finally, pyruvate can be metabolized into C4 aroma compounds: diacetyl, acetoin and 2,3-butanediol. These C4 compounds are primarily obtained from pyruvate produced by citrate catabolism (McKay and Baldwin, 1990). When pyruvate accumulates in the cell, their synthesis increases in order to prevent a putative toxic effect of high pyruvate content. Indeed, it has been demonstrated that mutant strains of *Streptococcus lactis* or *L. lactis* bv. diacetylactis deficient in lactate dehydrogenase produced higher amount of α-acetolactate and diacetyl in the presence of citrate (McKay and Baldwin, 1974; Monnet et al., 2000). To complete this observation, Zuljan et al. have demonstrated that a *L. lactis* strain which was no longer able to metabolize pyruvate into C4 compounds became sensitive to the addition of this organic acid at low pH (Zuljan et al., 2014).

Two molecules of pyruvate and one thiamin diphosphate are needed to form α-acetolactate plus CO_2 and the reaction is catalyzed by the acetolactate synthase (EC:2.2.1.6, encoded by the *alsS* gene in *O. oeni*; Hugenholtz, 1993; Garmyn et al., 1996; Olguín et al., 2009). The acetolactate synthase of *L. lactis* bv. diacetylactis showed a low affinity to pyruvate (Km = 50 mM), confirming that a high amount of pyruvate is needed to obtain C4 compounds (Snoep et al., 1992). Two pathways are then available to α-acetolactate: it can be metabolized into acetoin and CO_2 by the α-acetolactate decarboxylase (EC:4.1.1.5), or it can be spontaneously oxidated into diacetyl and CO_2 in the presence of oxygen. The α-acetolactate decarboxylase is encoded by the *alsD* gene in *O. oeni* and is organized in a single operon with the *alsS* gene (Garmyn et al., 1996). Moreover, the expression of this gene could be induced by the presence of ethanol (Olguín et al., 2009). Diacetyl is the major molecule which imparts a buttery aroma to wine, and it is primarily synthetized from pyruvate derived from citrate metabolism. Nevertheless, it has been proven than other metabolisms can contributes to its production, including sugar and malate metabolism (Mink et al., 2014, 2015; Sternes et al., 2017) The highest amount of diacetyl is detected during malolactic fermentation when almost all malic acid and more than half the

citrate concentration are consumed (Mink et al., 2014). this amount must not exceed 1 to 4 mg/L. At a concentration more than 7 mg/L, diacetyl will impart an undesirable buttery flavor to wine (Bartowsky and Henschke, 2004). Thus, controlling its production is of interest. Unfortunately, the regulation of citrate metabolism in *O. oeni* is to date imperfectly understood. This reflection will be the subject of a paragraph bellow in which the regulation of citrate metabolism in other LAB will be described, enabling a parallel with *O. oeni* to be drawn.

Finally, diacetyl can be reduced to acetoin which itself can be reduced to 2,3-butanediol. The reaction requires NADH or NADPH as a co-factor, depending on the LAB (Hugenholtz, 1993). According to a study on *L. lactis* bv. diacetylactis, these two reactions could be metabolized by the same enzyme, namely acetoin reductase (EC:1.1.1.304/1.1.1.47), and this enzyme may have a greater affinity for diacetyl (Crow, 1990). In the *O. oeni* PSU-1 genome, two genes are annotated as acetoin reductase: OEOE_0693 and OEOE_1602. According to previous studies (Cogan, 1981; Hugenholtz, 1993), this enzyme may be partially inhibited in presence of citrate.

3 A genomic insight into citrate metabolism: way of regulation pathway

The extreme diversity of the citrate locus in LAB was mentioned above. Indeed, the gene organization and the localization of the operon but also the genes within the locus are not the same depending on the species. In light of this diversity, regulation of citrate locus expression could be species-dependent; this may also be true because the growth environment of each LAB is very different, notably in terms of pH conditions. It has indeed been demonstrated that environment can impact the expression of the citrate locus in different ways depending on the species. In this section, the mechanisms of citrate locus regulation described in the literature for certain LAB will be detailed. The effect of environmental parameters on the expression of the operon will then be discussed.

3.1 Regulation of citrate locus expression

Previous studies have explored the regulatory mechanism of citrate locus expression in various LAB. Findings highlight an activator protein named CitI, CitR, or CitO acting at the transcriptional and/or the post-transcriptional level.

In *W. paramesenteroides*, the genes related to citrate metabolism are organized in a single plasmid-located cluster of 9.8 kb. Two divergent promoters located between *citI* and *citM* have been identified: the first (P*citI*) controls *citI* expression and the second (P*cit*) ensures the transcription of the whole *citMCDEFGRP* operon (Martín et al., 2000). In addition to the *citM, citP* and *citCDEFG* genes, which encode the key proteins involved in the citrate pathway, i.e., oxaloacetate decarboxylase, citrate permease and the different subunits of citrate lyase, respectively, this cluster includes two genes encoding putative regulators: *citI* and *citR*. CitI is a protein belonging to the SorC family. Its role in the expression of the *citMCDEFGRP* cluster has been explored (Martín et al., 2000; Martin et al., 2005). Indeed, the role of CitI as a transcriptional activator in *citMCDEFGRP* cluster expression has been revealed via heterologous expression in *E. coli*. The intergenic region citI-citM is rich in A/T bases (77%) with an intrinsic bending. Two operator sites recognized by CitI (O1 and O2) have been identified on this region and CitI is able to bind cooperatively to them. The affinity of CitI for its DNA operators is directly enhanced by citrate, resulting in increased RNA polymerase recruitment at Pcit and PcitI. In this way, in the absence of citrate, CitI interacts weakly with operator sites, resulting in a low level of expression of the citrate pathway enzymes such as the citrate permease which ensures the uptake of citrate inside the cell. When citrate is available in the environment, it is transported inside the cell and directly increases the affinity of CitI for its DNA operator, leading to an increase in the *cit* locus expression (Martin et al., 2005). It appears that similar operator sites can also be found on the citrate locus promoter regions of other LAB, including *O. oeni*. Thus, Martin et al. (2005) suggested that this regulatory mechanism may be similar in other LAB. Concerning the *citR* gene of this bacterium, the role of its product on *cit* cluster expression has not yet been investigated.

In addition, the *citMCDEFGRP* cluster expression in this bacterium is subjected to post-transcriptional regulation by a specific processing at the level of complex structures probably recognized by endonucleases (Martín et al., 2000). Thus, three different transcripts of the *cit* cluster have been detected: an 8.8 kb RNA including the transcript of all the *citMCDEFGRP* genes, a 6.1 kb RNA including the transcript from *citD* to *citP* and finally a 7.2 kb RNA including the transcript from *citM* to *citR* (Martín et al., 2000). The authors have suggested that this RNA processing might enable regulation of the synthesis of the different proteins in suitable proportions (Martín et al., 2000).

In *L. lactis* bv. diacetylactis, the genes encoding proteins involved in citrate metabolism are organized in two different clusters: the *citQRP* operon which is located on a plasmid and the *citMCDEFXG* operon which is integrated in the chromosome (Martín et al., 2004). This second cluster also includes the *citI* gene which is oriented in divergent direction. Promoter regions have been identified: before the IS element for *citQRP* cluster expression, before *citM* for *citMCDEFXG* expression and another one in a divergent direction before *citI* (de Felipe et al., 1994; Martín et al., 2004). The promoter enabling *citQRP* expression and the one before *citM* are very similar, rich in A/T bases (Martín et al., 2004). The two citrate clusters include two genes encoding regulatory proteins: *citI* and *citR*. The impact of CitR on permease gene expression has been explored by heterologous expression (de Felipe et al., 1994). This protein of 13.1 kDa is encoded by the 339 bp *citR* gene and shares homology with the *citR* of *W. paramesenteroides*. Overexpression of *citR* had no impact on the transcription of *citP*, whereas reporter gene activity decreased significantly. Thus, CitR could act as a repressor at a post-transcriptional level. Another experiment was conducted in which the *citR and citP* genes were both fused with the reporter gene; the construction was under the control of a constitutive promotor. This experiment revealed that the introduction of a frameshift mutation on *citR* led to decreased activity of the reporter gene. This finding implies that the coupled translation of *citR* and *citP* enhances the expression of *citP*. Thus, CitR in *L. lactis* bv. diacetylactis acts at a post-transcriptional level and may have two different impacts on the expression of *citP*. A secondary structure of the mRNA was detected before *citR* including its ribosome-binding site and the start codon. One of the

hypotheses is that CitR could help to stabilize this secondary structure, preventing the coupled translation of *citR* and *citP*. The impact of CitR on the second citrate cluster of *L. lactis* bv. diacetylactis has not yet been explored.

The *citMCDEFXG* of *L. lactis* bv. diacetylactis includes the *citI* gene between *citM* and *citC* in reverse orientation. This 930 bp gene encodes a 34.8 kDa regulatory protein named CitI. Its effect on the expression of the two *cit* clusters of *L. lactis* bv. diacetylactis has not yet been investigated. Nevertheless, Martín et al. (2004) have suggested that a post-transcriptional regulation of the *citI* expression is possible via an RNA-silencing mechanism, as both sense and antisense transcripts of this genomic location were detected by RT-PCR. Indeed, this gene can be transcribed from the promoter before *citM* (P1) and from its own promoter (P2; Figure 1). Furthermore, it has been demonstrated that citrate lyase activity increases at pH 5 compared to pH 7 and that more *citI* transcripts are detected in the acidic condition (Martín et al., 2004). Thus, a regulatory mechanism similar to that identified in *W. paramesenteroides* was proposed by the authors: CitI would seem to be a transcriptional activator of the *citMCDEFXG* cluster, whose expression would presumably be enhanced by a decrease in pH.

In the case of *E. faecalis*, there is another regulatory protein named CitO belonging to the GntR family and clustered in the FadR C-terminal Domain family. It has been shown to act as a transcriptional activator of the *cit* cluster expression in this bacterium, as no citrate metabolism could be detected when the *citO* gene was mutated (Blancato et al., 2008). Molecular modifications induced by citrate and metal ions (Ni^{2+}, Zn^{2+}) in the C-terminal domain of CitO are required for optimal transcriptional activation by CitO (Blancato et al., 2008). The authors have also identified two operator sites on the promoter region of *citO*, and citrate seems to interact with CitO, modulating its capacity to bind DNA. Similar to what has been suggested in the cases of *W. paramesenteroides* and *L. lactis* bv. diacetylactis, the *cit* cluster of this LAB could be the subject of post-transcriptional regulation, as four secondary structures have been identified on the operon and as smaller RNA were also detected (Blancato et al., 2008).

In *O. oeni*, no study has been undertaken to understand the role of CitR, the putative regulator included in its citrate operon. Compared to all the regulator proteins mentioned above, the CitR protein of *O. oeni* seems to be closest to the CitI protein of *L. lactis* bv. diacetylactis, as they share 52% of their amino acid identity. As previously mentioned, two putative operator sites for this protein have been proposed by Martin et al. (2005), presumably located between *citR* and *mae*. Concerning promoting regions, two putative promoters were identified with sequences which could be related to the −10 and −35 regions: the first one seemingly before *mae* and, similarly to other LAB, it could enable the entire operon transcription. This promoter is also rich in A/T bases, as described in *W. paramesenteroides* and in *L. lactis* bv. diacetylactis. Typical regulatory regions −35 and −10 were also found before *maeP*, meaning that the citrate operon could also be expressed from this putative promoter in this bacterium. Another promoter must be located before the *citR* gene, as it is divergently expressed. Nevertheless, identifying the −35 and −10 regions near this gene is not evident, nor is the ribosome binding site. Determining the +1 transcription start site would be necessary to precisely define the promoting area of *citR*. Similarly to what was found in other LAB, the *cit* cluster expression of *O. oeni* could be regulated post-transcriptionally.

3.2 Effect of environment on the citrate locus expression

As mentioned above, the environment can affect the expression of the citrate cluster in LAB. Indeed, in most LAB, citrate induces the expression of the operon. This positive effect of citrate has been reported in *W. paramesenteroides, Lc. mesenteroides, Limosilactobacillus panis*, and *E. faecalis* (Bekal-Si Ali et al., 1999; Martín et al., 2000; Blancato et al., 2008; Kang et al., 2013). On the contrary, in *L. lactis* bv. diacetylactis, the expression of the *cit* cluster is induced at low pH while citrate did not enhance the *cit* transcript level detected (Martín et al., 2004).

In *O. oeni*, a previous RT-qPCR study on the ATCC BAA-1163 strain has demonstrated that neither citrate nor pH had an effect on the expression of *mae, maeP*, or *citF* (Augagneur et al., 2007b). These results are not in accordance with transcriptomic analysis performed on RNA of the SD-2a strain, which demonstrated an up-regulation of the citrate lyase genes and *mae* at low pH (Liu et al., 2017). Regarding the sequence of the citrate operon in the ATCC BAA-1163 strain, one base deletion can be noted in the sequence of the *citR* gene compared to other strains, leading to the appearance of a premature stop codon (length of 256 amino acids instead of 320). Thus, the putative regulator CitR might be unfunctional in this strain and the conclusions drawn from the data collected on this strain would therefore not be generalizable to the whole species. Indeed, studies on *W. paramesenteroides* have shown the direct positive effect of citrate on the expression of the regulator *citI* specifically (Martín et al., 2000). If the regulator is unfunctional in the ATCC BAA-1163 strain of *O. oeni,* this might explain why no variation of the *cit* locus expression could be noted in the experiment conducted by Augagneur et al. (2007b), despite the addition of citrate and the acidic conditions. More experiments based on the characterization of different *O. oeni* strains would be necessary to confirm this hypothesis and to identify which environmental parameters affect the *cit* locus expression in this bacterium. Other RTqPCR and transcriptomic analyses on *O. oeni* grown in "wine-like" conditions have shown a significative induction of certain genes of the citrate locus by wine-related stresses, especially ethanol (Olguín et al., 2009, 2010; Bordas et al., 2015; Margalef-Català et al., 2016). Moreover, another study has demonstrated an over-expression of *citE* induced at low pH but also by the presence of fructose (Pretorius et al., 2019). The presence of phenolic compounds also seems to have an impact on *O. oeni* citrate metabolism and acetate production (Rozès et al., 2003; Campos et al., 2009). It would be of interest to characterize in further detail the impact of all these environmental parameters on the *cit* locus expression of *O. oeni*, especially on the expression of *citR* encoding the putative regulator. A deeper understanding of citrate metabolism regulation in *O. oeni* would help to better grasp one of the stress response mechanisms of this bacterium, as it has been reported in several instances that these genes are up-regulated during adaptation to wine (Bordas et al., 2015; Margalef-Català et al., 2016).

Concerning diacetyl, its production by *O. oeni* is influenced by the presence of oxygen, the redox potential of the wine and the concentration of pyruvate and citrate (Nielsen and Richelieu, 1998; Mink et al., 2015). Therefore, understanding the circumstances of citrate metabolism activation could allow for better control of the citrate-associated synthesis of products like diacetyl, which may impact positively but also negatively the aromatic profile of wines.

4 Beneficial effect of citrate on LAB growth and stress resistance

The citrate pathway is an unstable trait in LAB, as some of the key genes are plasmid-located in several species (Hugenholtz, 1993). Furthermore, it has been reported for some LAB that citrate itself does not support the growth of bacteria (García-Quintáns et al., 2008). However, citrate confers some interesting advantages on bacteria which are able to metabolize it. Indeed, this metabolism generates PMF and leads to the consumption of several scalar protons, helping to maintain pHi in an acidic environment (Poolman et al., 1991; Ramos et al., 1994). Furthermore, in heterofermentative LAB, pyruvate produced from citrate can be further metabolized into D-lactic acid to reoxidize cofactors resulting from sugar metabolism. Thus, cometabolism of carbohydrates and citrate can significantly enhance the growth of bacteria (Salou et al., 1994; Ramos and Santos, 1996; Kang et al., 2013).

4.1 Proton motive force generation

PMF is one of the main mechanisms by which energy is generated in LAB. PMF consists of a chemical (ΔpH) and an electrical gradient (ΔΨ), also called membrane potential. Two systems can generate PMF: the primary transport system, which consists of the translocation of one proton out of the cells and, in this case, the generation of chemical and electrical gradient is coupled, and the secondary transport system. Citrate metabolism belongs to the second category. In this case, pH gradient and membrane potential occur at two different steps of the metabolism. Indeed, membrane potential is generated by the transport of citrate into the cells while ΔpH occurs when citrate is metabolized (Ramos et al., 1994). The free energy released by PMF is strong enough to activate the F_0-F_1 ATPase to produce ATP (Poolman et al., 1991; Poolman, 1993; Ramos et al., 1994). To better describe this phenomenon, the example of *L. lactis* bv. diacetylactis will be taken and compared to that of *O. oeni*.

L. lactis bv. diacetylactis is used for milk fermentation and converts lactose to lactate, resulting in the acidification of the medium, from a pH of 7 to a pH of around 4 (García-Quintáns et al., 1998). It has been proven that citrate metabolism is induced at low pH in this bacterium, where the highest uptake rates were observed at pH 4.5 to 5.5 (Magni et al., 1994; Martín et al., 2004). The pKa of citrate are 3.13, 4.76 and 6.40 (Martell and Smith, 1982). Thus, when the pH of the medium is between 4.5 and 5.5, citrate will be principally found in the $Hcitrate^{2-}$ form. This form of citrate is the one that is taken up by the permease CitP (Figure 4; Magni et al., 1996). This transporter can act as a symporter, meaning that citrate is co-transported with one proton (Magni et al., 1996). It might also act as an antiporter, as has been described for *Lc. mesenteroides* and *L. lactis*; in this case, citrate is exchanged with one molecule of lactate (Figure 4; Marty-Tesset et al., 1996; Bandell et al., 1998; Pudlik and Lolkema, 2011a). In each case, the transport of citrate leads to the translocation of one negative charge into the cell, creating a negative electrical gradient inside (Magni et al., 1994; Marty-Tesset et al., 1996). Then, the decarboxylation of oxaloacetate into pyruvate leads to the consumption of a scalar proton and creates the second aspect of PMF: the pH gradient (Lolkema et al., 1995).

Oenococcus oeni grows in more acidic environments than *L. lactis* bv. diacetylactis, with the pH of wine reaching between 3 and 3.6. Thus, in wine, citrate is mainly found in the anionic form $H_2citrate^-$. This form of citrate is the particle transported by the permease CitP (Ramos et al., 1994). The latter acts as a uniporter leading to the internalization of one negative charge (ΔΨ) and it has been proven that citrate cannot be exchanged by one of the products of citrate metabolism, unlike what has been demonstrated in other LAB (Ramos et al., 1994; Marty-Tesset et al., 1996; Bandell et al., 1998). The second part of PMF is created by the consumption of scalar protons, which occur during the catabolism of citrate (Figure 4; Ramos et al., 1994). The generation of PMF is of importance as it is one of the only ways for *O. oeni* to produce energy in wine, because of sugar starvation. Thus, in the same way as malolactic fermentation, which represents the major source of PMF generation in *O. oeni*, citrate metabolism participates in the survival of the bacterium in a harsh environment such as wine.

4.2 Intracellular pH homeostasis

LAB grow in acidic environments, in particular *O. oeni* which has to survive in wine that can sometimes reach pH lower than 3. At low pH, many acids are found in their protonated form, meaning that they can enter the cells by simple passive diffusion. The consequence is a lowering of pHi, which can trigger the denaturation of proteins, decreasing enzyme activity and leading to the rigidification of the membrane, affecting transporter activity (Tourdot-Maréchal et al., 2000; Grandvalet et al., 2008). All of these changes modify cell homeostasis and can seriously affect the survival of bacteria. Extruding protons by the F_0 F_1-ATPase is one of the mechanisms used by LAB to maintain their pHi, but as it is energy-consuming it needs to be a temporary response. As mentioned above, citrate metabolism leads to the consumption of several protons and its catabolism in weaker acids such as lactate or acetate contributes to the maintain of pHi. It has also been reported that citrate metabolism relieved growth inhibition caused by an accumulation of lactate produced by glycolysis in the cytoplasm of *L. lactis,* thanks to the exchange of citrate against lactate by the permease CitP (Magni et al., 1999). Moreover, another study on *L. lactis* has demonstrated the beneficial effect of C4 compound synthesis against pyruvate accumulation which can become toxic at low pH. Indeed, the disruption of the *als* gene encoding the acetolactate synthase led to the loss of cell viability when grown at low pH in the presence of pyruvate, due to the cells' inability to regulate their pHi (Zuljan et al., 2014). In the same way, disruption of the *mae* gene in *L. lactis* leads to an intracellular oxaloacetate accumulation which significantly impacts growth, especially at low pH (Augagneur et al., 2007a; Pudlik and Lolkema, 2011b). There is no doubt that citrate metabolism is one of the stress response mechanisms used by LAB to resist in acidic environments.

4.3 Co-metabolism of citrate and glucose

LAB are able to ferment sugars from their environment to produce energy via two different pathways: homofermentative

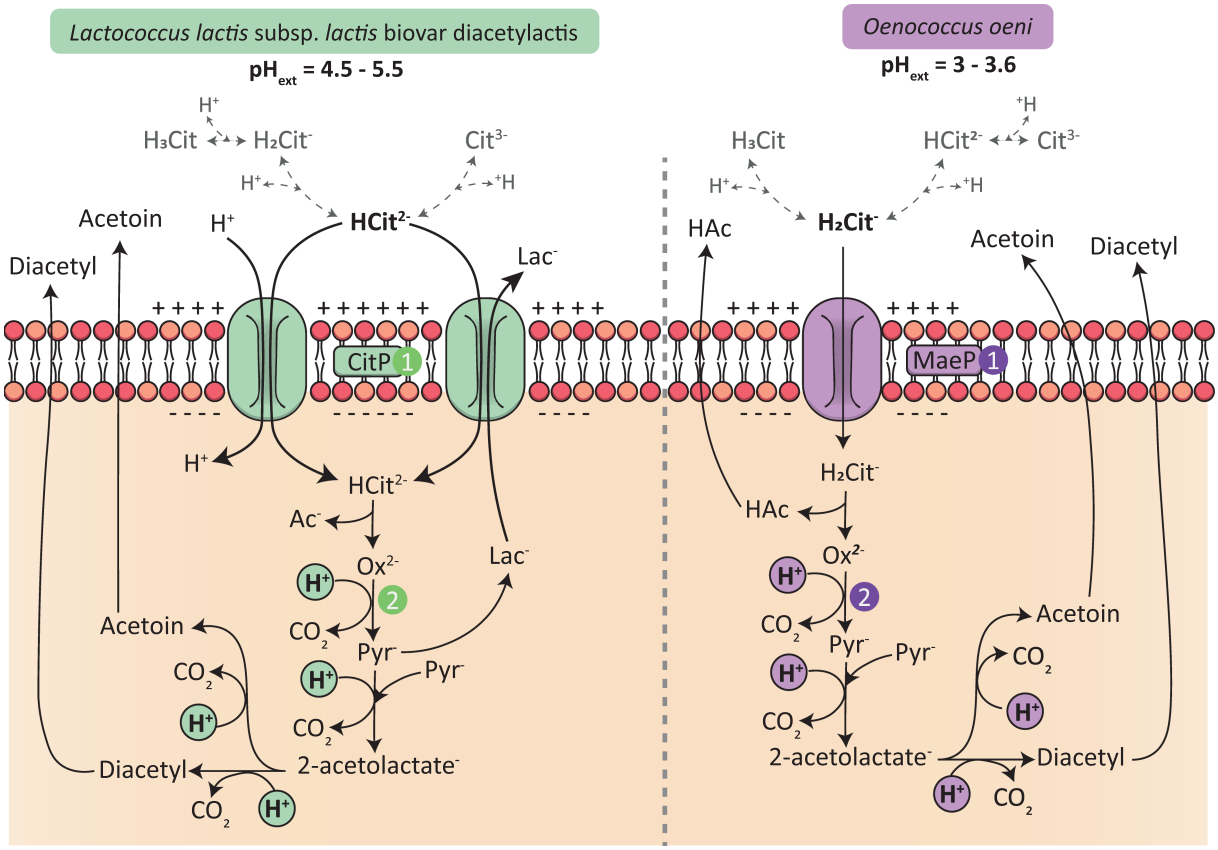

FIGURE 4
Generation of PMF in *Lactococcus lactis* bv. diacetylactis and in *Oenococcus oeni* by citrate metabolism. 1/ Internalization of citrate by either the permeases CitP or MaeP leads to the creation of an electrical gradient, inside negative (ΔΨ). Citrate forms are represented in gray, the majority form founded in each environment of the two LAB according to the extracellular pH is in bold 2/ Citrate metabolism drives the consumption of scalar protons leading to the creation of a ΔpH gradient, inside alkaline.

metabolism which corresponds to glycolysis (also called the Embden-Meyerhof-Parnas pathway) and which mainly leads to the production of lactic acid, and heterofermentative metabolism which uses the phosphoketolase pathway and produces lactic acid, but also ethanol, acetic acid and CO_2 (Kandler, 1983). Heterofermentative LAB can also be divided into two different groups: the facultatively heterofermentative, which are able to ferment sugars through glycolysis and the phosphoketolase pathway, and the obligately heterofermentative, such as *O. oeni*, which lack the main enzyme involved in the glycolysis pathway, resulting in the incapacity to use this metabolism (Salvetti et al., 2013).

The phosphoketolase pathway leads to the production of 1 or 2 molecules of ATP and is thus an energy source for LAB. Fructose and glucose, which are the most common hexoses founded in LAB environments, are metabolized to glyceraldehyde-3-P, acetyl-P and CO_2 and this reaction requires the reduction of two $NAD(P)^+$ (Figure 3). Glyceraldehyde-3-P is then used for the production of pyruvate which leads to the reduction of one extra NAD^+, although this one is quickly reoxidized under the action of the lactate dehydrogenase which produces lactate from pyruvate (Unden and Zaunmüller, 2009). The two first NAD(P)H produced by hexose fermentation also need to be reoxidized. This reoxidation is carried out by the conversion of acetyl-P to ethanol, but it appears that this pathway is very slow in *O. oeni* compared to the high activities of the enzymes of the phosphoketolase pathway (Maicas et al., 2002; Unden and Zaunmüller, 2009). Other pathways linked to sugar metabolism are used by the bacterium to reoxidize these cofactors: the erythritol, glycerol, and mannitol pathways (Maicas et al., 2002; Richter et al., 2003; Zaunmüller et al., 2006). Nevertheless, external electron acceptors may also be employed, as in the case of citrate metabolism. Indeed, citrate metabolism produces pyruvate, which can be converted by lactate dehydrogenase to D-lactate, thus enabling the reoxidation of one cofactor (Ramos and Santos, 1996; Zaunmüller et al., 2006). Consequently, it has been demonstrated that the growth of *O. oeni* is enhanced in medium containing both citrate and glucose, compared to a condition with only glucose (Salou et al., 1994; Ramos and Santos, 1996). A similar conclusion was drawn in a study on *Li. panis,* in which the addition of citrate caused a metabolic shift as more acetate was produced from glucose than ethanol, resulting in higher ATP production (Kang et al., 2013).

On the other hand, in homofermentative LAB, the association between citrate and sugar metabolisms appears only when citrate is exchanged by the end-product of glycolysis, i.e., lactate. In this case, it is the sugar metabolism which has a beneficial effect on citrate metabolism, as the addition of glucose enhances citrate uptake by bacteria (Pudlik and Lolkema, 2011a). Nevertheless, the co-metabolism of citrate and glucose also results in growth advantage in homofermentative LAB (Starrenburg and Hugenholtz, 1991; Sánchez et al., 2008).

5 A controversial effect of citrate metabolism highlighted in *Oenococcus oeni*

Several beneficial effects of citrate metabolism on LAB growth have been described above. However, a dual effect of citrate on *O. oeni* acid stress resistance has been highlighted (Augagneur et al., 2007b; Julliat et al., 2023). Indeed, while the addition of citrate in FT80m medium resulted in a higher final biomass and growth rate achieved at pH 5.3, the optimal pH for the growth of *O. oeni*, a significant inhibition effect was observed on bacterial growth in a pH 3.2 medium containing citrate (Augagneur et al., 2007b). In addition, an experimental evolution performed to improve *O. oeni* acid tolerance led to the appearance of fixed mutations in the *cit* locus. These mutations triggered down-regulation of citrate genes resulting in a slowdown in the rate of citrate consumption in the evolved populations tested. This study demonstrated that while the growth of the ancestral strain is impaired by the addition of citrate in pH 3 FT80m, that of evolved populations is not affected (Julliat et al., 2023). It demonstrated a correlation between citrate consumption rate and acid tolerance in *O. oeni*. The growth inhibition observed may be due to an inability of the bacterium to maintain its pHi. According to Augagneur et al. (2007b), citrate itself did not seem to directly affect the pHi maintenance. Consequently, the authors turned their attention to one of the products of citrate metabolism: acetate. This weak acid (pKa = 4.74) is primarily found in its protonated form at pH lower than 4.8 and can therefore easily re-enter the cells when the pH of the medium is low enough. Experiments conducted by Augagneur et al. (2007b) have shown a significant inhibitory effect of acetate addition on the growth of bacteria and, to a lesser extent, on the maintenance of pH gradient and membrane potential. Thus, the quick production of acetate from citrate metabolism but also sugar metabolism could become toxic for the cells. In addition, pyruvate production could also play a role in this case, as it has been shown in *L. lactis* that an accumulation of pyruvate that could no longer be metabolized into C4 compounds as a result of *alsS* mutation led to the loss of cell viability (Zuljan et al., 2014).

These studies may bring to light a controversial effect of citrate at low pH specific to the bacterium *O. oeni*. Nevertheless, it must be kept in mind the experiments conducted by Augagneur et al. (2007b) were performed on a laboratory complemented by 20 mM of citrate, corresponding to 3.8 g/L. This concentration is around 10-fold higher than what can be found in wine, meaning that the testing conditions were well removed from the real environment of the bacterium (Alexandre et al., 2008). Furthermore, the experiments were conducted using the laboratory strain ATCC BAA-1163. As noted above, this strain possesses a one-base deletion on the *citR* sequence compared to other strains, resulting in the appearance of a premature stop codon. It is thus possible that ATCC BAA-1163 has a particular behavior regarding citrate consumption.

No additional study has been carried out on *O. oeni* to demonstrate the effect on the bacterium of citrate addition at low pH. Nevertheless, other experiments have been conducted on other strains of *O. oeni* following the consumption of sugars and organic acids at low pH in presence of citrate. In these studies, the bacteria consumed all malic acid, whatever the pH (between 3 and 3.5 in some conditions tested) or the citrate concentration (0.5 g/L in the study of Pretorius et al., 2019 and between 5 to 8.5 g/L in the study of Viljakainen and Laakso, 2000). This was not the case in the study of Augagneur et al. (2007b) as the addition of citrate at pH 3.2 prevented the total malate consumption. This suggests that bacteria were not affected by the presence of citrate at low pH in the conditions tested by Viljakainen and Laakso (2000) and Pretorius et al. (2019). Other studies would be needed to generalize the controversial effect of citrate on the acid resistance of *O. oeni* observed by Augagneur et al. (2007b) and to determine whether this metabolism could have an impact on malolactic fermentation.

6 Conclusion and perspectives

This review aimed to summarize current understanding of citrate metabolism in LAB with a focus on the wine bacterium *O. oeni*. This metabolism requires 3 different complex proteins: a permease, a citrate lyase and finally an oxaloacetate decarboxylase (Hugenholtz, 1993; Bekal et al., 1998a; Drider et al., 2004). The genes encoding these enzymes are organized in a long citrate operon which can be included in a plasmid or integrated in the bacterial chromosome, depending on the LAB (de Felipe et al., 1994; Drider et al., 2004; Martin et al., 2005; Blancato et al., 2008). The regulation mechanism of the citrate locus expression has been described in some LAB, bringing to light the major role of a transcriptional/post-transcriptional activator encoded by a gene named *citI, citR*, or *citO,* depending on the LAB. We can note in passing that the different names assigned to the various regulatory proteins reveal a certain lack of relevance, as the *citR* encoding the regulatory protein found in *O. oeni* is genetically closer to *citI* than to the *citR* of *L. lactis* bv. diacetylactis.

Expression of the citrate locus may be induced by environmental parameters such as the presence of citrate or pH (Bekal-Si Ali et al., 1999; Martín et al., 2000, 2004; Blancato et al., 2008). In *O. oeni*, certain RT-qPCR and RNAseq studies have demonstrated the up-regulation of some citrate locus genes by wine-related stresses such as ethanol (Bordas et al., 2015; Margalef-Català et al., 2016), but further experimentation would be necessary to decrypt the regulation mechanism of the citrate operon in this specific species.

Citrate metabolism has a beneficial effect on growth and acid stress resistance in LAB. Nevertheless, a controversial effect of citrate has been highlighted on the acid stress resistance of the ATCC BAA-1163 strain of *O. oeni* (Augagneur et al., 2007b; Julliat et al., 2023). This effect could be strain-dependent, as no other study reported this kind of effect of citrate at low pH on this bacterium. It would be of interest to study citrate metabolism in different *O. oeni* strains to confirm this hypothesis. In addition, a complementary study could be undertaken in order to understand how citrate may be the object of growth inhibition in this strain. Augagneur et al. (2007b) suspected acetate production to be toxic, but pyruvate could also play an important role, as has been demonstrated in *L. lactis* (Zuljan et al., 2014). From a more general point of view, further knowledge is needed on the citrate metabolism of *O. oeni* and particularly on how this metabolism is regulated in the species. No study to date has been undertaken to describe the role of CitR, the putative regulator of the citrate operon in *O. oeni*, and little information is available concerning the effect of environment on the expression of the *cit* cluster. As far as previous studies have allowed us to ascertain, citrate metabolism does not seem to impact malolactic fermentation (Viljakainen and Laakso, 2000; Pretorius et al., 2019). However, to the extent that this metabolism may be strain-dependent, conducting fermentation with

different *O. oeni* strains at different pH and with different citrate concentrations following malate and citrate consumption could be a profitable way forward. Finally, as citrate metabolism leads to the production of diacetyl, a C4 compound responsible for the buttery aroma that is only desirable in small amounts in wine (Bartowsky and Henschke, 2004), a more precise understanding of how environmental conditions affect citrate metabolism could enable a better control of diacetyl production.

Author contributions

CE: Writing – review & editing. JC: Writing – review & editing, Funding acquisition. MF: Writing – review & editing, Funding acquisition. HA: Writing – review & editing, Supervision. CR: Writing – review & editing, Supervision. CG: Writing – review & editing, Supervision.

Funding

The authors declare financial support was received for the research, authorship, and/or publication of this article. This research was funded by Laffort (France) and the Institut Agro (France). The funders were involved in the writing of this article and the decision to submit it for publication.

Acknowledgments

The authors would like to thank Dominique Garmyn (Université de Bourgogne) for helpful discussions and assistance in proofreading this review.

Conflict of interest

The authors JC and MF were employed by Biolaffort.

The remaining authors declare that the research was conducted in the absence of any commercial or financial relationships that could be construed as a potential conflict of interest.

The author(s) declared that they were an editorial board member of Frontiers, at the time of submission. This had no impact on the peer review process and the final decision.

Publisher's note

References

Alexandre, H., Grandvalet, C., Guilloux-Benatier, M., Remize, F., and Tourdot-Maréchal, R. (2008). *Les bactéries lactiques en œnologie*. Paris, France: Lavoisier.

Augagneur, Y., Garmyn, D., and Guzzo, J. (2007a). Mutation of the oxaloacetate decarboxylase gene of *Lactococcus lactis* subsp. *lactis* impairs the growth during citrate metabolism. *J. Appl. Microbiol.* 104:071010063119003. doi: 10.1111/j.1365-2672.2007.03582.x

Augagneur, Y., Ritt, J.-F., Linares, D. M., Remize, F., Tourdot-Maréchal, R., Garmyn, D., et al. (2007b). Dual effect of organic acids as a function of external pH in *Oenococcus oeni*. *Arch. Microbiol.* 188, 147–157. doi: 10.1007/s00203-007-0230-0

Bandell, M., Lhotte, M. E., Marty-Teysset, C., Veyrat, A., Prévost, H., Dartois, V., et al. (1998). Mechanism of the citrate transporters in carbohydrate and citrate cometabolism in *Lactococcus* and *Leuconostoc* species. *Appl. Environ. Microbiol.* 64, 1594–1600. doi: 10.1128/AEM.64.5.1594-1600.1998

Bartowsky, E. J. (2005). *Oenococcus oeni* and malolactic fermentation – moving into the molecular arena. *Aust. J. Grape Wine Res.* 11, 174–187. doi: 10.1111/j.1755-0238.2005.tb00286.x

Bartowsky, E. J., and Henschke, P. A. (2004). The 'buttery' attribute of wine—diacetyl—desirability, spoilage and beyond. *Int. J. Food Microbiol.* 96, 235–252. doi: 10.1016/j.ijfoodmicro.2004.05.013

Bekal, S., Diviès, C., and Prévost, H. (1998a). Citrate lyases of lactic acid bacteria. *Lait* 78, 3–10. doi: 10.1051/lait:199811

Bekal, S., Van Beeumen, J., Samyn, B., Garmyn, D., Henini, S., Diviès, C., et al. (1998b). Purification of *Leuconostoc mesenteroides* citrate lyase and cloning and characterization of the *citCDEFG* gene cluster. *J. Bacteriol.* 180, 647–654. doi: 10.1128/JB.180.3.647-654.1998

Bekal-Si Ali, S., Diviès, C., and Prévost, H. (1999). Genetic organization of the *citCDEF* locus and identification of *mae* and *clyR* genes from *Leuconostoc mesenteroides*. *J. Bacteriol.* 181, 4411–4416. doi: 10.1128/JB.181.14.4411-4416.1999

Blancato, V. S., Repizo, G. D., Suárez, C. A., and Magni, C. (2008). Transcriptional regulation of the citrate gene cluster of *Enterococcus faecalis* involves the GntR family transcriptional activator CitO. *J. Bacteriol.* 190, 7419–7430. doi: 10.1128/JB.01704-07

Bonnin-Jusserand, M. (2011). *Etude du métabolisme des amines biogènes chez les bactéries lactiques du vin*. University of Burgundy (France) Language = French.

Bordas, M., Araque, I., Bordons, A., and Reguant, C. (2015). Differential expression of selected *Oenococcus oeni* genes for adaptation in wine-like media and red wine. *Ann. Microbiol.* 65, 2277–2285. doi: 10.1007/s13213-015-1069-2

Bott, M. (1997). Anaerobic citrate metabolism and its regulation in enterobacteria. *Arch. Microbiol.* 167, 78–88. doi: 10.1007/s002030050419

Campos, F. M., Figueiredo, A. R., Hogg, T. A., and Couto, J. A. (2009). Effect of phenolic acids on glucose and organic acid metabolism by lactic acid bacteria from wine. *Food Microbiol.* 26, 409–414. doi: 10.1016/j.fm.2009.01.006

Cogan, T. M. (1981). Constitutive nature of the enzymes of citrate metabolism in *Streptococcus lactis* subsp. *diacetylactis*. *J. Dairy Res.* 48, 489–495. doi: 10.1017/S002202990002197X

Contreras, A., Ribbeck, M., Gutiérrez, G. D., Cañon, P. M., Mendoza, S. N., and Agosin, E. (2018). Mapping the physiological response of *Oenococcus oeni* to ethanol stress using an extended genome-scale metabolic model. *Front. Microbiol.* 9:291. doi: 10.3389/fmicb.2018.00291

Crow, V. L. (1990). Properties of 2,3-butanediol dehydrogenases from *Lactococcus lactis* subsp. *lactis* in relation to citrate fermentation. *Appl. Environ. Microbiol.* 56, 1656–1665. doi: 10.1128/aem.56.6.1656-1665.1990

de Felipe, F. L., Magni, C., de Mendoza, D., and López, P. (1994). Citrate utilization gene cluster of the *Lactococcus lactis* biovar diacetylactis: organization and regulation of expression. *Mol. Gen. Genet.* 246, 590–599. doi: 10.1007/BF00298965

Drider, D., Bekal, S., and Prévost, H. (2004). Genetic organization and expression of citrate permease in lactic acid bacteria. *Genet. Mol. Res.* 3, 273–281.

García-Quintáns, N., Blancato, V., Repizo, G., Magni, C., and López, P. (2008). "Citrate metabolism and aroma compound production in lactic acid bacteria" in *Molecular aspects of lactic acid bacteria for traditional and new applications*. eds. Mayo, B.; López, P.; Pérez-Martínez, G. (Kerala, India: Research Signpost), 65–88.

García-Quintáns, N., Magni, C., de Mendoza, D., and López, P. (1998). The citrate transport system of *Lactococcus lactis* subsp. *lactis* biovar diacetylactis is induced by acid stress. *Appl. Environ. Microbiol.* 64, 850–857. doi: 10.1128/AEM.64.3.850-857.1998

Garmyn, D., Monnet, C., Martineau, B., Guzzo, J., Cavin, J.-F., and DiviÃs, C. (1996). Cloning and sequencing of the gene encoding α-acetolactate decarboxylase from *Leuconostoc oenos*. *FEMS Microbiol. Lett.* 145, 445–450. doi: 10.1111/j.1574-6968.1996.tb08614.x

Grandvalet, C., Assad-García, J. S., Chu-Ky, S., Tollot, M., Guzzo, J., Gresti, J., et al. (2008). Changes in membrane lipid composition in ethanol- and acid-adapted *Oenococcus oeni* cells: characterization of the *cfa* gene by heterologous complementation. *Microbiology* 154, 2611–2619. doi: 10.1099/mic.0.2007/016238-0

Gemelas, L., Degraeve, P., and Demarigny, Y. (2014). The citrate metabolism in homo- and heterofermentative LAB: a selective means of becoming dominant over other microorganisms in complex ecosystems. *Food Nutr. Sci.* 5, 953–969. doi: 10.4236/fns.2014.510106

Hugenholtz, J. (1993). Citrate metabolism in lactic acid bacteria. *FEMS Microbiol. Rev.* 12, 165–178. doi: 10.1111/j.1574-6976.1993.tb00017.x

Julliat, F., Eicher, C., Tourti, N., Glaser, P., Cabanel, N., Coulon, J., et al. (2023). Experimental evolution forcing *Oenococcus oeni* acid tolerance highlights critical role of the citrate locus. *Res. Microbiol.* 174:104048. doi: 10.1016/j.resmic.2023.104048

Kandler, O. (1983). Carbohydrate metabolism in lactic acid bacteria. *Antonie Van Leeuwenhoek* 49, 209–224. doi: 10.1007/BF00399499

Kang, T. S., Korber, D. R., and Tanaka, T. (2013). Contributions of citrate in redox potential maintenance and ATP production: metabolic pathways and their regulation in *Lactobacillus panis* PM1. *Appl. Microbiol. Biotechnol.* 97, 8693–8703. doi: 10.1007/s00253-013-5108-2

Kim, O. B., Richter, H., Zaunmüller, T., Graf, S., and Unden, G. (2011). Role of secondary transporters and phosphotransferase systems in glucose transport by *Oenococcus oeni*. *J. Bacteriol.* 193, 6902–6911. doi: 10.1128/JB.06038-11

Liu, L., Zhao, H., Peng, S., Wang, T., Su, J., Liang, Y., et al. (2017). Transcriptomic analysis of *Oenococcus oeni* SD-2a response to acid shock by RNA-Seq. *Front. Microbiol.* 8:1586. doi: 10.3389/fmicb.2017.01586

Lolkema, J. S., Poolman, B., and Konings, W. N. (1995). Role of scalar protons in metabolic energy generation in lactic acid bacteria. *J. Bioenerg. Biomembr.* 27, 467–473. doi: 10.1007/BF02110009

Magni, C., de Felipe, F. L., Sesma, F., López, P., and de Mendoza, D. (1994). Citrate transport in *Lactococcus lactis* biovar diacetylactis: expression of the plasmid-borne citrate permease P. *FEMS Microbiol. Lett.* 118, 75–82. doi: 10.1111/j.1574-6968.1994.tb06806.x

Magni, C., de Mendoza, D., Konings, W. N., and Lolkema, J. S. (1999). Mechanism of citrate metabolism in *Lactococcus lactis*: resistance against lactate toxicity at low pH. *J. Bacteriol.* 181, 1451–1457. doi: 10.1128/JB.181.5.1451-1457.1999

Magni, C., López, P., and Mendoza, D. (1996). The properties of citrate transport catalyzed by CitP of *Lactococcus lactis* ssp. *lactis* biovar diacetylactis. *FEMS Microbiol. Lett.* 142, 265–269. doi: 10.1111/j.1574-6968.1996.tb08441.x

Maicas, S., Ferrer, S., and Pardo, I. (2002). NAD(P)H regeneration is the key for heterolactic fermentation of hexoses in *Oenococcus oeni*. *Microbiology* 148, 325–332. doi: 10.1099/00221287-148-1-325

Margalef-Català, M., Araque, I., Bordons, A., Reguant, C., and Bautista-Gallego, J. (2016). Transcriptomic and proteomic analysis of *Oenococcus oeni* adaptation to wine stress conditions. *Front. Microbiol.* 7:1554. doi: 10.3389/fmicb.2016.01554

Martell, A. E., and Smith, R. M. (1982). *Critical stability constants: First supplement*. Boston, MA: Springer US.

Martin, M. G., Magni, C., de Mendoza, D., and López, P. (2005). CitI, a transcription factor involved in regulation of citrate metabolism in lactic acid Bacteria. *J. Bacteriol.* 187, 5146–5155. doi: 10.1128/JB.187.15.5146-5155.2005

Martín, M., Magni, C., López, P., and de Mendoza, D. (2000). Transcriptional control of the citrate-inducible *citMCDEFGRP* operon, encoding genes involved in citrate fermentation in *Leuconostoc paramesenteroides*. *J. Bacteriol.* 182, 3904–3912. doi: 10.1128/JB.182.14.3904-3912.2000

Martín, M. G., Sender, P. D., Peirú, S., de Mendoza, D., and Magni, C. (2004). Acid-inducible transcription of the operon encoding the citrate lyase complex of *Lactococcus lactis* biovar diacetylactis CRL264. *J. Bacteriol.* 186, 5649–5660. doi: 10.1128/JB.186.17.5649-5660.2004

Marty-Tesset, C., Posthuma, C., Lolkema, J. S., Schmitt, P., Divies, C., and Konings, W. N. (1996). Proton motive force generation by citrolactic fermentation in *Leuconostoc mesenteroides*. *J. Bacteriol.* 178, 2178–2185. doi: 10.1128/jb.178.8.2178-2185.1996

McKay, L. L., and Baldwin, K. A. (1974). Altered metabolism in a *Streptococcus lactis* C2 mutant deficient in lactic dehydrogenase. *J. Dairy Sci.* 57, 181–186. doi: 10.3168/jds.S0022-0302(74)84857-5

McKay, L. L., and Baldwin, K. A. (1990). Applications for biotechnology: present and future improvements in lactic acid bacteria. *FEMS Microbiol. Lett.* 87, 3–14. doi: 10.1111/j.1574-6968.1990.tb04876.x

Mills, D. A., Rawsthorne, H., Parker, C., Tamir, D., and Makarova, K. (2005). Genomic analysis of *Oenococcus oeni* PSU-1 and its relevance to winemaking. *FEMS Microbiol. Rev.* 29, 465–475. doi: 10.1016/j.fmrre.2005.04.011

Mink, R., Kölling, R., Sommer, S., Schmarr, H.-G., and Scharfenberger-Schmeer, M. (2015). Diacetyl formation by *Oenococcus oeni* during winemaking induced by exogenous pyruvate. *Am. J. Enol. Vitic.* 66, 85–90. doi: 10.5344/ajev.2014.14056

Mink, R., Sommer, S., Kölling, R., Schmarr, H.-G., and Scharfenberger-Schmeer, M. (2014). Time course of diacetyl formation during vinification with *Saccharomyces cerevisiae* and *Oenococcus oeni* co-cultivation: diacetyl formation during vinification. *Aust. J. Grape Wine Res.* 20, 194–198. doi: 10.1111/ajgw.12076

Monnet, C., Aymes, F., and Corrieu, G. (2000). Diacetyl and α-acetolactate overproduction by *Lactococcus lactis* subsp. *lactis* biovar diacetylactis mutants that are deficient in α-acetolactate decarboxylase and have a low lactate dehydrogenase activity. *Appl. Environ. Microbiol.* 66, 5518–5520. doi: 10.1128/AEM.66.12.5518-5520.2000

Mortera, P., Pudlik, A., Magni, C., Alarcón, S., and Lolkema, J. S. (2013). Ca^{2+}−citrate uptake and metabolism in *Lactobacillus casei* ATCC 334. *Appl. Environ. Microbiol.* 79, 4603–4612. doi: 10.1128/AEM.00925-13

Nielsen, J. C., and Richelieu, M. (1998). Control of flavor development in wine during and after malolactic fermentation by *Oenococcus oeni*. *Appl. Environ. Microbiol.* 65, 740–745. doi: 10.1128/AEM.65.2.740-745.1999

Olguín, N., Bordons, A., and Reguant, C. (2009). Influence of ethanol and pH on the gene expression of the citrate pathway in *Oenococcus oeni*. *Food Microbiol.* 26, 197–203. doi: 10.1016/j.fm.2008.09.004

Olguín, N., Bordons, A., and Reguant, C. (2010). Multigenic expression analysis as an approach to understanding the behaviour of *Oenococcus oeni* in wine-like conditions. *Int. J. Food Microbiol.* 144, 88–95. doi: 10.1016/j.ijfoodmicro.2010.08.032

Poolman, B. (1993). Energy transduction in lactic acid bacteria. *FEMS Microbiol. Rev.* 12, 125–147. doi: 10.1111/j.1574-6976.1993.tb00015.x

Poolman, B., Molenaar, D., Smid, E. J., Ubbink, T., Abee, T., Renault, P. P., et al. (1991). Malolactic fermentation: electrogenic malate uptake and malate/lactate antiport generate metabolic energy. *J. Bacteriol.* 173, 6030–6037. doi: 10.1128/jb.173.19.6030-6037.1991

Pretorius, N., Engelbrecht, L., and Du Toit, M. (2019). Influence of sugars and pH on the citrate metabolism of different lactic acid bacteria strains in a synthetic wine matrix. *J. Appl. Microbiol.* 127, 1490–1500. doi: 10.1111/jam.14401

Pudlik, A. M., and Lolkema, J. S. (2011a). Citrate uptake in exchange with intermediates in the citrate metabolic pathway in *Lactococcus lactis* IL1403. *J. Bacteriol.* 193, 706–714. doi: 10.1128/JB.01171-10

Pudlik, A. M., and Lolkema, J. S. (2011b). Mechanism of citrate metabolism by an oxaloacetate decarboxylase-deficient mutant of *Lactococcus lactis* IL1403. *J. Bacteriol.* 193, 4049–4056. doi: 10.1128/JB.05012-11

Qi, Y., Wang, H., Chen, X., Wei, G., Tao, S., and Fan, M. (2021). Altered metabolic strategies: elaborate mechanisms adopted by *Oenococcus oeni* in response to acid stress. *J. Agric. Food Chem.* 69, 2906–2918. doi: 10.1021/acs.jafc.0c07599

Ramos, A., Poolman, B., Santos, H., Lolkema, J. S., and Konings, W. N. (1994). Uniport of anionic citrate and proton consumption in citrate metabolism generates a proton motive force in *Leuconostoc oenos*. *J. Bacteriol.* 176, 4899–4905. doi: 10.1128/jb.176.16.4899-4905.1994

Ramos, A., and Santos, H. (1996). Citrate and sugar cofermentation in *Leuconostoc oenos*, a 13C nuclear magnetic resonance study. *Appl. Environ. Microbiol.* 62, 2577–2585. doi: 10.1128/aem.62.7.2577-2585.1996

Repizo, G. D., Blancato, V. S., Mortera, P., Lolkema, J. S., and Magni, C. (2013). Biochemical and genetic characterization of the *Enterococcus faecalis* oxaloacetate decarboxylase complex. *Appl. Environ. Microbiol.* 79, 2882–2890. doi: 10.1128/AEM.03980-12

Richter, H., Hamann, I., and Unden, G. (2003). Use of the mannitol pathway in fructose fermentation of *Oenococcus oeni* due to limiting redox regeneration capacity of the ethanol pathway. *Arch. Microbiol.* 179, 227–233. doi: 10.1007/s00203-003-0519-6

Rozès, N., Arola, L., and Bordons, A. (2003). Effect of phenolic compounds on the co-metabolism of citric acid and sugars by *Oenococcus oeni* from wine. *Lett. Appl. Microbiol.* 36, 337–341. doi: 10.1046/j.1472-765X.2003.01323.x

Salou, P., Loubiere, P., and Pareilleux, A. (1994). Growth and energetics of *Leuconostoc oenos* during cometabolism of glucose with citrate or fructose. *Appl. Environ. Microbiol.* 60, 1459–1466. doi: 10.1128/AEM.60.5.1459-1466.1994

Salvetti, E., Fondi, M., Fani, R., Torriani, S., and Felis, G. E. (2013). Evolution of lactic acid bacteria in the order *Lactobacillales* as depicted by analysis of glycolysis and pentose phosphate pathways. *Syst. Appl. Microbiol.* 36, 291–305. doi: 10.1016/j.syapm.2013.03.009

Sánchez, C., Neves, A. R., Cavalheiro, J., dos Santos, M. M., García-Quintáns, N., López, P., et al. (2008). Contribution of citrate metabolism to the growth of *Lactococcus lactis* CRL264 at low pH. *Appl. Environ. Microbiol.* 74, 1136–1144. doi: 10.1128/AEM.01061-07

Schneider, K., Dimroth, P., and Bott, M. (2000). Biosynthesis of the prosthetic group of citrate lyase. *Biochemistry* 39, 9438–9450. doi: 10.1021/bi000401r

Sender, P. D., Martín, M. G., Peirú, S., and Magni, C. (2004). Characterization of an oxaloacetate decarboxylase that belongs to the malic enzyme family. *FEBS Lett.* 570, 217–222. doi: 10.1016/j.febslet.2004.06.038

Snoep, J. L., Teixeira de Mattos, M. J., Starrenburg, M. J., and Hugenholtz, J. (1992). Isolation, characterization, and physiological role of the pyruvate dehydrogenase complex and alpha-acetolactate synthase of *Lactococcus lactis* subsp. *lactis* bv. Diacetylactis. *J. Bacteriol.* 174, 4838–4841. doi: 10.1128/jb.174.14.4838-4841.1992

Starrenburg, M. J. C., and Hugenholtz, J. (1991). Citrate fermentation by *Lactococcus* and *Leuconostoc* spp. *Appl. Environ. Microbiol.* 57, 3535–3540. doi: 10.1128/aem.57.12.3535-3540.1991

Sternes, P. R., Costello, P. J., Chambers, P. J., Bartowsky, E. J., and Borneman, A. R. (2017). Whole transcriptome RNAseq analysis of *Oenococcus oeni* reveals distinct intra-specific expression patterns during malolactic fermentation, including genes involved in diacetyl metabolism. *Int. J. Food Microbiol.* 257, 216–224. doi: 10.1016/j.ijfoodmicro.2017.06.024

Tourdot-Maréchal, R., Gaboriau, D., Beney, L., and Diviès, C. (2000). Membrane fluidity of stressed cells of *Oenococcus oeni*. *Int. J. Food Microbiol.* 55, 269–273. doi: 10.1016/S0168-1605(00)00202-6

Unden, G., and Zaunmüller, T. (2009). "Metabolism of sugars and organic acids by lactic acid Bacteria from wine and must" in *Biology of microorganisms on grapes, in must and in wine*. eds. H. König, G. Unden and J. Fröhlich (Berlin, Heidelberg: Springer Berlin Heidelberg), 135–147.

Viljakainen, S. K., and Laakso, S. V. (2000). The use of malolactic *Oenococcus oeni* (ATCC 39401) for deacidification of media containing glucose, malic acid and citric acid. *Eur. Food Res. Technol.* 211, 438–442. doi: 10.1007/s002170000217

Wagner, N., Tran, Q. H., Richter, H., Selzer, P. M., and Unden, G. (2005). Pyruvate fermentation by *Oenococcus oeni* and *Leuconostoc mesenteroides* and role of pyruvate dehydrogenase in anaerobic fermentation. *Appl. Environ. Microbiol.* 71, 4966–4971. doi: 10.1128/AEM.71.9.4966-4971.2005

Yang, X., Zhao, L., Chen, Q., Wang, N., Shi, K., and Liu, S. (2022). Functional verification of the citrate transporter gene in a wine lactic acid bacterium, *Lactiplantibacillus plantarum*. *Front. Bioeng. Biotechnol.* 10:894870. doi: 10.3389/fbioe.2022.894870

Yang, K., Zhu, Y., Qi, Y., Zhang, T., Liu, M., Zhang, J., et al. (2019). Analysis of proteomic responses of freeze-dried *Oenococcus oeni* to access the molecular mechanism of acid acclimation on cell freeze-drying resistance. *Food Chem.* 285, 441–449. doi: 10.1016/j.foodchem.2019.01.120

Zaunmüller, T. (2008). *Identifizierung von Hexosecarriern und Regulation des Phosphoketolasewegs in Oenococcus oeni*. University Johannes Gutenberg-Universität Mainz (Germany) (language = Deutsch).

Zaunmüller, T., Eichert, M., Richter, H., and Unden, G. (2006). Variations in the energy metabolism of biotechnologically relevant heterofermentative lactic acid bacteria during growth on sugars and organic acids. *Appl. Microbiol. Biotechnol.* 72, 421–429. doi: 10.1007/s00253-006-0514-3

Zuljan, F. A., Repizo, G. D., Alarcon, S. H., and Magni, C. (2014). α-Acetolactate synthase of *Lactococcus lactis* contributes to pH homeostasis in acid stress conditions. *Int. J. Food Microbiol.* 188, 99–107. doi: 10.1016/j.ijfoodmicro.2014.07.017

frontiers | Frontiers in Microbiology

TYPE Original Research
PUBLISHED 07 March 2024
DOI 10.3389/fmicb.2024.1335989

OPEN ACCESS

EDITED BY
Maria Filippa Addis,
University of Milan, Italy

REVIEWED BY
Leticia Barrientos,
Autonomous University of Chile, Chile
Jesús Muñoz-Rojas,
Meritorious Autonomous University of Puebla, Mexico

*CORRESPONDENCE
Veronica Godoy-Carter
✉ v.godoycarter@northeastern.edu

RECEIVED 09 November 2023
ACCEPTED 16 February 2024
PUBLISHED 07 March 2024

CITATION
Reverdy A, Hathaway D, Jha J, Michaels G, Sullivan J, McAdoo DD, Riquelme C, Chai Y and Godoy-Carter V (2024) Insights into the diversity and survival strategies of soil bacterial isolates from the Atacama Desert. *Front. Microbiol.* 15:1335989. doi: 10.3389/fmicb.2024.1335989

Insights into the diversity and survival strategies of soil bacterial isolates from the Atacama Desert

Alicyn Reverdy[1], Daniel Hathaway[1], Jessica Jha[1], Gabriel Michaels[1], Jeffrey Sullivan[1], Daniela Diaz McAdoo[2], Carlos Riquelme[2], Yunrong Chai[1] and Veronica Godoy-Carter[1]*

[1]Northeastern University, Boston, MA, United States, [2]Facultad de Ciencias Básicas, Universidad de Antofagasta, Antofagasta, Chile

The Atacama Desert, the driest, with the highest radiation, and one of the most ancient deserts in the world, is a hostile environment for life. We have a collection of 74 unique bacterial isolates after cultivation and confirmation by 16S rRNA gene sequencing. Pigmentation, biofilm formation, antimicrobial production against *Escherichia coli* MG1655 and *Staphylococcus aureus* HG003, and antibiotic resistance were assessed on these isolates. We found that approximately a third of the colonies produced pigments, 80% of isolates formed biofilms, many isolates produce growth inhibiting activities against *E. coli* and/or *S. aureus*, and many were resistant to antibiotics. The functional characterization of these isolates gives us insight into the adaptive bacterial strategies in harsh environments and enables us to learn about their possible use in agriculture, healthcare, or biotechnology.

KEYWORDS

extremophiles, microbial diversity, Atacama Desert, biofilm, antimicrobial production, antibiotic resistance, pigments

Introduction

Extreme environments are challenging for life, yet bacteria have developed strategies for survival. One location in Chile characterized by its extreme environment is the Atacama Desert, located in northern Chile at the border with Bolivia and Argentina spanning about 128,000 km^2. Bound by mountain ranges that prevent precipitation, the Atacama Desert is one of the most ancient and the driest temperate deserts in the world (Rundel and Villagra, 2007; Bull et al., 2018). Described as an extremobiosphere, the hyper-arid Atacama Desert contains a chain of Andean volcanoes, large salt flats, high mineral deposits, and Altiplano lakes (Rundel and Villagra, 2007; Rampelotto, 2013). Ranging between 2,000 and over 5,000 meters above sea level, the region experiences the highest levels of UV radiation in the world (Cordero et al., 2014, 2018) and low levels of oxygen, as well as large temperature fluctuations and extremely low precipitation levels (Rundel and Villagra, 2007; Bull et al., 2018; Cordero et al., 2018). Thus, the Atacama Desert is of increasing interest for understanding the microbial diversity and strategies to survive in extreme conditions including alkaline or acidic pH, temperature variabilities, water stress, and high UV radiation (Bull and Asenjo, 2013; Orellana et al., 2018), conditions that resemble those of other planets (Parro et al., 2011).

Extremophiles are bacteria that adjust to and survive in hostile environments once thought too harsh to sustain life (Rampelotto, 2013). These bacteria are categorized into two types: those that require the extreme condition, and those that tolerate extreme conditions, but can also grow optimally in "standard" conditions (Rampelotto, 2013). To thrive in harsh conditions, extremophiles use a variety of strategies to maintain their communities. These strategies have been extensively reviewed and include accumulation of certain molecules to counteract imbalances produced by the extreme conditions, production of specially designed enzymes and cell membranes, and enhanced DNA-repair mechanisms (Meyer, 2000; Gallardo et al., 2016; Órdenes-Aenishanslins et al., 2016; Narsing Rao et al., 2017; Mandakovic et al., 2020). Other such strategies include biofilm formation and production of inhibitory substances, antimicrobial activities, and pigment production (Hassan and Fridovich, 1980; Meyer, 2000; Hall-Stoodley et al., 2004; Azua-Bustos et al., 2012; Gallardo et al., 2016; Gerardin et al., 2016; Órdenes-Aenishanslins et al., 2016; Narsing Rao et al., 2017; Mandakovic et al., 2020). Biofilm is a community of surface attached bacterial cells encased in a self-produced, protective matrix that primarily consists of protein, exopolysaccharide, and extracellular DNA (Hall-Stoodley et al., 2004; Vlamakis et al., 2013). Biofilms enhance nutrient sharing, cell-cell communication (Hall-Stoodley et al., 2004; Vlamakis et al., 2013), and provide a protective barrier against antimicrobials, UV damage, and other pathogens (Hall-Stoodley et al., 2004; de Carvalho, 2017; Hall and Mah, 2017). As such, biofilm-producing bacteria are one of the leading causes of human and plant pathogenesis, consistent with its role as a bacterial survival strategy (Hall-Stoodley et al., 2004; Vlamakis et al., 2013).

Bacterial production of inhibitory substances is a competitive advantage since it allows the antimicrobial producing bacteria to fend off other colonizers and protect the population from further harm (Gerardin et al., 2016). For this reason, the search for novel antibiotics from environmental isolates is a very active area of research. The hope is to discover antibiotics to use against specific pathogenic bacteria without harming the general microbiome (Azua-Bustos and González-Silva, 2014; Lewis, 2017). Many groups have isolated and identified new compounds produced by *Actinobacteria* from the Atacama Desert, supporting the study of extremophiles for novel antibiotic discovery (Okoro et al., 2009; Rateb et al., 2011a; Santhanam et al., 2012a,b; Undabarrena et al., 2016; Goodfellow et al., 2018). But because bacteria are exposed to antimicrobials produced in their environment, they are apt to develop strategies for surviving these challenges (Ferri et al., 2017; Lewis and Caboni, 2017). Identifying naturally resistant bacteria will provide us in the future with mechanistic models to better understand how bacteria become antibiotic resistant as well as insights into how to combat this rapidly increasing problem. Indeed, antibiotic resistance has created a billion-dollar problem in the healthcare system (Ferri et al., 2017).

Microbial diversity studies from the Atacama Desert have only been published within the last 15 years (Bull et al., 2016). Overall, there is still a large gap in knowledge of the microbial diversity in the Atacama Desert. With better sequencing technology and increased characterization of cultivable isolates, we will gain a more complete view of what and how extremophiles live in their environment. Additionally, investigating which bacterial communities live in different locations is essential for understanding how they contribute to the environmental ecology and drive global dynamics.

Here, we provide a comprehensive picture of the microbial diversity and investigation into the survival strategies of bacteria living in the Atacama Desert. We sampled from 18 locations within the Atacama Desert. Further, we cultivated 74 unique isolates and performed characterization assays to identify pigment production, biofilm formation, production of inhibitory substances, and antibiotic resistance as probable survival mechanisms. In this study we provide insights into bacterial diversity and the strategies that bacteria use to survive in extreme environments.

Results

Locations and environmental sampling

The Atacama Desert exhibits the most extreme environment in Chile (Cordero et al., 2014, 2018; Bull et al., 2018). For this reason, we were curious to see what bacteria were present to identify what strategies they may use to survive in such a harsh environment. During the months of May and June of 2018, we traveled to 18 locations in the Atacama Desert (**Figure 1** and **Supplementary Figure 1**). Each high-altitude location is distinct in its characteristics: fully barren to presence of low grasses and high to low mineral and salt content (**Supplementary Table 1** and **Supplementary Figure 1**).

Specific sampling locations were chosen for their unique characteristics, high altitude, near water, barren, high salinity, etc. At each location, environmental soil samples between 1 and 5 cm were collected. The exact coordinates were recorded at each sampling location (**Supplementary Table 1**). Samples were then processed to cultivate bacterial isolates (**Figure 2**).

Cultivation and isolation of unique isolates

Our next goal for gaining insights into the behavior of bacteria in the Atacama Desert was to cultivate and isolate single bacterial colonies from the samples that we collected. We found that, in general, isolates grew much better on the R2 medium than on the LB or 1:100 LB media plates. This was to be expected because bacteria from these locations are more accustomed to growing in low nutrient environments. We surmised that different colony morphology would be a good way as a first approximation to distinguish one isolate from the other. Therefore, isolates were further purified and examined on solid medium based on visual morphology differences.

Results of the 16S rRNA gene sequencing identified 74 unique isolates out of the 142 purified colonies (52%) across all sample locations (**Supplementary Table 2**). The isolates belonged to 27 unique genera (19%) and closely related to 74 species (52%). Unique was defined as any isolate different to another within a given sample. For example, if two isolates were identified to be *Enterobacter* sp. from one location, but one was from a soil sample and another was from a moss sample, then they were considered unique. However, if two *Enterobacter* sp. isolates from a location

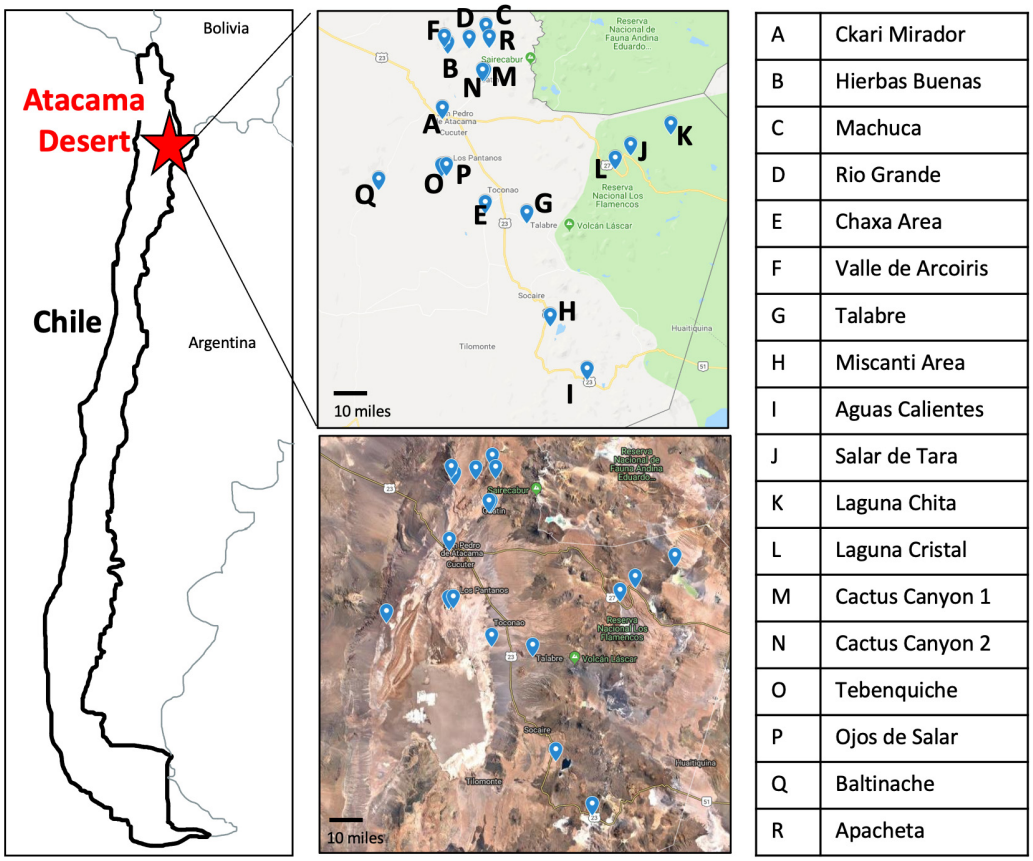

A	Ckari Mirador
B	Hierbas Buenas
C	Machuca
D	Rio Grande
E	Chaxa Area
F	Valle de Arcoiris
G	Talabre
H	Miscanti Area
I	Aguas Calientes
J	Salar de Tara
K	Laguna Chita
L	Laguna Cristal
M	Cactus Canyon 1
N	Cactus Canyon 2
O	Tebenquiche
P	Ojos de Salar
Q	Baltinache
R	Apacheta

FIGURE 1
Map of the 18 sampling locations across the Atacama Desert. Sampling sites have clear geographical distinction as seen by Google Maps imaging. Letter key identifies the name of sampling location labeled on the maps.

were both from a soil sample and both had a percent identification above 97% by 16SrRNA, then they were considered sisters and non-unique. A distribution of the unique and non-unique isolates from the different sampling locations was made using the above definition (**Figure 3**).

Though 16S rRNA is not enough to identify species, 97% was used as the threshold of similarity that an isolate was closely related to a given species, though 98.65% has also been used (Yoon et al., 2017). In our case, any percent identity below 97% indicates that the isolate is likely a novel species, which we may be undercounting. Interestingly, 34% of our isolates had a percent identity below 97%, and 4% of all isolates had a percent identity below 90%. This suggests that we may have at least 48 new species within our collection (**Supplementary Table 2**).

Of all the culturable isolates, the most abundant genus was *Bacillus* sp. Forty-three isolates belonged to this genus and it was found in 13 locations (**Supplementary Table 2**). Bacteria closely related to *Bacillus simplex* were the most abundant among the enriched culturable species, and they were found in 10 locations (**Supplementary Table 2** and **Table 1**). The next most abundant enriched culturable genus was *Arthrobacter*. Fourteen isolates (9.8% of all isolates) were found in 7 locations (**Supplementary Table 2**). These data could mean that *Bacillus* and *Arthrobacter* are non-discriminatory, can live in many diverse locations and are easily culturable.

Together, our data demonstrates success in bacterial cultivability from the extreme environments of the Atacama Desert. These isolates are representatives of where they came from and allow for the characterization of unknown species and identification of whether any of the known closely related species have unique characteristics because they were isolated from an extreme environment.

Pigment producing isolates

We then sought to investigate the capabilities of the Atacama Desert extremophiles we had cultivated, isolated, and closely identified by 16S rRNA. We surmised that by defining certain characteristics of these bacteria, we would gain insights into their strategies for survival in extreme environments. The first easily identifiable characteristic was that 34.5% of our isolates produced pigment (**Figure 4A** for quantification and **Figure 4B** representative isolates), most of which were cell bound. Of these isolates, 69.4% produced a yellow pigment, 26.5% produced an orange pigment, and 4.1% produced a pink pigment. Pigment production by bacteria is thought to be a protective mechanism against UV radiation (Azua-Bustos et al., 2012; Órdenes-Aenishanslins et al., 2016; de Carvalho, 2017; Narsing Rao et al., 2017). Many *Actinobacteria* and *Cyanobacteria* from salt flats and

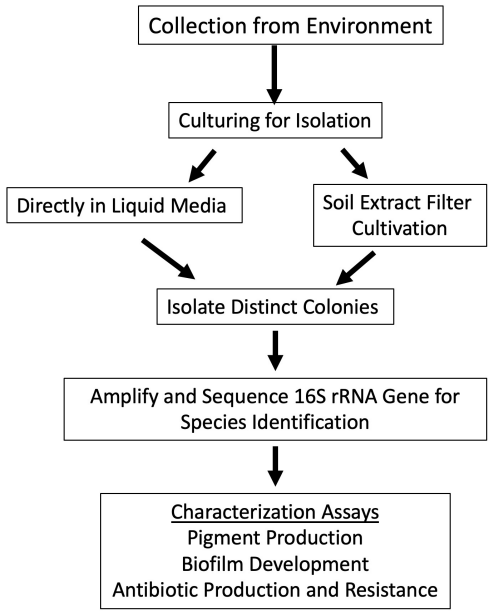

FIGURE 2
Schematic approach used for sample analysis and colony isolation. Samples were collected from locations in **Figure 1**. Samples were cultured to isolate individual bacterial species. This was done by two methods: inoculating the sample directly into culture medium or by scraping concentrated sample from soil extract filter disk and depositing it onto R2 agar plate. Bacterial colony growth was observed, and colonies were isolated until purity. Colony PCR of the 16S rRNA gene was used to identify closely related species of the colony isolates with different morphologies. Colony isolates were then assayed for pigment production, biofilm production, and antimicrobial production and resistance.

hyper-arid locations produce protective pigments (Bull and Asenjo, 2013; Narsing Rao et al., 2017). The Atacama Desert is known for its extreme levels of UV radiation (Demergasso et al., 2010; Cordero et al., 2018). It is plausible that these bacteria produce pigments to protect themselves from the DNA-damaging UV that they are exposed to while living in the Atacama Desert. We attempted to measure the UV resistance of some of our isolates, but it is a difficult endeavor since the pigments are secondary metabolites produced late in stationary phase. In fact, most of the isolates tested were UV-sensitive when growing exponentially compared to *Escherichia coli* (data not shown). Pigment isolation would allow determination of its functional role.

Prominent biofilm formation is correlated to more extreme environments

To assess whether biofilm formation was used as a survival strategy in the extremophiles of our collection, we performed biofilm assays. Briefly, cells were inoculated into R2 medium and incubated statically for 5 days at 25°C in glass tubes. Using a standard crystal violet (CV) assay as indicated in Materials and methods (O'Toole, 2011). Eighty percent of the142 isolates assayed under our conditions, attached to surfaces (**Figure 5**). This was determined by any value greater or equal to 0.05 AU, a value in which CV-stained cells were visible on the glass. The isolates closely related to *Bacillus simplex* exhibited the greatest biofilm production.

Also, of interest were the isolates that produced a pellicle or clumped biofilm. Isolates that produced a visible pellicle, a biofilm formed at the air-liquid interface (Vlamakis et al., 2013), were KMK, KMM, KME, APH, AC2F, and STB (**Supplementary Figure 2**). Additionally, KMK, RVC, AC2F, and APH produced a visible clumped biofilm while shaking. These are types of biofilms that might not be accurately quantified using the CV assay but are important examples of biofilm producers.

When comparing the amount of biofilm produced by isolates from the different locations, the ones from the most extreme environments were more likely to form biofilms. The bacteria inhabiting Laguna Chita had the most prominent biofilms; they attached to surfaces well. The location with the greatest number of biofilm formers was Salar de Tara (**Figure 5**). These locations are next to each other, are located at high elevation (> 4,200 meters above sea level), and are barren (**Supplementary Figure 1** and **Supplementary Table 1**). The bacteria from these locations may use biofilm to facilitate nutrient sharing, protect against the high UV radiation, and enhance colonization. It is also of note that three isolates from Ckari Mirador produced pellicles/clumped biofilms. This location is exceptionally dry within the Atacama Desert and biofilm may be used by these isolates to enhance their survival in this extreme environment.

Together, our data indicate that biofilm production is a strategy that bacteria use to survive in the extreme environments found in the Atacama Desert.

Extremophiles produce growth inhibitors against Gram-positive and Gram-negative bacteria

To identify isolates that produced growth inhibitors or antimicrobials, we performed a zone of inhibition assay against Gram-positive *Staphylococcus aureus* HG003 and Gram-negative *Escherichia coli* MG1655 as representatives of their respective groups. Isolates were grown shaking until late stationary phase and then spotted onto lawns of the target bacteria. Plates were incubated at 30°C, and the zones of inhibitions were measured after one and four days of growth.

There were two types of inhibition phenomena: haloing and clearing (**Figure 6A**). Haloing was when there was a visible ring of inhibition, however the target bacteria still grew. Most of the isolates demonstrated this phenomenon. Possible explanations for this haloing could be a result of inhibition then gained resistance by the target bacteria, or due to different growth rates where the test isolate grew after the target bacterium resulting in a delayed killing. Regardless, the haloing demonstrated an inhibition of the target bacterium by the test isolate. Further analysis of the resistant isolates would provide insights to any mechanism of resistance if the growth inhibiting compound were an antibiotic. The other phenomenon, clearing, suggests the produced antimicrobial is more potent. The isolates that demonstrated clearing are indicated by stars or pound signs

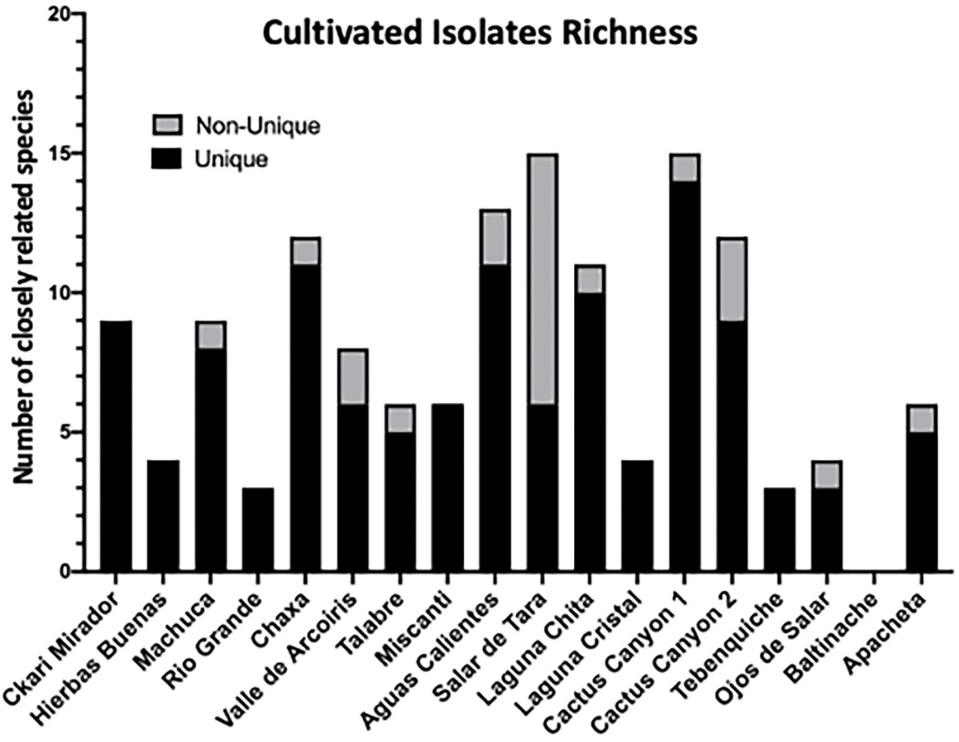

FIGURE 3
Among cultivable bacteria 74 unique colony species were isolated and identified. 142 distinct isolates based on colony morphology were isolated including 74 unique bacterial species. Isolates were cultured from environmental samples as described in Materials and methods. The strain identity of colony isolates with different morphologies were distinguished based on the 16S rRNA gene of each colony isolate amplified via PCR and sequenced. The 16S rRNA gene sequence was aligned to the NCBI database to identify colony genus, and the closest related species and/or strain using 97% identity as species separation and confidence. Distribution of isolates across sampling locations. Unique is defined as a bacterial isolates within the same location that has no other representative. Non-unique refers to the same closely related species found in different samples from the same location.

(Figure 6A, B). Results show that many isolates produced growth inhibiting compounds against *S. aureus* and *E. coli* (Figure 6B). 16 isolates inhibited the growth of *S. aureus*, while 13 exhibited a challenge to *E. coli*. A loss of inhibition after 4 days showed that the target bacteria grew resistant to the challenge.

Of the isolates, TQA (closely related to *Pseudomonas koreensis*, ID: 98.32), TQB (closely related to *Pseudomonas azotoformans*, ID: 99.26%) and 710$AA (closely related to *Pseudomonas brassicacearum*, ID: 99.7) produced the most potent inhibitory compounds against both *S. aureus* and *E. coli* (Figure 6). This was seen by large clearing zones of inhibition (Figure 6A). Of more interest are isolates 316*CB$ (closely related to *Hafnia alvei*, ID: 98.1%), and 312*AB$ (closely related to *Hafnia alvei*, ID: 99.9%), both of which demonstrated killing against only the Gram-negative *E. coli* (Figure 6B). The identification of Gram-negative-specific antimicrobial compounds are of particular interest for drug discovery groups (Lewis, 2017).

Together, these data demonstrate that the chosen isolates produced growth inhibitory substances against *S. aureus* and *E. coli*. Antimicrobial production is an expected strategy that provides competitive advantage in an extreme environment.

Extremophiles are naturally resistant to commercial antibiotics

Coming from remote environmental samples, none of these isolates have been exposed to commercially available antibiotics. Many of these isolates were also identified as genera that have developed multi-drug resistances (Supplementary Table 2; Santajit and Indrawattana, 2016). Such examples include *Enterobacter* sp., *Acinetobacter* sp., and *Pseudomonas* sp (Supplementary Table 2). We were curious as to whether any of the isolates were inherently resistant to commercial antibiotics; thus, we performed a minimum inhibitory concentration (MIC) assay using antibiotics with different mechanisms of action. The MIC was measured for the same 21 isolates from Supplementary Table 3 used in the antimicrobial production assay. We determined the MIC for ampicillin (targets cell wall), vancomycin (targets cell wall), rifampicin (targets RNA polymerase), kanamycin (targets 30S ribosomal subunit), tetracycline (targets 30S ribosomal subunit), spectinomycin (targets 30S ribosomal subunit), and chloramphenicol (targets 50S ribosomal subunit) at a range of 200 to 0.2 μg/mL (Lewis, 2013). The MIC was defined as the lowest concentration of antibiotic that completely inhibited growth.

TABLE 1 Cultivated isolates.

Closely related species	ID	Location	References
Aeromonas aquatica strain MX16A	98.00	Laguna Chita	Beaz-Hidalgo et al., 2015
Agrobacterium rhizogenes strain K599	89.57	Valle de Arcoiris	Valdes Franco et al., 2016
Aeromonas sp. AU20	93.19	Salar de Tara	Anda et al., 2015
Bacillus atrophaeus SQA-17	96.39, 99.05, 100	Ckari Mirador, Cactus Canyon 2, Laguna Chita	
Bacillus atrophaeus strain GQJK17	97.99, 98.03, 98.68	Valle del Arcoiris, Laguna Chita, Chaxa,	Ma et al., 2018
Bacillus megaterium strain JX285	100	Miscanti	Huang et al., 2019
Bacillus mycoides strain Gnyt1	99.71	Miscanti	Xiaomei and Yao, 2020
Bacillus simplex NBRC 15720 = DSM 1321	99.03, 98.19, 99.61, 99.13, 98.33, 88.70, 95.77 99.28, 94.67, 96.15, 98.61 98.49, 97.48, 99.01, 98.49, 98.31, 98.60, 95.69, 87.26, 94.37, 97.75, 99.81	Talabre, Cactus Canyon, Salar de Tara, Cactus Canyon 1, Laguna Chita, Rio Grande, Valle del Arcoiris, Aguas Calientes, Ckari Mirador, Miscanti	Gutierrez-Luna et al., 2020
Bacillus sp. X1(2014)	97.31	Miscanti	
Bacillus subtilis strain DKU_NT_03	99.99, 99.81, 95.90, 97.22, 96.50	Talabre, Aguas Calientes, Salar de Tara, Cactus Canyon 1, Laguna Cristal	Gutierrez-Luna et al., 2020
Bacillus subtilis strain SG6	97.20	Cactus Canyon 1	Zhao et al., 2014
Bacillus thuringiensis strain c25	97.93	Ojos de Salar	Shrestha et al., 2015
Bacillus thuringiensis strain SCG04-02	97.93	Ojos de Salar	Fu et al., 2017
Brevundimonas sp. LM2	96.79, 95.91	Chaxa, Cactus Canyon 1	Chen et al., 2020
Enterobacter sp.	98.93, 93.82, 98.54, 98.62, 98.53, 98.66, 99.90, 99.90	Cactus Canyon 1, Cactus Canyon 2, Tebenquiche, Laguna Cristal, Laguna Chita, Chaxa	Mafakheri et al., 2021
Janthinobacterium agaricidamnosum NBRC102515 = DSM 9628	96.58	Ckari Mirador	Graupner et al., 2015
Microbacterium oryzae strain MB-10	99.90	Cactus Canyon 2	Deb and Das, 2020
Planococcus rifietoensis strain M8	98.14, 97.01	Cactus Canyon 2, Chaxa	See-Too et al., 2016b
Pseudomonas azotoformans strain S4	97.15, 99.26	Tebenquiche, Rio Grande	Fang et al., 2016
Pseudomonas brassicacearum strain L13-6-12	99.70	Hierbas Buenas	Zachow et al., 2017
Pseudomonas fluorescens NCIMB 11764	87.03	Cactus Canyon 1	Silby et al., 2009
Pseudomonas koreensis strain D26	98.32	Tebenquiche	Lin et al., 2016
Pseudomonas protegens strain FDAARGOS_307	99.90	Cactus Canyon 1	Ramette et al., 2011
Pseudomonas sp. L10.10	97.40	Laguna Chita	See-Too et al., 2016a
Pseudomonas sp. M30-35	96.10	Laguna Chita	He et al., 2018
Rahnella aquatilis strain HX2	99.32	Machuca	Guo et al., 2012
Serratia fonticola strain GS2	96.52	Chaxa	Jung et al., 2017
Serratia liquefaciens strain FDAARGOS_125	99.80	Laguna Chita	Caneschi et al., 2019

Results demonstrated that many isolates had high MICs to multiple antibiotics (**Figure 6C** and **Supplementary Table 4**). High MIC suggested resistance while low MIC suggested susceptibility to a particular antibiotic. Overall, the isolates had the highest MICs to ampicillin and the lowest MICs to kanamycin (**Figure 6C** and **Supplementary Table 4**). The isolates with the highest MICs were TQB (closely related to *Pseudomonas azotoformans*: 99.26%) and MA2B (*Microbacterium* sp. ID: 99.2%) (**Figure 6C** and **Supplementary Table 4**). For TQB, its lowest MIC was 6.25 μg/mL against kanamycin and tetracycline (**Supplementary Table 4**). TQB also had growth at 200 μg/mL antibiotic concentration for four antibiotics (ampicillin, vancomycin, spectinomycin, and chloramphenicol) indicating it was not susceptible to these antibiotics at all (**Supplementary Table 4**). For MA2B, its lowest MIC was 12.5 μg/mL against vancomycin (**Supplementary Table 4**). The most susceptible isolate

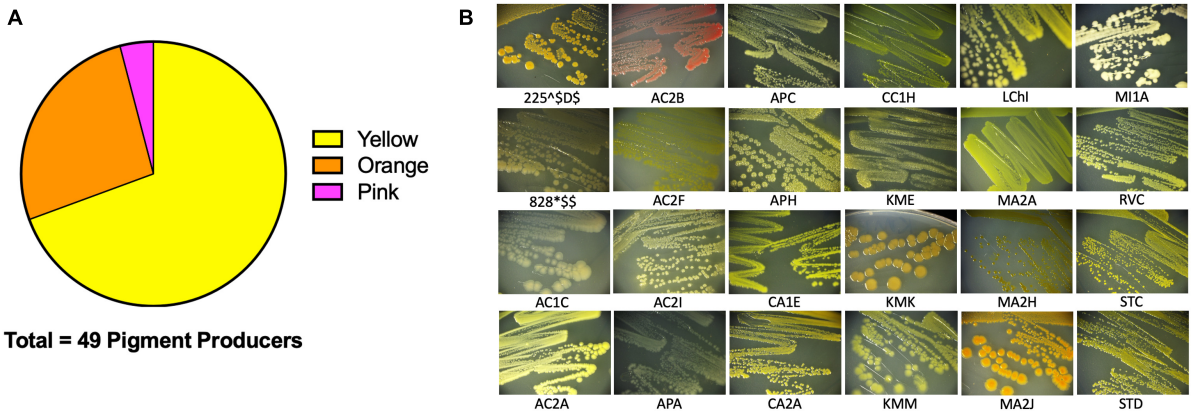

FIGURE 4
Extremophiles produce pigment. Pigment production was observed in colonies over 7 days. **(A)** 49/142 colony isolates produce pigments. **(B)** Sample images of pigmented colonies after 7 days of growth on R2 minimal medium agar at 25°C.

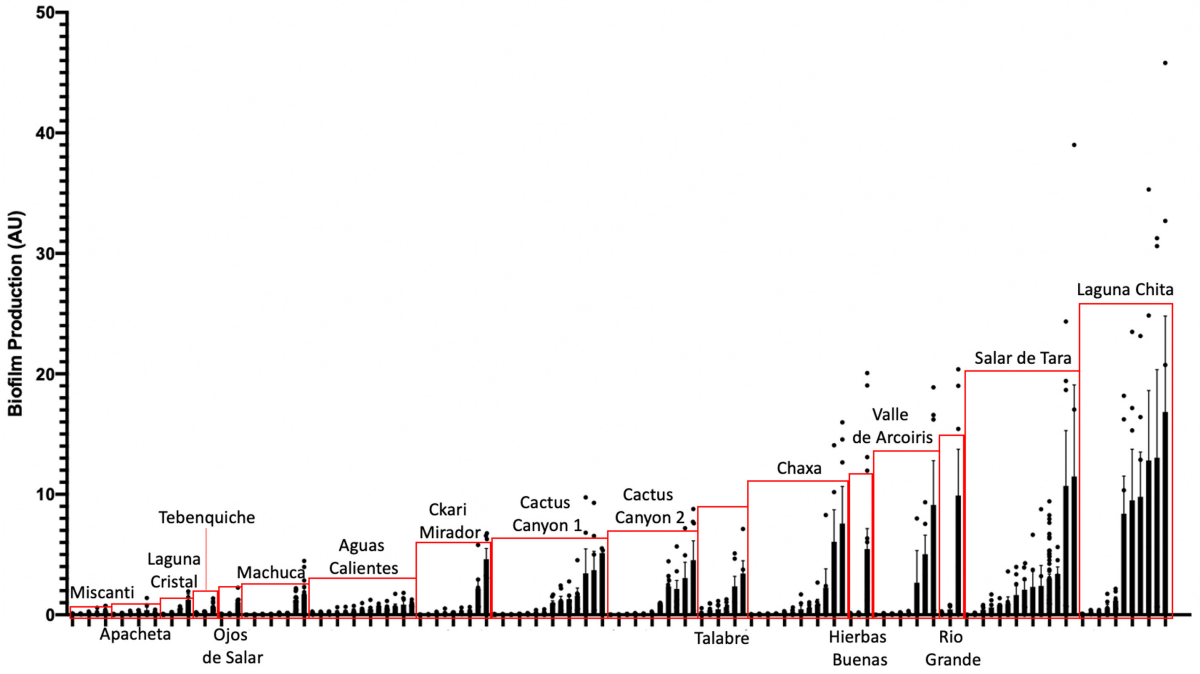

FIGURE 5
Extremophiles produce biofilm in more extreme environments. Colonies were assayed for biofilm formation by inoculating cells into R2 liquid medium in glass culture tubes. Cultures were grown statically at 25°C and quantified after 5 days of growth using the crystal violet (CV) staining assay (O'Toole, 2011). Biofilms were stained with 0.1% CV. Solubilized CV was then quantified using a spectrophotometer at OD_{595}. OD_{595} was standardized by cell count (OD_{600}) to quantify the amount of biofilm produced per cell (AU). Bars represent the average of two or more independent experiments for each individual isolate, dots represent biological replicates ($n \geq 6$), and error bars represent standard deviation. Red boxes highlight isolates from the same location.

was MA2J (closely related to *Exiguobacterium antarcticum* B7 ID: 98.7%) (Figure 6C and Supplementary Table 4). Its highest MIC was 6.25 μg/mL against spectinomycin and chloramphenicol (Supplementary Table 4). What gives us confidence for this assay is that isolates from the same genera had the same MIC patterning (Figure 6C). Examples include the *Enterobacter* sp. isolates (727**B*, CC2A, LAD, TQC, LCrF, LChC, CA1D, and 602^A) and the *Pseudomonas* sp. isolates (TQA, TQB, and 710$$A).

Together, these data demonstrate that isolates from remote extreme environments with little to no encounter with commercial antibiotics, have multidrug resistances.

Discussion

In this study, we provide insights into the diversity and functionality of culturable environmental isolates from Atacama

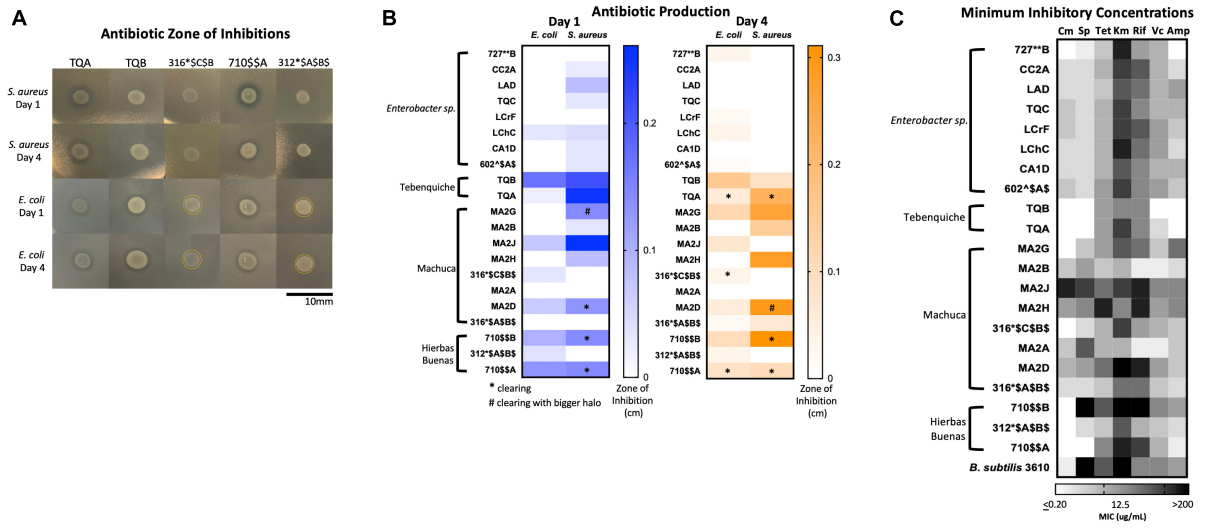

FIGURE 6
Extremophiles produce antimicrobials against *S. aureus* and *E. coli* and are naturally resistant to commercial antibiotics. **(A)** Images of select isolates demonstrating antimicrobial production. Clearing can be seen in isolates TQA, TQB, and 710$$A. Yellow circle delineates haloing. **(B)** Antimicrobial production assay demonstrated by a challenge assay in which a select set of isolates inhibit the growth of either *S. aureus* or *E. coli* or both. The zones of inhibition were measured after one and 4 days of incubation at 25°C. Stars indicate clearing and pound signs indicate clearing with a larger halo. Heatmap represents the average of three independent experiments each including three biological replicates (n = 9). **(C)** Minimum inhibition concentration (MIC) assay of select isolates demonstrated resistance to commercial antibiotics (Cm, chloramphenicol; Sp, spectinomycin; Tet, tetracycline; Km, kanamycin; Rif, rifampicin; Vc, vancomycin; Amp, ampicillin). In a 96-well plate, a select set of isolates were subjected to antibiotic challenge in 2-fold dilution in a range 200–0.2 μg/mL. Cells were inoculated into R2 medium and grown statically at room temperature for 3 days. Growth was quantified by plate reader at OD600. The MIC was determined as the lowest concentration at which cell growth was completely inhibited. Heatmap represents the average MIC across three independent experiments in singlet (n = 3).

Desert (**Figures 1–4** and **Supplementary Figures 1, 2**). We identified the dominant phyla to be *Actinobacteria* and *Proteobacteria* in Atacama soils (**Supplementary Table 2**). A culture-dependent strategy and cultivated bacteria from the collected samples led to the isolation of 74/142 unique species (**Supplementary Table 2** and **Table 1**).

Before this study, no one as far as we could find had reported the presence of bacteria in any of our locations except for Chaxa, Tebenquiche, and Miscanti (Demergasso et al., 2004, 2008; Dorador et al., 2018). These studies, however, were on water samples. Here, we add to the collection of data that others have provided to increase the understanding of the microbial diversity in new locations within the Atacama Desert.

The isolates that we cultivated must be extremotolerant bacteria; those that can tolerate extreme conditions but can also successfully grow under "normal" physiological conditions (Rampelotto, 2013). Being that we cultivated under the latter conditions, it is highly probable that other bacteria can be cultivated from these samples using more selective conditions.

Many previous studies lacked research on bacteria physiology (Demergasso et al., 2004, 2008, 2010; Drees et al., 2006; Dorador et al., 2010, 2018; Bull et al., 2016; Mandakovic et al., 2018a,b; Schulze-Makuch et al., 2018; Uritskiy et al., 2019). Being that a third of our isolates produced a pigment, there is strong likelihood that it is made for protection in its environment (**Figure 4**). One example of pigments used for survival is the production of pyocyanin and pyoverdine from *Pseudomonas* sp. Pyocyanin is a blue-green pigment produced by *Pseudomonas* sp. that acts an antimicrobial, but also has been shown to have siderophore activity to uptake environmental iron (Hassan and Fridovich, 1980; Jayaseelan et al., 2014). Pyoverdine, is a yellow-green pigment and siderophore secreted by *Pseudomonas* sp. during iron starvation as a way to sequester iron(III) (Meyer, 2000). Indeed, the identified *Pseudomonas* genera isolates were seen to produce a secreted yellow pigment as exemplified by TQA, TQB, RGA, APA, and 710$$A (data not shown). Other groups have also seen that *Actinobacteria* and *Cyanobacteria* from the Atacama Desert produce melanins, scytonemin, carotenoids, chlorophylls, and other pigments (Azua-Bustos et al., 2012; Bull and Asenjo, 2013).

To date, no one has shown biofilm production data of microbial isolates from the Atacama Desert. 80% of our isolates produced a biofilm and there were many distinct types of biofilms produced (**Figure 5** and **Supplementary Figure 2**). The bacteria from these locations may use biofilm as a survival strategy to facilitate nutrient sharing, protect against the high UV index, and enhance colonization. The two locations of high biofilm production, Laguna Chita and Salar de Tara, were devoid of plant life. The presence of biofilm-producing bacteria may also provide plant-promoting effects to the few low grasses that do live in the area.

Our study showed that some isolates produce antimicrobials against Gram-positive *S. aureus* and Gram-negative *E. coli* (**Figure 6**). This was not surprising because the most dominant phylum was *Actinobacteria* (35.9%) and because many other groups have been working with these antibiotic producers (Okoro et al., 2009; Rateb et al., 2011a,b; Santhanam et al., 2012a,b; Undabarrena et al., 2016; Goodfellow et al., 2018).

Lastly, we found that many isolates had high MICs against commercially produced antibiotics indicating inherent antibiotic resistance (**Figure 6C**). Being from remote environments, these isolates have theoretically not encounter commercial antibiotics

until now. Because they are resistant to them, they must have intrinsic strategies to resist the antibiotic challenge. We believe this resistance has developed by three possible means: 1. they face antibiotic challenge in their environments, 2. mutagenesis because of being subjected to high levels of UV radiation, and 3. they are extremophiles and have strategies to withstand exogenous stress.

Many commercially available antibiotics were originally discovered to be produced by soil bacteria. Vancomycin, for example, was discovered from soil isolate *Streptomyces orientalis* (Levine, 2006). It is, therefore, not surprising that our isolates had relatively high MICs to this antibiotic (**Figure 6C** and **Supplementary Table 4**) since they are isolated form the soil. Environmental bacteria use antimicrobial production as a competitive advantage, and they must develop ways to resist these challenges and outcompete the bacteria producing them. Our isolates were most likely exposed to similar type of antimicrobials in the soil and therefore, have developed resistance mechanisms that enable their growth when challenged with commercial antibiotics (Hibbing et al., 2010).

Mutagenesis is the result of a variety of genomic insults coming from diverse sources including reactive oxygen species, methylating agents, or ionizing radiation (Chatterjee and Walker, 2017). UV radiation is one of the most damaging abiotic factors to the cell that directly damages the DNA by formation of thymidine dimers (Chatterjee and Walker, 2017; Cordero et al., 2018). As a result, mutations occur, which could be favorable to the survival of bacterial species. Antibiotic resistance is one advantage that can be gained by mutagenesis (Li et al., 2019). Therefore, the more UV that the bacteria are exposed to, the higher the probability that they will accumulate mutations to confer antibiotic resistance.

The third explanation for higher resistance is that these extremophiles inherently have strategies to survive stress. These bacteria may have improved their cell membranes, enzymes, DNA repair machineries, among other adaptations that allow them to resist chemical challenges in addition to the condition they already survive (Hibbing et al., 2010; Orellana et al., 2018). Efflux pumps, for example, have been found to increase antibiotic resistance and tolerance and are also found in many high metal tolerant extremophiles (Lewis, 2017; Orellana et al., 2018). Such examples include *Arthrobacter* sp., and *Flavobacterium* sp., which were genera isolated and used in the MIC assay (**Supplementary Table 4** and **Figure 6C**; Orellana et al., 2018). Studies have also shown that extremophiles from the Atacama Desert have high resistance to arsenic due to the arsenic-rich Atacama brooks and soils (Escalante et al., 2009; Azua-Bustos et al., 2012). Examples from our isolate list include *Pantoea*, *Serratia*, *Hafnia*, *Microbacterium*, *Exiguobacterium*, and *Pseudomonas* (**Supplementary Tables 2**; Orellana et al., 2018). Indeed, our most resistant isolates were TQB (closely related to *Pseudomonas azotoformans*: 99.26%) and MA2B (*Microbacterium* sp. ID: 99.2%) (**Figure 6C**). Their resistance mechanisms for high metals and arsenic toxicity may lead to their naturally occurring antibiotic resistance.

Conclusion

There are many reviews covering the advantages of extremophiles, especially in the light of bioremediation (Azua-Bustos and González-Silva, 2014; Bull et al., 2016; Orellana et al., 2018). It is important to go beyond microbial diversity analyses and isolate individual bacteria to learn what they are really doing. Cultivation is obviously a challenge but learning from extremophiles will allow us to understand the adaptation mechanisms that microbes use to survive in their environments. Their more sophisticated machineries will give insight into the metabolic and synthesis pathways that their non-extreme and pathogenic relatives utilize. This will lead to discoveries of new enzymes, pigments, and compounds that can be used in biotechnology, agriculture, and healthcare.

Materials and methods

Sample preparation and storage

Environmental samples were collected during the months of May and June of 2018. At each location soils were sampled from in between 1 and 5 cm and collected into sterile 2 mL microcentrifuge tubes using sterile tools. The date and exact coordinates were recorded at each sampling location (**Supplementary Table 1**). It is important to note that samples from Chaxa, Miscanti, Aguas Calientes, and Salar de Tara were taken from outside of the national parks. Samples, e.g., soil, water, moss, etc. were maintained at room temperature while in the field. Once brought to the laboratory, 20% (v/v) glycerol in water was added and stored at −80°C.

Bacteria isolate cultivation

Bacterial cultivation was performed using two approaches: direct cultivation and soil extract filter cultivation (**Figure 2**). For direct cultivation, ∼100 mg of soil was added directly to liquid cultivation medium. Four media were used: Luria Benton (LB) liquid and solid agar, 1:100 diluted LB liquid and solid agar, R2 liquid and solid agar (BD Difco, Franklin Lakes, NJ, USA). Liquid cultures and plates were incubated at room temperature overnight. Liquid cultures that had visible growth, as seen by turbidity, were deposited onto the surface of solid agar plates of the same medium for colony formation. All cultures and plates were grown statically at room temperature.

The vacuum filter disks were collected to trap and concentrate any bacteria that were in the soil onto the filter paper. A sterile stick was used to scrape the filter disk and was resuspended into 100 μL of sterile water. The resuspension was then plated onto R2 medium agar plates. Plates were incubated at room temperature for colony formation.

Colonies were struck onto R2 solid agar plates until single distinct colonies were observed. After obtaining all our isolates, potential sisters were removed by the following steps. First, colonies of the same morphology from the same location were removed. Second, colonies of the same morphology across the entire isolate collection were removed. At this point, isolates were stocked in 20% (v/v) glycerol in water and stored at −80°C.

For all subsequent cultivation and assays, R2 solid agar and liquid medium were used and incubated at 25°C. Isolates were observed to grow well in these conditions. Isolates were named

according to a numbering system based on location, sample number, and medium type.

Species identification

To identify the species of each cultivated isolate we amplified and sequenced the 16S rRNA gene from the bacterial chromosome. A single colony was resuspended in 20 μL of water and then used as the template in the polymerase chain reaction (PCR) reaction. The 16S rRNA gene was amplified using OneTaq Polymerase Master Mix (Fisher Scientific, Agawam, MA) and bacteria specific 16S rRNA gene primers 8F (5′-AGAGTTTGATCCTGGCTCAG-3′) and 1492R (5′-GGTTACCTTGTTACGACTT -3′) (Galkiewicz and Kellogg, 2008). For those isolates that colony PCR was not successful, genomic DNA was extracted using chemical extraction and used as the template for PCR amplification (Sambrook and Josehp, 2001). The PCR products were sent for purification and Sanger Sequencing service at Eurofins Genomics (Louisville, KY, USA). Sequences were identified using NCBI Nucleotide Blast alignment.

We chose a 97% percent identity to determine the more closely related species. If the identity is lower than 97%, the isolate is considered a different and/or unidentified species. To identify unique isolates, we defined a sister isolate as any isolate similar in colony morphology to another isolate within a given sample. This was confirmed by 16S rRNA sequencing. If the percent identity was not available, then both isolates were kept. If both percent identities were above 97%, the isolate with the lower percent identity was removed.

Pigment identification

Pigment production was observed by tracking morphology over the course of 7 days. Samples were categorized into yellow, orange, and pink pigment production. Results were reported as a percentage of all the isolates that produced a pigment.

Biofilm production assay

Isolates were grown overnight in R2 liquid medium shaking at 25°C. Biofilm assay cultures were then inoculated 1:1,000 into R2 liquid medium in small glass culture tubes and grown statically at room temperature. All strains were tested for biofilms after 5 days of static growth. At harvest, the OD600 was measured by spectrophotometer to quantify cell density. Quantification of biofilm production was done by adaptation of published protocols (O'Toole, 2011). Briefly, cultures were decanted and rinsed with phosphate buffer saline (PBS). Any leftover liquid was pipetted out, and the tubes dried for 10 min in a fume hood. Each tube was filled with 0.1% (w/v) crystal violet stain and incubated for 15 min at room temperature. The stain was decanted, and the tubes were twice washed with PBS. Excess liquid was pipetted out and dried for 10 min under a flow hood. The remaining dye adhered to the biofilm was then dissolved in 30% (v/v) acetic acid in water for 15 min. This solution solubilized the dye. The crystal violet was measured at OD_{595}. All experiments were performed in biological triplicates. R2 liquid medium was used as a blank control and the isolate 225*C, a known-biofilm producer, was used as a positive control in each experiment. For quantification of biofilm production, all OD_{595} values were subtracted by the blank control OD595 value. This new value was then divided by the isolate's respective OD600 value to standardize all the cultures by cell count. Outliers were removed by Grubbs outlier test. Replicates were averaged, and the standard deviation of the mean was calculated to evaluate error.

Antimicrobial production assay

Test isolates were sub-cultured 1:100 from saturated cultures into R2 liquid medium in triplicate glass tubes. The cultures grew shaking at 25°C for 20 hrs. Lawns of *S. aureus* HG003 and *E. coli* MG1655 were prepared by sub-culturing cells 1:100 from saturated cultures into LB liquid medium. Bacterial cells were grown shaking at 30°C for 1 h until reaching about OD_{600} = 0.1, which were then diluted to an OD_{600} = 0.02 in R2 liquid medium. The diluted cells were used to flood R2 solid agar plates and further dried in a flow hood for 30 min. 3 μL of the environmental isolates' saturated cultures were spotted onto the *E. coli* and *S. aureus* lawns. For comparison purposes, ampicillin (25 mg/mL) was spotted as a positive control since the strains are ampicillin susceptible, and R2 liquid medium was spotted as a negative control. Plates were incubated at 25°C. After one and four days of incubation, the zones of inhibition were measured from the edge of the grown colony to the edge of the inhibition zone. Three independent experiments each with biological triplicates were performed. The average zone of inhibition was calculated for all three experiments (n = 9).

Minimum inhibitory concentration (MIC) dilution assay

Selected isolates were challenged against commercial antibiotics ampicillin, rifampicin, vancomycin, kanamycin, tetracycline, spectinomycin, and chloramphenicol (all purchased from Fisher Scientific, Agawam, MA, USA or Sigma Millipore, St. Louis, MO, USA) in 96-well plates. Media was supplemented with antibiotic in a 2-fold dilution ranging from 200 to 0.2 μg/mL final concentration. Rifampicin was diluted 2-fold in a range 164 μg/mL to 0.2 μg/mL final concentration. Cells were inoculated at a 1:100 dilution from a saturated culture. Wells with no antibiotic, no cells, and R2 supplemented with antibiotic vehicle were included as positive, negative, and vehicle effect controls. *Bacillus subtilis* NCBI 3610 was used as a control strain with known MICs to these antibiotics. Assay plates were covered with a sealing film and incubated at room temperature for 3 days. After 3 days, isolate growth was quantified using a plate reader at OD600. The MIC was determined as the concentration that fully inhibited growth. The experiment was performed three independent times each in biological singlet. The MIC was calculated to be the average from the three experiments.

Data availability statement

The original contributions presented in the study are included in the article/**Supplementary material**, further inquiries can be directed to the corresponding author.

Author contributions

AR: Conceptualization, Investigation, Methodology, Writing – original draft. DH: Investigation, Writing – original draft. JJ: Investigation, Writing – original draft. GM: Investigation, Writing – original draft. JS: Investigation, Writing – original draft. DM: Writing – original draft. CR: Methodology, Resources, Writing – original draft. YC: Investigation, Resources, Supervision, Writing – original draft. VG-C: Conceptualization, Data curation, Formal Analysis, Funding acquisition, Investigation, Methodology, Project administration, Resources, Supervision, Validation, Writing – original draft, Writing – review & editing.

Funding

The authors declare financial support was received for the research, authorship, and/or publication of this article. This work was funded by Northeastern University (NU) Global Experience Office, and the NU Scholars Programs. VG-C was funded by a stipend from NuSci, an Inclusive Excellence grant from HHMI, YC was supported by a National Science Foundation grant (MCB1651732), and AR was supported by the NU Provost Dissertation Completion Fellowship.

Acknowledgments

We would like to thank Jonna Iacono, Director of Office of Undergraduate Research and Fellowships, at Northeastern University for co-leading the trips to Chile. We are thankful to the Northeastern University undergraduate students that participated in the Dialogue of Civilizations courses to Chile (2017 and 2018). The students performed sample collection, bacterial growth and colony purification, DNA isolation, and PCR amplifications while in Chile as part of the course. We would also like to thank Joey Lehman Morris for being an active participant in the science aspect of the course while teaching students about the art of landscape photography. Special thanks to OneSeed guide Sofia Mardones and to our most patient and knowledgeable driver Guillermo Maluenda. We would also like to thank Paul Mueller and Hannah Meiseles for bioinformatics assistance, and the students at University of Antofagasta for lab support while in Chile. We would like to thank Dr. Slava Epstein from Northeastern University Department of Biology and Dr. D. Mark Welch from Marine Biological Laboratory Woods Hole, MA for insightful discussion and revisions of the manuscript. Finally, thanks to the VG-C and Chai Lab members for continuous discussion and support.

Conflict of interest

The authors declare that the research was conducted in the absence of any commercial or financial relationships that could be construed as a potential conflict of interest.

The authors declared that they were an editorial board member of Frontiers, at the time of submission. This had no impact on the peer review process and the final decision.

Publisher's note

Supplementary material

The Supplementary Material for this article can be found online at: https://www.frontiersin.org/articles/10.3389/fmicb.2024.1335989/full#supplementary-material

SUPPLEMENTARY FIGURE 1
Images of sampling locations. Images taken at the time of sampling in each location. The sample place name is indicated.

SUPPLEMENTARY FIGURE 2
Images of unique biofilm producers. Side view images taken of unique biofilm producers. Pellicle biofilms were produced after 5 days of static incubation at 25°C in R2 liquid medium. Shaking biofilms were observed as excess matrix and cell clumping. Cells were grown overnight shaking at 25°C in R2 liquid medium. Crystal violet-stained biofilms were imaged after 5 days of static incubation at 25°C in R2 liquid medium.

References

Anda, M., Ohtsubo, Y., Okubo, T., Sugawara, M., Nagata, Y., Tsuda, M., et al. (2015). Bacterial clade with the ribosomal RNA operon on a small plasmid rather than the chromosome. *Proc. Natl. Acad. Sci. U S A.* 112, 14343–14347. doi: 10.1073/pnas.1514326112

Azua-Bustos, A., and González-Silva, C. (2014). Biotechnological applications derived from microorganisms of the Atacama desert. *Biomed. Res. Int.* 2014:909312. doi: 10.1155/2014/909312

Azua-Bustos, A., Urrejola, C., and Vicuña, R. (2012). Life at the dry edge: microorganisms of the Atacama desert. *FEBS Lett.* 586, 2939–2945.

Beaz-Hidalgo, R., Latif-Eugenín, F., Hossain, M., Berg, K., Niemi, R., Rapala, J., et al. (2015). Aeromonas aquatica sp. nov., Aeromonas finlandiensis sp. nov. and Aeromonas lacus sp. nov. isolated from finnish waters associated with cyanobacterial blooms. *Syst. Appl. Microbiol.* 38, 161–168. doi: 10.1016/j.syapm.2015.02.005

Bull, A., Andrews, B., Dorador, C., and Goodfellow, M. (2018). Introducing the Atacama desert. *Antonie Van Leeuwenhoek* 111, 1269–1272.

Bull, A., and Asenjo, J. (2013). Microbiology of hyper-arid environments: recent insights from the Atacama desert. *Chile. Antonie Van Leeuwenhoek* 103, 1173–1179. doi: 10.1007/s10482-013-9911-7

Bull, A., Asenjo, J., Goodfellow, M., and Gómez-Silva, B. (2016). The Atacama desert: technical resources and the growing importance of novel microbial diversity. *Annu Rev Microbiol.* 70, 215–234. doi: 10.1146/annurev-micro-102215-095236

Caneschi, W., Sanchez, A., Felestrino, ÉB, Lemes, C., Cordeiro, I., et al. (2019). Serratia liquefaciens FG3 isolated from a metallophyte plant sheds light on the evolution and mechanisms of adaptive traits in extreme environments. *Sci. Rep.* 9:18006. doi: 10.1038/s41598-019-54601-4

Chatterjee, N., and Walker, G. (2017). Mechanisms of DNA damage, repair, and mutagenesis. *Environ. Mol. Mutagen* 58, 235–263.

Chen, Q., Meyer, W., Zhang, Q., and White, J. (2020). 16S rRNA metagenomic analysis of the bacterial community associated with turf grass seeds from low moisture and high moisture climates. *PeerJ* 8:e8417. doi: 10.7717/peerj.8417

Cordero, R., Damiani, A., Jorquera, J., Sepúlveda, E., Caballero, M., Fernandez, S., et al. (2018). Ultraviolet radiation in the Atacama desert. *Antonie Van Leeuwenhoek* 111, 1301–1313.

Cordero, R., Seckmeyer, G., Damiani, A., Riechelmann, S., Rayas, J., Labbe, F., et al. (2014). The world's highest levels of surface UV. *Photochem. Photobiol. Sci.* 13, 70–81.

de Carvalho, C. (2017). Biofilms: microbial strategies for surviving UV exposure. *Adv. Exp. Med. Biol.* 996, 233–239.

Deb, S., and Das, S. (2020). Draft genome sequence of microbacterium oryzae strain MB-10, isolated from a rice field in India. *Microbiol. Resour. Announc.* 9:e01532-19. doi: 10.1128/MRA.01532-19

Demergasso, C., Casamayor, E., Chong, G., Galleguillos, P., Escudero, L., and Pedrós-Alió, C. (2004). Distribution of prokaryotic genetic diversity in athalassohaline lakes of the Atacama desert, Northern Chile. *FEMS Microbiol. Ecol.* 48, 57–69. doi: 10.1016/j.femsec.2003.12.013

Demergasso, C., Dorador, C., Meneses, D., Blamey, J., Cabrol, N., and Escudero, L. (2010). Prokaryotic diversity pattern in high-latitude ecosystems of the Chilean Altiplano. *J. Geophys. Res.* 115:G00D09. doi: 10.1029/2008JG000836

Demergasso, C., Escudero, L., Casamayor, E., Chong, G., Balagué, V., and Pedrós-Alió, C. (2008). Novelty and spatio-temporal heterogeneity in the bacterial diversity of hypersaline Lake Tebenquiche (Salar de Atacama). *Extremophiles* 12, 491–504. doi: 10.1007/s00792-008-0153-y

Dorador, C., Fink, P., Hengst, M., Icaza, G., Villalobos, A., Vejar, D., et al. (2018). Microbial community composition and trophic role along a marked salinity gradient in Laguna Puilar, Salar de Atacama, Chile. *Antonie Van Leeuwenhoek* 111, 1361–1374. doi: 10.1007/s10482-018-1091-z

Dorador, C., Vila, I., Remonsellez, F., Imhoff, J., and Witzel, K. (2010). Unique clusters of Archaea in Salar de Huasco, an athalassohaline evaporitic basin of the Chilean Altiplano. *FEMS Microbiol. Ecol.* 73, 291–302. doi: 10.1111/j.1574-6941.2010.00891.x

Drees, K., Neilson, J., Betancourt, J., Quade, J., Henderson, D., Pryor, B., et al. (2006). Bacterial community structure in the hyperarid core of the Atacama Desert, Chile. *Appl. Environ. Microbiol.* 72, 7902–7908. doi: 10.1128/AEM.01305-06

Escalante, G., Campos, V., Valenzuela, C., Yañez, J., Zaror, C., and Mondaca, M. (2009). Arsenic resistant bacteria isolated from arsenic contaminated river in the Atacama Desert (Chile). *Bull. Environ. Contam Toxicol.* 83, 657–661.

Fang, Y., Wu, L., Chen, G., and Feng, G. (2016). Complete genome sequence of *Pseudomonas* azotoformans S4, a potential biocontrol bacterium. *J. Biotechnol.* 227, 25–26. doi: 10.1016/j.jbiotec.2016.04.020

Ferri, M., Ranucci, E., Romagnoli, P., and Giaccone, V. (2017). Antimicrobial resistance: a global emerging threat to public health systems. *Crit. Rev. Food Sci. Nutr.* 57, 2857–2876.

Fu, Y., Wu, Y., Yuan, Y., and Gao, M. (2017). Complete genome sequence of Bacillus thuringiensis Serovar rongseni reference strain SCG04-02, a Strain Toxic to Plutella xylostella. *Genome Announc.* 5:e0691-17. doi: 10.1128/genomeA.00691-17

Galkiewicz, J., and Kellogg, C. (2008). Cross-kingdom amplification using bacteria-specific primers: complications for studies of coral microbial ecology. *Appl. Environ. Microbiol.* 74, 7828–7831. doi: 10.1128/AEM.01303-08

Gallardo, K., Candia, J., Remonsellez, F., Escudero, L., and Demergasso, C. (2016). The ecological coherence of temperature and salinity tolerance interaction and pigmentation in a non-marine vibrio isolated from salar de Atacama. *Front. Microbiol.* 7:1943. doi: 10.3389/fmicb.2016.01943

Gerardin, Y., Springer, M., and Kishony, R. (2016). A competitive trade-off limits the selective advantage of increased antibiotic production. *Nat. Microbiol.* 1:16175. doi: 10.1038/nmicrobiol.2016.175

Goodfellow, M., Nouioui, I., Sanderson, R., Xie, F., and Bull, A. (2018). Rare taxa and dark microbial matter: novel bioactive actinobacteria abound in Atacama Desert soils. *Antonie Van Leeuwenhoek* 111, 1315–1332. doi: 10.1007/s10482-018-1088-7

Graupner, K., Lackner, G., and Hertweck, C. (2015). Genome sequence of mushroom soft-rot pathogen Janthinobacterium agaricidamnosum. *Genome Announc.* 3:e0277-15. doi: 10.1128/genomeA.00277-15

Guo, Y., Jiao, Z., Li, L., Wu, D., Crowley, D., Wang, Y., et al. (2012). Draft genome sequence of Rahnella aquatilis strain HX2, a plant growth-promoting rhizobacterium isolated from vineyard soil in Beijing. *China. J. Bacteriol.* 194, 6646–6647. doi: 10.1128/JB.01769-12

Gutierrez-Luna, F. M., Lopez-Bucio, J., Altamirano-Hernandez, J., Valencia-Cantero, E., de la Cruz, H. R., Macias-Rodriguez, L., et al. (2020). Plant growth-promoting rhizobacteria modulate root system architecture in Arabidopsis Thaliana through volatile organic compound emission. *Symbiosis* 51, 75–83.

Hall, C., and Mah, T. (2017). Molecular mechanisms of biofilm-based antibiotic resistance and tolerance in pathogenic bacteria. *FEMS Microbiol. Rev.* 41, 276–301.

Hall-Stoodley, L., Costerton, J., and Stoodley, P. (2004). Bacterial biofilms: from the natural environment to infectious diseases. *Nat. Rev. Microbiol.* 2, 95–108.

Hassan, H., and Fridovich, I. (1980). Mechanism of the antibiotic action pyocyanine. *J. Bacteriol.* 141, 156–163.

He, A., Niu, S., Zhao, Q., Li, Y., Gou, J., Gao, H., et al. (2018). Induced salt tolerance of perennial ryegrass by a novel bacterium strain from the rhizosphere of a desert shrub Haloxylon ammodendron. *Int. J. Mol. Sci.* 19:469. doi: 10.3390/ijms19020469

Hibbing, M., Fuqua, C., Parsek, M., and Peterson, S. (2010). Bacterial competition: surviving and thriving in the microbial jungle. *Nat. Rev. Microbiol.* 8, 15–25. doi: 10.1038/nrmicro2259

Huang, F., Zhang, Y., Zhang, L., Wang, S., Feng, Y., and Rong, N. (2019). Complete genome sequence of Bacillus megaterium JX285 isolated from Camellia oleifera rhizosphere. *Comput Biol Chem.* 79, 1–5. doi: 10.1016/j.compbiolchem.2018.12.024

Jayaseelan, S., Ramaswamy, D., and Dharmaraj, S. (2014). Pyocyanin: production, applications, challenges and new insights. *World J. Microbiol. Biotechnol.* 30, 1159–1168. doi: 10.1007/s11274-013-1552-5

Jung, B., Khan, A., Hong, S., Park, G., Park, Y., Park, C., et al. (2017). Genomic and phenotypic analyses of Serratia fonticola strain GS2: a rhizobacterium isolated from sesame rhizosphere that promotes plant growth and produces N-acyl homoserine lactone. *J. Biotechnol.* 241, 158–162. doi: 10.1016/j.jbiotec.2016.12.002

Levine, D. (2006). Vancomycin: a history. *Clin. Infect Dis.* 42, S5–S12.

Lewis, K. (2013). Platforms for antibiotic discovery. *Nat. Rev. Drug Discov.* 12, 371–387.

Lewis, K. (2017). New approaches to antimicrobial discovery. *Biochem. Pharmacol.* 134, 87–98.

Lewis, K., and Caboni, M. (2017). The making of a pathogen. *Cell Host Microbe* 21, 653–654.

Li, X., Gu, A., Zhang, Y., Xie, B., Li, D., and Chen, J. (2019). Sub-lethal concentrations of heavy metals induce antibiotic resistance via mutagenesis. *J. Hazard. Mater.* 369, 9–16. doi: 10.1016/j.jhazmat.2019.02.006

Lin, H., Hu, S., Liu, R., Chen, P., Ge, C., Zhu, B., et al. (2016). Genome sequence of *Pseudomonas* koreensis CRS05-R5, an antagonistic bacterium isolated from rice paddy field. *Front. Microbiol.* 7:1756. doi: 10.3389/fmicb.2016.01756

Ma, J., Wang, C., Wang, H., Liu, K., Zhang, T., Yao, L., et al. (2018). Analysis of the complete genome sequence of Bacillus atrophaeus GQJK17 reveals its biocontrol characteristics as a plant growth-promoting rhizobacterium. *Biomed. Res. Int.* 2018, 9473542. doi: 10.1155/2018/9473542

Mafakheri, H., Taghavi, S., Zarei, S., Kuzmanovic, N., and Osdaghi, E. (2021). Occurrence of crown gall disease on Japanese Spindle (Euonymus japonicas var. green rocket) caused by Agrobacterium rosae in Iran. *Plant Dis.* Online ahead of print. doi: 10.1094/PDIS-03-21-0580-PDN

Mandakovic, D., Cintolesi, Á, Maldonado, J., Mendoza, S. N., Aïte, M., Gaete, A., et al. (2020). Genome-scale metabolic models of Microbacterium species isolated from a high altitude desert environment. *Sci. Rep.* 10:5560. doi: 10.1038/s41598-020-62130-8

Mandakovic, D., Maldonado, J., Pulgar, R., Cabrera, P., Gaete, A., Urtuvia, V., et al. (2018a). Microbiome analysis and bacterial isolation from Lejía Lake soil in Atacama desert. *Extremophiles* 22, 665–673. doi: 10.1007/s00792-018-1027-6

Mandakovic, D., Rojas, C., Maldonado, J., Latorre, M., Travisany, D., Delage, E., et al. (2018b). Structure and co-occurrence patterns in microbial communities under acute environmental stress reveal ecological factors fostering resilience. *Sci. Rep.* 8:5875.

Meyer, J. (2000). Pyoverdines: pigments, siderophores and potential taxonomic markers of fluorescent *Pseudomonas* species. *Arch. Microbiol.* 174, 135–142. doi: 10.1007/s002030000188

Narsing Rao, M., Xiao, M., and Li, W. (2017). Fungal and bacterial pigments: secondary metabolites with wide applications. *Front Microbiol.* 8:1113. doi: 10.3389/fmicb.2017.01113

Okoro, C., Brown, R., Jones, A., Andrews, B., Asenjo, J., Goodfellow, M., et al. (2009). Diversity of culturable actinomycetes in hyper-arid soils of the Atacama desert, Chile. *Antonie Van Leeuwenhoek* 95, 121–133.

Órdenes-Aenishanslins, N., Anziani-Ostuni, G., Vargas-Reyes, M., Alarcón, J., Tello, A., and Pérez-Donoso, J. (2016). Pigments from UV-resistant Antarctic bacteria as photosensitizers in dye sensitized solar cells. *J. Photochem. Photobiol. B* 162, 707–714. doi: 10.1016/j.jphotobiol.2016.08.004

Orellana, R., Macaya, C., Bravo, G., Dorochesi, F., Cumsille, A., Valencia, R., et al. (2018). Living at the frontiers of life: extremophiles in chile and their potential for bioremediation. *Front. Microbiol.* 9:2309. doi: 10.3389/fmicb.2018.02309

O'Toole, G. (2011). Microtiter dish biofilm formation assay. *J. Vis. Exp.* 47:2437.

Parro, V., de Diego-Castilla, G., Moreno-Paz, M., Blanco, Y., Cruz-Gil, P., Rodríguez-Manfredi, J., et al. (2011). A microbial oasis in the hypersaline Atacama subsurface discovered by a life detector chip: implications for the search for life on Mars. *Astrobiology* 11, 969–996. doi: 10.1089/ast.2011.0654

Ramette, A., Frapolli, M., Fischer-Le Saux, M., Gruffaz, C., Meyer, J., Défago, G., et al. (2011). *Pseudomonas* protegens sp. nov., widespread plant-protecting bacteria producing the biocontrol compounds 2,4-diacetylphloroglucinol and pyoluteorin. *Syst. Appl. Microbiol.* 34, 180–188. doi: 10.1016/j.syapm.2010.10.005

Rampelotto, P. (2013). Extremophiles and extreme environments. *Life* 3, 482–485.

Rateb, M., Houssen, W., Arnold, M., Abdelrahman, M., Deng, H., Harrison, W., et al. (2011a). Chaxamycins A-D, bioactive ansamycins from a hyper-arid desert Streptomyces sp. *J. Nat. Prod.* 74, 1491–1499. doi: 10.1021/np200320u

Rateb, M., Houssen, W., Harrison, W., Deng, H., Okoro, C., Asenjo, J., et al. (2011b). Diverse metabolic profiles of a Streptomyces strain isolated from a hyper-arid environment. *J. Nat. Prod.* 74, 1965–1971. doi: 10.1021/np200470u

Rundel, P. W., and Villagra, P. E. (2007). *Arid and Semi-Arids Ecosystems in Regional Environments Series*. Oxford: Oxford University Press.

Sambrook, J., and Josehp, R. D. W. (2001). *Molecular Cloning: a Laboratory Manual*, 3rd Edn. Cold Spring Harbor, NY: Cold Spring Harbor Laboratory Press.

Santajit, S., and Indrawattana, N. (2016). Mechanisms of antimicrobial resistance in ESKAPE pathogens. *Biomed. Res. Int.* 2016:2475067.

Santhanam, R., Okoro, C., Rong, X., Huang, Y., Bull, A., Andrews, B., et al. (2012a). Streptomyces deserti sp. nov., isolated from hyper-arid Atacama desert soil. *Antonie Van Leeuwenhoek* 101, 575–581. doi: 10.1007/s10482-011-9672-0

Santhanam, R., Okoro, C., Rong, X., Huang, Y., Bull, A., Weon, H., et al. (2012b). Streptomyces atacamensis sp. nov., isolated from an extreme hyper-arid soil of the Atacama desert, Chile. *Int. J. Syst. Evol. Microbiol.* 62(Pt 11), 2680–2684. doi: 10.1099/ijs.0.038463-0

Schulze-Makuch, D., Wagner, D., Kounaves, S., Mangelsdorf, K., Devine, K., de Vera, J., et al. (2018). Transitory microbial habitat in the hyperarid Atacama desert. *Proc. Natl. Acad. Sci. U S A.* 115, 2670–2675. doi: 10.1073/pnas.1714341115

See-Too, W., Convey, P., Pearce, D., Lim, Y., Ee, R., Yin, W., et al. (2016a). Complete genome of Planococcus rifietoensis M8(T), a halotolerant and potentially plant growth promoting bacterium. *J. Biotechnol.* 221, 114–115. doi: 10.1016/j.jbiotec.2016.01.026

See-Too, W., Lim, Y., Ee, R., Convey, P., Pearce, D., Yin, W., et al. (2016b). Complete genome of *Pseudomonas* sp. strain L10.10, a psychrotolerant biofertilizer that could promote plant growth. *J. Biotechnol.* 222, 84–85. doi: 10.1016/j.jbiotec.2016.02.017

Shrestha, A., Sultana, R., Chae, J., Kim, K., and Lee, K. (2015). Bacillus thurigienses C25 which is rich in cell wall degrading enzymes efficiently controls lettuce drop caused by Sclerotinia minor. *Eur. J. Plant Pathol.* 142, 577–589.

Silby, M., Cerdeño-Tárraga, A., Vernikos, G., Giddens, S., Jackson, R., Preston, G., et al. (2009). Genomic and genetic analyses of diversity and plant interactions of *Pseudomonas* fluorescens. *Genome Biol.* 10:R51. doi: 10.1186/gb-2009-10-5-r51

Undabarrena, A., Beltrametti, F., Claverías, F., González, M., Moore, E., Seeger, M., et al. (2016). Exploring the diversity and antimicrobial potential of marine actinobacteria from the comau fjord in Northern Patagonia. Chile. *Front. Microbiol.* 7:1135. doi: 10.3389/fmicb.2016.01135

Uritskiy, G., Getsin, S., Munn, A., Gomez-Silva, B., Davila, A., Glass, B., et al. (2019). Halophilic microbial community compositional shift after a rare rainfall in the Atacama desert. *ISME J.* 13, 2737–2749. doi: 10.1038/s41396-019-0468-y

Valdes Franco, J., Collier, R., Wang, Y., Huo, N., Gu, Y., Thilmony, R., et al. (2016). Draft genome sequence of Agrobacterium rhizogenes strain NCPPB2659. *Genome Announc.* 4:e0746-16. doi: 10.1128/genomeA.00746-16

Vlamakis, H., Chai, Y., Beauregard, P., Losick, R., and Kolter, R. (2013). Sticking together: building a biofilm the Bacillus subtilis way. *Nat. Rev. Microbiol.* 11, 157–168. doi: 10.1038/nrmicro2960

Xiaomei, Y., and Yao, T. (2020). Comparative genomic analysis of Bacillus mycoides Gnyt1 strain. *Res. Sq.* doi: 10.21203/rs.3.rs-15751/v1

Yoon, S., Ha, S., Kwon, S., Lim, J., Kim, Y., Seo, H., et al. (2017). Introducing EzBioCloud: a taxonomically united database of 16S rRNA gene sequences and whole-genome assemblies. *Int. J. Syst. Evol. Microbiol.* 67, 1613–1617. doi: 10.1099/ijsem.0.001755

Zachow, C., Müller, H., Monk, J., and Berg, G. (2017). Complete genome sequence of *Pseudomonas* brassicacearum strain L13-6-12, a biological control agent from the rhizosphere of potato. *Stand Genomic Sci.* 12:6. doi: 10.1186/s40793-016-0215-1

Zhao, Y., Selvaraj, J., Xing, F., Zhou, L., Wang, Y., Song, H., et al. (2014). Antagonistic action of Bacillus subtilis strain SG6 on Fusarium graminearum. *PLoS One* 9:e92486. doi: 10.1371/journal.pone.0092486

frontiers | Frontiers in Microbiology

TYPE Original Research
PUBLISHED 15 May 2024
DOI 10.3389/fmicb.2024.1323765

OPEN ACCESS

EDITED BY
Maria Filippa Addis,
University of Milan, Italy

REVIEWED BY
Janak Raj Joshi,
Montana State University, United States
Riccardo Melis,
Porto Conte Ricerche, Italy

*CORRESPONDENCE
Renata Wawrzyniak
✉ renata.wawrzyniak@gumed.edu.pl
Krzysztof Waleron
✉ krzysztof.waleron@gumed.edu.pl

RECEIVED 18 October 2023
ACCEPTED 30 April 2024
PUBLISHED 15 May 2024

CITATION
Smoktunowicz M, Wawrzyniak R, Jonca J, Waleron M and Waleron K (2024) Untargeted metabolomics coupled with genomics in the study of sucrose and xylose metabolism in *Pectobacterium betavasculorum*. *Front. Microbiol.* 15:1323765. doi: 10.3389/fmicb.2024.1323765

Untargeted metabolomics coupled with genomics in the study of sucrose and xylose metabolism in *Pectobacterium betavasculorum*

Magdalena Smoktunowicz[1], Renata Wawrzyniak[2]*, Joanna Jonca[3], Małgorzata Waleron[3] and Krzysztof Waleron[1]*

[1]Department of Pharmaceutical Microbiology, Faculty of Pharmacy, Medical University of Gdańsk, Gdańsk, Poland, [2]Department of Biopharmaceutics and Pharmacodynamics, Faculty of Pharmacy, Medical University of Gdańsk, Gdańsk, Poland, [3]Laboratory of Plant Protection and Biotechnology, Intercollegiate Faculty of Biotechnology University of Gdańsk and Medical University of Gdańsk, University of Gdańsk, Gdańsk, Poland

Introduction: *Pectobacterium betavasculorum* is a member of the *Pectobacerium genus* that inhabits a variety of niches and is found in all climates. Bacteria from the *Pectobacterium* genus can cause soft rot disease on various plants due to the secretion of plant cell wall degrading enzymes (PCWDEs). The species *P. betavasculorum* is responsible for the vascular necrosis of sugar beet and soft rot of many vegetables. It also infects sunflowers and artichokes. The main sugar present in sugar beet is sucrose while xylose is one of the main sugars in artichoke and sunflower.

Methods: In our work, we applied *metabolomic* studies coupled with genomics to investigate the metabolism of *P. betavasculorum* in the presence of xylose and sucrose as the only carbon source. The ability of the strains to use various sugars as the only carbon source were confirmed by the polypyridyl complex of Ru(II) method in 96-well plates.

Results: Our studies provided information on the metabolic pathways active during the degradation of those substrates. It was observed that different metabolic pathways are upregulated in the presence of xylose in comparison to sucrose.

Discussion: The presence of xylose enhances extracellular metabolism of sugars and glycerol as well as stimulates EPS and IPS synthesis. In contrast, in the presence of sucrose the intensive extracellular metabolism of amines and amino acids is promoted.

KEYWORDS

***Pectobacterium betavasculorum*, plant pathogen, metabolomics, GC-MS, sucrose, xylose**

1 Introduction

The bacteria of the genus *Pectobacterium* inhabit a wide spectrum of ecological niches and have been isolated from soil, water, plants, and insects (Ma et al., 2007; Glasner et al., 2008). They can degrade plant cell walls through the secretion of plant cell wall degrading enzymes (PCWDEs) (Hugouvieux-Cotte-Pattat et al., 2014). *Pectobacterium* is considered as one of the top 10 bacterial pathogens that causes the harvest loss of potatoes and other vegetables both on the field and during transport or storage (Mansfield et al., 2012).

However, representatives of this genus have also been found to cause disease symptoms of many other plants crops and ornamentals. The host range of inhabited and infected plants varies between *Pectobacterium* species (Ma et al., 2007; Charkowski, 2018).

Our attention caught the species *P. betavasculorum*, which is responsible for the vascular necrosis of sugar beet (Thomson et al., 1981). This group of bacteria was first described as a subspecies of *E. carotovora* subsp. *betavasculorum*, and then elevated to the species level *P. betavasculorum* (Gardan et al., 2003). The first records of this microorganism were from the USA, Mexico, La Reunion and Romania (Gardan et al., 2003). The species were recently isolated in Asia (Ozturk et al., 2019). *P. betavasculorum* is one of the most important causes of sugar beet root rot symptoms in Iran (Nedaienia and Fassihian, 2011), and South Korea (Jee et al., 2020). Based on the 16S rRNA sequences from different environmental studies, the map of locations recorded for this taxon was created (Figure 1) (Rodrigues et al., 2017). Its most favorable growth temperature is 28 ± 2°C. Disease symptoms in the form of black streaks and rotting develop within 2–10 days in leaves, stems, roots, fruits, and tubers, also in plants such as cucumber, bean, melon, tomato, squash, corn, potato, eggplant, carrots, turnips, garlic, and onions. Moreover, red beet and date palm fruit were presented as potential new hosts of *P. betavasculorum* (Saleh et al., 2008).

More detailed studies of the pathogenicity of *P. betavasculorum* revealed that this species causes rot and root vascular necrosis of sugar beet root and is casually isolated from sunflower, artichoke, and potato (Gardan et al., 2003). Due to its high sucrose content, sugar beet is a biennial plant used for sugar production. It reaches its highest sucrose content (15–20% of fresh weight) in the storage root at the end of the first, vegetative year of development (Getz, 2000). Sucrose is the primary sugar transported in the phloem of most plants (Stein and Granot, 2019). Xylose is the main component of xylan, a hemicellulose which is a major component of plant cell walls (Zhang et al., 2021). Xylan comprises about 30% of many economically important plants (birch for example). In the case of sunflower, it is 26 and 17.7% in artichoke (Fortunati et al., 2016; Pesce et al., 2020). Sunflower leaves and flowers contain glucose and xylose as the main sugars. Additionally, lesser amounts of galactose, mannose, and arabinose are also present (Fortunati et al., 2016). All those sugars are accessible to bacteria colonizing these plants, including *P. betavasculorum*.

Even though *P. betavasculorum* causes losses in sugar beet or sunflower, and thus in crops crucial for the production not only of food but also of raw materials for biofuels or biodegradable polymers, this species is not very well studied compared to other taxa. One reason may be that, so far, no rapid detection and identification methods have been developed. Therefore, the metabolism of *P. betavasculorum*, has not yet been well investigated by modern omics methods. The mere fact that *P. betavasculorum* is growing mostly on sugar beet may indicate a metabolism adapted for the colonization of this plant species (Borowska-Beszta et al., 2024).

Therefore, in our research, we conducted genomic and metabolomic studies in order to verify if *P. betavasculorum* strains adapted to inhabit and infect the plants containing high concentrations of sucrose or xylose, in their tissues. The observed metabolic changes, combined with biochemical and physiological tests, may enable pathway determination, regulatory inference and understanding of the adaptative abilities of *P. betavasculorum*.

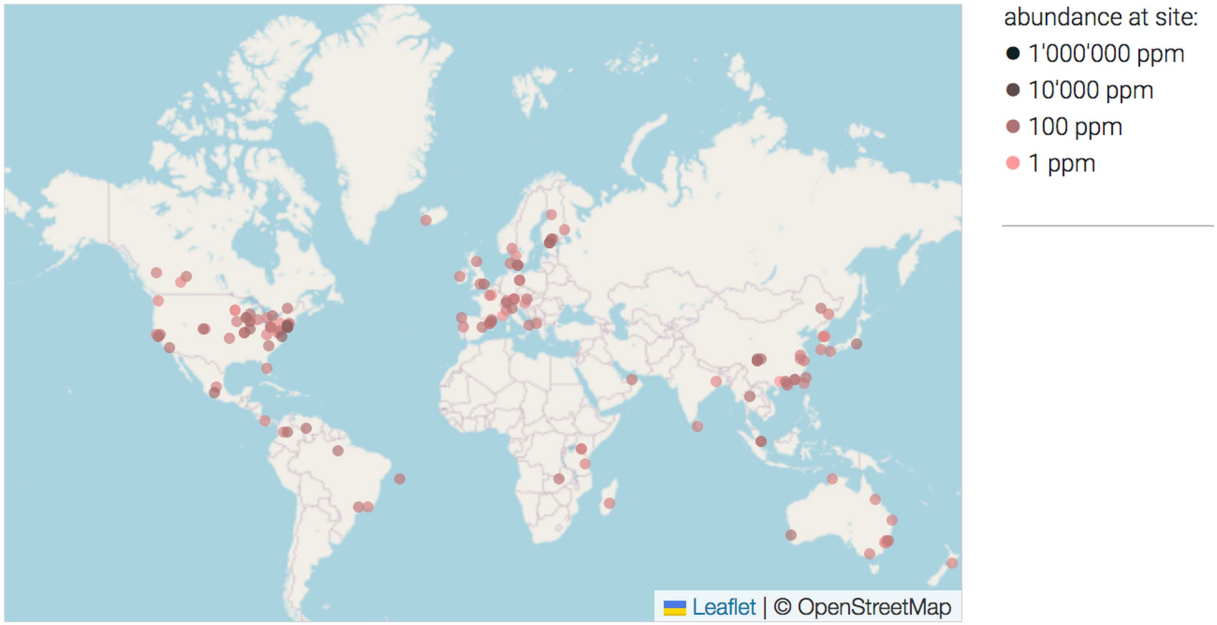

FIGURE 1
The map of locations where *P. betavasculorum* was found based on the 16S rRNA sequences from different environmental studies (Rodrigues et al., 2017). The intensity of the dot color reflect the aboundance on the site. ● = 1 ppm, ● = 100 ppm, ● = 10,000 ppm.

2 Materials and methods

2.1 Materials

Strains of *P. betavasculorum* used in the study: B2 = IFB5269 = CFBP 2122^T = SCRI479 = NCPPB2795^T = 43762ATCC isolated from sugar beet; B5 = IFB5271 = CFBP1520 isolated from sunflower and B6 = IFB5272 = Sf142-2 isolated from artichoke. The strains were obtained from the Laboratory of Plant Protection and Biotechnology, Intercollegiate Faculty of Biotechnology of University of Gdansk and Medical University of Gdansk (IFB collection).

2.2 The ability to use sugars as the only organic carbon source

The ability of the strains to use sugars as the only carbon source was tested by the polypyridyl complex of Ru(II) method in 96-well plates (Jońca et al., 2021). For the experiment, 0.5% solutions of monosaccharides in the minimal medium M63 base were prepared (Miller, 1972). The following sugars were used: cellobiose, trehalose, sorbitol, sucrose, glucose and xylose. Aliquots 200 µL of the appropriate sugar solution, 2.5 µL of 5 mg/mL of ruthenium dye solution and 5 µL of a bacterial suspension of 0.5 McFarland (McF) optical density were added to each well. For each sugar solution, the sterility of the work was checked by adding only the nutrient solution and the ruthenium dye (negative control) to the well. The plates were incubated for 72 h at 28°C. Absorbance was read at 600 nm and in case of fluorescence samples were excited at 480 nm, and the fluorescence intensity was measured at 610 nm on the Infinite M200 Pro Tecan (Männedorf, Switzerland).

2.3 Testing the ability to form polysaccharides on a medium supplemented with various sugars

For the purposes of the experiment, a medium with the following composition was prepared: 2 g/L tryptone, 10 g/L sugar, 5 g/L sodium chloride, 1 g/L yeast extract, 0.300 g/L potassium hydrogen phosphate, 0.080 g/L bromothymol blue, 15 g/L agar. The final pH at 25°C was 7.1 ± 0.2. Sugars used in the experiment were glucose, mannitol, sucrose, galactose, xylose, maltose, ribose, rhamnose, isomaltulose. Bacteria grown overnight on Muller Hinton II (MHII) plates (Graso, Biotech, Poland) were suspended in the phosphate buffered saline (PBS) to the optical density of 0.5 McFarland (McF). The plates were inoculated by the spot method, 5 µL of the prepared bacterial suspension was placed on the plates. This allowed for a large number of bacteria to grow and produce metabolites at a single location. The plates were then incubated for 48 h. After that time, the plates were inverted and incubated again for 24 h to check for polysaccharide production.

2.4 Untargeted metabolomic analyses of biomass and media samples

For metabolomics analysis, bacteria were cultured on MS medium (Murashige and Skoog medium) without sugar content as a base. It is the most commonly used medium in laboratory experiments on plant tissue cultures and was selected to imitate the conditions of the *in vitro* plant growth. Carbon sources were added to the medium: 1% sucrose and 1% xylose, respectively. For each sugar, cultures were set in three biological replicates. Cultures were carried out for 72 h at 28°C and afterwards centrifuged (12,000 × g, 10 min). From the obtained supernatant, 1 mL of culture medium were taken in three technical replicates. Subsequently, the bacterial biomass samples were collected also in three technical replicates.

For the extraction of metabolites, 900 µL of methanol:chloroform: water mixture (10,3,1, v:v) were added to 900 µL of biomass from the bottom of the tube and to 900 µL of the nutrient medium after the bacteria cultivation. After centrifugation (13,000 × g, 15 min, 4°C), 300 µL of the obtained supernatants were concentrated by rotary vacuum and evaporated to the dryness. Afterwards, a two-step derivatization procedure was performed before analytical measurements with the use of gas chromatography–mass spectrometry (GC-MS) technique. The detailed procedure of sample preparation was displayed in Figure 2.

Quality Control (QC) samples, constituting a pool of an equal volume of all bacterial biomass or media samples, were prepared in the same manner as previously described (Figure 2). QC samples were analyzed throughout the sequence runs to ensure proper control of the system's stability and analytical reproducibility.

The prepared bacterial biomass and media extracts were analyzed with the use of gas chromatography coupled with triple quadrupole mass spectrometry (GC-QqQ/MS) in two separate sequence runs. Chromatographic separations were performed with the use of Zebron ZB-5MS column (30 m × 0.25 mm, 0.25 µm). The GCMS-TQ8030 (Shimadzu, Japan) equipped with electron ionization source (EI) was used in the study. Both chromatographic and mass spectrometer parameters are described in detail in Table 1. The prepared bacterial biomass or media extracts were analyzed in a randomized order along with QC samples. Data acquisition was conducted using GC/MS Solution Software version 4.01 (Shimadzu, Japan).

Peak detection and deconvolution of the acquired raw data were performed using the Automated Mass Spectrometry Deconvolution and Identification System (AMDIS) freeware[1] (Stein, 1999; Du and Zeisel, 2013). The retention index (RI) for each detected compound was calculated by normalization of its retention time (RT) by the RT and RI of the closest eluting n-alkane, included in the standard mixture of even n-alkanes (C10-C40). This mixture was analyzed at the beginning of each sequence run. The deconvoluted data sets were multialigned with the use of MassProfiler Professional B.02.01 software (Agilent Technologies, Waldbronn, Germany). The obtained data matrices were normalized using intensity of internal standard. Identification of compounds detected with the GC-MS technique was based on RI, RT, and mass spectra present in the NIST 14 and in-house spectral libraries. Data matrices obtained after processing, include 9 samples (3 biological replicates in 3 technical replicates) for each growth condition. In the case of biomass extracts, data matrix contained 97 variables, namely detected metabolites. In the case of media extracts, dataset contained 114 variables, namely detected metabolites.

The Shapiro–Wilk test was first used to check the normality of data distribution and then *t*-test or U Mann–Whitney test (depending on data distribution) were applied. Additionally, to

1 http://www.amdis.net

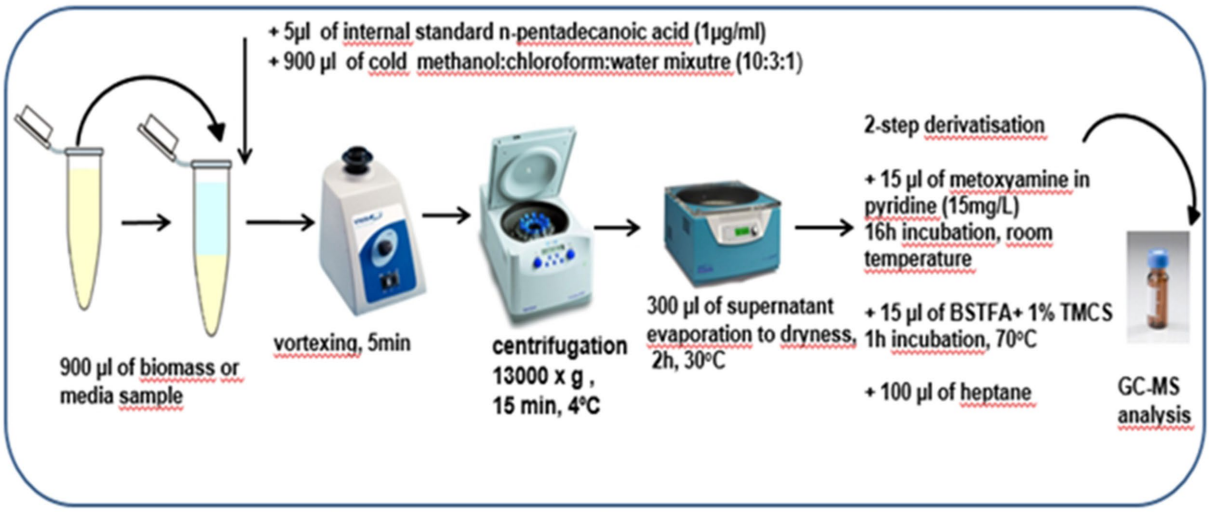

FIGURE 2
The detailed preparation procedure for biomass and media samples before analytical measurements with the use of GC-MS technique.

TABLE 1 Chromatographic and mass spectrometer parameters of the GC-MS method.

Method parameter	The optimized value
Temperature gradient	60–320°C
Temperature gradient rate	8°C/min
Injection volume	1 µL
Injection temperature	250°C
Carrier gas	hel
Total flow rate of carrier gas	10 mL/min
Pressure of carrier gas	53.5 kPa
Interface temperature	300°C
Mass range (*m/z*)	50–600
Ion source voltage	70 eV
Ion source temperature	200°C

evaluate the homogeneity of variance between groups, Levene's test was used. Subsequently, based on results of performed test the standard *t*-test in case of equal variances or Welch's *t*-test in case of unequal variances were applied. Furthermore, the multivariate statistical analyses were performed, including Principal Component Analysis (PCA) and Orthogonal Partial Least Squares Discriminant analysis (OPLS-DA). PCA, as unsupervised method was performed to verify the quality of analytical measurements and general trends in the dataset. OPLS-DA is a supervised method which was applied to selected statistically significant variables which were able to discriminate the compared groups. All multivariate models were built on previously prepared datasets with the use of Pareto scaling and logarithmic transformation. The OPLS-DA models were k-fold cross-validated. The validation parameters included R^2, Q^2 and *p* CV-ANOVA. Statistical analyses, including both univariate and multivariate tests, were performed in Matlab (MATLAB 2016a, The MathWorks Inc., Natick, MA) and SIMCA P 16.0.1 (Sartorius stedim biotech, Umeå, Sweden) in order to evaluate metabolic changes in different growth conditions of *Pectobacterium betavasculorum*. The statistically significant metabolic changes observed in biomass and media extracts were selected based on both *p*-value < 0.05 after multiple testing with the use of FDR (False Discovery Rate) Benjamini-Hochberg method and Variable Importance in Projection (VIP) value > 1.0. Metaboanalyst 5.0[2] a web-based platform were used for comprehensive interpretation of biochemical pathways in which identified metabolites are involved. MetaboAnalyst provides metabolic pathway evaluation by integration of pathway enrichment and pathway topology analyses.

2.5 Genomic analysis

Genomic and metabolomic analyses were performed with the use of Pathway Tools Software v27.0.[3] As the reference, the publicly available genome of *P. betavasculorum* NCPPB2795^T strain isolated from sugar beet was used. All found metabolites were evaluated, including metabolites that were not statistically significant, with the use of Pathway Tools software.

3 Results

3.1 Testing the ability to use sugars as the only carbon source

Three strains were tested: B2 - isolated from sugar beet, B5 - isolated from sunflower; and B6 - isolated from artichoke. The bacterial growth and metabolic activity were tested on the

2 http://www.metaboanalyst.ca
3 http://bioinformatics.ai.sri.com/ptools/, accessed on 12 October 2023.

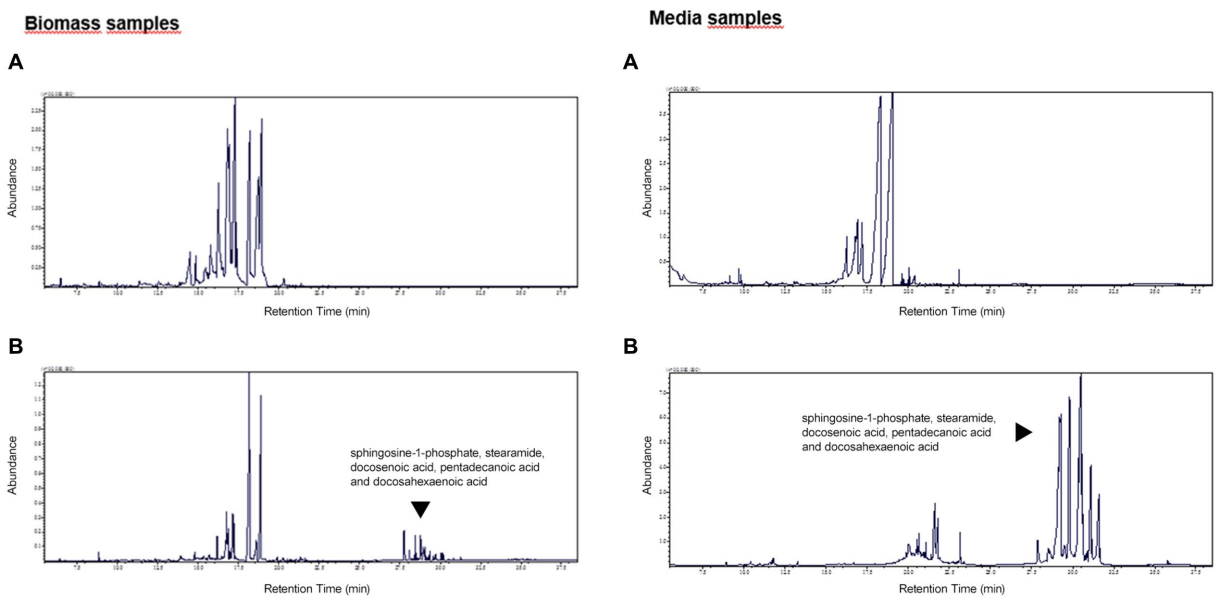

FIGURE 3
The exemplary metabolomic profiles for biomass and media extracts of *P. betavasculorum* in the presence of xylose **(A)** and sucrose **(B)**. The y-axis represents the abundance of detected compounds. The y-axis represents the retention time (RT) of detected compounds.

following sugars: cellobiose, trehalose, sorbitol, sucrose, xylose, and glucose (Supplementary Figure S1). The highest *P. betavasculorum* growth and metabolic activity observed as a high absorbance (OD > 0.6), as well as high fluorescence ($F > 50$), were demonstrated in the medium with the addition of sorbitol (Supplementary Figure S1C) and sucrose (Figure 1D). Sugars that have been used as a carbon source for growth but have been used to a lesser extent for other metabolic processes are trehalose (Supplementary Figure S1B) and xylose (Supplementary Figure S1F). On the other hand, sugars used to support growth (OD = 0.3–0.4) and basic life processes ($F < 16$) are cellobiose (Supplementary Figure S1A) and glucose (Supplementary Figure S1E). Interestingly, the B6 strain isolated from artichoke showed higher metabolic activity on the sugars, while the B5 strain isolated from sunflower showed a higher growth rate and lesser fluorescence intensity than the B6 strain. The B2 strain, isolated from sugar beet, showed intermediate values of absorbance and fluorescence.

3.2 Testing the ability to form polysaccharides on a medium with various sugars

The ability of *P. betavasculorum* strains to produce exopolysaccharides in the presence of the following sugars was investigated: glucose, mannitol, sucrose, galactose, xylose, maltose, ribose, rhamnose and isomaltulose (Supplementary Table S1). The addition of bromothymol blue to the medium made it possible to observe the change in pH of the medium. The intensive production of mucus was observed on media supplied with two sugars: xylose and sucrose. The obtained results were used to design metabolomics studies.

3.3 Metabolic signatures of *Pectobacterium betavasculorum* in different growth conditions

Determination of both bacterial biomass and media metabolomic signatures was performed to evaluate the metabolite changes at intracellular and extracellular levels. After data processing, 97 and 114 metabolites were identified in bacterial biomass and media samples, respectively (Supplementary Tables S2, S3). When bacteria were cultivated in the presence of sucrose, 50 metabolites were common for metabolomic profiles of bacterial biomass and media extracts. These metabolites are derived mainly from carbohydrates and amino acid metabolic pathways. Exemplary metabolites that were unique for media extract include hypoxanthine, mannose, galactose, indole-3-pyruvic acid, adipic acid and docosenoic acid. On the other hand, metabolites that were detected only in bacterial biomass include, for instance, aconitic acid, maleic acid, phenylacetic acid and meso-erythritol. If xylose was the only source of organic carbon, 51 common metabolites associated mainly with carbohydrates and amino acids metabolism, were detected in both bacterial biomass samples and culture media extracts. The group of metabolites unique for culture media extracts contains, for instance, lactose, galactose, stearamide, indole-3-pyruvic acid, adipic acid and docosenoic acid. However, metabolites detected only in bacterial biomass samples include, for example, dihydroxybenzoic acid, aconitic acid, serine, maleic acid and 5-hydroxy-tryptophan.

The exemplary metabolomic profiles of biomass and media extracts in the presence of xylose or sucrose were presented in Figure 3. It can be noticed that in the presence of sucrose, the obtained metabolomic profiles for both bacterial biomass and media samples are enriched for more hydrophobic compounds, such as: sphingosine-1-phosphate, stearamide, docosenoic acid, pentadecanoic acid and docosahexaenoic acid, mainly related to fatty acid metabolism. As

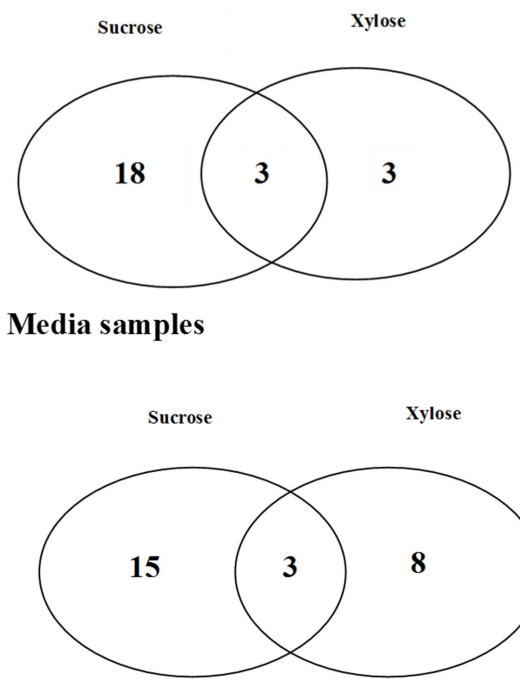

FIGURE 4
The Venn diagrams representing the number of common and unique metabolites which were found statistically significant in bacterial biomass samples and media extracts for different growth conditions.

shown in Figures 3, 4, these compounds are more abundant in media samples which can be related to intensive extracellular metabolic reactions.

The metabolomic signatures of *P. betavasculorum* metabolism in different conditions of growth were compared and summarized in Tables 2, 3 as well as Figure 4. It should be underlined that more statistically significant metabolites were detected in the presence of sucrose than xylose, both in bacterial biomass (18 versus 3) and media extracts (15 versus 8). In the case of bacterial biomass, among selected statistically significant metabolites, three metabolites, namely, 5-hydroxy-L-tryptophan, arabinose and fructose were common for both growth conditions. However, in case of the media extracts, common metabolites for both growth conditions include creatinine, galactofuranose and glucopyranose. The significant metabolites that were unique if xylose constituted the only source of organic carbon, include lyxose, sucrose and xylitol in the bacterial biomass samples as well as norvaline, glycerol, arabinopyranose, threitol, mannopyranoside, arabinose, propanediamine and nicotinic acid mononucleotide in culture media extracts. The results of PCA and validated OPLS-DA models were presented in Supplementary material section 2.

In order to identify the network of the observed metabolite changes, the pathway analysis in Metaboanalyst 5.0 (see footnote 2) was performed (Figures 5, 6). Observed metabolite changes in the presence of xylose and sucrose in bacterial biomass samples were related mainly to glycerolipid, galactose, starch metabolism and pentose phosphate pathway reactions. The changes were similar in the media extracts with the exception of additional differences in purine metabolism (Figure 6).

Obtained results were additionally analyzed using the Pathway Tools Software v27.0.[4] For culture media extracts and biomass data, 33 and 25 compounds were identified in the custom database created from *P. betavasculorum* NCPPB2795^T genome, respectively (Supplementary Tables S4, S5). The analysis revealed that in the biomass samples, metabolic processes involved in alcohol degradation and lipid synthesis were only active in sucrose-containing medium (Figure 7A). The opposite could be observed in case of bacterial medium (Figure 7B). Other processes that showed a greater activity in sucrose-containing biomass samples than xylose-containing biomass samples were processes of amino acid synthesis and degradation, and cofactor synthesis (Figure 7A). The metabolomic datasets were also analyzed for Pathway Perturbation Score (PPS) and Differential Pathway Perturbation Score (DPPS) which attempt to measure the overall extend of pathways down or upregulation. The 20 pathways of the highest DPPS detected in biomass extracts containing sucrose were listed in Supplementary Table S6 and visualized in Supplementary Figure S2. They included pathways of sucrose and glycogen degradation. In biomass extracts containing xylose, those pathways were also upregulated (Supplementary Table S7; Supplementary Figure S3). Media extracts of sucrose-containing samples indicated the activity of enzymes involved in purine metabolism and upregulation of nucleotide degradation pathways as well as pathways of cardiolipin and phospholipids biosynthesis (Supplementary Table S8; Supplementary Figure S4). In contrast, media extracts containing xylose had increased activity of enzymes involved in the metabolism of sugars such as sucrose, trehalose, mannose, D-xylose and lactose (Supplementary Table S9; Supplementary Figure S5). Glycogen degradation pathway was also upregulated.

4 Discussion

P. betavasculorum is unique among *Pectobacterium* genus in its ability to colonize plants which contain high sucrose (sugar beet) and xylose (sunflower and artichoke) content (Borowska-Beszta et al., 2024). In our work, we conducted metabolomic and genomic studies to shed some light on its adaptation potential and metabolic pathways which become upregulated in the presence of those sugars. Our investigation showed that *P. betavasculorum* strains were able to utilize both, sucrose and xylose as the only carbon source. It is indicative of their ability to colonize hosts with a high content of those sugars.

P. betavasculorum was able to grow on xylose and sucrose as the only organic carbon source (Supplementary Figures S1D,F). Genomic analysis confirmed the presence of sucrose and xylose degradation pathways in its genome (Supplementary Figure S6) as well as the pathway of glycogen degradation (Supplementary Figure S7). The results of growth assays agreed with the metabolomic, coupled with genomic, analysis of pathways upregulated during bacterial growth. In general, *P. betavasculorum* strains exhibited higher metabolic activity in the presence of sucrose than xylose. Those results were not

4 http://bioinformatics.ai.sri.com/ptools/, accessed on 14 August 2023.

TABLE 2 Statistically significant metabolites detected in bacterial biomass samples of *Pectobacterium betavasculorum* cultivated in the presence of xylose or sucrose as a source of organic carbon.

Metabolite	RT	Identification	VIP	*p* value
Butane	9.9	103,73,45	1.47	0.000333
8,10-Dioxaheptadecane	12.3	129,97,57	1.49	0.000333
2-Methylbutyrate	12.6	159,75,73	1.48	0.000333
2-Hydroxyisocaproic acid	14.8	189,117,75	1.55	0.000333
Glycerol	15.2	293,205,147	1.43	0.000333
Galactofuranose	16.6	319, 217,73	1.61	0.000333
Erythro-Pentonic acid	17.2	306,147,73	1.6	0.000547
d-Ribose	17.3	305,191,217	1.28	0.021198
Lyxopyranoside	17.9	305,204,133	1.42	0.000333
Threitol	18.1	307,205,103	1.2	0.021198
Ribitol	18.4	319,307,103	1.65	0.000547
2-Deoxy ribose	18.6	218,129,73	1.5	0.000333
Serine	18.8	218,204,73	1.55	0.000547
5-Hydroxy-L-tryptophan	18.8	220,204,146	1.47	0.000333
Arabinose	18.9	333, 217,191	1.5	0.000333
Mannose, 6-deoxy	18.9	393,204,73	1.39	0.000333
Arabinopyranose	19.1	333,217,204	1.38	0.000333
Gulose	19.8	435,204,73	1.48	0.000333
Glucopyranoside	19.8	409,187,101	1.35	0.000333
Fructose	20.1	437,204,73	1.36	0.000333
Mannopyranose	20.2	377, 204,73	1.08	0.006096
Lyxose	20.7	333,204,73	1.33	0.014908
Sucrose	28.6	361,217,73	1.26	0.000333
Xylitol	29.0	307,103,73	1.54	0.000333

Metabolites detected only in presence of sucrose are marked in green. Metabolites detected only in presence of xylose are marked in blue. Metabolites common for both growth conditions are marked in orange. RT, retention time; VIP, variable importance in projection.

surprising as sucrose provides a more readily available source of energy for growth as it is a dimer of glucose and fructose.

Sucrose can be transported into the cell and hydrolysed, or it can be hydrolysed extracellularly and converted into polymers (Gering and Brückner, 1996). For example, *Erwinia amylovora* can utilize sucrose via secreted levansucrase (Bogs and Geider, 2000). The main classes of enzymes involved in the breakdown of sucrose are hydrolases and phosphorylases whereas glycosyl-nucleotide glycosyltransferases synthesize carbohydrate polymers (Reid and Abratt, 2005). These polymers act as pathogenicity factors or can serve as an alternative energy source when other nutrients become depleted (Gering and Brückner, 1996).

Extracellular sucrose can enter to the periplasm of Gram-negative bacteria via channels in the outer membrane created by porins, then is transported through the inner (cell) membrane. The sucrose-related pathway includes the membrane-bound phosphoenolpyruvate:sugar phosphotransferase systems (PTS), which causes sugar transport as well as phosphorylation (Costa-Riu et al., 2003). The hydrolysis of the phosphorylated disaccharide in the cytosol is performed by enzymes with sugar specificity, such as sucrose hydrolase. The product β-D-glucose-6-phosphate can enter glycolysis, and D-fructose-6-phosphate is an intermediate in glycolysis (Meadow et al., 1990).

The gene of the PTS transporter (KP22_RS13800), as well as sucrose-6-phosphate hydrolase (KP22_RS13795), are both present in the *P. betavasculorum* genome (Supplementary Figure S5). What is more, metabolomic analysis of bacterial biomass confirmed that this pathway was upregulated (Supplementary Figure S2). Another upregulated pathway involved in sucrose catabolism was a hydrolysis of sucrose-by-sucrose invertase [β-D-fructofuranoside fructohydrolase (EC 3.2.1.26)], the product of the KP22_RS13795 gene of *P. betavasculorum*. Unsurprisingly, the glycolysis pathway was also upregulated.

The enzymes responsible for intracellular polysaccharide degradation or synthesis are encoded by the operon *glg*. This includes *glg*A (glycogen synthase), *glg*B (branching enzyme), *glg*C and D (two subunits of ADP-Glc pyrophosphorylase, ADP-Glc-PP) and *glg*P (or *phs*G, glycogen phosphorylase). The crucial regulating point of intracellular polysaccharide (IPS) biosynthesis is the generation of ADP-glucose, catalyzed by ADP-Glc-PP. This reaction is allosterically regulated by the intermediates, activators fructose-6-phosphate (F6P) or fructose-1,6-bisphosphate (F-1, 6-bP) and inhibitors AMP, ADP or Pi. This corresponds to the conditions of high and low energy supply, respectively. Studies have shown that transcript levels of the *glg* operon are upregulated under

TABLE 3 Statistically significant metabolites detected in media extracts of *Pectobacterium betavasculorum* cells cultivated in the presence of xylose or sucrose as a source of organic carbon.

Metabolite	RT	Identification	VIP	*p* value
4-Imidazoleacrylic acid (Trans-urocanic)	9.9	309,235,73	1.21	0.011671
Norvaline	10.7	251,108,91	1.14	0.020229
Glycerol	15.1	293,205,147	1.41	1.7 × 10−4
Creatinine	15.3	329,115,73	1.09	0.00388
Arabinopyranose	18.4	305,207,204,73	1.48	1.7 × 10−4
Threitol	18.4	307,205,103	1.38	1.7 × 10−4
Mannopyranoside	18.6	377,204,73	1.5	1.7 × 10−4
Arabinofuranose	18.9	393,217,73	1.29	1.7 × 10−4
2-Deoxy ribose	18.9	218,129,73	1.39	0.006291
Galactofuranose	18.9	319,217,73	1.03	0.009699
Arabinose	19.2	333, 217,191	1.32	0.006291
Fructose	19.4	437,204,73	1.51	1.7 × 10−4
Glucopyranoside	19.8	409,187,101	1.48	1.7 × 10−4
Sorbose	20.3	437,204,73	1.5	1.7 × 10−4
Galactose	20.6	320,204,191,73	1.49	1.7 × 10−4
Galactinol	20.8	421,307,217	1.15	0.000174
Hypoxanthine	20.8	280,265,73	1.18	0.006291
Mannose	20.8	204,191,73	1.17	0.020229
Talose	20.8	217,204,191,73	1.51	1.7 × 10−4
Glucopyranose	21.01	204,191,147	1.04	0.000339
Propanediamine	21.1	196,154,72	1.06	0.038965
Galactofuranoside	22.4	217,205,101	1.15	0.006291
Maltose	27.8	361,204,191	1.39	1.7 × 10−4
Sucrose	28.1	361,217,73	1.45	1.7 × 10−4
Lactose	29.4	361,204,73	1.43	1.7 × 10−4
Nicotinic acid mononucleotide	31.02	235,147,73	1.29	0.006476

Metabolites detected only in presence of sucrose are marked in green. Metabolites detected only in presence of xylose are marked in blue. Metabolites common for both growth conditions are marked in orange. RT, retention time; VIP, variable importance in projection.

glucose-limiting conditions and downregulated with excess of glucose. However, the presence of sucrose results in decreased *glg* operon expression compared to glucose. Sucrose is usually converted into soluble and insoluble exopolysaccharides (EPS) by glucosyltransferases, forming glucose homopolymers called glucans. Glucans promote bacterial attachment and biofilm accumulation, which undoubtedly enhances the virulence of the species (Staat and Schachtele, 1974; Burne et al., 1996; Khalikova et al., 2005; Klahan et al., 2018). It has been shown that the activity of these exoenzymes, as well as the internalization of sucrose by PTS, have a profound effect on the regulation of bacterial genes, both through the release of monosaccharides, as glucose or fructose, and PTS-dependent regulation of gene expression (Verhaeghe et al., 2021).

P. betavasculorum contains the *glg* operon genes in its genome and a complete pathway of glycogen synthesis and degradation (Supplementary Figure S7). Metabolomic analysis revealed that this pathway was upregulated in the presence of sucrose in bacterial biomass (Supplementary Figure S2). It suggests the production of IPS. The pathway was not found upregulated in the bacterial media samples (Supplementary Figure S4). However, our studies show that *P. betavasculorum* produces EPS in a sucrose-supplemented medium. It may suggest a different EPS composition than IPS.

Several other pathways were also found upregulated. N-acetylglucosamine is a component of bacterial cell wall. However, it can also play a role in cell signaling in bacterial pathogenesis (Ansari et al., 2022). What is more, poly-β-1,6-N-acetyl-d-glucosamine (PGA) is a crucial component of *Pectobacterium* biofilm (Pérez-Mendoza et al., 2011). Cardiolipin is a component of bacterial membranes. It is synthesized in response to osmotic stress to which bacteria are undoubtedly subjected during infection of sugar beet root (Romantsov et al., 2009). Putrescine and agmatine provide protection against acid stress (del Rio et al., 2016). Upregulation of those pathways may play a role in *P. betavasculorum* adaptation to colonization of sugar beet. It is worth noting that neither agmatine nor putrescine pathways were found upregulated in xylose-supplemented media samples.

Many bacteria species use an active transport system for the uptake of xylose into the cell (Oh and Kim, 1998). Xylose is initially converted to xylulose. In the case of bacteria, xylose to xylulose isomerisation process is performed by xylose isomerase (Zhao et al., 2020). Xylose is

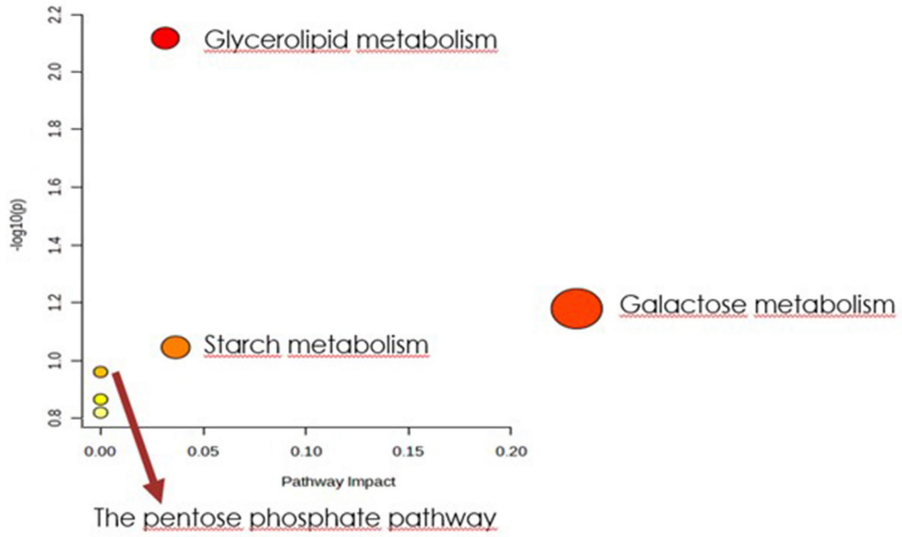

FIGURE 5
Biochemical evaluation of metabolic pathways in bacterial biomass samples. The x-axis represents the pathway impact value computed with the use of pathway topological analysis. The y-axis is the-log of the *p*-value obtained from pathway enrichment analysis. The pathways that were most significantly changed are characterized by both a high-log(p) value and high impact value (top right region).

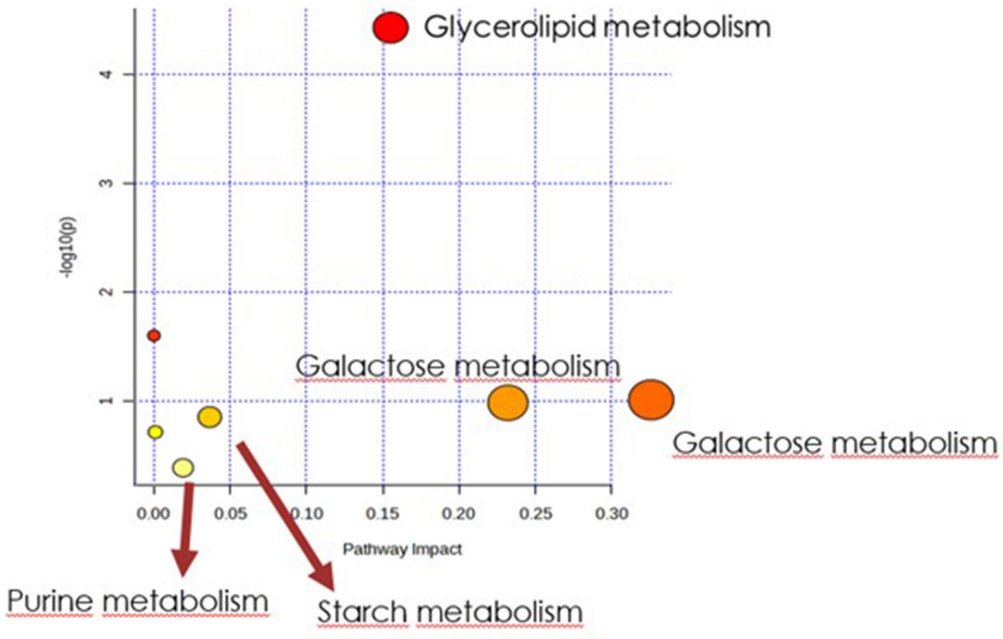

FIGURE 6
Biochemical evaluation of metabolic pathways in culture media extracts. The x-axis represents the pathway impact value computed with the use of pathway topological analysis. The y-axis is the log of the *p*-value obtained from pathway enrichment analysis. The pathways that were most significantly changed are characterized by both a high-log(p) value and high impact value (top right region).

utilized through three alternative metabolic pathways: the isomerase pathway; the oxidoreductase pathway; and the oxidative pathway, also called as the non-phosphorylative pathway. Among the bacteria of the order *Enterobacteriales*, the isomerase pathway is the main pathway. The isomerase pathway converts xylose into xylulose, then it is phosphorylated to xylulose phosphate an intermediate of the pentose phosphate pathway (Domingues et al., 2021). Genes coding for xylose isomerase and phosphatase enzymes are induced by xylose and repressed by glucose as well as the other usable substrates, according to the to use xylose as the carbon source (Vivek et al., 2022). This pathway is characteristic for prokaryotes (Lawlis et al., 1984; Lokman et al., 1991; Rygus et al., 1991; Stephens et al., 2007). The oxidoreductase

FIGURE 7
Metabolic pathways identified in PathwayTools *P. betavasculorum* NCPPB 2795 genome database based on the biomass **(A)** and medium **(B)** metabolomics data. Blue color indicates sucrose containing samples whereas green pertains to the samples supplemented with xylose. Each experiment was repeated three times and conducted in triplicate.

pathway is present mainly in eukaryotic organisms where the xylose is converted to xylitol, which is subsequently dehydrogenated and phosphorylated to xylulose phosphate, entering the pentose phosphate pathway (Wong et al., 1991; Desai and Rao, 2010).

P. betavasculorum possesses genes of xylose isomerase *xyl*A as well as xylulokinase *xyl*B (Supplementary Figure S6), which together convert D-xylose to D-xylulose-5-phosphate. It was consistent with the metabolomic studies results as this pathway was found upregulated in bacteria grown in xylose supplemented medium (Supplementary Figure S3). Moreover, a putative xylose reductase gene (WP_039325299) is present in *P. betavasculorum* genome, suggesting that this bacterium can produce xylitol from xylose. Xylitol was indeed detected in bacteria grown in xylose supplemented medium samples. The xylose reductase pathway is more thermodynamically advantageous than the xylose isomerase pathway and thus allows faster assimilation of xylose (Mouro et al., 2020). It may be the adaptation of *P. betavasculorum* to infecting plants with high lignocellulose content.

Sucrose degradation pathways as well as pathways involved in glycogen metabolism were found to be upregulated during growth in xylose-supplemented medium. It suggests intensive production of IPS and EPS. Those findings agree with phenotypic tests which confirmed that in the presence of xylose, *P. betavasculorum* strains produced significant amounts of EPS. Produced EPS may differ in composition to the EPS produced in sucrose supplemented medium. Such differences in EPS composition might be due to a host specific adaptation. However, to support this hypothesis, further studies on the composition of EPS derived from different sugars are necessary.

In the presence of xylose, *P. betavasculorum* exhibited enhanced extracellular metabolism of sugars and glycerol. In contrast, the presence of sucrose promoted intensive extracellular metabolism of amines and amino acids. The latter change in the metabolism the *P. betavasculorum* might maintain proper intracellular carbon and nitrogen levels, that is crucial to maximize nutrient utilization and cell growth. Among systems regulating carbon and nitrogen pools are the regulatory phosphotransferase systems that serve as a sensor responsible for metabolism tuning depending on the nutrients availability. It has been shown that PTS is required for EPS production and controls central carbon metabolism via the tricarboxylic acid (TCA) cycle (Sánchez-Cañizares et al., 2020).

To conclude, untargeted metabolomic studies combined with physiological and genomic analyses provided valuable information about metabolic pathways upregulated during the growth in the presence of xylose and sucrose, two main sugars found in *P. betavasculorum* native hosts. Our studies revealed that bacteria from the *P. betavasculorium* species may successfully utilize sucrose and xulose for growth and metabolism, and the formation of both, IPS and EPS.

Data availability statement

The original contributions presented in the study are included in the article/Supplementary material, further inquiries can be directed to the corresponding authors.

Author contributions

MS: Conceptualization, Data curation, Methodology, Writing – original draft. RW: Conceptualization, Data curation, Methodology, Visualization, Writing – original draft, Writing – review & editing. JJ: Methodology, Data curation, Visualization, Writing – review & editing. MW: Conceptualization, Data curation, Funding acquisition, Supervision, Project administration, Writing – review & editing. KW: Conceptualization, Data curation, Funding acquisition, Supervision, Project administration, Writing – review & editing.

Funding

The author(s) declare that financial support was received for the research, authorship, and/or publication of this article. This work was supported by the National Science Centre, projects OPUS9-2015/17/B/NZ9/01730 and OPUS18-2019/35/B/NZ9/01973. SM was supported by project POWR.03.02.00-00-I035/16-00 co-financed by the European Union through the European Social Fund under the Operational Programme Knowledge Education Development 2014–2020.

Conflict of interest

The authors declare that the research was conducted in the absence of any commercial or financial relationships that could be construed as a potential conflict of interest.

Publisher's note

Supplementary material

The Supplementary material for this article can be found online at: https://www.frontiersin.org/articles/10.3389/fmicb.2024.1323765/full#supplementary-material

References

Ansari, S., Kumar, V., Bhatt, D. N., Irfan, M., and Datta, A. (2022). N-Acetylglucosamine sensing and metabolic engineering for attenuating human and plant pathogens. *Bioengineering* 9:64. doi: 10.3390/BIOENGINEERING9020064

Bogs, J., and Geider, K. (2000). Molecular analysis of sucrose metabolism of *Erwinia amylovora* and influence on bacterial virulence. *J. Bacteriol.* 182, 5351–5358. doi: 10.1128/jb.182.19.5351-5358.2000

Borowska-Beszta, M., Smoktunowicz, M., Horoszkiewicz, D., Jonca, J., Waleron, M. M., Gawor, J., et al. (2024). Comparative genomics, pangenomics, and phenomic studies of *Pectobacterium betavasculorum* strains isolated from sugar beet, potato, sunflower, and artichoke: insights into pathogenicity, virulence determinants, and adaptation to the host plant. *Front. Plant Sci.* 15:1352318. doi: 10.3389/fpls.2024.1352318

Burne, R. A., Chen, Y. Y. M., Wexler, D. L., Kuramitsu, H., and Bowen, W. H. (1996). Cariogenicity of Streptococcus mutans Strains with Defects in Fructan Metabolism Assessed in a Program-fed Specific-pathogen-free Rat Model. 75, 1572–1577. doi: 10.1177/00220345960750080801

Charkowski, A. O. (2018). The changing face of bacterial soft-rot diseases. *Annu. Rev. Phytopathol.* 56, 269–288. doi: 10.1146/annurev-phyto-080417-045906

Costa-Riu, N., Burkovski, A., Krämer, R., and Benz, R. (2003). PorA represents the major cell wall channel of the gram-positive bacterium *Corynebacterium glutamicum*. *J. Bacteriol.* 185, 4779–4786. doi: 10.1128/JB.185.16.4779-4786.2003

del Rio, B., Linares, D., Ladero, V., Redruello, B., Fernandez, M., Martin, M. C., et al. (2016). Putrescine biosynthesis in *Lactococcus lactis* is transcriptionally activated at acidic pH and counteracts acidification of the cytosol. *Int. J. Food Microbiol.* 236, 83–89. doi: 10.1016/J.IJFOODMICRO.2016.07.021

Desai, T. A., and Rao, C. V. (2010). Regulation of arabinose and xylose metabolism in *Escherichia coli*. *Appl. Environ. Microbiol.* 76, 1524–1532. doi: 10.1128/AEM.01970-09

Domingues, R., Bondar, M., Palolo, I., Queirós, O., de Almeida, C. D., and Cesário, M. T. (2021). Xylose metabolism in Bacteria-opportunities and challenges towards efficient lignocellulosic biomass-based biorefineries. *Appl. Sci.* 11:8112. doi: 10.3390/app11178112

Du, X., and Zeisel, S. H. (2013). Spectral deconvolution for gas chromatography mass spectrometry-based metabolomics: current status and future perspectives. *Computational and Structural Biotechnology Journal*, 4, e201301013. doi: 10.5936/CSBJ.201301013

Fortunati, E., Luzi, F., Puglia, D., and Torre, L. (2016). Extraction of Lignocellulosic Materials From Waste Products. *Multifunctional Polymeric Nanocomposites Based on Cellulosic Reinforcements*, 1–38. doi: 10.1016/B978-0-323-44248-0.00001-8

Gardan, L., Cécile, G., Christen, R., and Samson, R. (2003). Elevation of three subspecies of *Pectobacterium carotovorum* to species level: *Pectobacterium atrosepticum* sp. nov., *Pectobacterium betavasculorum* sp. nov. and *Pectobacterium wasabiae* sp. nov. *Int. J. Syst. Evol. Microbiol.* 53, 381–391. doi: 10.1099/ijs.0.02423-0

Gering, M., and Brückner, R. (1996). Transcriptional regulation of the sucrase gene of *Staphylococcus xylosus* by the repressor ScrR. *J. Bacteriol.* 178, 462–469. doi: 10.1128/jb.178.2.462-469.1996

Getz, H. P. (2000). Sucrose accumulation and synthesis in sugar beet. *Developments in Crop Science*, 26(C), 55–77. doi: 10.1016/S0378-519X(00)80004-5

Glasner, J. D., Marquez-Villavicencio, M., Kim, H. S., Jahn, C. E., Ma, B., Biehl, B. S., et al. (2008). Niche-specificity and the variable fraction of the *Pectobacterium* pan-genome. *Mol. Plant-Microbe Interact.* 21, 1549–1560. doi: 10.1094/mpmi-21-12-1549

Hugouvieux-Cotte-Pattat, N., Condemine, G., and Shevchik, V. E. (2014). Bacterial pectate lyases, structural and functional diversity: bacterial pectate lyases. *Environ. Microbiol. Rep.* 6, 427–440. doi: 10.1111/1758-2229.12166

Jee, S., Choi, J. G., Lee, Y. G., Kwon, M., Hwang, I., and Heu, S. (2020). Distribution of *Pectobacterium* species isolated in South Korea and comparison of temperature effects on pathogenicity. *Plant Pathol.* 36, 346–354. doi: 10.5423/PPJ.OA.09.2019.0235

Jońca, J., Stachowska, A., Chylewska, A., Turecka, K., Waleron, K., and Waleron, M. (2021). Practical considerations in the application of a polypyridyl complex of Ru(II) in physiological and biochemical studies of *Pectobacterium* spp. and other bacteria. *Eur. J. Plant Pathol.* 159, 371–383. doi: 10.1007/s10658-020-02168-6

Khalikova, E., Susi, P., and Korpela, T. (2005). Microbial Dextran-Hydrolyzing Enzymes: Fundamentals and Applications. *Microbiology and Molecular Biology Reviews*, 69, 306–325. doi: 10.1128/MMBR.69.2.306-325.2005/ASSET/395B13D1-848A-4622-A4C4-EF05BD492D7A/ASSETS/GRAPHIC/ZMR0020520880002.JPEG

Klahan, P., Okuyama, M., Jinnai, K., Ma, M., Kikuchi, A., Kumagai, Y., et al (2018). Engineered dextranase from Streptococcus mutans enhances the production of longer isomaltooligosaccharides. *Bioscience, Biotechnology, and Biochemistry*, 82, 1480–1487. doi: 10.1080/09168451.2018.1473026

Lawlis, V. B., Dennis, M. S., Chen, E. Y., Smith, D. H., and Henner, D. J. (1984). Cloning and sequencing of the xylose isomerase and xylulose kinase genes of *Escherichia coli*. *Appl. Environ. Microbiol.* 47, 15–21. doi: 10.1128/aem.47.1.15-21.1984

Lokman, B. C., van Santen, P., Verdoes, J. C., Krüse, J., Leer, R. J., Posno, M., et al. (1991). Organization and characterization of three genes involved in D-xylose catabolism in *Lactobacillus pentosus*. *Mol. Gen. Genet.* 230, 161–169. doi: 10.1007/BF00290664

Ma, B., Hibbing, M. E., Kim, H.-S., Reedy, R. M., Yedidia, I., Breuer, J., et al. (2007). Host range and molecular phylogenies of the soft rot enterobacterial genera pectobacterium and dickeya. *Phytopathology* 97, 1150–1163. doi: 10.1094/PHYTO-97-9-1150

Mansfield, J., Genin, S., Magori, S., Citovsky, V., Sriariyanum, M., Ronald, P., et al (2012). Top 10 plant pathogenic bacteria in molecular plant pathology. *Molecular Plant Pathology*, 13, 614–629. doi: 10.1111/j.1364-3703.2012.00804.x

Meadow, N. D., Fox, D. K., and Roseman, S. (1990). The bacterial phosphoenolpyruvate: glycose phosphotransferase system. *Annu. Rev. Biochem.* 59:542,

Miller, J. H. (1972). *Experiments in molecular genetics*. Cold Spring Harbor: Cold Spring Harbor Laboratory Press.

Mouro, A., Santos, A. A. D., Agnolo, D. D., Gubert, G. F., Bon, E. P. S., Rosa, C. A., et al. (2020). Combining xylose reductase from *Spathaspora arborariae* with xylitol dehydrogenase from *Spathaspora passalidarum* to promote xylose consumption and fermentation into xylitol by *Saccharomyces cerevisiae*. *Fermentation* 6:72. doi: 10.3390/FERMENTATION6030072

Nedaienia, R., and Fassihian, A. (2011). Host range and distribution of *Pectobacterium betavasculorum*, the causal agent of bacterial vascular necrosis and root rot of sugarbeet in Fars province. *Iranian J Plant Pathol* 47, 179–185,

Oh, D. K., and Kim, S. Y. (1998). Increase of xylitol yield by feeding xylose and glucose in *Candida tropicalis*. *Appl. Microbiol. Biotechnol.* 50, 419–425. doi: 10.1007/s002530051314

Ozturk, M., Eroglu, Z., and Soylu, S. (2019). First report of *Pectobacterium betavasculorum* associated with bacterial vascular necrosis and root rot disease of sugar beet in Turkey. *New Dis. Rep.* 39:20. doi: 10.5197/j.2044-0588.2019.039.020

Pérez-Mendoza, D., Coulthurst, S. J., Sanjuán, J., and Salmond, G. P. C. (2011). N-Acetylglucosamine-dependent biofilm formation in *Pectobacterium atrosepticum* is cryptic and activated by elevated c-di-GMP levels. *Microbiology* 157, 3340–3348. doi: 10.1099/mic.0.050450-0

Pesce, G. R., Fernandes, M. C., and Mauromicale, G. (2020). Globe artichoke crop residues and their potential for bioethanol production by dilute acid hydrolysis. *Biomass and Bioenergy*, 134, 105471. doi: 10.1016/J.BIOMBIOE.2020.105471

Reid, S. J., and Abratt, V. R. (2005). Sucrose utilisation in bacteria: genetic organisation and regulation. *Appl. Microbiol. Biotechnol.* 67, 312–321. doi: 10.1007/s00253-004-1885-y

Rodrigues, J. F., Schmidt, T. S. B., Tackmann, J., and von Mering, C. (2017). MAPseq: highly efficient k-mer search with confidence estimates, for rRNA sequence analysis. *Bioinformatics* 33, 3808–3810. doi: 10.1093/bioinformatics/btx517

Romantsov, T., Guan, Z., and Wood, J. M. (2009). Cardiolipin and the osmotic stress responses of bacteria. *Biochim. Biophys. Acta Biomembr.* 1788, 2092–2100. doi: 10.1016/J.BBAMEM.2009.06.010

Rygus, T., Scheler, A., Allmansberger, R., and Hillen, W. (1991). Molecular cloning, structure, promoters and regulatory elements for transcription of the *Bacillus megaterium* encoded regulon for xylose utilization. *Arch. Microbiol.* 155, 535–542. doi: 10.1007/BF00245346

Saleh, O., Huang, P. Y., and Huang, J.-S. (2008). Bacterial vessel necrosis and root rot of sugar beet in Egypt. *J. Phytopathol.* 144, 225–230. doi: 10.1111/j.1439-0434.1996.tb01520.x

Sánchez-Cañizares, C., Prell, J., Pini, F., Rutten, P., Kraxner, K., Wynands, B., et al. (2020). Global control of bacterial nitrogen and carbon metabolism by a PTSNtr-regulated switch. *Proc. Natl. Acad. Sci.* 117, 10234–10245. doi: 10.1073/pnas.1917471117

Staat, R. H., and Schachtele, C. F. (1974). Evaluation of Dextranase Production by the Cariogenic Bacterium Streptococcus mutans. *Infection and Immunity*, 9, 467–469. doi: 10.1128/IAI.9.2.467-469.1974

Stein, O., and Granot, D. (2019). An overview of sucrose synthases in plants. *Front. Plant Sci.* 10:95. doi: 10.3389/fpls.2019.00095

Stein, S. E. (1999). An integrated method for spectrum extraction and compound identification from gas chromatography/mass spectrometry data. *J Am Soc Mass Spectrom*, 10, 770–781. doi: 10.1016/S1044-0305(99)00047-1

Stephens, C., Christen, B., Fuchs, T., Sundaram, V., Watanabe, K., and Jenal, U. (2007). Genetic analysis of a novel pathway for D-xylose metabolism in *Caulobacter crescentus*. *J. Bacteriol.* 189, 2181–2185. doi: 10.1128/JB.01438-06

Thomson, S. V., Hildebrand, D. C., and Schroth, M. N. (1981). Identification and nutritional differentiation of the *Erwinia* sugarbeet pathogen from members of *Erwinia carotovora* and *Erwinia chrysanthemi*. *Phytopathology* 71, 1037–1042. doi: 10.1094/Phyto-71-1037

Verhaeghe, T., Aerts, D., Diricks, M., Soetaert, W., and Desmet, T. (2021). The quest for a thermostable sucrose phosphorylase reveals sucrose 6′-phosphate phosphorylase as a novel specificity. *Appl. Microbiol. Biotechnol.* 98, 7027–7037. doi: 10.1007/s00253-014-5621-y

Vivek, N., Haseena, K. V., Tenali, S. N., Fernandez, M., Adlakha, N., Devendra, L., et al (2022). Sustainable technologies for platform and drop-in chemicals: production and applications. *Advanced Catalysis for Drop-in Chemicals*, 1–29. doi: 10.1016/B978-0-12-823827-1.00004-3

Wong, H. C., Ting, Y., Lin, H. C., Reichert, F., Myambo, K., Watt, K. W., et al. (1991). Genetic organization and regulation of the xylose degradation genes in *Streptomyces rubiginosus*. *J. Bacteriol.* 173, 6849–6858. doi: 10.1128/jb.173.21.6849-6858.1991

Zhang, W., Qin, W., Li, H., and Wu, A. M. (2021). Biosynthesis and transport of nucleotide sugars for plant hemicellulose. *Front. Plant Sci.* 12:723128. doi: 10.3389/fpls.2021.723128

Zhao, Z., Xian, M., Liu, M., and Zhao, G. (2020). Biochemical routes for uptake and conversion of xylose by microorganisms. *Biotechnol. Biofuels* 13:21. doi: 10.1186/s13068-020-1662-x

frontiers | Frontiers in Microbiology

TYPE Original Research
PUBLISHED 21 May 2024
DOI 10.3389/fmicb.2024.1356733

OPEN ACCESS

EDITED BY
Ilana Kolodkin-Gal,
Reichman University, Israel

REVIEWED BY
Pundrik Jaiswal,
National Institutes of Health (NIH), United States
Valdir Cristovao Barth,
University of São Paulo, Brazil

*CORRESPONDENCE
Valerie J. Carabetta
carabetta@rowan.edu

RECEIVED 16 December 2023
ACCEPTED 22 April 2024
PUBLISHED 21 May 2024

CITATION
Carr RA, Tucker T, Newman PM, Jadalla L, Jaludi K, Reid BE, Alpheaus DN, Korrapati A, Pivonka AE and Carabetta VJ (2024) Nε-lysine acetylation of the histone-like protein HBsu influences antibiotic survival and persistence in *Bacillus subtilis*. *Front. Microbiol.* 15:1356733. doi: 10.3389/fmicb.2024.1356733

Nε-lysine acetylation of the histone-like protein HBsu influences antibiotic survival and persistence in *Bacillus subtilis*

Rachel A. Carr[1], Trichina Tucker[1], Precious M. Newman[1], Lama Jadalla[2], Kamayel Jaludi[2], Briana E. Reid[1], Damian N. Alpheaus[1], Anish Korrapati[1], April E. Pivonka[1] and Valerie J. Carabetta[1]*

[1]Department of Biomedical Sciences, Cooper Medical School of Rowan University, Camden, NJ, United States, [2]Rowan-Virtua School of Osteopathic Medicine, Stratford, NJ, United States

Nε-lysine acetylation is recognized as a prevalent post-translational modification (PTM) that regulates proteins across all three domains of life. In *Bacillus subtilis*, the histone-like protein HBsu is acetylated at seven sites, which regulates DNA compaction and the process of sporulation. In Mycobacteria, DNA compaction is a survival strategy in response antibiotic exposure. Acetylation of the HBsu ortholog HupB decondenses the chromosome to escape this drug-induced, non-growing state, and in addition, regulates the formation of drug-tolerant subpopulations by altering gene expression. We hypothesized that the acetylation of HBsu plays similar regulatory roles. First, we measured nucleoid area by fluorescence microscopy and in agreement, we found that wild-type cells compacted their nucleoids upon kanamycin exposure, but not exposure to tetracycline. We analyzed a collection of HBsu mutants that contain lysine substitutions that mimic the acetylated (glutamine) or unacetylated (arginine) forms of the protein. Our findings indicate that some level of acetylation is required at K3 for a proper response and K75 must be deacetylated. Next, we performed time-kill assays of wild-type and mutant strains in the presence of different antibiotics and found that interfering with HBsu acetylation led to faster killing rates. Finally, we examined the persistent subpopulation and found that altering the acetylation status of HBsu led to an increase in persister cell formation. In addition, we found that most of the deacetylation-mimic mutants, which have compacted nucleoids, were delayed in resuming growth following removal of the antibiotic, suggesting that acetylation is required to escape the persistent state. Together, this data adds an additional regulatory role for HBsu acetylation and further supports the existence of a histone-like code in bacteria.

KEYWORDS

acetyl, acetylation, antibiotic resistance, bacteria, nucleoid-associated protein, tolerance, persisters

1 Introduction

Antibiotic resistance is a pressing concern in global public health, created by the rapid acquisition of resistance genes by bacteria. According to the 2019 Center for Disease Control and Prevention (CDC) antibiotic resistance threats report, more than 2.8 million antibiotic-resistant infections occur each year, leading to more than 35,000 deaths (CDC, 2019). There

is a direct relationship between the use of antibiotics and the emergence of drug-resistant bacterial strains (Llor and Bjerrum, 2014). Drug resistance may evolve by *de novo* mutations or be acquired by horizontal gene transfer (HGT), which occurs via conjugation, bacteriophage transduction, or transformation, all resulting in the recombination of foreign DNA into host chromosomes (Sun, 2018; Lerminiaux and Cameron, 2019). HGT is a significant clinical concern because the transfer of resistance genes can occur between environmental or human-associated bacteria and pathogens, which then promotes the dissemination of resistance. These resistance genes are selected for when a population of bacteria is challenged by antibiotic exposure, which allows such resistant strains to dominate the population.

From a genetically identical population of cells, different subpopulations can have different growth rates and gene expression patterns, and the selection of these subpopulations contributes to antibiotic survival. A common physiologic characteristic of bacteria is dormancy, which is a state they enter when encountering external biological stressors. This feature allows specialized cells to survive in a hostile environment, where they enter a cycle of reduced metabolic activity and activate protective stress responses, such as the general stress or SOS response (Rittershaus et al., 2013; Harms et al., 2016). The presence of true resistance genes is irrelevant in such populations. This phenomenon is referred to as bacterial persistence. In a population, persister cells are spontaneously formed at a basal rate and this rate is influenced by adverse environmental conditions, such as a hostile host environment or sublethal concentrations of antibiotics. Persister formation occurs devoid of any new genetic modifications. Instead, a shift in global gene expression is responsible, creating a dormancy-related profile characterized by the inhibition of genes responsible for cell growth and division, while increasing the expression of stress-related genes (Harms et al., 2016). Even small variations in gene expression can cause the rise of antibiotic-tolerant subpopulations. Following removal of the stress, persisters escape from the dormant state and return to their normal metabolic functions. This capability of persisters to alternate between an active and inactive state is a key factor of antibiotic ineffectiveness and leads to prolonged and relapsing infections (Gollan et al., 2019).

N^{ε}-lysine acetylation is recognized as a prevalent post-translational modification (PTM) that regulates proteins across all three domains of life. The level of acetylation is controlled by the action of lysine acetyltransferases (KATs), which transfer an acetyl group from a donor molecule, usually acetyl-CoA, to the target lysine sidechain amine. This action is reversed by the deacetylases, which are either Zn^{+}-dependent lysine deacetylases (KDACs) or NAD^{+}-dependent sirtuins (Christensen et al., 2019b). Some known functions of acetylation in bacteria are to control enzymatic activity, modulate protein stability, and regulate gene expression (Carabetta and Cristea, 2017; VanDrisse and Escalante-Semerena, 2019; Christensen et al., 2019a,b). In eukaryotes, the histones are responsible for chromatin compaction and regulation of various DNA transactions, such as DNA replication and gene expression. The N-terminal tails of the histones are highly modified by PTMs, which correlates to the degree of gene expression (Bannister and Kouzarides, 2011). This regulatory process has been referred to as the "histone code." In general, lysine acetylation is associated with chromatin loosening and allows the DNA to be more accessible for RNA polymerase, which promotes transcription. The removal of the acetyl groups restores the positively charged lysine residues and strengthens the interaction between histones and DNA, which reduces gene expression (Strahl and Allis, 2000; Patel and Wang, 2013). Therefore, the level of chromatin compaction is correlated with the level of gene expression.

Bacteria have nucleoid-associated proteins (NAPs) that are considered functional equivalents of histones and are responsible for the compaction of the chromosome and regulation of DNA processes (Ohniwa et al., 2011). The HU family, also known as the DNABII family, are the most widely conserved NAPs in bacteria. The HU family of proteins constitutes of a class of non-specific, DNA-binding proteins that actively participate in a wide range of biological processes, such as protecting the chromosome from thermal denaturation, DNA compaction, and gene expression (Stojkova et al., 2019; Carabetta, 2021). In *Bacillus subtilis,* the HU-family ortholog is HBsu, which is acetylated at seven lysine residues *in vivo* (Carabetta et al., 2019). Many of the modification sites of these proteins are predicted to have direct contact with DNA, likely influencing their DNA binding activity. Acetylation of HBsu regulates DNA compaction and the process of sporulation (Carabetta et al., 2019; Luu et al., 2022). As HBsu is the major NAP in *B. subtilis* (Micka and Marahiel, 1992; Ohniwa et al., 2011), additional processes which involve chromosomal dynamics or gene expression are likely also influenced by its acetylation.

In Mycobacteria, the HU-family ortholog is HupB, which is non-essential in *Mycobacterium smegmatis* (Sakatos et al., 2018). In *M. smegmatis*, the chromosomal DNA is diffusely spread throughout the cell, and when these bacteria are exposed to the antibiotic fusidic acid, their chromosome condenses into a single, dense structure (Scutigliani et al., 2018). This behavior was also observed in *Mycobacterium tuberculosis* cells that were treated with a variety of antibiotics. DNA condensation decreases over time during drug exposure, indicating that drug-induced DNA condensation is reversible. Therefore, DNA condensation likely represents an important survival strategy in the presence of environmental stresses in Mycobacteria. In further support of this, DNA condensation was also observed in response to nutrient starvation (Scutigliani et al., 2018). As NAPs are responsible for chromosomal compaction in bacteria, they are likely important regulatory factors of this stress response. Sakatos et al., using high-throughput microfluidic imaging, observed multiple drug-resistant subpopulations when *M. smegmatis* cells were exposed to sub-lethal levels of isoniazid. These subpopulations, referred to as large and small colony variants (LCVs and SCVs, respectively), differ in cell size, division times, and transcriptional profiles. The differences between these two populations are not due to gene mutations, but rather epigenetics. It was observed that following isoniazid exposure, a *hupB* deletion strain resulted in a specific loss of drug-resistant subpopulations and did not influence the growth kinetics of the entire population. RNA-seq analysis revealed that the loss of *hupB* influences gene expression, with the upregulation of 77 genes (Sakatos et al., 2018). In *Mycobacterium* spp., it was found that when HupB is acetylated DNA binding affinity is decreased (Ghosh et al., 2016) and deacetylation has the opposite effect (Anand et al., 2017). HupB contains six methylated and acetylated sites, and three were identified that impacted DNA binding (Sakatos et al., 2018). Mutation of one of the identified lysine sites to the unmodified mimic arginine (K86R), resulted in a significant reduction of SCVs when exposed to isoniazid in comparison to wild-type. These findings suggest that epigenetic regulation in bacteria,

involving the modifications of histone-like proteins, have global effects on gene expression that can influence antibiotic resistance and other essential cellular properties.

We hypothesized that acetylation of the histone-like proteins in Gram-positive bacteria play similar roles as they do in Mycobacteria. Thus, we determined the role that HBsu acetylation plays in *B. subtilis* during antibiotic challenge. We found that like *M. smegmatis* and *M. tuberculosis*, wild-type cells compact their nucleoids upon challenge with the aminoglycoside antibiotic kanamycin and that deacetylation of HBsu at specific sites is required for this compaction. We propose that nucleoid compaction is a survival strategy of bacteria when challenged with specific antibiotics and that HU family proteins may be important mediators of this response. We next examined the role of HBsu acetylation during drug survival by performing time-kill assays. We utilized a collection of HBsu mutants that contain lysine substitutions that mimic the acetylated (glutamine) or unacetylated (arginine) forms of the protein. Interfering with HBsu acetylation led to faster killing kinetics than wild-type. However, the number of cells that survived following 2 h of kanamycin or vancomycin exposure were similar among all strains, possibly representing persisters. Finally, we determined that interfering with the acetylation status of HBsu led to an increase in persister cell formation, following 5 h of exposure to kanamycin. This was different than what was observed for *M. smegmatis*. Although there was an increased number of persisters, the recovery from the semi-dormant persistent state was significantly delayed for many acetylation mutant strains. Together, this data adds an additional regulatory role for HBsu acetylation in survival following drug exposure, which further supports the existence of a histone-like code in bacteria.

2 Materials and methods

2.1 Bacterial strains, media, and growth conditions

All strains used in this study were constructed as previously described (Carabetta et al., 2019) and are listed in Table 1. These mutant strains have an identified lysine acetylation site (K3, K18, K37, K41, K75, K80, and K86) mutated to either glutamine (acetylated mimic) or arginine (deacetylated mimic) at the native locus. Liquid and agar Luria Broth (LB) were prepared according to standard protocols. Bacteria were grown in LB media at 37°C with aeration, with growth monitored by a Klett colorimeter. When appropriate, kanamycin, vancomycin, and tetracycline were added at final concentrations of 5, 12.5, and 25 μg/mL, respectively.

2.2 Fluorescence microscopy and data analysis

Cells were grown overnight at 30°C on LB plates and inoculated into fresh media the next morning. Specifically, cells were pre-grown in 5 mL LB for 2 h and after this period, the culture was split in half and subcultured into LB with or without kanamycin, tetracycline, or vancomycin. This extended pre-growth period allows for cells to enter exponential growth phase and increases cell numbers for subsequent analysis. After 20 min of growth, 300 μL of cells were harvested and nucleoids stained with a final concentration of 2 mM 4′, 6-diamidino-2-phenylindole (DAPI) for 5 min at room temperature. Cells were collected by centrifugation, washed once 300 μL of phosphate buffered saline (PBS, 10 mM potassium phosphate, pH 7.4, 0.15 M NaCl), and resuspended in 100 μL of PBS. 1 μL of cells was placed on 1% agarose pads for fluorescence microscopy, performed using a Nikon Eclipse Ti2 inverted wide-field microscope. Measurement of nucleoid area was performed using the NIS-Elements AR (Nikon) automated General Analysis feature (version 5.21.02). Using this software, thresholds based on DAPI intensity were manually applied to create a binary layer that identified the nucleoids as regions of interest for automated analysis. After initial thresholding was applied for wild-type cells that clearly separated the nucleoids from the background, the same filters were used for all images. The general analysis tool was used to measure nucleoid length, width, and area. At least 800 cells were analyzed for each strain, including multiple images from at least four biological replicates. The measurements generated were exported to Microsoft Excel for further processing. Large nucleoid lengths (> 3.2 μM) were excluded from analysis, which likely represented out of focus cells or those not differentiated as individual cells by the automated analysis program. The cutoffs for length and width measurements were determined as described previously (Carabetta et al., 2019). For each strain and growth condition, cumulative distribution plots were made by sequentially organizing the calculated nucleoid areas from low to high and plotting those values against their cumulative fraction. The cumulative distribution curves were plotted using the ggplot2 package in R (version 4.3.2, R Core Team, 2021). Nucleoid area distributions were compared between mutants and the wild-type in the presence or absence of kanamycin. The nonparametric, Kolmogorov–Smirnov test was used to determine if the two comparative samples came from the same distribution (Karson, 1968) and was performed in R, using the stats package. A p value <0.05 was considered statistically significant.

TABLE 1 Strains used in this study.

Strain	Relevant genotype[1]	Source/Ref
BD630	*his leu8 metB5*	Lab strain
BD7484	*hbsK80R*	Carabetta et al. (2019)
BD7493	*hbsK86Q*	Carabetta et al. (2019)
BD7506	*hbsK86R*	Carabetta et al. (2019)
BD8119	*hbsK37Q*	Carabetta et al. (2019)
BD8120	*hbsK37R*	Carabetta et al. (2019)
BD8147	*hbsK41Q*	Carabetta et al. (2019)
BD8148	*hbsK41R*	Carabetta et al. (2019)
BD8190	*hbsK18R*	Carabetta et al. (2019)
BD8219	*hbsK18Q*	Carabetta et al. (2019)
BD8333	*hbsK75R*	Carabetta et al. (2019)
BD8387	*hbsK3R*	Carabetta et al. (2019)
BD8398	*hbsK75Q*	Carabetta et al. (2019)
BD8576	*hbsK80Q*	Carabetta et al. (2019)
BD8577	*hbsK3Q*	Carabetta et al. (2019)

[1]All strains are in the BD630 background.

2.3 Time-kill assays

Cells were grown overnight at 30°C on LB plates, inoculated into LB media the next morning, and pre-grown for 2 h at 37°C, with aeration, as above. Following pre-growth, cells were serially diluted and plated on LB plates for initial cell count determination. Next, cells were diluted into flasks containing LB with or without kanamycin, tetracycline, or vancomycin. Growth was monitored by Klett colorimetry. Every 30 min for 2 h, cells were serially diluted and plated on LB plates to determine cell survival following antibiotic exposure. Percent survival was determined as colony-forming units (CFUs)/mL following antibiotic treatment/initial colony counts (CFUs/mL). All experiments were completed at least three independent times.

2.4 Persistence assays

Cells were grown overnight at 30°C on LB plates, inoculated into LB media the next morning, and pre-grown for 1 h at 37°C, with aeration to allow for entry into exponential growth phase. Following pre-growth, kanamycin was added to each culture. After 5 h of growth in the presence of antibiotic, cells were serially diluted and plated on LB plates for determination of colony counts (CFU/mL) to identify the surviving persistent population (Windels et al., 2019). All experiments were completed at least three independent times.

2.5 Persistence recovery assays

Cells were pre-grown in 1 mL of LB media for 1 h. Following pre-growth, kanamycin or vancomycin was added and cultures incubated overnight at 37°C, with aeration, to ensure that only viable, persistent cells would be assayed. The next morning, cells were washed three times with 1 mL LB media lacking antibiotics, resuspended in 1 mL LB, and 150 µL were added per well in a white, 96-well optical plate (ThermoFisher Scientific), in technical triplicates. The plate was sealed with a Breath-Easy sealing membrane [Research Products International (RPI)] and grown with shaking at 37°C in a Varioskan Lux (ThermoFisher Scientific) plate reader. Optical density measurements at 600 nm (OD_{600}) were recorded every 10 min for 8 h. A background subtract step, using the data from wells containing only sterile media, was performed using SkanIT software (version 7.0.2), before exportation to Microsoft Excel for further analysis. Each experiment was completed two independent times.

3 Results

3.1 Wild-type cells compact their nucleoids upon exposure to kanamycin

It was previously demonstrated that when challenged with antibiotics, Mycobacteria respond by compacting their DNA, possibly for additional protection from drug-induced oxidative stress (Scutigliani et al., 2018). However, it is unknown if this is a universal bacterial response to drug challenge. Wild-type *B. subtilis* cells were harvested following 20 min of growth in the presence or absence of the aminoglycoside antibiotic kanamycin, and nucleoids visualized by staining with DAPI. In LB media, before cell division, the nucleoids were diffused and appeared to be almost the same size as the cell (Figure 1A). However, when wild-type cells were challenged with kanamycin, the nucleoids became more rounded and compacted, and stained more intensely with DAPI (Figure 1A), in agreement with our previous observations (Carabetta et al., 2019). Quantification of the nucleoid areas of cells in the presence of kanamycin showed that the population distribution curve was shifted to the left when compared to cells in the absence of the drug, indicating a significant reduction in nucleoid size across the population (Figure 1B, p value = $2.54e^{-7}$). Next, we looked at the response of wild-type cells to another bactericidal antibiotic, the glycopeptide vancomycin, and a bacteriostatic drug tetracycline. In response to tetracycline, the distribution of nucleoid areas was similar to wild-type without drug (Supplementary Figure S1, p value = 0.6385), and no compaction was observed. For vancomycin, the distribution was statistically different from wild-type without drug (p value = 0.0004), but was slightly shifted to the right, rather than compacted (Supplementary Figure S1). We speculate that these differences might be related to the mechanism of killing, specifically the generation of reactive oxygen species (ROS), which will be discussed below. This data indicated that *B. subtilis* cells can compact their chromosome in response to antibiotic exposure, although it was drug specific, suggesting this response is conserved between the Actinobacteria and Firmicutes.

3.2 HBsu acetylation regulates nucleoid compaction in response to drug challenge

Since wild-type cells compacted their nucleoids in response to drug challenge, we reasoned that this was likely due to HBsu, as it is known to be involved in DNA compaction (Micka and Marahiel, 1992; Köhler and Marahiel, 1997; Schibany et al., 2020) and is the predominant NAP in this *B. subtilis* (Ohniwa et al., 2011). In addition, we previously showed that lysine acetylation at key sites in HBsu regulates nucleoid compaction in cells grown in minimal media (Carabetta et al., 2019). With this in mind, we next explored the role of lysine acetylation of HBsu during drug challenge. For these analyses, we utilized a collection of strains in which the lysine acetylation site (K3, K18, K37, K41, K75, K80, and K86) was mutated to glutamine (K → Q) or arginine (K → R) to mimic the fully acetylated or deacetylated state, respectively (Carabetta et al., 2019). Cells were grown in the presence and absence of kanamycin for 20 min and nucleoids stained with DAPI for visualization and quantification. A time of 20 min was selected to observe early responses to antibiotic challenge. Compared to wild-type cells, *hbsK3Q* and *hbsK75Q* did not compact their nucleoids properly in response to kanamycin (compare Figures 2A,E to Figure 1B), suggesting that some level of deacetylation of these sites is required for this response. For the *hbsK18Q*, *hbsK80Q*, and *hbsK86Q* strains, there was a response similar to wild-type, where the nucleoid became compacted in the presence of kanamycin (Figures 2B,F,G). Note that in LB media, some of the Q mutants may lead to global decondensation of the chromosome in the absence of drug, such as *hbsK86Q*, making the response to drug seem more extreme than that seen with wild-type (compare Figure 2G with Figure 1B). Surprisingly, the *hbsK37Q* and *hbsK41Q* strains had an opposite response, in that the nucleoid was decondensed in response to kanamycin challenge (Figures 2C,D). This suggested that acetylation

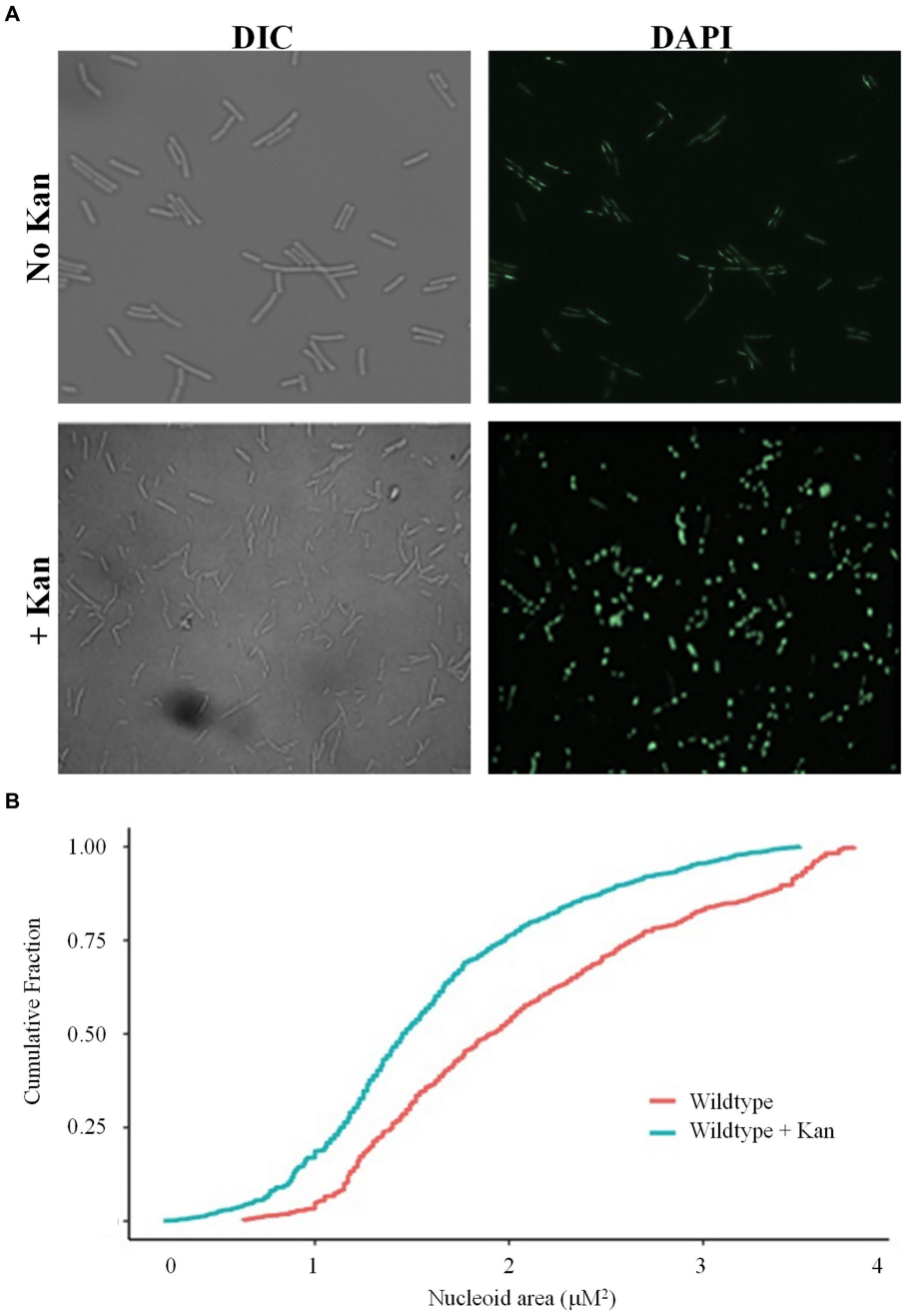

FIGURE 1
Wild-type cells compact their nucleoids in response to kanamycin challenge. **(A)** Wild-type cells (BD630) were pre-grown in LB media for 2 h, then incubated with or without 5 μg/mL kanamycin for 20 min, and nucleoids stained with DAPI. Representative microscopy images are displayed. DIC, Differential interference contrast. **(B)** Cumulative distribution plots are displayed, where the 50th percentile represents the median of the population distribution. Nucleoid areas of at least 800 cells were analyzed. The distributions with and without kanamycin were significantly different (*p* value = $2.54e^{-7}$), as determined by the Kolmogorov–Smirnov test.

of these two sites relaxes the chromosome. The fact that they have the opposite response suggested that acetylation of K37 or K41 may be required to decondense the chromosome to escape from this drug-induced state.

In an *hbsK3R* and *hbsK41R* mutant, there were very small differences visually with or without kanamycin (Figures 3A,D), although by statistical analyses, the distributions were significantly different. However, these subtle changes in distribution are unlikely to be biologically significant. The nucleoids of these mutants were already compacted compared to wild-type (Figure 1B), so there were minor differences with and without drug. This supports that acetylation at K41 may be required to escape from the compacted state. For K3, the fully acetylated and deacetylated forms did not have an appropriate response, suggesting that some intermediate level of acetylation is required *in vivo*. For the *hbsK18R*, *hbsK75R*, *hbsK80R*, and *hbsK86R* mutants there was still a response where the nucleoids

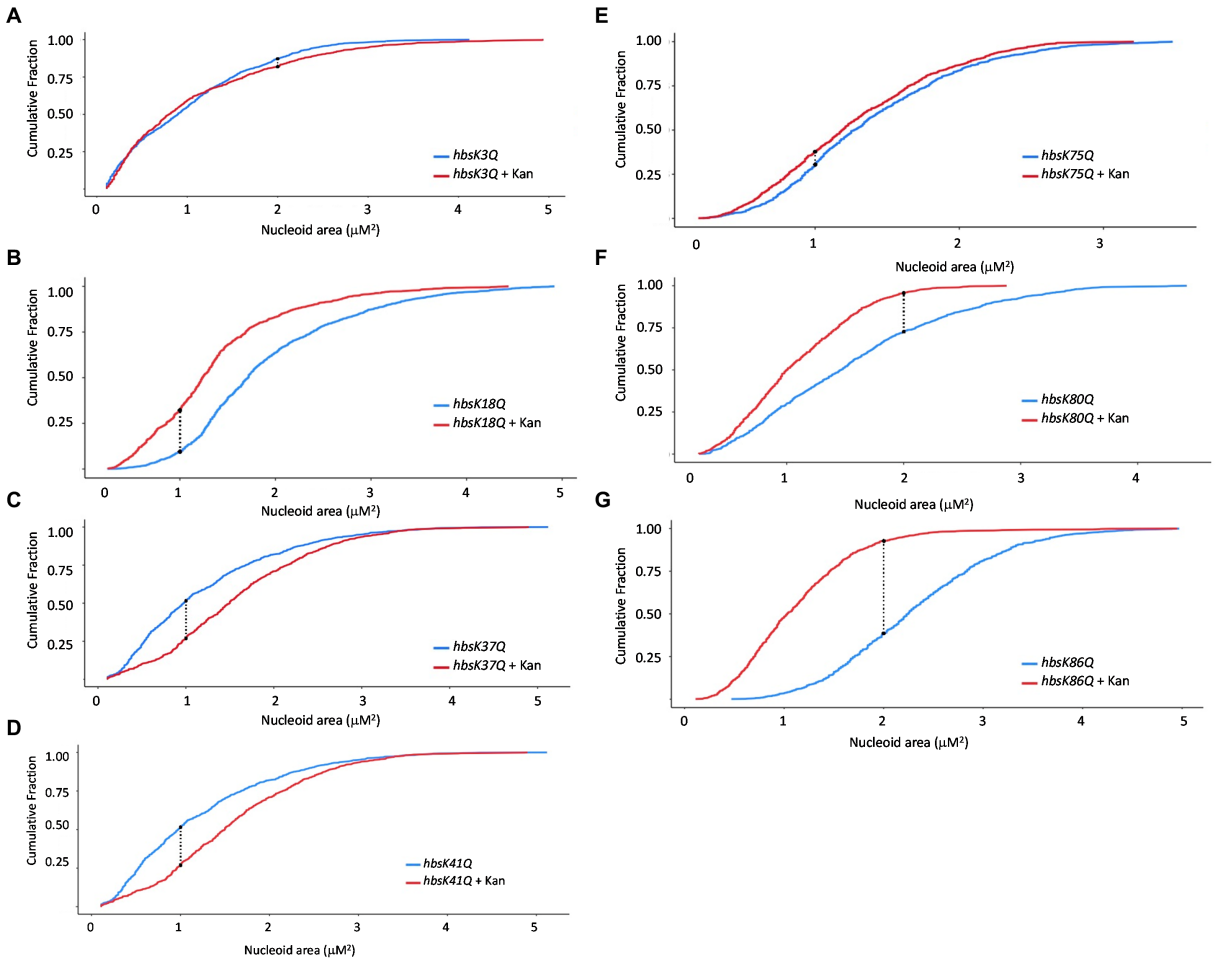

FIGURE 2
The impact of HBsu acetylation on nucleoid compaction following kanamycin exposure. *hbsK3Q* (BD8577, **A**), *hbsK18Q* (BD8219, **B**), *hbsK37Q* (BD8119, **C**), *hbsK41Q* (BD8147, **D**), *hbsK75Q* (BD8398, **E**), *hbsK80Q* (BD8576, **F**), and *hbsK86Q* (BD7493, **G**) cells were pre-grown in LB media for 2 h, then incubated with or without 5 μg/mL kanamycin for 20 min, and nucleoids stained with DAPI. Cumulative distribution plots are displayed, where the 50th percentile represents the median of the population distribution. Nucleoid areas of at least 800 cells were analyzed. The population distributions of nucleoid area in all strains, except for *hbsK3Q* (p value = 0.0682), were significantly different ± kanamycin, with the *hbsK75Q* p value = 0.005 and for all others, p values <2.2e^{-16}.

were more compacted in the presence of kanamycin (Figures 3B,E–G). Taken together, this suggests that the acetylation status of K18, K80, and K86 is not important for nucleoid compaction in the context of antibiotic challenge, and K75 must be deacetylated for this response. The *hbsK37R* mutant behaved exactly like the *hbsK37Q* mutant, where the nucleoid was decondensed when faced with antibiotic challenge. As K37 is not predicted to directly contact the DNA (Carabetta et al., 2019), perhaps mutation of this residue to any amino acid disrupts an important regulatory protein–protein interaction.

3.3 HBsu acetylation influences the rate of killing during antibiotic exposure

As we observed that some mutants do not properly compact their nucleoids, we next determined if this observation impacted cell survival during antibiotic challenge. Mutant cells were grown overnight and diluted into fresh media with and without kanamycin, after which cell survival was analyzed every 30 min for 2 h. For wild-type cells, ~50% of the population was killed by 30 min of drug exposure, which steadily decreased over 2 h, ending with less than 5% survival (Figure 4; Supplementary Table S1). For the Q substitution mutants, all strains had a faster killing rate, especially in the first 30 min, when compared to wild-type cells, regardless of whether their nucleoids were properly compacted (Figure 4A). The percentage of survival decreased below 15% within 30 min of exposure to kanamycin. By one 1.5 h, the survival of all mutants was less than 5% (Supplementary Table S1). This suggested that the level of nucleoid compaction alone does not impact the rate of killing or overall survival of the population. Most of the R substitution mutants followed a similar pattern, with survivability decreased below 15% within 30 min of exposure to kanamycin (Figure 4B; Supplementary Table S2). The *hbsK3R* and *hbsK18R* mutants had an intermediate phenotype, where it took 1 h to decrease the population numbers below 15%. At the 2-h time point, for all strains there was on average 0.5–3.4% survival, which likely represents the viable persistent subpopulation. Next, we selected the *hbsK3Q* strain, which did not properly compact the nucleoid, and the *hbsK41Q* strain, which had expanded nucleoids in

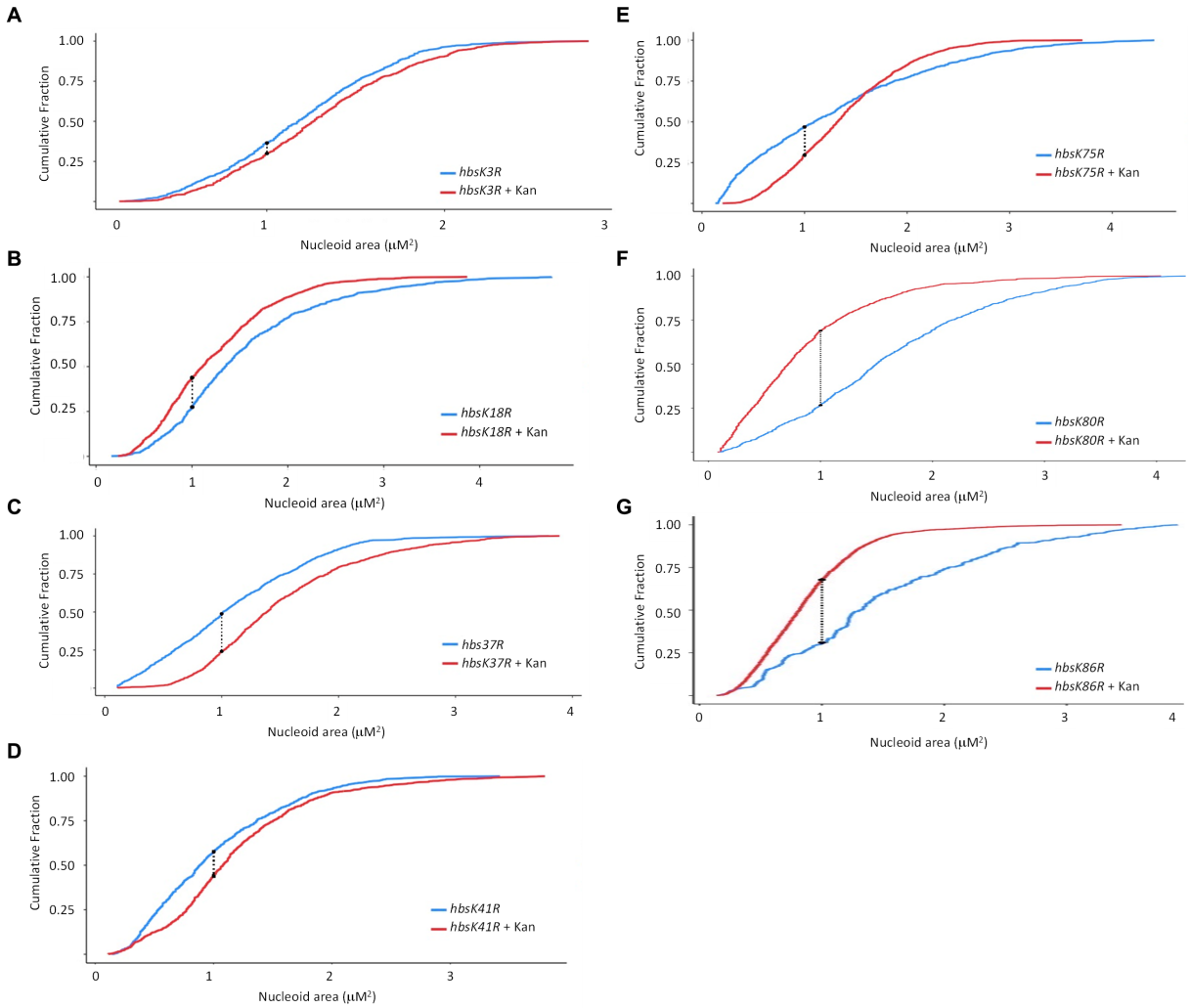

FIGURE 3
The impact of HBsu deacetylation on nucleoid compaction following kanamycin exposure. *hbsK3R* (BD8387, **A**), *hbsK18R* (BD8190, **B**), *hbsK37R* (BD8120, **C**), *hbsK41R* (BD8148, **D**), *hbsK75R* (BD8333, **E**), *hbsK80R* (BD7484, **F**), and *hbsK86R* (BD7506, **G**) cells were pre-grown in LB media for 2 h, then incubated with or without 5 μg/mL kanamycin for 20 min, and nucleoids stained with DAPI. Cumulative distribution plots are displayed, where the 50th percentile represents the median of the population distribution. The population distributions of nucleoid area in all strains were significantly different ± kanamycin: *hbsK3R* (p value = 0.005), *hbsK18R* (p value = $3.16e^{-12}$), *hbsK37R* (p value < $2.2e^{-16}$), *hbsK41R* (p value < $1.1e^{-15}$), *hbsK75R* (p value < $2.2e^{-16}$), *hbsK80R* (p value < $2.2e^{-16}$), and *hbsK86R* (p value < $2.2e^{-16}$).

the presence of kanamycin, to analyze the survival kinetics following vancomycin exposure. As seen with kanamycin, the *hbsK3Q* and the *hbsK3R* strains displayed faster killing kinetics than the wild-type following vancomycin exposure (Figure 5; Supplementary Table S3). The *hbsK41Q* had faster kinetics as well, but the *hbsK41R* strain looked like wild-type and actually had a 2–3-fold increase in percentage of survivors at the later timepoints (Supplementary Table S3). The reason for this difference compared to kanamycin exposure is unclear but does suggest that it would be beneficial for cells to have K41 deacetylated when challenged with drugs. These findings confirm that the extent of nucleoid compaction does not influence the rate of killing following exposure to bactericidal drugs.

We also examined the survival of these mutant strains against the bacteriostatic drug tetracycline (Figure 6). At 2 h, there was only a 20% reduction in survival, which was variable among replicates, in viability for wild-type cells (Figure 6; Supplementary Table S4). The *hbsK18Q*, *hbsK41Q*, and *hbsK86Q* mutants were relatively similar to wild-type (Figure 6A; Supplementary Table S4). The *hbsK37Q* displayed an increased rate of killing after 1 h of exposure, whereas *hbsK3Q*, *hbsK75Q*, and *hbsK80Q* were rapidly killed, with *hbsK80Q* being the most severe. The opposite mutant, *hbsK80R* followed a similar pattern to the wild-type, suggesting that in wild-type cells, K80 is mostly deacetylated (Figure 6B, Supplementary Table S5). In addition, K18 is normally acetylated, as *hbsK18Q* cells were similar to wild-type, while the *hbsK18R* mutant cells were rapidly killed (Figure 6). The *hbsK86R* mutant was like wild-type, while all other mutants were rapidly killed in the presence of tetracycline. It is unknown whether the response to bacteriostatic and bactericidal drugs is the same, but our data suggests that HBsu may be important for more than nucleoid compaction and that acetylation influences these functions differently.

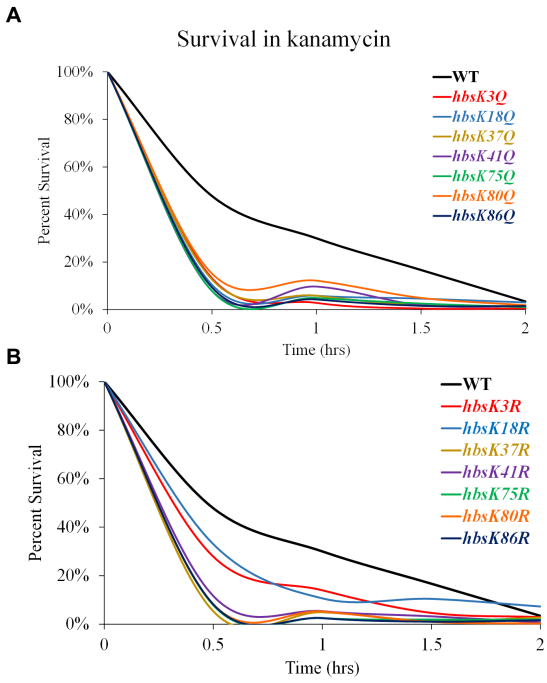

FIGURE 4
Interfering with HBsu acetylation leads to faster killing in the presence of kanamycin. Cells were pre-grown in LB media, then incubated with or without 5 μg/mL kanamycin for 2 h, with viable counts determined every 30 min. Percent survival at each timepoint was determined as CFUs/mL following kanamycin treatment/initial colony counts (CFUs/mL). **(A)** Wildtype (BD630), *hbsK3Q* (BD8577), *hbsK18Q* (BD8219), *hbsK37Q* (BD8119), *hbsK41Q* (BD8147), *hbsK75Q* (BD8398), *hbsK80Q* (BD8576), and *hbsK86Q* (BD7493). **(B)** Wildtype (BD630), *hbsK3R* (BD8387), *hbsK18R* (BD8190), *hbsK37R* (BD8120), *hbsK41R* (BD8148), *hbsK75R* (BD8333), *hbsK80R* (BD7484), and *hbsK86R* (BD7506).

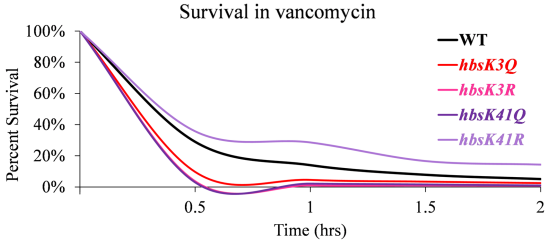

FIGURE 5
Interfering with HBsu acetylation leads to faster killing in the presence of vancomycin. Cells were pre-grown in LB media, then incubated with or without 12.5 μg/mL vancomycin for 2 h, with viable counts determined every 30 min. Percent survival at each timepoint was determined as CFUs/mL following vancomycin treatment/initial colony counts (CFUs/mL). Wildtype (BD630), *hbsK3Q* (BD8577), *hbsK41Q* (BD8147), *hbsK3R* (BD8387), and *hbsK41R* (BD8148).

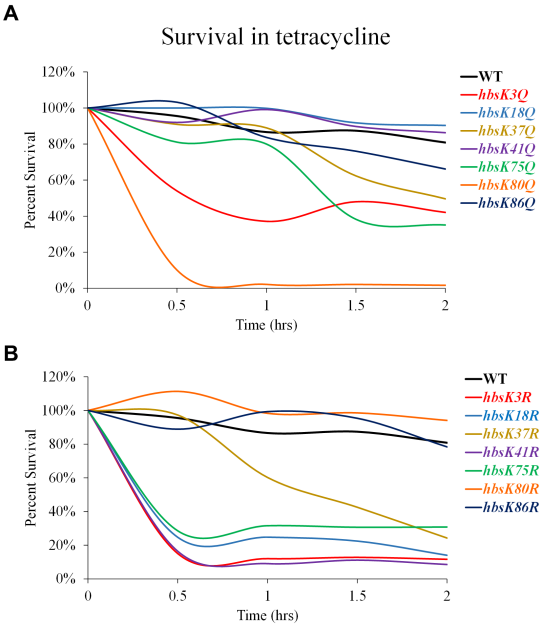

FIGURE 6
Interfering with HBsu acetylation alters survival in the presence of tetracycline. Cells were pre-grown in LB media, then incubated with or without 25 μg/mL tetracycline for 2 h, with viable counts determined every 30 min. Percent survival at each timepoint was determined as CFUs/mL following tetracycline treatment/initial colony counts (CFUs/mL). **(A)** Wildtype (BD630), *hbsK3Q* (BD8577), *hbsK18Q* (BD8219), *hbsK37Q* (BD8119), *hbsK41Q* (BD8147), *hbsK75Q* (BD8398), *hbsK80Q* (BD8576), and *hbsK86Q* (BD7493). **(B)** Wildtype (BD630), *hbsK3R* (BD8387), *hbsK18R* (BD8190), *hbsK37R* (BD8120), *hbsK41R* (BD8148), *hbsK75R* (BD8333), *hbsK80R* (BD7484), and *hbsK86R* (BD7506).

3.4 The effects of HBsu acetylation on the formation of persistent cells

So far, our data suggested that the acetylation of HBsu impacts survival during antibiotic stress. One explanation is that acetylation regulates DNA compaction, which we have provided evidence for above, and another possibility that HBsu regulates gene expression and the development of antibiotic-tolerant subpopulations, as found for the HBsu ortholog in *M. smegmatis* (Sakatos et al., 2018). To test this idea, wild-type and mutant cells were pre-grown in LB and subsequently exposed to kanamycin for 5 h before plating to assess survivors, which represent the persistent population. In comparison to wild-type, the *hbsK18Q* mutant exhibited a 2.55-fold increase in persisters, the *hbsK75Q* mutant showed a 1.98-fold increase, and the *hbsK41Q* mutant had a 2.26-fold increase, while all other Q mutants were only modestly increased compared to wild-type (Figure 7A). The *hbsK41R* mutant showed a similar increase to the *hbsK41Q* mutant of 2.34-fold. For the remaining R mutants, *hbsK37R* showed a 3-fold increase, *hbsK86R* had a 2-fold increase, and *hbsK80R* exhibited a 2.9-fold increase (Figure 7B). It should be noted that our data were highly variable among replicates, so we cannot draw strong conclusions. However, if we accept that the patterns were consistent among replicates, then this data suggested that in wild-type cells, K18 and K75 are deacetylated, while K37, K80, and K86 are acetylated in persistent cells. The acetylation status at K41 was unclear, but there is likely some level of acetylation required. Perhaps, cells with this acetylation pattern are more likely to enter the persistent state, which is based upon which genes are expressed. Understanding HBsu acetylation and its consequent effects is important for determining the

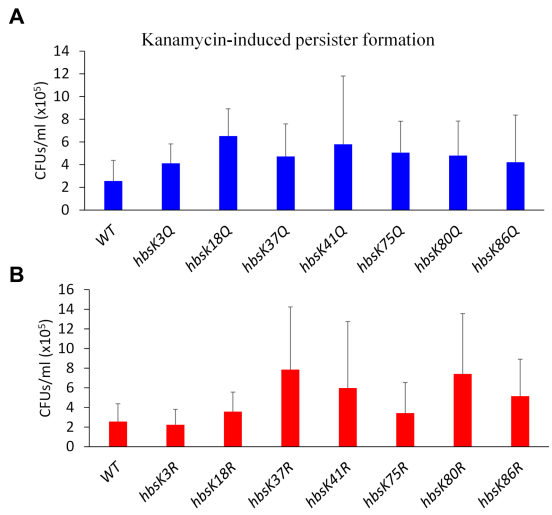

FIGURE 7
The influence of HBsu acetylation the formation of persisters. Cells were pre-grown in LB media for 1 h, and then exposed to 5 μg/mL kanamycin for 5 h. Serial dilutions were plated to determine survivors (CFUs/mL), which likely represented persisters. The data shown is an average of at least three independent replicates with standard deviation displayed. **(A)** Wildtype (BD630), *hbsK3Q* (BD8577), *hbsK18Q* (BD8219), *hbsK37Q* (BD8119), *hbsK41Q* (BD8147), *hbsK75Q* (BD8398), *hbsK80Q* (BD8576), and *hbsK86Q* (BD7493). **(B)** Wild-type (BD630), *hbsK3R* (BD8387), *hbsK18R* (BD8190), *hbsK37R* (BD8120), *hbsK41R* (BD8148), *hbsK75R* (BD8333), *hbsK80R* (BD7484), and *hbsK86R* (BD7506). CFU, Colony forming unit; WT, Wildtype.

specific role of acetylation and its connection to bacterial persistence which holds implications for developing strategies to regulate persistence in clinically relevant bacteria.

3.5 HBsu acetylation is required for recovery from the persistent state

While the overall numbers of persisters were increased in the presence of altered HBsu acetylation, we next determined if the cells that survived could properly escape from the semi-dormant, persistent state. Following the formation of persister cells in the presence of kanamycin and vancomycin, cells were washed and diluted into media without drugs and monitored for growth for 8 h in a multimode plate reader. The persisters from wild-type cells in the presence of kanamycin began growing within the first 30 min following dilution into fresh media (Figure 8A). The same was observed for *hbsK41Q* mutant cells. For all the other Q mutants, the persisters did grow, but at a slower rate than wild-type. The slowest growth rate was observed for the *hbsK75Q* strain (Figure 8A). For the deacetylated mimics, *hbsK37R* was similar to wild-type, while all the other mutants delayed growth significantly (Figure 8B). The *hbsK80R* and *hbsK75R* strains did not resume growth until after 5 h, while the *hbsK3R* and *hbsK86R* strains resumed growth between 6 and 7 h. The *hbsK18R* and *hbsK41R* strains resumed growth close to 8 h. As the *hbsK37R* strain did not delay growth and is the only one of the seven that does not have nucleoid compaction phenotype (Carabetta et al., 2019), this data suggested that nucleoid compaction is necessary to enter the persistent state and decompaction is required for escape.

Similar observations were made when the persister cells were harvested from vancomycin-treated cultures. Wild-type cells began growing after a 4-h delay (Figure 8C). The *hbsK3Q* strain began growing an hour earlier, while the *hbsK18Q*, *hbsK37Q*, *hbsK41Q*, *hbsK75Q*, and *hbsK80Q* strains began growth between 4 and 5 h. The *hbsK86Q* strain was the most delayed, beginning to grow at 5.5 h. For the opposite mutants, the *hbsK37R* strain began growth earlier than wild-type, but all other R mutants were delayed, beginning to grow after 5 h (Figure 8D). The largest defect was observed with the *hbsK41R* mutant, with growth only being observed close to 8 h. Together, these findings support that idea that K41 must be acetylated for decompaction of the chromosome to occur, as in either vancomycin or kanamycin, the *hbsK41R* mutants, had a severe phenotype.

4 Discussion

DNA compaction is widely acknowledged as an effective strategy employed by bacteria in response to environmental stressors (Boor, 2006; Hołówka and Zakrzewska-Czerwińska, 2020). Given the diverse environments that bacteria inhabit, ranging from extreme heat to cold or nutrient-rich to poor, DNA compaction is a rapid and practical mechanism to protect the chromosome from insults and enhance survival chances. Compaction of the nucleoid is crucial not only for spatial organization but also efficient segregation of replicated DNA during cell division, regulation of bacterial responses to environmental changes, and gene expression. Under stressful conditions, DNA compaction not only provides heightened protection but also affords bacteria the ability to conserve space and energy. This streamlined energy usage becomes crucial when bacteria must redirect their resources more efficiently, prioritizing tasks such as maintenance and response to stresses. *Escherichia coli, Helicobacter pylori, Deinococcus radiodurans*, and *B. subtilis* transiently condense their chromosomal DNA in response to different stresses to preserve genome integrity (Wolf et al., 1999; Smith et al., 2002; Eltsov and Dubochet, 2005; Ceci et al., 2007). Furthermore, recently, it was shown *M. tuberculosis* condenses the chromosome in response to the stressors of nutrient starvation and antibiotic treatment, and this response was important to survival (Scutigliani et al., 2018). However, it was unclear whether this response to antibiotic challenge represented a universal survival strategy in bacteria. Here, we showed that wild-type cells, when challenged with kanamycin, compacted the nucleoid as compared to cells not challenged (Figure 1). This suggested that nucleoid compaction may also be a bacterial survival strategy when challenged with antibiotics, perhaps to protect the DNA from drug-induced oxidative damage. Aminoglycosides target the bacterial ribosome but are also thought to induce the production of ROS, which is part of their killing mechanism (Kohanski et al., 2008). However, wild-type cells did not compact the nucleoid when challenged with tetracycline or vancomycin (Supplementary Figure S1). Tetracyclines and other bacteriostatic drugs do not lead to the production of hydroxyl radicals (Kohanski et al., 2007). In *Staphylococcus aureus*, exposure to vancomycin did lead to the production of hydroxyl radicals but following 3 h of treatment (Kohanski et al., 2007). For our microscopy studies, we examined cells after 20 min of exposure, to look for early responses and to ensure adequate cell numbers for quantification (Figure 1; Supplementary Figure S1). We propose that nucleoid

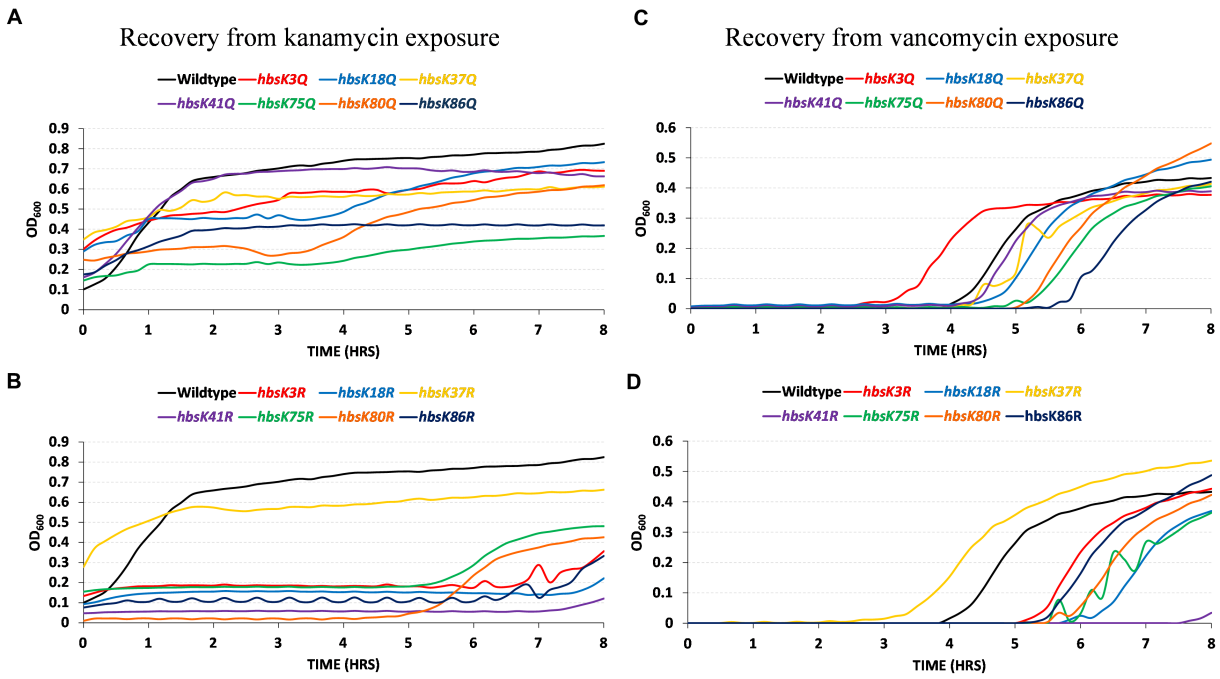

FIGURE 8
HBsu acetylation influences recovery from the persistent state. Persistent cells were prepared in the presence of kanamycin **(A,B)** and vancomycin **(C,D)**, as described in the Materials and Methods section. Cell pellets were washed three times in LB without antibiotics and added to a 96-well plate. Growth was monitored by OD_{600} determination every 10 min for 8 h in a microplate reader. The curves plotted are the averages of six determinations (three technical replicates for each of two biological replicates). **(A,C)** Wild-type (BD630), *hbsK3Q* (BD8577), *hbsK18Q* (BD8219), *hbsK37Q* (BD8119), *hbsK41Q* (BD8147), *hbsK75Q* (BD8398), *hbsK80Q* (BD8576), and *hbsK86Q* (BD7493). **(B,D)** Wild-type (BD630), *hbsK3R* (BD8387), *hbsK18R* (BD8190), *hbsK37R* (BD8120), *hbsK41R* (BD8148), *hbsK75R* (BD8333), *hbsK80R* (BD7484), and *hbsK86R* (BD7506).

compaction is a response to antibiotic-induced oxidative stress, and we predict that examination of cells following prolonged exposure to vancomycin would result in compacted nucleoids. The identity of the protein(s) that senses the stress and signals to condense the chromosome is currently unknown. We propose that one signal is HBsu acetylation, and then the signaling proteins would be those enzymes that modify HBsu, or other histone-like proteins in other species. With candidate enzymes identified, these ideas can be further explored. Additionally, further studies are required to confirm if chromosomal condensation is a response only to bactericidal drugs that induce oxidative stress or DNA damage (Kohanski et al., 2007).

The NAPs are the likely drivers of the DNA compaction response, as they are responsible for chromosome dynamics and organization. In addition, it is well established that they are important for adaptation to unfavorable conditions, including sudden stressors (Atlung and Ingmer, 1997; Nguyen et al., 2009; Mangan et al., 2011; Datta et al., 2019; Hołówka and Zakrzewska-Czerwińska, 2020). For both *M. tuberculosis* and *B. subtilis*, acetylation of the HU family proteins regulates DNA compaction. Here, we showed that mutation of specific acetylation sites of HBsu eliminates the nucleoid compaction response to drug challenge (Figure 2). Based on our findings, some level of acetylation at K3 was required for a proper response, and deacetylation at K75 was important. Acetylation at sites K18 and K80 were unimportant for nucleoid compaction under these conditions. For *hbsK41R* there were very small differences in the presence of absence of kanamycin, which should suggest that K41 must be acetylated (Figure 3). However, the *hbsK41Q* mutant resulted in a rightward shift, toward larger, expanded nucleoids. While this was unexpected, we propose that acetylation at K41 is required to decondense the chromosome to escape from this drug-induced state. This suggestion was supported by our data that showed that *hbsK41R* persisters from kanamycin or vancomycin-treated cells significantly delayed the entry into growth following removal of the antibiotic stress (Figures 8B,D). Another unusual observation was that both K37 mutants had distribution curves that were right shifted in the presence of drug. K37 was the only site where mutation to arginine did not lead to a compacted nucleoid in minimal media (Carabetta et al., 2019). The K37 persister cells escaped from the persistent state similar or earlier than wild-type (Figure 8), further suggesting that a relaxed chromosome is needed to escape the persistent state. K37 is not predicted to make direct contact with the chromosome (Figure 9). In this model, the DNA molecule is threaded through the extended "arms" on top of HBsu, and likely wraps down around it, which induces a severe bend in the DNA molecule that compacts and organizes the chromosome (Swinger and Rice, 2007). K37 points in the opposite direction of where the DNA molecule lies. It seems likely that the acetylation status at K37 does not influence chromosomal dynamics by direct DNA binding. Instead, we propose that this is an important interface for protein–protein interactions, and introduction of a non-native amino acid abolishes this interaction. By this model, the unknown protein would be regulatory in nature, in that it modulates the DNA binding activity of HBsu, possibly through acetylation of the other sites. It will be interesting to study the influence of the known HBsu acetyltransferases, YfmK and YdgE (Carabetta et al., 2019), and examine the possible contribution of the two known deacetylases in *B. subtilis,* AcuC and SrtN (Gardner and

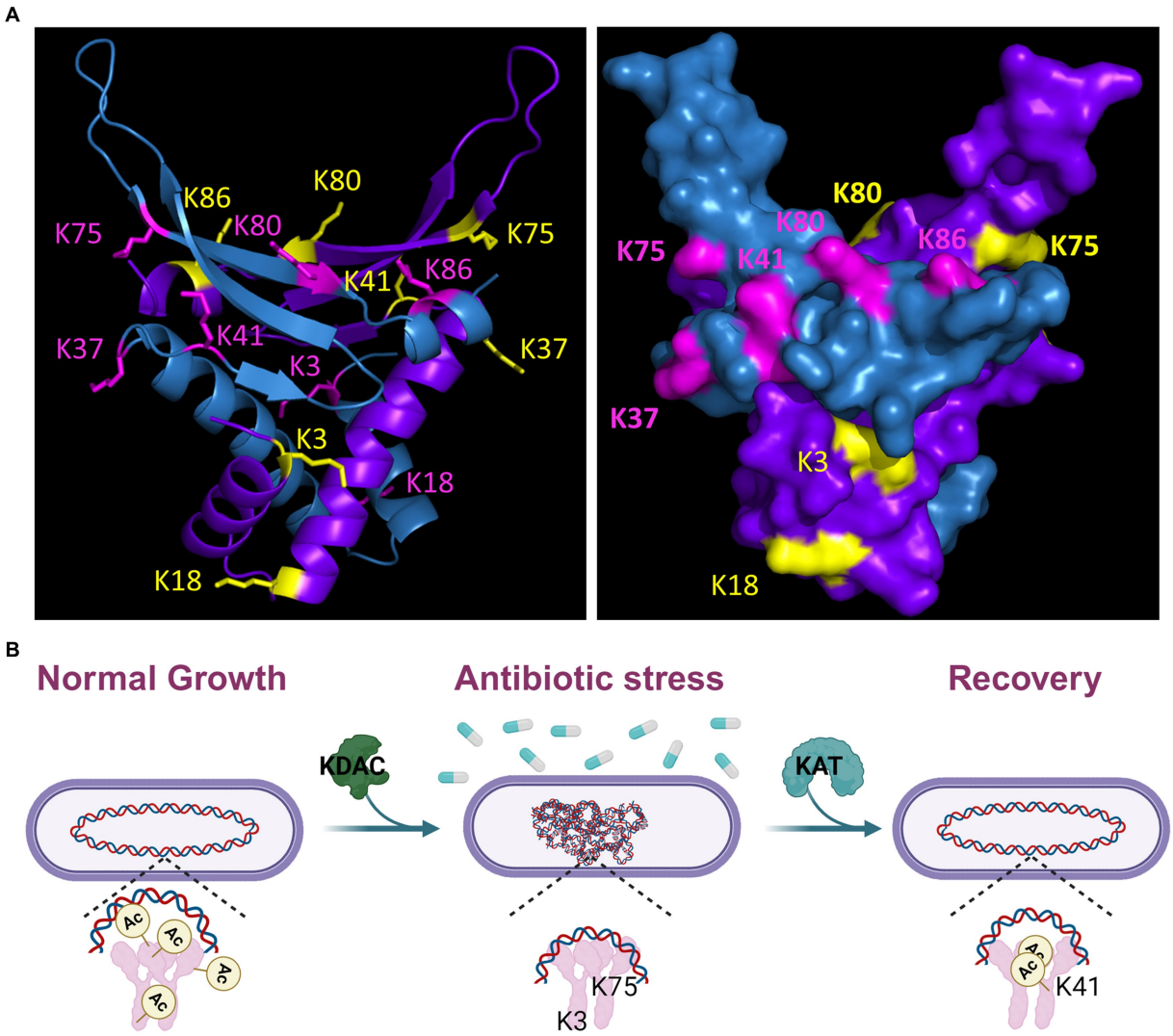

FIGURE 9
Model of HBsu response to antibiotic stress. **(A)** A *B. subtilis* HBsu structural model was generated in PyMOL using the *B. stearothermophilus* ortholog as a template (PDB 1HUU). The HBsu homodimer is displayed, with one monomer colored in cyan with the acetylated lysine sites (K3, K18, K37, K41, K75, K80, and K86) labeled in pink, and the other monomer colored purple with the acetylated sites labeled yellow. The left panel is a ribbon diagram, and the right shows a space-filling model. Reproduced and modified with permission from Carabetta et al. (2019). **(B)** During normal, exponential phase growth, HBsu is acetylated in specific patterns over the chromosome (left). In response to antibiotic stress, possibly only those that induce the formation of ROS, HBsu is deacetylated by an unknown KDAC, especially important at K3 and K75, which leads to a more compacted nucleoid (middle). This compaction may protect against further damage and/or change the transcriptional program to aid in survival. When the stress is removed, an unknown KAT acetylates HBsu and acetylation at K41 is likely an important early event to trigger the reentry into growth (right).

Escalante-Semerena, 2009). In addition, little is known about how these enzymes themselves are regulated and it is worth determining which one(s) are responsible setting the proper acetylation pattern on HBsu during times of stress.

In *M. tuberculosis*, the lack of nucleoid condensation is associated with decreased survival and recovery from the persistent state (Scutigliani et al., 2018). Interestingly, nearly all mutants tested displayed increased rates of killing in the presence of kanamycin and vancomycin (Figures 4, 5). The faster rate of death observed in the mutants could be due to the lack of significant compaction of the nucleoid for the *hbsK3Q and hbsK75Q* mutants. Nucleoid compaction is a protective response, whereby NAPs bind along the entire chromosome, compact the chromosome, and protect it from insults (Stojkova et al., 2018; Hołówka and Zakrzewska-Czerwińska, 2020). The DNA compaction response is also important for damage repair, such as double-stranded break repair (Shechter et al., 2013) and DNA replication initiation (Karaboja and Wang, 2022), which could also be the underlying reason for increased death rates. These possibilities are not mutually exclusive and further studies will be required to determine the exact underlying mechanism. Nonetheless, acetylation at K3 and K75 likely leads to a significant reduction in DNA binding affinity, as these sites likely contact the DNA molecule (Figure 9), thus making chromosome compaction less efficient or not effective. However, strains that did properly compact their nucleoids also exhibited faster death rates. As acetylation could influence multiple aspects of HBsu functions, other possibilities for reduced survival are that there is improper stress response signaling, or changes in gene expression of proteins that promote survival. Indeed, the *E. coli* HU

orthologs, HupA and HupB were found to control gene expression, where the regulon consists of ~350 genes, including many involved in stress responses (Oberto et al., 2009). Note that the regulon of HBsu is currently unknown and future investigations should be performed to determine if the acetylation status of HBsu alters gene expression during times of stress.

In *M. smegmatis*, it was found that acetylation of HupB regulates the emergence of a specific slow-growing, drug-tolerant subpopulation, likely by controlling gene expression (Sakatos et al., 2018). Specifically, mutation of K86, which is modified by both acetylation and methylation in this species, to the unmodified mimic resulted in a loss of the SCV subpopulation. Here, we found that acetylation of HBsu at K18, K41, and K75 led to at least 2-fold increases in the number of persisters (Figure 7A). This would be predicted based upon the data from *M. smegmatis*. Surprisingly, we did not see decreases in persisters in any mutants but observed increased numbers for some of the R mutants, specifically at K37, K41, K80, and K86 (Figure 7B). It is unclear if SCVs or LCVs exist in *B. subtilis*, so this could be one explanation for the observed differences. Although our data was highly variable, there was a suggestion that the acetylation status of HBsu influences gene expression, making the transition into the persistent state more likely. However, once in the persistent state, altering the acetylation status of HBsu makes the escape more challenging (Figure 8). Our data suggests that acetylation of HBsu is required to escape the persistent state, with K41 possibly being the most important site. All the R mutants, except for *hbsK37R* were delayed in re-entering growth, and we propose that this is because the nucleoids were highly compacted, which did allow for the resumption of DNA replication or transcription due to lack of access to the chromosome. In addition, our data suggests that while DNA compaction may be an important response as an attempt to maintain genome integrity, it is of most benefit to the persistent population. A more in-depth transcriptomic analysis of these persisters is warranted to fully understand the influence of HBsu acetylation on persister cell formation and survival.

The persistent subpopulation is what makes pathogens able to remain dormant and survive antibiotic challenge in patients. Initially thought to be rare, persister cells are non-growing cells capable of withstanding drug concentrations many times higher than the minimum inhibitory concentration (Bigger, 1944; Sakatos et al., 2018). The clinical implication of bacterial persistence is treatment failure, which can result in chronic infections. The persisters represent only a subpopulation, meaning that while the majority of the infection will be killed by antibiotics, the persisters survive. When the antibiotic stress is removed, i.e., due to the completion of a regimen, the persisters can grow and divide again, leading to recurrent infections. In addition, when persisters survive the initial antibiotic exposure, there is an increased likelihood of acquiring resistance through genetic mutation or HGT, possibly from interactions with the native microbiota (Huemer et al., 2020). Alarmingly, this dual threat not only allows persisters to survive standard treatment, but also contributes to the emergence of more resistant bacterial strains, limiting the effectiveness of available antibiotics.

As chronic infections are a significant healthcare burden and increase morbidity and mortality for patients, it would be worthwhile to further explore how modulation of the acetylation status of the histone-like proteins influences drug-tolerant sub-populations in both Gram-negative and -positive bacteria. If it is found that interfering with DNA condensation or gene expression reduces survival or eliminates drug-tolerant subpopulations, the design of novel drugs that block or interfere with histone-like protein acetylation could be pursued. In fact, in *M. smegmatis,* the acetyltransferase Eis acetylates HupB, which limits its DNA-binding capability. Scutigliani et al. (2018) showed that treatment of *M. smegmatis* with fusidic acid to induce DNA condensation, followed by Eis inhibitors led to drug synergy and more efficient killing. They proposed that by inhibiting acetylation, the nucleoid remained compacted, and the cells could not escape from the dormant persistent state (Scutigliani et al., 2018). We observed that some acetylation mutants in combination with tetracycline displayed synergistic effects, leading to rapid killing in the presence of a bacteriostatic drug. There have been previous reports of tetracyclines having synergistic effects and enhancing the potency of other drugs (Mawabo et al., 2015; Cacace et al., 2023). If we consider the HBsu mutations as a phenotypic mimic of a hypothetical drug that interferes with chromosomal compaction or organization, the combination of this hypothetical drug with tetracyclines might represent a novel strategy to augment and enhance treatment with bacteriostatic agents.

A drug that interferes with HU-family protein acetylation could potentially treat infections by killing actively growing cells and eliminating some persistent subpopulations, creating a more effective treatment option. Our findings suggest that acetylation of K41 is required to decondense the nucleoid and escape the persistent state (Figures 2, 3, 7, 8). If this finding is validated, identification of the appropriate acetyltransferase responsible for K41 acetylation during antibiotic stress could reveal a new target for novel drug design. Our lab has identified five potential enzymes (Carabetta et al., 2019). This drug could be used in an analogous fashion to those in *M. smegmatis*, where it may be more effective at killing in combination with aminoglycosides or tetracylcines. It is worth noting that in the Gram-positive pathogenic bacterium *S. aureus*, a recent report identified acetylation sites on the HBsu ortholog (Hsa) as K3, K18, K38, K67, K75, K80, K83, and K86 (Tan et al., 2022). Based on our data, if we assume chromosome compaction is a universal bacterial response to drug-induced stress, we predict that K38 acetylation of HSa plays a similar role as K41 acetylation of HBsu for recovery from a drug-induced, persistent state. If these predictions hold true, it is possible that we could identify broad-spectrum drug targets that can be used in the fight against drug-resistant infections.

5 Conclusion

As more largescale proteomic analyses of bacterial PTMs were published, it became clear that the HU-family of proteins were routinely identified among the modified proteins in diverse species (Carabetta, 2021). The HU-family of proteins is the most widely conserved NAP among bacteria, and this includes the conservation of the regulation by PTMs. In *B. subtilis,* we identified seven novel acetylation sites. So far, we know that some level of acetylation is required at six of those sites, all except for K37, for proper chromosomal compaction during growth (Carabetta et al., 2019). K37 is the only site that is not predicted to directly contact the DNA (Figure 9), which suggests that it may represent an important protein–protein interface, where acetylation can regulate this interaction.

We also examined the impact of HBsu acetylation on sporulation and found that K41 acetylation is not important and deacetylation at K3 is required for normal sporulation frequency. For all other sites, some level of acetylation is needed. The patterns of acetylation required for resistance properties of mature spores were different (Luu et al., 2022). This data suggested that there may be sporulation-specific regulation of acetyltransferases or deacetylases that set the HBsu acetylation patterns, both before and after chromosomal packing into the mature spore. Here, we have expanded upon those findings. Our current model is that during exponential growth, HBsu is acetylated in specific, but currently unknown, patterns over the entire chromosome (Figure 9B). We propose that local areas on the chromosome contain highly acetylated HBsu species and these regions contain genes that are actively transcribed, analogous to eukaryotic histones. In response to antibiotic stress, possibly only those that induce the formation of ROS, HBsu is deacetylated by an unknown KDAC, which begins the compaction process. Our data suggests that K3 and K75 deacetylation is particularly important. This compaction may protect against further DNA damage. However, as most of the mutants displayed faster killing kinetics in the presence of drug, regardless of their nucleoid compaction state, we suggest that HBsu plays additional roles, possibly by altering the transcriptional program to ensure survival. When the stress is removed, an unknown KAT acetylates HBsu. Acetylation of K41 is particularly important and seems to be a signal to resume growth and decondense the chromosome. In the persistent subpopulation (Figure 7), K18 and K75 were deacetylated, while K37, K80, K86 were acetylated. Perhaps this acetylation pattern regulates gene expression or important protein–protein interactions and allows for cells to remain in a slow growing, metabolically inactive state. One thing is for certain, there are different acetylation patterns of HBsu that have phenotypic consequences depending on the growth conditions, which lends further support for the existence of a histone-like code in bacteria. The missing piece of information for all these studies is an understanding of how HBsu acetylation influences gene expression. Currently, we do not know where HBsu specifically binds on the chromosome during growth or under stress conditions, and we do not know the members of its regulon. This information must be determined next, using largescale omics studies, like RNA-seq, ChIP-seq, and Hi-C. With this information available, we can examine the effects of our collection of acetylation mutant strains to determine the influence of acetylation on gene expression during different developmental fates or during stressful conditions. If protein acetylation of HBsu influences the transition into the persistent state, recovery from persistence, or contributes to antibiotic survival, the identification of novel molecules that can inhibit this process, by targeting an acetyltransferase, deacetylase, or HBsu itself, could become new antimicrobial weapons against Gram-positive infections. A mechanism to target or eliminate the persistent population would tremendously reduce the risk of recurrent infections for patients and would lead to more efficient treatment. This promising and exiting possibility deserves further exploration.

Data availability statement

The original contributions presented in the study are included in the article/Supplementary material, further inquiries can be directed to the corresponding author.

Author contributions

RC: Validation, Visualization, Writing – original draft, Writing – review & editing, Formal analysis, Investigation, Project administration. TT: Formal analysis, Investigation, Writing – review & editing. PN: Formal analysis, Investigation, Writing – review & editing. LJ: Formal analysis, Investigation, Writing – original draft. KJ: Formal analysis, Investigation, Writing – original draft. DA: Formal analysis, Investigation, Writing – original draft. AK: Formal analysis, Investigation, Visualization, Writing – original draft. AP: Formal analysis, Investigation, Writing – review & editing. VC: Conceptualization, Funding acquisition, Resources, Supervision, Validation, Visualization, Writing – original draft, Writing – review & editing. BR: Investigation, Visualization, Writing – original draft, Writing – review & editing.

Funding

The author(s) declare that financial support was received for the research, authorship, and/or publication of this article. This work was supported by grant R35GM138303 from the National Institute of General Medical Sciences awarded to VC. Research reported in this publication was supported by the National Institute of General Medical Sciences of the National Institutes of Health under Award Number T34GM136492.

Acknowledgments

We would like to thank members of the Carabetta lab for critical reading of the manuscript. Figure 9B was created using Biorender.com.

Conflict of interest

The authors declare that the research was conducted in the absence of any commercial or financial relationships that could be construed as a potential conflict of interest.

Publisher's note

Author disclaimer

The content is solely the responsibility of the authors and does not necessarily represent the official views of the National Institutes of Health.

Supplementary material

The Supplementary material for this article can be found online at: https://www.frontiersin.org/articles/10.3389/fmicb.2024.1356733/full#supplementary-material

References

Anand, C., Garg, R., Ghosh, S., and Nagaraja, V. (2017). A Sir2 family protein Rv1151c deacetylates HU to alter its DNA binding mode in *Mycobacterium tuberculosis*. *Biochem. Biophys. Res. Commun.* 493, 1204–1209. doi: 10.1016/j.bbrc.2017.09.087

Atlung, T., and Ingmer, H. (1997). H-NS: a modulator of environmentally regulated gene expression. *Mol. Microbiol.* 24, 7–17. doi: 10.1046/j.1365-2958.1997.3151679.x

Bannister, A. J., and Kouzarides, T. (2011). Regulation of chromatin by histone modifications. *Cell Res.* 21, 381–395. doi: 10.1038/cr.2011.22

Bigger, J. (1944). Treatment of staphylococcal infections with penicillin by intermittent sterilization. *Lancet* 244, 497–500. doi: 10.1016/S0140-6736(00)74210-3

Boor, K. J. (2006). Bacterial stress responses: what doesn't kill them can make them stronger. *PLoS Biol.* 4:e23. doi: 10.1371/journal.pbio.0040023

Cacace, E., Kim, V., Varik, V., Knopp, M., Tietgen, M., Brauer-Nikonow, A., et al. (2023). Systematic analysis of drug combinations against gram-positive bacteria. *Nat. Microbiol.* 8, 2196–2212. doi: 10.1038/s41564-023-01486-9

Carabetta, V. J. (2021). Addressing the possibility of a histone-like code in bacteria. *J. Proteome Res.* 20, 27–37. doi: 10.1021/acs.jproteome.0c00442

Carabetta, V. J., and Cristea, I. M. (2017). Regulation, function, and detection of protein acetylation in bacteria. *J. Bacteriol.* 199:e00107-17. doi: 10.1128/JB.00107-17

Carabetta, V. J., Greco, T. M., Cristea, I. M., and Dubnau, D. (2019). YfmK is an N(epsilon)-lysine acetyltransferase that directly acetylates the histone-like protein HBsu in *Bacillus subtilis*. *Proc. Natl. Acad. Sci. USA* 116, 3752–3757. doi: 10.1073/pnas.1815511116

CDC (2019). "Biggest threats and data|Antibiotic/AntimicrobialResistance|CDC. Available at: https://www.cdc.gov/drugresistance/biggest-threats.html#acine (Accessed September 20, 2023).

Ceci, P., Mangiarotti, L., Rivetti, C., and Chiancone, E. (2007). The neutrophil-activating Dps protein of *Helicobacter pylori*, HP-NAP, adopts a mechanism different from *Escherichia coli* Dps to bind and condense DNA. *Nucleic Acids Res.* 35, 2247–2256. doi: 10.1093/nar/gkm077

Christensen, D. G., Baumgartner, J. T., Xie, X., Jew, K. M., Basisty, N., Schilling, B., et al. (2019a). Mechanisms, detection, and relevance of protein acetylation in prokaryotes. *MBio* 10:e02708-18. doi: 10.1128/mBio.02708-18

Christensen, D. G., Xie, X., Basisty, N., Byrnes, J., McSweeney, S., Schilling, B., et al. (2019b). Post-translational protein acetylation: an elegant mechanism for bacteria to dynamically regulate metabolic functions. *Front. Microbiol.* 10:1604. doi: 10.3389/fmicb.2019.01604

Datta, C., Jha, R. K., Ganguly, S., and Nagaraja, V. (2019). NapA (Rv0430), a novel nucleoid-associated protein that regulates a virulence operon in *Mycobacterium tuberculosis* in a supercoiling-dependent manner. *J. Mol. Biol.* 431, 1576–1591. doi: 10.1016/j.jmb.2019.02.029

Eltsov, M., and Dubochet, J. (2005). Fine structure of the *Deinococcus radiodurans* nucleoid revealed by cryoelectron microscopy of vitreous sections. *J. Bacteriol.* 187, 8047–8054. doi: 10.1128/jb.187.23.8047-8054.2005

Gardner, J. G., and Escalante-Semerena, J. C. (2009). In *Bacillus subtilis*, the sirtuin protein deacetylase, encoded by the *srtN* gene (formerly *yhdZ*), and functions encoded by the *acuABC* genes control the activity of acetyl coenzyme a synthetase. *J. Bacteriol.* 191, 1749–1755. doi: 10.1128/JB.01674-08

Ghosh, S., Padmanabhan, B., Anand, C., and Nagaraja, V. (2016). Lysine acetylation of the *Mycobacterium tuberculosis* HU protein modulates its DNA binding and genome organization. *Mol. Microbiol.* 100, 577–588. doi: 10.1111/mmi.13339

Gollan, B., Grabe, G., Michaux, C., and Helaine, S. (2019). Bacterial persisters and infection: past, present, and progressing. *Ann. Rev. Microbiol.* 73, 359–385. doi: 10.1146/annurev-micro-020518-115650

Harms, A., Maisonneuve, E., and Gerdes, K. (2016). Mechanisms of bacterial persistence during stress and antibiotic exposure. *Science* 354:aaf4268. doi: 10.1126/science.aaf4268

Hołówka, J., and Zakrzewska-Czerwińska, J. (2020). Nucleoid associated proteins: the small organizers that help to cope with stress. *Front. Microbiol.* 11:590. doi: 10.3389/fmicb.2020.00590

Huemer, M., Mairpady Shambat, S., Brugger, S. D., and Zinkernagel, A. S. (2020). Antibiotic resistance and persistence: implications for human health and treatment perspectives. *EMBO Rep.* 21:e51034. doi: 10.15252/embr.202051034

Karaboja, X., and Wang, X. (2022). HBsu is required for theinitiation of DNA replication in *Bacillus subtilis*. *J. Bacteriol.* 204:e0011922. doi: 10.1128/jb.00119-22

Karson, M. (1968). Handbook of methods of applied statistics. *J. Am. Stat. Assoc.* 63, 1047–1049. doi: 10.1080/01621459.1968.11009335

Kohanski, M. A., Dwyer, D. J., Hayete, B., Lawrence, C. A., and Collins, J. J. (2007). A common mechanism of cellular death induced by bactericidal antibiotics. *Cell* 130, 797–810. doi: 10.1016/j.cell.2007.06.049

Kohanski, M. A., Dwyer, D. J., Wierzbowski, J., Cottarel, G., and Collins, J. J. (2008). Mistranslation of membrane proteins and two-component system activation trigger antibiotic-mediated cell death. *Cell* 135, 679–690. doi: 10.1016/j.cell.2008.09.038

Köhler, P., and Marahiel, M. A. (1997). Association of the histone-like protein HBsu with the nucleoid of *Bacillus subtilis*. *J. Bacteriol.* 179, 2060–2064. doi: 10.1128/jb.179.6.2060-2064.1997

Lerminiaux, N. A., and Cameron, A. D. S. (2019). Horizontal transfer of antibiotic resistance genes in clinical environments. *Can. J. Microbiol.* 65, 34–44. doi: 10.1139/cjm-2018-0275

Llor, C., and Bjerrum, L. (2014). Antimicrobial resistance: risk associated with antibiotic overuse and initiatives to reduce the problem. *Ther. Adv. Drug Saf.* 5, 229–241. doi: 10.1177/2042098614554919

Luu, J., Mott, C. M., Schreiber, O. R., Giovinco, H. M., Betchen, M., and Carabetta, V. J. (2022). Nε-lysine acetylation of the histone-like protein HBsu regulates the process of sporulation and affects the resistance properties of *Bacillus subtilis* spores. *Front. Microbiol.* 12:782815. doi: 10.3389/fmicb.2021.782815

Mangan, M. W., Lucchini, S., Ó Cróinín, T., Fitzgerald, S., Hinton, J. C. D., and Dorman, C. J. (2011). Nucleoid-associated protein HU controls three regulons that coordinate virulence, response to stress and general physiology in *Salmonella enterica* serovar typhimurium. *J. Gen. Microbiol.* 157, 1075–1087. doi: 10.1099/mic.0.046359-0

Mawabo, I. K., Noumedem, J. A. K., Kuiate, J. R., and Kuete, V. (2015). Tetracycline improved the efficiency of other antimicrobials against gram-negative multidrug-resistant bacteria. *J Infect Public Heal* 8, 226–233. doi: 10.1016/j.jiph.2014.09.001

Micka, B., and Marahiel, M. A. (1992). The DNA-binding protein HBsu is essential for normal growth and development in *Bacillus subtilis*. *Biochimie* 74, 641–650. doi: 10.1016/0300-9084(92)90136-3

Nguyen, H. H., De La Tour, C. B., Toueille, M., Vannier, F., Sommer, S., and Servant, P. (2009). The essential histone-like protein HU plays a major role in *Deinococcus radiodurans* nucleoid compaction. *Mol. Microbiol.* 73, 240–252. doi: 10.1111/j.1365-2958.2009.06766.x

Oberto, J., Nabti, S., Jooste, V., Mignot, H., and Rouviere-Yaniv, J. (2009). The HU regulon is composed of genes responding to anaerobiosis, acid stress, high osmolarity and SOS induction. *PLoS One* 4:e4367. doi: 10.1371/journal.pone.0004367

Ohniwa, R. L., Ushijima, Y., Saito, S., and Morikawa, K. (2011). Proteomic analyses of nucleoid-associated proteins in *Escherichia coli*, *Pseudomonas aeruginosa*, *Bacillus subtilis*, and *Staphylococcus aureus*. *PLoS One* 6:e19172. doi: 10.1371/journal.pone.0019172

Patel, D. J., and Wang, Z. (2013). Readout of epigenetic modifications. *Annu. Rev. Biochem.* 82, 81–118. doi: 10.1146/annurev-biochem-072711-165700

R Core Team (2021). "R: A language and environment for statistical computing". R Foundation for Statistical Computing, Vienna, Austria.

Rittershaus, E. S., Baek, S. H., and Sassetti, C. M. (2013). The normalcy of dormancy: common themes in microbial quiescence. *Cell Host Microbe* 13, 643–651. doi: 10.1016/j.chom.2013.05.012

Sakatos, A., Babunovic, G. H., Chase, M. R., Dills, A., Leszyk, J., Rosebrock, T., et al. (2018). Posttranslational modification of a histone-like protein regulates phenotypic resistance to isoniazid in mycobacteria. *Sci. Adv.* 4:eaao1478. doi: 10.1126/sciadv.aao1478

Schibany, S., Hinrichs, R., Hernández-Tamayo, R., and Graumann, P. L. (2020). The major chromosome condensation factors Smc, HBsu, and gyrase in *Bacillus subtilis* operate via strikingly different patterns of motion. *mSphere* 5:e00817-20. doi: 10.1128/mSphere.00817-20

Scutigliani, E. M., Scholl, E. R., Grootemaat, A. E., Khanal, S., Kochan, J. A., Krawczyk, P. M., et al. (2018). Interfering with DNA decondensation as a strategy against mycobacteria. *Front. Microbiol.* 9:2034. doi: 10.3389/fmicb.2018.02034

Shechter, N., Zaltzman, L., Weiner, A., Brumfeld, V., Shimoni, E., Fridmann-Sirkis, Y., et al. (2013). Stress-induced condensation of bacterial genomes results in re-pairing of sister chromosomes: implications for double strand DNA break repair. *J. Biol. Chem.* 288, 25659–25667. doi: 10.1074/jbc.M113.473025

Smith, B. T., Grossman, A. D., and Walker, G. C. (2002). Localization of UvrA and effect of DNA damage on the chromosome of *Bacillus subtilis*. *J. Bacteriol.* 184, 488–493. doi: 10.1128/jb.184.2.488-493.2002

Stojkova, P., Spidlova, P., Lenco, J., Rehulkova, H., Kratka, L., and Stulik, J. (2018). HU protein is involved in intracellular growth and full virulence of *Francisella tularensis*. *Virulence* 9, 754–770. doi: 10.1080/21505594.2018.1441588

Stojkova, P., Spidlova, P., and Stulik, J. (2019). Nucleoid-associated protein HU: a lilliputian in gene regulation of bacterial virulence. *Front. Cell. Infect. Microbiol.* 9:159. doi: 10.3389/fcimb.2019.00159

Strahl, B. D., and Allis, C. D. (2000). The language of covalent histone modifications. *Nature* 403, 41–45. doi: 10.1038/47412

Sun, D. (2018). Pull in and push out: mechanisms of horizontal gene transfer in bacteria. *Front. Microbiol.* 9:2154. doi: 10.3389/fmicb.2018.02154

Swinger, K. K., and Rice, P. A. (2007). Structure-based analysis of HU-DNA binding. *J. Mol. Biol.* 365, 1005–1016. doi: 10.1016/j.jmb.2006.10.024

Tan, L., Yang, Y., Shang, W., Hu, Z., Peng, H., Li, S., et al. (2022). Identification of lysine succinylome and acetylome in the vancomycin-intermediate *Staphylococcus aureus* XN108. *Microbiol. Spect.* 10, e03481–e03422. doi: 10.1128/spectrum.03481-22

VanDrisse, C. M., and Escalante-Semerena, J. C. (2019). Protein acetylation in bacteria. *Ann. Rev. Microbiol.* 73, 111–132. doi: 10.1146/annurev-micro-020518-115526

Windels, E. M., Michiels, J. E., Fauvart, M., Wenseleers, T., Van den Bergh, B., and Michiels, J. (2019). Bacterial persistence promotes the evolution of antibiotic resistance by increasing survival and mutation rates. *ISME J.* 13, 1239–1251. doi: 10.1038/s41396-019-0344-9

Wolf, S. G., Frenkiel, D., Arad, T., Finkel, S. E., Kolter, R., and Minsky, A. (1999). DNA protection by stress-induced biocrystallization. *Nature* 400, 83–85. doi: 10.1038/21918

Frontiers in Microbiology

Explores the habitable world and the potential of microbial life

The largest and most cited microbiology journal which advances our understanding of the role microbes play in addressing global challenges such as healthcare, food security, and climate change.

Discover the latest Research Topics

See more →

Frontiers

Avenue du Tribunal-Fédéral 34
1005 Lausanne, Switzerland
frontiersin.org

Contact us

+41 (0)21 510 17 00
frontiersin.org/about/contact